

UNCLASSIFIED

AD NUMBER

AD804727

LIMITATION CHANGES

TO:

Approved for public release; distribution is unlimited.

FROM:

Distribution authorized to U.S. Gov't. agencies and their contractors;  
Administrative/Operational Use; 06 SEP 1966.  
Other requests shall be referred to Federal Aviation Administration, Washington, DC 20591.

AUTHORITY

FAA notice, 2 Jul 1973

THIS PAGE IS UNCLASSIFIED

804727

PHASE III PROPOSAL  
AIRFRAME DESIGN  
REPORT PART B

AR 112

NOV 1957



V2-B2707-β-2

Phase II Proposal

① Supersonic Transport Development Program •  
Phase II Proposal  
BOEING MODEL 2707

Volume II-6-2

AIRFRAME DESIGN REPORT.  
PART B  
COMPONENT DESIGN

⑭ V2-B2707-6-2

September 6, 1966

D D C  
RECEIVED  
JAN 13 1967  
BY

⑩  
⑪  
⑫

PREPARED BY

*John E. Johnson*

APPROVED BY

*H. ...*

⑮  
Contract FA-SS-66-5 ✓

Prepared for  
FEDERAL AVIATION AGENCY  
Office of Supersonic Transport Development Program

"THIS DOCUMENT CONTAINS SENSITIVE, COMPETITIVE, AND PROPRIETARY DATA, AND IS NOT TO BE REPRODUCED OR RELEASED OUTSIDE OF YOUR ORGANIZATION OR USED FOR ANY PURPOSE OTHER THAN SUPERSONIC TRANSPORT EVALUATION WITHOUT THE WRITTEN PERMISSION OF EITHER THE FEDERAL AVIATION AGENCY, OFFICE OF SUPERSONIC TRANSPORT DEVELOPMENT, ATTENTION: 55-30 OR THE BOEING COMPANY, SUPERSONIC TRANSPORT DIVISION, ATTENTION: CONTRACT ADMINISTRATION"

112 097

THE **BOEING** COMPANY  
SUPERSONIC TRANSPORT DIVISION

FAA

6

ISSUE NO. A 105

**BLANK PAGE**

## CONTENTS

	Page
1.0 INTRODUCTION AND SUMMARY	1
1.1 INTRODUCTION	1
1.2 SUMMARY	1
2.0 STRUCTURAL DESIGN	7
2.1 STRUCTURAL DESIGN APPROACH	7
2.2 AIRFRAME DESIGN, GENERAL	7
2.3 FATIGUE AND FAIL-SAFE	9
2.4 STRUCTURAL ACCESS	9
2.5 ENGINEERING-MANUFACTURING COORDINATED DOLLAR SIGN SURFACES	9
3.0 DESIGN DESCRIPTION	13
3.1 WING CONSTRUCTION	13
3.2 FUSELAGE	48
3.3 HORIZONTAL STABILIZER	80
3.4 VERTICAL AND VENTRAL FINS	93
3.5 LANDING GEAR	109
3.6 STRUCTURAL INSPECTION AND REPAIR	125
4.0 STRESS ANALYSIS	135
4.1 METHODS OF ANALYSIS	135
4.2 WING STRESS ANALYSIS	135
4.3 FUSELAGE STRESS ANALYSIS	178
4.4 EMPENNAGE STRESS ANALYSIS	205
4.5 LANDING GEAR STRESS ANALYSIS	226
4.6 PROPULSION POD STRESS ANALYSIS	241
5.0 FATIGUE ANALYSIS	258
5.1 FATIGUE CRITERIA	258
5.2 FATIGUE ENVIRONMENT	258
5.3 S-N CURVES	262
5.4 FATIGUE ANALYSIS PROCEDURE	262
5.5 FATIGUE ANALYSIS RESULTS	267
5.6 ONE-G STRESSES	267

**B-2707 PHASE III PROPOSAL DOCUMENTATION INDEX**

VOLUME I	VOLUME III	VOLUME V
<b>SUMMARY</b> V1-B2707	<b>ENGINE CONTRACTORS ONLY</b>	<b>MANAGEMENT/ MANUFACTURING</b> V5-B2707
Phase III Proposal Summary -1		Configuration Management Plan -1
Boeing Model 2707 Warranties Program -2		Data Management Plan -2
		Master Program Plan -3
<b>VOLUME II</b>		Detail Work Plan -4
<b>AIRPLANE TECHNICAL REPORT</b> V2-B2707		Procurement Program -5
System Engineering Report -1	<b>VOLUME IV</b>	Cost & Schedules Control Program -6
Mockup Plan -2	<b>SYSTEM INTEGRATION</b> V4-B2707	Facilities Program -7
Aerodynamic Design Report -3	Operational Suitability -1	Program Management -8
Airplane Performance (GE) -4	Sonic Boom Program -3	Manufacturing Program -9
Airplane Performance (P&W) -5	Airport & Community Noise Program -4	
Airframe Design Report -6-1	Internal Noise Program -5	<b>VOLUME VI</b>
Part A Weight & Balance	System Safety Plan -6	<b>COST</b> V6-B2707
<b>Airframe Design Report -6-2</b>	Training & Training Equipment Program -7	Cost Baseline Report Summary Data -1
Part B Component Design	Human Engineering Program -8	Cost Baseline Report Cost Support Data -2
Airframe Design Report- Part C -7	Test Integration & Management -10	
Design Criteria Loads	Integrated Test Program -11	<b>VOLUME VII</b>
Aerodynamic Heating Flutter	Simulation Program -12	<b>ECONOMICS</b> V7-B2707
Airframe Design Report- Part D -8	Flight Simulator Program -13	Economic Summary -1
Materials and Processes	Flight Test Program -14	Economic Summary - For Government Use Only -2
Airframe Design Report- Part E -9	Maintainability Program -15	
Structural Tests	Reliability Program -16	
Systems Report-Part A -10	Quality Control Program -17	
Environmental Control Electric	Value Engineering Program -18	
Navigation and Communications	Standardization Program -19	
Systems Report-Part B -11	Product Support Program -20	
Hydraulics	Quality Assurance Program -21	
Landing Gear		
Auxiliary Systems		
Propulsion Report-Part A -12		
Engine, Inlet, & Controls		
Propulsion Report-Part B -13		
Engine Installation		
Fuel System		
Exhaust System		
Propulsion Report-Part C -14		
Engine Evaluation		

## 1.0 INTRODUCTION AND SUMMARY

### 1.1 INTRODUCTION

This document is Part B, Component Design, of the Airframe Design Report and one of a series of documents under Volume II, Technical/Airplane, called for by the FAA Request for Proposal for Phase III of the Supersonic Transport Development Program. The Airframe Design Report is published in five parts:

Part A, Weight and Balance  
(V2-B2707-6-1)

Part B, Component Design  
(V2-B2707-6-2)

Part C, Design Criteria, Loads, Aerodynamic Heating, Flutter  
(V2-B2707-7)

Part D, Material and Processes  
(V2-B2707-8)

Part E, Structural Tests  
(V2-B2707-9)

This book describes the production version of the B-2707. Minimal differences will exist between the production and prototype airplanes because of availability of materials, processes, and facilities.

Section 2.0 contains a general discussion of the structural design. *is presented*

Section 3.0 contains a complete description of structural design features of the wing, fuselage, empennage, control surfaces, and landing gear, including drawings of all major assemblies. Figure 1-1 is a three-view drawing of the B-2707. *is included*

Section 4.0 contains a preliminary stress analysis, including methods of analysis, stress levels, member sizes, allowable stresses, and analysis and description of fail-safe designs. An analysis of structure designed by sonic or high-temperature effects is included. *discusses*

Section 5.0 contains a fatigue analysis, *includes* including fatigue criteria and environment, analysis procedure, fatigue damage summaries, fatigue analysis results, and 1-g stress levels.

### 1.2 SUMMARY

The structural arrangement of the B-2707, as shown in Fig. 1-2, with its variable sweep wing and integrated tail, has the following outstanding structural features:

- Excellent slow-speed characteristics are achieved by continuous full-span, leading-edge and trailing-edge, high-lift wing devices uninterrupted by engine inlets or exhausts.
- A deep wing is possible as a result of the fully integrated wing and horizontal tail, along with attendant advantages of maximum space for systems and fuel containment and a more efficient primary structure. Space within the trailing edge permits a more efficient flap system.
- The integrated wing-tail airfoil allows a deeper lower-fuselage lobe with decreased structural weight, increased stiffness, and more space for fuel, cargo, and landing gear stowage.
- The design of the aft-retracting landing gear allows continuity of the side fuselage structure.
- The double-pivoting fuselage nose provides forward and side vision superior to present commercial jet transports.
- Aft engine location eliminates exposure of the fuselage and tail surface to high temperatures from engine exhausts and minimizes exposure of structure to high-sonic levels.
- The integrated wing planform allows a fixed horizontal tail.

- The four-post landing gear allows unit gear loads to be reduced to a value consistent with commercial subsonic jets. Compatibility with existing airport pavement is therefore ensured.
- A high degree of landing safety is ensured because the airplane can be landed at design sink rates with one or both front main gears retracted, and at a reduced sink rate with both rear gears retracted.
- The extended forebody design provides a forward ground-contact surface in the event of a nose-gear-up landing.
- The long stroke on the aft gear provides soft-landing characteristics and reduces dynamic loads.

Titanium 6Al-4V is used extensively throughout the airframe structure. Its selection evolved from company studies begun before 1958 of materials for supersonic flight. Titanium 6Al-4V has the following advantages:

- It is the most thoroughly proved of all titanium alloys.
- It has high fracture toughness at high-strength levels for all operational environments, permitting a structural design with good fail-safe characteristics.
- Optional heat treatments provide maximum strength-to-weight ratios for each application.
- Weldability is excellent.

Improved high-strength steels are used in certain moderate temperature areas having extremely high loads and are of the same heat-treat levels as used on present Boeing commercial transports.

Skin stringer construction is used throughout all primary structure; this construction has the following advantages:

- Highest strength-weight compression efficiency in heavy- and medium-load applications.
- Proved construction from the standpoint of reliability and ease of manufacture.
- Structure that is easily inspected and repaired.
- Durable structure resistant to damage.

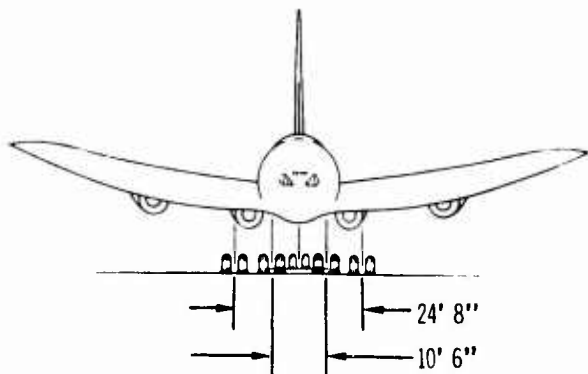
Bonded, metal-face honeycomb panels, with high-temperature adhesives, are used extensively for light-gage secondary structure. This application is an extension of technology being used on commercial and military airplanes. The following advantages are obtained:

- Lowest weight construction for lower-load applications.
- Best known resistance to lightning-strike penetration. This quality provides much greater safety than minimal gage skins used as fuel tank coverings. Lightning-strike resistance in fuel compartments, where honeycomb construction is not used, is provided by the thick skins required for strength considerations.
- Superior sonic-resistant qualities.
- Excellent aerodynamic smoothness under operational environment.
- Inherent thermal insulation qualities. This minimizes weight of fuel compartment walls by elimination of insulation.

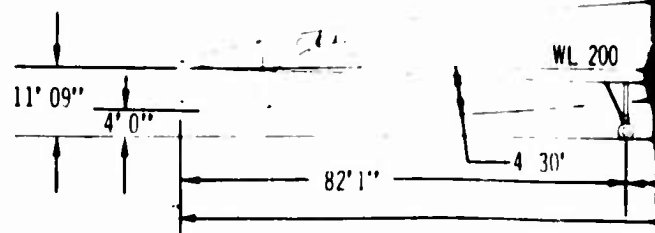


CONTROL AIRFOIL DATA		
BUTTOCK LINE	% SEMI-SPAN	l c
67.50	10.64	2.70
186	29.32	2.78
375	59.10	2.80
634.469	100	3.00

ξ AIRPLANE

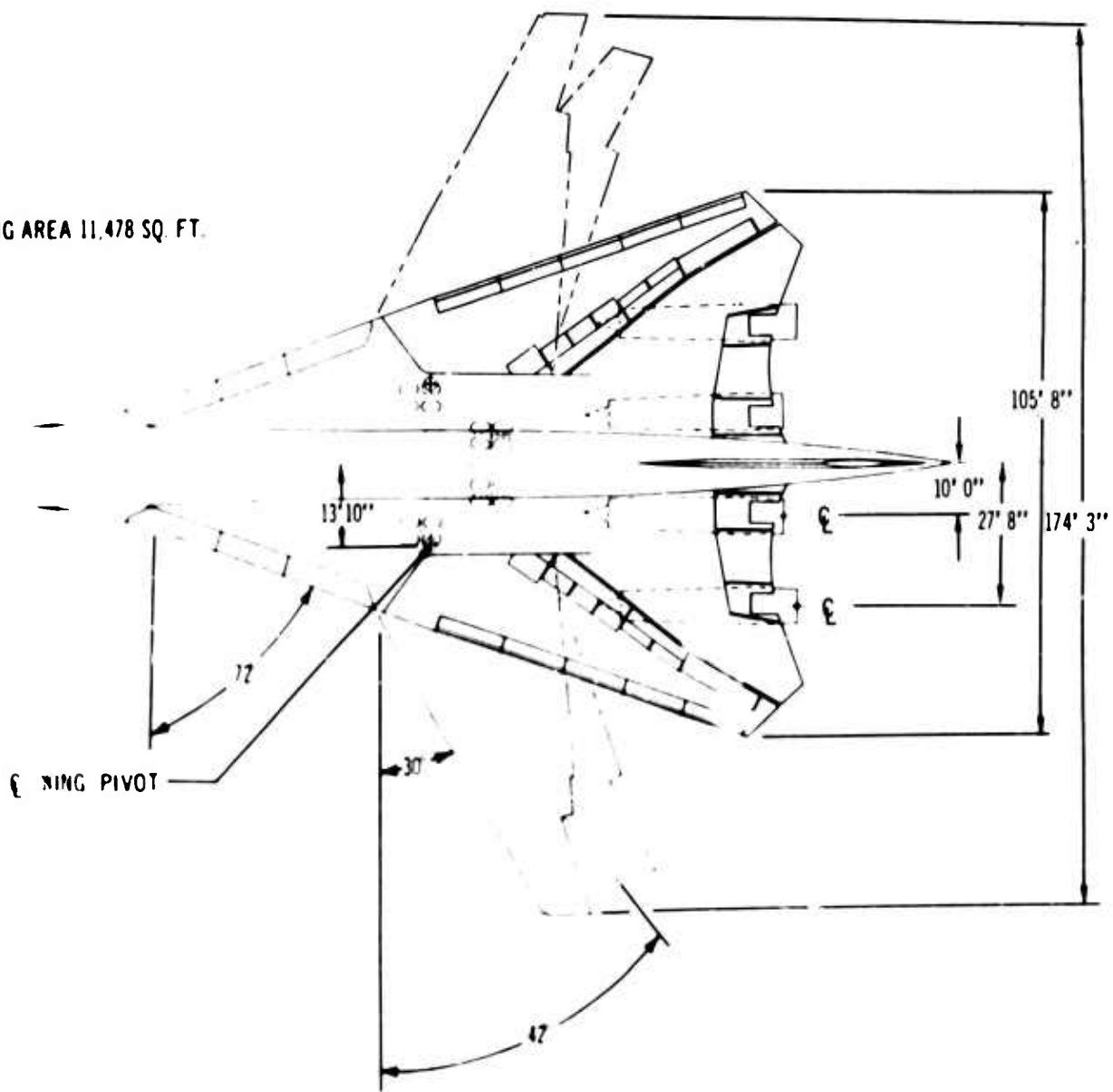


WING REFERENCE PLANE



A

TOTAL WING AREA 11,478 SQ. FT.



VERTICAL STABILIZER AREA 875 SQ. FT.

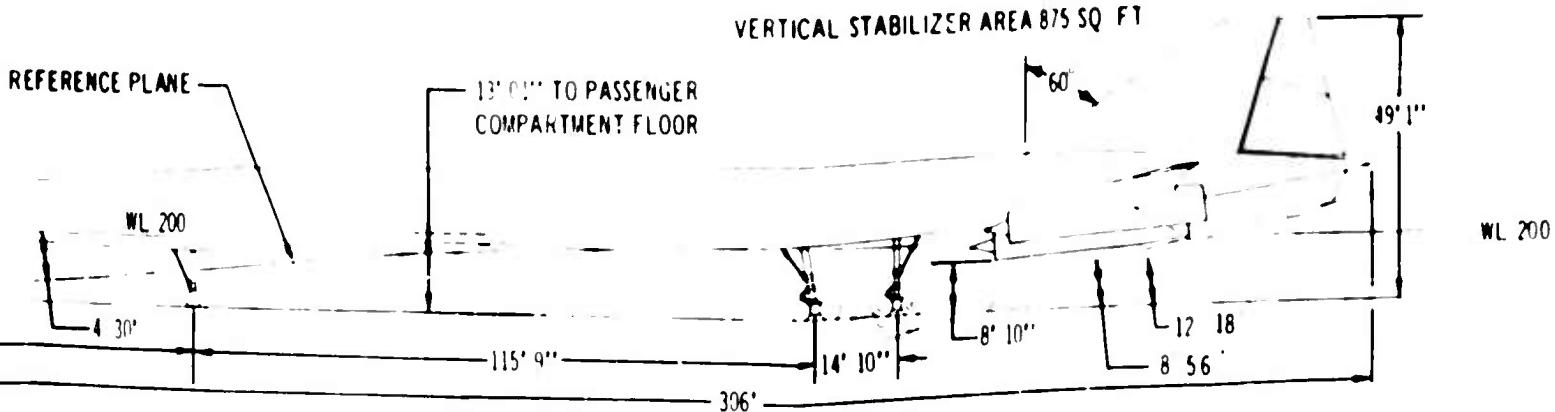
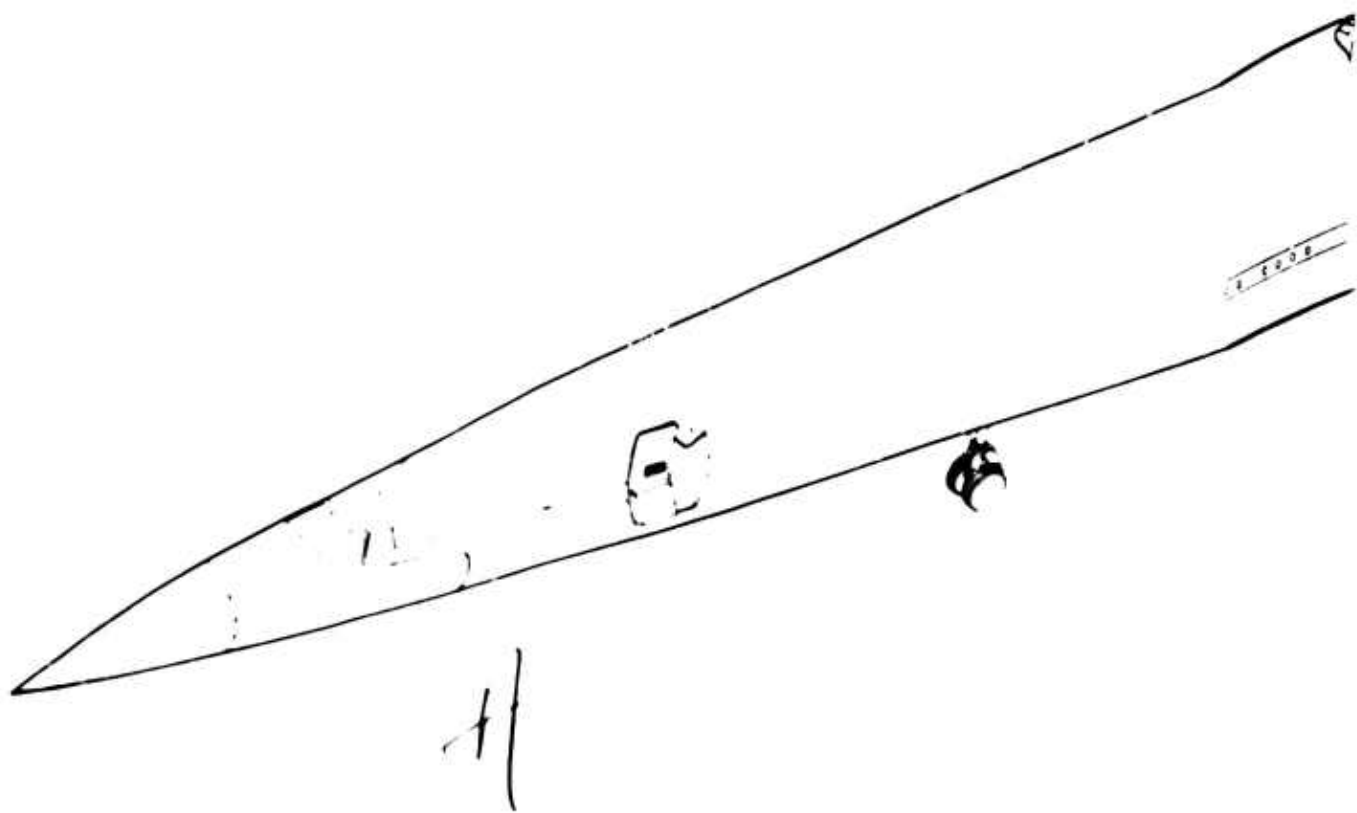
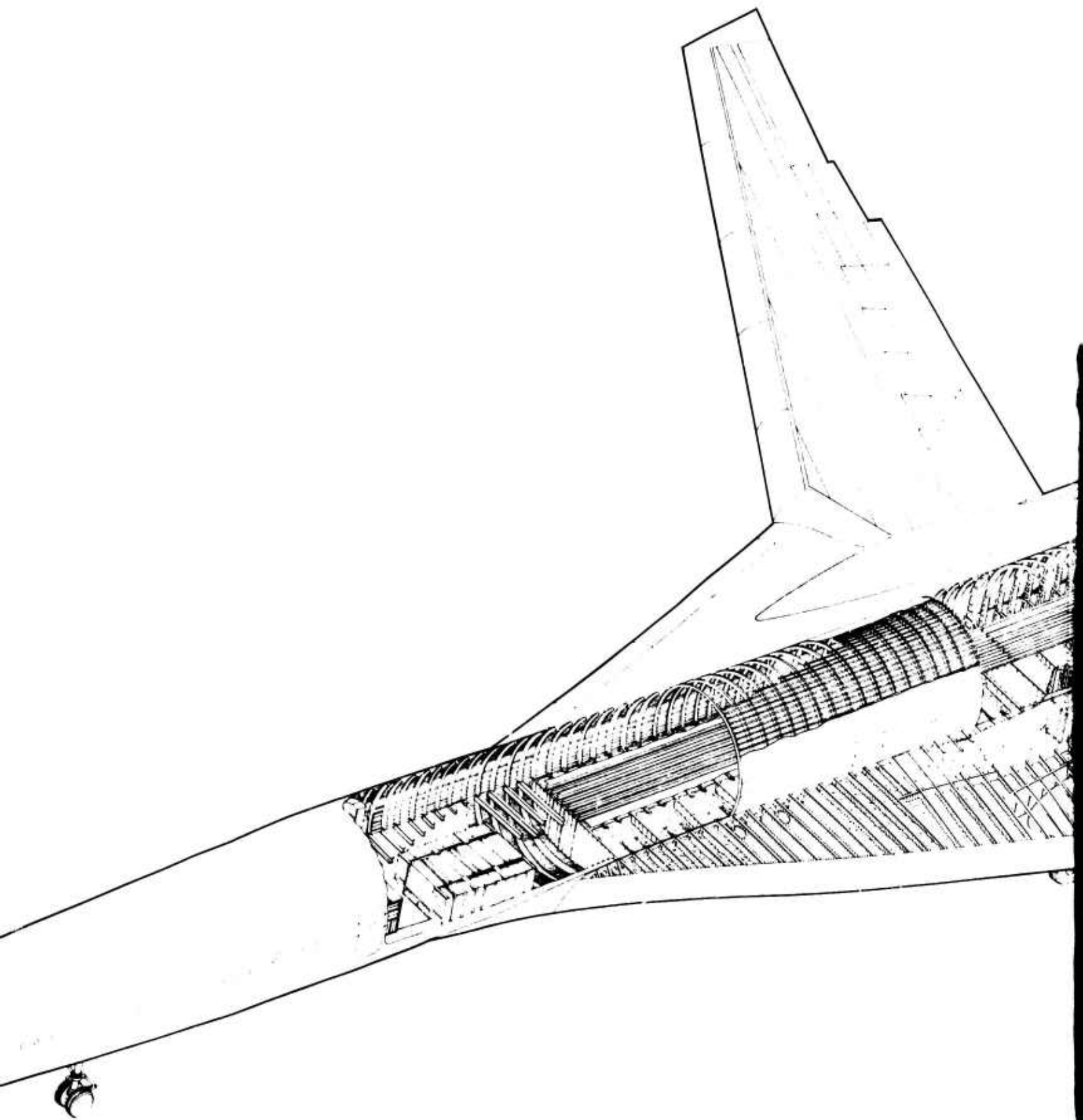


Figure 1-1. Airplane Three-View

V2-B2707-6-2

B





B

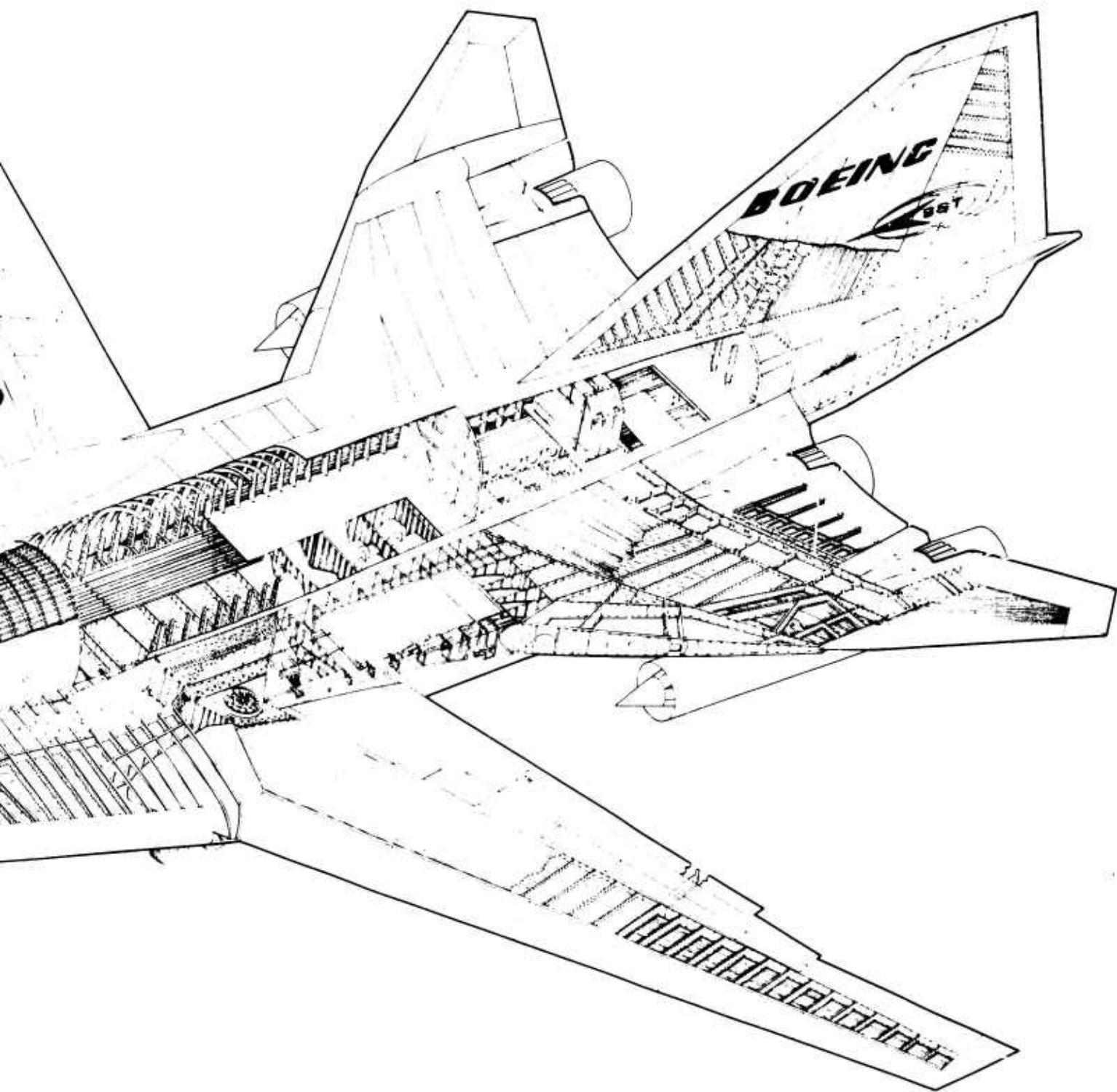


Figure 1-2. Airplane Structure Arrangement

V2-B2707-6-2

C

**BLANK PAGE**

## 2.0 STRUCTURAL DESIGN

### 2.1 STRUCTURAL DESIGN APPROACH

Comprehensive design development and study programs were conducted during Phase II-C along with structural and material testing to establish an optimum structural design. The objective of these studies was to refine the structural features of the configuration such as the wing-pivot area, wing-stabilizer interconnects, movable nose, and landing gear and combine them into a safe, economical, structural design that will meet or exceed the environmental and operational requirements. The results of these studies constitute the proposed structural design and are detailed in this book.

The company's experience in commercial transport design greatly facilitated obtaining the best structural configuration for all regimes of flight and airline operation. Design personnel on the B-2707 Program held key positions on previous commercial programs. Coordination was maintained with company commercial programs such as the 707 and 727 programs and also with customer airlines to keep abreast of current operational experience. In areas such as the wing-pivot where operational experience is limited, extensive test programs, structural analysis, and design studies were initiated.

Inasmuch as maintenance costs are among the highest recurring expenses in all airline operations, maintainability is a primary structural design parameter. Design features are constantly monitored to ensure provisions for inspection, servicing, repair, adjustment, and removal and replacement.

Mockups have been used in the development of the structural configuration of the B-2707 to optimize space with regard to structural and systems requirements. Mockups have been used extensively to establish crew vision requirements for design of the movable-nose section; mockups will also be used to effectively manage structural and system interfaces throughout Phase III.

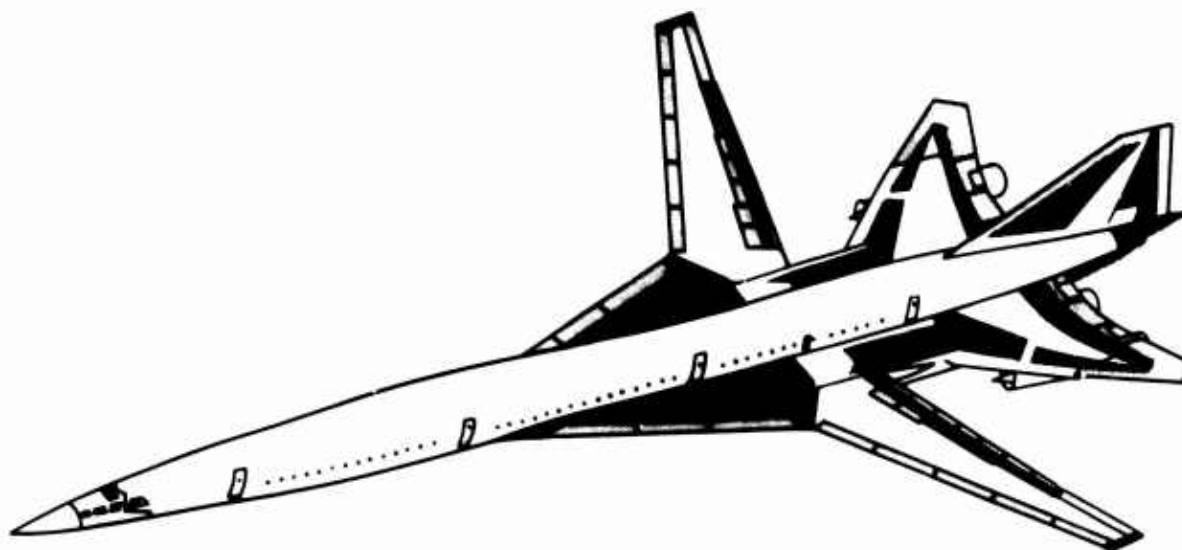
### 2.2 AIRFRAME DESIGN, GENERAL

Skin and stringer construction is used in structural boxes of both the wing and tail and the semimonocoque fuselage shell. This construction is a logical extension of design concepts of subsonic commercial transports and is compatible with inspection and repair methods used on present subsonic jets. Titanium 6Al-4V has been selected as the primary structural material; this selection is discussed in Part D, Materials and Processes (V2-B2707-8), of the Airframe Design Report.

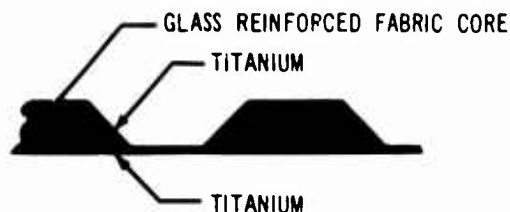
Thin gage titanium 6Al-4V sine wave webs are used extensively throughout the wing and tail in rib construction and in the fuselage floor beams. The webs are welded to flange material producing a lightweight, shear-resistant, economical structure. These webs, when used in fuel compartments, provide effective resistance to fuel slosh.

Lightweight honeycomb construction is used in secondary structural applications such as flaps, slats, spoilers, elevons, wing strake, rudder, elevators, doors, panels, and leading edges of the horizontal and vertical tail. Figure 2-1 illustrates the uses of honeycomb. Honeycomb is the most efficient means of meeting the requirements of aerodynamic smoothness, panel loading, and thermal insulation. It also permits greater spacing of supporting structure, with more uninterrupted space for systems and fuel storage, and improved airflow around aerodynamic surfaces. It has superior resistance to lightning strikes and is an excellent thermal insulator for fuel tanks, eliminating the use of additional insulating materials.

Honeycomb's proved quality of being highly fatigue-resistant makes it ideal for structural surfaces located in areas of high sonic levels, such as control surfaces in the vicinity of the engine exhaust. When used as external panels, it is also highly resistant to aerodynamic flutter.




**FULL DEPTH HONEYCOMB**



**HONEYCOMB PANELS**

**LEGEND**

 FULL DEPTH HONEYCOMB

 BONDED HONEYCOMB PANELS

**BONDED STRUCTURE COMPARISON**

MODEL	AREA, SQ FT	
	ALUMINUM - BONDED HONEYCOMB	TITANIUM - BONDED HONEYCOMB
KC - 135	890	
707 - 320	1070	
727	600	
B-2707		13,080

*Figure 2-1. Honeycomb Usage*  
V2-B2707-6-2



Honeycomb construction consists of titanium faces with glass-reinforced fabric core bonded with high-temperature-resistant polyimide adhesives. Face sheets vary in thickness to suit load requirements, with 0.006 in. as the minimum gage. A wide-overlap edge design with increased edge thickness prevents moisture penetration. The honeycomb core is a nonperforated type that prevents venting of the entire panel cavity and moisture accumulation.

### 2.3 FATIGUE AND FAIL-SAFE

The design objective is a fatigue life of 50,000 hours with minimum maintenance. This objective is achieved by careful consideration of the following:

- Material selection
- Operating stress levels
- Design details, including all joints and attachments
- Corrosion prevention including material compatibility
- Past airplane service-life experience

Comprehensive testing completed and scheduled in support of development and selection of various fatigue-resistant designs are discussed in Part E, Structural Tests, V2-B2707-9; and Part D, Materials and Processes (V2-B2707-8) of the Airframe Design Report.

In addition to fatigue resistance, Boeing criteria require fail-safety in the design of basic structure. It is obtained through the use of load paths such as the following:

- Wing and tail multistiffener multiple panels for primary structure

- Numerous fuselage longitudinal stringers designed with fail-safe straps attached to the skin
- Wing-pivot dual lug structure

Where fail-safe criteria are not feasible, safe-life criteria are applied.

### 2.4 STRUCTURAL ACCESS

Nonstructural access provisions are used for structural and system inspection, service, and repairs (see Fig. 2-2). Easily visible markings on all doors and openings are provided, with maximum use of the Air Transport Association indexing system. For each mechanically attached removable panel, identical bolts are used for each fastener diameter.

### 2.5 ENGINEERING-MANUFACTURING COORDINATED DOLLAR SIGN SURFACES

Engineering and Manufacturing will agree on key tooling index surfaces early in the design stage. The surfaces and pertinent tooling information will be published jointly by Engineering and Operations in a pictorial document. Tooling will be fabricated by indexing the tool faces to these surfaces which are designated dollar sign (\$) surfaces.

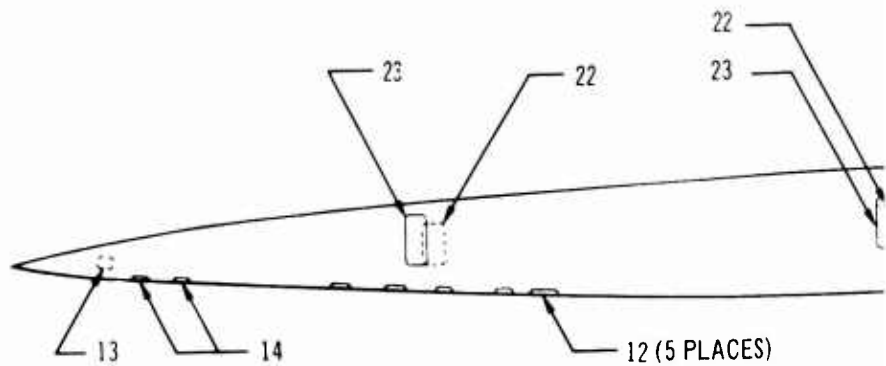
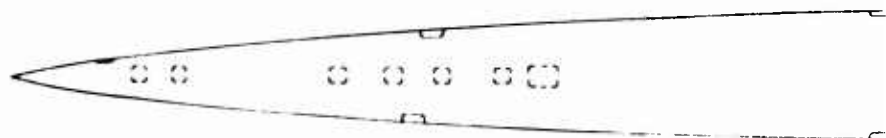
The design will provide for changes in structural member sizes or thickness caused by airplane growth or other changes with no effect on dollar sign surfaces. This results in minimum tooling changes and minimum program costs. A similar practice is used on company subsonic jets.

A description of the dollar sign tooling philosophy and selected typical surfaces for the Model B-2707 is shown in the Manufacturing Program, V5-B2707-9.

ACCESS FOR

- 1 FUEL TANK
- 2 ELEVATOR ACTUATOR
- 3 PIVOT ACTUATOR EQUIPMENT
- 4 AIR CONDITIONING
- 5 AUXILIARY DRIVE SYSTEM
- 6 ACTUATOR-AUXILIARY ELEVATOR
- 7 CONTROLS SYSTEM
- 8 WING PIVOT
- 9 POWER TAKEOFF-AUXILIARY DRIVE SYSTEM
- 10 ENGINE INLET COWL
- 11 SLAT TRACK SUPPORT BEARINGS
- 12 EQUIPMENT
- 13 ATR PACKAGES
- 14 NOSE PIVOT
- 15 NOSE DROOP SUPPORT BEARINGS
- 16 FUEL & ANTENNA
- 17 HYDRAULICS SYSTEM
- 18 CONTROLS SYSTEM & FUEL ADAPTER (R.H.) -  
FUEL ADAPTER (L.H.)
- 19 OIL TANK
- 20 THRUST REVERSER
- 21 INSPECTION
- 22 GALLEY SERVICE
- 23 ENTRY
- 24 ESCAPE
- 25 INTERNAL DRIVE MECHANISM
- 26 RUDDER ACTUATOR
- 27 RUDDER HINGE
- 28 DRIVE SHAFT COUPLING -  
AUXILIARY DRIVE SYSTEM

NOTE: (WING & HORIZONTAL TAIL)  
R.H. - UPPER SURFACE ACCESS  
L.H. - LOWER SURFACE ACCESS



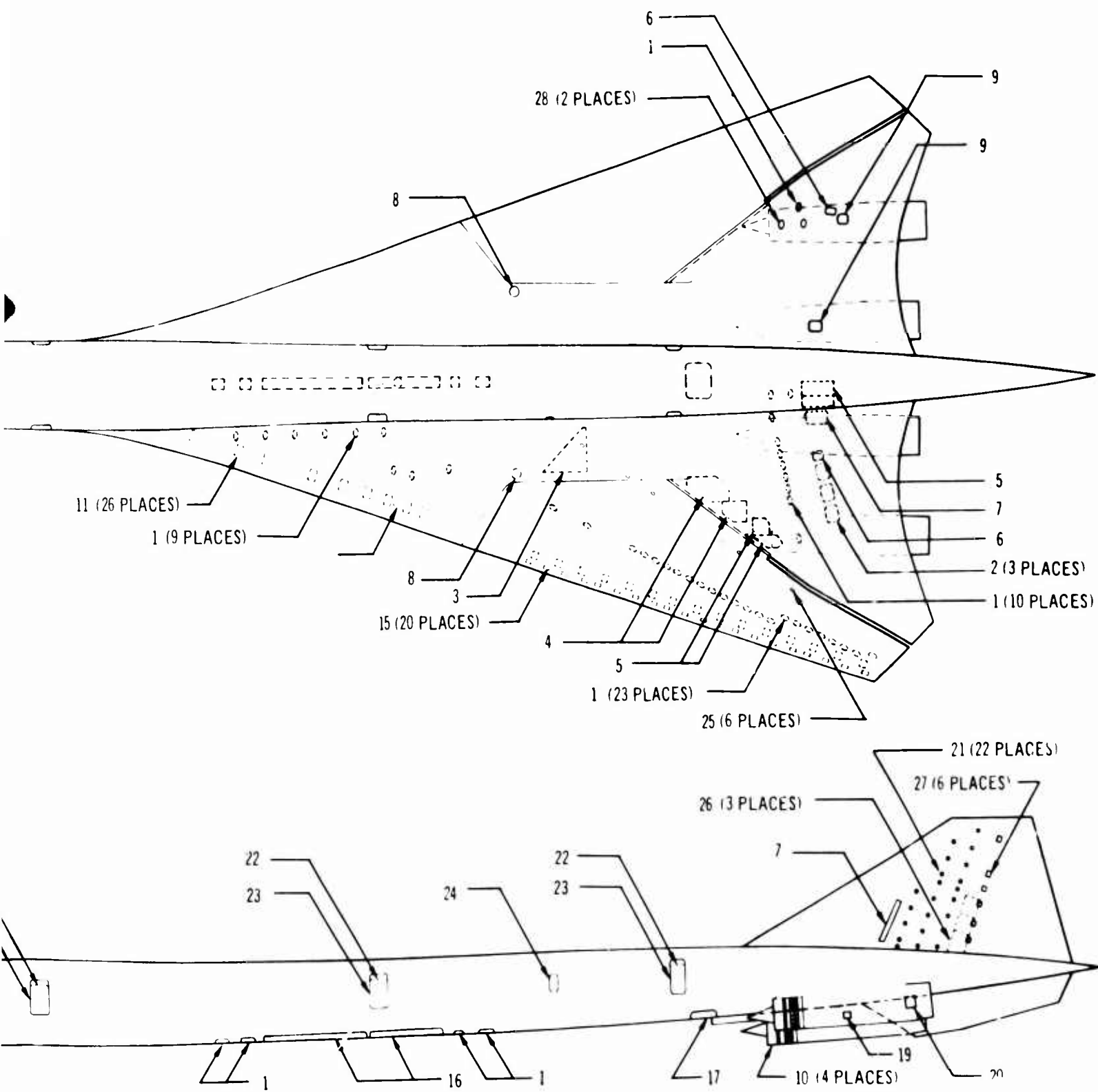


Figure 2-2. Service and Maintenance Access

3

### 3.0 DESIGN DESCRIPTION

#### 3.1 WING CONSTRUCTION

The wing definition is shown in Fig. 3-1. The wing is pivoted at approximately 29 percent of the wing semispan (wings aft). The wing and stabilizer are an integrated design such that in the aft position the wing and stabilizer form a single, large, airfoil section for the major portion of the wing. The elevon and outboard section of the wing (aileron area) form separate surfaces. This design results in much greater depth of structure for both the wing and stabilizer than is possible with nonintegrated wing-stabilizer design.

In the high-speed cruise configuration, the wings are swept aft to an angle of 72 degrees measured at the wing leading edge. In the subsonic speed configuration, the wings are swept forward to leading edge angles as low as 30 degrees. As the wing is swept forward from the aft position, the flaps move rearward providing a smooth wing-airfoil section. At the 42-degree wing position, the outboard flaps may be lowered. At the 30-degree position, the inboard flaps and the leading edge slats may be used.

Figure 3-2 shows the structural arrangement of the wing. The major features of the wing are the following:

- A movable outboard section
- The main structural box, inboard of the pivot, extending continuously through the fuselage
- A large, forward, inboard section (strake)
- Support of the main landing gears from the primary wing box
- Fuel carried in the three major wing sections
- Trailing edge flaps from the side of the fuselage outboard to the aileron

For the primary wing-bending material (titanium 6Al-4V), the upper panel surface uses

a special heat treatment providing a high-compression yield strength. For the lower panel surface, critical in tension, another special heat treatment is used to obtain high fracture toughness and long fatigue life. Certain components, such as flap tracks, use a high-strength steel.

The primary wing-bending structure is a conventional skin and stringer configuration, using two spars.

The wing box has skin and stringers that are relatively thick, with close stiffener spacing. The selected rib spacing of this structure gives a high strength-to-weight ratio. Other advantages are as follows:

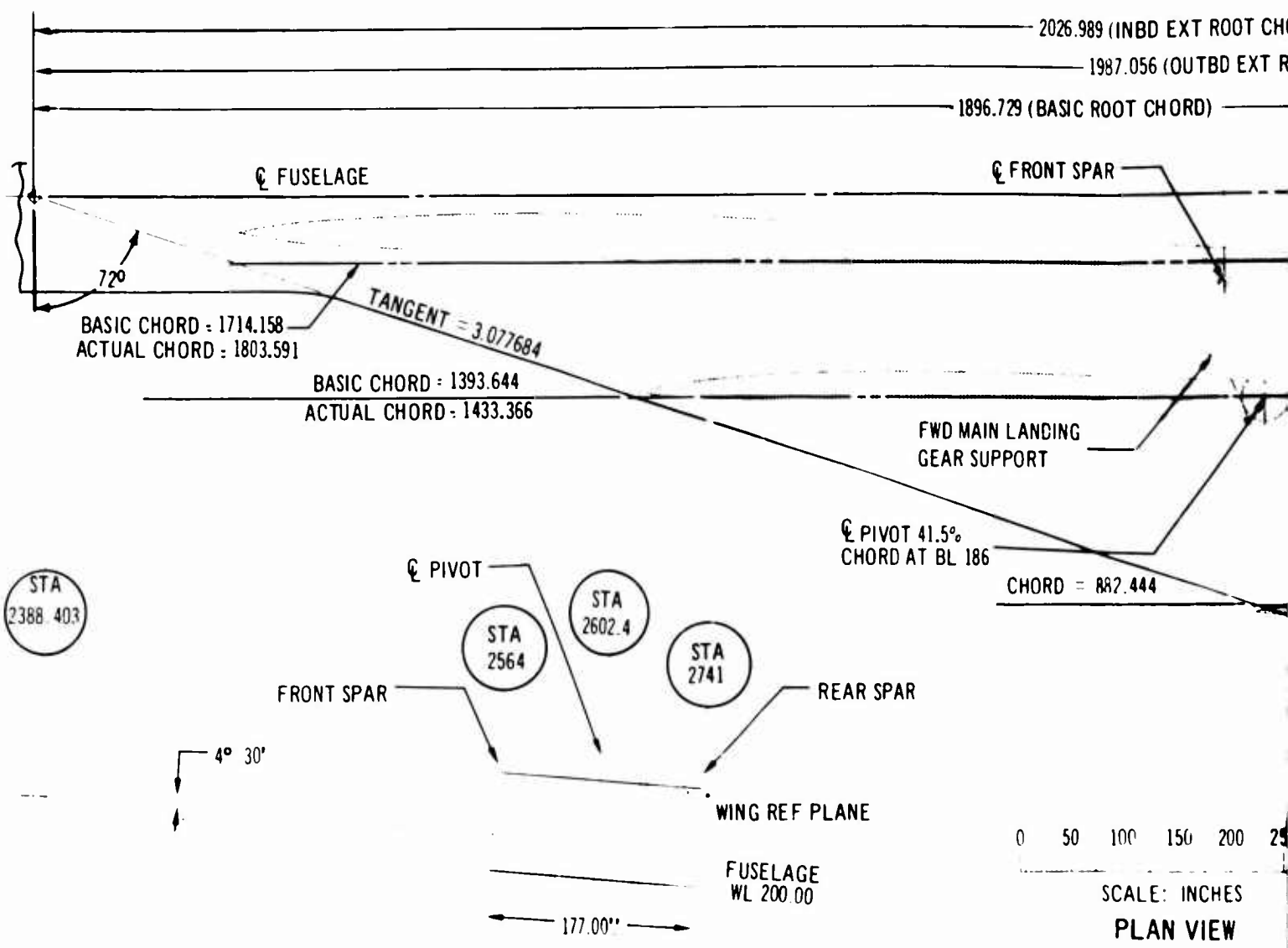
- The internal structure can be inspected through man-size nonstructural access doors (see Fig. 2-2).
- Repair is easily accomplished.
- The structure can be produced at reasonable cost.
- A reliable, quality product can be produced because the design is not a great departure from previous manufacturing experience.

#### 3.1.1 Outboard Variable-Sweep Portion

##### 3.1.1.1 Wing Box

For the primary wing-box structure, the two spars are built of extruded chord sections with stiffened webs, tapered in the spanwise direction.

The upper and lower surfaces are stiffened by Z-section stringers mechanically joined to the skin panels by titanium fasteners and supported by ribs as shown in Fig. 3-3. Both the stringers and skins are tapered in thickness in the spanwise direction either by machining or chem-milling. Stringer spacing varies as determined by considerations of structural efficiency, fail safety, and aerodynamic smoothness.

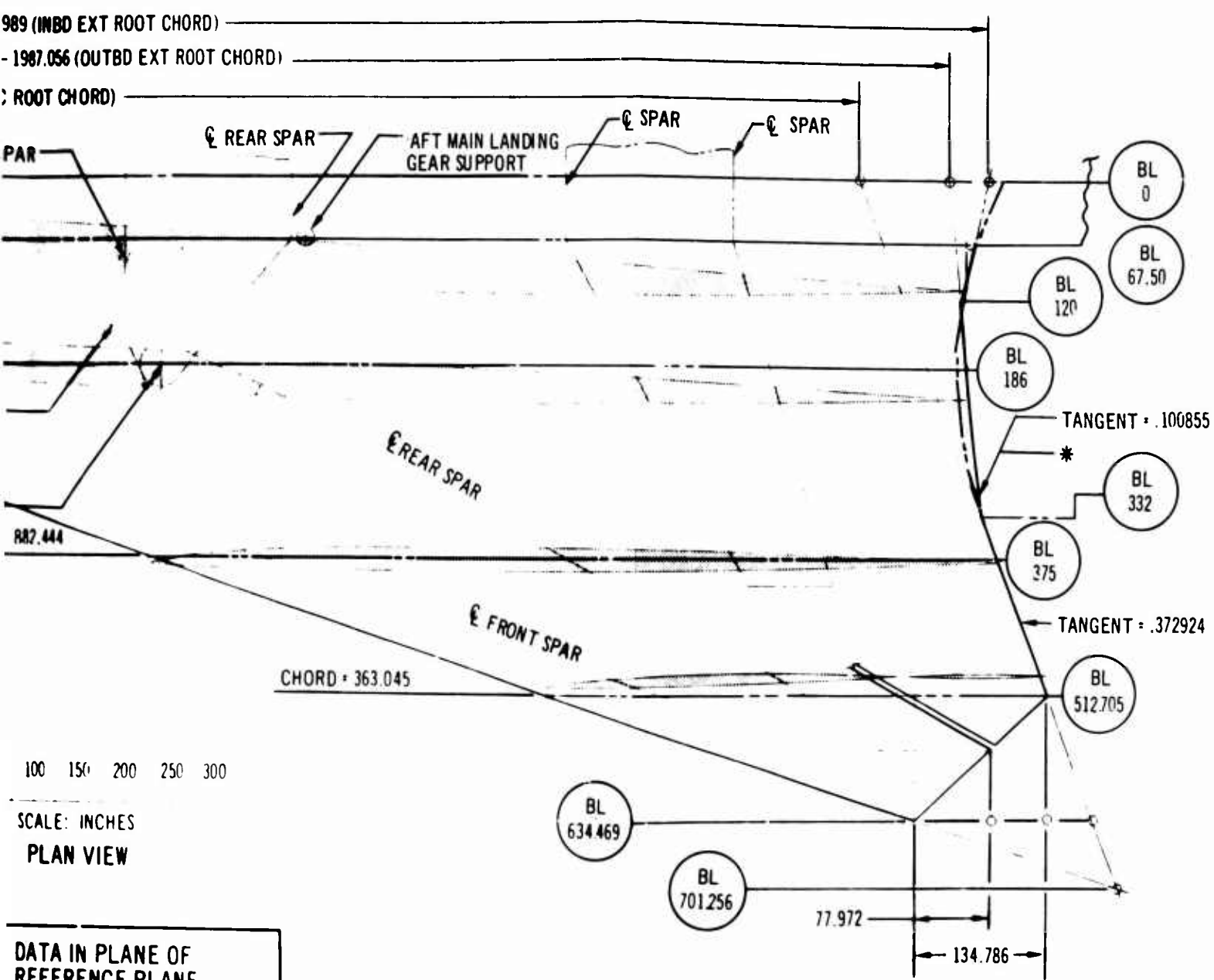


L.H. SIDE VIEW OF BODY

CONTROL AIRFOIL DATA		
BUTTOCK LINE	° SEMI-SPAN	t/c
67.50	10.64	2.70
186	29.32	2.78
375	59.10	2.80
634.469	100	3.00

WING DATA IN PLANE WING REFERENCE PLANE		
SURFACE	INTEGRAL	
	WING	
AREA (FT <sup>2</sup> )	9000	
L.E. SWEEP	72°	
ASPECT RATIO	1.242	
DIHEDRAL	0°	
INCIDENCE TO WL		4° 30'

*Handwritten signature*

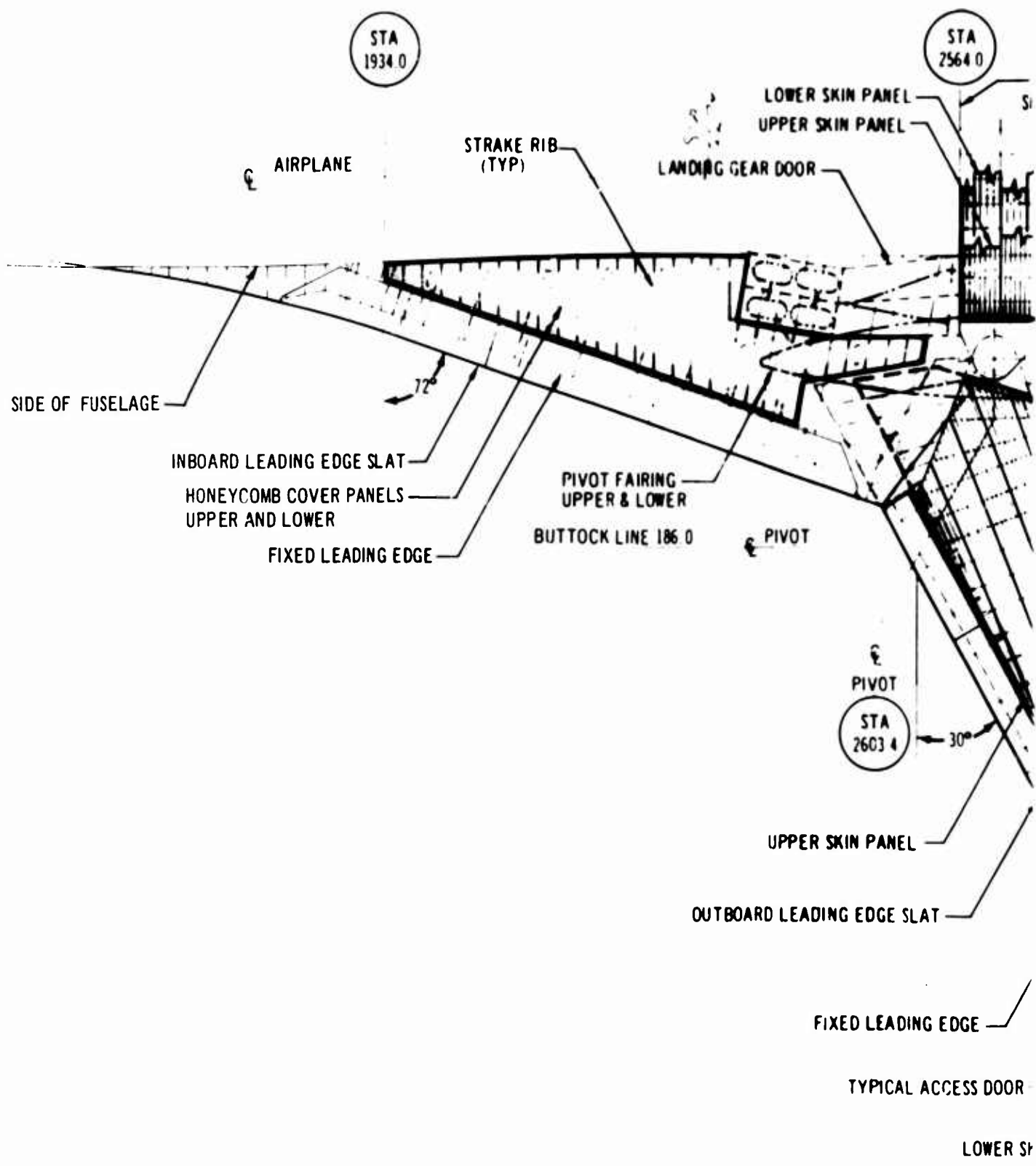


\* TRAILING EDGE MODIFIED LOCALLY TO SIMPLIFY LOFT

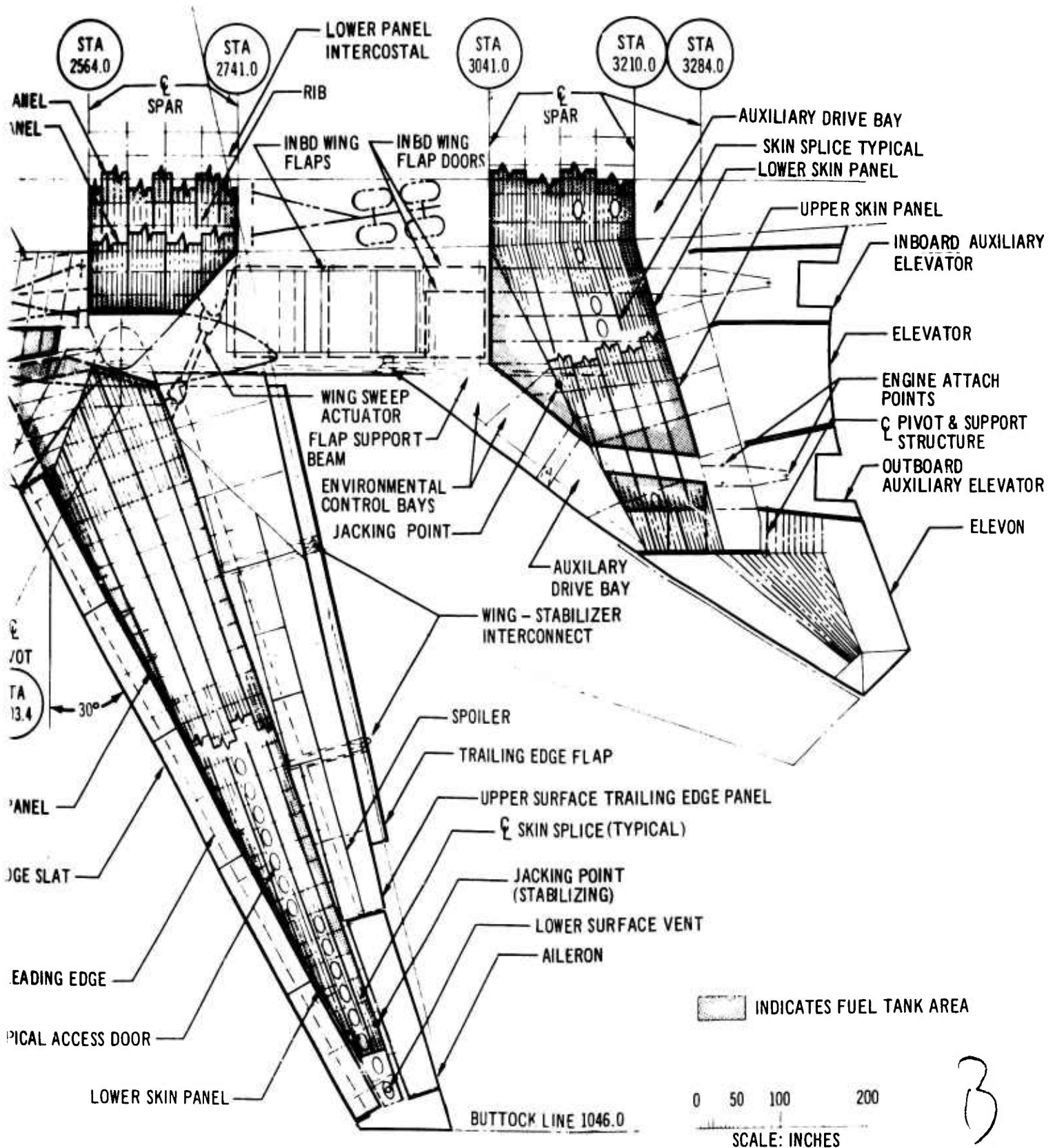
DATA IN PLANE OF REFERENCE PLANE	
INTEGRAL WING	
WING	HORIZ. STAB.
9000	2478
72°	60° & 55°
TIO 1.242	3.510
0°	0°
0 WL	4° 30'

Figure 3-1. Wing Definition

B



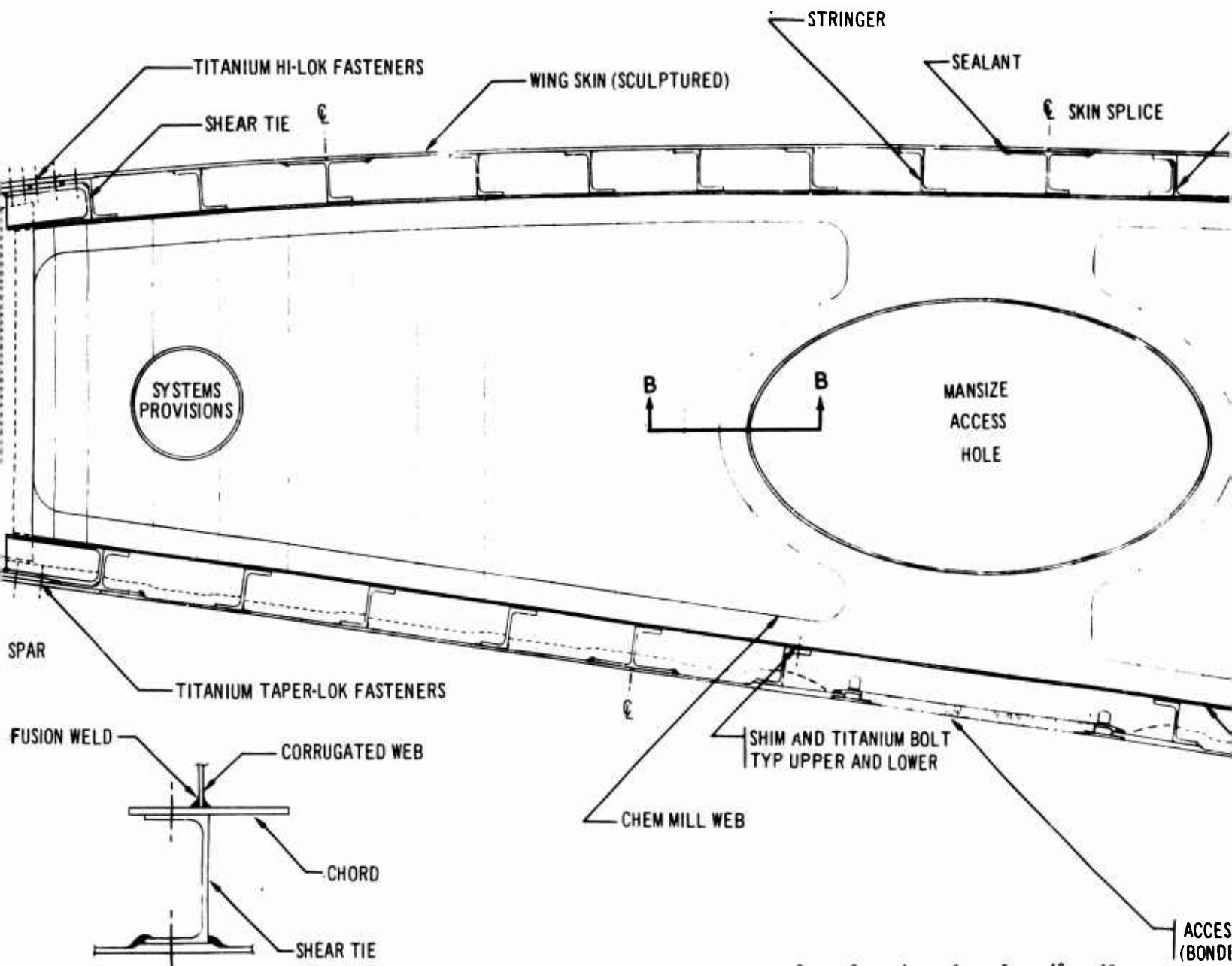
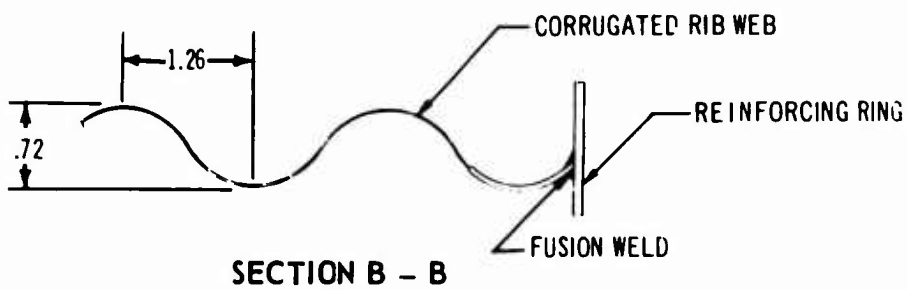
A



106

Figure 3-2. Wing and Horizontal-Tail Structure Diagram





SCALE: INCHES

SECTION C - C

SECTION A - A

*A*

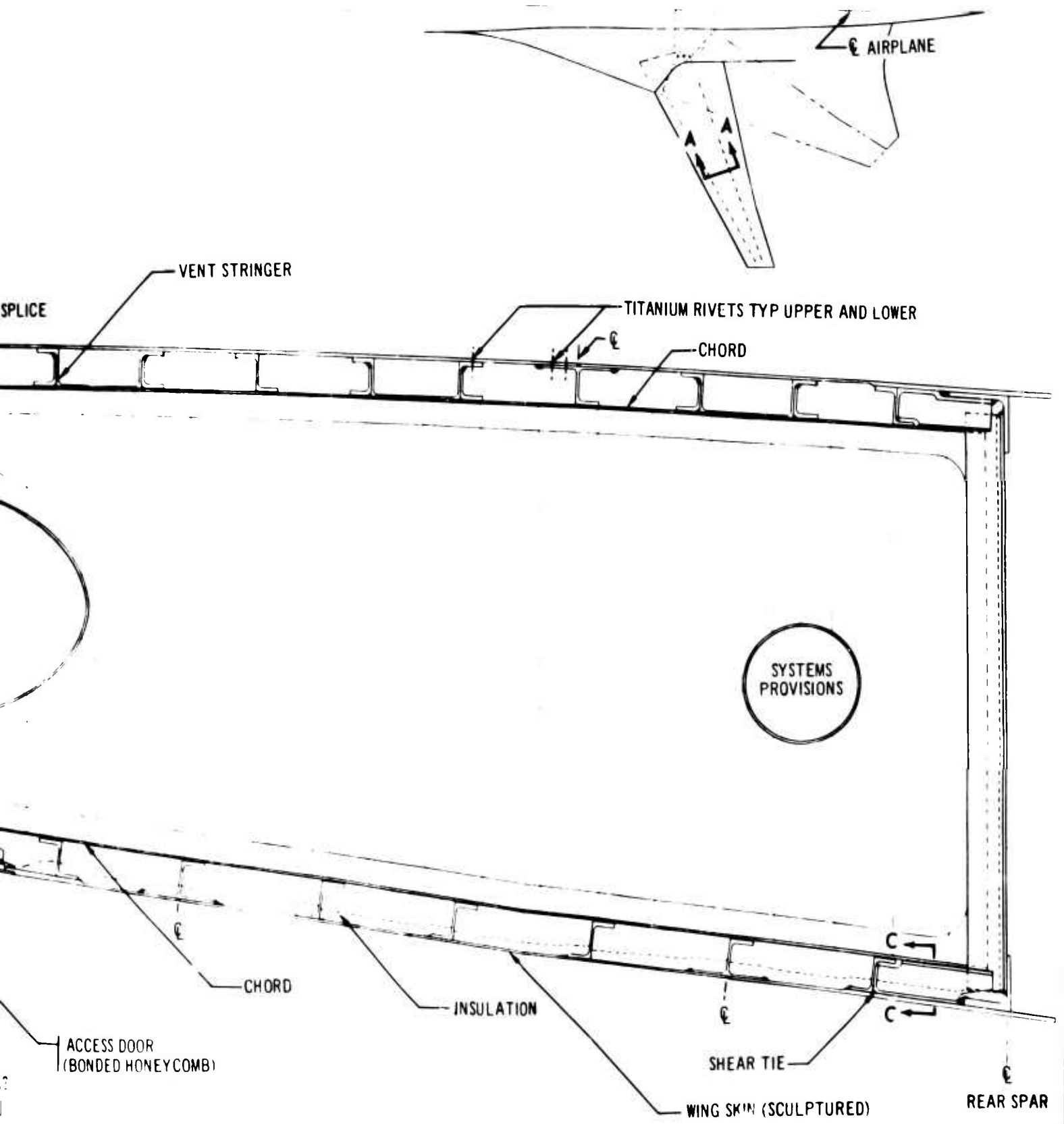


Figure 3-3. Typical Rib

The upper and lower surfaces are divided into a number of skin panels of limited width to provide fail-safety. These panels are joined by titanium fasteners.

The typical wing ribs in the inner-spar area are spaced at approximately 27 in. and are of built-up construction of light-gage corrugated webs that are fusion welded to a flange cap. At concentrated-load locations, special ribs are used.

The inspar area serves as an integral fuel tank. A lightweight, fuel-tank insulation material is added to the lower surface. Filleted tank sealant is used at all skin splices. The titanium rivets used to attach the wing stringers to the upper- and lower-skin panels are self-sealing, consistent with current practices. Access to the fuel cells is provided through nonstructural clamp-or doors of honeycomb construction.

Forward of the wing front spar, the fixed structure is fabricated of light-gage sheet, riveted to light-gage nose ribs that maintain contour and carry shear loads to the front spar. This assembly is installed by titanium fasteners (see Fig. 3-4). Access is provided through removable honeycomb panels in the lower surface.

#### 3.1.1.2 Slats

The double-segment, leading-edge slats are supported on heat-treated steel tracks located as shown in Fig. 3-5. Needle-bearing track rollers are used. Light-gage honeycomb construction with machined rib formers is used. Replaceable rub strips, mechanically attached, are provided at contact areas between surfaces. Hailstone resistance is provided by increasing the skin gage at the slat nose.

#### 3.1.1.3 Spoilers and Movable Trailing-Edge Panels

Spoilers, trailing-edge flaps, and an aileron occupy the area aft of the rear spar (See Fig. 3-6). The spoilers are simple built-up honeycomb structures with ribs and machined spars, hinged from support fittings attached to the rear spar (see Fig. 3-7). Antifriction hinge bearings are used. Each spoiler is actuated by hydraulic power. The honeycomb upper-surface trailing-edge panels, aft of the spoiler, are actuated to be compatible with flap position and wing sweep such as to give a faired upper-surface airfoil in the subsonic cruise condition (see Fig. 3-6).

#### 3.1.1.4 Flaps

Three double-segmented, double-slotted, trailing-edge flaps are used (see Fig. 3-6). The forward segment of each flap is supported by three high-heat-treated steel tracks that cantilever from the rear spar (see Figs. 3-8 and 3-9). Each main segment is actuated by two screw actuators. The aft segment is movable, relative to the main section, and moves on steel tracks. Actuation is accomplished by mechanically picking up the motion of the flap screws. Flap segments are constructed of light-gage honeycomb panel structures and extruded, machined, longitudinal members assembled with titanium fasteners (see Fig. 3-10). Access panels, attached by bolts, are provided in the lower surface. Conventional track roller bearings are used.

#### 3.1.1.5 Aileron and Trailing-Edge Fixed Panels

The aileron is fully powered. Fixed areas of the wing trailing-edge structure and the aileron (see Fig. 3-11) are fabricated of light-gage honeycomb construction. Hinge bearings are the conventional antifriction type.

#### 3.1.1.6 Wing Tip

The wing tip is an interchangeable, light-gage honeycomb assembly.

#### 3.1.1.7 Wing-to-Stabilizer Interconnect

Two shear-connection attach points are used between the wing and the horizontal tail (see Fig. 3-12). The function of this connection is to ensure aerodynamic alignment between the wing and stabilizer in supersonic cruise. The design is such that the inboard connection engages before the outboard connection as the wing sweeps aft. This is to minimize any possible mismatch during that operation. A funnel arrangement is used to ensure engagement. The outer shear connection is located at the outboard engine. Both shear connections serve a dual purpose by acting as wing flap supports.

#### 3.1.2 Inboard Fixed Portion

##### 3.1.2.1 Wing Box

The inboard box structural details are similar to those of the outboard box structure. One difference, as shown in Figs. 3-2 and 3-13, is that wing ribs are replaced by fuselage floor beams and intercostals that are attached to spanwise beams. The basic wing box is permanently attached to the fuselage by forged fittings attached to the front and rear spar, which are carefully

**BLANK PAGE**

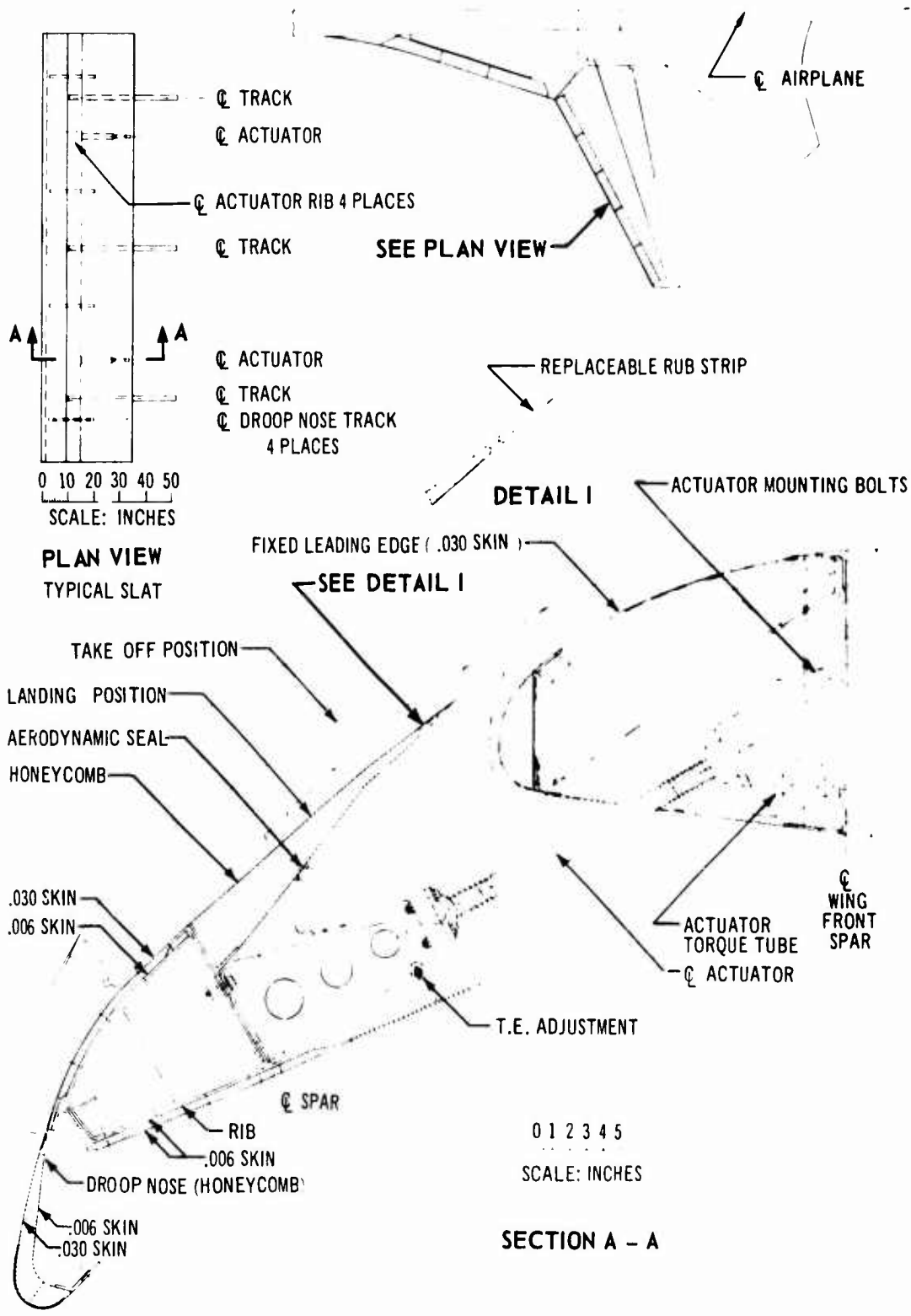


Figure 3-4. Typical Structure of Outboard Slat

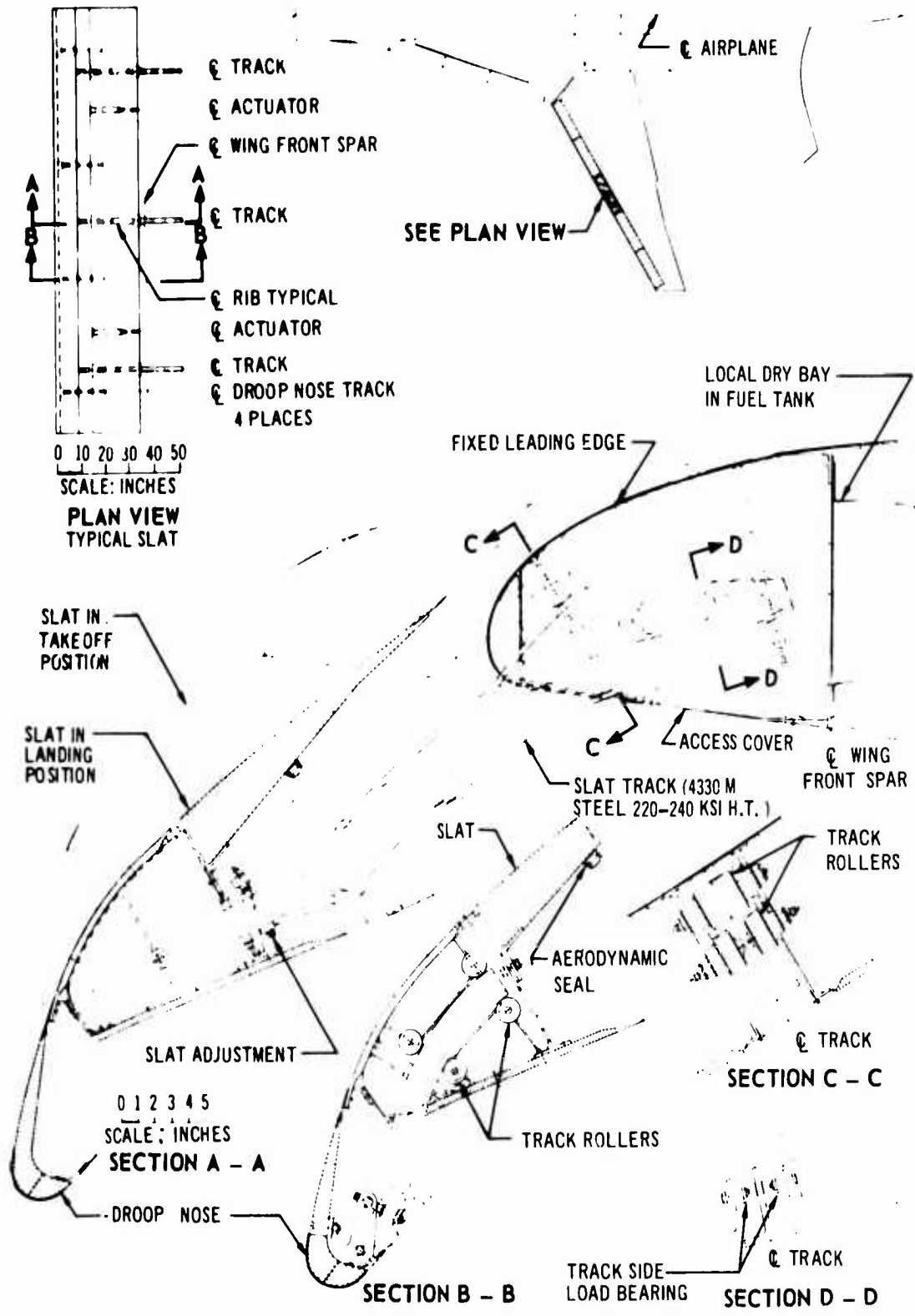
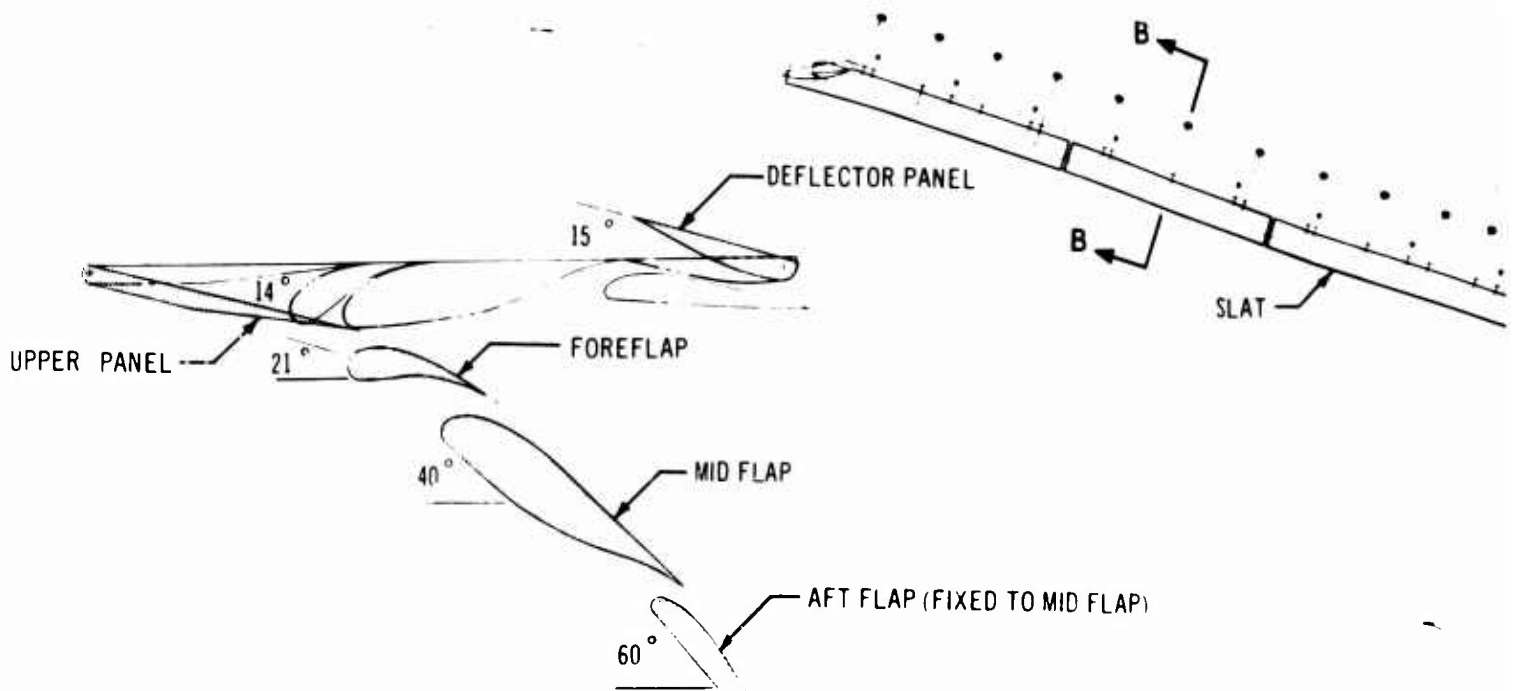
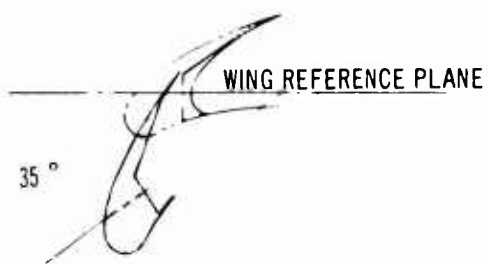


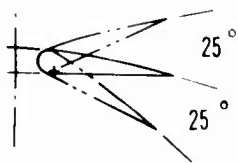
Figure 3-5. Support Structure of Outboard-Wing-Portion Leading Edge Slat



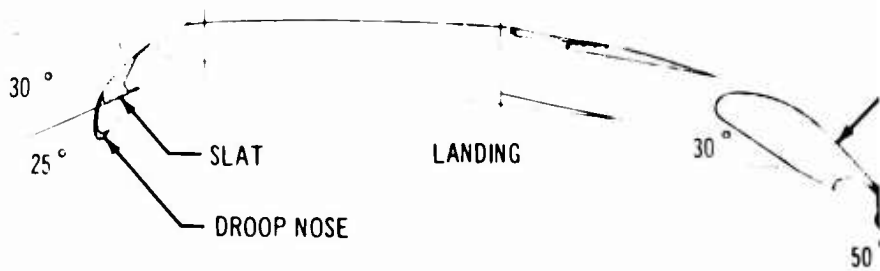
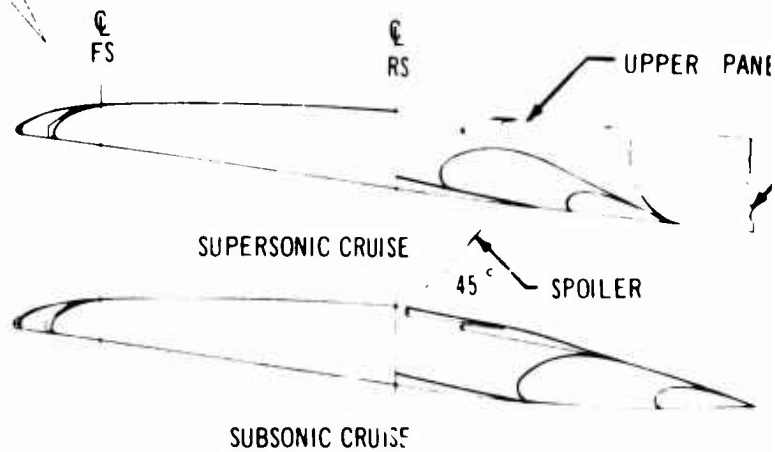
SECTION D - D



SECTION B - B



SECTION A - A



SECTION C - C

H

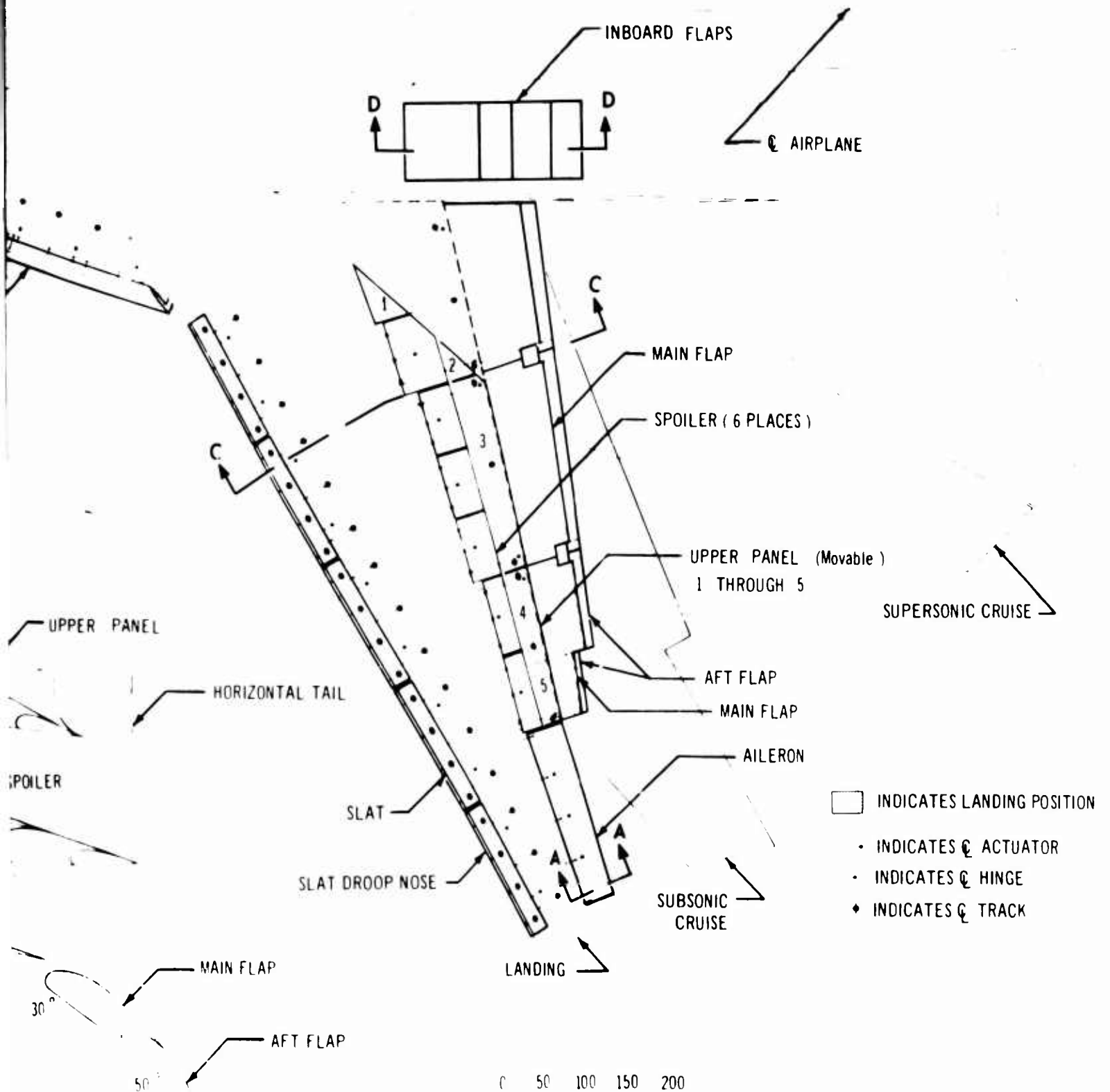


Figure 3-6. Control Surface Diagram



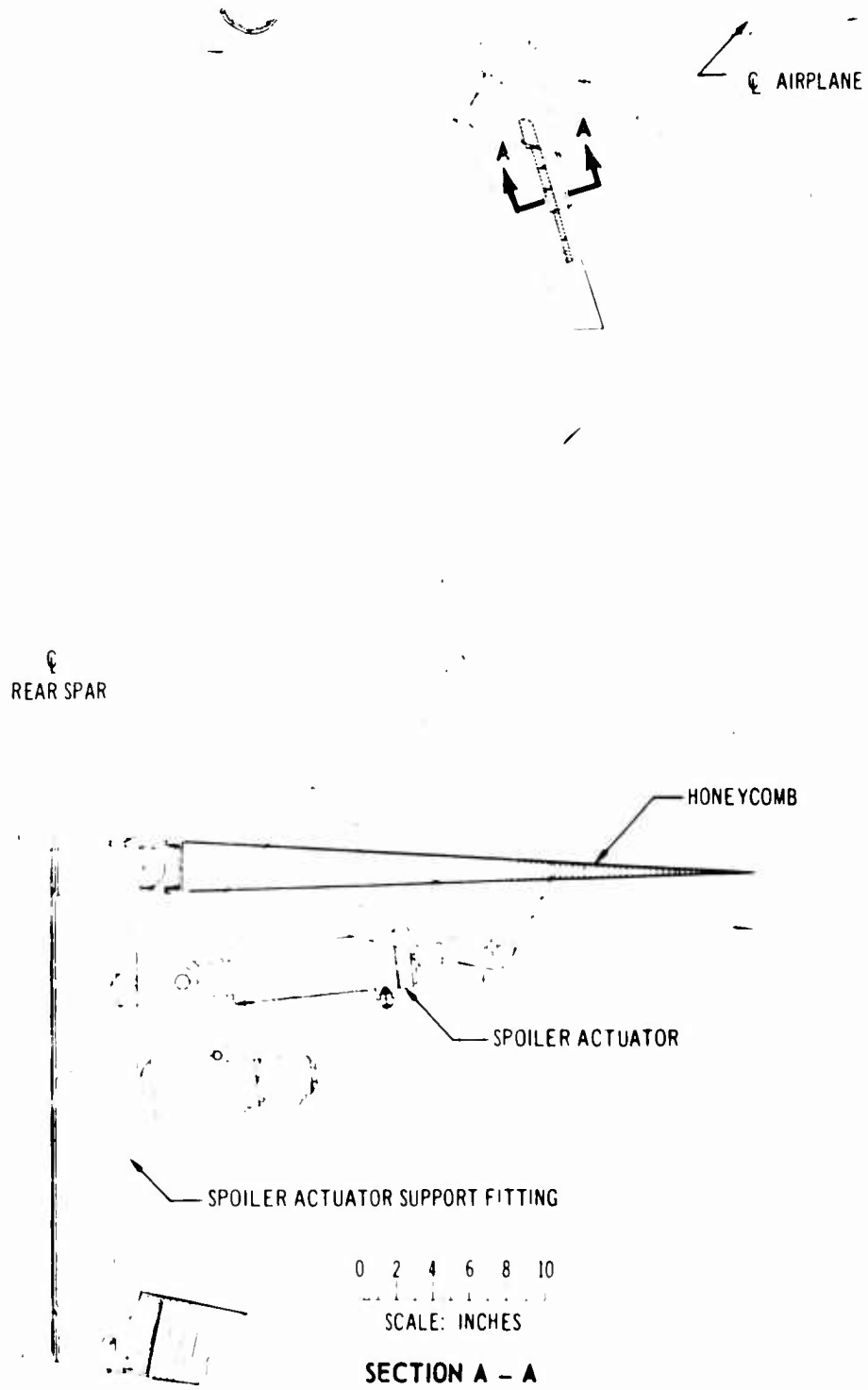
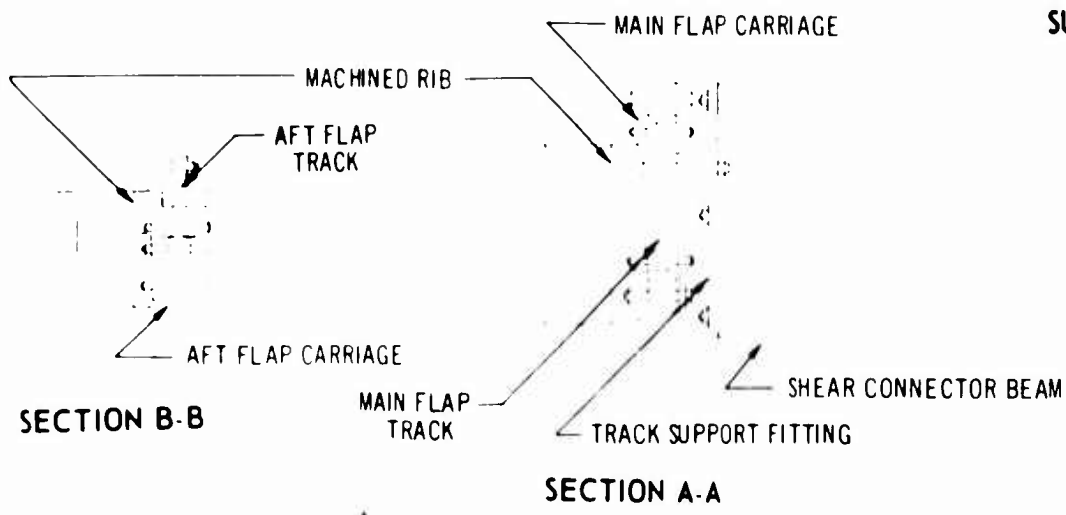
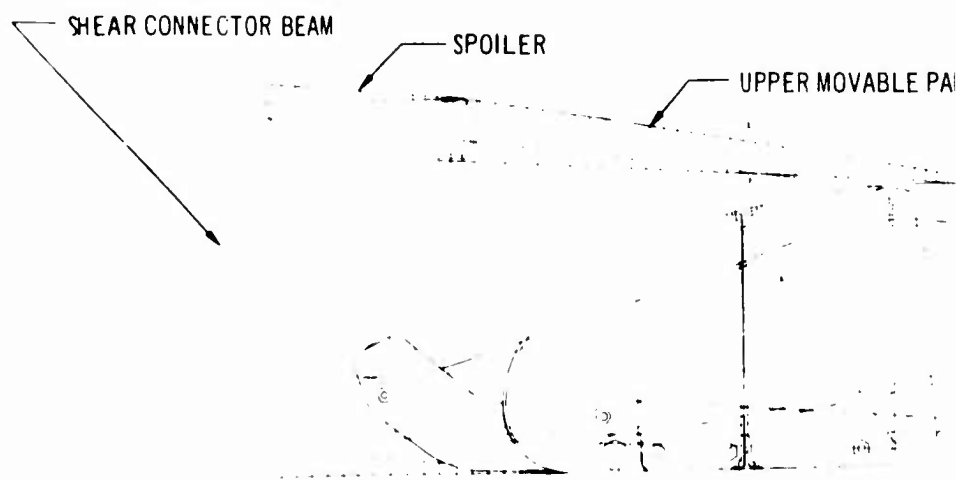
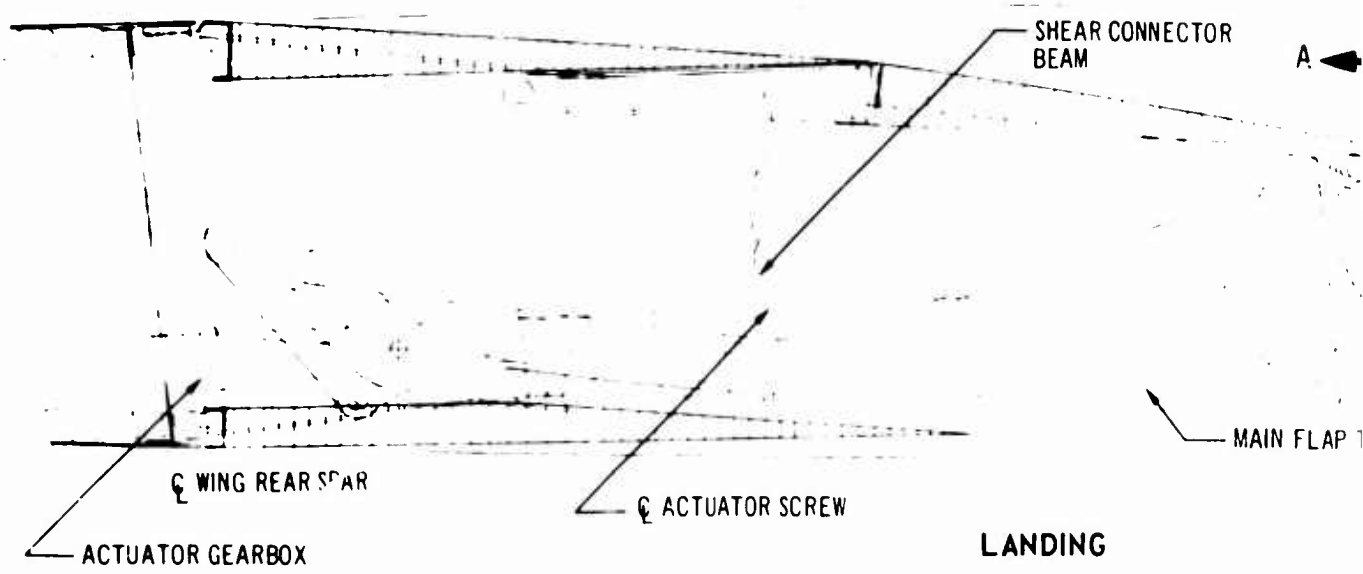


Figure 3-7. Spoiler Cross Section

V2-B2707-6-2



**SUBSONIC CRUISE**

0 5 10

SCALE: INCHES

**SECTION C-C**

*Handwritten signature or initials.*

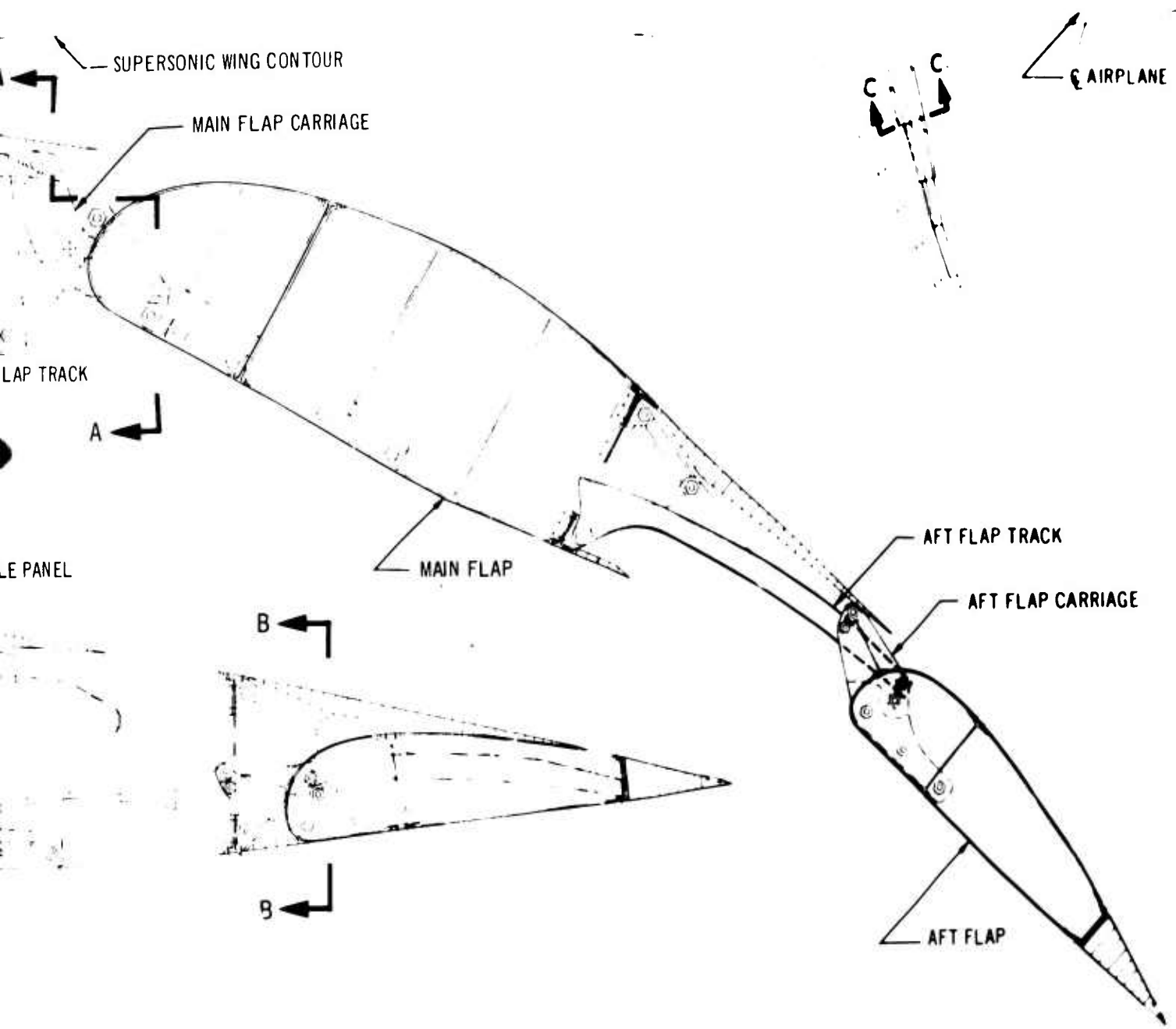


Figure 3-8. Outboard-Wing-Portion End Flap Track

B

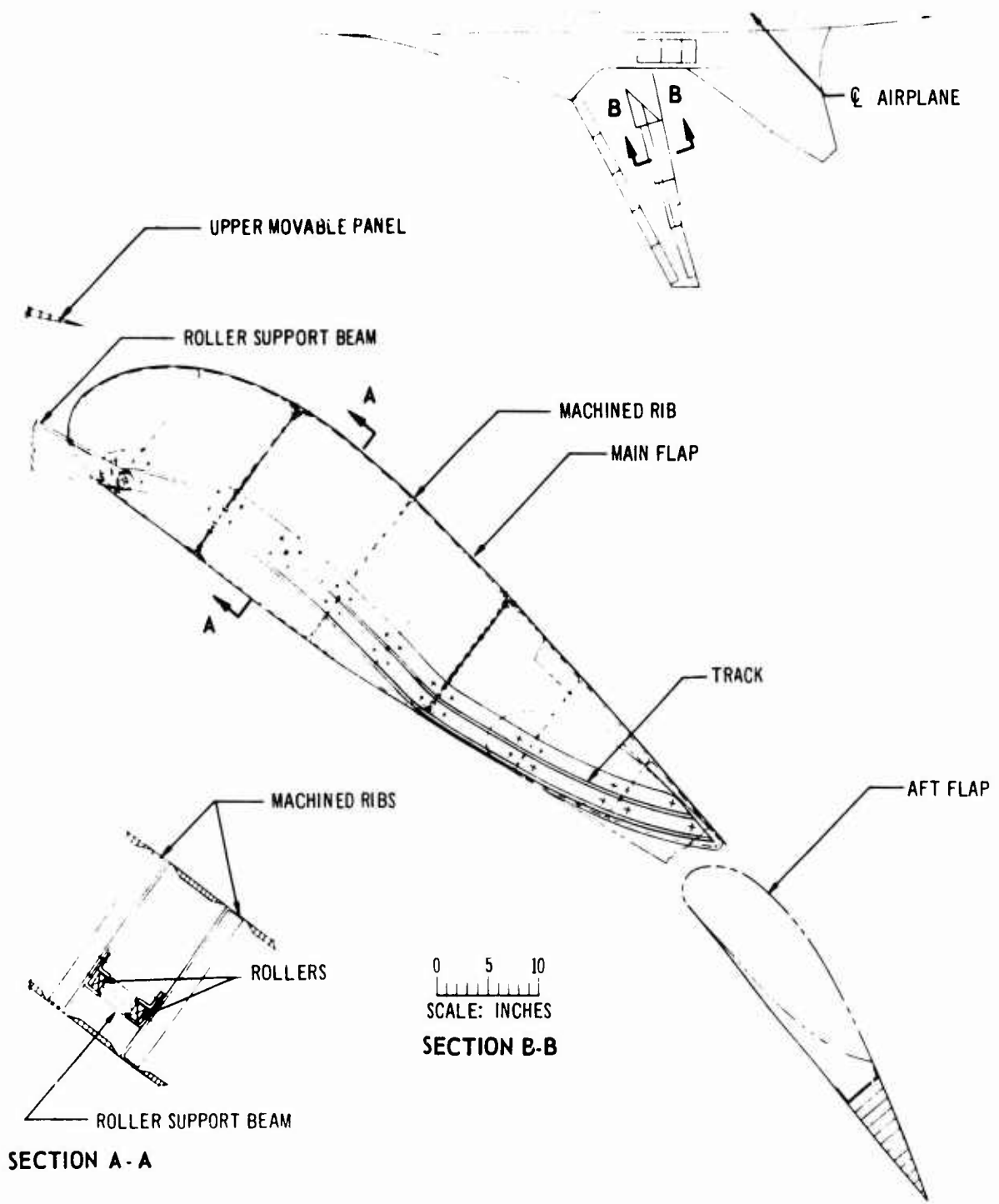
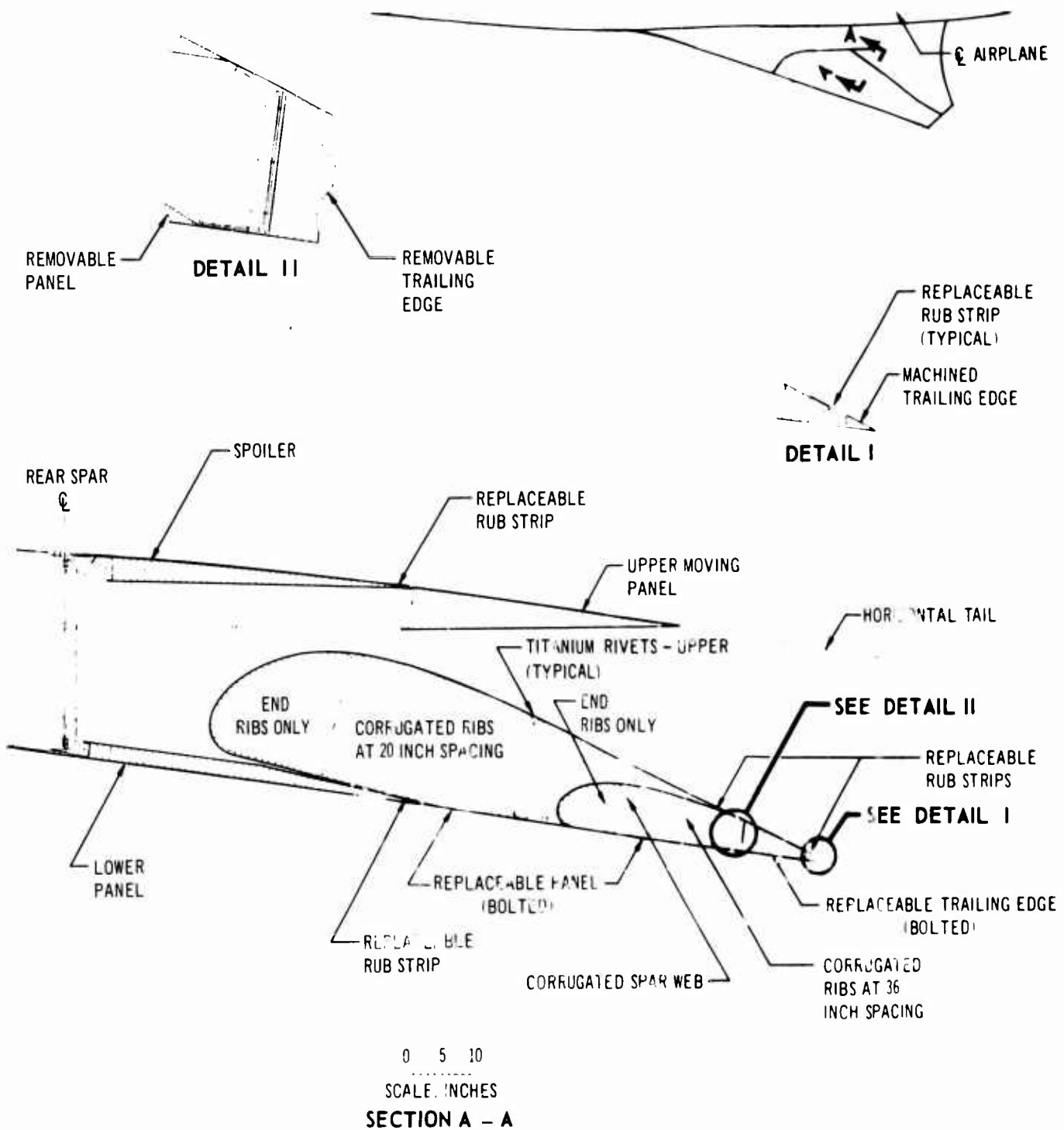


Figure 3-9. Outboard-Wing-Portion Center Flap Track

V2-B2707-6-2



TYPICAL HONEYCOMB PANEL SKIN 006 TITANIUM  
FOR TYPICAL EDGE CONSTRUCTION SEE FIGURE 3-15

Figure 3-10. Outboard-Wing-Portion Flap Trailing Edge

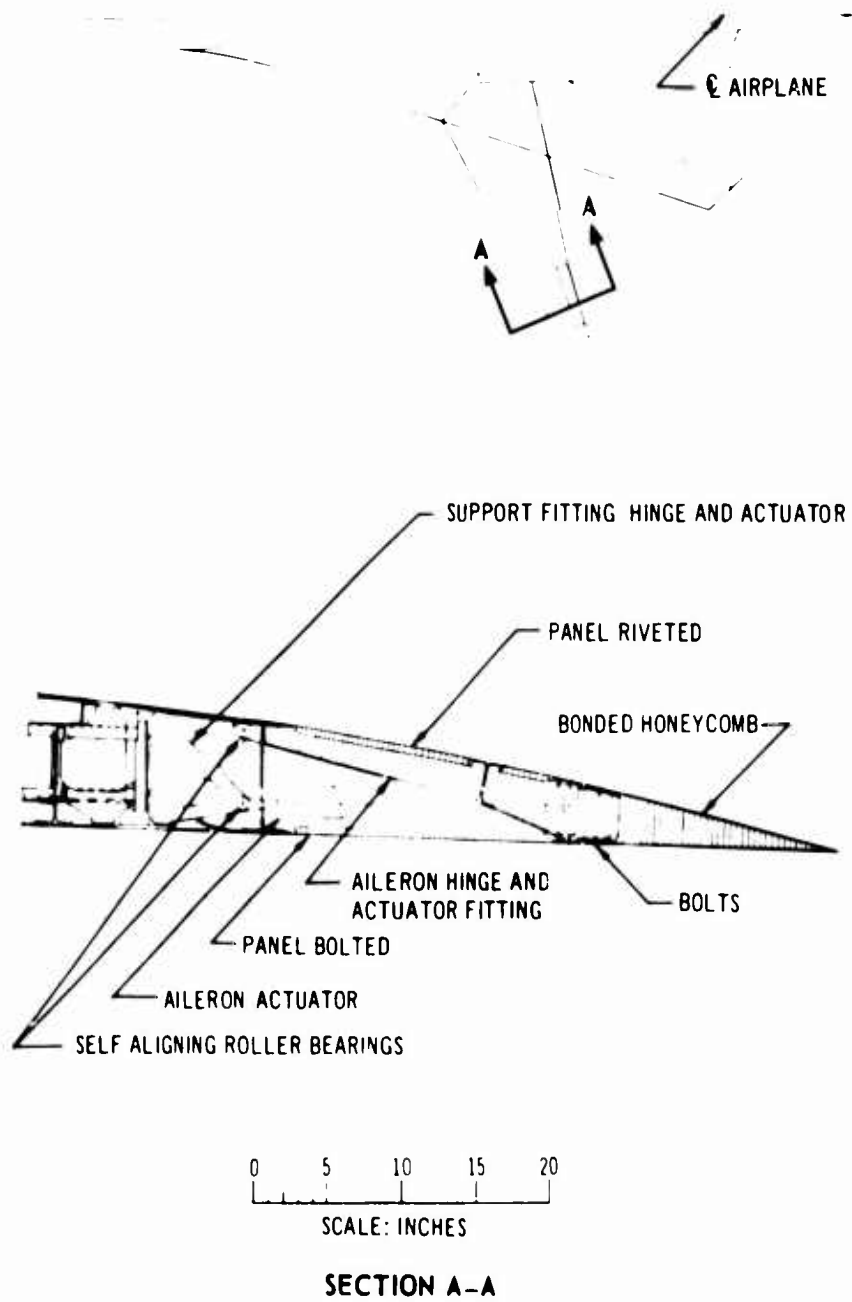
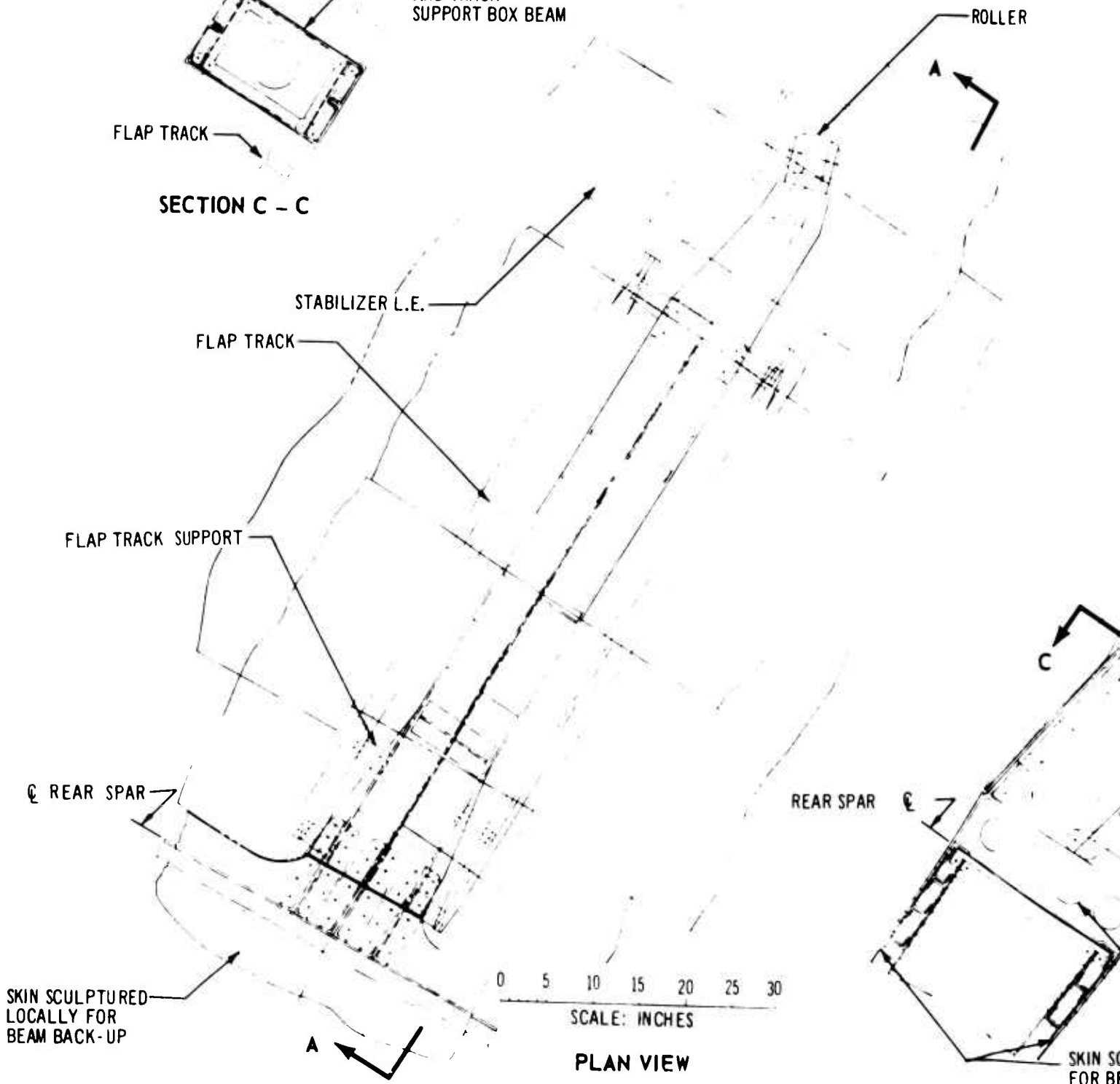
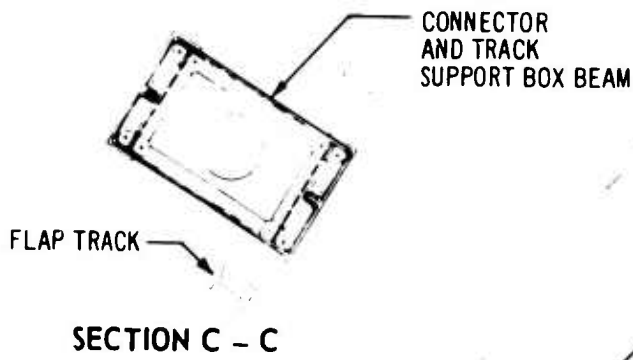


Figure 3-11. Aileron Support Structure

V2-B2707-6-2



H

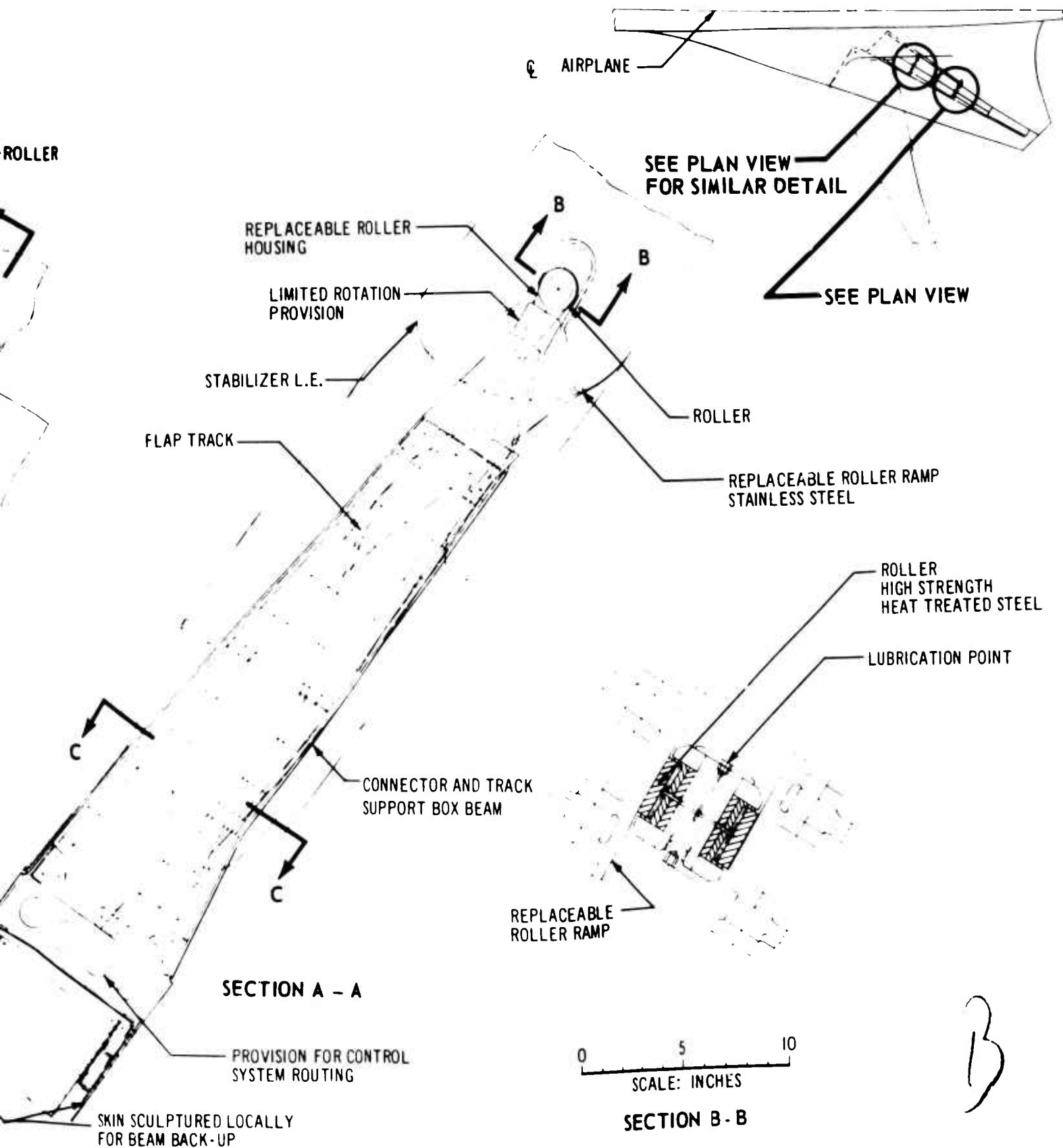
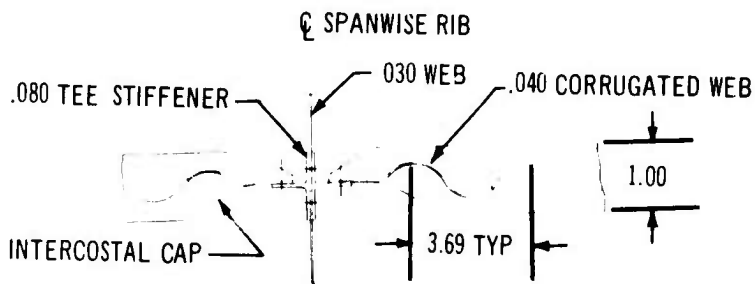
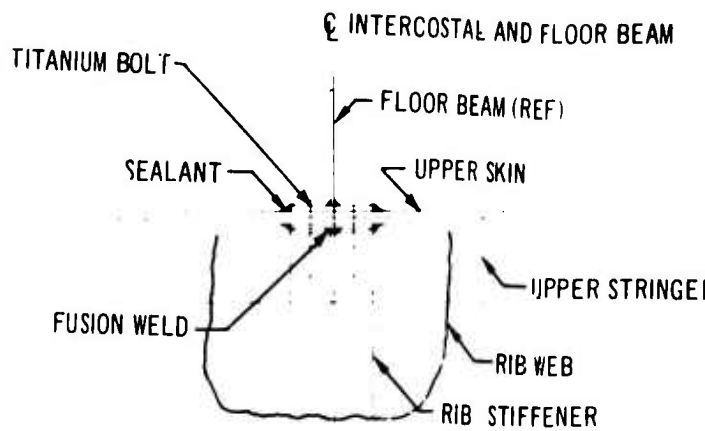


Figure 3-12. Wing-Stabilizer Shear Connector

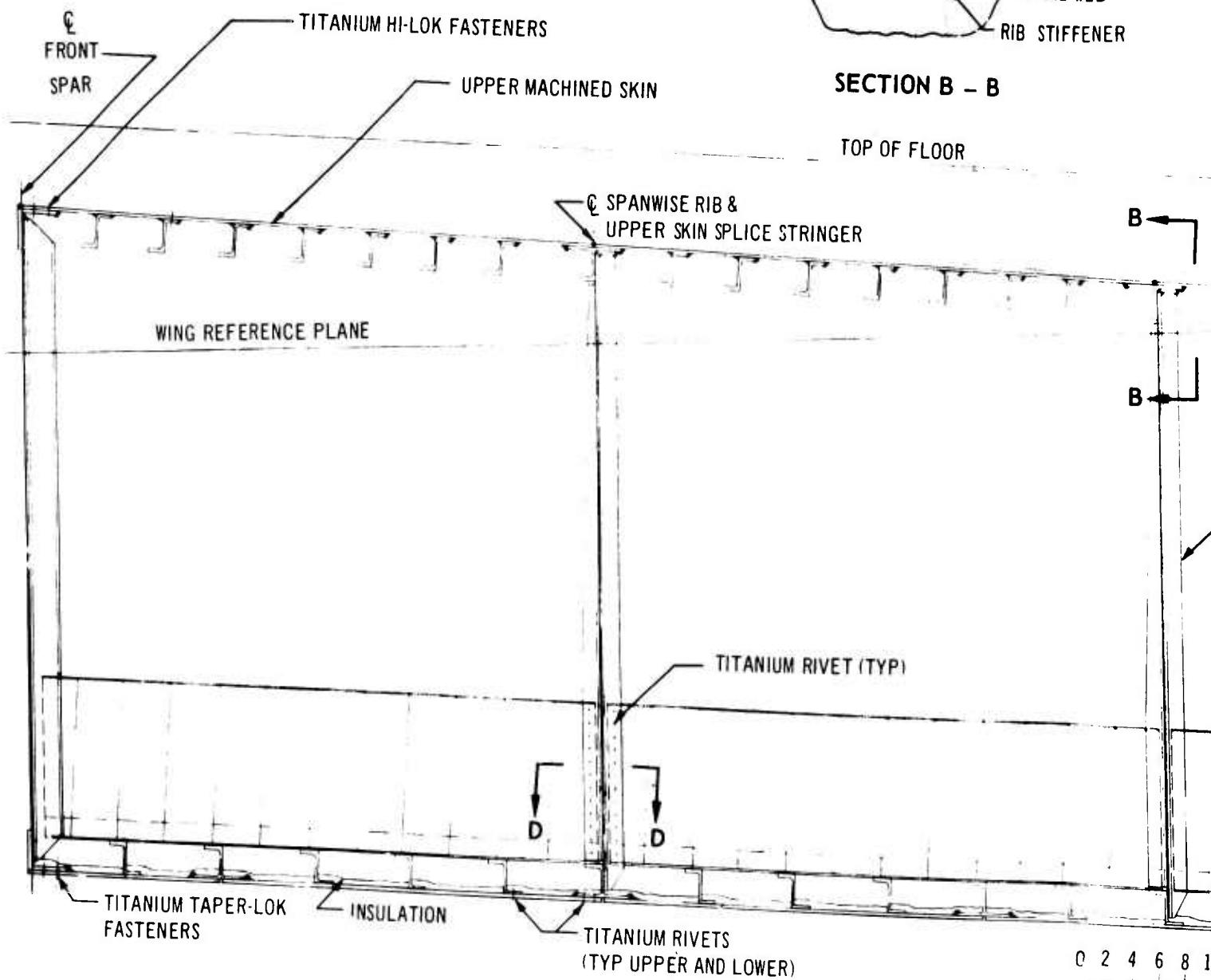




SECTION D - D

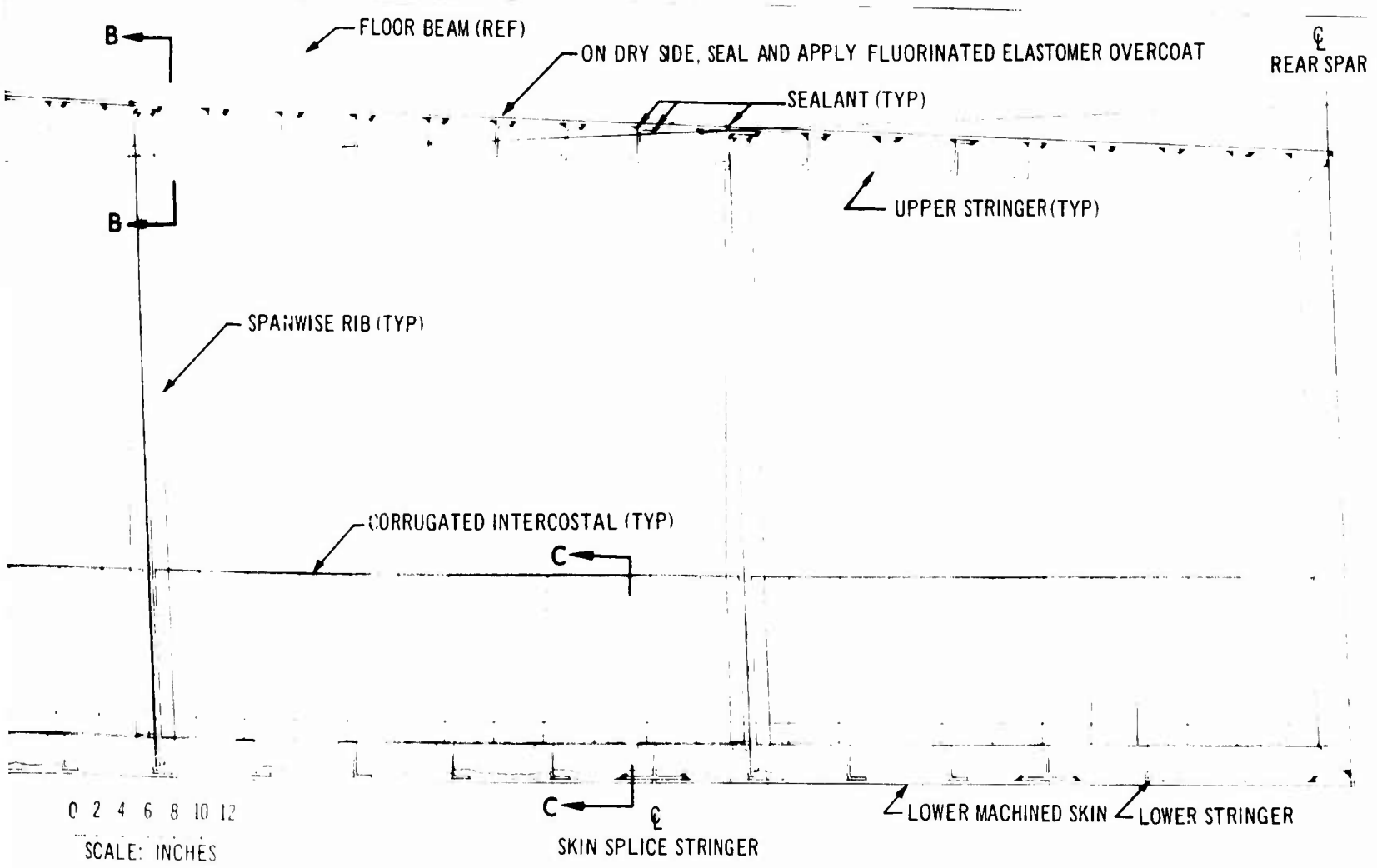
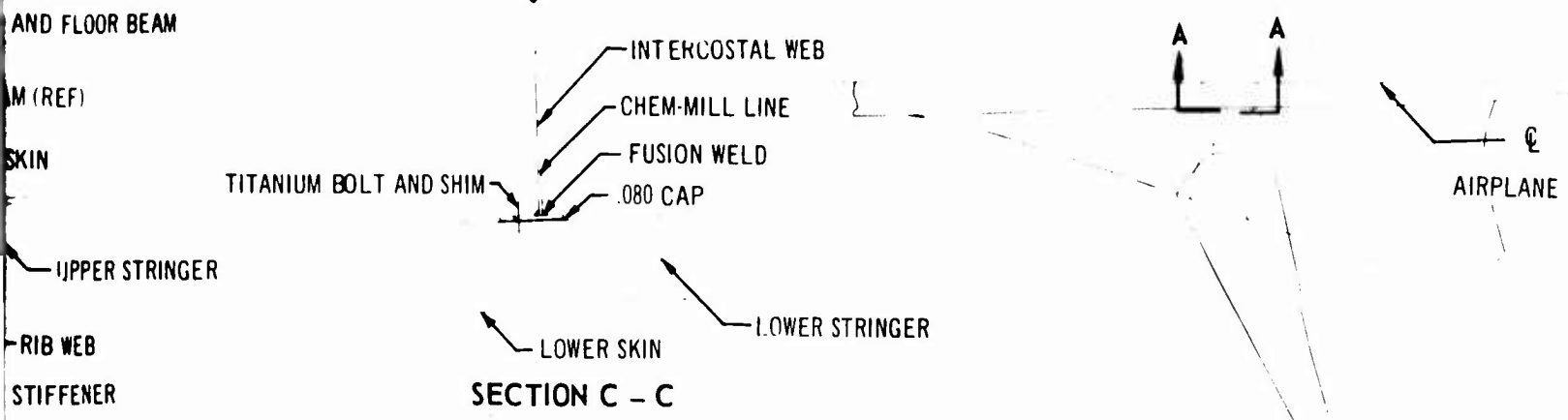


SECTION B - B



0 2 4 6 8 1  
SCALE: INCHES  
SECTION A - A

A



0 2 4 6 8 10 12  
SCALE: INCHES

Figure 3-13. Wing-Inside Fuselage Section

B

tailored for consistent wing and fuselage deflection. Further definition of this structure, including the side of the fuselage rib, is found in the fuselage structural description in Par. 3.2.

The upper and lower skin panels and fasteners are fillet sealed at the spars and skin splices. Inside the fuselage, a triple seal is provided between the fuselage compartment and the fuel tank. This is accomplished by sealing all stringers, fasteners, and skin splices on both the wet and dry side and applying a fluorinated elastomer overcoat to the dry side. Insulation is applied to the complete lower surface of the fuel tank. In addition, insulation is applied to the upper, inside surface, outboard of the side of the fuselage.

#### 3.1.2.2 Gear Support

The outboard main landing gear is attached to the front spar of the wing at two trunnion bearings located at the rugged wing-pivot structure (see Fig. 3-14). The landing gear side-brace backup structure is near the side of the fuselage at the stiff wing-to-fuselage attachment fittings. Loads are distributed into the primary wing-box structure through large forgings and rib assemblies. The inboard main gear is attached to the wing rear spar and fuselage. The design provides for failure of the gear without rupture of the structural box.

#### 3.1.2.3 Forward Inboard Section (Strake)

The large inboard structural assembly, forward of the primary wing box, is continuously attached to the side of the fuselage at the strake surfaces and at each strake rib location. The aft connection is made along the front spar of the primary wing box.

The exterior honeycomb panels are supported by typical ribs of corrugated web design as shown in Fig. 3-15. Spars, tank end ribs, and wheel-well beams are of a built-up web-stiffener design. Forward of the auxiliary spar, the fixed leading-edge area is covered by light-gage sheet, stiffened by spanwise stringers and die-formed ribs.

The strake area aft of the leading-edge auxiliary spar serves as an integral fuel tank. Fillet tank sealing is used around the edges of the large honeycomb panels. The titanium face honeycomb panels provide a fuel-impervious tank wall with excellent insulating properties. Access to the area is provided by nonstructural clamp-on doors located in the lower surface.

#### 3.1.2.4 Landing Gear Doors

Each outboard main landing gear retracts into a well within the strake and is enclosed by four main landing gear doors and two small gear strut doors. The main doors are hinged along the wheel-well side walls and operated hydraulically, and sequenced to open before gear extension and to close when the gear is fully extended. The small strut doors open with gear extension and remain open while the gear is down.

All doors are sandwich construction with honeycomb core and titanium sheet faces similar to those shown in Fig. 3-16. Door latches are provided to hold doors to contour when they are closed and subjected to airload. In the event of failure of the main hydraulic system, opening of the forward main gear doors is provided by a separate hydraulic system and separate actuator. The wheel doors can be manually disconnected and opened for ground servicing. Hinge and latch pins have dry film lubrication. When closed, doors are sealed by glass-cloth-reinforced fluorocarbon rubber seals around the edges.

#### 3.1.2.5 Slats

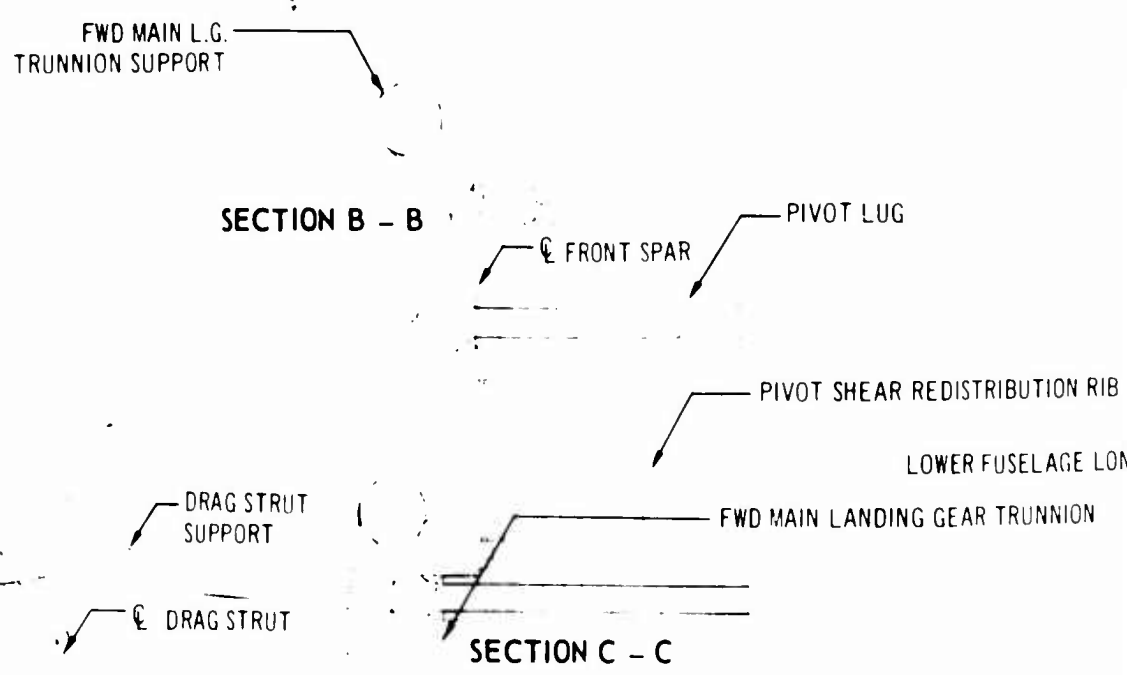
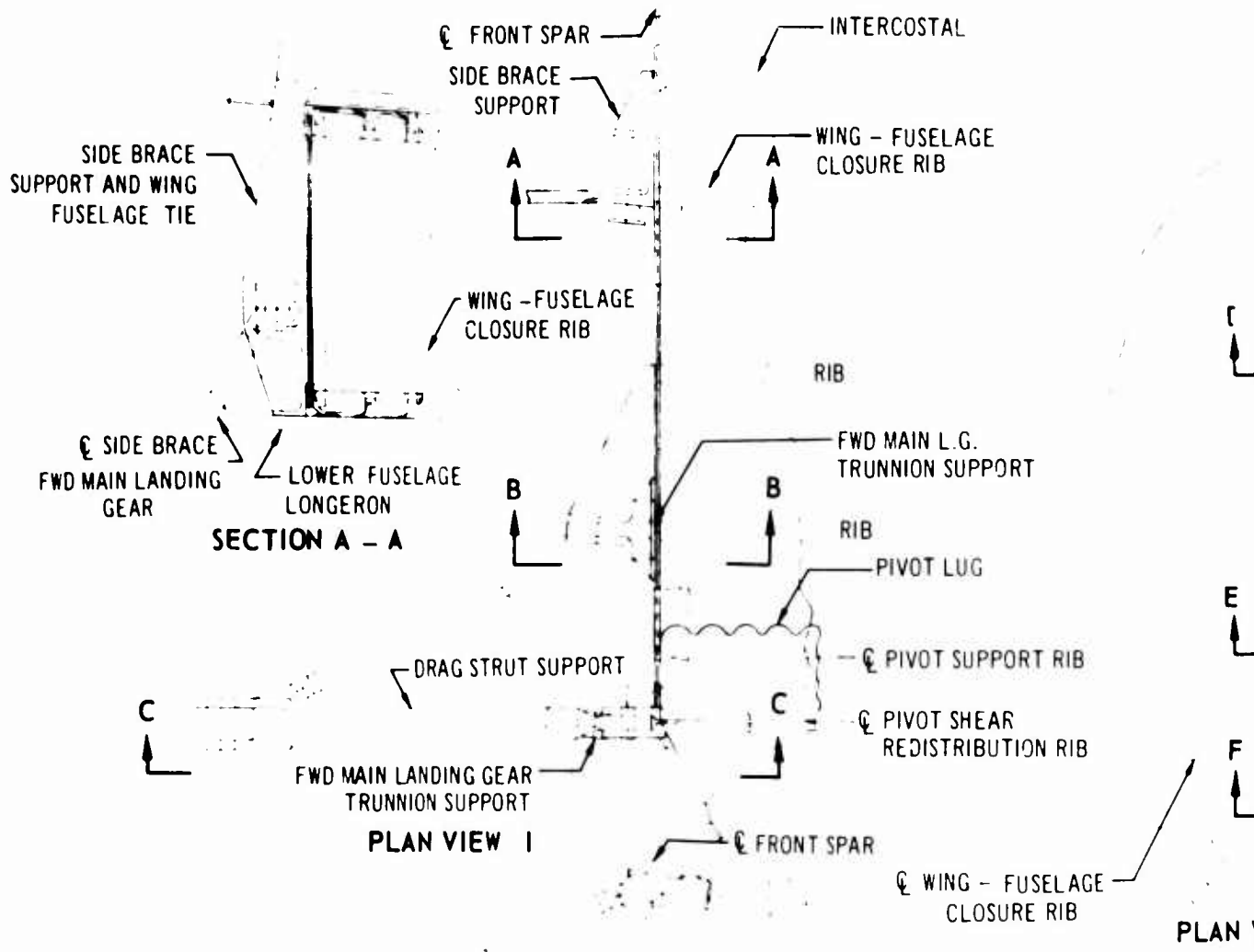
The single-segment, leading-edge slats for the inboard wing portion are supported on steel tracks located as shown in Fig. 3-17. Needle-bearing track rollers, and light-gage honeycomb construction is used (see Fig. 3-18). Hail protection is provided by reinforcement of the nose area. Replaceable rub strips, mechanically attached, are provided at contact areas between surfaces.

#### 3.1.2.6 Flap

The inboard end of the inboard flap is supported from the side of the fuselage; the outboard end is supported by a beam structure that runs from the wing pivot aft to the horizontal tail, as shown in Fig. 3-19. The outboard edge of the flap closure doors are also supported along this beam.

The inboard flap is supported and actuated by a linkage system as shown in Fig. 3-20.

In addition to serving as a conventional high-lift device, the inboard flap also acts as a deflector to prevent engine inlet ingestion of foreign material. The surface panel construction is honeycomb material, supported by conventional inner rib and spar structure as shown in Fig. 3-21. The lower surface is bolted to allow replacement. Use of titanium skins and the glass-fiber core construction will provide a durable



*A*

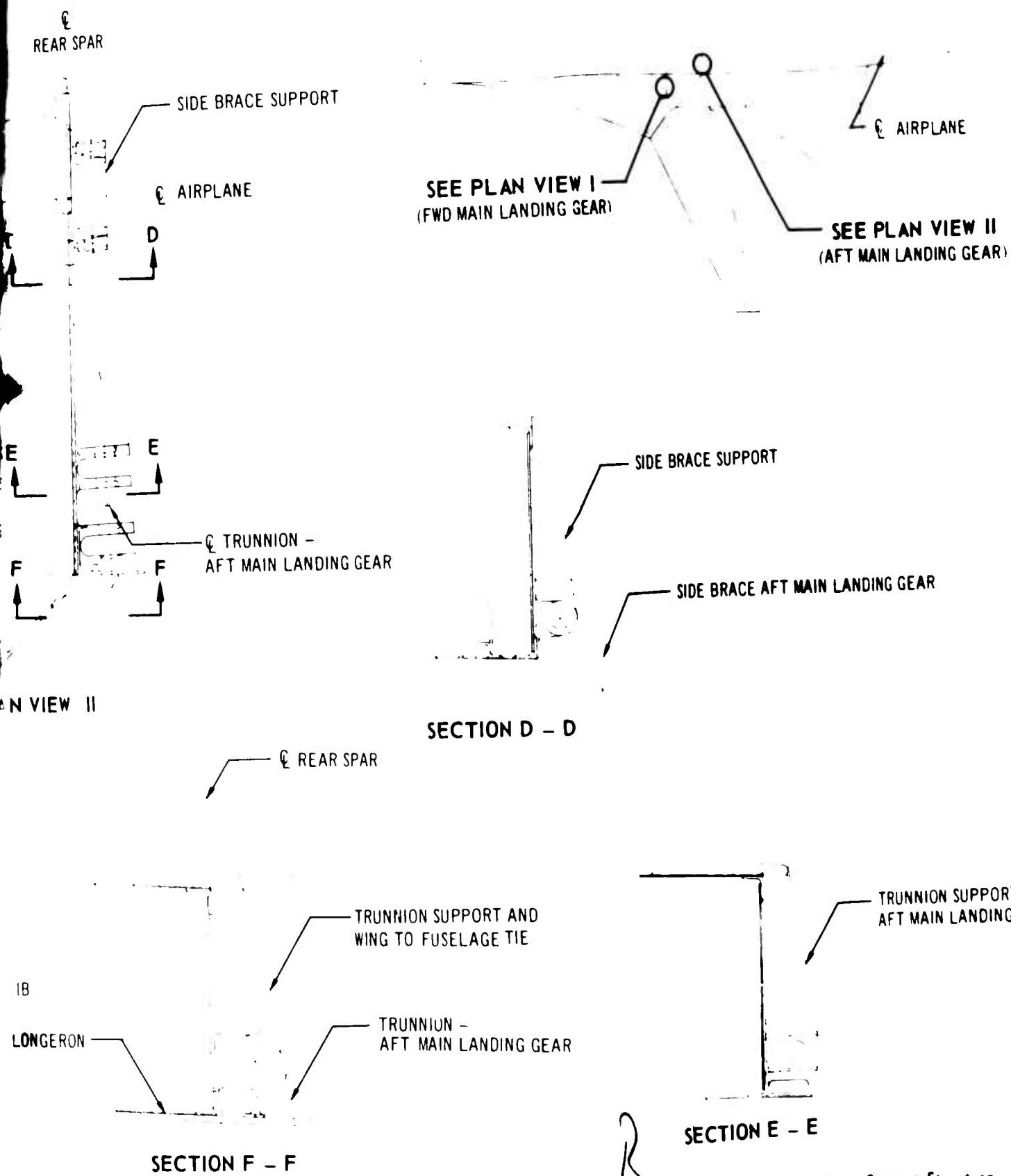
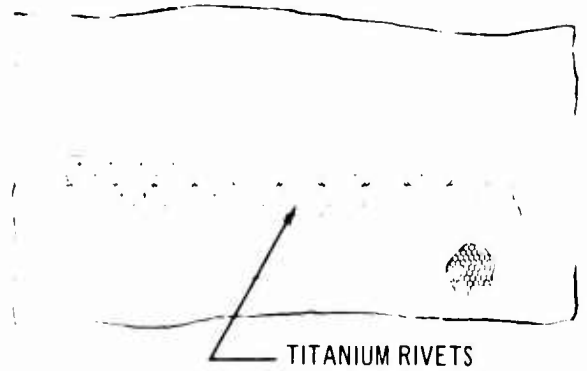
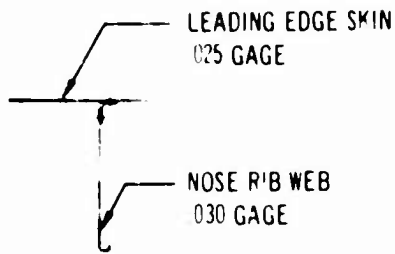
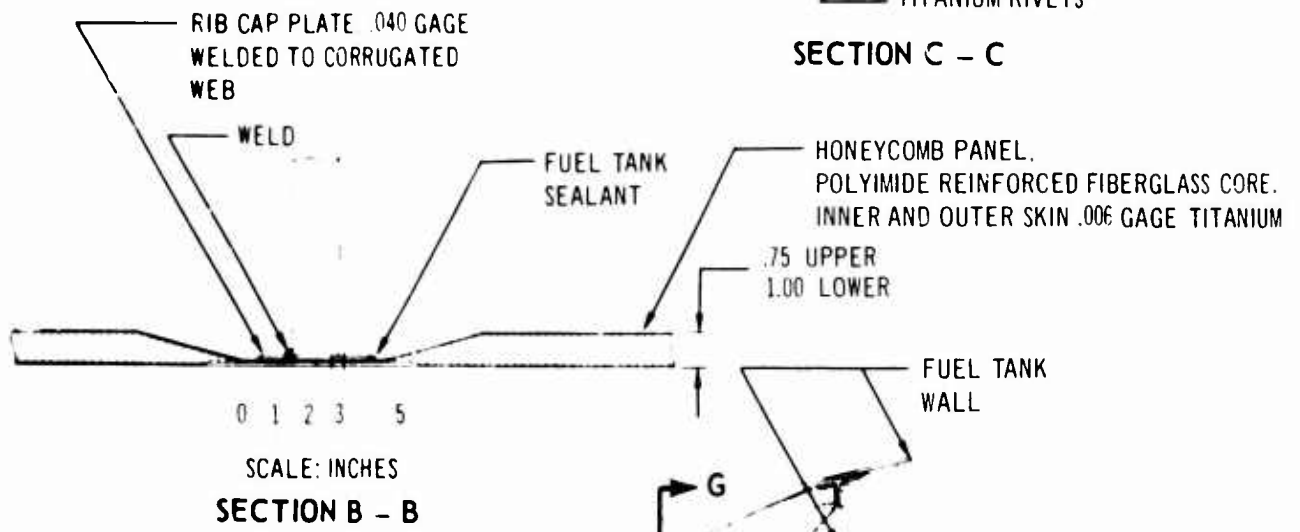


Figure 3-14. Landing Gear Support Structure

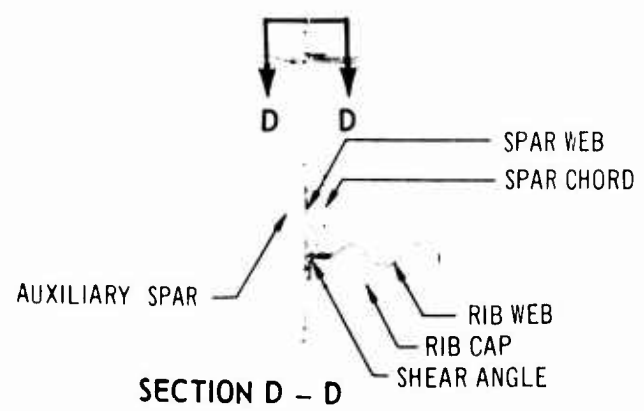
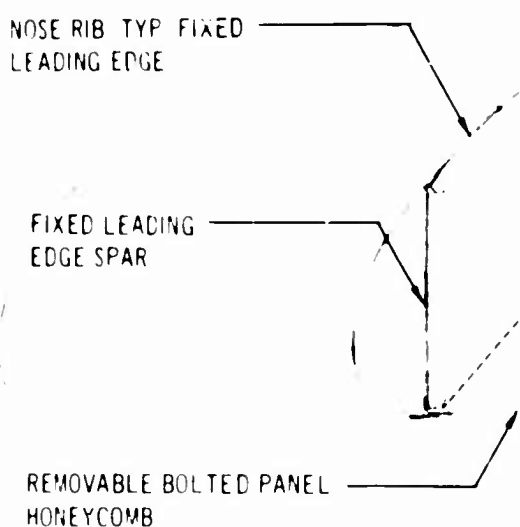


**SECTION G - G**

**SECTION C - C**

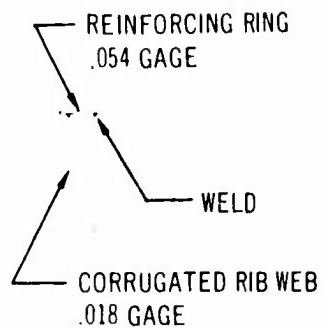


**SECTION B - B**

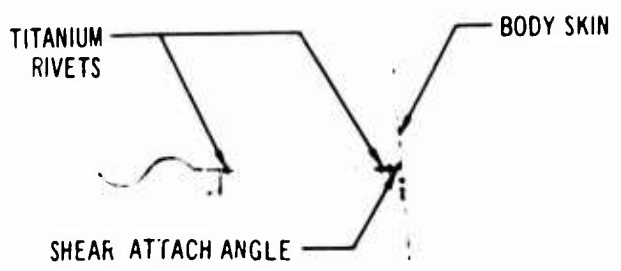
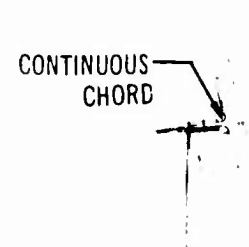
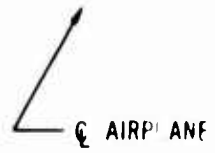


**SECTION D - D**

*Handwritten signature*

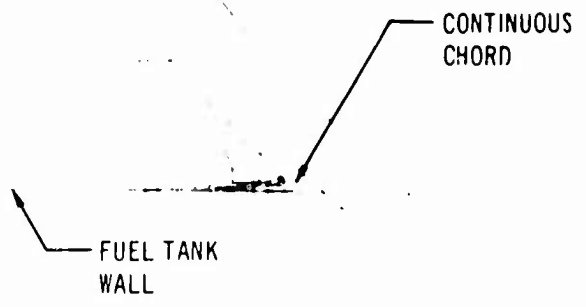
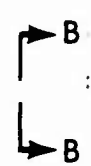
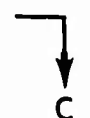
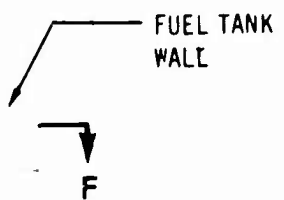


SECTION E - E



SECTION F - F

ACCESS HOLE  
12" x 20"



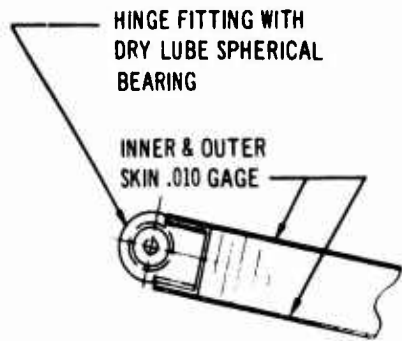
0 1 2 3 5 10

SCALE: INCHES

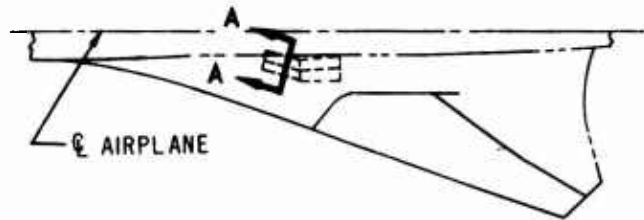
SECTION A - A

Figure 3-15. Typical Strake Rib

B



DETAIL I



ACTUATOR (ONE AT EACH DOOR)

STRAKE WING UPR SURFACE

WHEEL - WELL BULKHEAD

HONEYCOMB CORE  
POLYIMIDE REINF. FIBERGLASS

DETAIL II

SEE DETAIL I

SEE DETAIL II

ACTUATOR FITTING



SECTION B - B



SECTION A A

Figure 3-16. Forward Landing Gear Doors



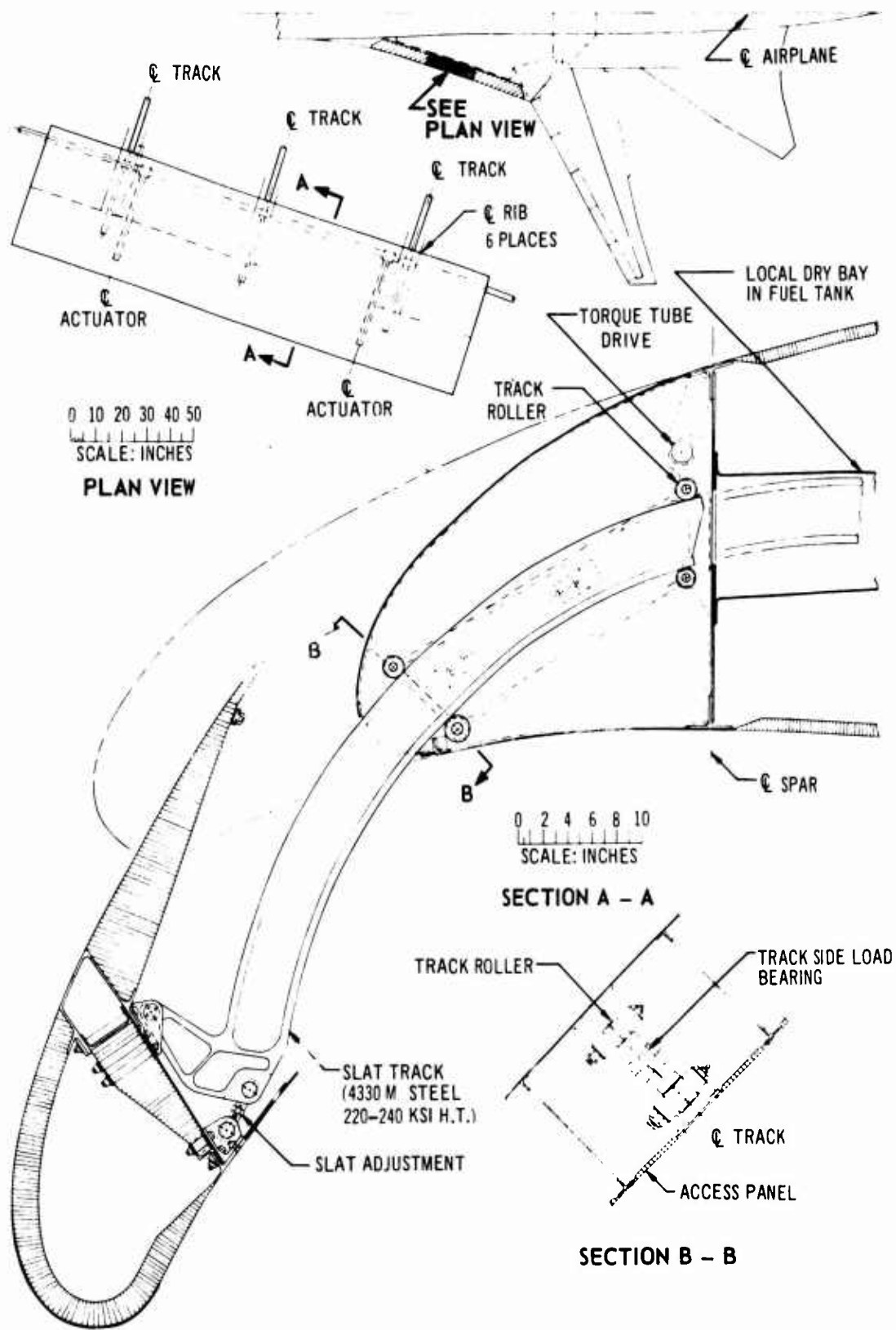


Figure 3-17. Support Structure of Inboard-Wing-Portion Leading Edge Slat

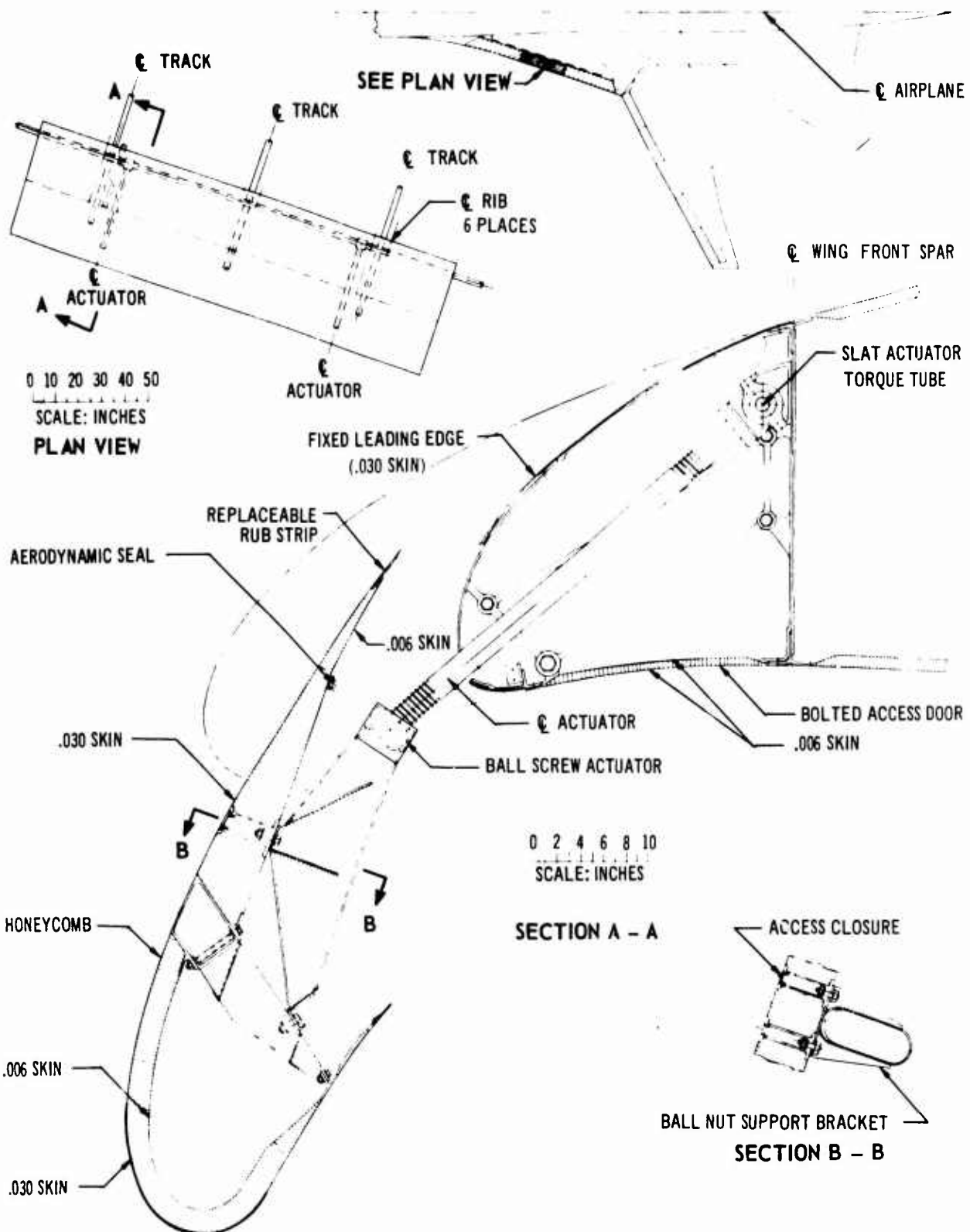
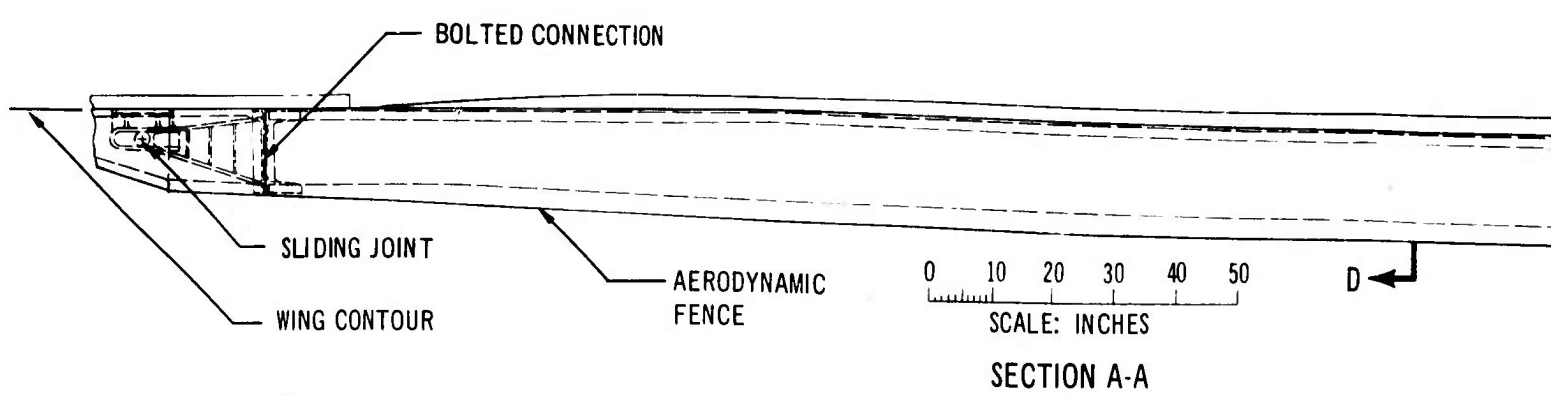
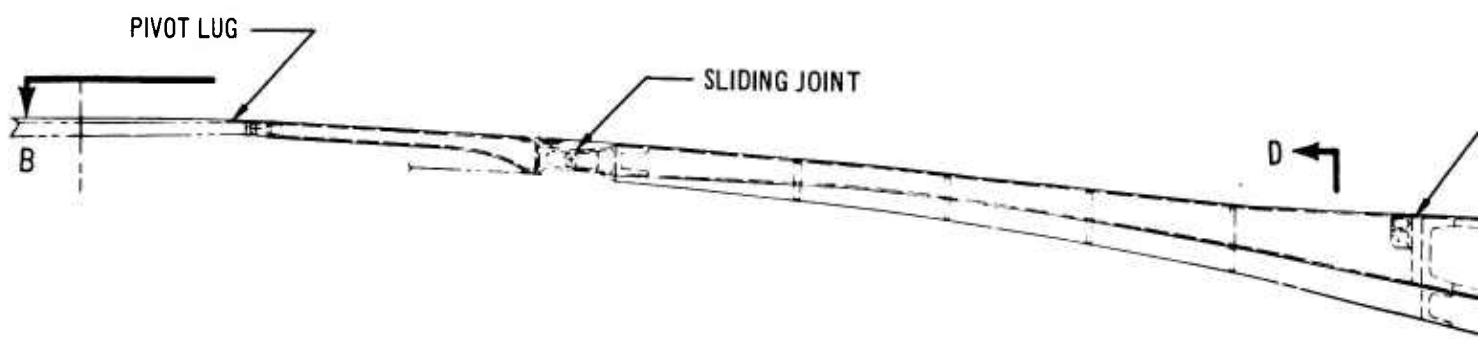
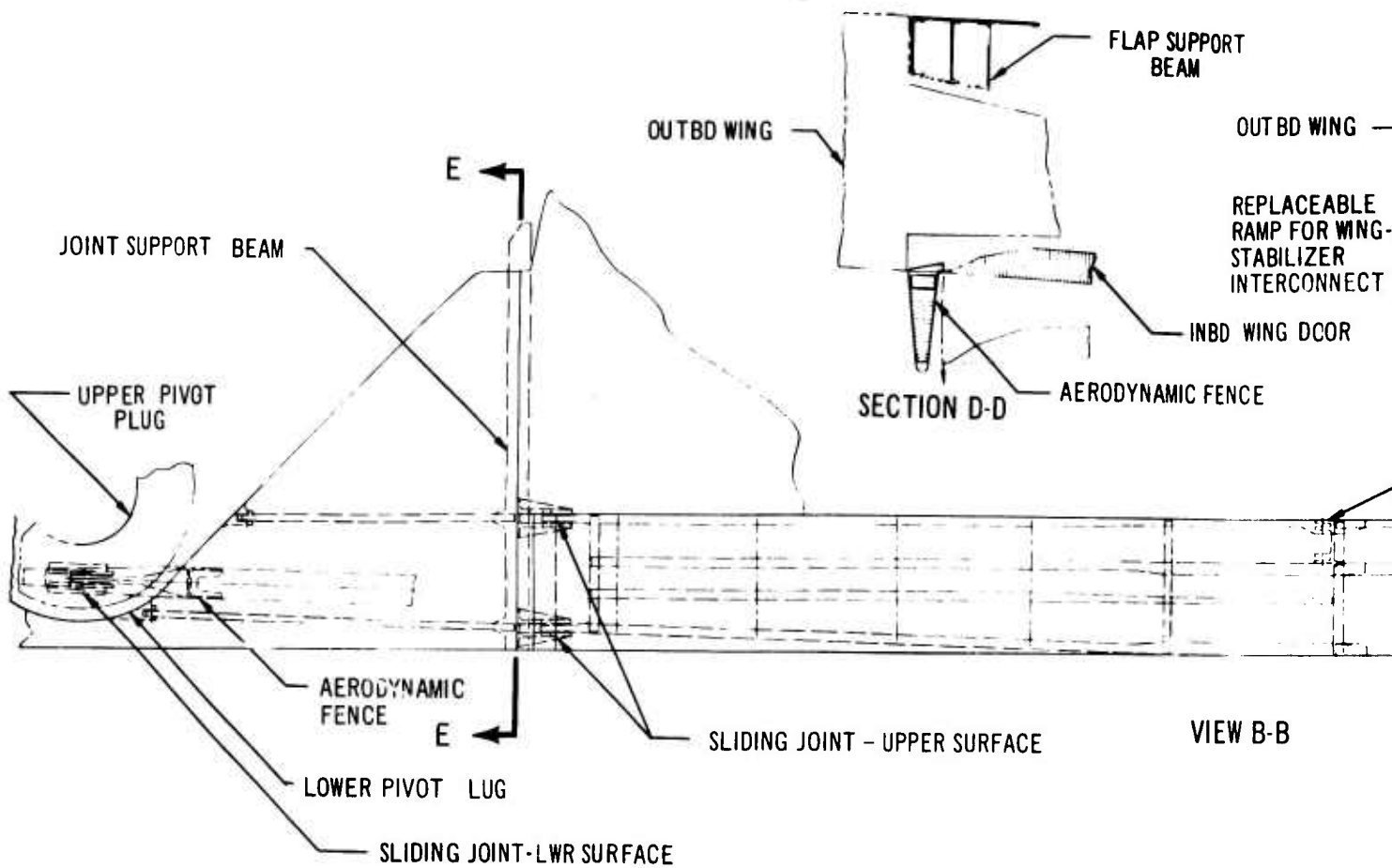


Figure 3-18. Typical Structure of Inboard-Wing-Portion Leading Edge Slat

V2-B2707-6-2



A

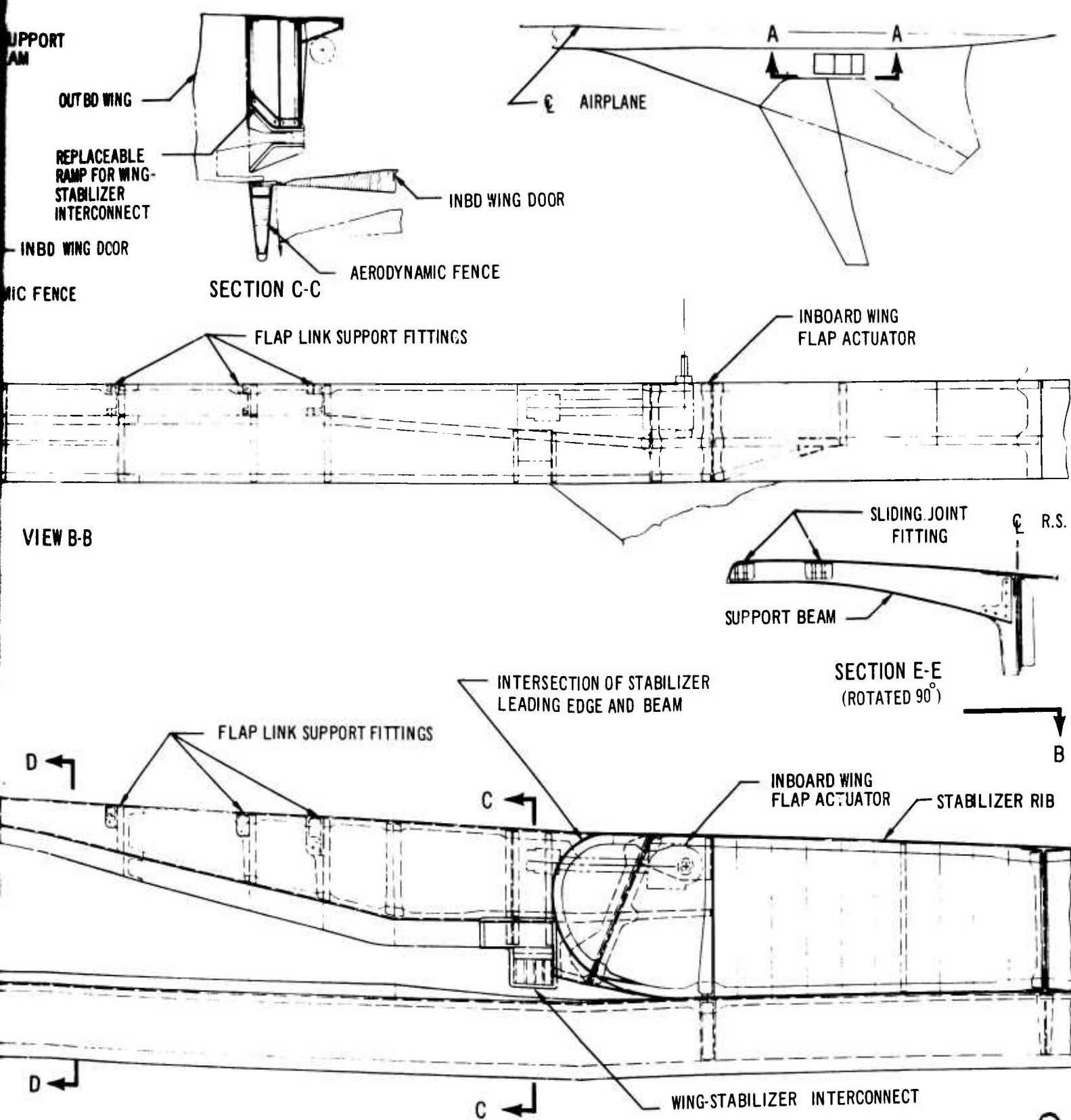
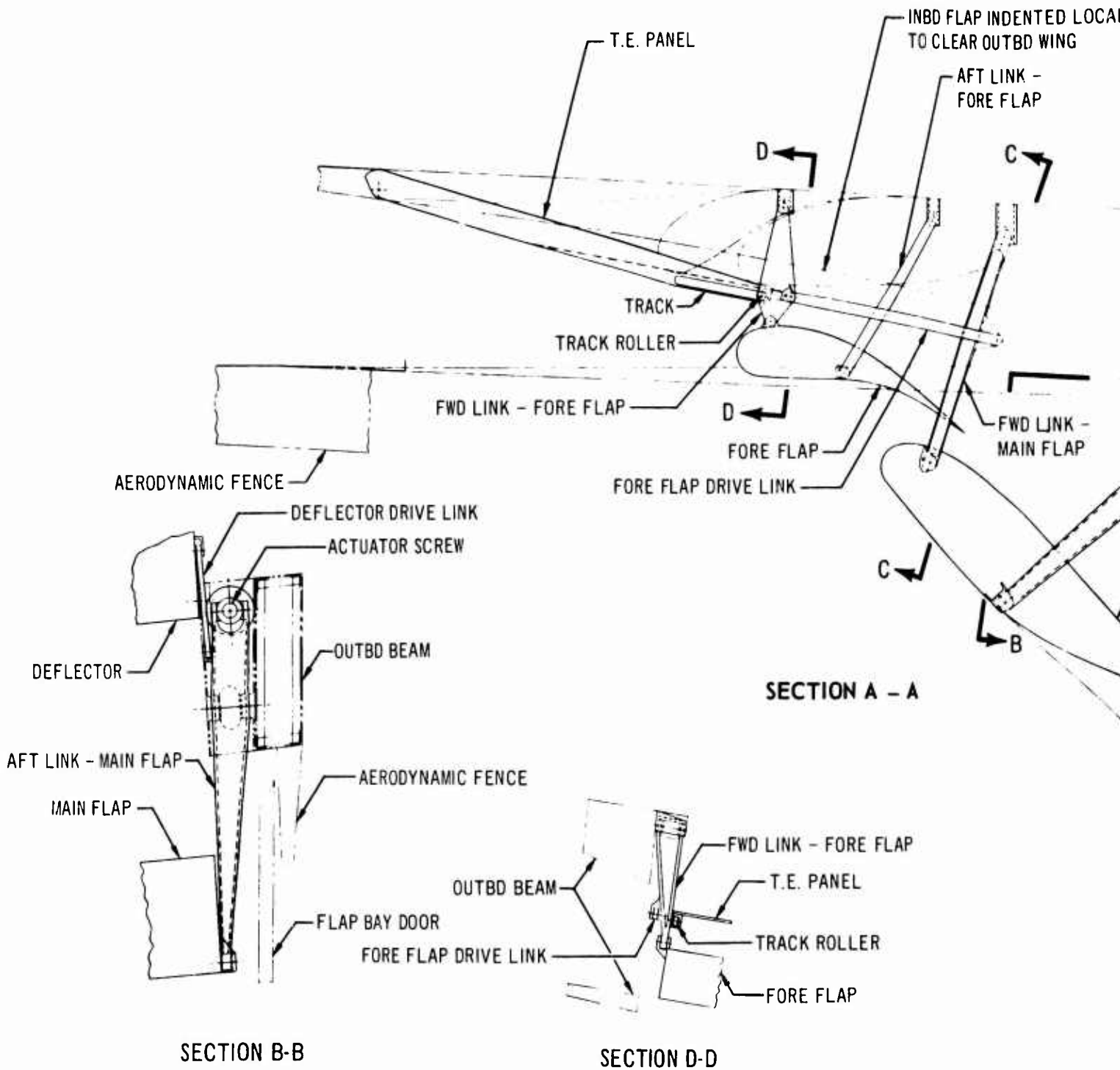


Figure 3-19. Outboard Support Beams of Inboard Wing Portion



A

FLAP INDENTED LOCALLY  
NEAR OUTBD WING

AFT LINK -  
FORE FLAP

FWD LINK -  
MAIN FLAP

AFT LINK -  
MAIN FLAP

MAIN FLAP

AFT FLAP

DEFLECTOR

DEFLECTOR DRIVE LINK

ACTUATOR SCREW

HORIZONTAL STABILIZER  
(REF)

FLAP BAY DOOR  
AFT SEGMENT

AIRPLANE

OUTBD BEAM

FWD LINK -  
MAIN FLAP

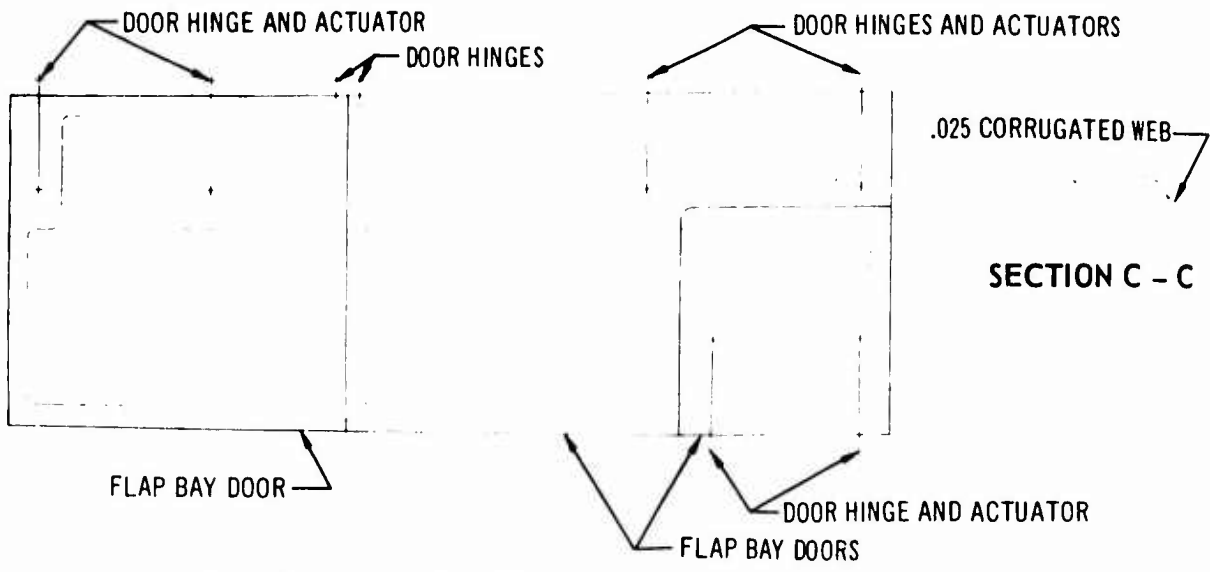
FORE FLAP  
DRIVE LINK

MAIN FLAP

0 10 20 30 40  
SCALE: INCHES

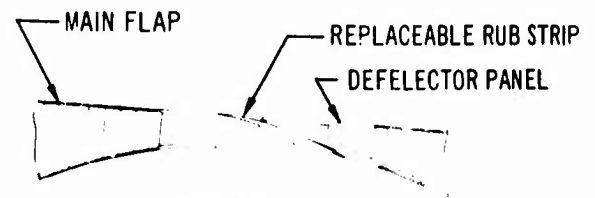
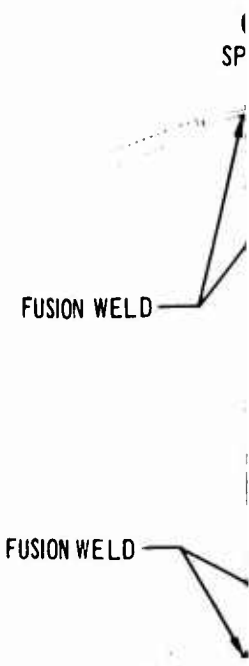
SECTION C-C

Figure 3-20. Trailing-Edge Flap Mechanism of Inboard Wing Portion

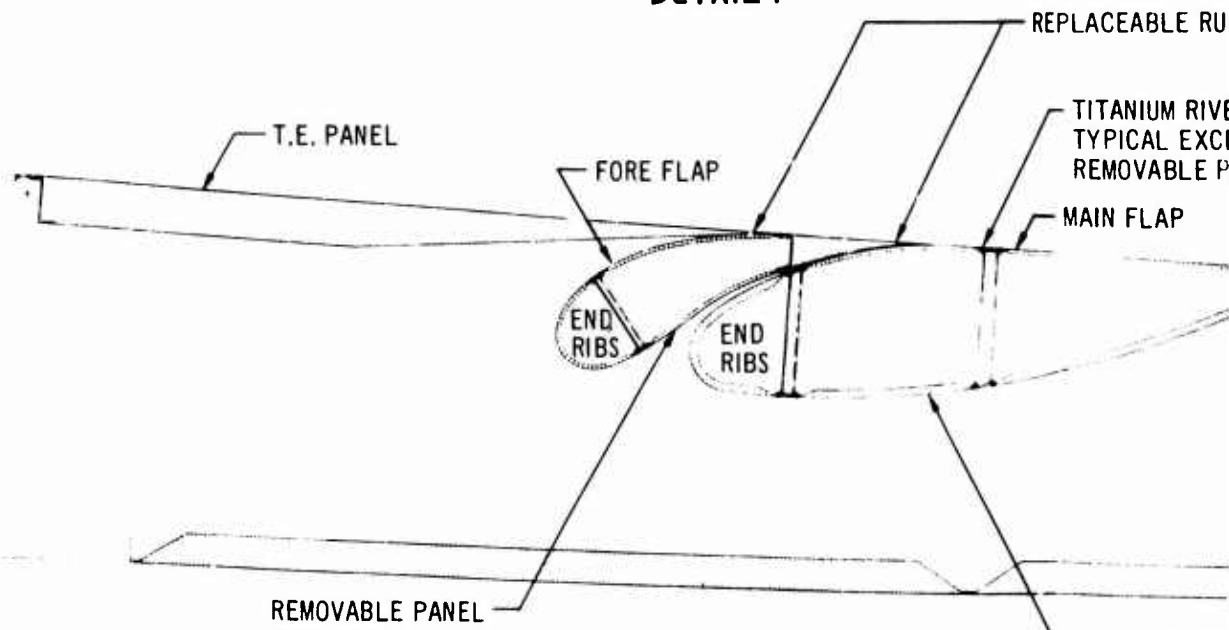


0 20 40 60 80 100

SCALE: INCHES  
 PLAN VIEW  
 LOWER SURFACE



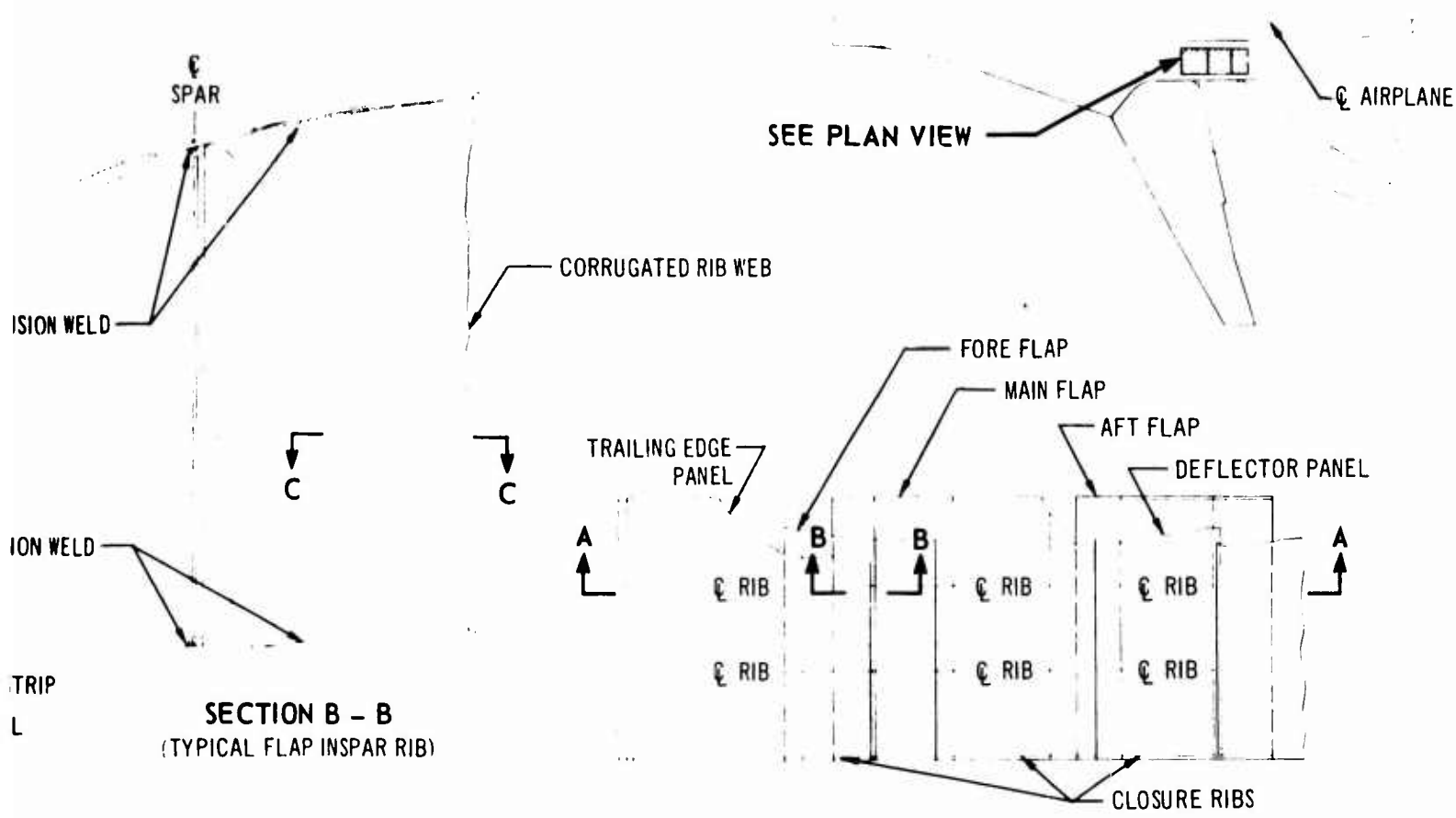
DETAIL I



0 5 10 15 20 25 30 35 40

SCALE: INCHES  
 SECTION A - A

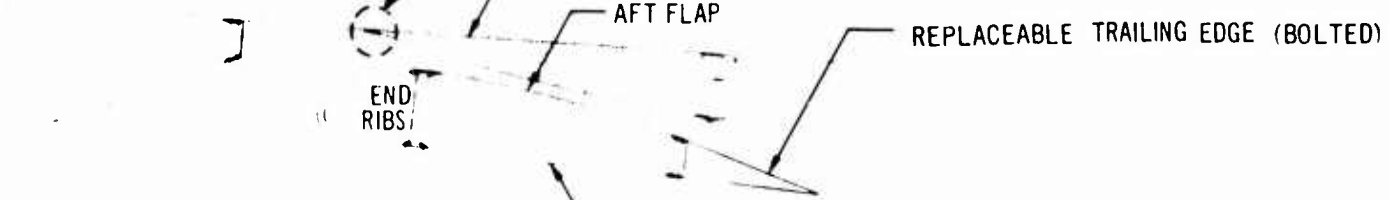
A



REPLACEABLE RUB STRIP

TITANIUM RIVETS  
TYPICAL EXCEPT FOR  
REMOVABLE PANELS

MAIN FLAP



REMOVABLE PANEL (BOLTED)  
TYPICAL HONEYCOMB PANEL SKIN .006 TITANIUM

REMOVABLE PANEL (BOLTED)

FLAP BAY DOOR (3 SEGMENTS)

Figure 3-21. Trailing-Edge Structure of Inboard Wing Portion



long-life surface, much tougher than aluminum construction in use on subsonic jet aircraft. Replaceable rubbing strips, attached by mechanical fasteners, are provided at points of contact.

### 3.1.3 Wing Pivot

#### 3.1.3.1 Actuator Support

The wing-pivot, screw-actuator support structure is mounted on the rear spar of the outboard and inboard sections of the wing box as shown in Fig. 3-22. Dual load path fail-safe provisions are incorporated in the design. The major portion of the structure is composed of heavy forgings.

#### 3.1.3.2 Wing Pivot

The wing pivot design is shown in Figs. 3-23 and 3-24. The pivot design consists of an upper and lower journal bearing mounted in the outboard-wing-section pivot lugs. A large plug is mounted in the journal bearing that bears on the inboard-wing-section lugs. In this manner the wing bearing loads are transmitted through the pivot. A thrust bearing between the outboard wing lugs and the upper plug transmits vertical load from the outboard tank end rib through the pivot (see Fig. 3-24). Bolts and a shear transfer plate transmit the vertical load to the inboard curved spar. Torsion loading is transmitted as a couple load in the journal bearing. The upper and lower wing lugs have upper and lower members, each of which is capable of carrying 80 percent of limit load times a dynamic magnification factor of 1.15. In this manner, fail-safe design is obtained. Control system and fuel lines are routed through the pivot centerline. Studies (Ref. 1) and mockups show that this configuration gives the simplest and most reliable system design.

The journal bearing consists of two surfaces of self-lubricating 0.012-in.-thick Teflon fiber interweave fabric bonded to stainless steel races. Sizing of the components and operating stress levels are selected to give long, trouble-free service life. One bearing surface is spherical to provide for misalignment. The other bearing surface is cylindrical to prevent transmittal of vertical loads through the bearing. Bearing rotation can occur on either of two surfaces; the spherical or the cylindrical. The center race floats, distributing the wear to two surfaces. This results in excellent pivot-bearing wear life. The sliding motion takes place between the steel and the Teflon-fabric surface.

The wing vertical shear loads are carried on a replaceable Teflon-bronze bearing, sliding on a replaceable steel strip, at the upper, outboard area of the pivot (see View I, Fig. 3-24).

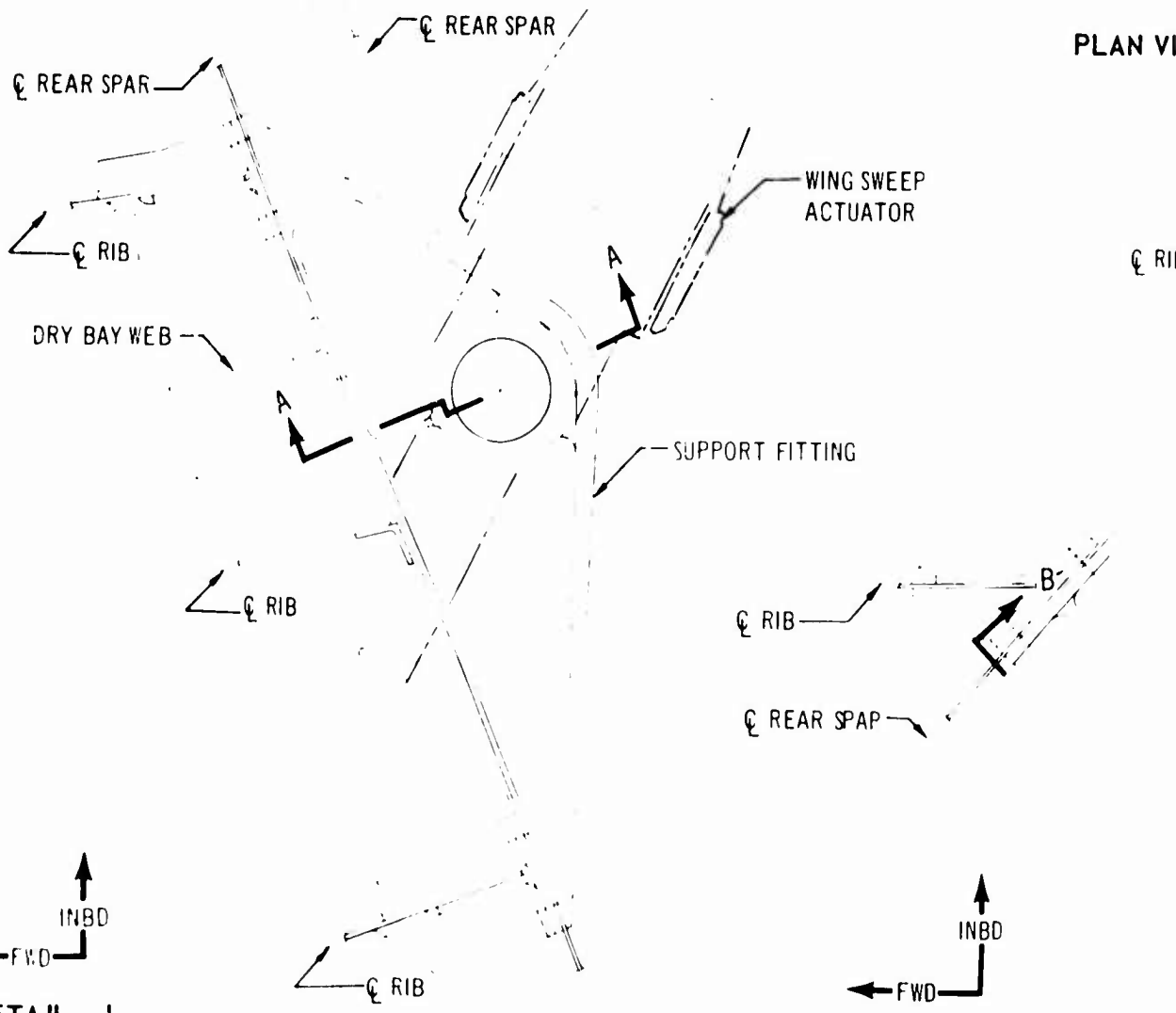
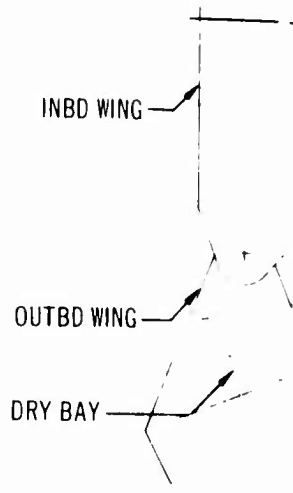
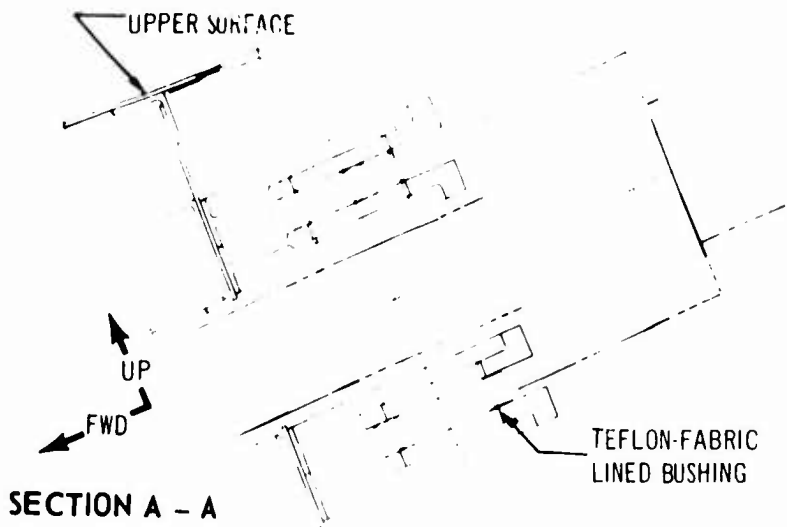
Bearing pressures are low, giving long-wear life. No lubrication is required. These thrust bearings are in segments and can be replaced without disassembly of the wing-pivot journal bearing.

Simple seals, compatible with the airplane environment, are provided to preclude bearing contamination.

The pivot-bearing components are designed to give a long trouble-free service life. Company bearing development tests are discussed in Part E, Structural Tests (V2-B2707-9), of the Airframe Design Report. Tests of quarter-scale and full-scale pivot bearings demonstrate that the pivot bearings will function satisfactorily for the operational life of the airplane. The full-scale bearing has been tested under simulated airplane variable loadings and environments for 30,100 ground-air-ground cycles without showing appreciable wear. Because of the thinness of the Teflon bearing material, bearing wear does not impair the functioning or reliability of the assembly, or adversely affect wing stiffness.

As part of the bearing test program, a reliable, easy method of checking the pivot wear condition has been developed. The method consists of measuring the electrical capacitance across the bearing. The bearing configuration is exceptionally suited to this method of check. A local thin or worn area of the bearing can be reliably and simply detected. Wear tests show that after the initial warning, as detected by the electrical capacitance measurement, appreciable wear life remains in the bearing. This will allow the airplane operator to schedule a routine bearing replacement at his convenience. Aerodynamic forces on the wing tend to move the wing forward, giving a high margin of wing actuator power available to move the wings forward in case of an increase in bearing friction.

Electrical bonding across the pivot, from the outboard section to the inboard section of the wing, is provided by a metal-to-metal pressure rub strip attached to the pivot-bearing lug structure. Electrical tests involving simulated lightning strikes are scheduled (Refs. 2 and 3).



DETAIL I

DETAIL II

A

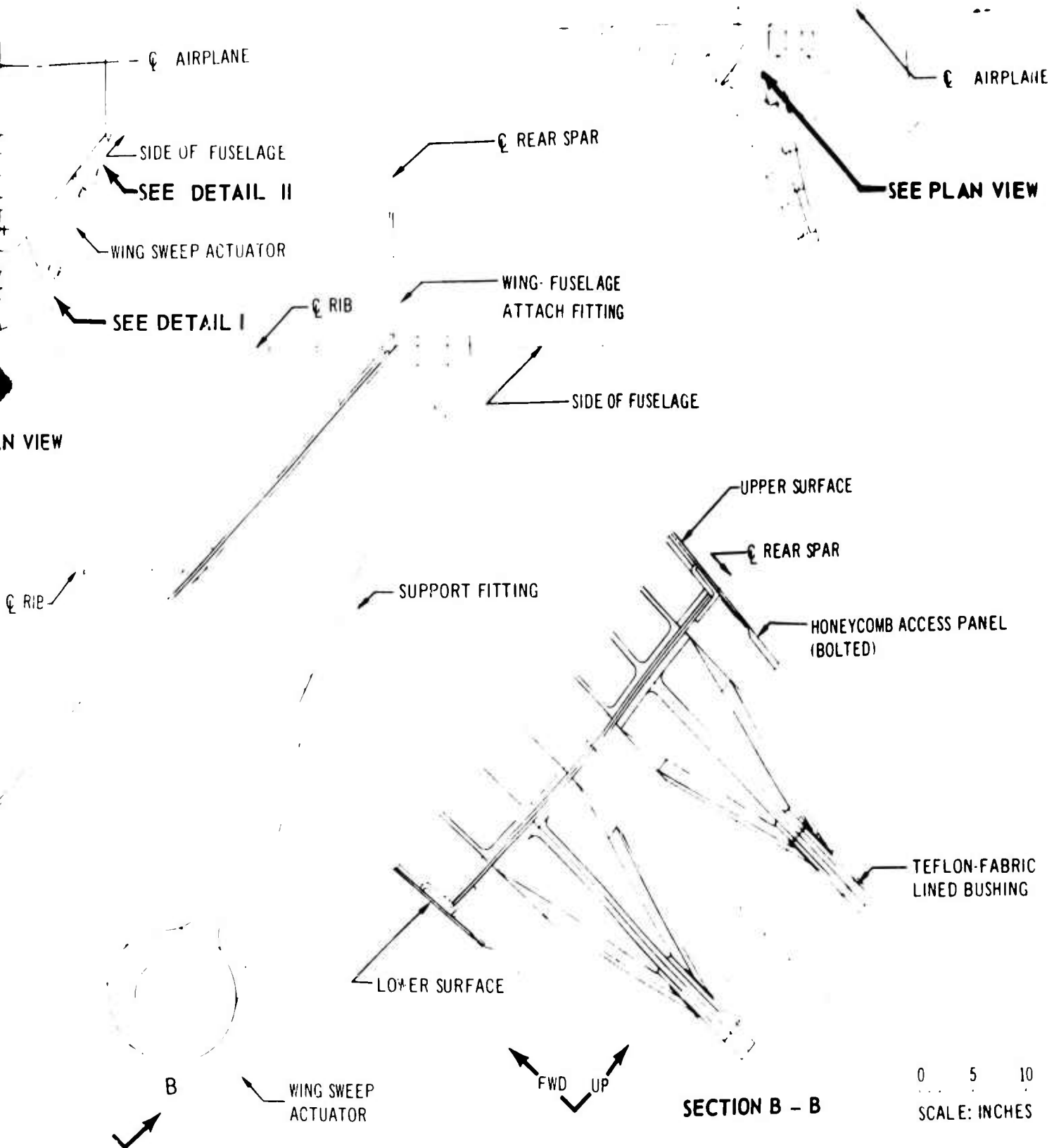


Figure 3-22. Sweep Actuator Support

V2-B2707-6-2

B

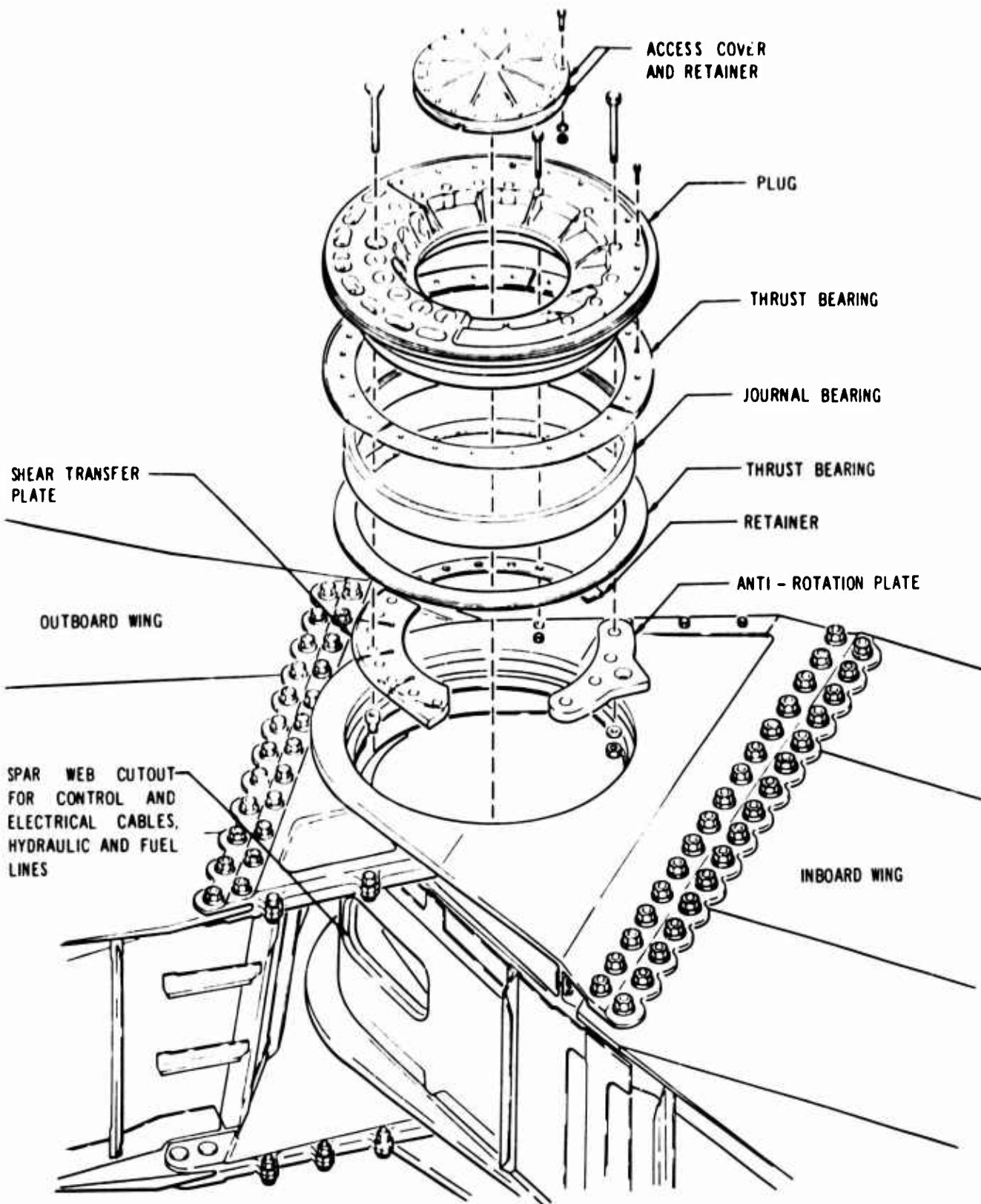
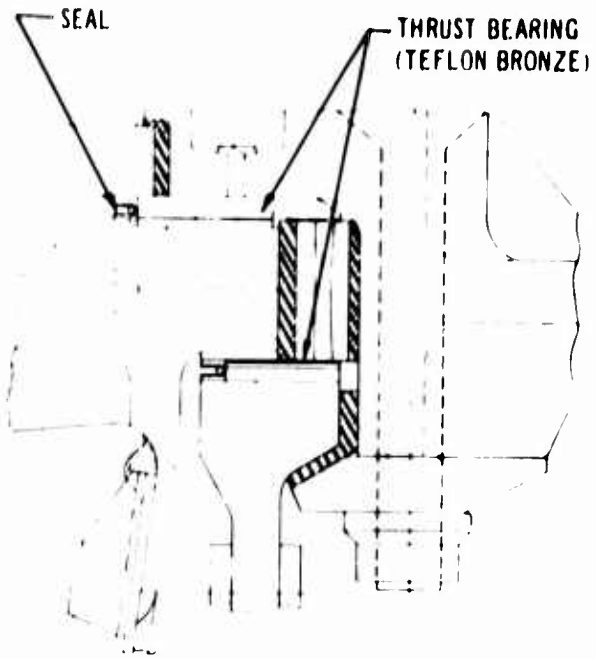


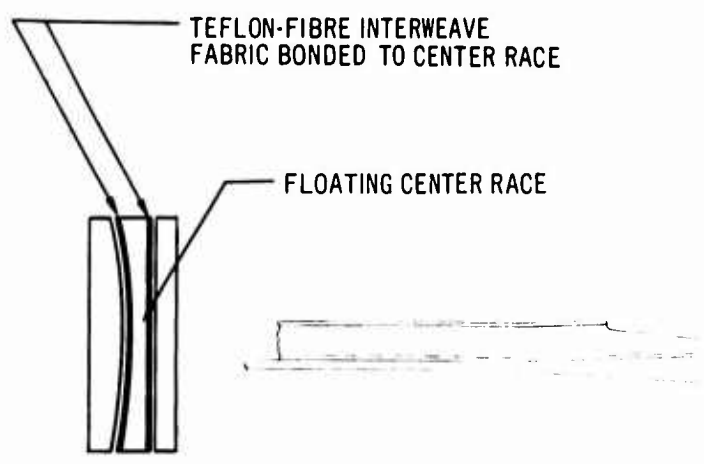
Figure 3-23. Pivot Arrangement

V2-B2707-6-2

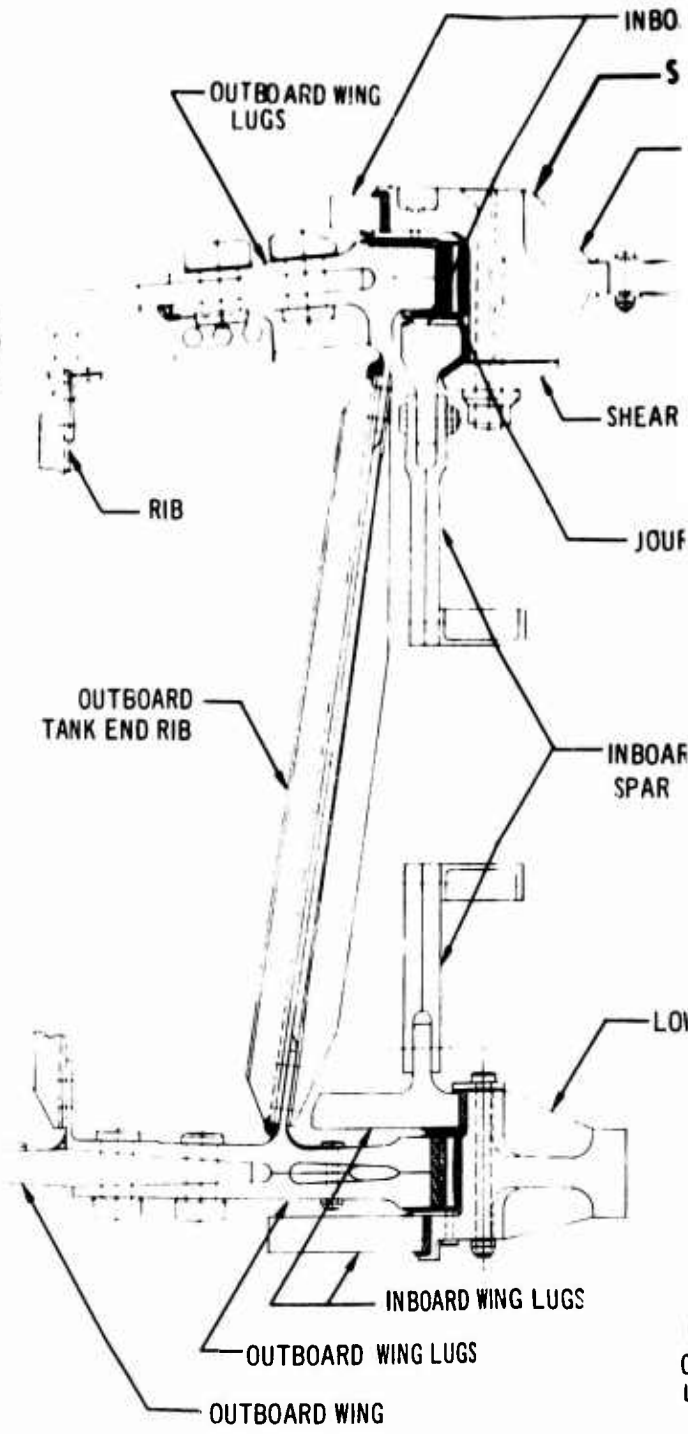


INDICATES REPLACEABLE  
TITANIUM SLEEVE

DETAIL I



DETAIL II  
STEEL JOURNAL BEARING



A

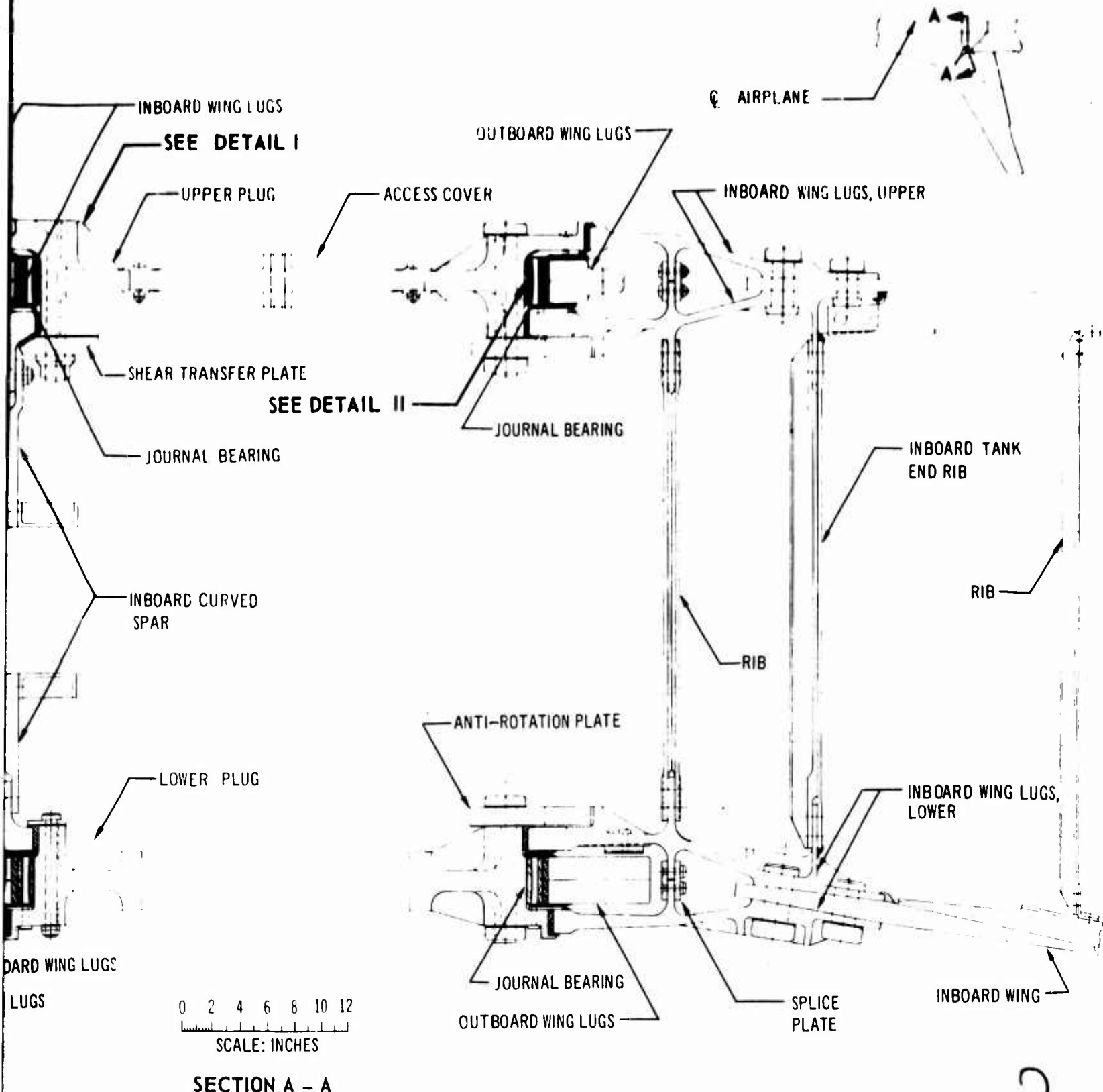


Figure 3-24. Section Through Pivot

Access doors for complete inspection of primary structure and systems in the pivot area are provided as shown in Fig. 2-2.

To conduct a complete inspection or replacement of the pivot bearing assembly, the following procedure is recommended. The outboard wing is jacked into jig position, relieving bearing loads. After removal of the pivot fairing and outer thrust bearing assemblies, the plug retainer bolts are removed. This allows the plug (see Fig. 2-23) to be removed using a simple puller. The antirotation plate, shear transfer plate, and retainer are removed with the plug retainer bolts. The inner thrust bearings are removed allowing the installation of the bearing puller. The journal bearing is cooled with liquid nitrogen and removed by the bearing puller. The bearing removal is accomplished without separating the outboard wing section from the inboard wing section. For replacement, the journal bearing assembly is cooled with liquid nitrogen and inserted in place.

### 3.2 FUSELAGE

The fuselage structural arrangement is shown in Fig. 3-25. The deep fuselage provides the following advantages:

- High dynamic stiffness with minimum weight
- Space for cargo, fuel, continuous-wing center section, and aft main gear
- Improved lower-lobe frame design

The inboard profile drawing in the System Engineering Report (V2-B2707-1) shows the space arrangement.

To facilitate manufacturing, the fuselage is divided into six sections as shown in Fig. 3-25. This figure shows boundaries of the pressurized volume. The movable forebody allows excellent subsonic crew vision.

Pressurized compartment access doors are the inward-opening plug type. Full and visible markings with the maximum use of the Air Transport Association indexing system are provided on access doors and openings. Service doors are retained to the airplane.

A cargo-restraining and pressure-safety bulkhead is located at the forward end of the aft cargo compartment. It protects the passengers, systems, and equipment from the aft cargo. In the event of a decompression in the cargo compartment, the bulkhead retains cabin pressure.

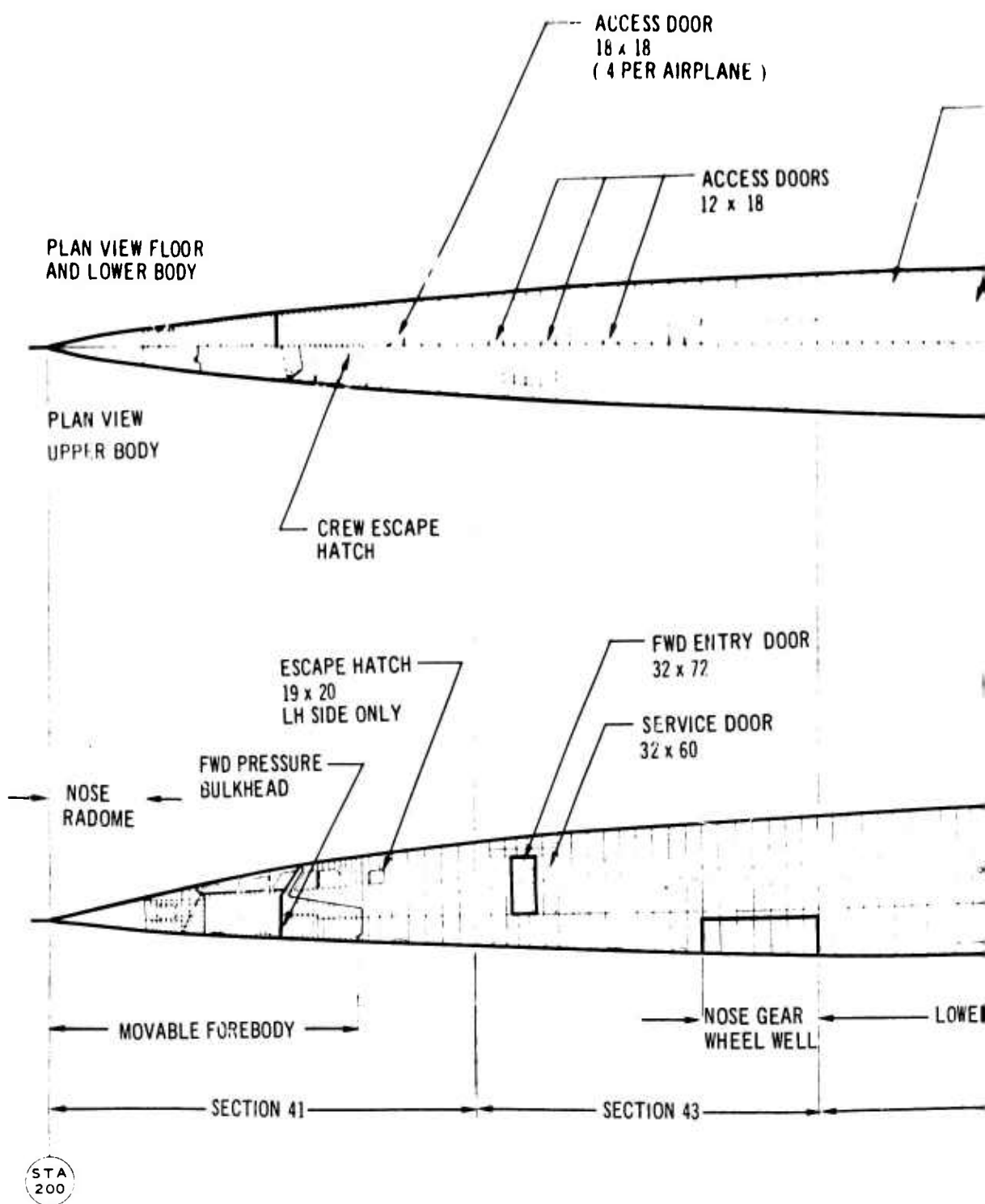
Major assemblies are described in detail in the following paragraphs.

#### 3.2.1 Movable Forebody

Movable forebody construction details are shown in Fig. 3-26. The movable forebody provides the best compromise of vision, drag, maintainability, weight, and reliability that extensive study, testing, and mockup evaluation could develop.

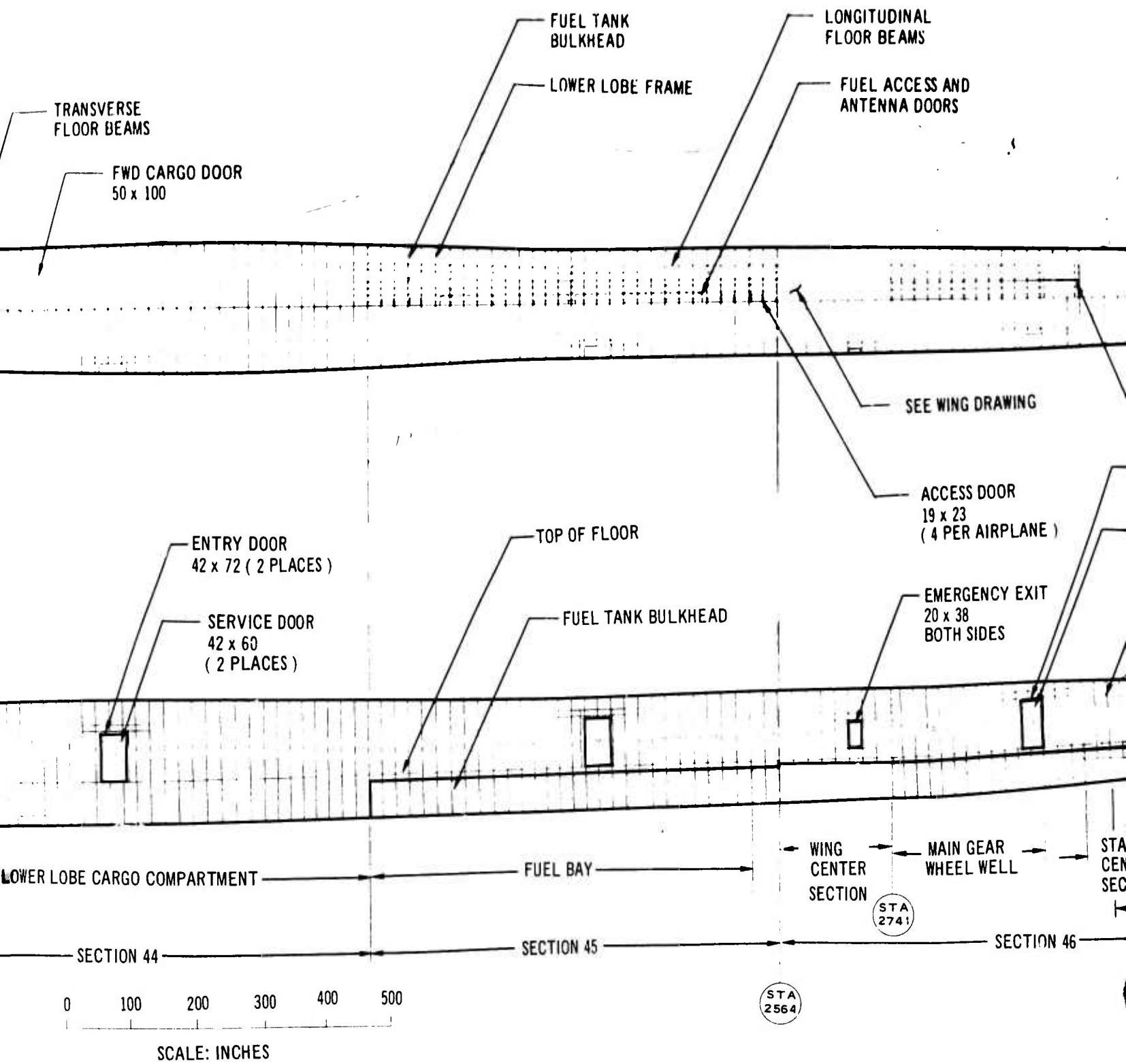
The forebody design is of conventional skin, frame, and longeron construction. This provides efficient structure and resists hail damage.

The forebody is operated about a fixed hinge by means of a ball-bearing, screw-type actuator. The actuator is normally powered by two electric motors each operated from a separate power source. Operation time is 15 sec down and 15 sec up. Loss of either motor results in operation at twice the normal operating time. As an emergency feature, in the event that both motors fail, a manual disconnect allows a free fall of the forebody. A rate-limiting device restricts free fall to prevent a large impact load on the down stop. To eliminate the possibility of the forebody extending during supersonic cruise, a mechanical device lock the forebody in the up position. The forward section of the forebody rotates about a pivot forward of the forebody windows. Sequencing of the forward section is accomplished by a torque shaft, extending forward from the gear box, that actuates the aft section. Rotation of this shaft actuates a ball screw-type actuator that moves the forward section at the same rate as the aft section. This allows the weather radar antenna and pitot probe to maintain alignment during forebody actuation and provides suitable ground clearance for runway and taxiway markers and snow banks. Slides attached to the forebody engage with rails that are mounted on the forward pressure bulkhead. The rails provide reaction for side loads. The forebody structure is designed for actuation up to Mach 0.90 or 375 knots calibrated air-speed (CAS).



A





B

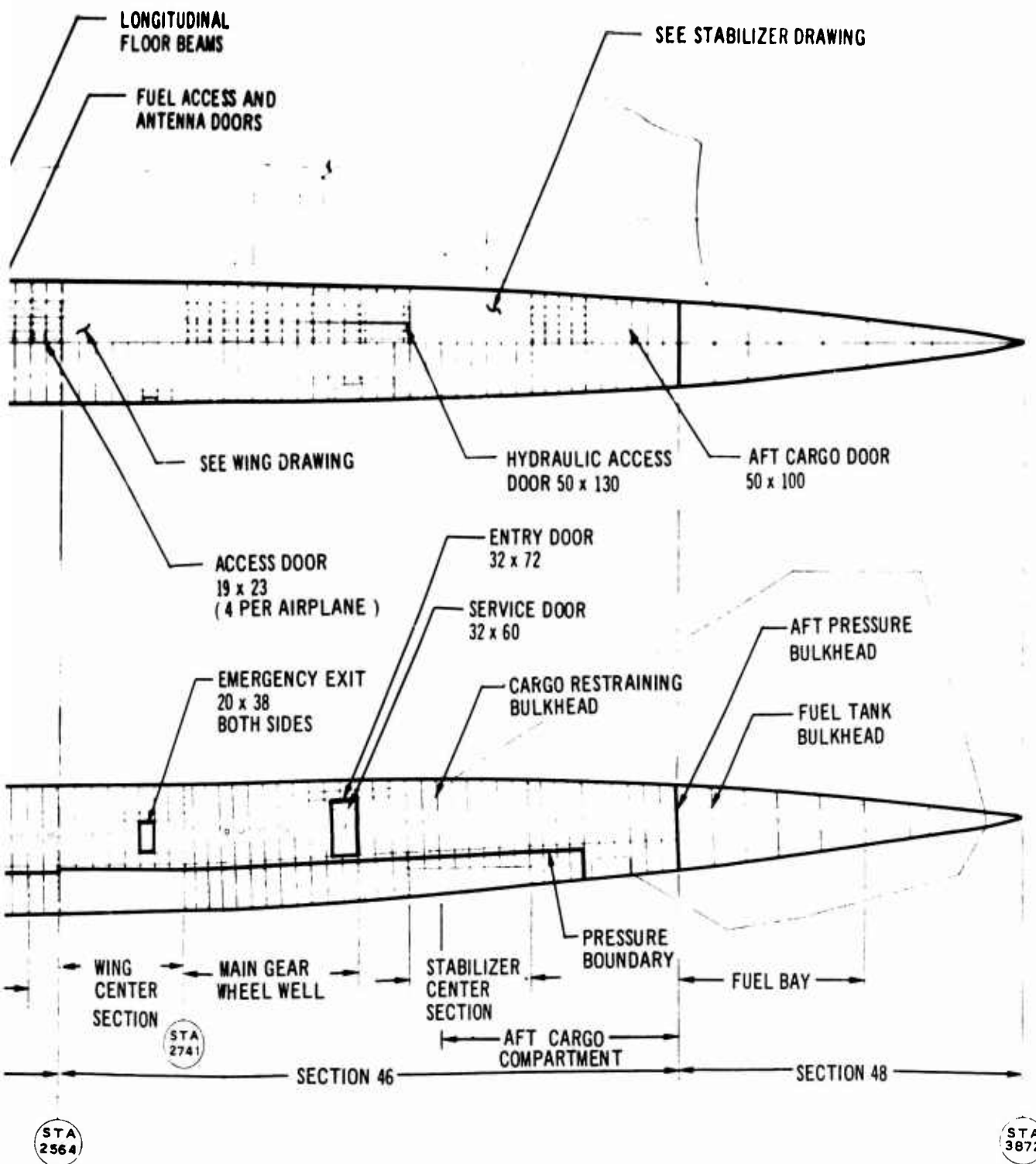
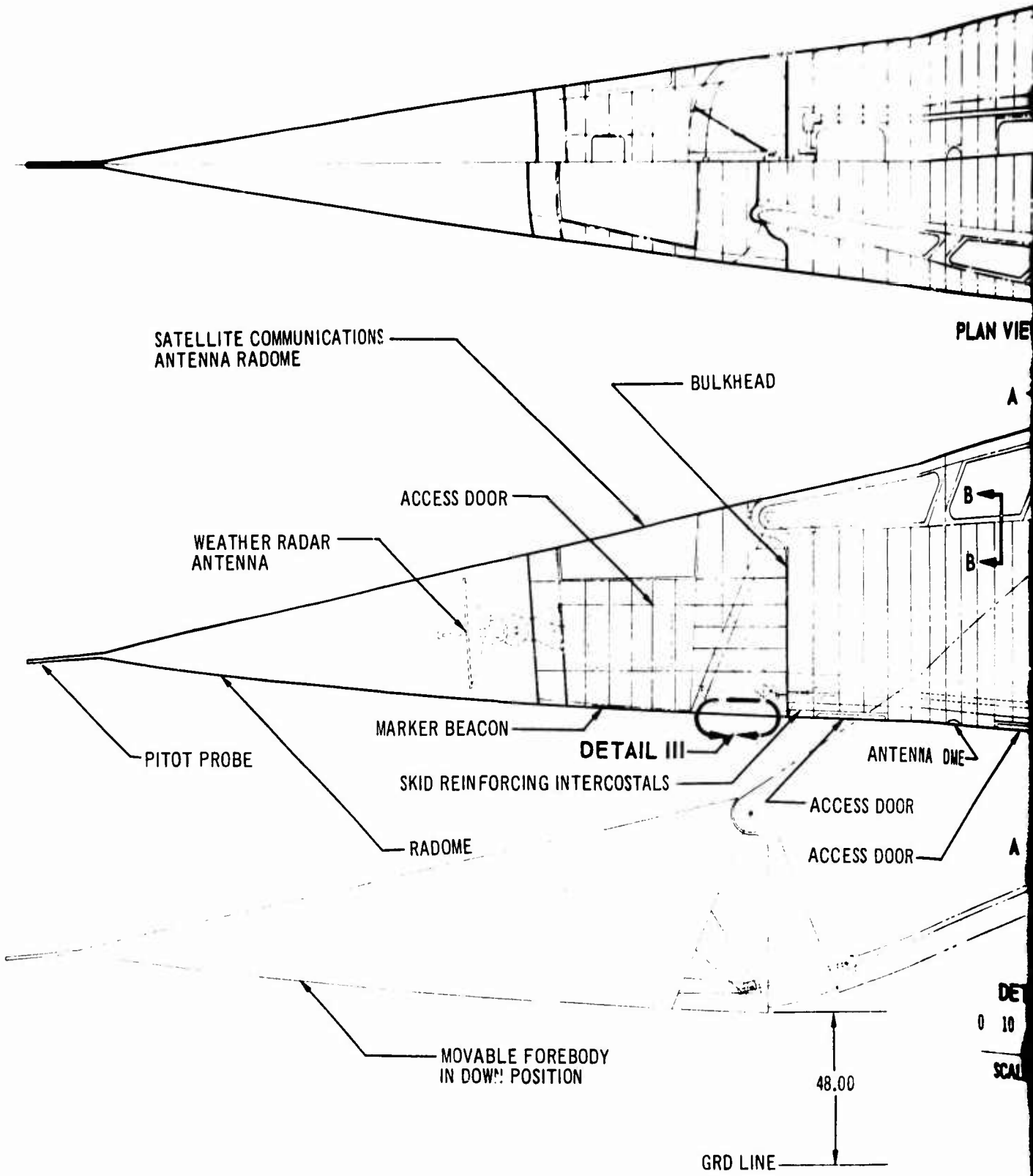


Figure 3-25. Fuselage Structure Diagram

C



PLAN VIEW

A

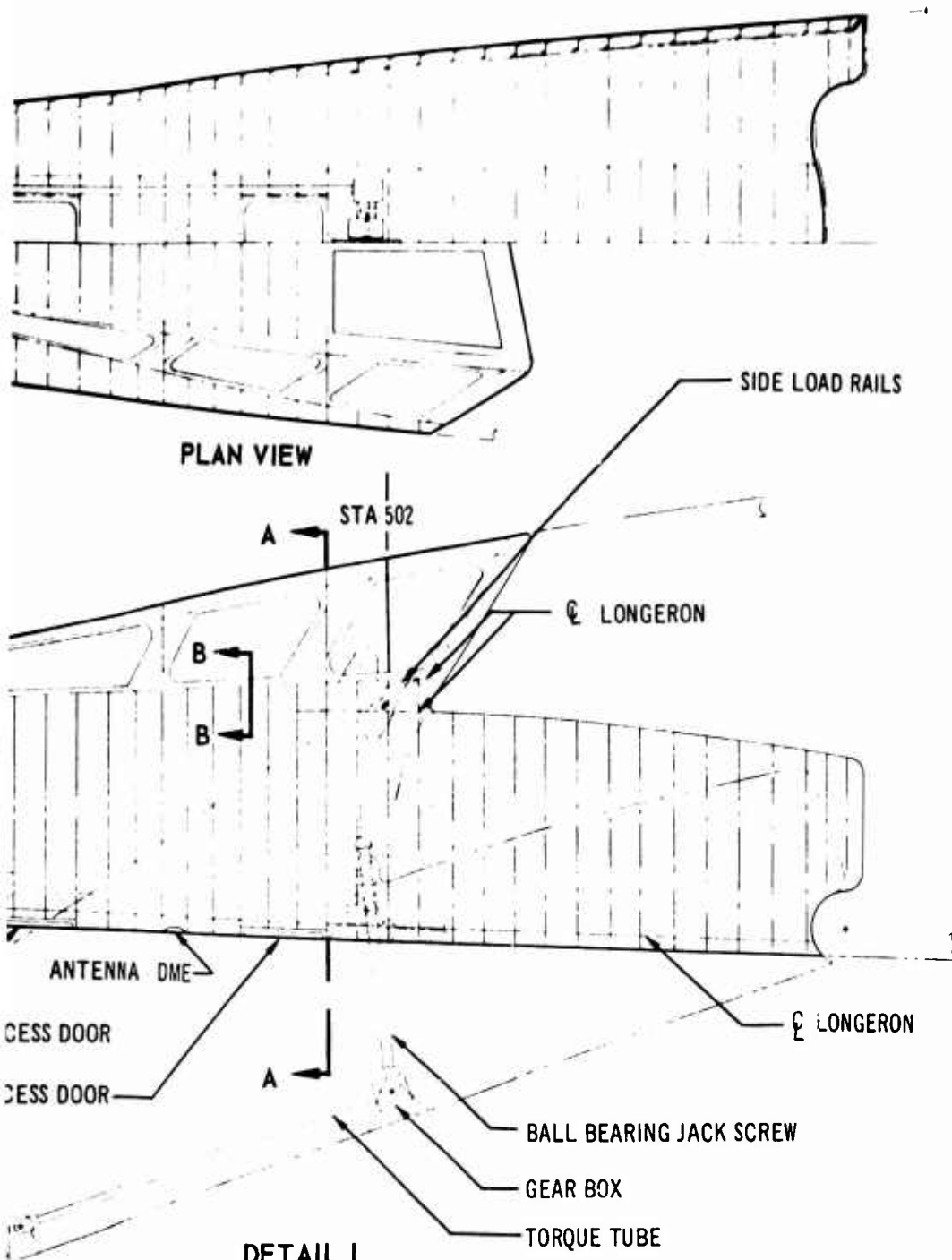
B

B

A

DE  
0 10  
SCALE

A

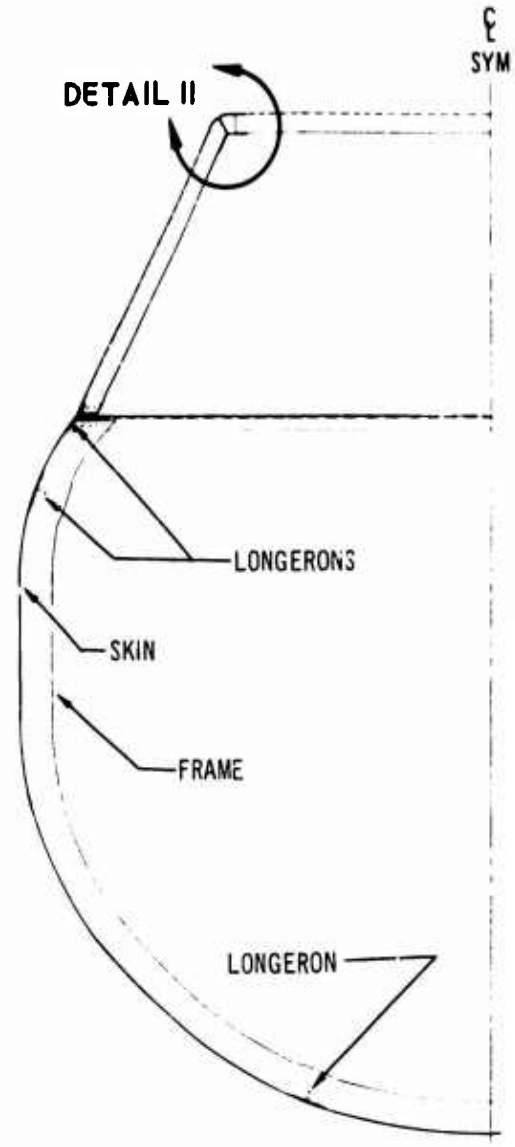


PLAN VIEW

DETAIL I

0 10 20 30 40

SCALE INCHES



DETAIL II

SECTION A - A

0 4 8 12 16

SCALE INCHES

B

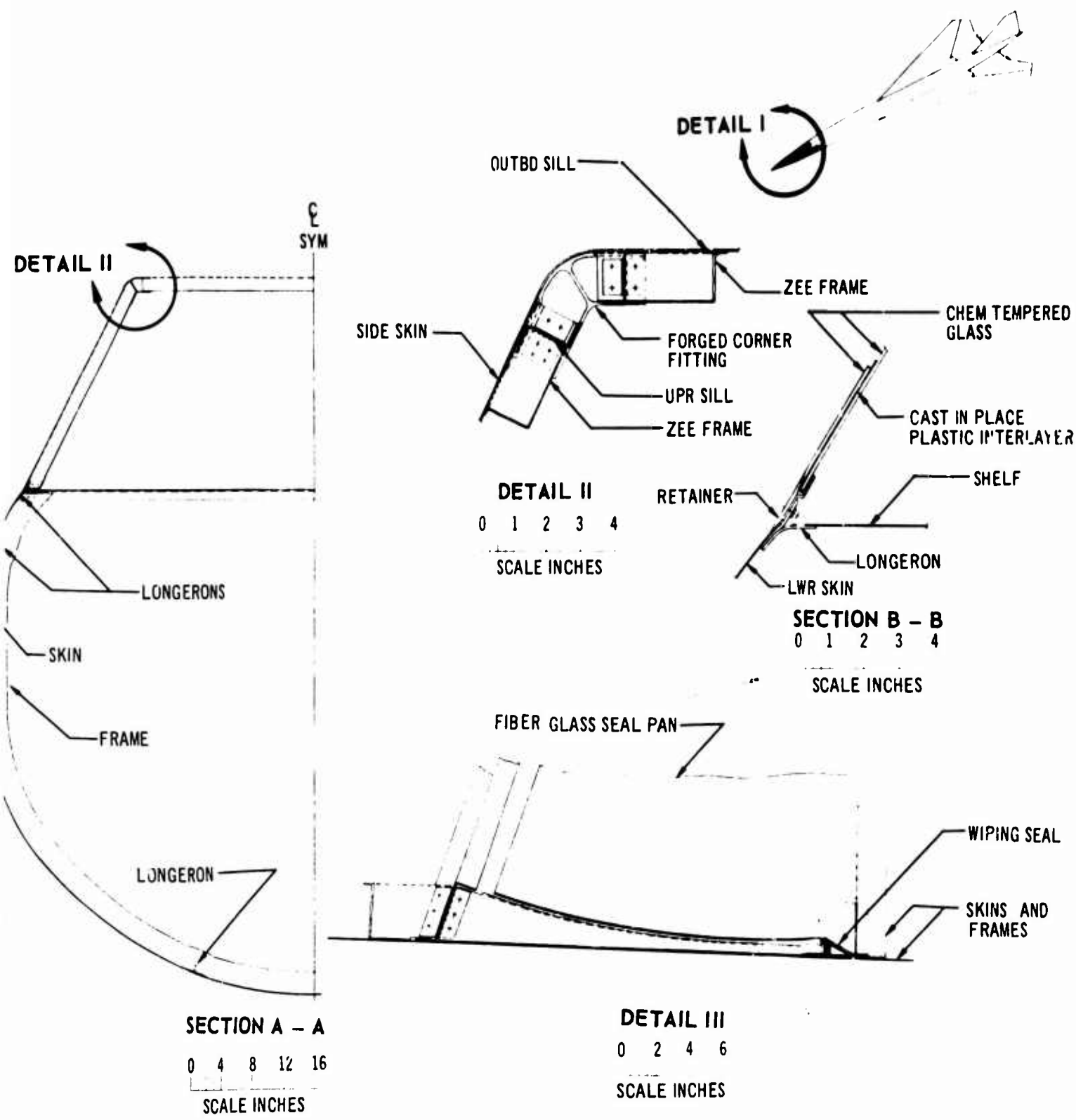


Figure 3-26. Forebody General Arrangement

A seal is maintained between the fuselage and the aft section of the forebody during the full range of travel to reduce aerodynamic drag and noise caused by air circulation. The forward section is also sealed with the aft section. The ability of the forebody to function under extreme operating environment will be verified by test (see Part B, Hydraulics, Landing Gear, Auxiliary Systems (V2-B2707-11), of the Systems Report). Nose radome information is contained in Part A, Environmental Control, Electric, Navigation and Communication (V2-B2707-10), of the System Report.

Windows in the forebody, as shown in Fig. 3-26, provide cruise vision as defined in the V2-B2707-11 document. Laminated assemblies of chemically tempered glass, similar to Corning Glass Co. 0315 high-strength, high-temperature material, are used. Stannous oxide coating is applied on the inner surface of the aft side window and aft portions of the upper windows to reduce infrared absorption during supersonic cruise. Materials such as Dow-Corning XR63449 interlayer are currently being evaluated for the interlayer portion of the laminated assemblies. Defogging of the side windows is accomplished by blowing air on the inner surface.

A nose-gear-up landing that will minimize danger to the flight crew and passengers can be accomplished by the B-2707 airplane. In the event of a nose-gear-up landing, initial contact will be on the main gear. The forebody in the extended position will contact the runway approximately 15 ft aft of the probe. A portion of the lower forebody will abrade and deform to absorb energy before contact of the reinforced structure as shown in Fig. 3-27. The reinforced structure consists of two longerons supported by a bulkhead and closely spaced vertical frames. The forebody screw actuator and support structure are designed to resist the ground load condition; therefore damage is confined to the forebody section. The fuel-containing areas are well clear of the runway and are approximately 130 ft aft of the nose contact point.

Trade studies supporting the forebody design and configuration can be found in Boeing Document D6A10187-1, SST Engineering Trade Studies Summary (Ref. 4).

### 3.2.2 Flight Deck Structure

The forward section of the pressurized fuselage is composed of the flight deck and electronics

compartment as shown in Fig. 3-28. Conventional skin, stringer, frame construction is used. Dual load-path, fail-safe construction of window posts is shown in Fig. 3-29. Each of the two tension members of the post is capable of sustaining one and one half times the operating load. Insulation material of polyimide-laminated fiber glass is used between each section of the side post to protect the critical interlayer materials used in the laminated windshields from high external temperatures. All titanium outer window retainers are lined with insulation material of polyimide-laminated fiber glass.

The structural arrangement of stringers, frames, and tear straps results in containment of skin cracks within the limits required to prevent fuselage depressurization. Below the crew compartment side windows, the structure consists of skin, closely spaced frames, the window sill, and the floor edge member. These closely spaced frames provide high tear resistance against crack growth induced by hoop tension stresses in the skin. Hoop stress in the 0.032 skin at 11.12-psi cabin pressure is 15,500 psi and fore and aft stress is 7,700 psi. Critical crack length for the hoop stress of 15,500 psi is 28 in., approximately four times the frame spacing. The critical crack length for the fore and aft stress of 7,700 psi is 112 in., approximately three times the distance between the window sill beam and the floor. Crack growth testing on similar panels has shown that the rate of crack growth at these stress levels is extremely low and any crack will be detected long before it becomes critical.

Aft of the side windows, the structure consists of frame and stringer supported monocoque, similar to that used throughout the fuselage. The fail-safe capability of the flight deck structure will be demonstrated by full-size testing during Phase III. Testing to date has shown that this type of system has high tear resistance and long service life. In addition, future testing of the Phase II-C crew compartment, now under construction, will verify the tear resistance of this specific design (see Part E, Structural Tests (V2-B2707-9), of the Airframe Design Report). In all other areas of the pressurized compartment, the stringer and frame spacing restricts the blow-out area to approximately 42 sq in.

Access to the area under the flight deck floor is provided by removable panels. Crew escape hatches are provided on the airplane top center-

line and aft of the windows on the left-hand side (see Fig. 3-28). The side hatch is hinged on the aft side to provide ventilation or the ground and oral communication for the crew.

### 3.2.3 Flight Deck Windshields

Vision from the crew compartment with the forebody extended is superior to that provided by any current commercial subsonic jet transport. Vision, as affected by light transmission and reflections, was established as satisfactory by extensive windshield testing and by numerous flights performed by pilots in the B-2707 simulator at the Boeing Kent facility (see Part B, Hydraulics, Landing Gear, Auxiliary Systems (V2-B2707-11) of the Systems Report).

The windshield construction is shown in Fig. 3-29. The windshields are plug type designed to withstand three factors of pressure on the primary laminated windshield. The three glass panes provide three separate fail-safe paths capable of 1.5 factors pressure each. High-strength, chemically tempered glass similar to Corning Glass Co. 0315 is used. Testing to demonstrate that thermal-shock margins are adequate is included in the window procurement specification. The laminated windows are designed to utilize the best possible interlayer material for each application. This interlayer material provides the best shock attenuation required for bird-proofing the windshields. The polyvinyl butyraldehyde (P. V. B.) material requires temperature control to maintain bird-proofing capability. An interlayer material, Dow Corning XR63449, being evaluated for the side windows is a cast-in-place type for high-temperature application. The interlayer for the forward windshield is P. V. B. as used in subsonic aircraft.

To maintain temperature control for the P. V. B. and reduced temperature for the crew compartment environment, a passive system of coatings, insulation, and air gaps is used. This system was evaluated by a thermal test during Phase II-C. The coatings are low infrared-emittance, vacuum-deposited gold film. The air gap between the outer pane and the laminated assembly is vented by a closed system to ambient pressure. The low-pressure air reduces convected heat transmission to the inner laminated assembly. Insulation of the windshield laminated assembly from the support structure is provided by polyimide-laminated fiber glass, which is used for windshield retaining and as the interlayer insert.

This material will allow full torquing of retaining fasteners without cold flow and resulting bolt loosening.

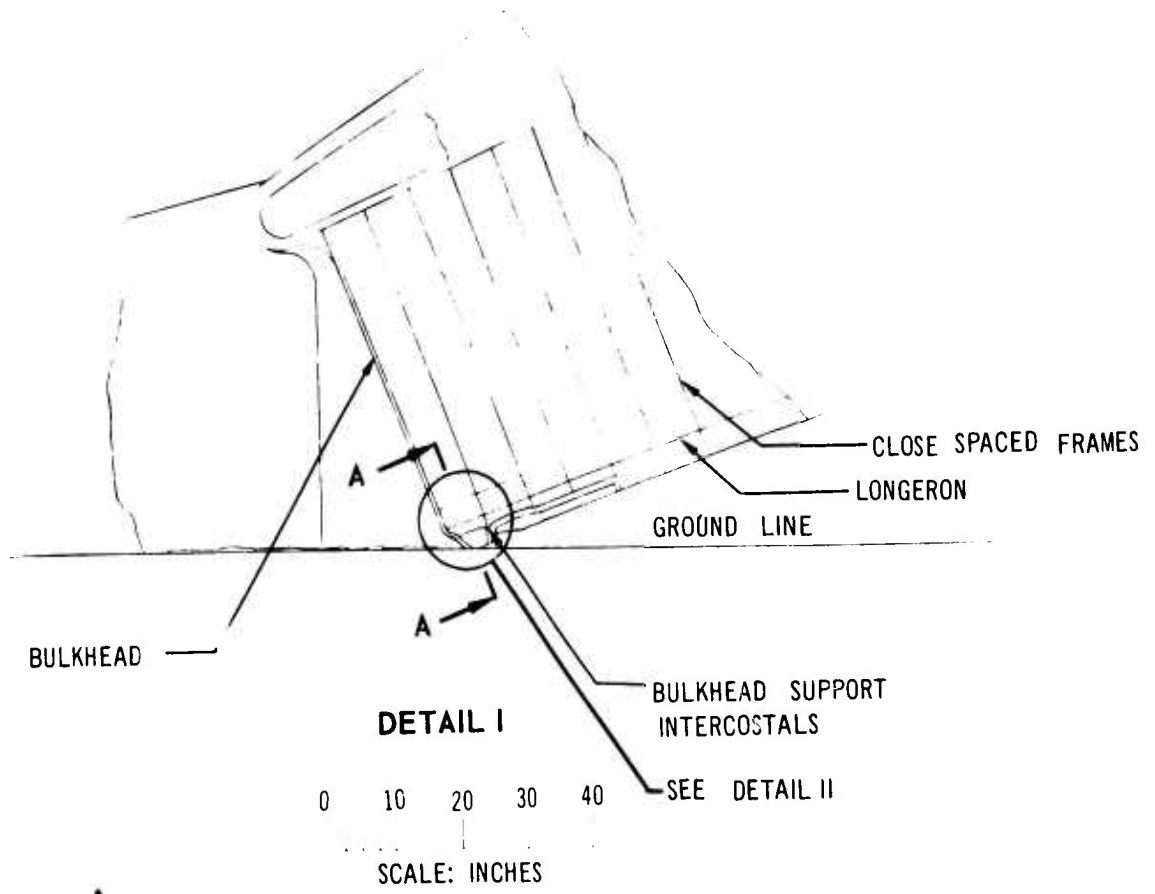
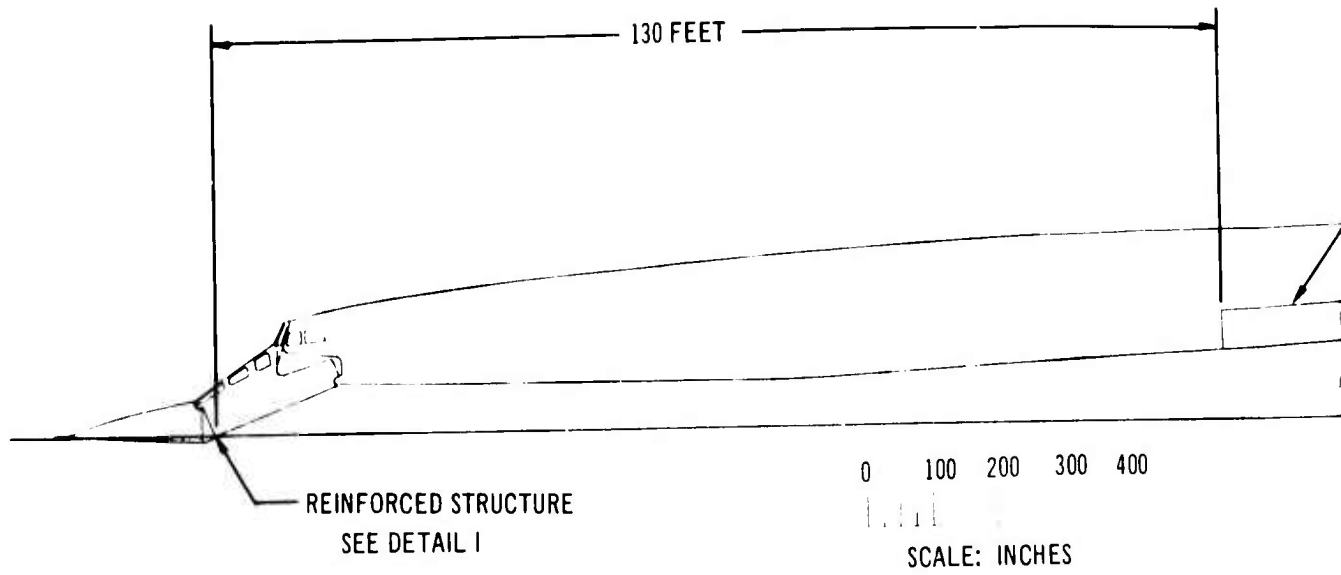
The coatings are used principally to reduce heat transmission, except for the forward windshield where the forward coating is also used for de-icing. The electrical power required for de-icing is applied to a monolithic pane rather than to a laminated assembly, eliminating delamination and chipping problems often associated with windshield design. Two power connections to each bus bar improve service life of the windshields. Coating of the laminated assembly provides temperatures consistent with interlayer bird proofing requirements for subsonic cold-environment operation and for defogging. The low power required for defogging minimizes differential thermal-expansion problems.

The windshield installation utilizes dry seals throughout. The temperature sensors are separately installed, allowing replacement without replacing windshields. The laminated assembly is plug type for increased safety and is installed inside the flight deck. Windshield maintenance is a prime consideration in this design, and a time study indicates a maximum of three hours required for replacement of the windshield laminated assembly.

### 3.2.4 Fuselage Shell

The fuselage shell is of conventional semi-monocoque skin-stringer construction stabilized by ring frames. A fuselage cross section at a typical frame is shown in Fig. 3-30. The structural arrangement is similar to the 707 and 727 and provides improved fail-safe construction, as well as ease of fabrication, inspection, and repair. The structure also gives high-strength efficiency for basic panel loading. Main frames and bulkheads are provided at points of load concentration. Close stringer spacing provides the required aerodynamic smoothness under normal flight loads and temperatures.

All skin splices are flush butt type. Tension fatigue-critical skin splices shown in Fig. 3-31 utilize flush-head rivets installed with an improved fatigue-resistant rivet installation technique (see Part D, Materials and Processes (V2-B2707-8), of the Airframe Design Report). Where fatigue requirements dictate reduced stresses, skin pad-up will be accomplished by chem-milling. Completion of the development



71



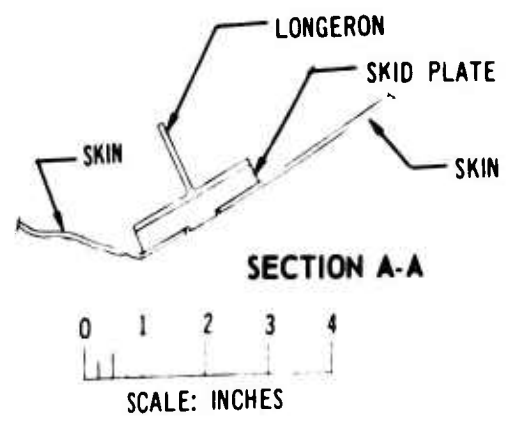
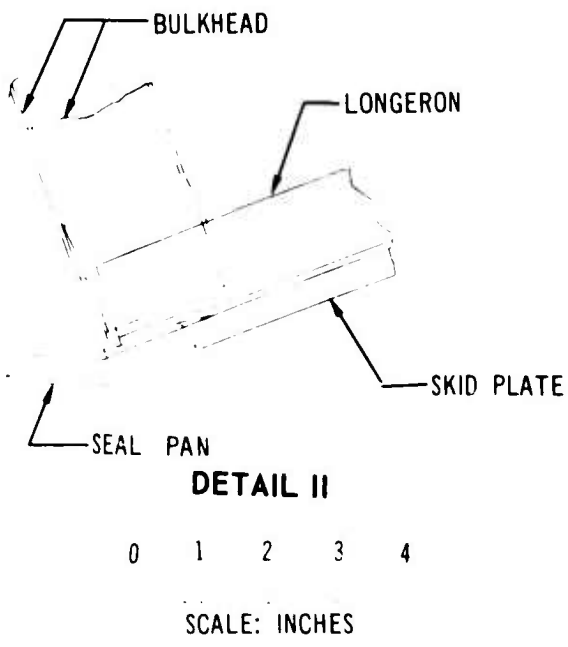
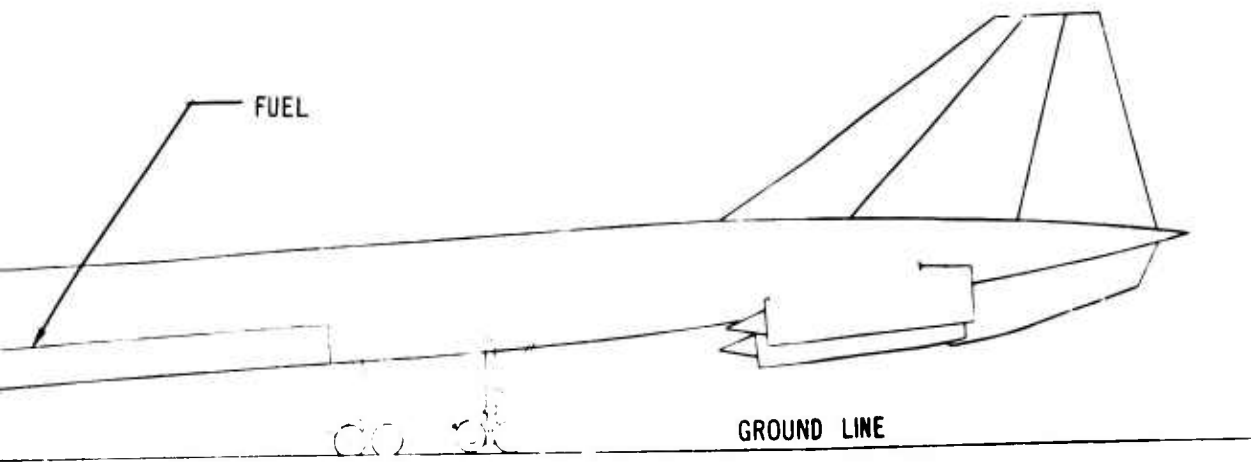
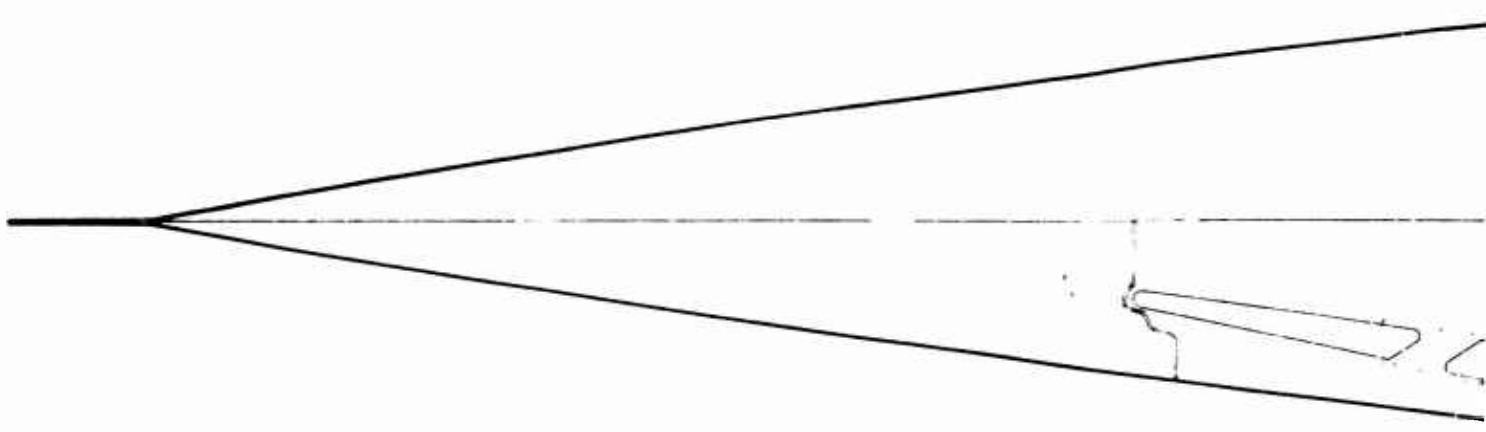


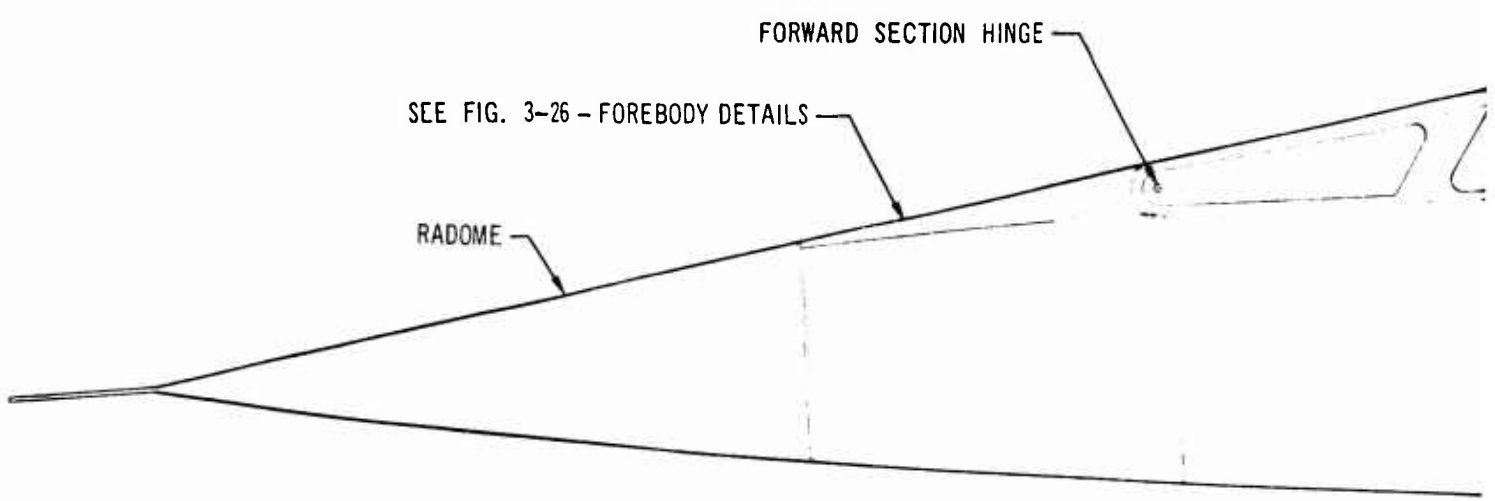
Figure 3-27. Nose Wheels-Up Landing



FOREBODY W

PLAN VII

FLIGHT DECK W



SEE FIG. 3-26 - FOREBODY DETAILS

FORWARD SECTION HINGE

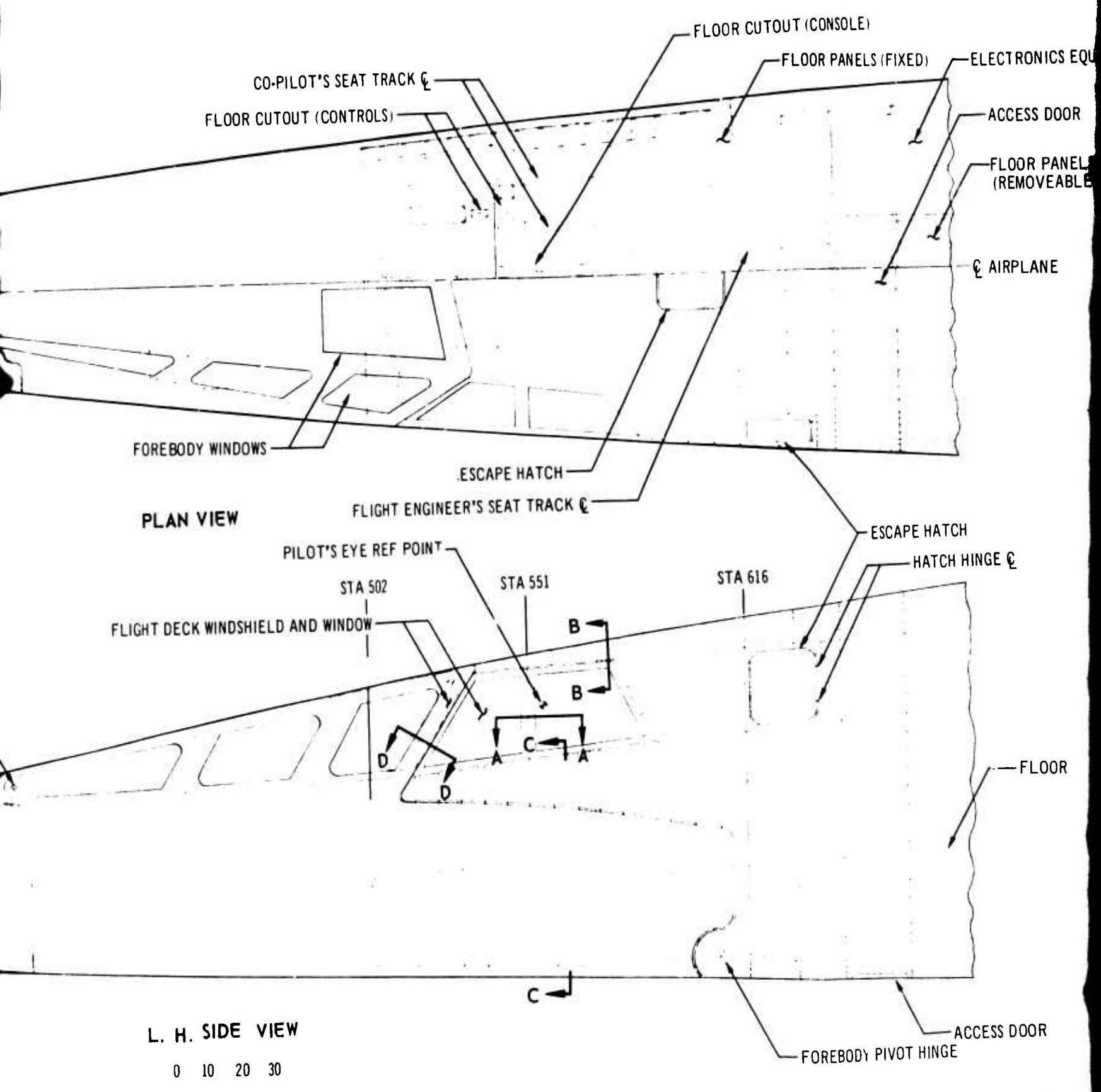
RADOME

L. H. SIC

0 10

SCALE

A



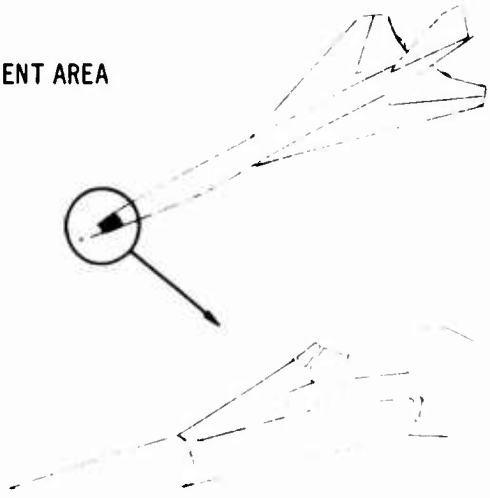
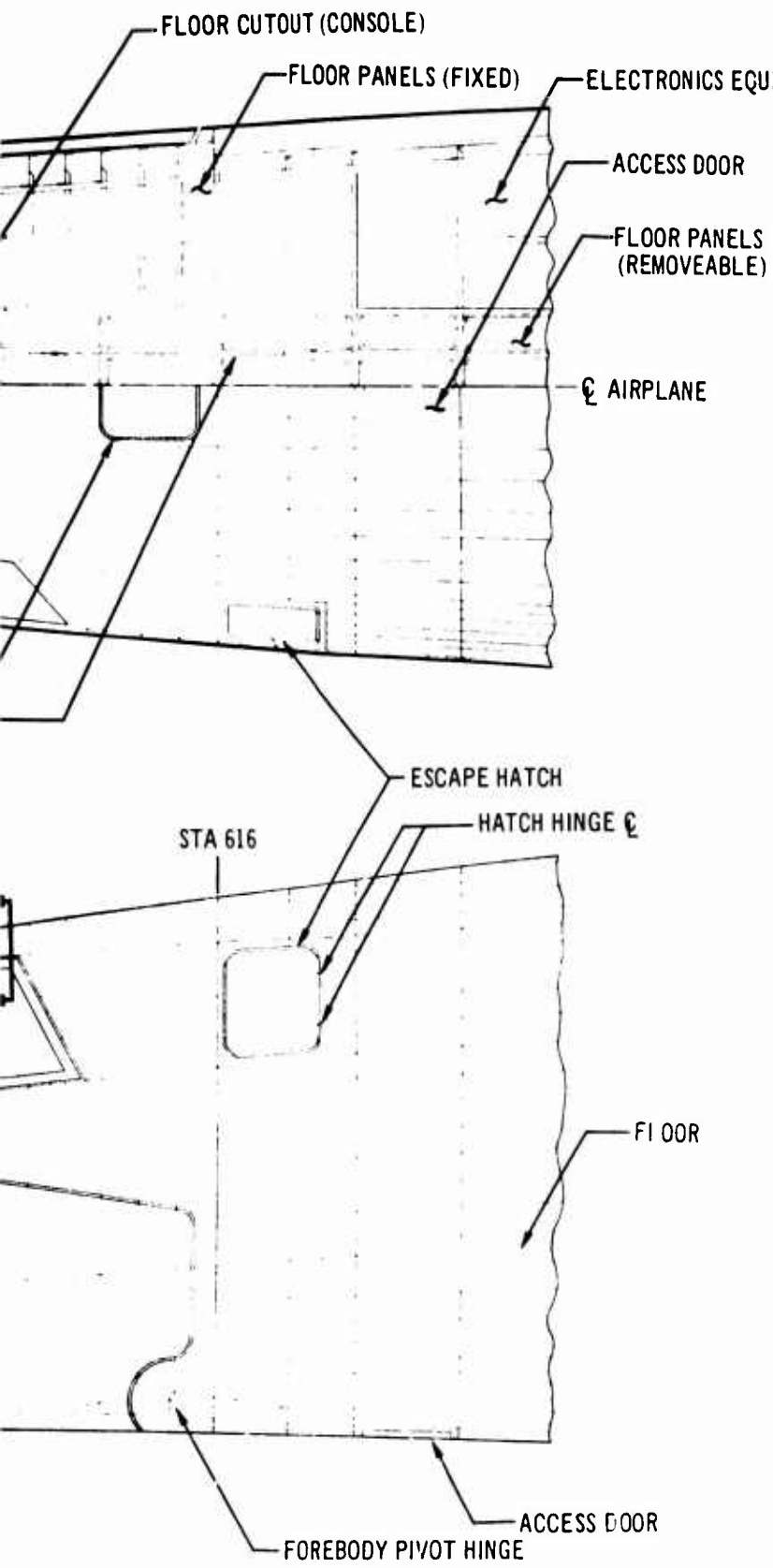
L. H. SIDE VIEW

0 10 20 30

SCALE-INCHES

3

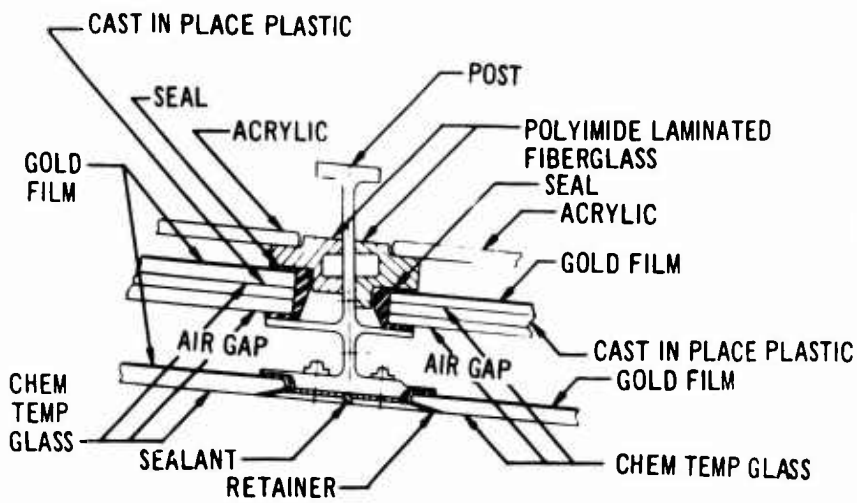
Figure 3-28



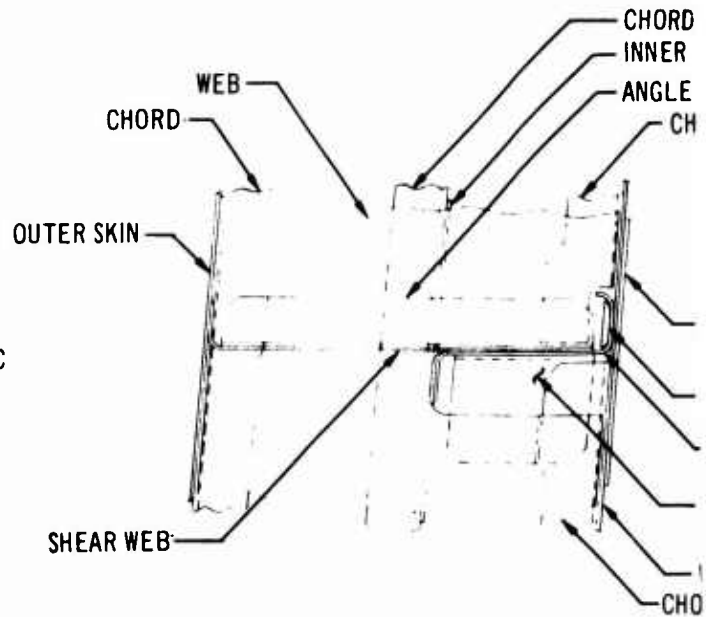
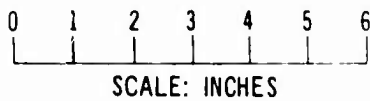
FOR SECTIONS SEE FIG. 3-29

C

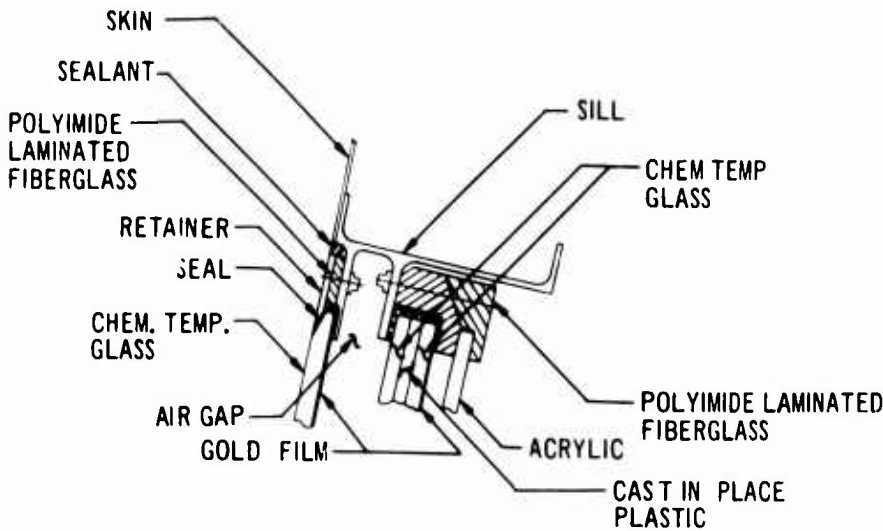
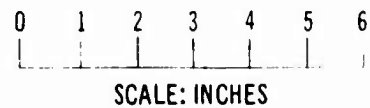
Figure 3-28. Flight Deck Structural Arrangement



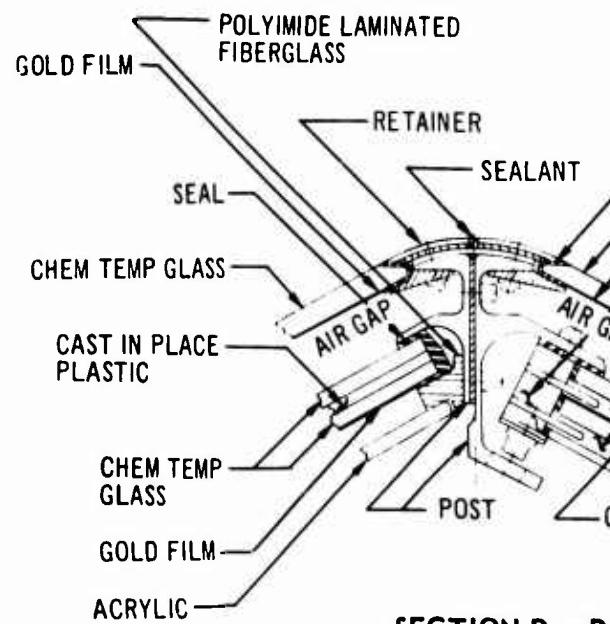
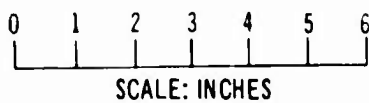
SECTION A - A



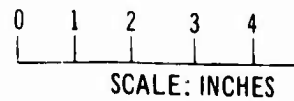
SECTION F - F



SECTION B - B



SECTION D - D



*A*

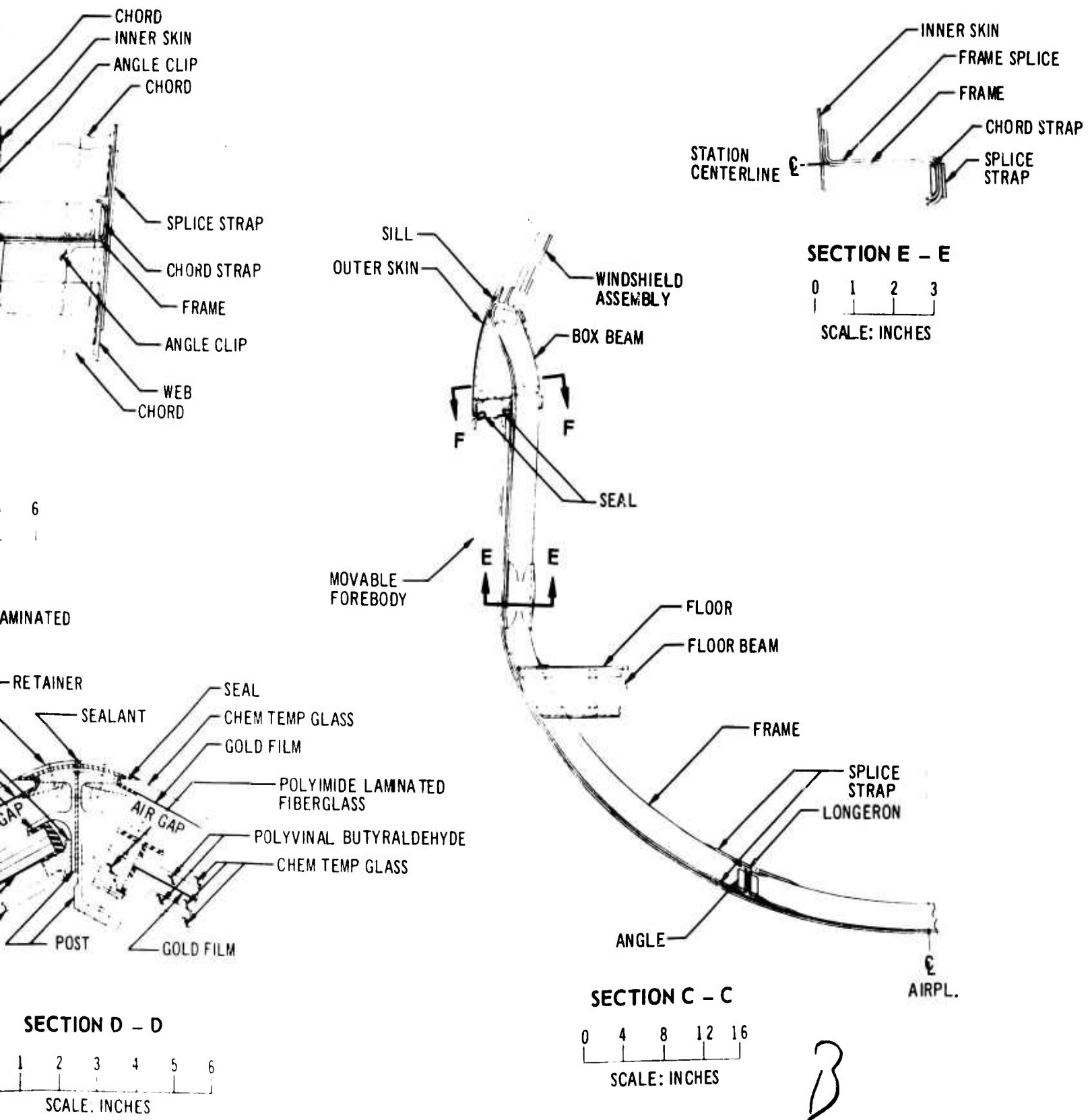


Figure 3-29. Flight Deck Structural Details

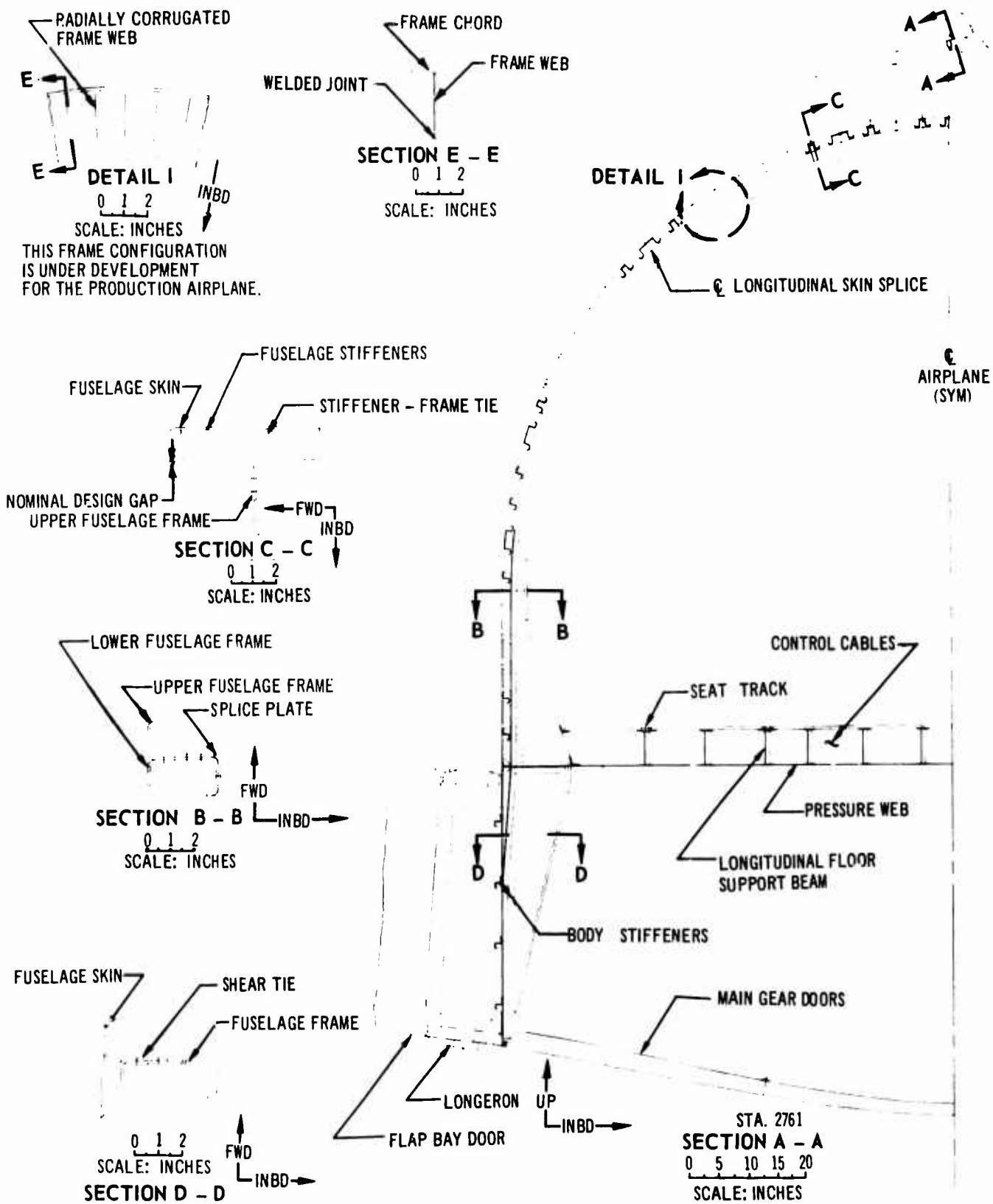


Figure 3-30. Wheel-Well Fuselage Frame

V2-B2707-6-2

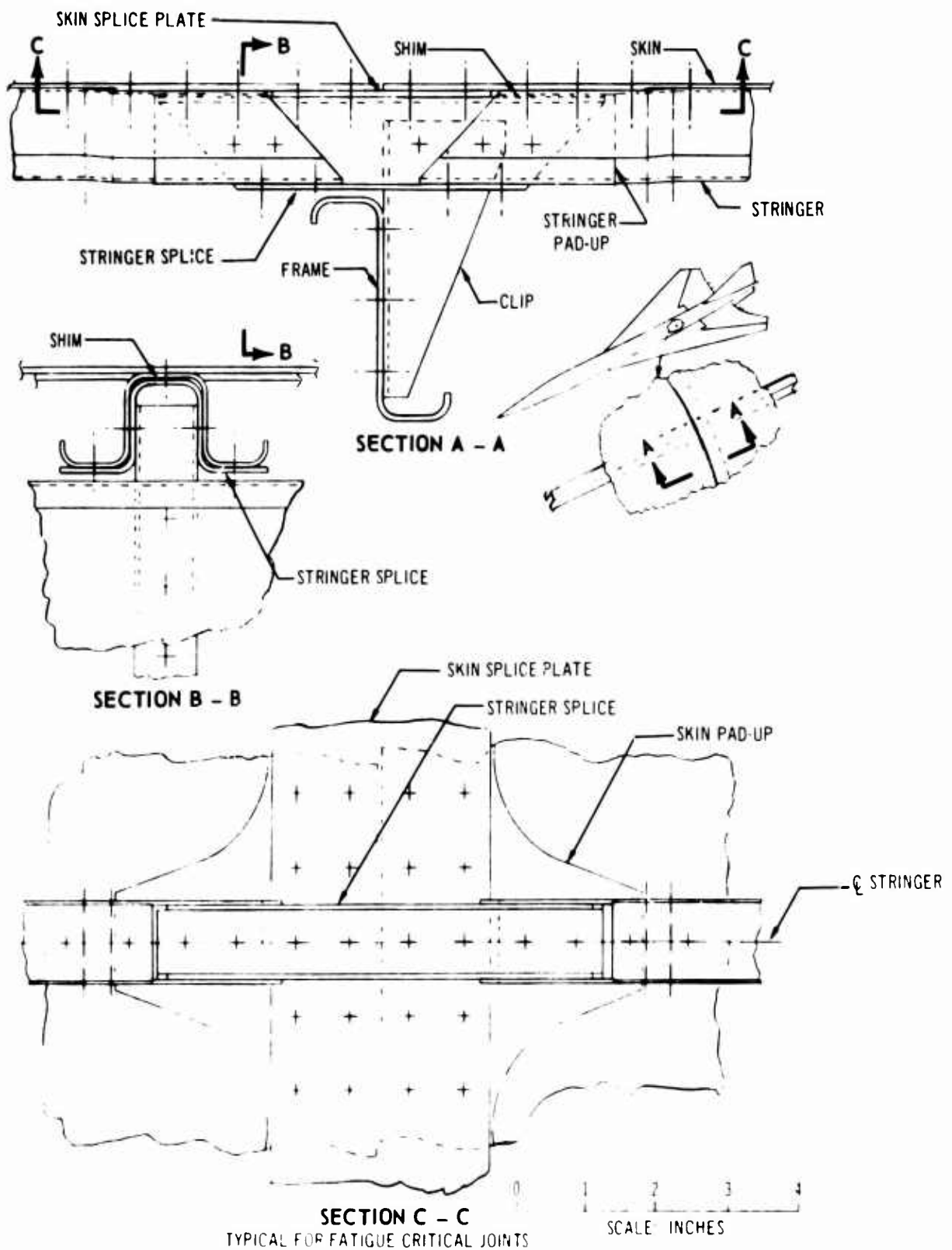


Figure 3-31. Skin Stringer Splice

V2-B2707-6-2



of high-temperature adhesive bonding will provide an alternative method of skin pad-up. Tear-stopper straps are riveted. Their locations are determined by the relationship of skin thickness, fuselage radius, and skin heat-treat condition. Most skins are tapered in thickness to save weight. Skins are reinforced around cutouts and edges by sculpturing and bonded doublers.

Stringers are formed hat or Z-sections tapered in thickness for weight optimization. Z-sections are used on the lower and side panels; hat sections are used in the top of the fuselage. Skin and stringer splices at tension fatigue-critical areas are padded-up by sculpturing or by a bonded reinforcement as shown in Fig. 3-31 and are joined with rivets using the improved fatigue-resistant rivet installation technique.

Fuselage frames are spaced at 21-in. intervals through the fuselage. The upper frame segment is a formed sheet metal Z-section that stabilizes the skin panels. The remaining part of the frame is built-up sheet metal construction required for support of the passenger cabin floor and lower-lobe cargo or fuel. The frame splice joining the upper and lower frame segments is shown in Fig. 3-30. A nominal design gap between the frame and stringers is used to achieve external smoothness. The stringer-to-frame attachment is shown in Fig. 3-30.

An improved upper-frame configuration is under development for weight optimization. The frame segment is a welded I-beam assembly. The frame chords are sheet metal strips welded to a thin-gage corrugated web.

### 3.2.5 Aft-Main-Landing Gear Wheel Well

The aft-main-landing-gear wheel well is behind the wing rear spar. It is enclosed by the pressure deck at the top, fuselage beam at the sides, and wheel well doors at the bottom (see Fig. 3-30).

The full-depth beam at the sides of the wheel well forms the fuselage shell. This beam provides uninterrupted structure for shear and bending fuselage loads. The bottom of the beam is a longeron consisting of a series of longitudinal chords. Segmentation of the chords eliminates the stress concentrations in the wing skin and chords that would occur because of spanwise load pickup. The chords also provide a fail-safe design for body bending.

Between the wing rear spar and the stabilizer front spar, the keel member is built into a torque box that supports the inboard flap and the landing-gear drag strut. This wheel-well beam is stabilized by five bulkheads and intermediate frames. Bulkheads are of conventional built-up construction as shown in Fig. 3-32. Loads are carried by a shear web beam that is contoured to provide clearance for the landing gear. The bulkheads have been designed with multiple load paths to achieve fail-safe design. Structure to support the landing-gear door-center closure member is provided at the centerline of the airplane.

### 3.2.6 Fuel Compartment Lower Lobe

The arrangement of the lower lobe is established by the transition from the beam at the side of the fuselage to the basic fuselage contour as shown in Figs. 3-33, 3-34, and 3-35.

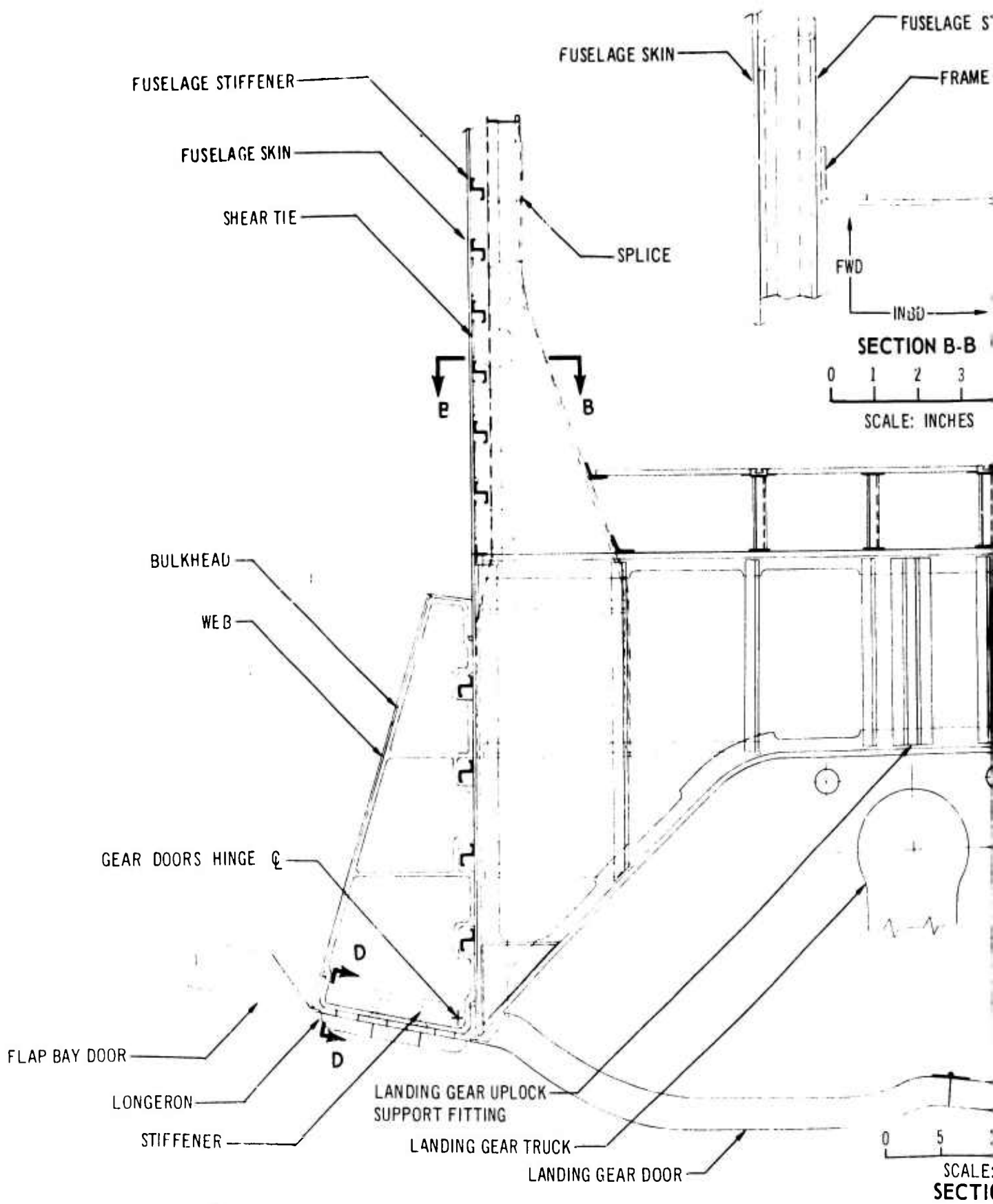
This transition provides greater fuel volume than a circular lower-lobe section. It also provides longitudinal structural continuity. The compartment is divided into nine bladder fuel cells. Positive assurance that the fuel will not enter the passenger compartment is provided by three barriers: fuel cells, the titanium pressure web, and the sealed titanium floor panels.

The design provides for access doors and antennas on the bottom centerline of the airplane. The arrangement consists of two longitudinal beams to carry fuselage bending loads as shown in Figs. 3-33, 3-34, and 3-35. These longitudinal beams also serve as fuel tank supports. The fuel support floor consists of titanium honeycomb panels and has sealed internal access doors as shown in Fig. 3-35.

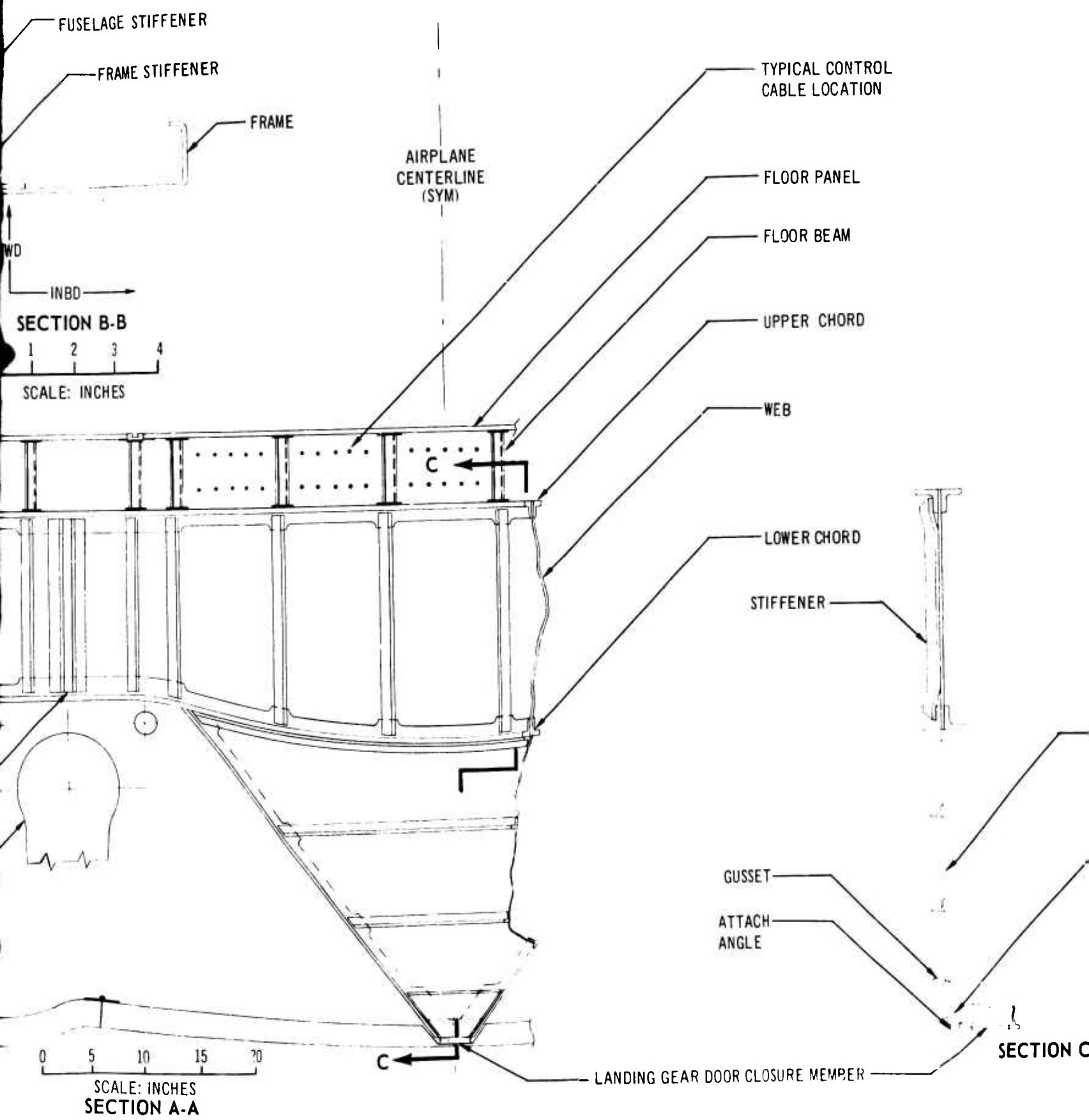
### 3.2.7 Fuel Compartment Bulkheads

The fuselage fuel compartment is divided by ten bulkheads into 63-in.-long bays containing separate but interconnected bladder-type fuel cells.

Figure 3-36 depicts a typical intermediate fuel bulkhead. The bulkhead consists of a sculptured web stiffened with formed Z-sections and framed with a channel around the periphery. These stiffeners support the floor beams. Reinforced cutouts are provided in the bulkhead webs for fuel lines. Individual shear ties connect each of the lower stiffeners and a short section of the lower skin to the frame channel of the bulkhead. The



*A*



B

TYPICAL CONTROL  
CABLE LOCATION

FLOOR PANEL

FLOOR BEAM

UPPER CHORD

WEB

LOWER CHORD

STIFFENER



BUSSET

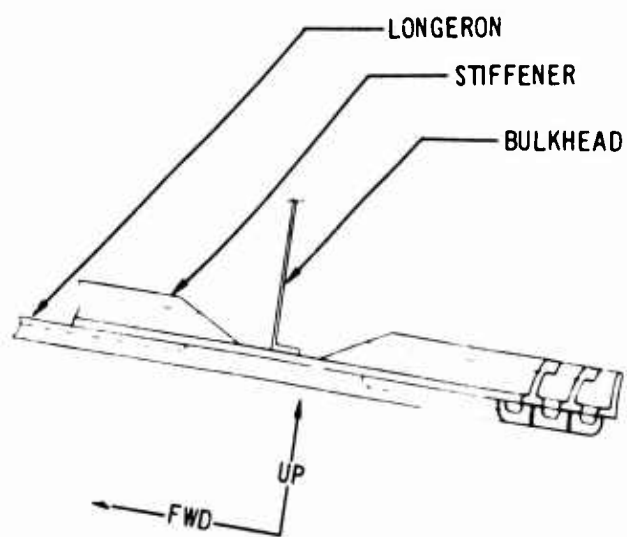
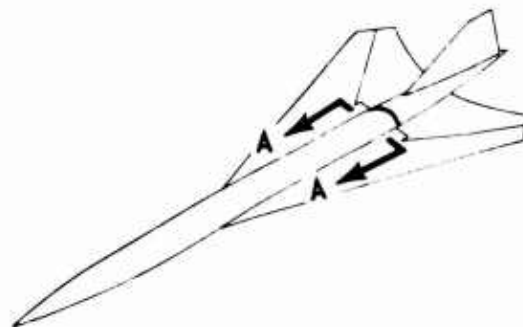
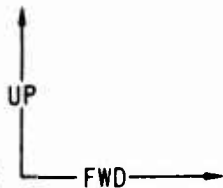
ATTACH  
ANGLE

R CLOSURE MEMBER

LANDING GEAR DOOR  
CLOSURE MEMBER SUPPORT

SUPPORT SIDE ANGLE

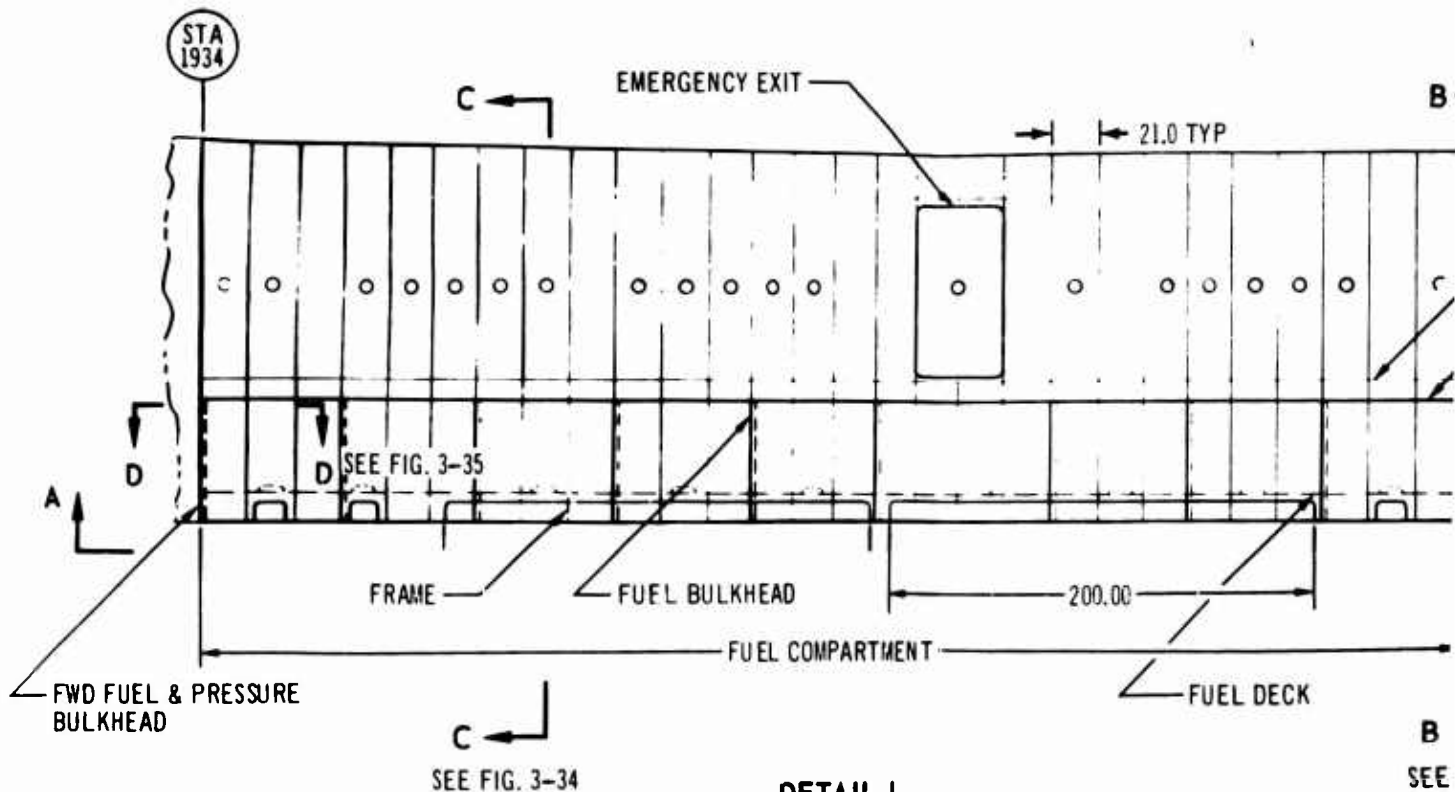
SECTION C-C



SECTION D - D

C

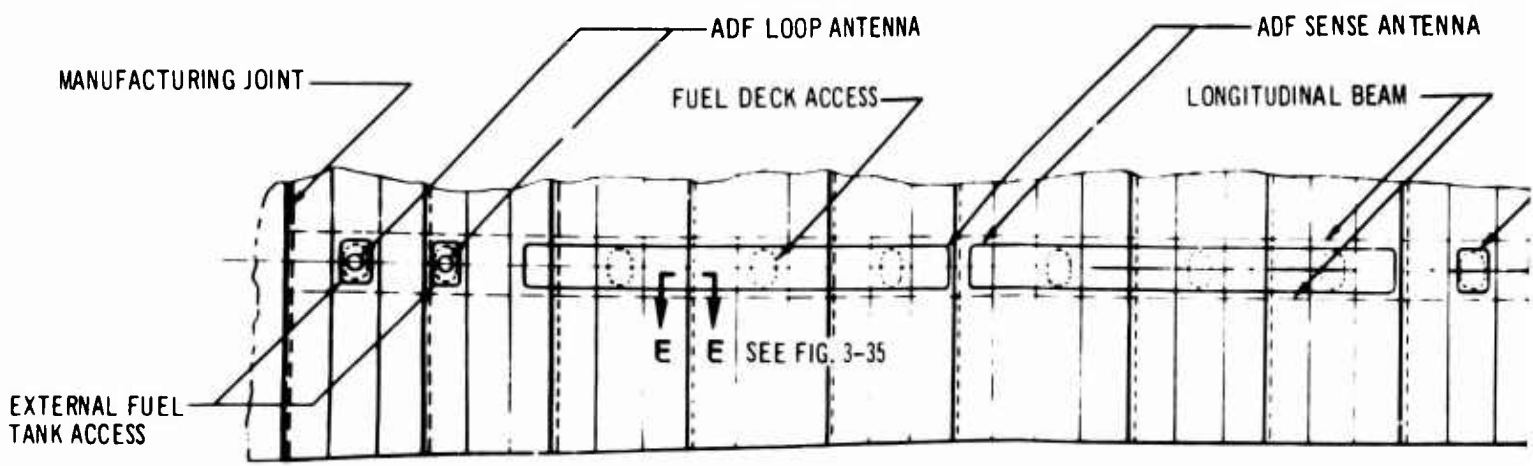
Figure 3-32. Aft-Main-Gear Wheel Well Bulkhead



SEE FIG. 3-34

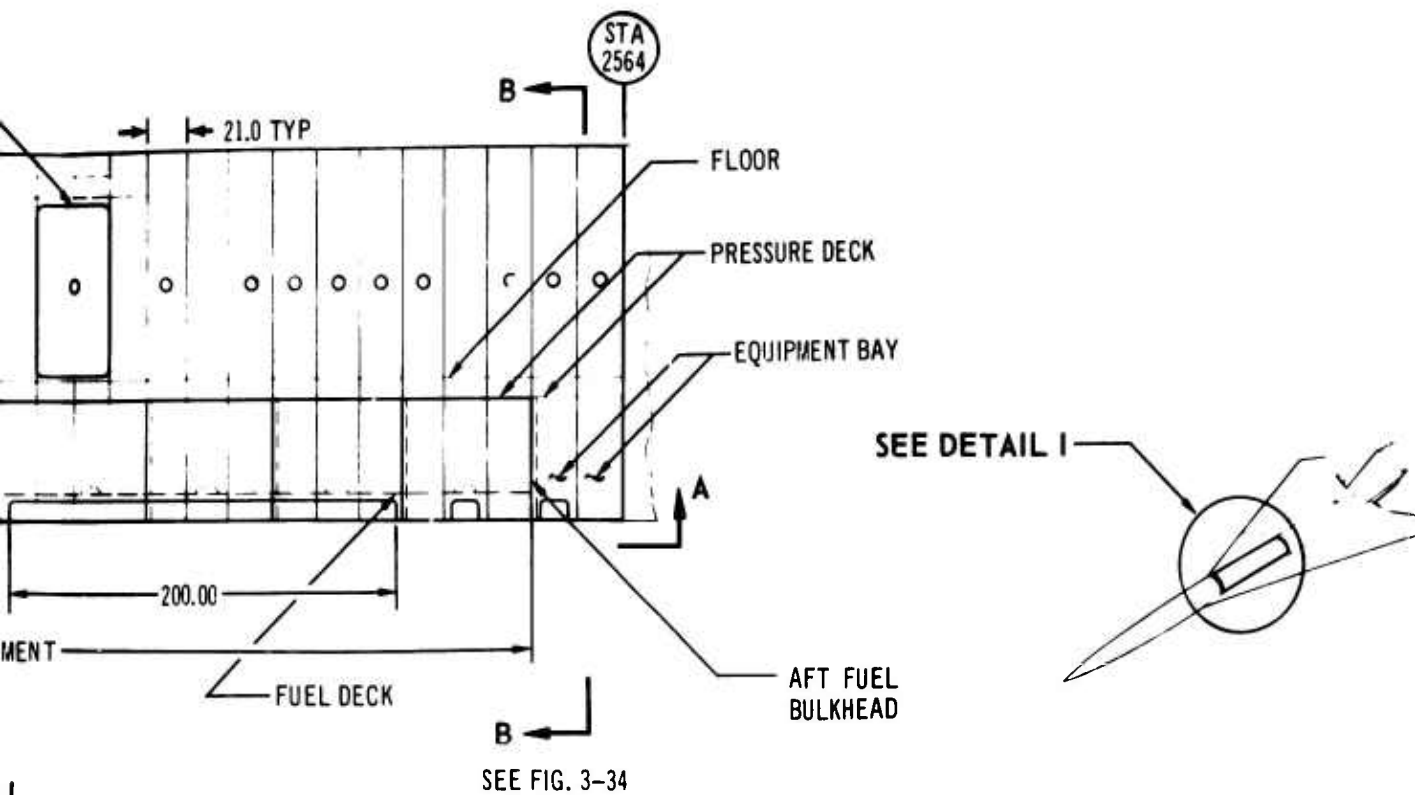
**DETAIL I**

SCALE: NONE

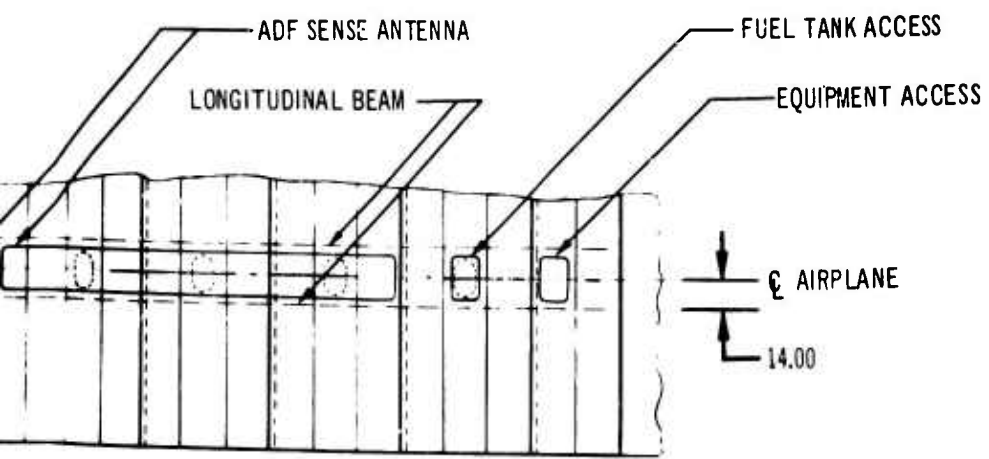


V. 'A - A

*A*



I  
NE

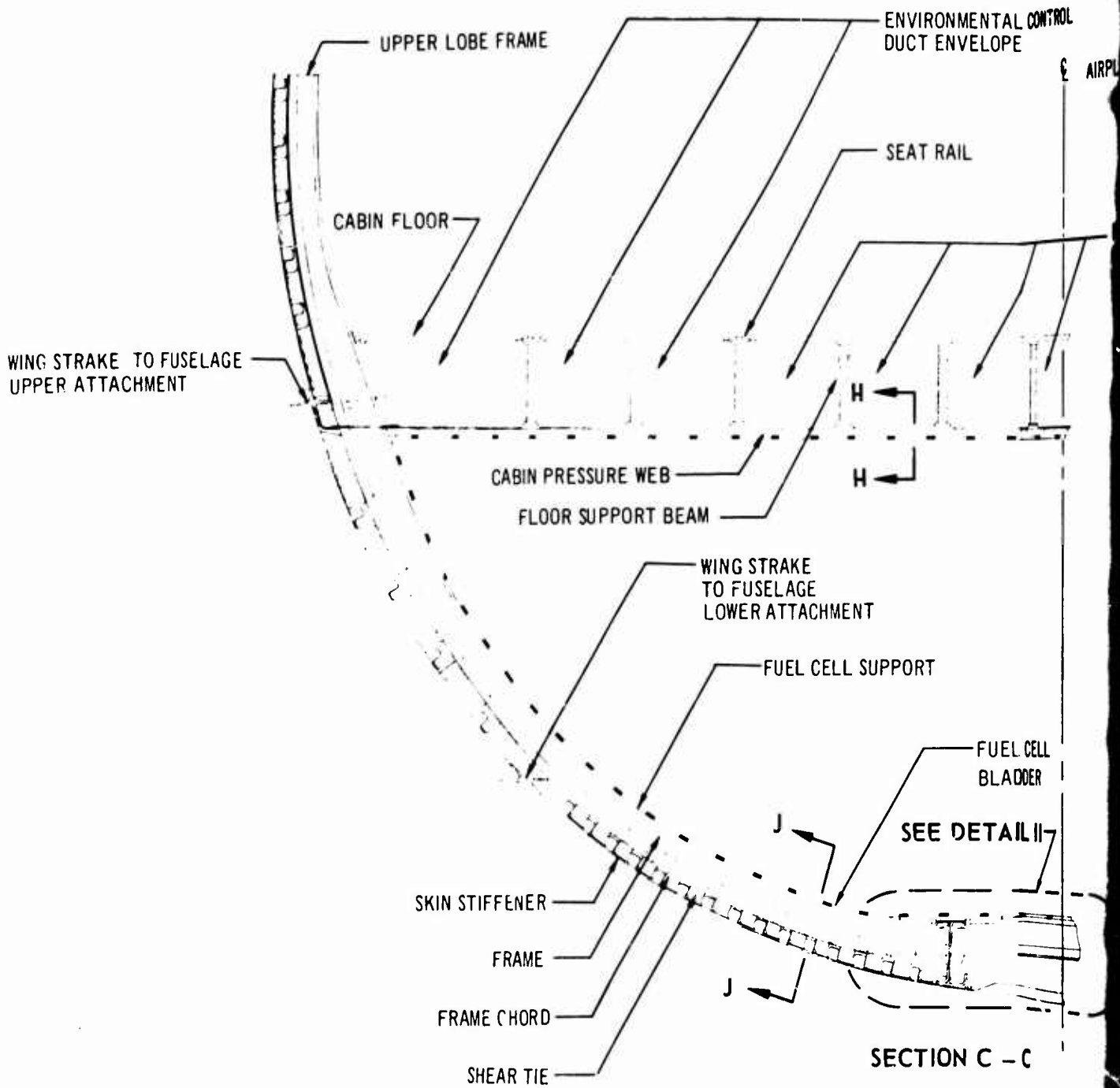


- A

B

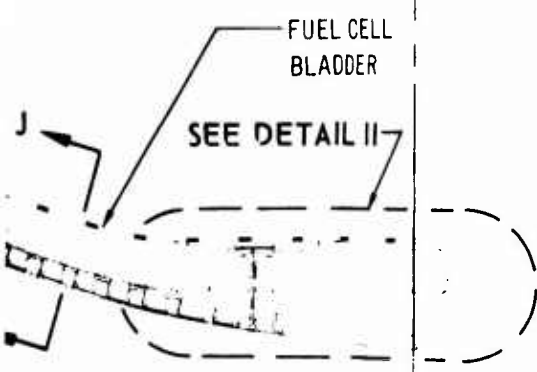
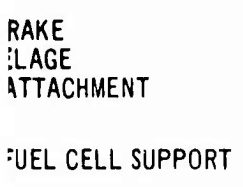
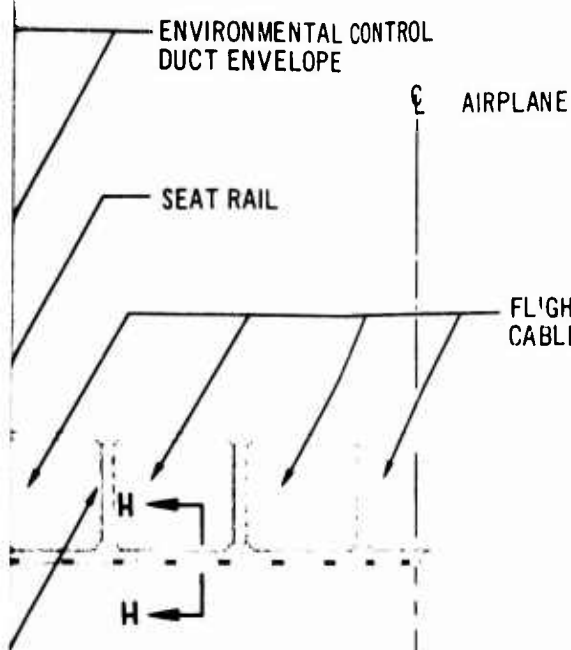
Figure 3-33. Fuel Compartment Lower Lobe

V2-B2707-6-2



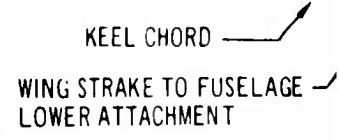
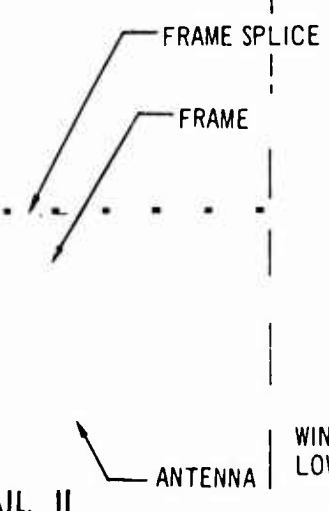
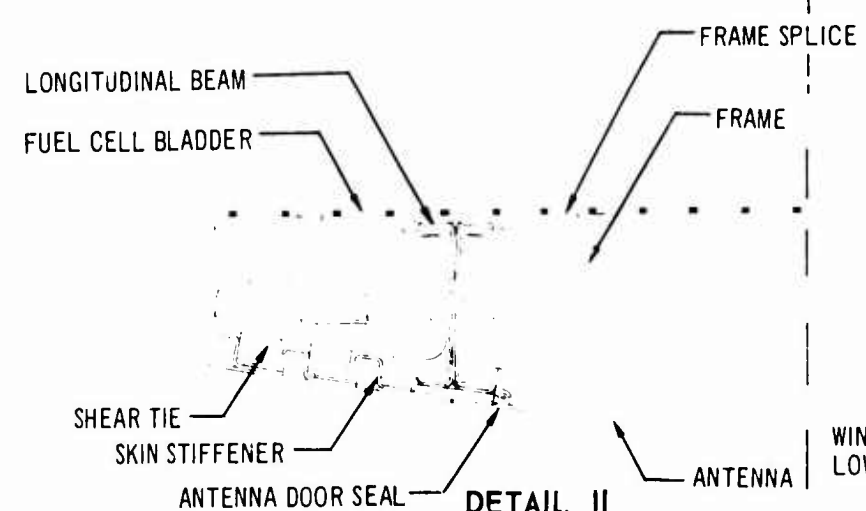
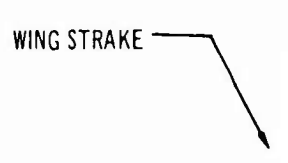
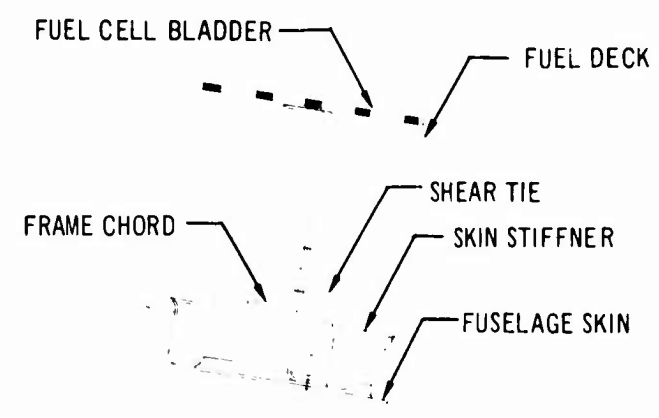
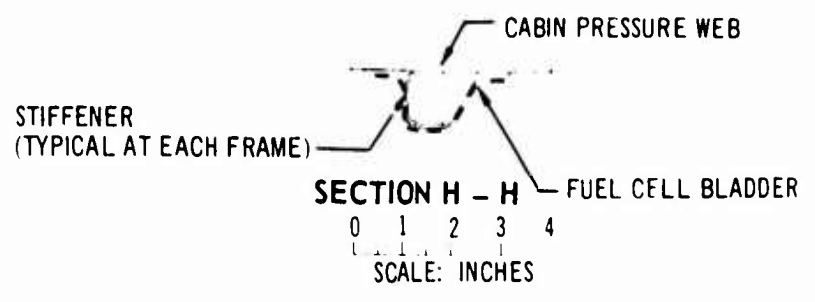
0 4 8 12 16  
SCALE: INCHES

A



SECTION C - C

0 4 8 12 16  
SCALE: INCHES



3



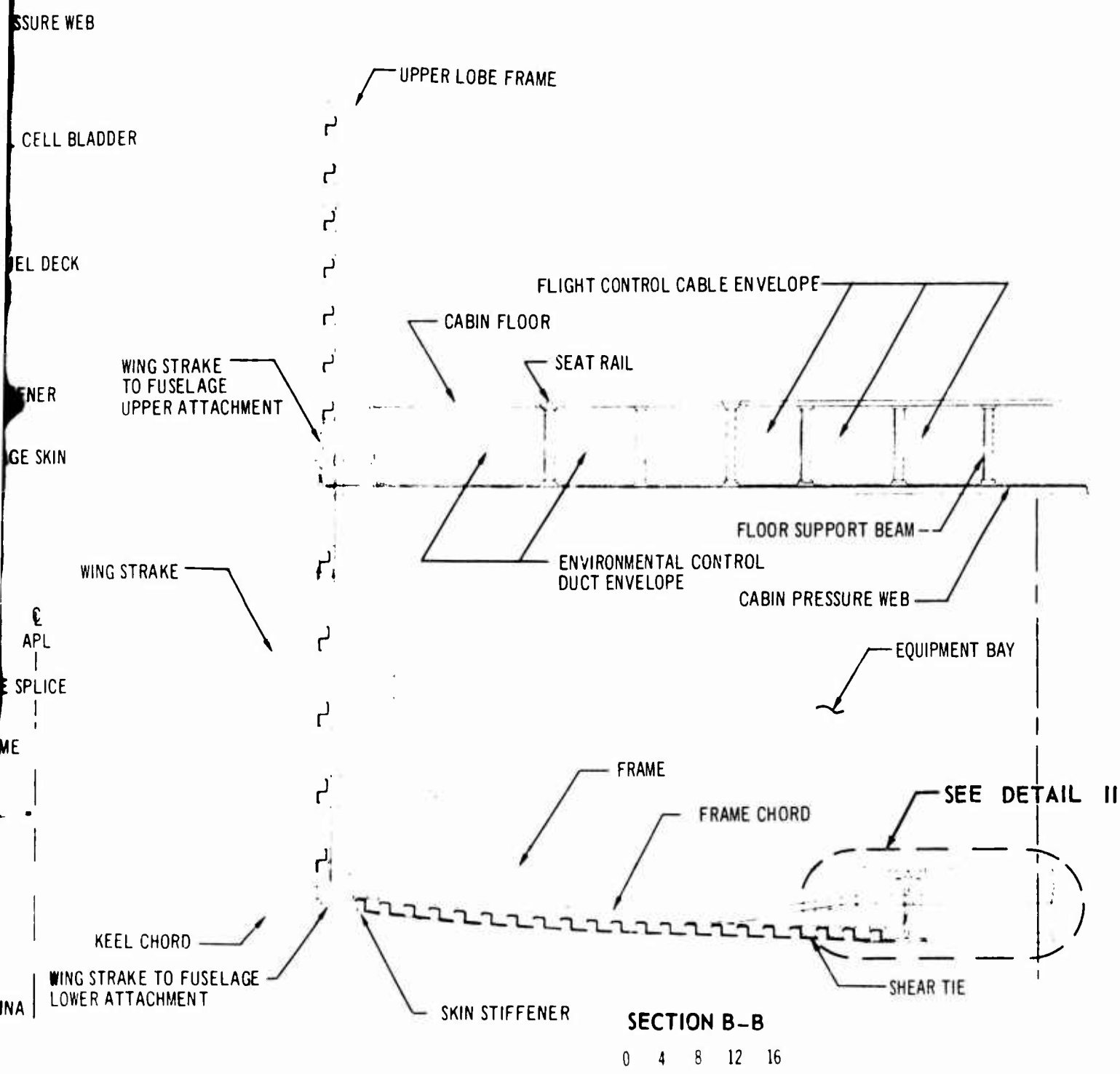
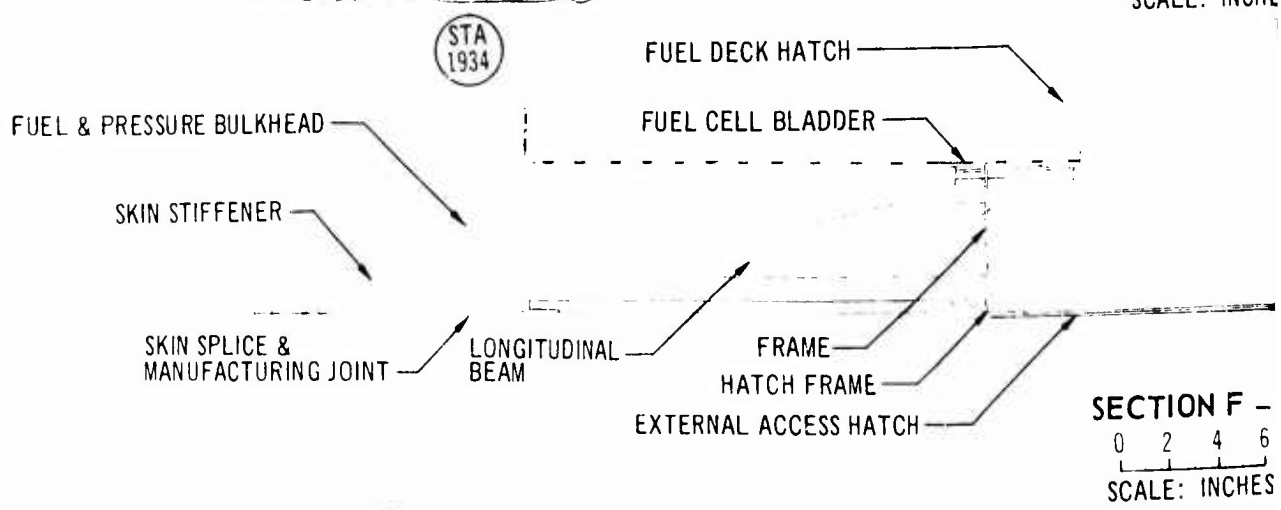
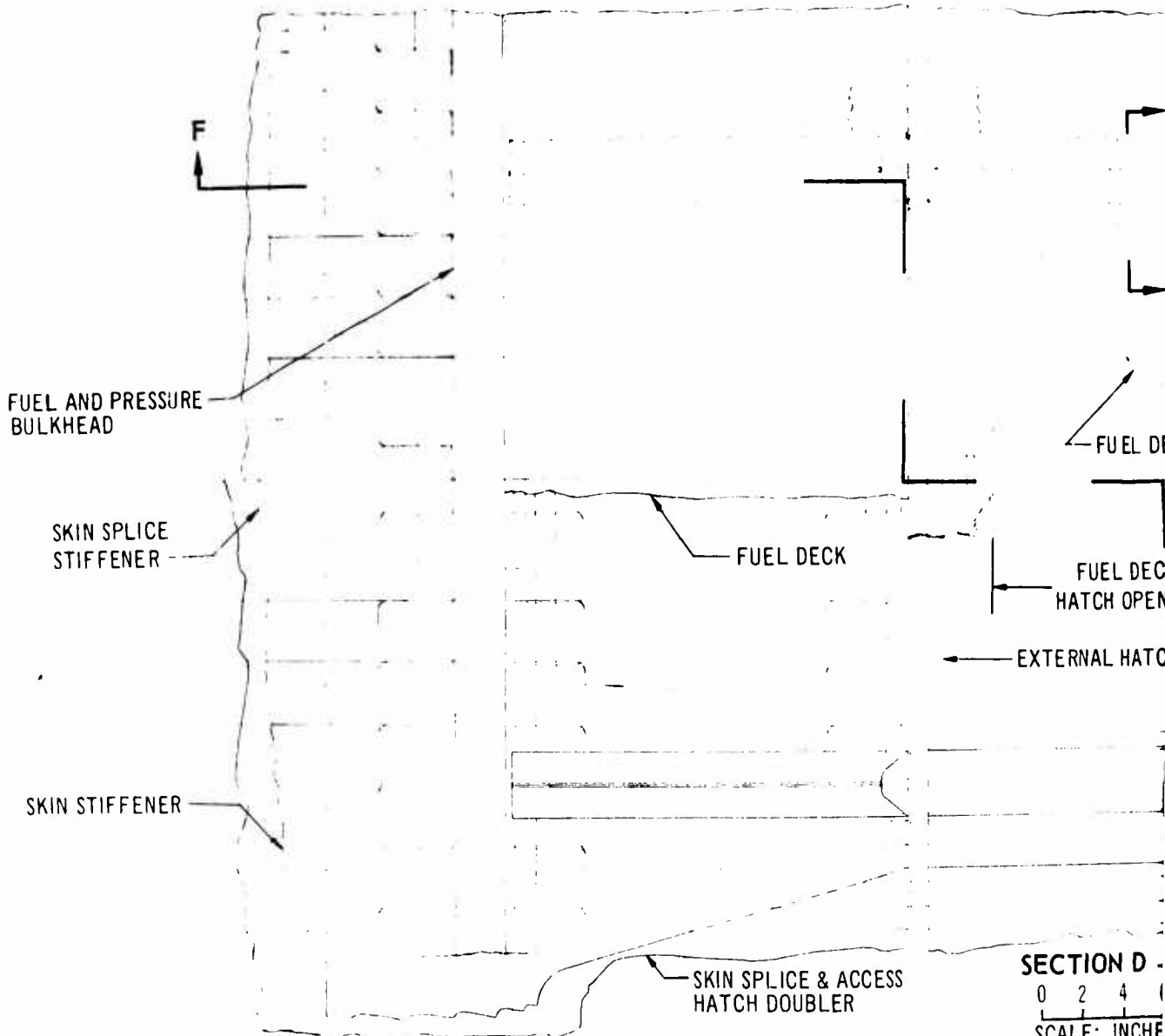
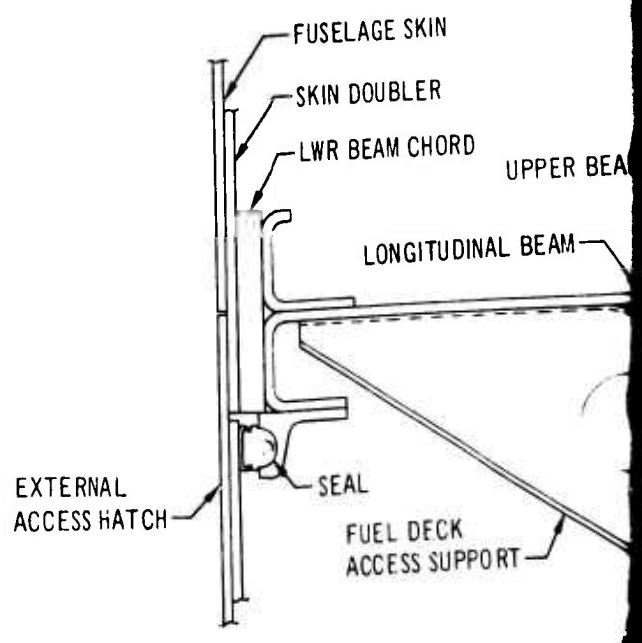
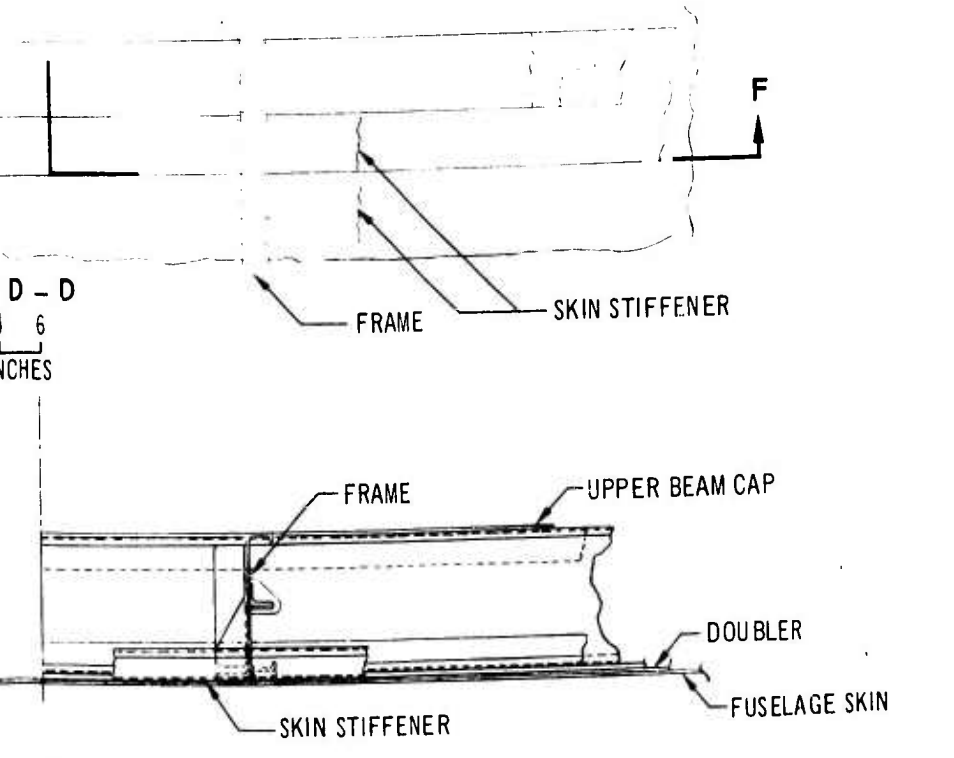
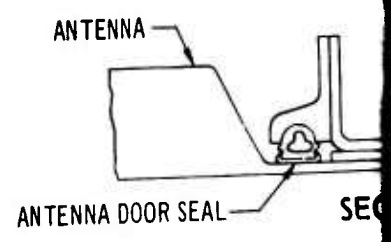
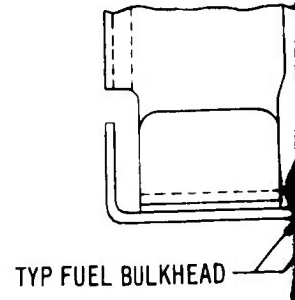
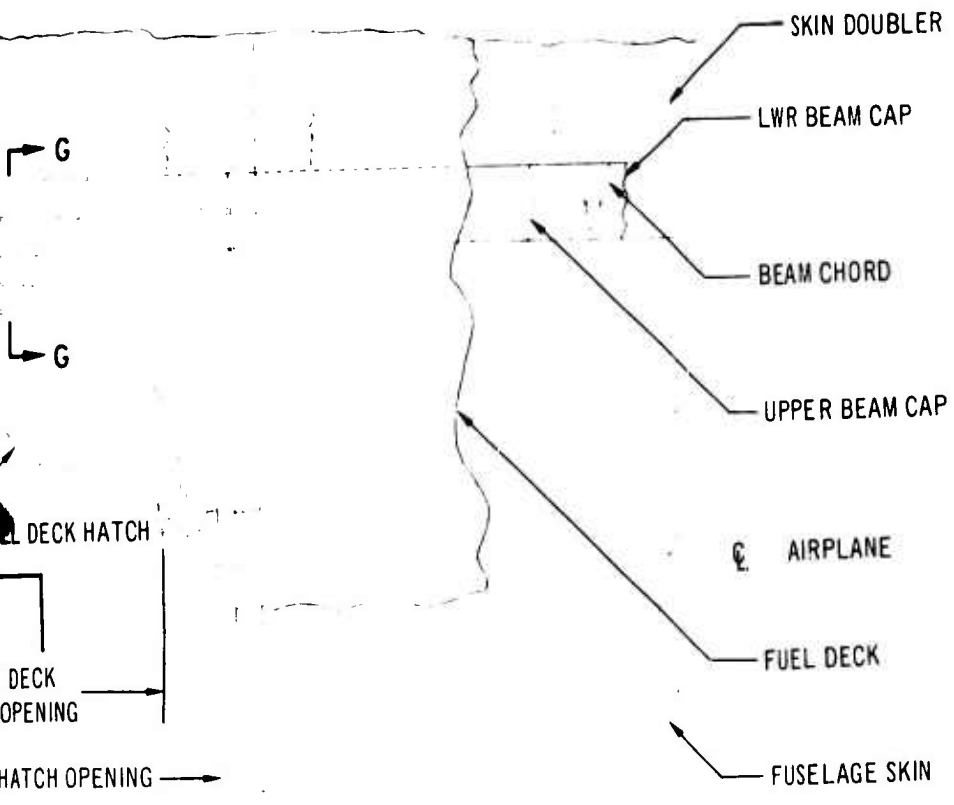


Figure 3-34. Fuel Compartment Frames



A



SECTION G

B

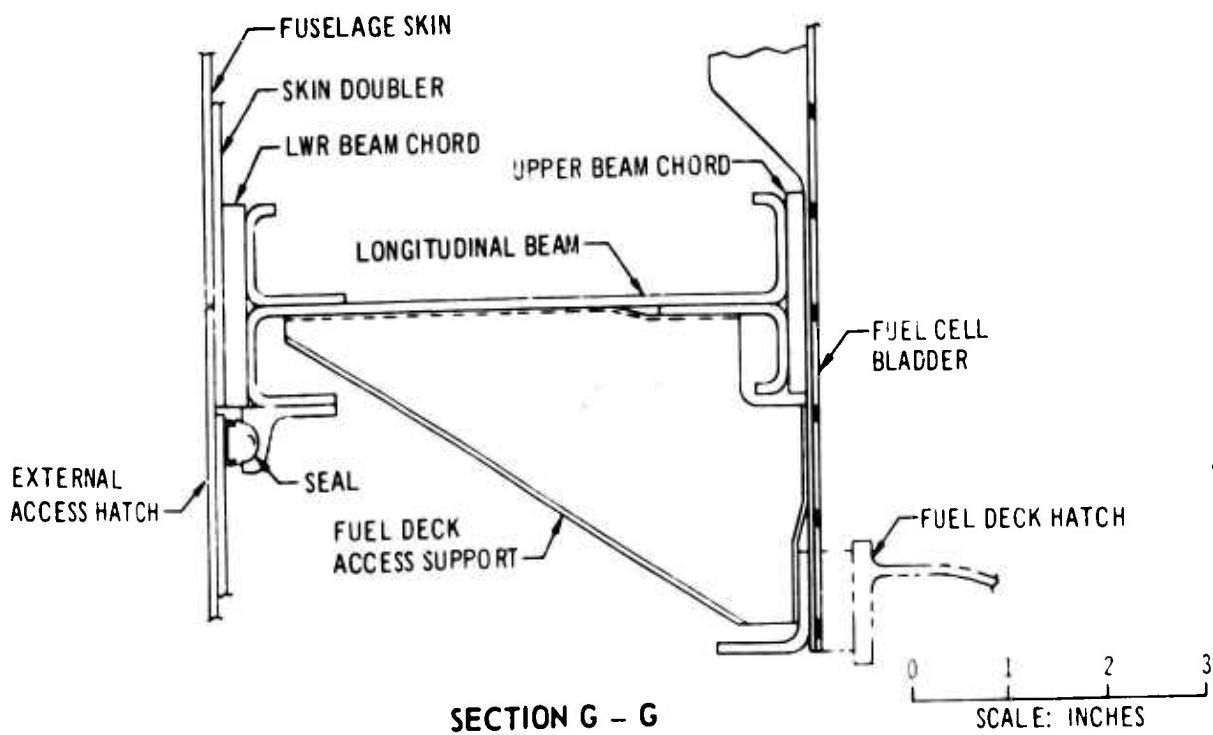
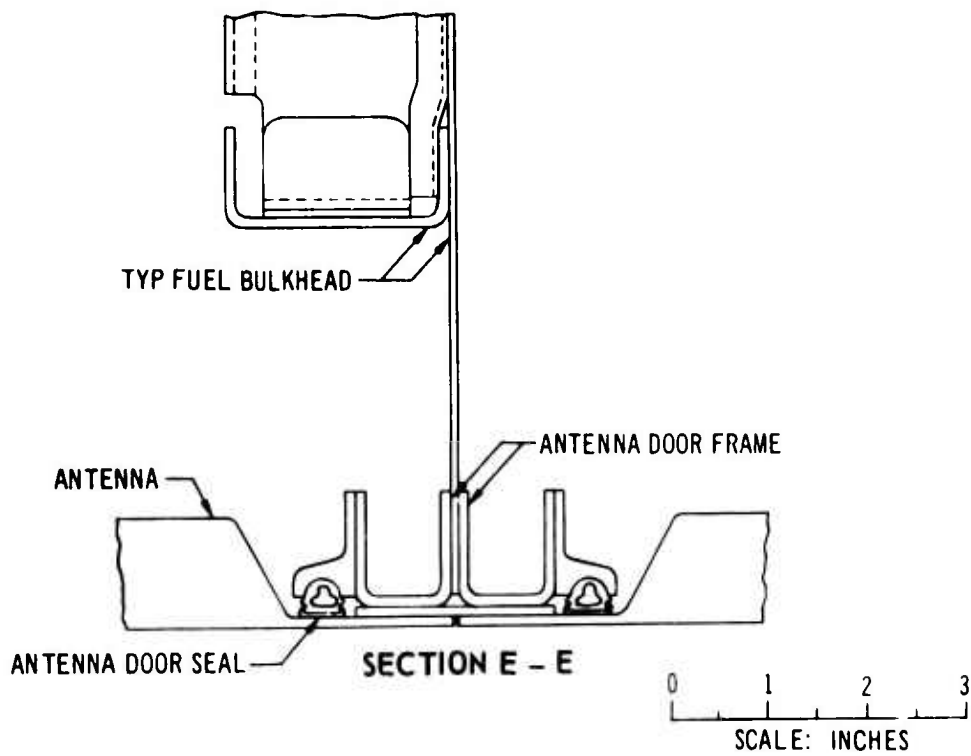
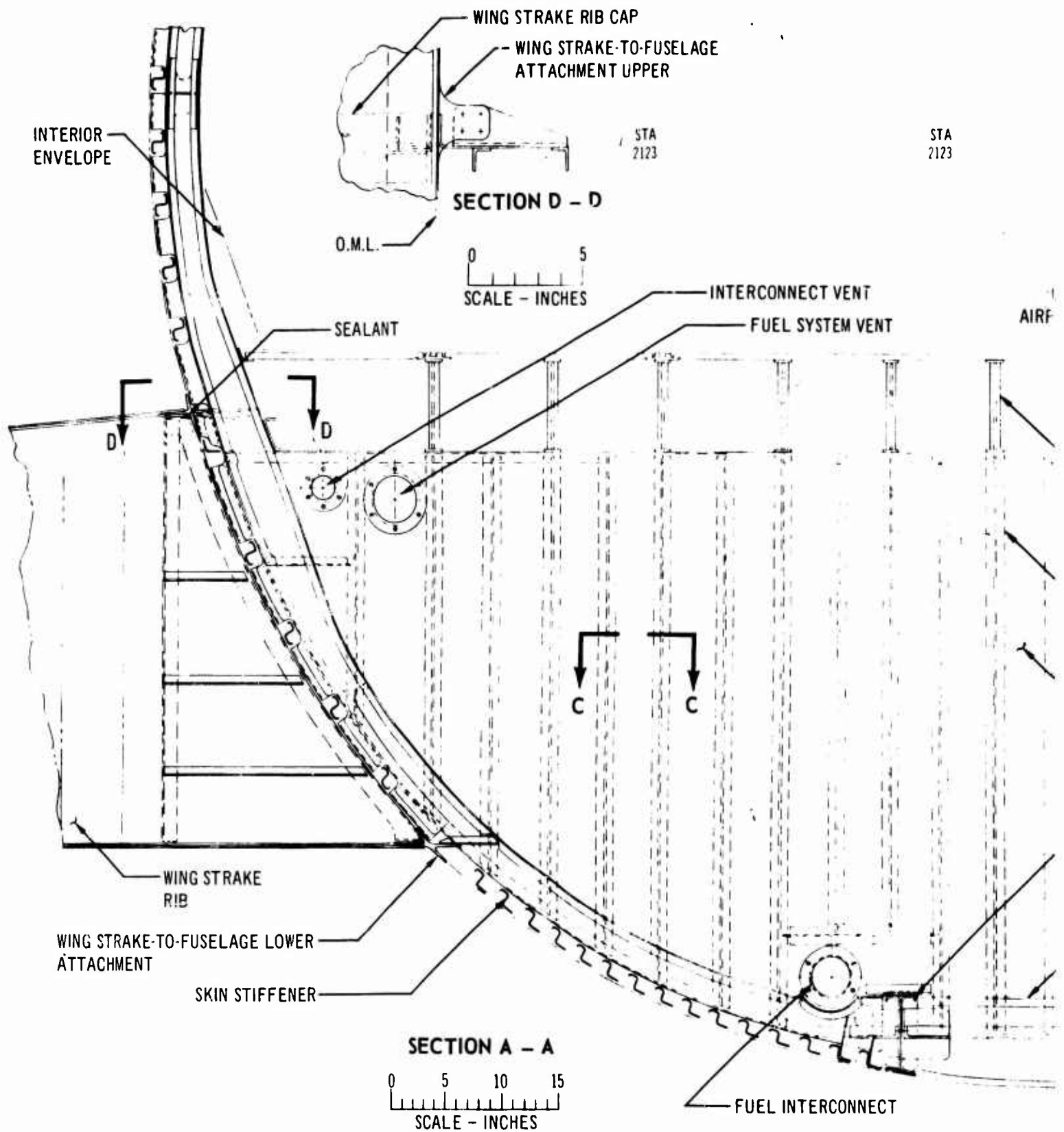


Figure 3-35. Fuel Compartment Access Hatches

C



A

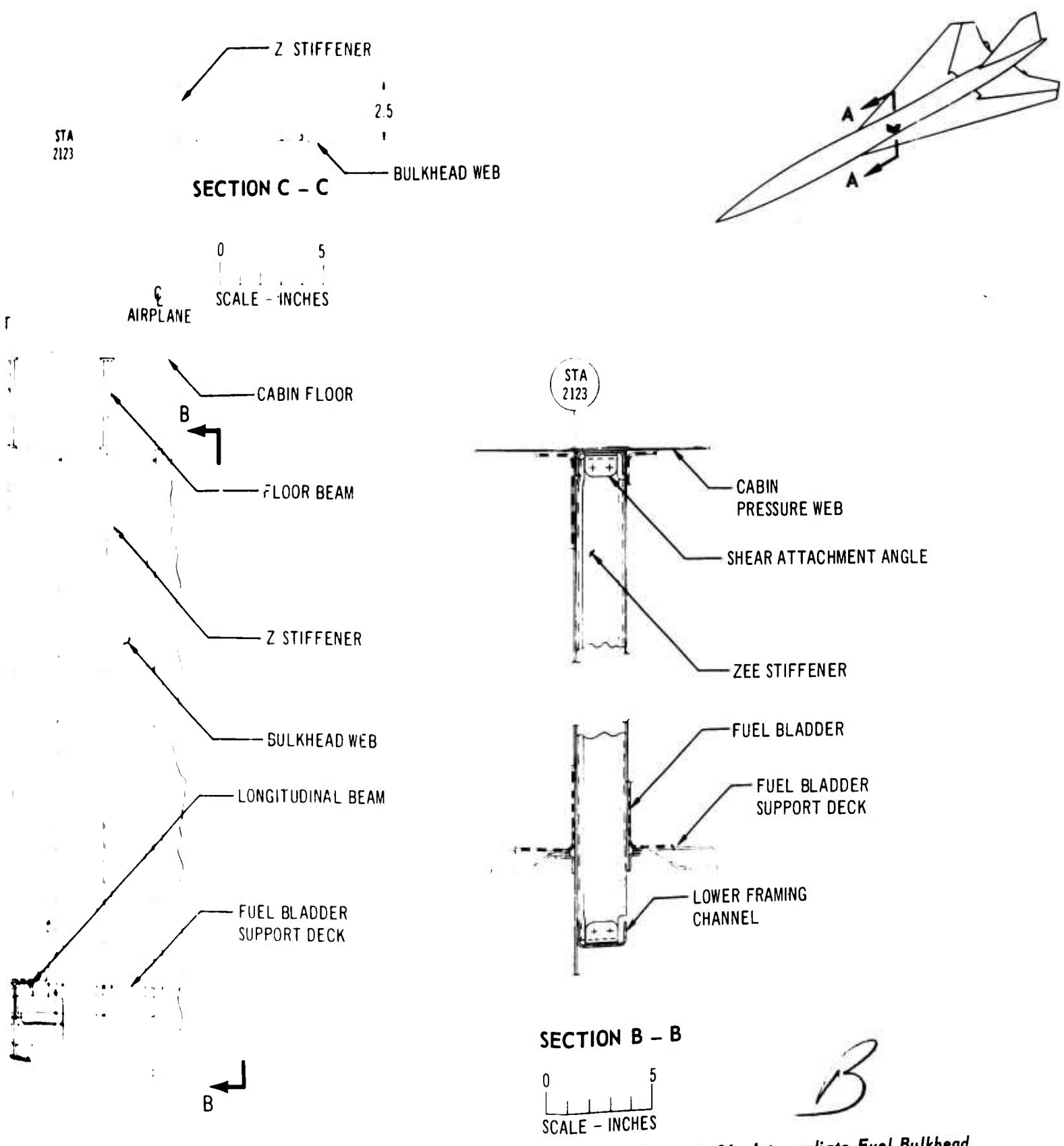


Figure 3-36. Intermediate Fuel Bulkhead

lower lobe is reinforced at the strake frame attachment. A section of the upper-lobe frame web overlaps the bulkhead web and provides shear ties in the area covered by the strake.

### 3.2.8 Passenger Cabin Floors, Floor Beams, and Pressure Webs

The passenger cabin floor consists of removable panels supported by transverse beams in the forward portion of the cabin and by longitudinal beams where the lower lobe is unpressurized. The transverse beams (shown in Fig. 3-37) are a welded corrugated web construction modified to a shear-resistant-web type of I-beam in the center portion to provide for control cable grommets. The longitudinal beams (shown in Fig. 3-38) are spaced approximately on 10-in. centers. These beams are also of the welded corrugated web construction.

Floor panel construction is varied to meet the traffic requirements of the area. A typical floor panel assembly is shown in Fig. 3-38. The titanium floor panels provide a service life better than the panels used on current commercial subsonic jets.

Cabin air pressure is carried by a titanium web attached to the lower chord of the longitudinal beams located over the fuel compartment and the wheel well. A flat waffle doubler is bonded on the lower surface of the pressure web. The doubler provides tear stoppers to limit the maximum pressure escape area. This combination provides fatigue resistance for minimum weight.

The titanium floor panels and pressure web provide a double fire barrier over the fuel compartment for increased safety.

### 3.2.9 Passenger Cabin Windows

Two panes of load-carrying glass are used in the fail-safe passenger windows shown in Fig. 3-39. The inner primary load-carrying pane is chemically tempered glass with a heat-reflecting gold coating on both surfaces. The fail-safe outer pane is chill-tempered soda-lime glass with a coating of heat-reflecting gold on the inner surface. The cavity between panes is vented to ambient through a desiccant. These structural panes were successfully tested for ultimate load, fatigue life, and impact load (see Sec. 4.0).

The cabin air pressure can be maintained at a safe level by the environmental control system with a fuselage opening equivalent to the window area (see Part A, Environmental Control, Electric, Navigation and Communication (V2-B2707-13), of the System Report).

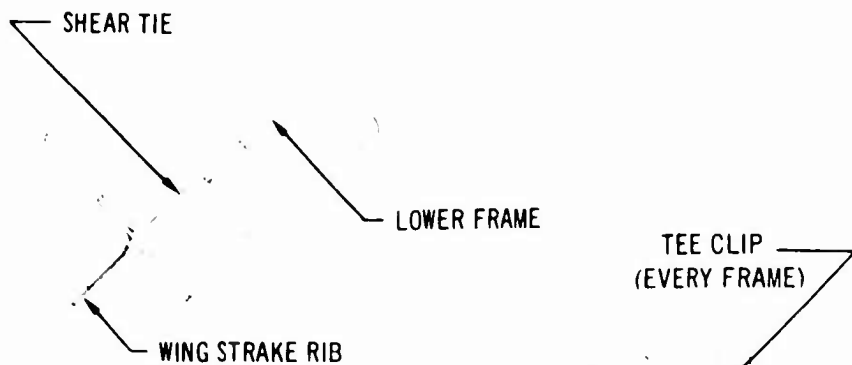
Cleaning and repair are easily accomplished from the inside of the airplane. Window glass replacement is achieved by removal of five clips on each windowpane.

### 3.2.10 Passenger, Service, and Cargo Doors

Four passenger doors, four service doors, and two cargo compartment doors are provided in the airplane. The size and location of these doors are shown in Fig. 3-25. All of the doors are improved derivations of the doors used on the 707 and 727. They combine the structural, mechanical, and seal features with innovations for temperature and higher operating pressure.

The following features are basic to all doors:

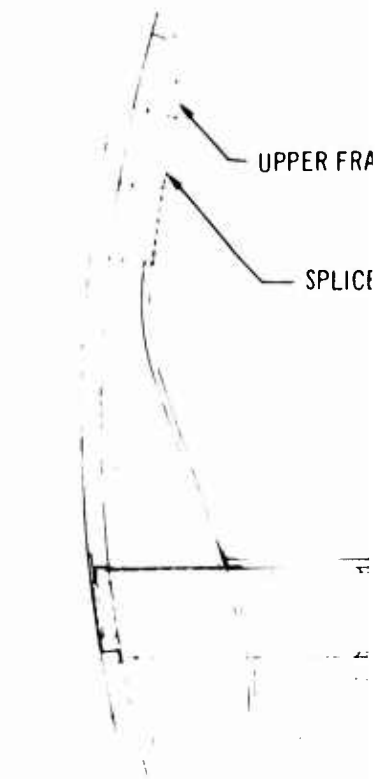
- The doors are plug type and are driven by fuselage pressure against fixed stops. These stops, as well as the door latches, are designed so that a fitting failure does not disturb door safety. Door hinges do not carry any loads except during actual door opening.
- Doors are isolated from fuselage loads and deflections by framing, which is designed to carry ultimate loads around the door. As a result, long service life, minimized heat transfer into the passenger cabin, and the structural rigidity to ensure emergency door operation are provided.
- Positive indication of locked doors is provided by observation of the door handle position and door flushness. Door lock indication is provided to the pilot's station by a light. Design strength of the lock and latch system is so arranged that first failure is ensured at the operating handle.
- Doors are damped at either end of travel to protect the door and fuselage structure from damage.
- Auxiliary locks in the door-open position provide stability against ground winds.



**SECTION B - B**  
 0 1 2 4  
 SCALE: INCHES

WING STRAKE-TO-FUSELAGE  
 UPPER SURFACE  
 ATTACHMENT

TEE CLIP  
 (EVERY FRAME)



**DETAIL II**  
 0 1 2 3 4  
 SCALE: INCHES

**DETAIL II**

ANGLE STIFFENER

WING STRAKE-TO-FUSELAGE  
 LOWER SURFACE  
 ATTACHMENT

**DETAIL I**

0 1 2 3 4  
 SCALE: INCHES

WING STRAKE

**B**

**SECTION**

0 4  
 SCALE

*A*



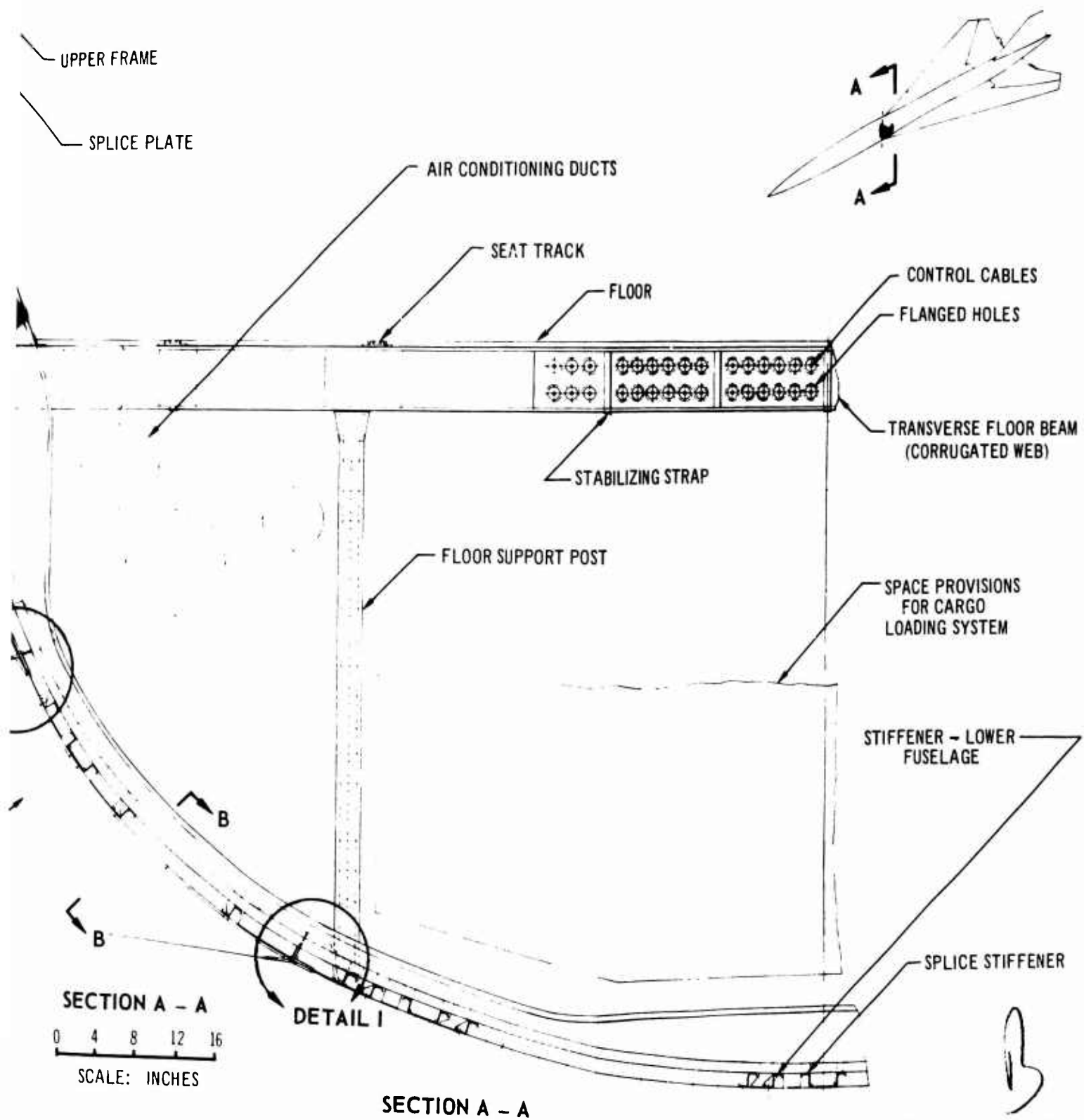
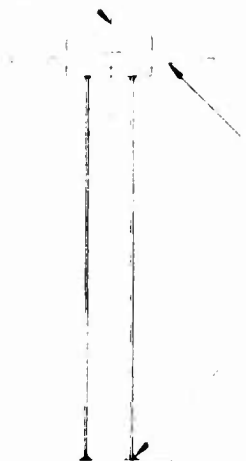


Figure 3-37. Fuselage-Frame Cargo Compartment

CSK BOLT



REMOVABLE SEAT TRACK (ALUMINUM)

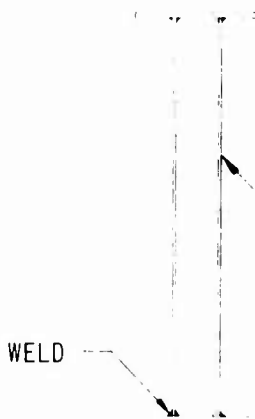
WELD

TYPICAL FLOOR BEAM WITH SEAT TRACK

0 1 2 3 4 5 6

SCALE: INCHES

SECTION D - D



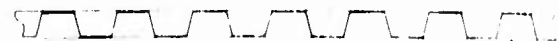
CORRUGATED WEB

TYPICAL LONGITUDINAL FLOOR BEAM

0 1 2 3 4 5 6

SCALE: INCHES

SECTION E - E

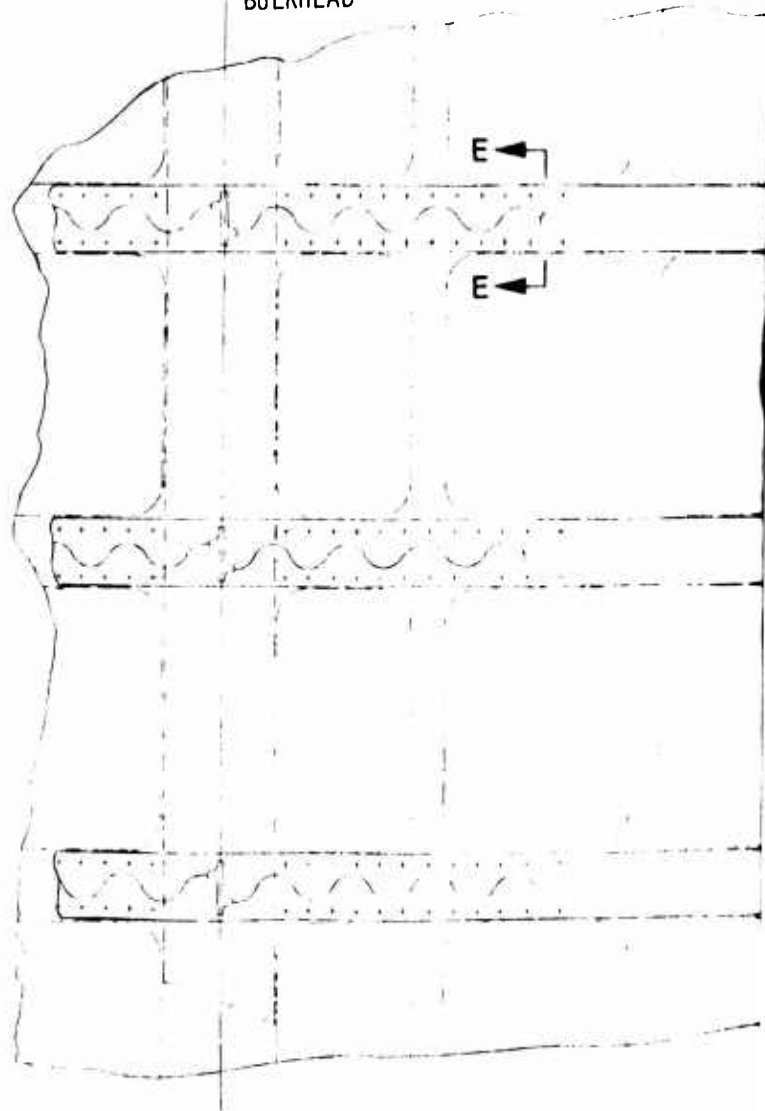


PASSENGER FLOOR PANEL

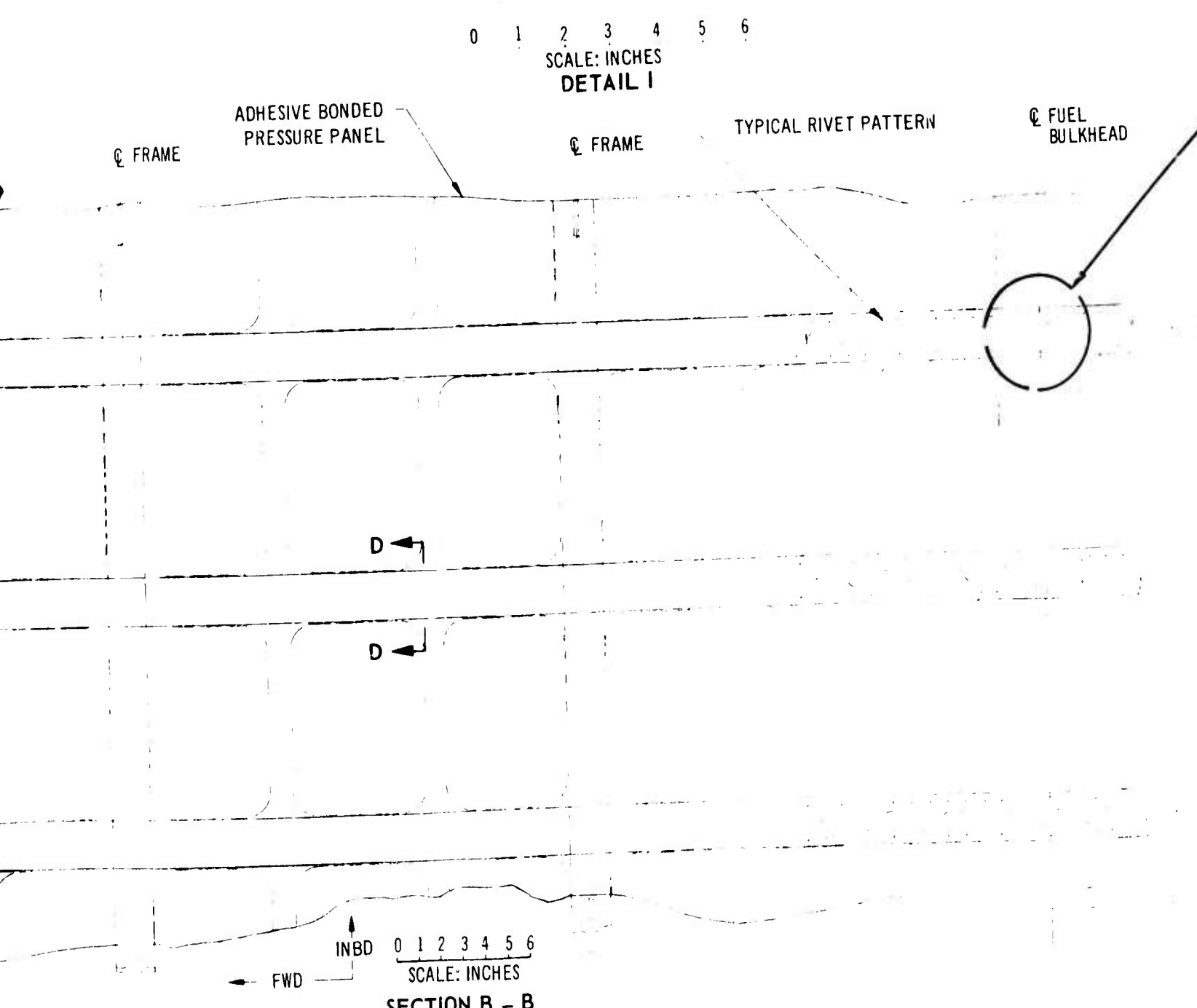
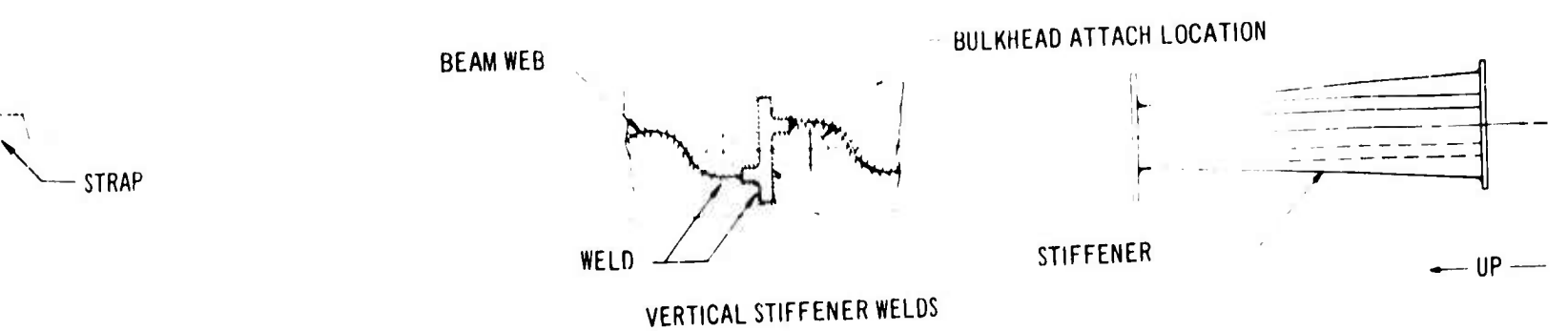
0 1 2 3 4 5 6

SCALE: INCHES  
SECTION C - C  
(ROTATED)

FUEL BULKHEAD

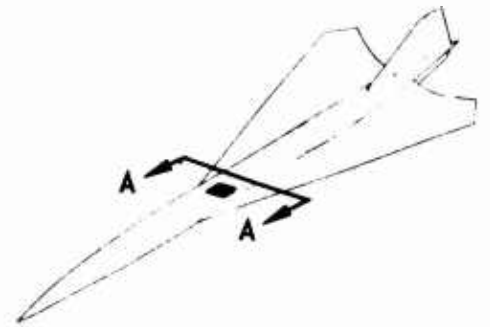
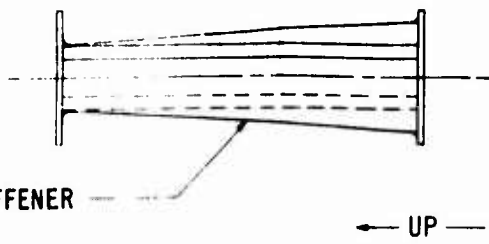


A

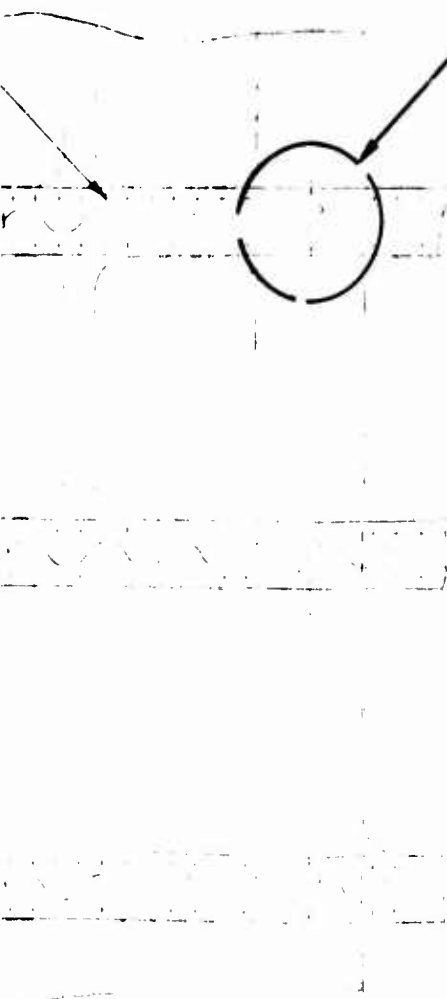


B

AD ATTACH LOCATION



RIVET PATTERN



DETAIL I

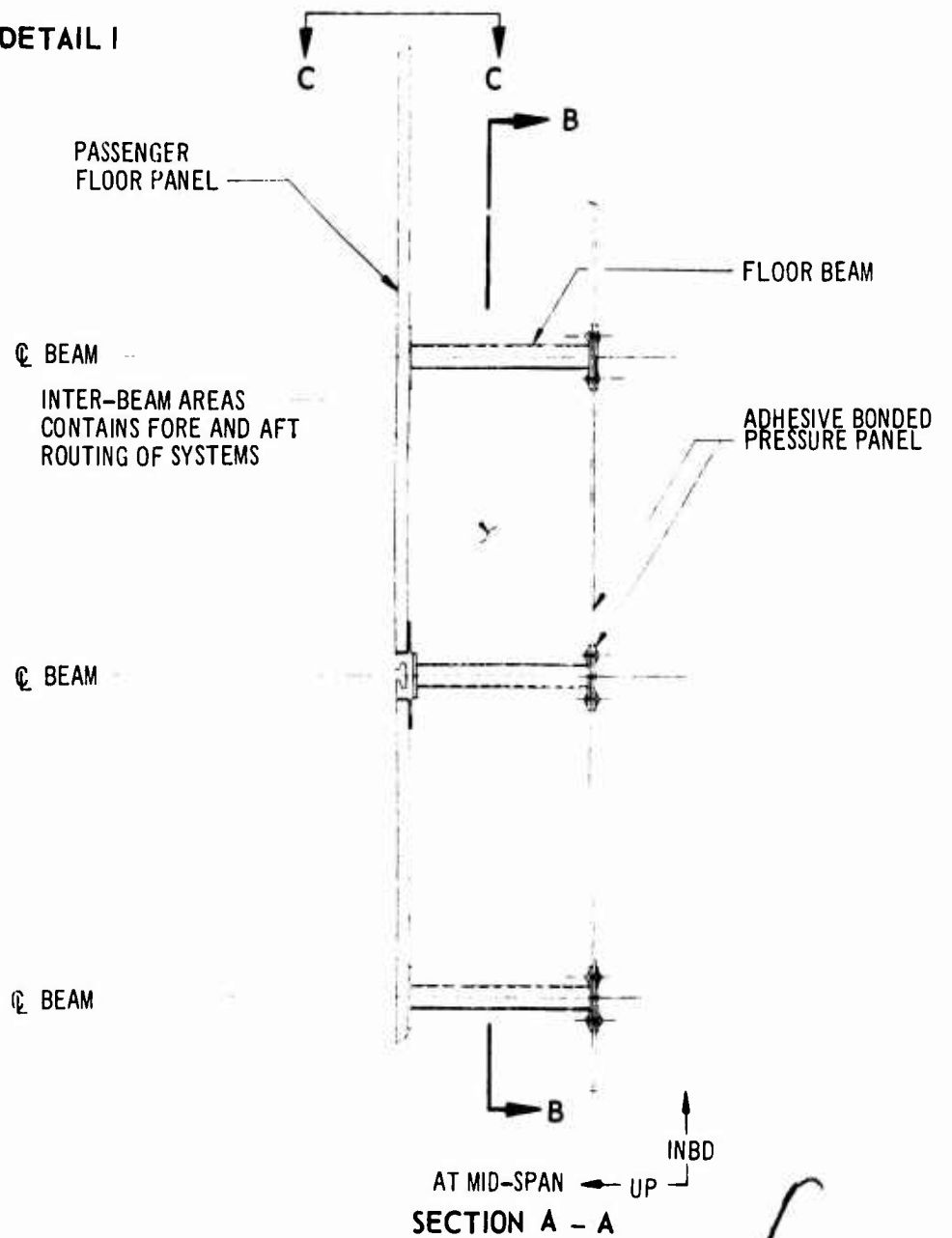
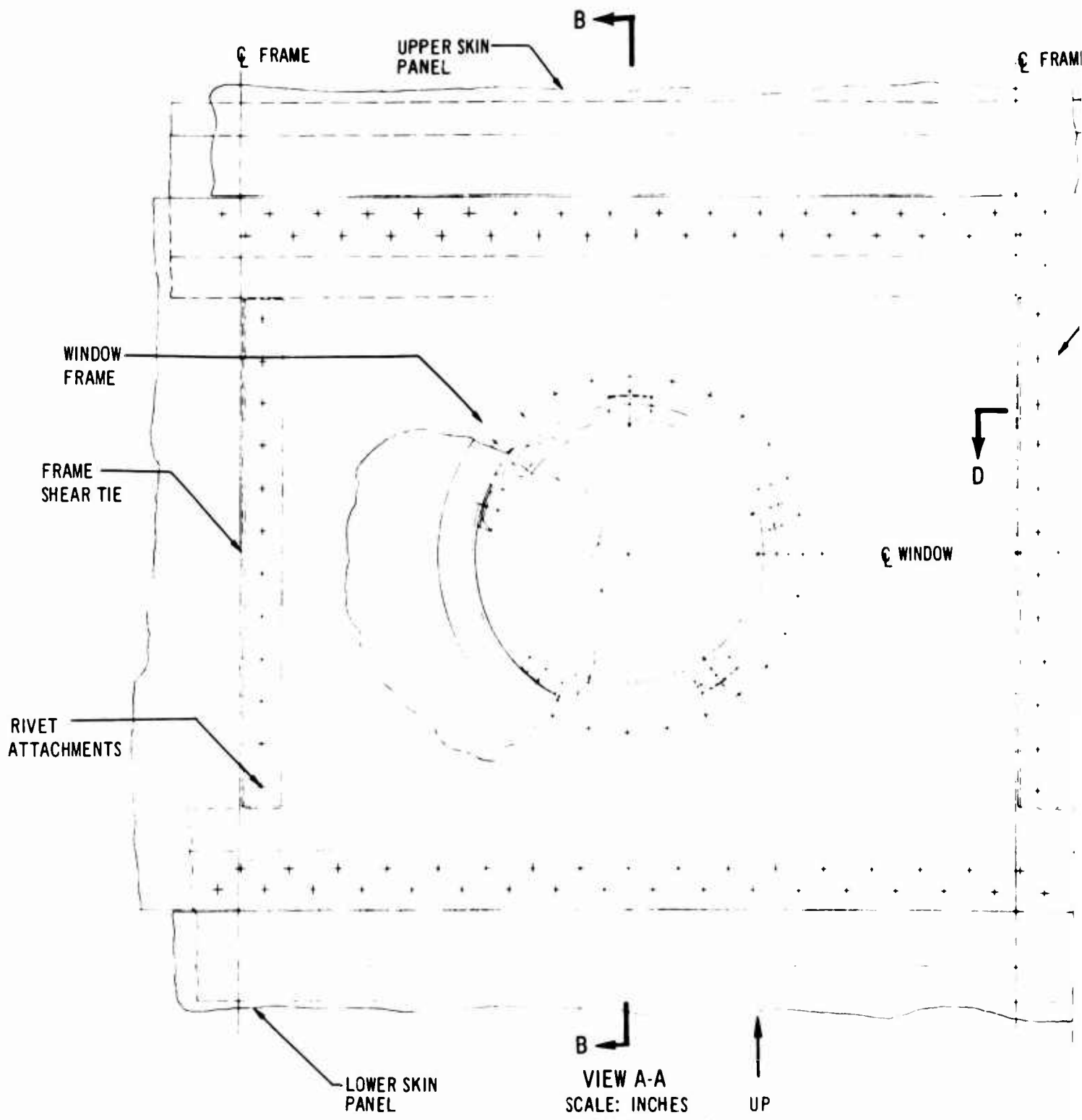


Figure 3-38. Floor Structure



*A*

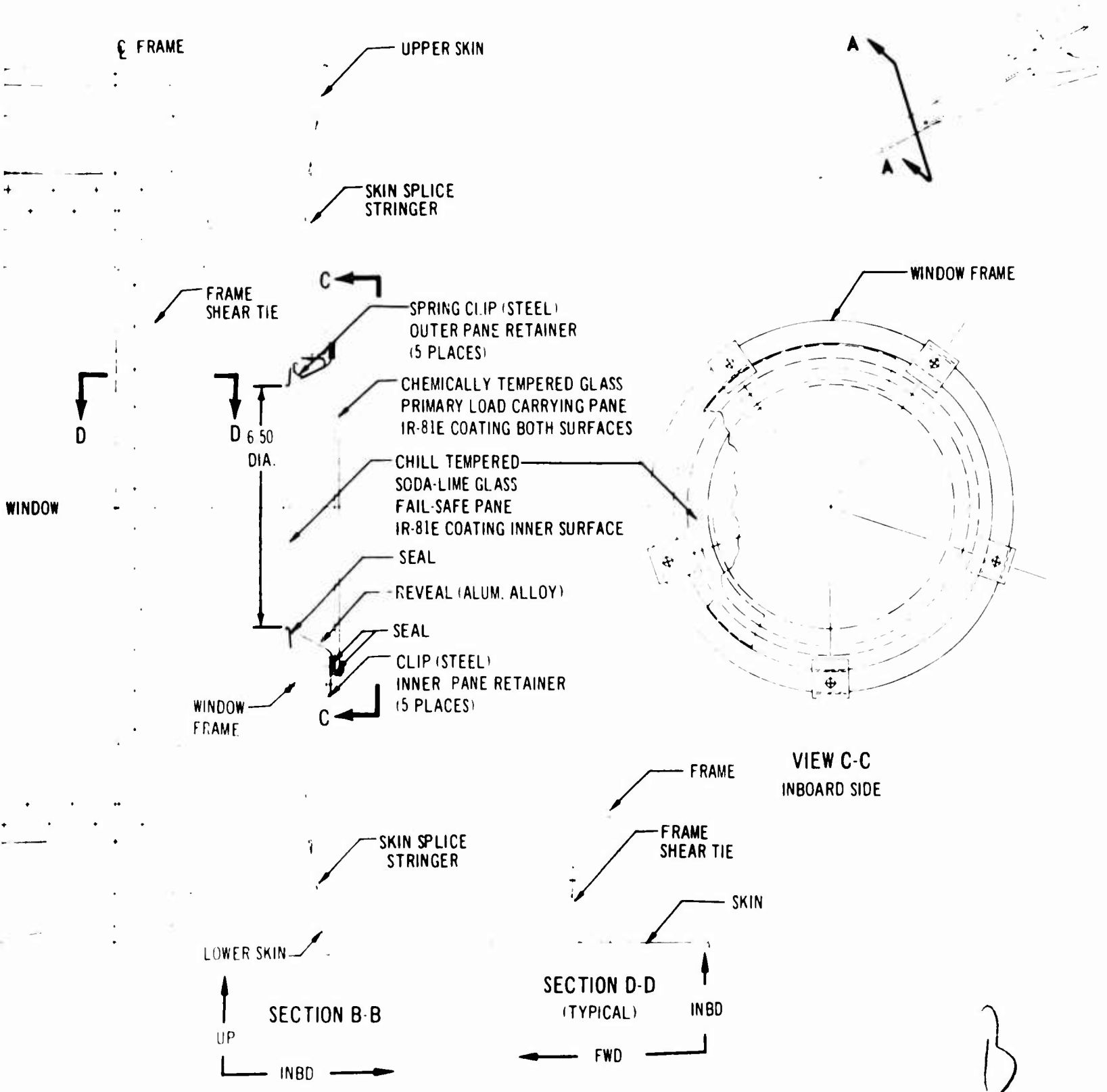


Figure 3-39. Passenger Window

- Door seals are made of fluorocarbon rubber reinforced with glass cloth. All seal retainers are designed for quick replacement.
- Bearings are oversize for low bearing pressure and are made from high-temperature materials that do not require lubrication
- Maximum level of interchangeability is achieved by use of numerical control-tooling panelization techniques and by built-in adjustability at primary fitup points. Adjustable stops provide for flushness with fuselage contours. Linkages with length adjustments ensure proper mechanical fit and smooth operation.
- Doors have external handles flush with fuselage contours. Internal handles are thermally insulated from the door structure to prevent injury during supersonic, high-temperature flight. The external handle will be cool upon landing.
- Manual operation forces of all doors will be within the capability of cabin attendants. Such features as hinge lines selected to be nearly vertical, low seal-deflection forces, and handle lengths keep the operating forces at approximately 30 pounds.
- Where door sill areas are subject to high traffic wear and possible damage, replaceable scuff plates are provided.

#### 3.2.10.1 Passenger and Service Doors

Passenger and service doors are hinged at the front and open with an inward-outward motion typical of the 707 and 727. A typical passenger door is shown in Fig. 3-40. These doors can be opened or closed from inside or outside of the airplane by operating handles mounted on either side of the door. Viewing ports in all doors permit observation by attendants before operating the doors.

The following actions occur when the door is opened from inside the airplane:

a. A handle in the door is rotated. This action, through mechanical linkages performs the following:

- (1) Unlocks the door latches.

- (2) Folds the upper and lower door edges (gates) inboard to make the overall height of the door less than the height of the door cutout. The gates are important safety features because they provide generous clearances that allow the doors to clear the opening when framing is distorted one inch because of an accident.

- (3) Drives the door inboard to a canted position that breaks the seal and overpowers any loads caused by passengers pressed against the door.

b. The canted door is then manually pushed edgewise through the door opening, being guided by the hinge linkages to a position parallel to the side of the fuselage.

#### 3.2.10.2 Cargo Compartment Doors

Each cargo compartment door is sized for the easy entry of standard cargo containers and loading systems. Each door has two sections as shown in Fig. 3-41. The sections open downward with hinges at the outboard edges and a mating joint on the bottom centerline of the airplane. The right-hand door is unlatched and opened before the left-hand door is opened. A reverse procedure closes the doors.

The following actions occur in opening the cargo doors:

a. The handle on the right-hand door is rotated by pulling downward. This action, through mechanical linkages, rotates cam latches translating the door off the stops and allowing it to swing open. A spring-loaded damper counterbalances the weight of the door during the initial downward opening. At full-down position, an overcenter linkage allows the damper to assist the cargo attendant in manually swinging the door to full open.

b. The left-hand door is opened by pulling a handle, which can be reached after the right-hand door is opened. The remaining operations are similar to those required in opening the right-hand door.

Cam latches that accomplish the normal door closure provide the restraint to hold the door in place against upward-acting loads. The rollers of the cam latches engage the upper face of the cam to transfer the inward-acting loads to fuselage framing structure.

**BLANK PAGE**



### 3.2.11 Landing Gear Doors

The aft main landing gear and the nose gear retract into wells within the body and are enclosed by landing gear doors. The nose gear doors consist of a right and left wheel-well door and a right and left strut door. Each main gear has four doors serving the same functions. All doors are hinged along their outboard edge and open along the airplane bottom centerline. The wheel-well doors are operated hydraulically and sequenced to open before gear extension and to close again when the gear is fully extended. The strut doors, slaved to the strut, open on gear extension and remain open while the gear is down. Wheel-well and strut doors for the aft main gear door are in two segments, hinged together to fold so that exposure to aerodynamic forces is minimized.

All doors are of sandwich construction with honeycomb core and titanium sheet faces similar to those shown in Fig. 3-16. Door latches are provided to hold doors to contour when they are closed and subjected to airload. In the event of a failure of a main hydraulic system, opening of the aft main gear doors is provided by a separate hydraulic system and separate actuators. The wheel doors can be manually disconnected and opened for ground servicing. Hinge and latch pins have dry film lubrication. All doors when closed are sealed by glass-cloth-reinforced fluorocarbon rubber seals around edges.

### 3.2.12 Wing-Strake-to-Fuselage Attachment

The wing strake, that portion of the wing forward of the front spar, is rigidly attached to the fuselage. Strake shear loads are transferred directly to the fuselage shell at each strake rib by a continuous attachment between the strake rib web and the fuselage skin. Strake bending loads, carried by the strake surfaces and ribs, are transferred to the fuselage frames. The carry-through structure for the strake upper surface is the transverse floor beam, the fuselage pressure web, and bulkheads. The carry-through structure for the strake lower surface is the lower segment of each fuselage frame or bulkhead. The fuselage lower lobe is deeper than earlier configurations. This change produced weight saving in fuselage framing, because the more circular lower lobe is more efficient for carrying pressure loads. A second benefit of a deeper lower lobe is more cargo and fuel volume.

Figures 3-37 and 3-36 display the two typical areas of strake attachment. Figure 3-37 shows this attachment in the area of the forward cargo compartment. Figure 3-36 shows this attachment in the fuselage fuel-tank area. Flight and inertial strake-to-fuselage loads are small because of the deep section of the integrated wing-tail design. In the area (shown in Fig. 3-36), the strake upper surface joins the fuselage close to, but never above, the passenger floor.

Structural components are efficient for the following reasons:

- a. The wing strake ribs are aligned with the fuselage frames to achieve a direct strake-to-fuselage load path.
- b. The strake-to-fuselage attaching members provide structural strength to strake and fuselage shells and also serve as fuselage skin-panel splices.
- c. The strake-to-fuselage attaching members receive extensive machining to tailor their contours, consistent with the high fatigue-life requirements established for this airplane.
- d. The continuous attachment of wing to fuselage uniformly distributes the thermal stresses resulting from the temperature difference between the cool cabin interior and the hot exterior.

### 3.2.13 Wing-Center-Section-to-Fuselage Attachment

The wing center-section-to-fuselage attachment is a continuous, fixed structural joint as shown in Fig. 3-42.

The front and rear spars of the wing center sections, which are continuous through the fuselage, are attached to fuselage frames with forged fittings. These fittings are located at the side of the fuselage and extend from the lower surface of the wing to approximately 36 in. above the cabin floor where they are spliced to the fuselage frames. The fuselage frames are designed to absorb all angular and lateral deflections induced by wing flexure and introduce this deformation into the fuselage structure fore and aft of the wing center section with very low secondary stresses. Front and rear spar fitting fail-safety is achieved by providing alternative load paths forward and aft of the spar systems via longitudinal members, fuselage skin panels, and frames.

The fuselage frames between the spars are attached to the wing by fittings that bolt through the wing skin to fittings on the wing rib located at the side of the fuselage.

All primary members of the wing-to-fuselage attachment can be readily inspected visually. The front spar fitting is attached to the forward side of the spar web with the lower portion being visible from inside the equipment bay. The rear spar fitting is attached to the aft side of the spar web with the lower portion being visible from inside the wheel well. The intermediate-frame-to-wing fittings and the upper portions of the front and rear spar fittings can be inspected from the cabin interior.

A chordwise wing rib is located in line with the flat side of the fuselage as shown in Fig. 3-42. Use of this rib as an integral part of the fuselage in the region of the wing cutout improves structural efficiency.

Wing fore and aft loads are transmitted to the fuselage by means of a shear redistribution member mounted on the upper wing skin and by the keel beam.

Space is provided between the passenger floor and top of the wing skin for passage of systems with no cutouts in wing structure.

#### 3.2.14 Stabilizer-Center-Section-to-Fuselage Attachment

The stabilizer and wing center sections are similarly attached to the fuselage, except for the stabilizer rear spar attachment. The stabilizer rear spar is continuous through the fuselage and is attached by a single pin at each side of fuselage. The fuselage bulkhead at the stabilizer rear spar is a lower-lobe pressure bulkhead and supports the longitudinal pressure deck beams. Pressure is retained by a web attached to the floor beams above the stabilizer. The unpressurized area below the pressure web is used for systems and equipment.

#### 3.2.15 Aft Body Structure

The aft body consists of a pressure bulkhead, three bladder-cell fuel bays, two integral fuel bays, and a tail cone. Each fuel bay is separated by a bulkhead.

##### 3.2.15.1 Fin-Front-Spar Pressure Bulkhead

The aft pressure bulkhead, as shown in Fig.

3-43, is utilized as a multiple-load-carrying structure to perform multiple functions at minimum weight. It forms the aft end of the pressure compartment and at the same time provides primary support for the vertical and ventral fins and supports the aft bladder fuel cells. Fail-safe straps bonded to the bulkhead web provide reduced size panels and minimize crack length. Fuel pressure loads during crash conditions are less than normal cabin pressure loads. This results in bulkhead strength in excess of crash requirements. It is sealed for cabin pressure and, as an added safety feature, provides a secondary barrier for fuel and vapors. The primary barrier is provided by the bladder fuel cells located immediately aft of the bulkhead.

##### 3.2.15.2 Bladder Cell Fuel Bay

This area consists of three bladder fuel bays and supporting bulkheads. The sidewall construction is closely spaced body circumferential frames supporting the body skin. A typical fuel bulkhead is shown in Fig. 3-44. The upper part of the bulkhead is sheet stiffener design. The remainder utilizes honeycomb construction to minimize weight and provide smooth surfaces for the bladder fuel cell support, thus eliminating a requirement for backing boards. Vertical and ventral fin support by the bulkhead results in efficient dual use of the structure.

##### 3.2.15.3 Integral Fuel Bay

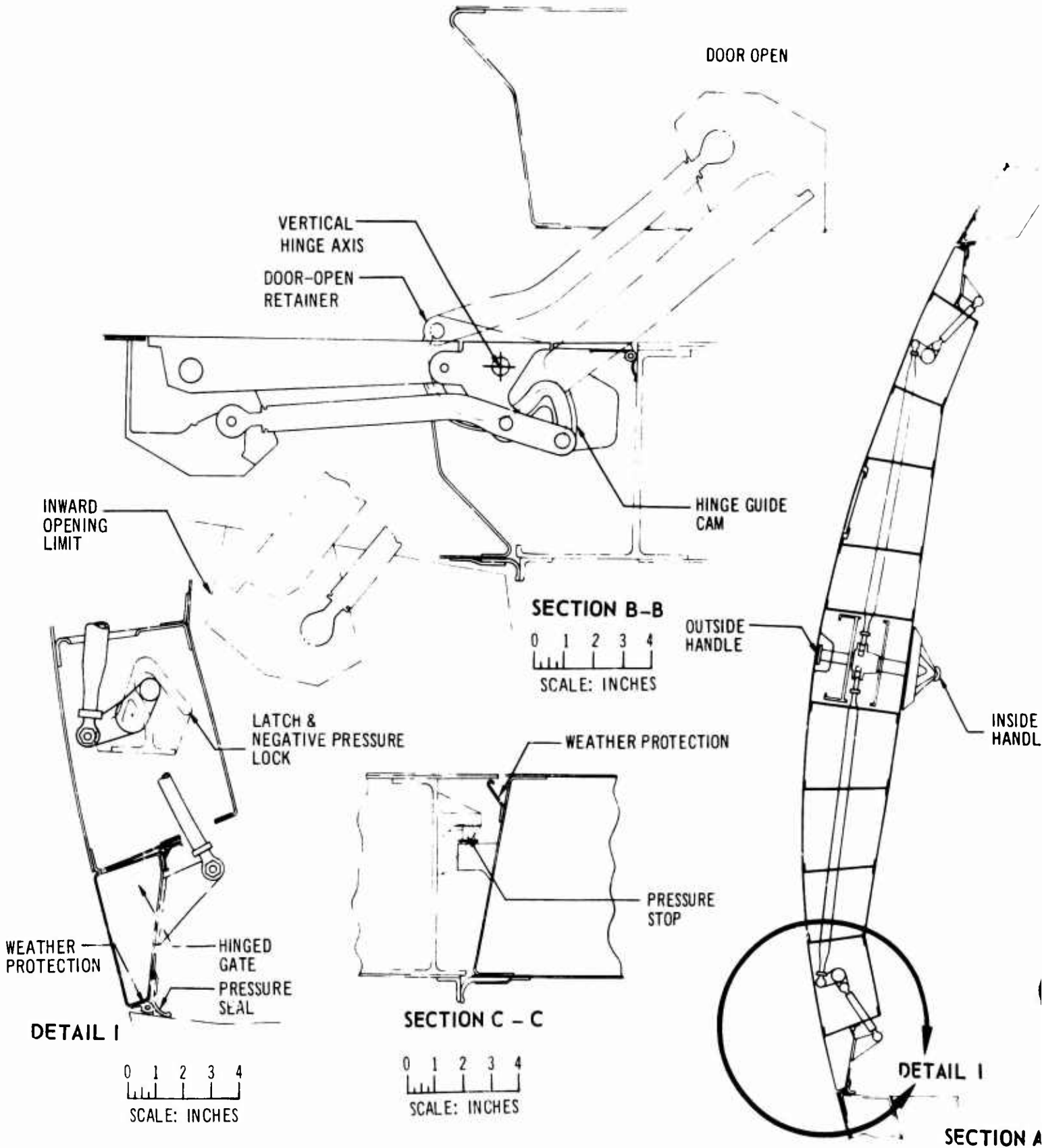
This area consists of three honeycomb bulkheads as described in the previous paragraph. The tank sidewalls are of curved metal face honeycomb construction. The tanks are of integral design and sealed with fillet sealant.

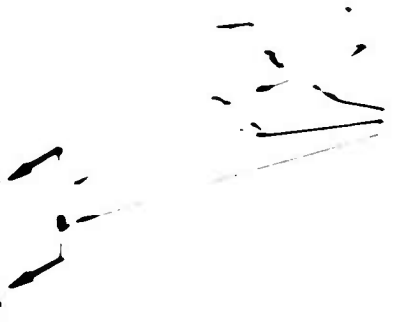
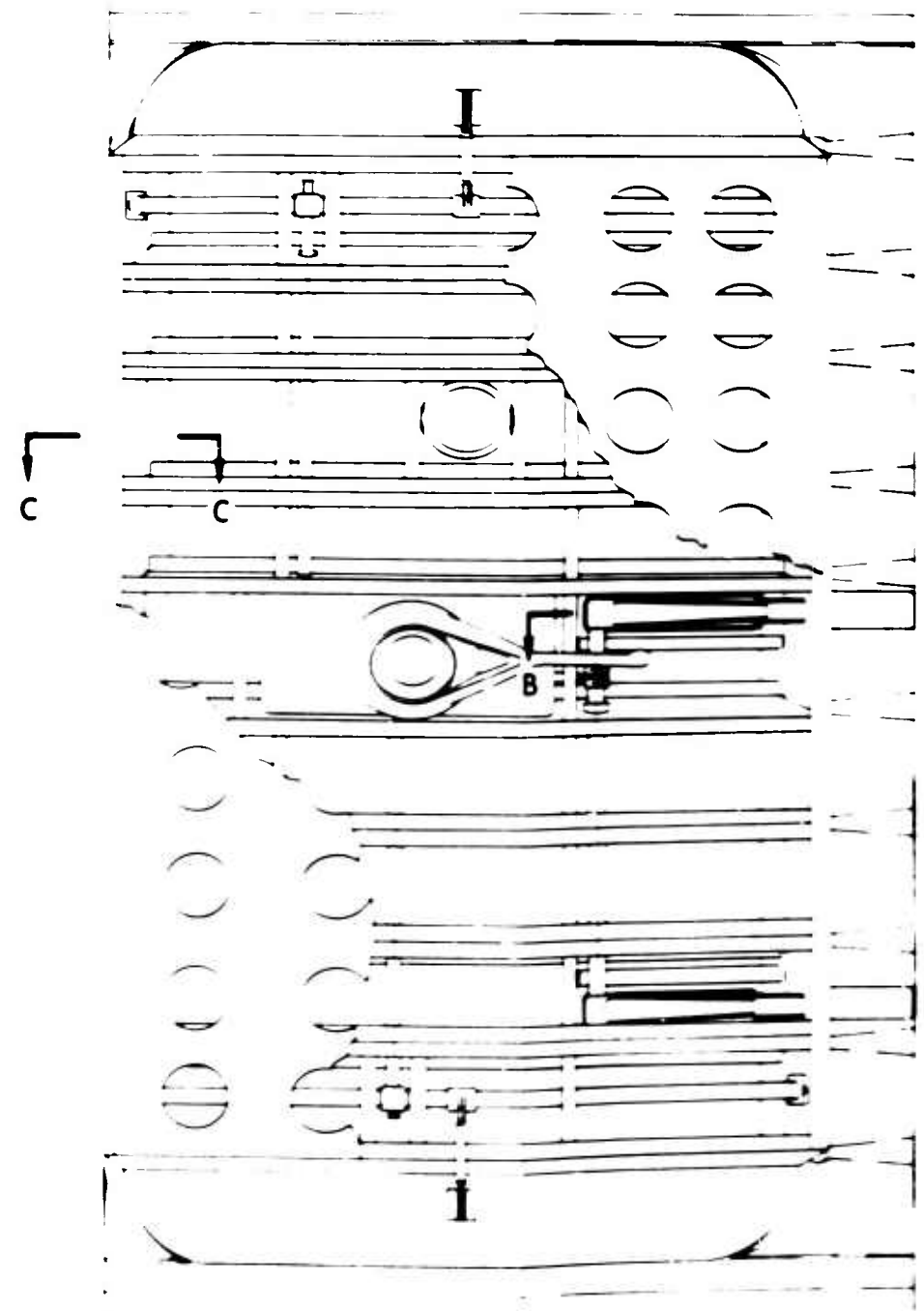
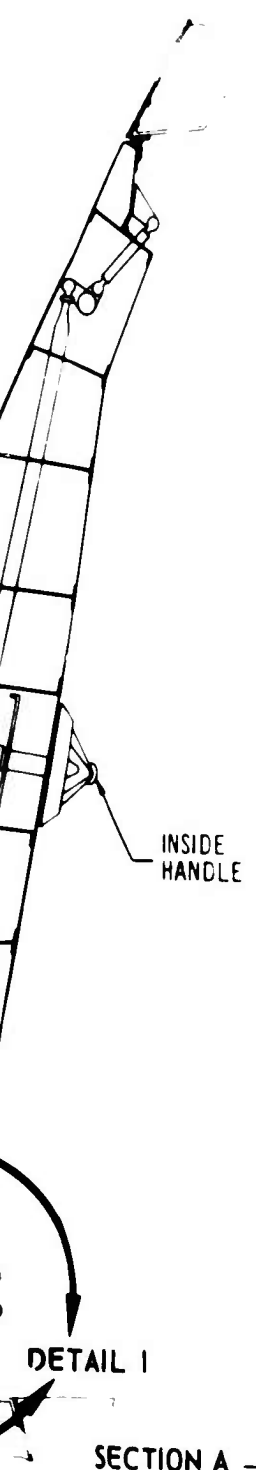
##### 3.2.15.4 Sonic Resistance

The aft body side walls are subjected to sound pressure levels as shown in Part C, Design Criteria, Loads, Aerodynamic Heating, Flutter (V2-B2707-7) design report of the airframe. Sonic resistance is provided by honeycomb panels in the aft area and skins supported by closely spaced circumferential frames in the forward area. Testing of the structure to withstand the sonic environment is reported in Part E, Structural Tests (V2-B2707-9) of the Airframe Design Report.

#### 3.3 HORIZONTAL STABILIZER

The general arrangement of the horizontal stabilizer is shown in Fig. 3-2. It is a fixed stabilizer permanently attached to the fuselage. It provides excellent carry-through with adequate depth for

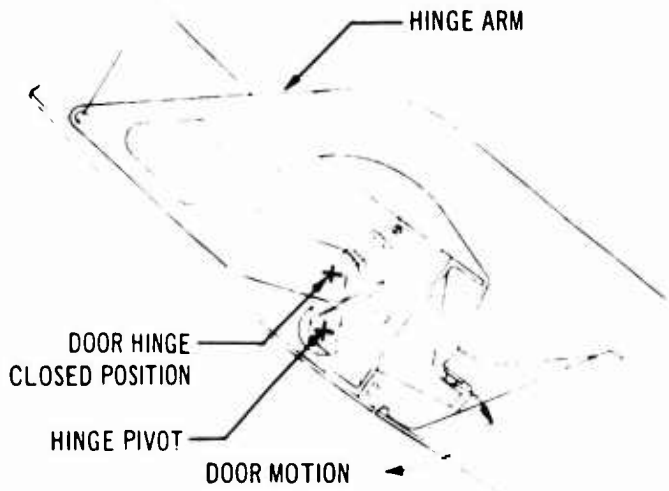




SCALE 1/2" = 1'-0"

Figure 3-40. Passenger Door  
V2-B2707-6-2

3

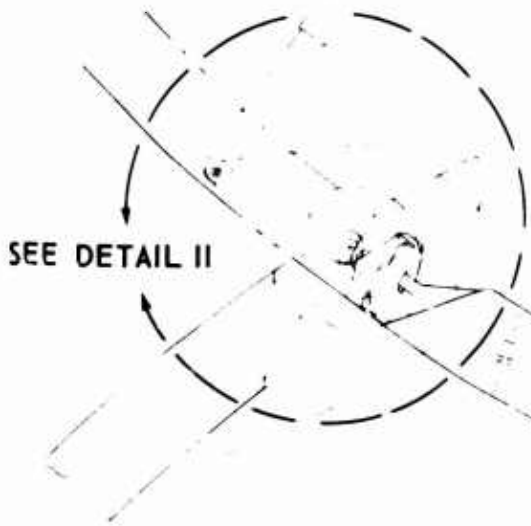


**DETAIL II**

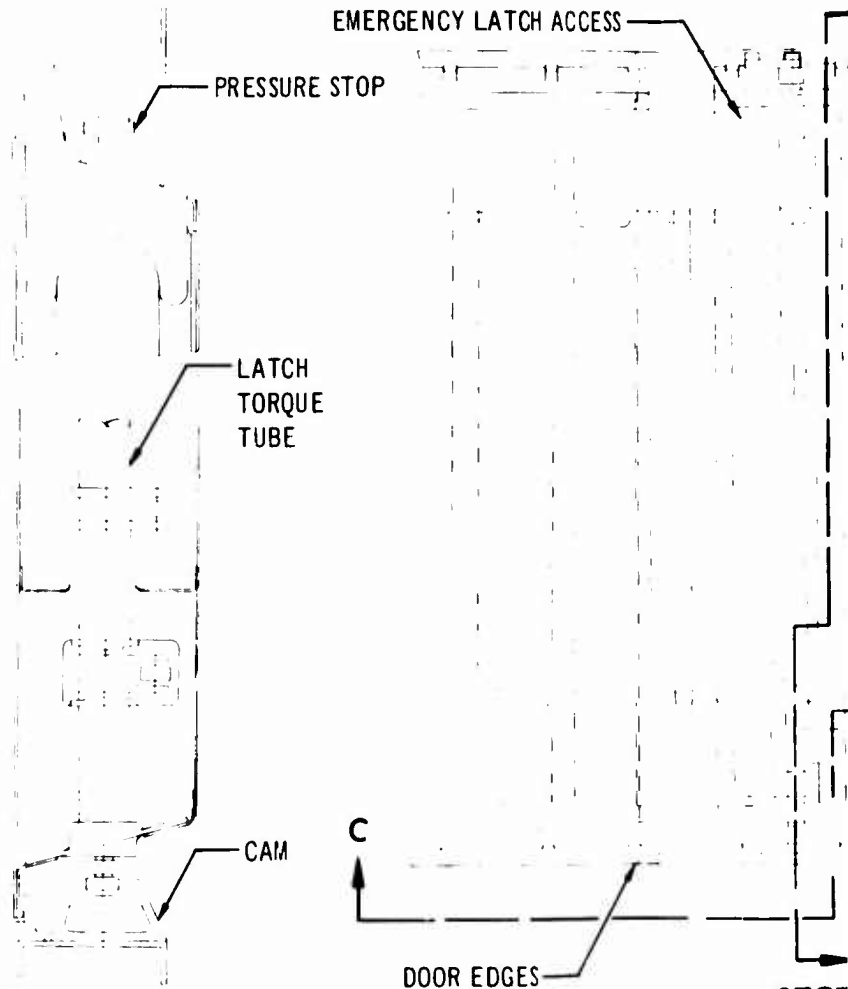


SCALE: INCHES

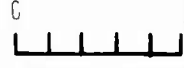
DAMPER & DOOR RETAINER



DOOR MOTION



**SECTION B - B**



SCALE: INCHES

LEFT SIDE DOOR LOCK & HANDLE

SECT

DOOR

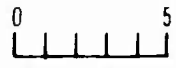
CAM

DOOR EDGES

PRESSURE STOP

GUIDE & NEGATIVE  
PRESSURE ROLLER

**DETAIL I**



SCALE: INCHES

Handwritten mark resembling the number 11.

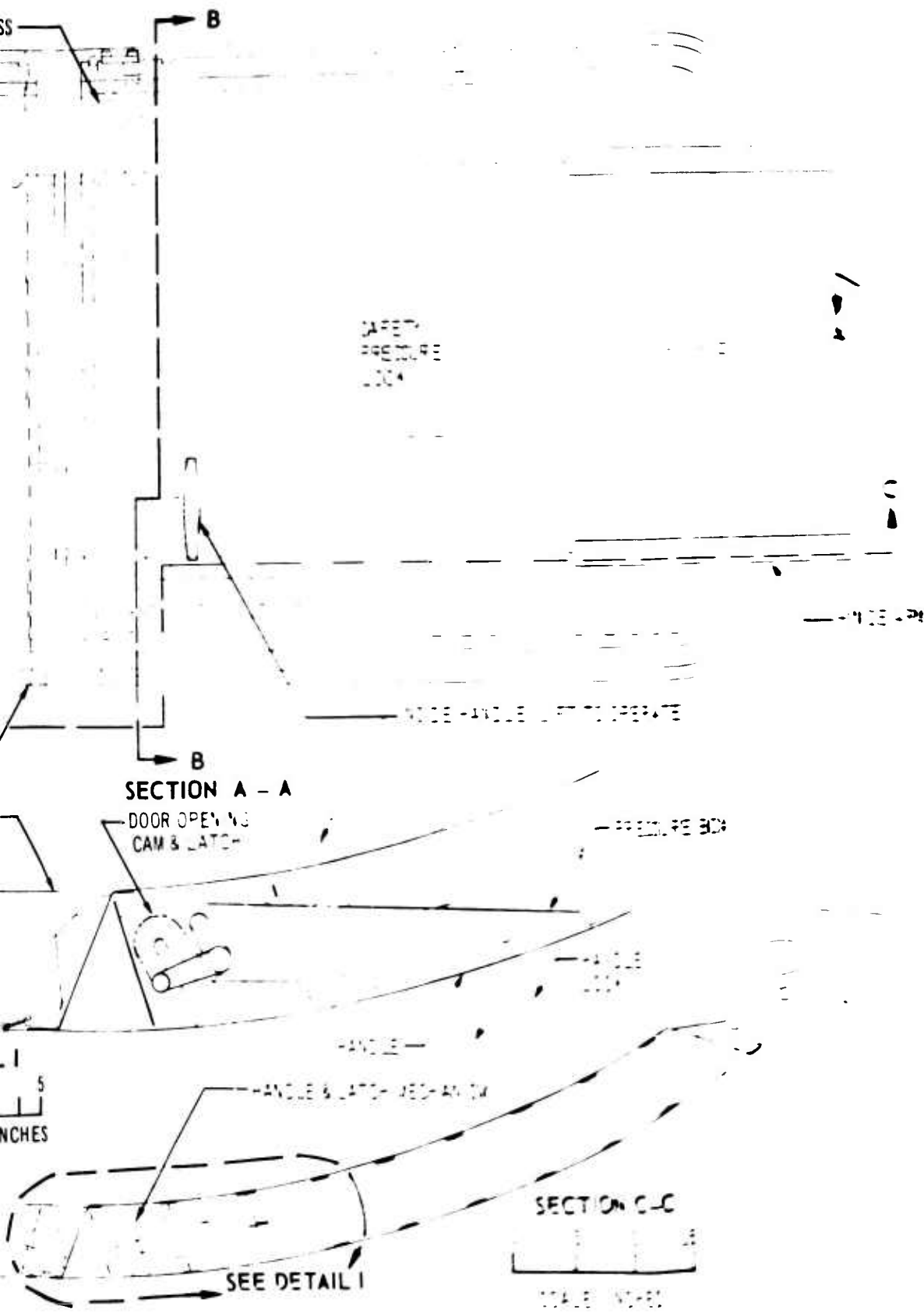
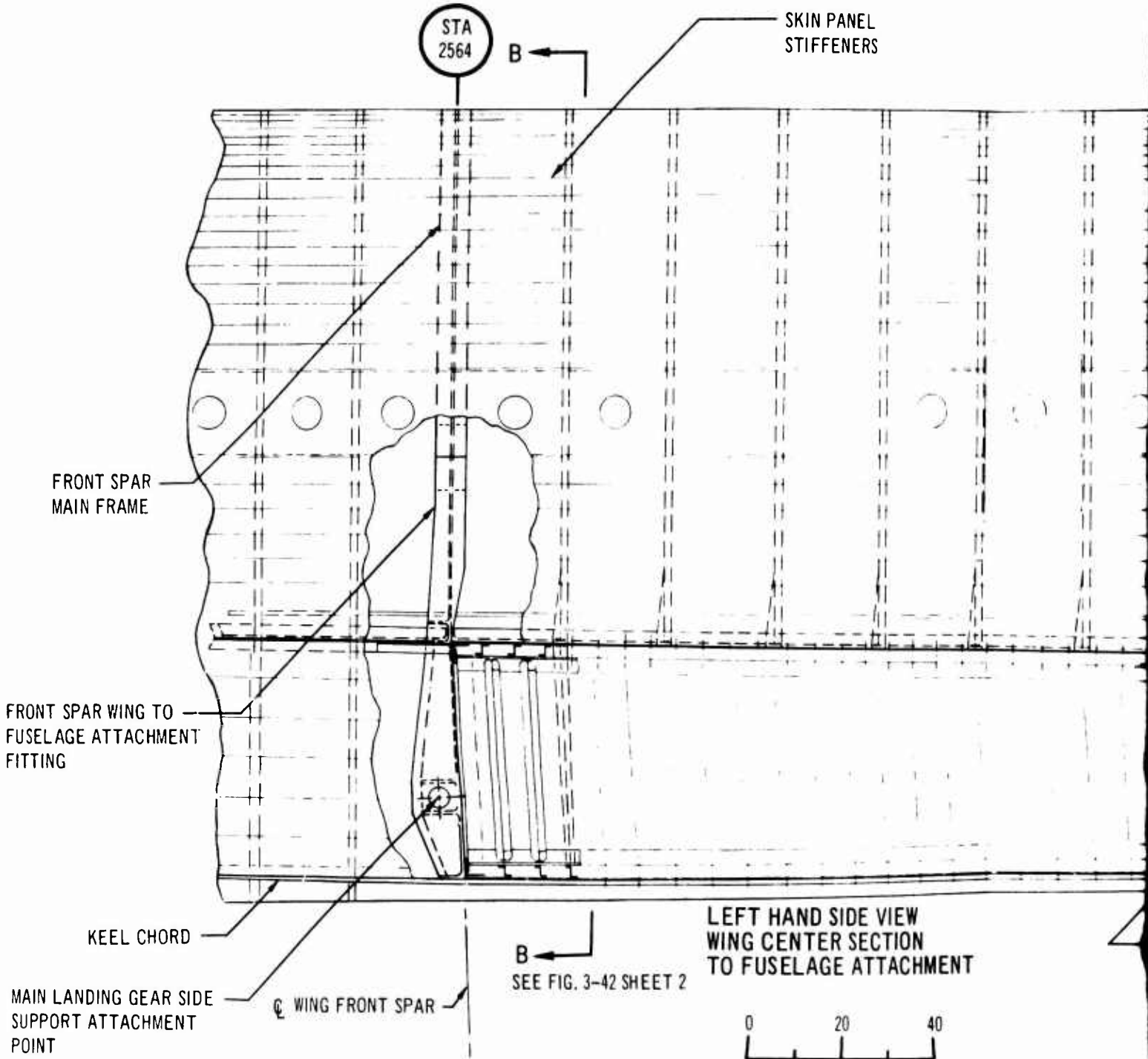
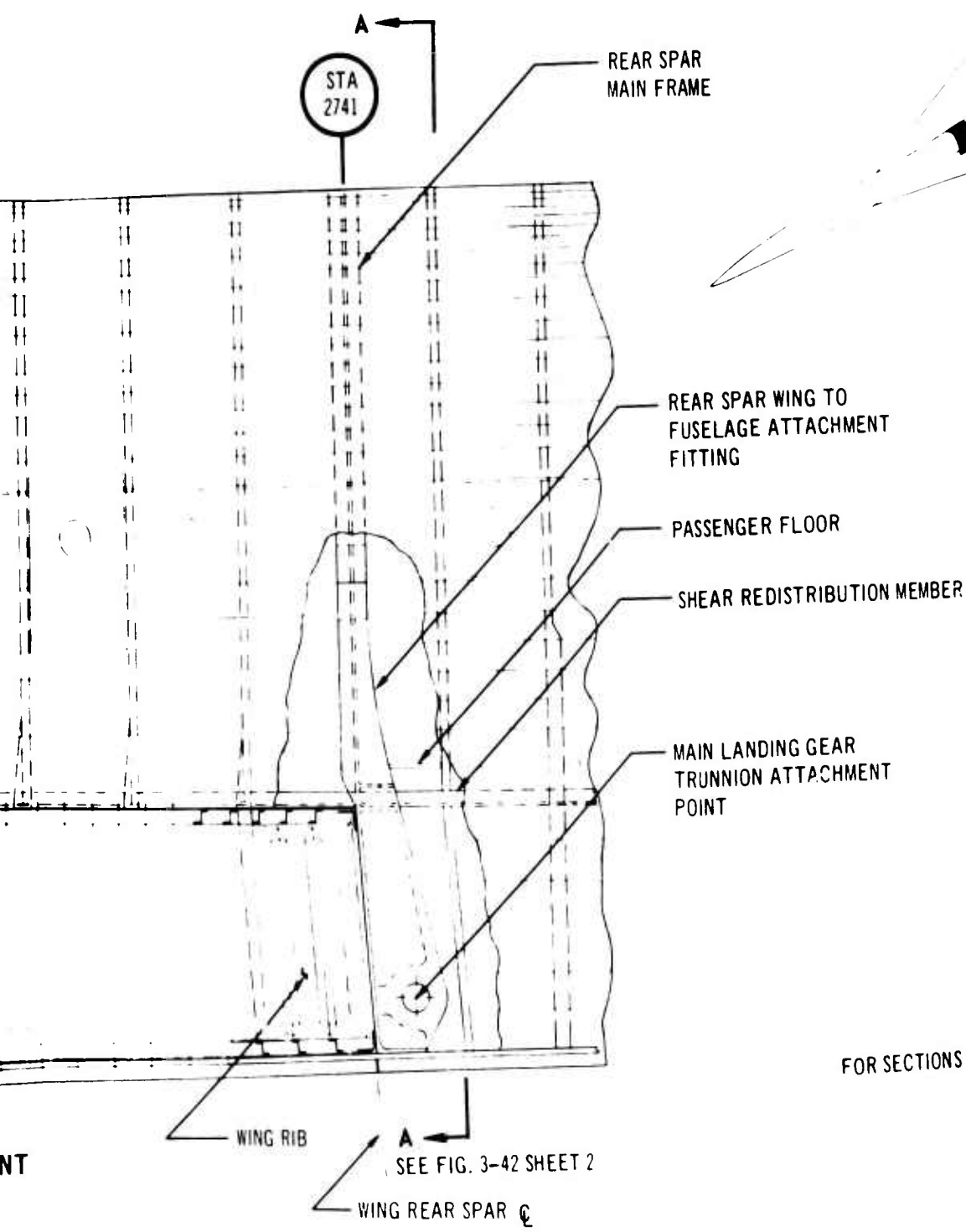


Figure 3-41. Cargo Compartment Door

V2-B2707-6-2



A



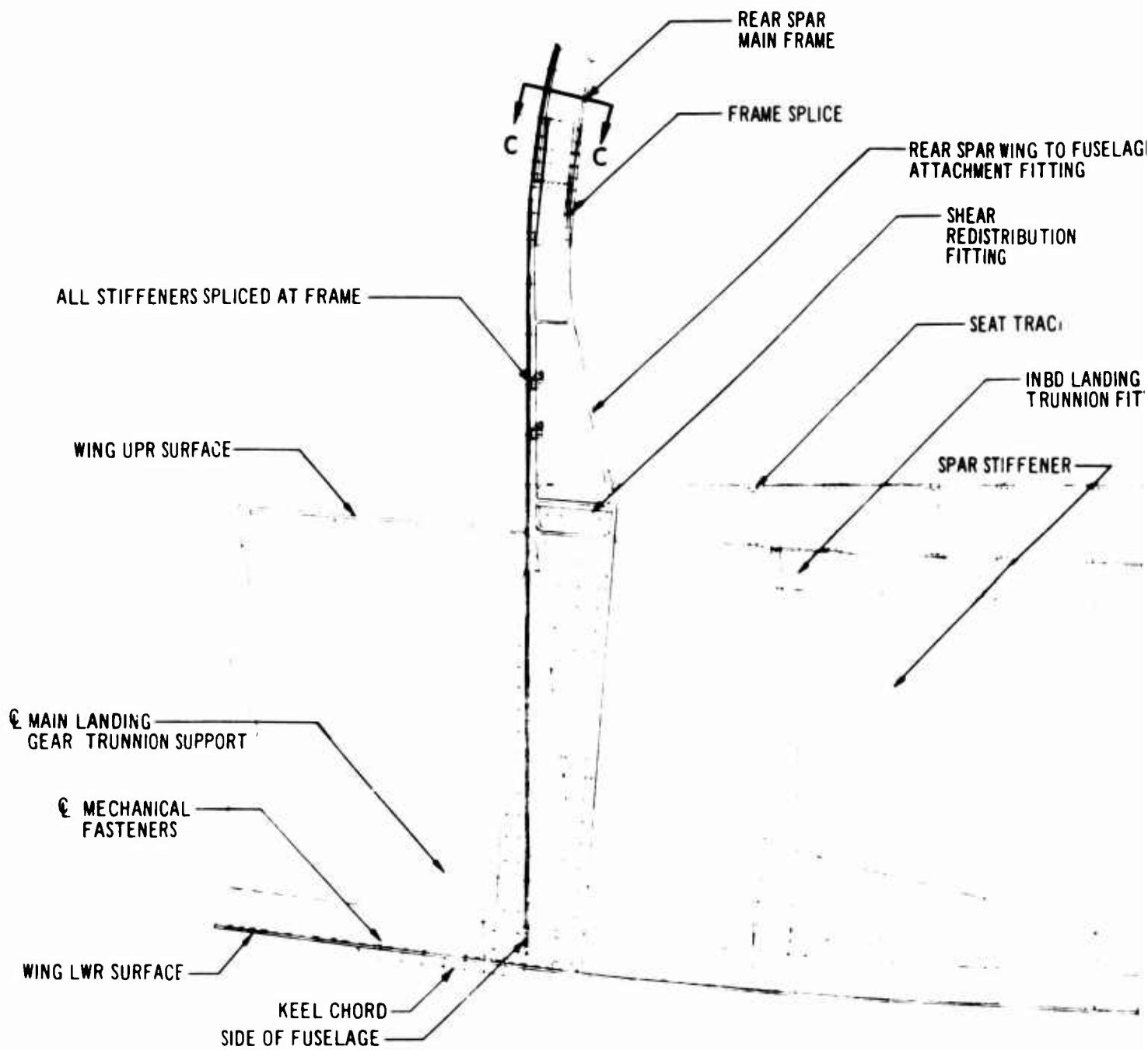
FOR SECTIONS SEE SHEET 2

SEE FIG. 3-42 SHEET 2

B

Figure 3-42. Wing-Center-Section-to-Fuselage Attachment





SECTION A - A  
 REAR SPAR ATTACHMENT

A

AIRPLANE

SECTION C - C

SPAR WING TO FUSELAGE  
ATTACHMENT FITTING

SHEAR  
REDISTRIBUTION  
FITTING

SEAT TRACK

INBOARD LANDING GEAR  
TRUNNION FITTING

SPAR STIFFENER

CABIN FLOOR

CORRUGATED SHEAR WEB  
FLOOR BEAM

UPPER SPAR CHORD

REAR SPAR WEB

MAIN LANDING GEAR  
SIDE SUPPORT FITTING

WING LOWER SURFACE  
LOWER SPAR CHORD

SKIN PANEL STIFFENER

FUSELAGE SKIN

TENSION  
FASTENERS

SHEAR  
REDISTRIBUTION  
MEMBER

WING RIB

FUSELAGE  
FRAME

FRAME SPLICE

SHEAR TIE

INTERMEDIATE  
STUB FRAME  
ATTACHMENT

CABIN  
PRESSURE  
DECK

WING SKIN  
STIFFENER

SECTION B - B

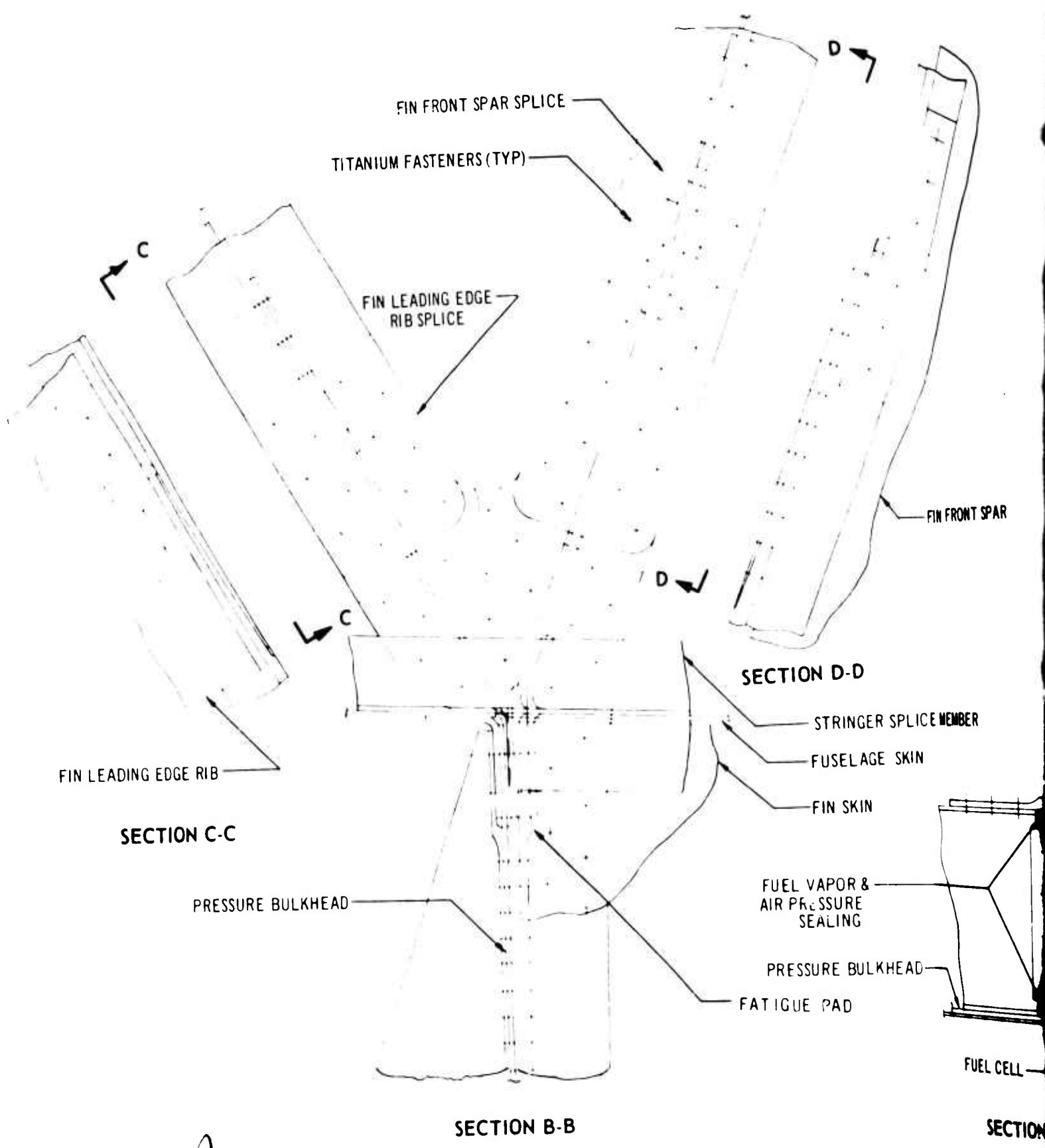
INTERMEDIATE ATTACHMENT FITTING

0 5 10 15  
SCALE: INCHES

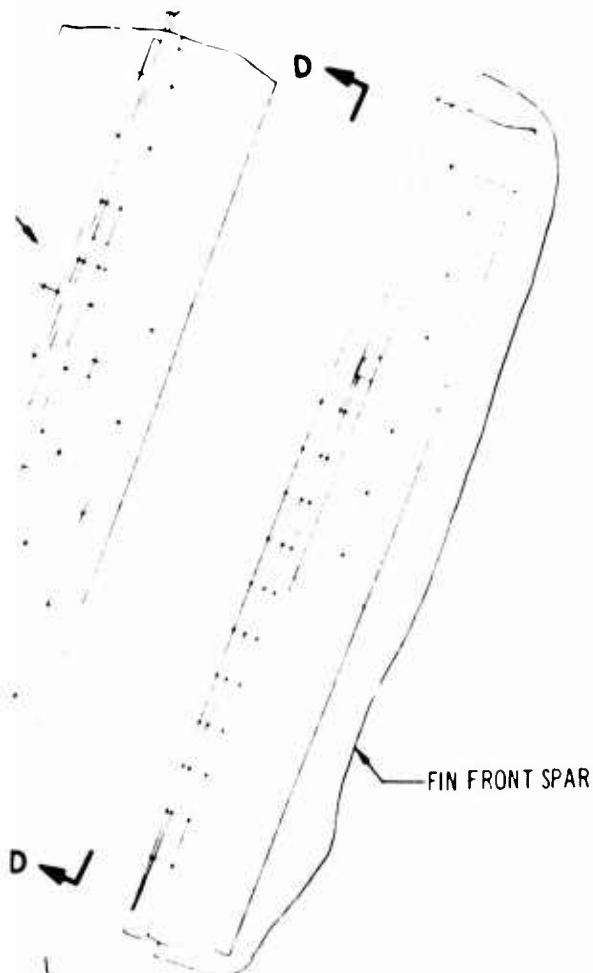
Figure 3-42. (Continued)

V2-B2707-6-2

B



A



SECTION D-D

STRINGER SPLICE MEMBER

FUSELAGE SKIN

FIN SKIN

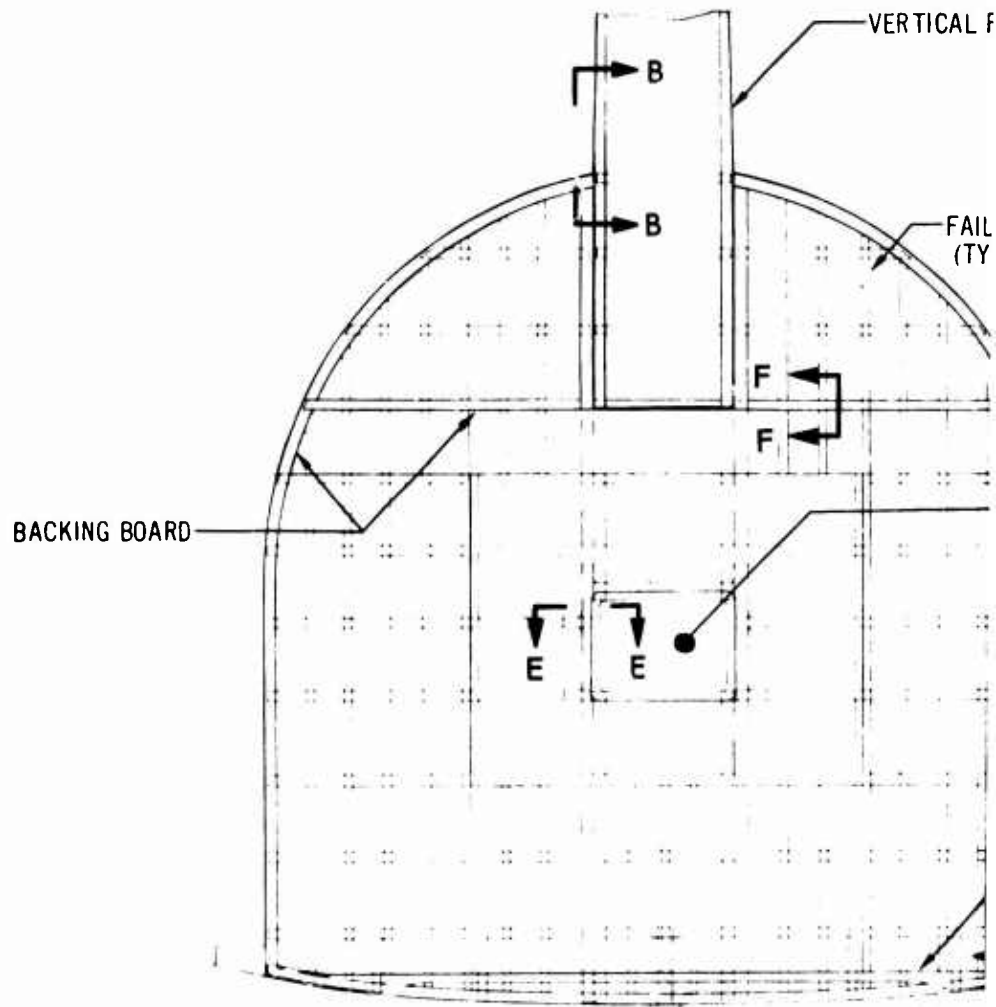
FUEL VAPOR &  
AIR PRESSURE  
SEALING

PRESSURE BULKHEAD

FATIGUE PAD

FUEL CELL

SECTION E-E



BACKING BOARD

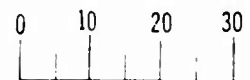
VERTICAL FIN

FAIL (TY

SEE H-H

VENTRAL FIN

FIN FRONT SPAR PRESSURE  
BULKHEAD AT STATION 3405



SCALE: INCHES

SECTION A-A

B

VERTICAL FIN

FAIL SAFE STRAP (TYPICAL)

ACCESS DOORS

BACKING BOARD

H H

BACKING BOARD

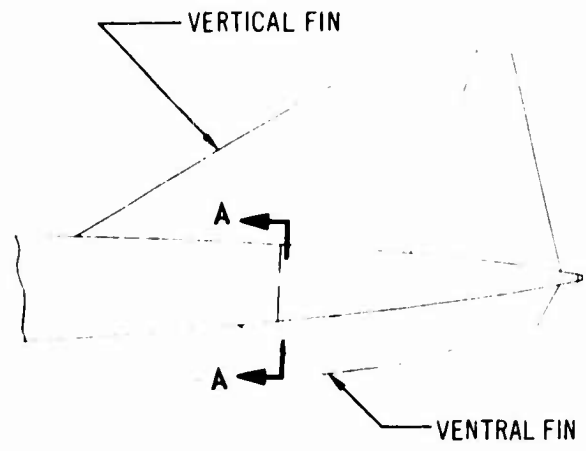
SEE H-H

STABILIZER

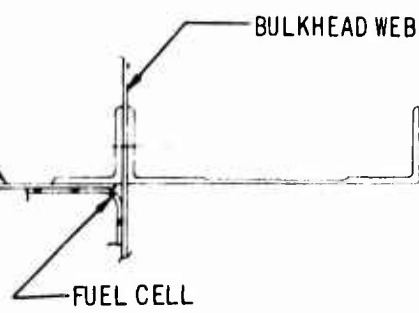
VENTRAL FIN

ASSURE  
ION 3405

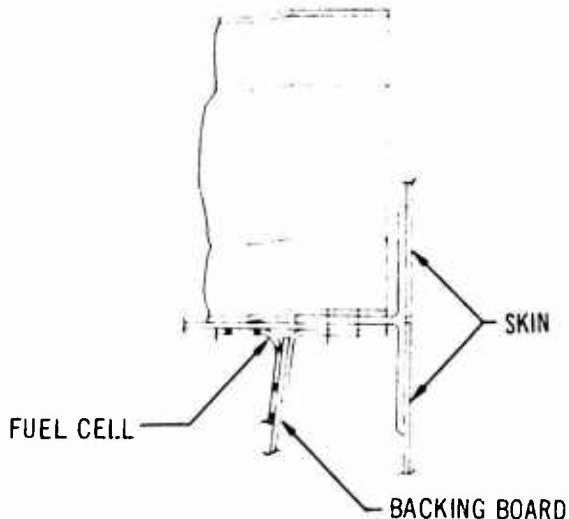
30



NO SCALE



SECTION F-F



SECTION H-H

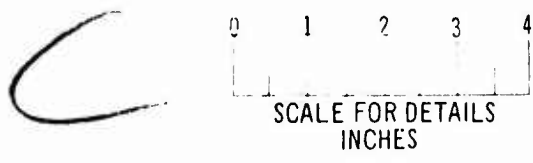
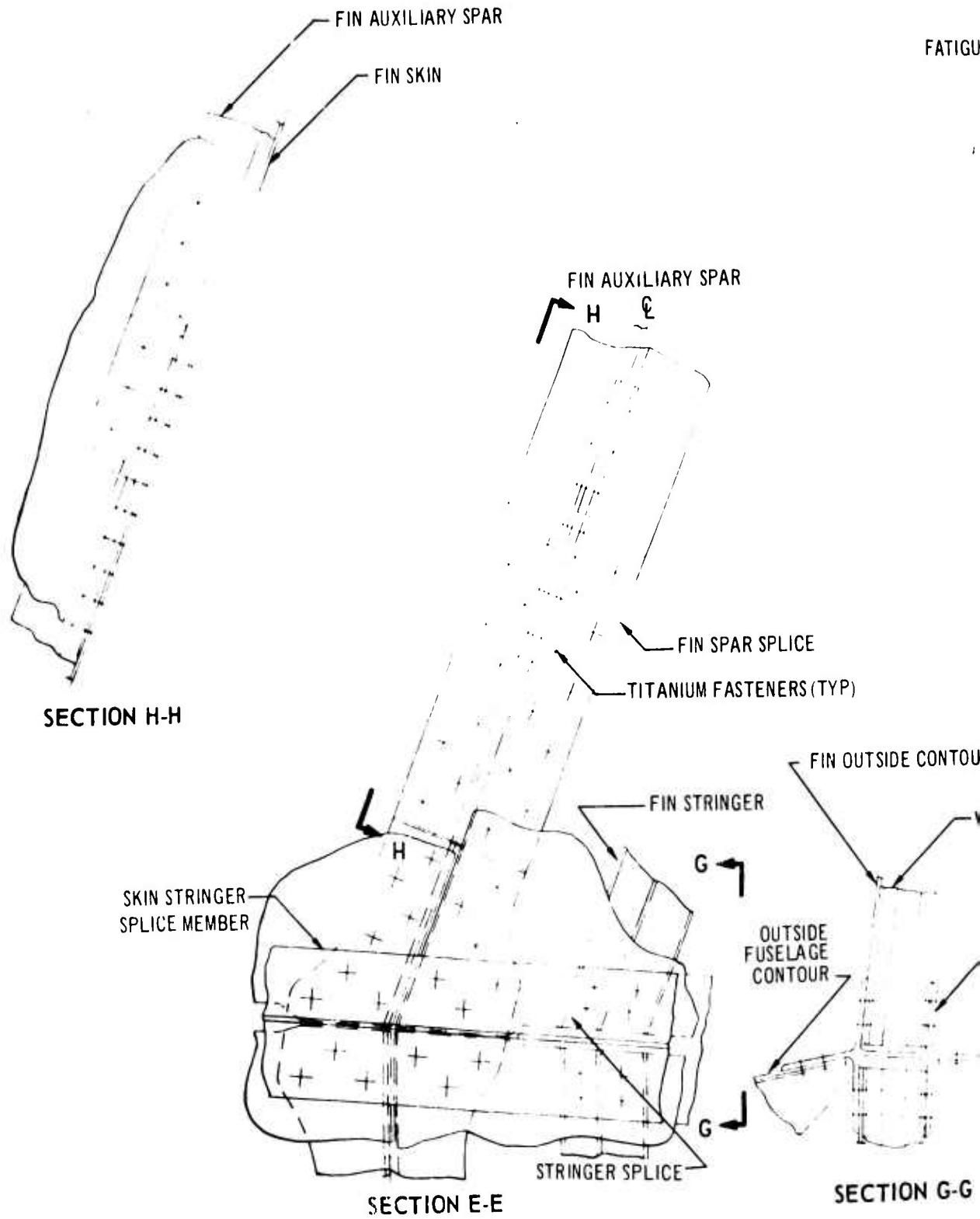
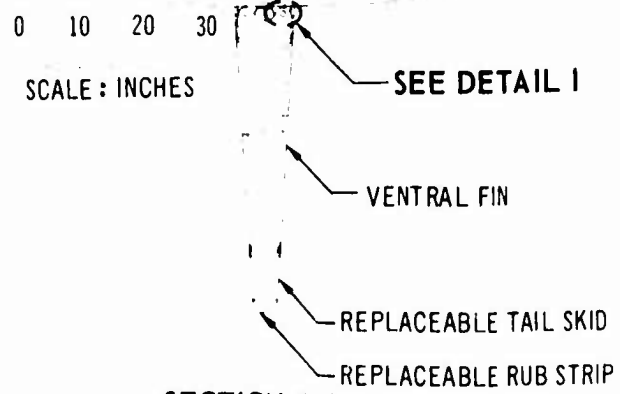
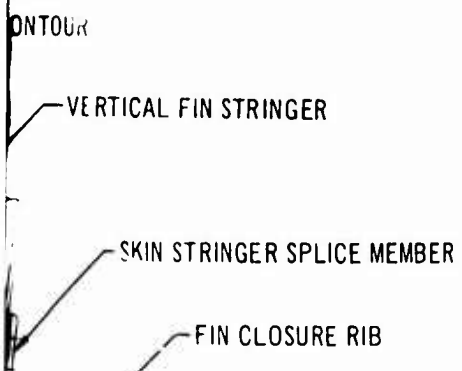
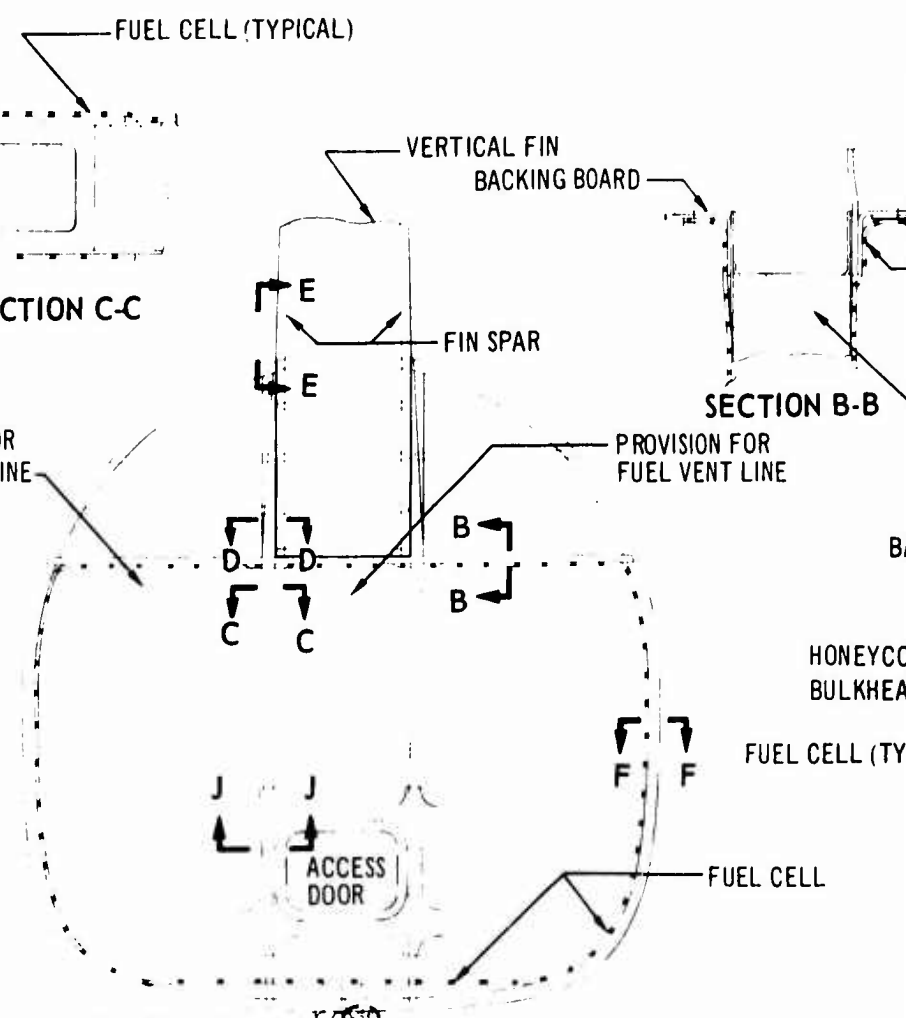
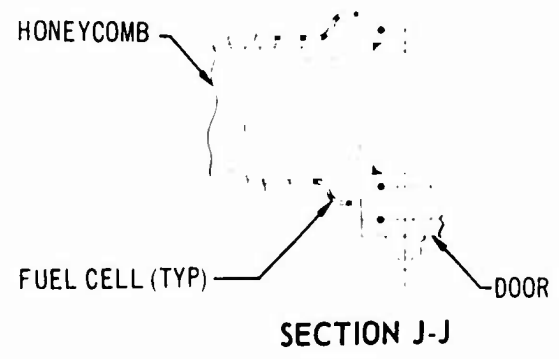
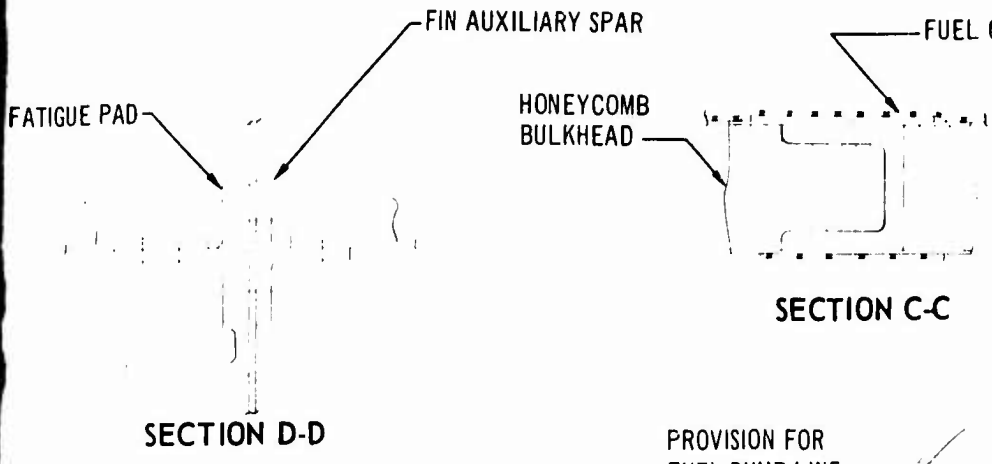


Figure 3-43. Fin-Spar Pressure Bulkhead





SCALE FOR DETAILS: INCHES

0 1 2 3 4

B

YPICAL)

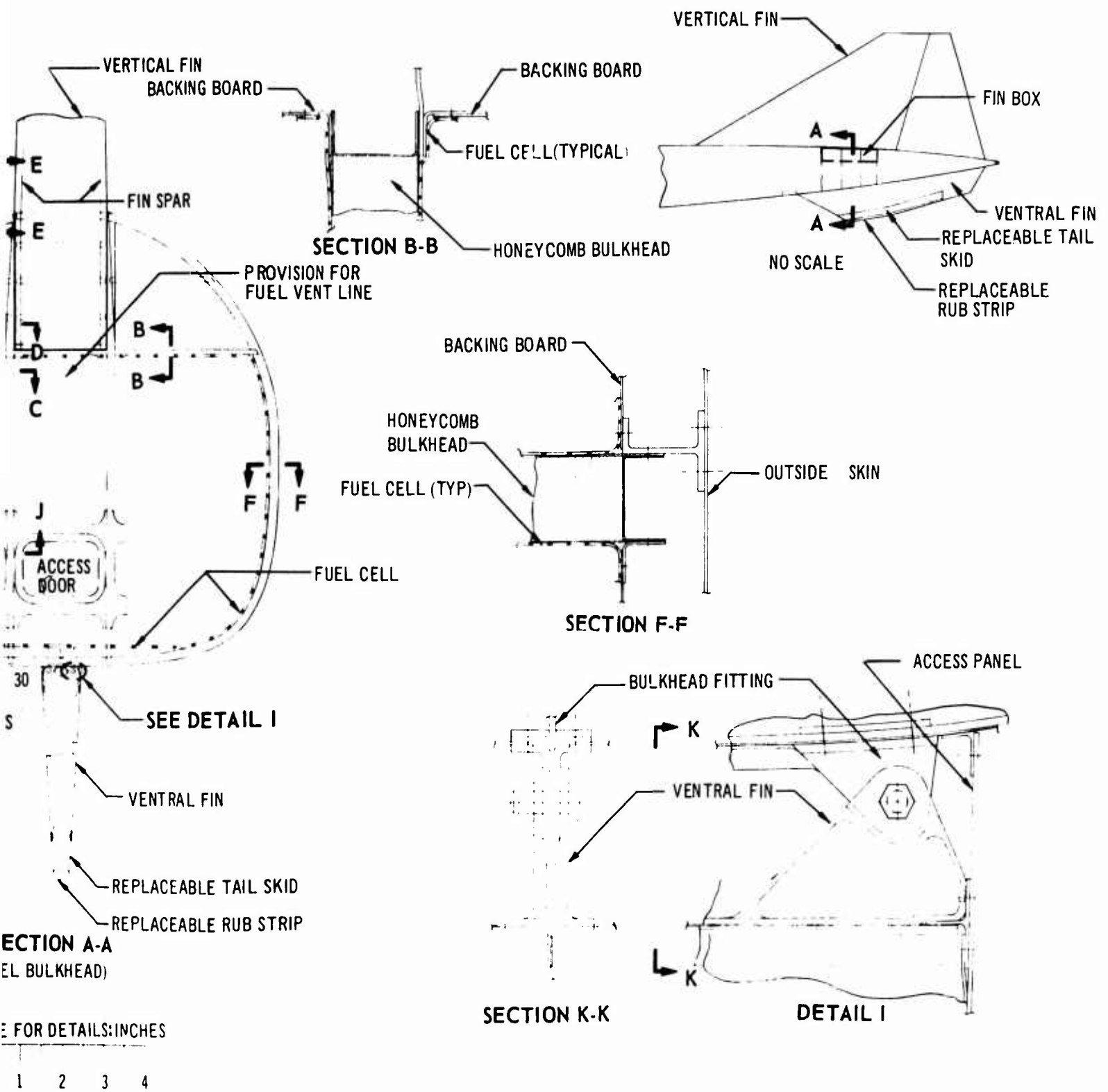


Figure 3-44. Fin-Spar Fuel Bulkhead

C



efficient structure and integral fuel-storage capacity.

Engine sonic and thermal exposure of the stabilizer has been minimized by the aft placement of the engines. Sonic level exposure is shown in Part C, Design Criteria, Loads, Aerodynamic Heating, Flutter (V2-B2707-7), of the Airframe Design Report. Sonic resistance is provided by stiffened skins and honeycomb panels. Adequacy of the structure to withstand sonic environment is demonstrated by testing as shown in Part E, Structural Tests (V2-B2707-9), of the Airframe Design Report.

### 3.3.1 Structural Box

A three-spar structural box allows the use of efficient skin-stringer construction as load-carrying surfaces as shown in Fig. 3-45. Fail safety is provided by multiple panels on both upper and lower surfaces and by multiple attachments to body frames and bulkheads. Rib design utilizes sine wave construction to provide efficient lightweight structure. Where concentrated loads are applied, ribs are constructed of chords and stiffened shear webs with machined forgings. Mechanical fasteners are used for assembly means. Access is provided to all areas for maintenance and for inspection and repair.

The structure of the primary box closely resembles Boeing subsonic wing structure in type of construction and general design and integral fuel tank requirements.

The stabilizer carry-through structure within the fuselage is a continuation of the box structure design. It contains integral fuel and is sealed both internally and externally to provide a double seal. Body pressure loads are transmitted to the stabilizer structure by supports from the cargo deck.

### 3.3.2 Leading Edge

Widely spaced ribs in the leading-edge area allow systems installation. Honeycomb panels span these ribs to provide lightweight covers with excellent aerodynamic smoothness. The extreme leading edge of the stabilizer, which is protected by the wing during high-speed conditions, has chem-milled sculptured skins for hail resistance at low speeds. This feature is similar to that of the wing leading edge of the 707, which has extra thickness on the leading edge. Honeycomb access doors on the lower surface are de-

signed to give access for maintenance of systems and structures as shown in Fig. 3-46. The depth of the stabilizer gives adequate space for systems routing and easier maintenance.

### 3.3.3 Interconnect Structure

The interconnect fittings, as shown in Fig. 3-47, ensure wing-to-stabilizer alignment when the wings are swept aft. Each fitting is supported on two ribs which form the sides of a torsion box. These ribs also support large systems installations and the leading-edge cover panels.

### 3.3.4 Elevator Structure and Support

The elevator cross section is shown in Fig. 3-45. Hinges and actuators are located to provide maximum mechanical advantages. The multiple hinges and actuator supports provide fail-safe design. Access panels in machine-sculptured skins provide for servicing actuators and controls. Honeycomb panels and sine wave ribs are efficient, lightweight components of the elevator torsion box.

### 3.3.5 Engine Support

Engine support is provided by fittings attached to the structural box as shown in Fig. 3-48 (GE) and 3-49 (P&WA). Space within the diverter between engine and stabilizer is used to obtain maximum depth support beams for increased structural efficiency.

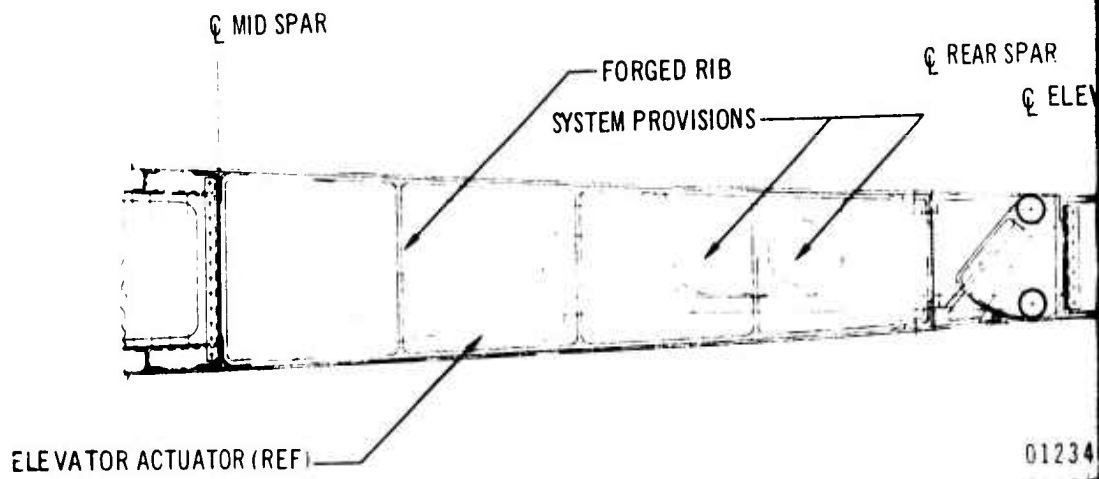
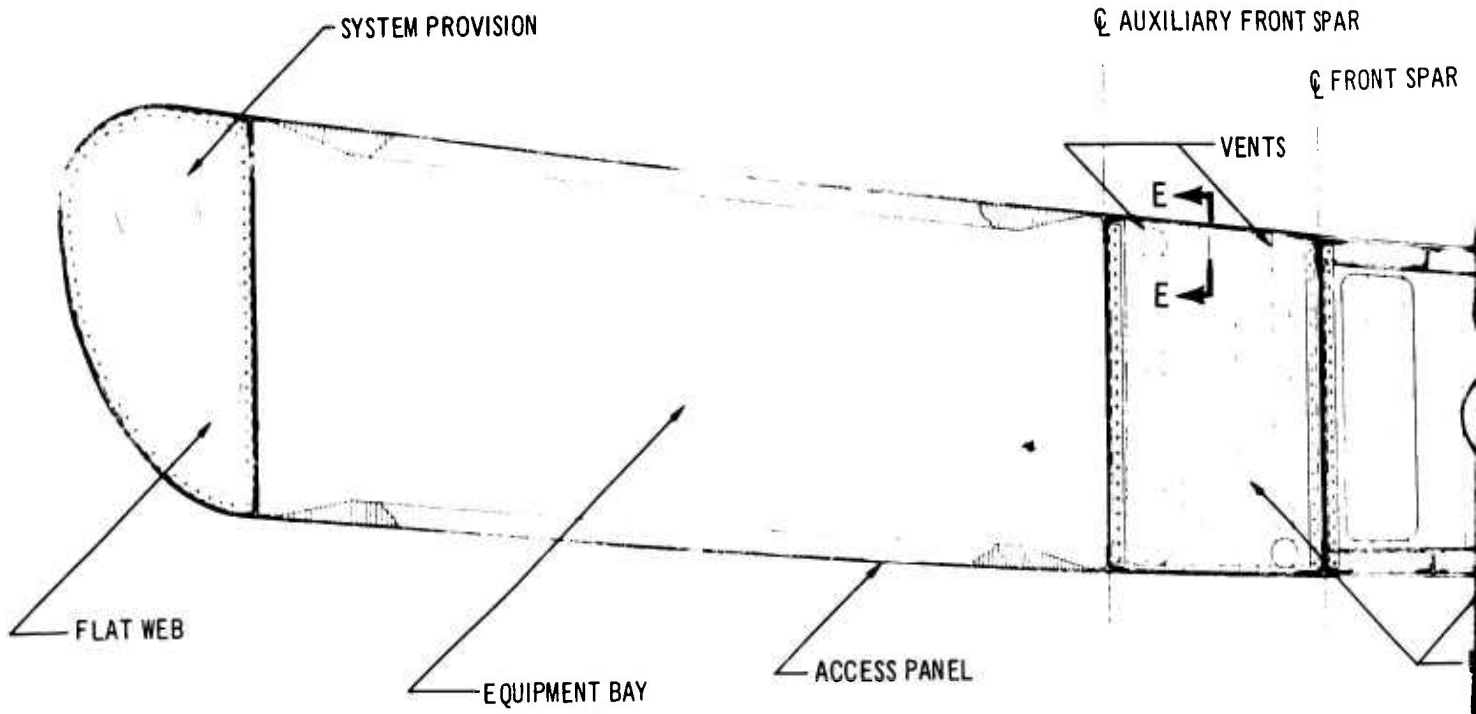
For extreme landing or engine seizure conditions, the nacelles are designed to break free from the box structure without damaging the fuel tank.

### 3.3.6 Elevon Structure Support

The tip elevon support structure as shown in Fig. 3-50 is designed with double ribs at both support points. Each rib has multiple bearings in multiple lugs to provide fail-safe design. The actuator arms extend above the stabilizer surface to provide rigidity to the actuation system and adequate moment capability. The actuators are anchored to the structural box and the system is covered by an aerodynamic fairing. Access to the actuators is by removing sections of the fairing. The elevon is a multispar box with nonbuckling covers as primary structure. Honeycomb panels, supported on ribs, and full-depth honeycomb leading and trailing edges complete the structure.

## 3.4 VERTICAL AND VENTRAL FINS

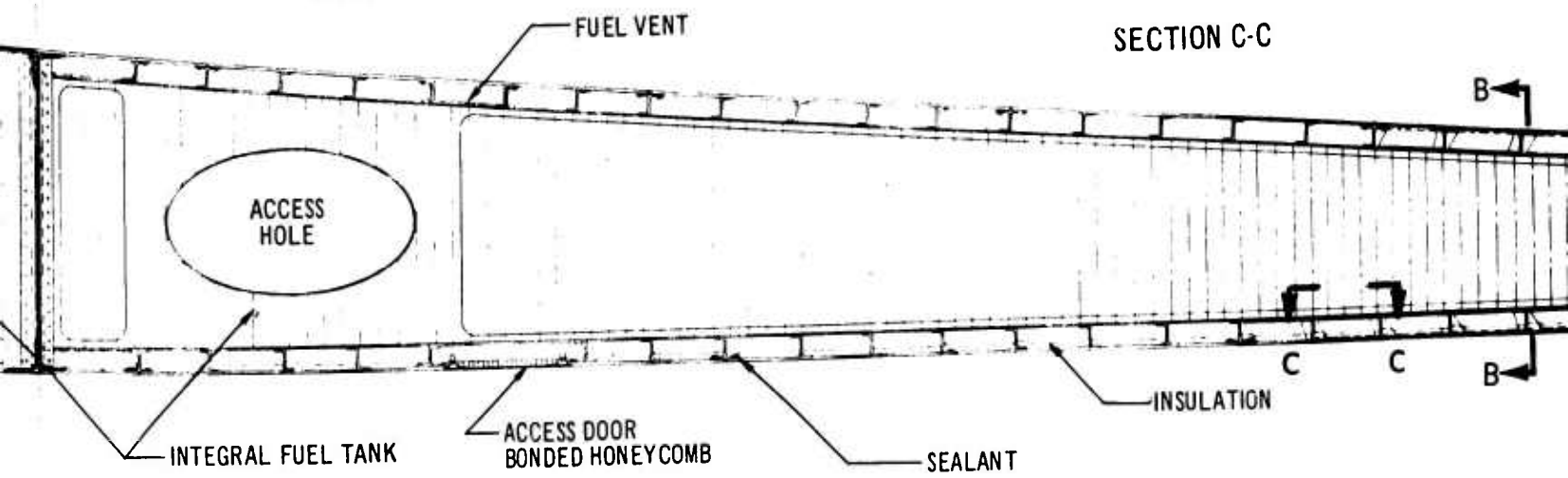
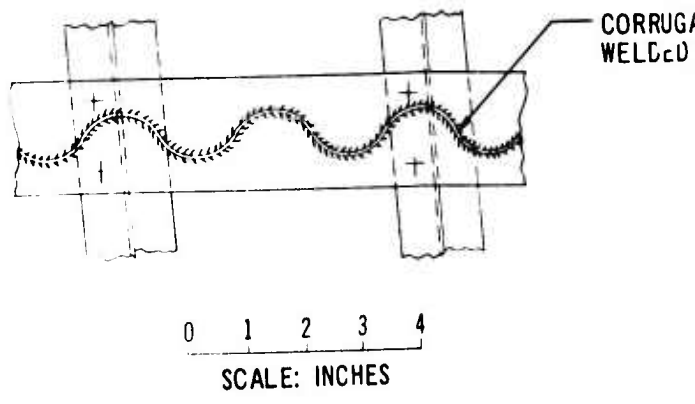
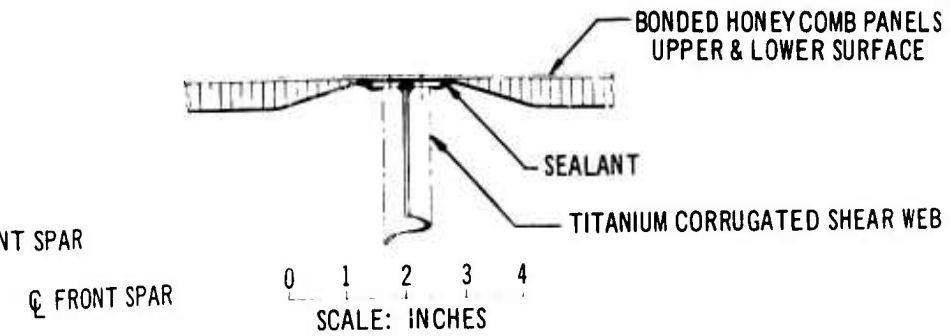
The general arrangement of the fins is shown in Fig. 3-51. The vertical fin is attached to the



01234

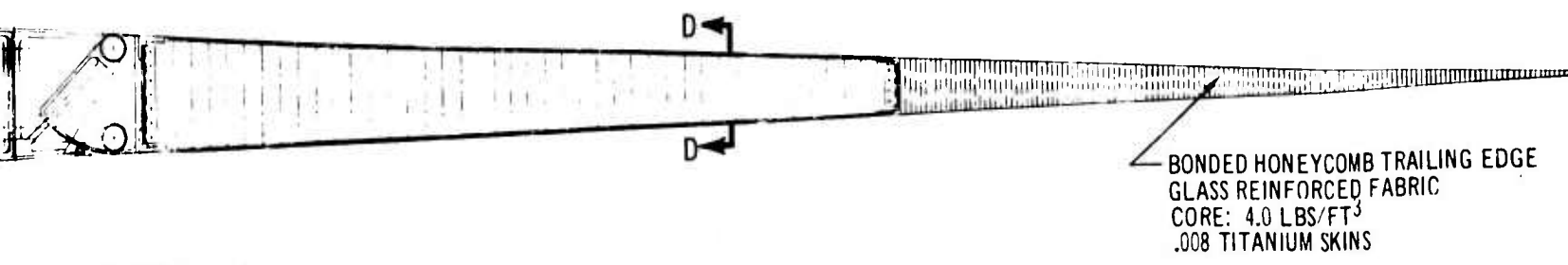
SCALE:  
SECTION

A



0 1 2 3 4 5 10  
 SCALE: INCHES  
 SECTION A-A CONTINUED

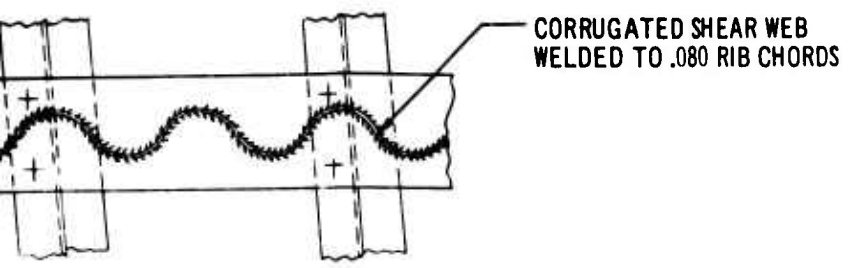
REAR SPAR  
 ELEVATOR HINGE



0 1 2 3 4 5 10  
 SCALE: INCHES  
 SECTION A-A

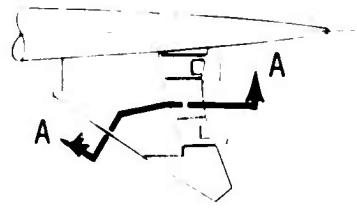
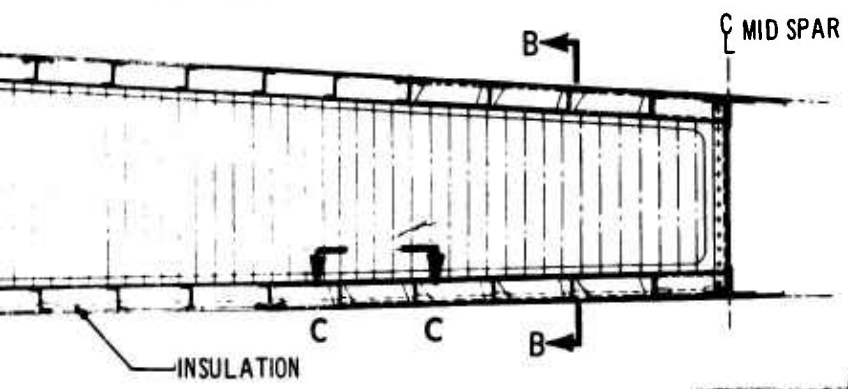
B

Figure 3-45.



0 1 2 3 4  
SCALE: INCHES

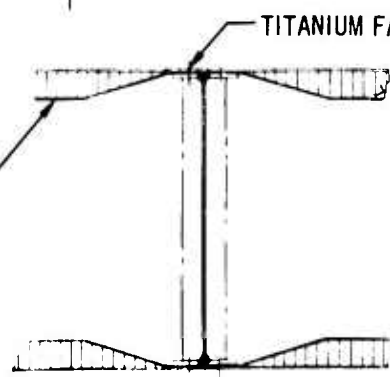
SECTION C-C



TITANIUM  
FASTENERS



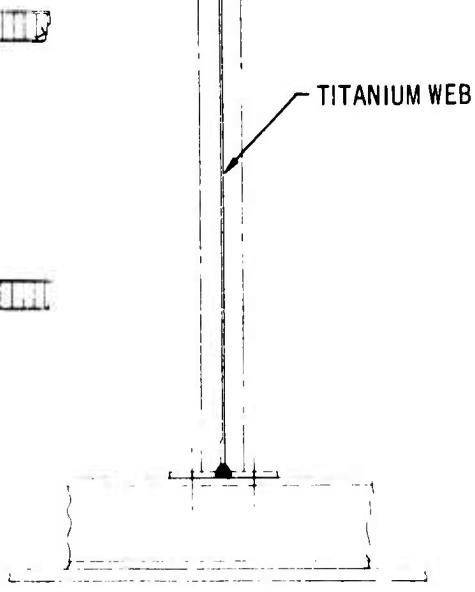
BONDED HONEYCOMB



0 1 2 3 4  
SCALE: INCHES

SECTION D-D

TITANIUM WEB



0 1 2 3 4  
SCALE: INCHES  
SECTION B-B

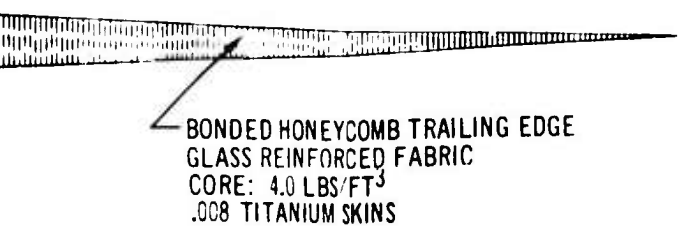
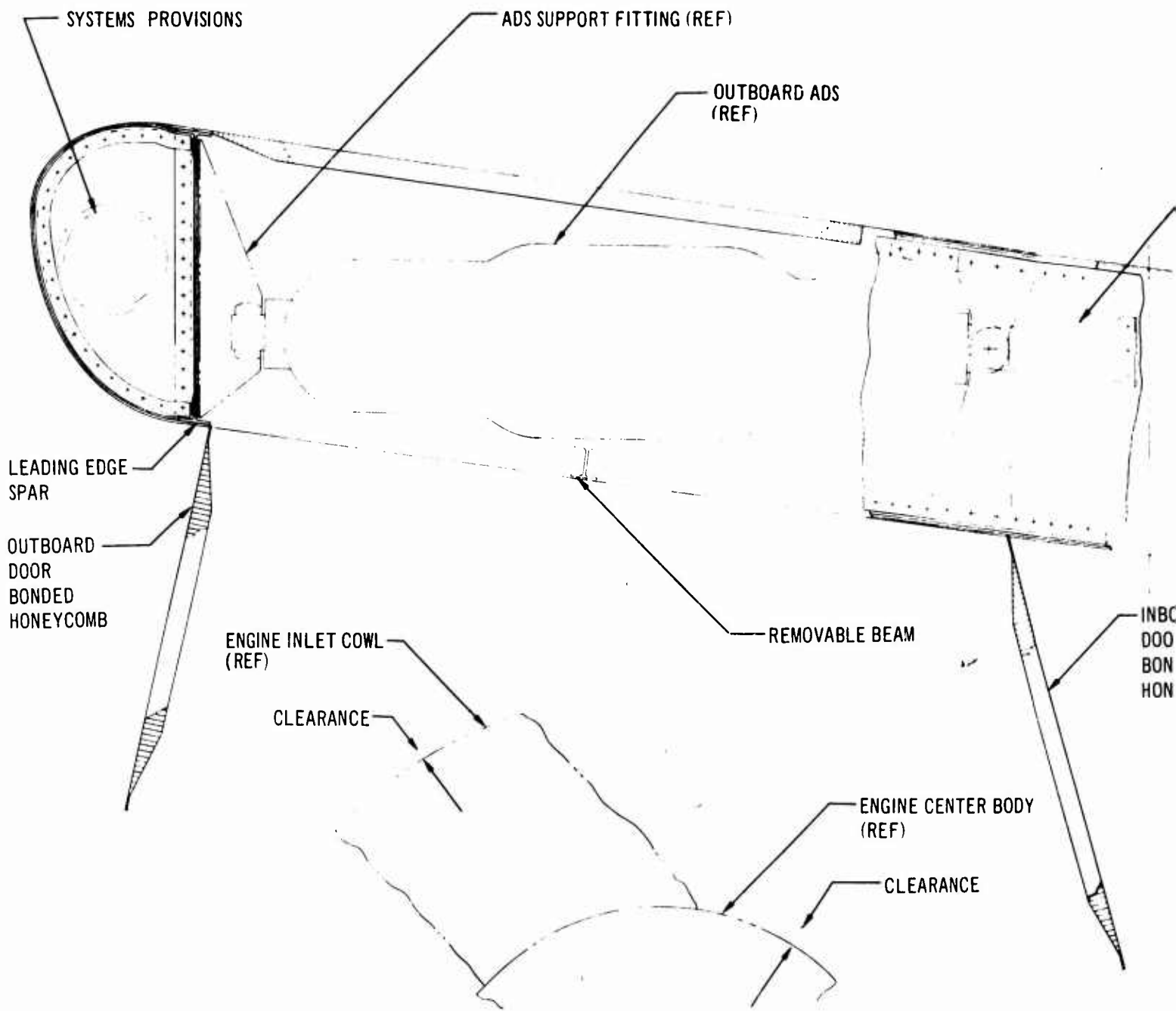


Figure 3-45. Stabilizer Structure Details

V2-B2707-6-2



SYSTEMS PROVISIONS

ADS SUPPORT FITTING (REF)

OUTBOARD ADS (REF)

LEADING EDGE SPAR

OUTBOARD DOOR BONDED HONEYCOMB

ENGINE INLET COWL (REF)

REMOVABLE BEAM

INBOARD DOOR BONDED HONEYCOMB

CLEARANCE

ENGINE CENTER BODY (REF)

CLEARANCE

0 5 10  
SCALE: INCHES

SECTION A - A

A

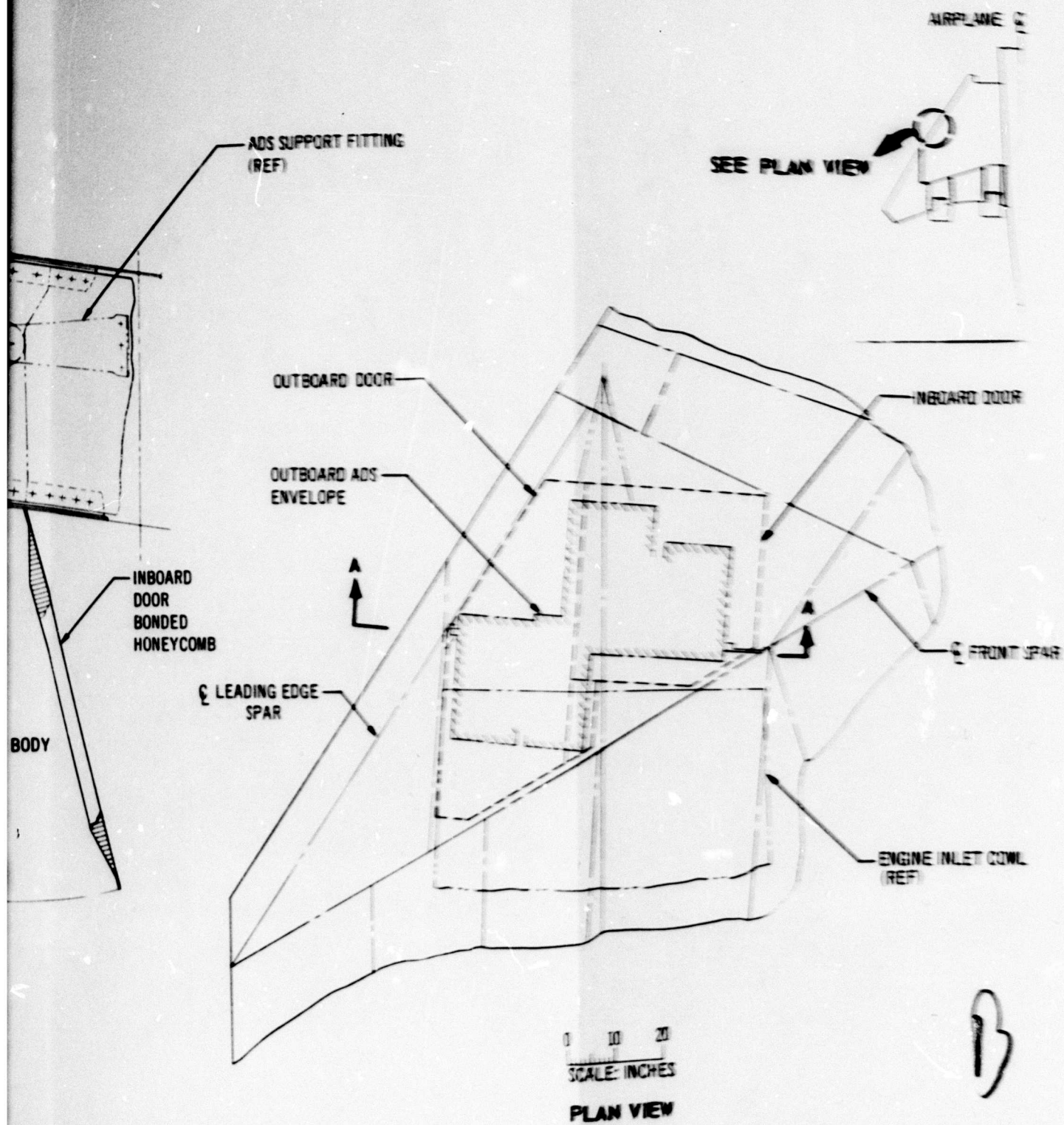
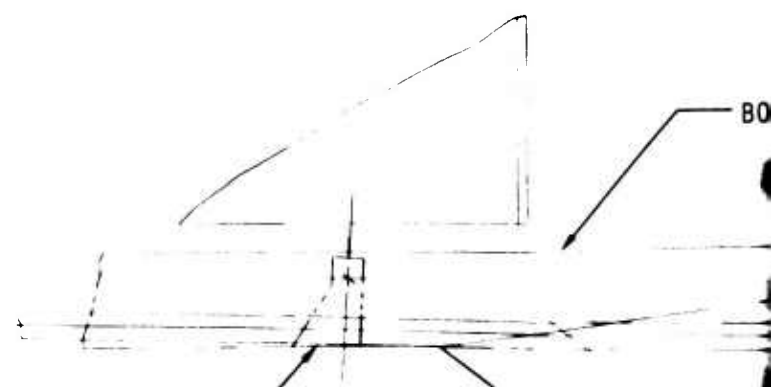


Figure 3-46. Installation and Access of Outboard Auxiliary Drive System

V2-B2707-6-2



INTERCONNECT FITTING  
INBOARD

LEADING EDGE  
BEAM

☉ SUPPORT  
INTERC

AUX. SPAR ☉

☉ FRONT SPAR

SUPPORT FITTING

INTERCONNECT  
STABILIZER

TITANIUM

☉ LEADING EDGE  
BEAM

B

B

SUPPORT FITTING

0 2 4 8

SCALE: INCHES

SECTION A-A

WEAR PLATE

0 2 4

SCALE: INCHES

SECTION

A

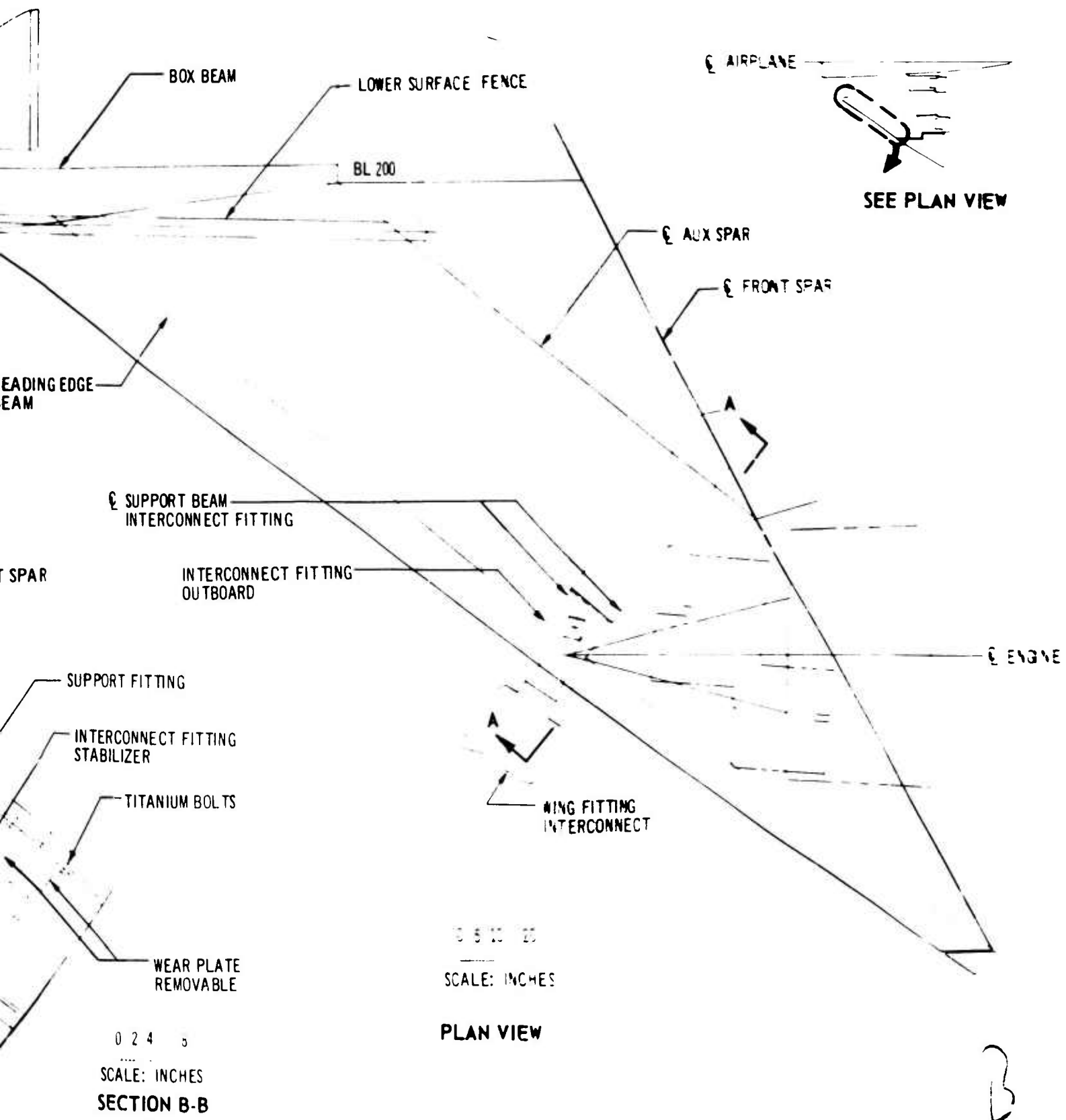


Figure 3-47. Wing-Stabilizer Interconnect



☉ SUPPORT RIB

☉ FRONT SPAR

MID SPAR

FRONT SPAR

TITANIUM FASTENERS (TYP)

ENGINE ATTACH POINT

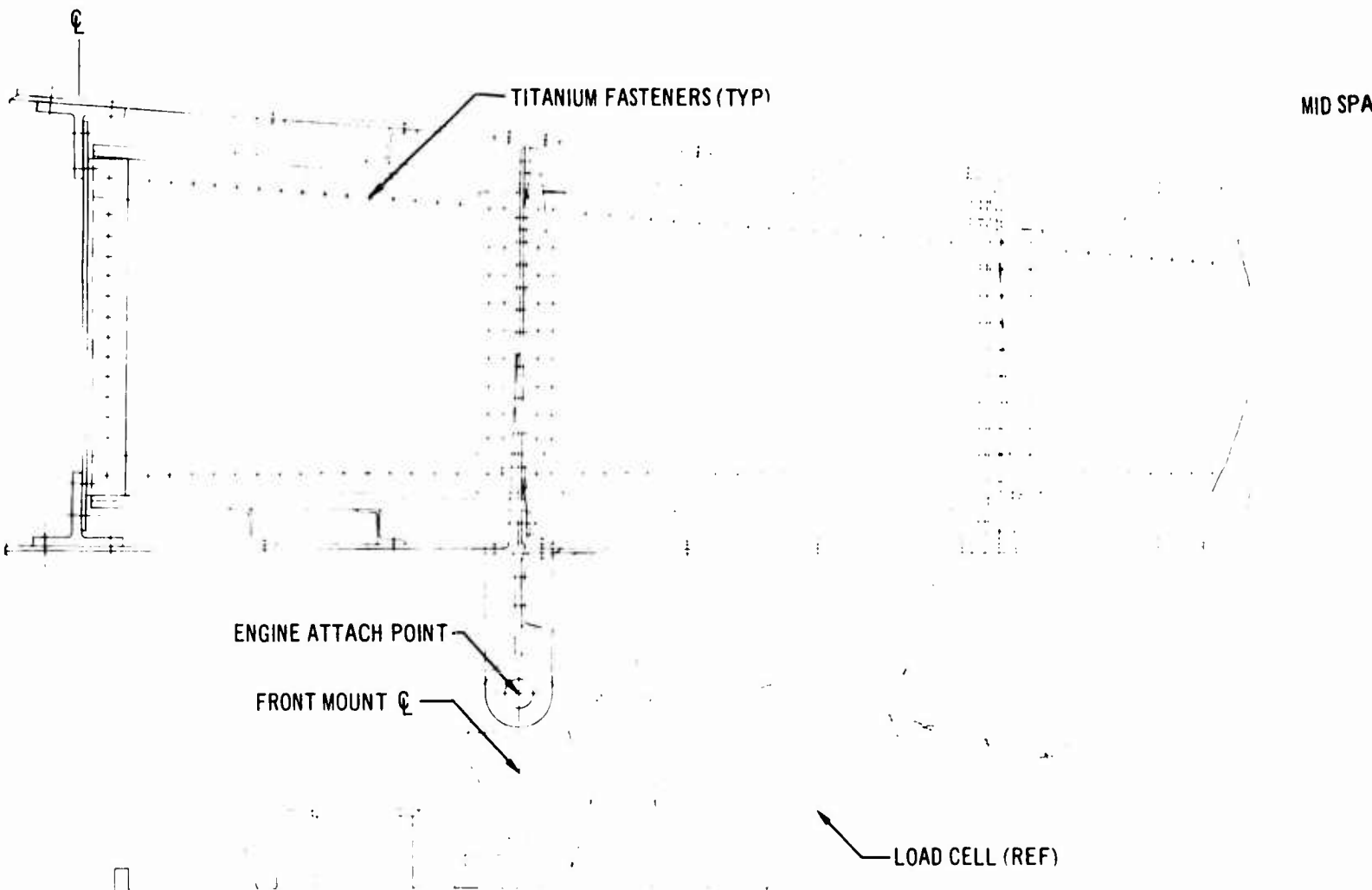
FRONT MOUNT ☉

LOAD CELL (REF)

0 5

SCALE: INCHES  
SECTION A-A

A



☞ SUPPORT RIB

☞ FRONT SPAR

FRONT SPAR

MID SPAR

TITANIUM FASTENERS (TYP)

ENGINE ATTACH POINT

FRONT MOUNT ☞

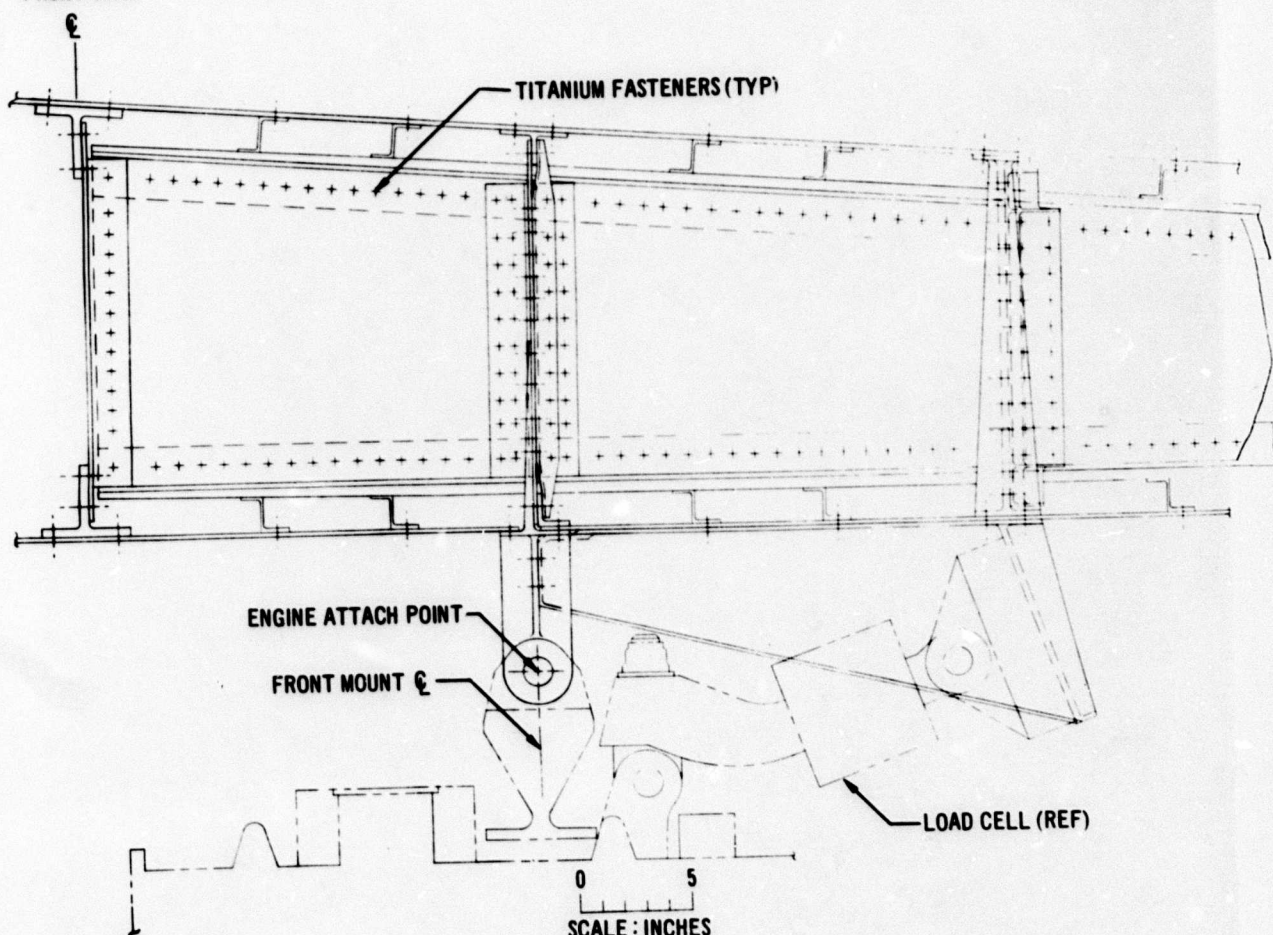
LOAD CELL (REF)

0 5

SCALE : INCHES

SECTION A-A

A



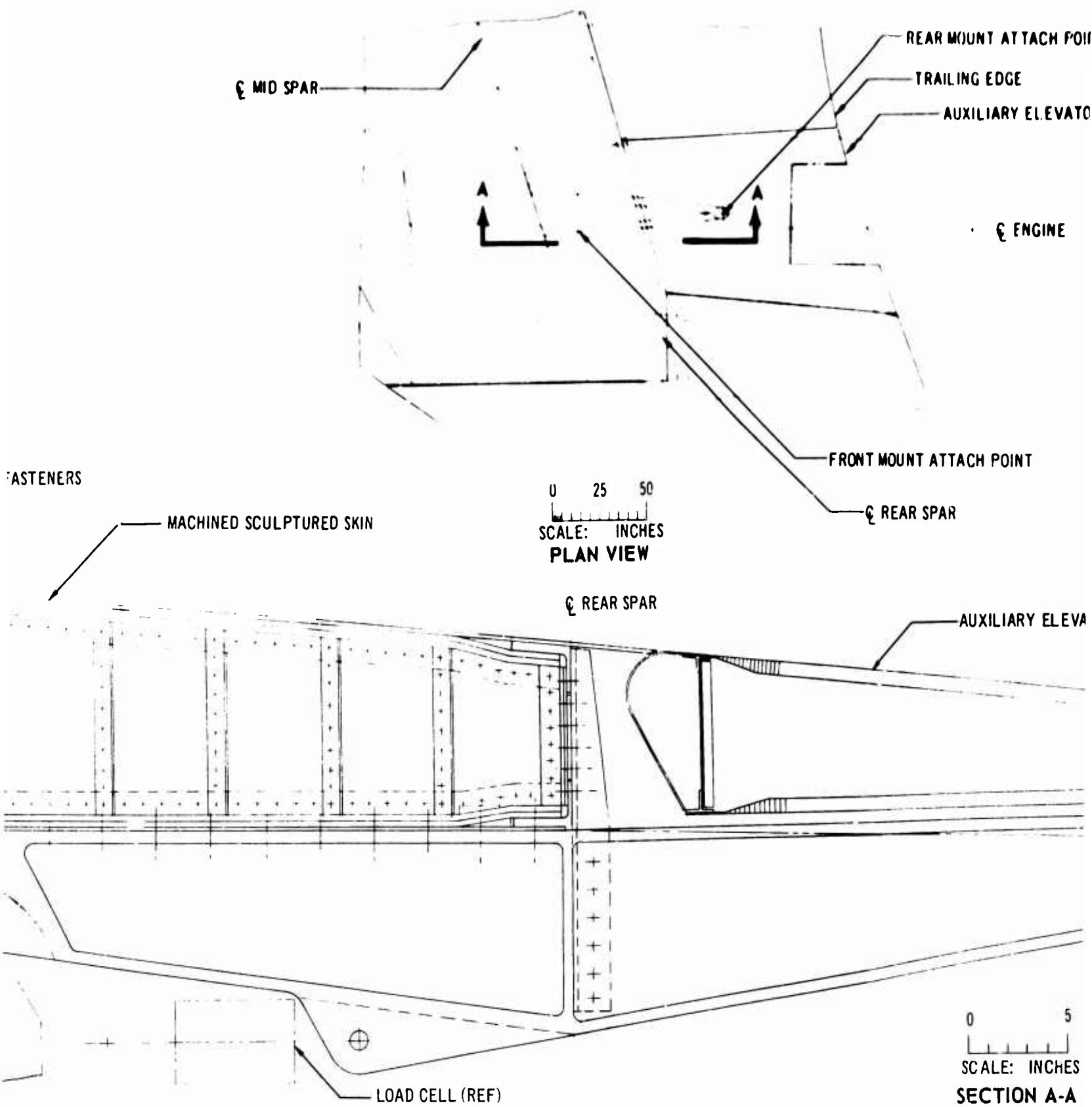


Figure 3-

B

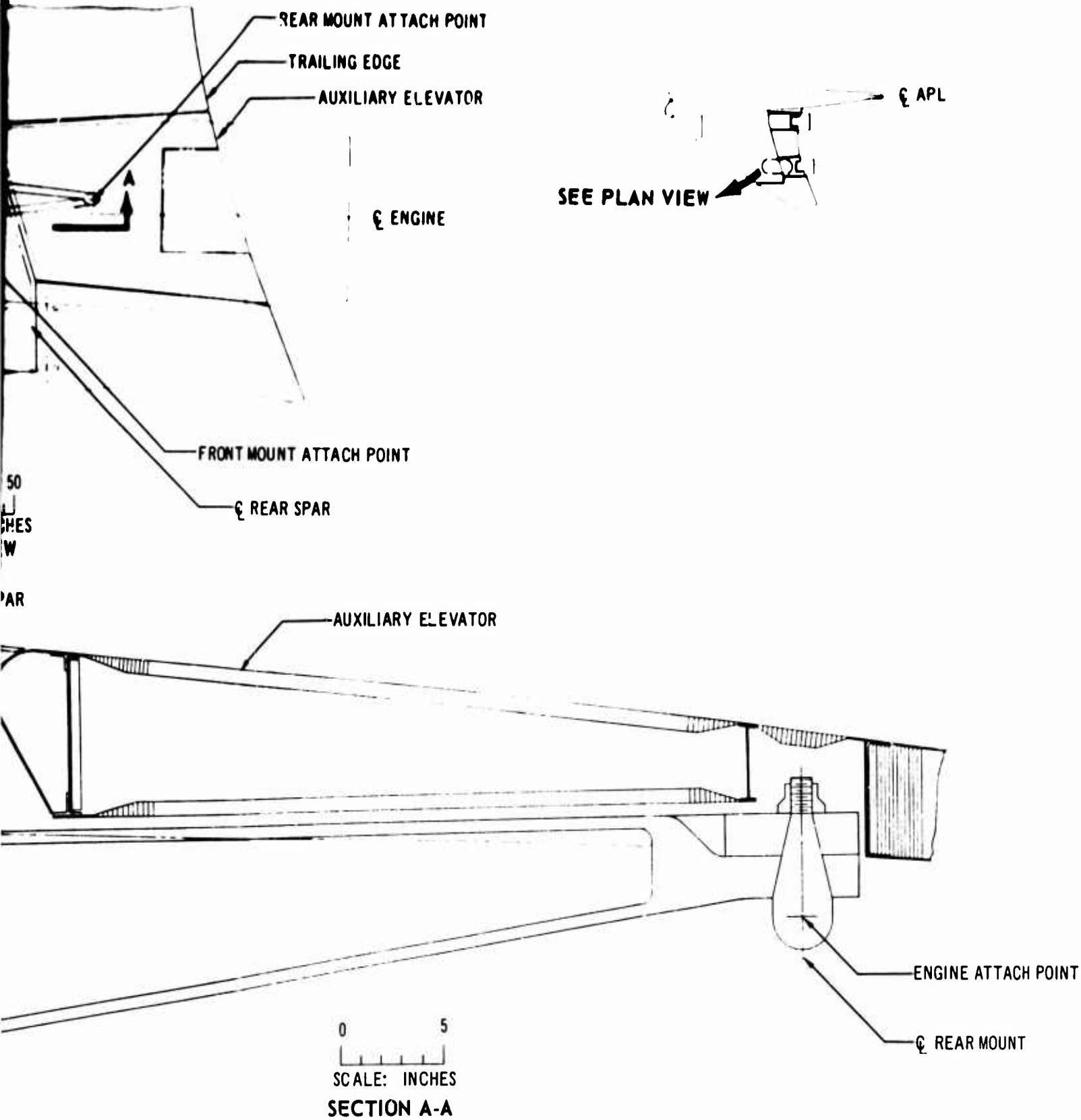
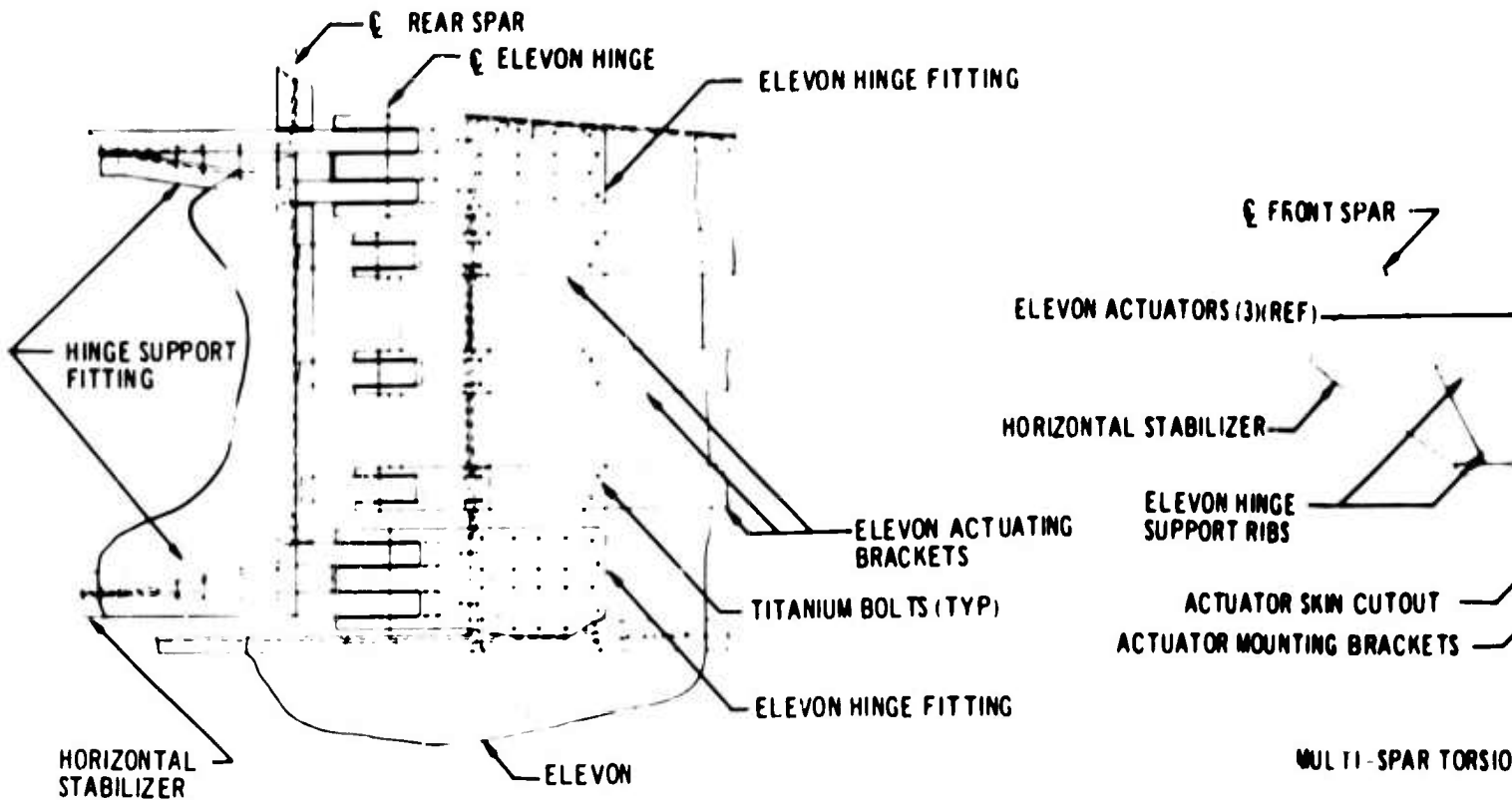
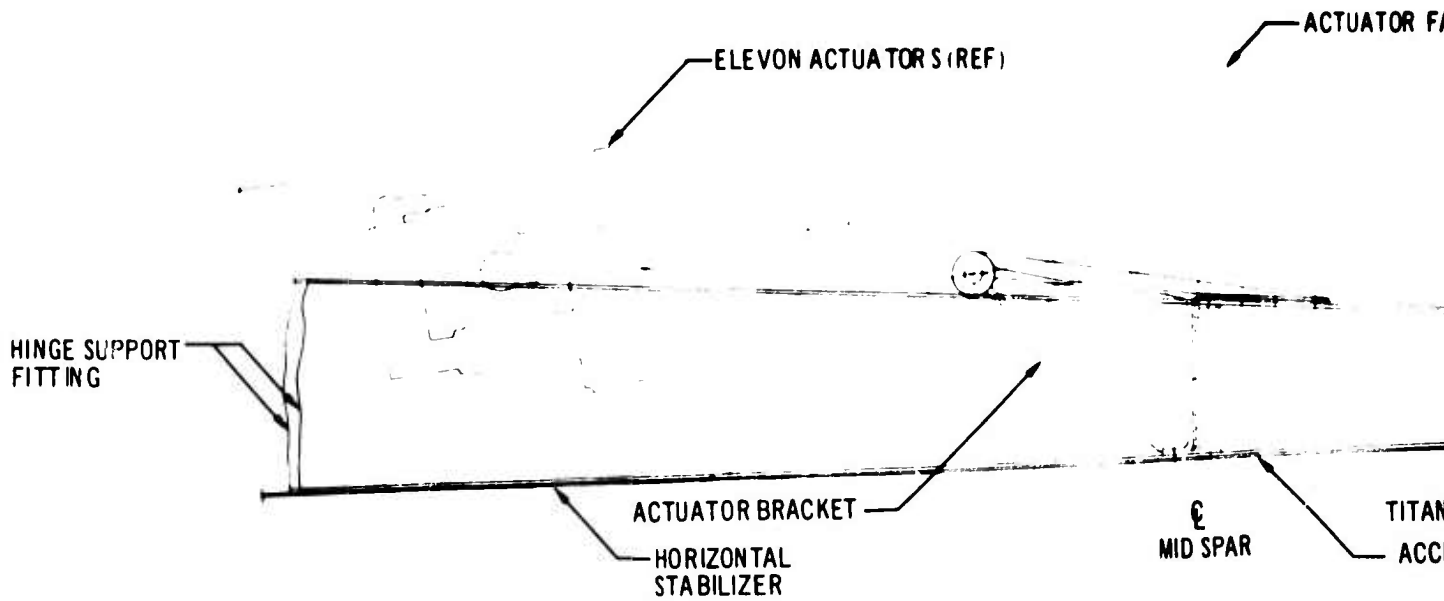


Figure 3-49. Support Beam of Pratt and Whitney Outboard Engine

C



0 5 10  
 SCALE: INCHES  
 SECTION B-B



A

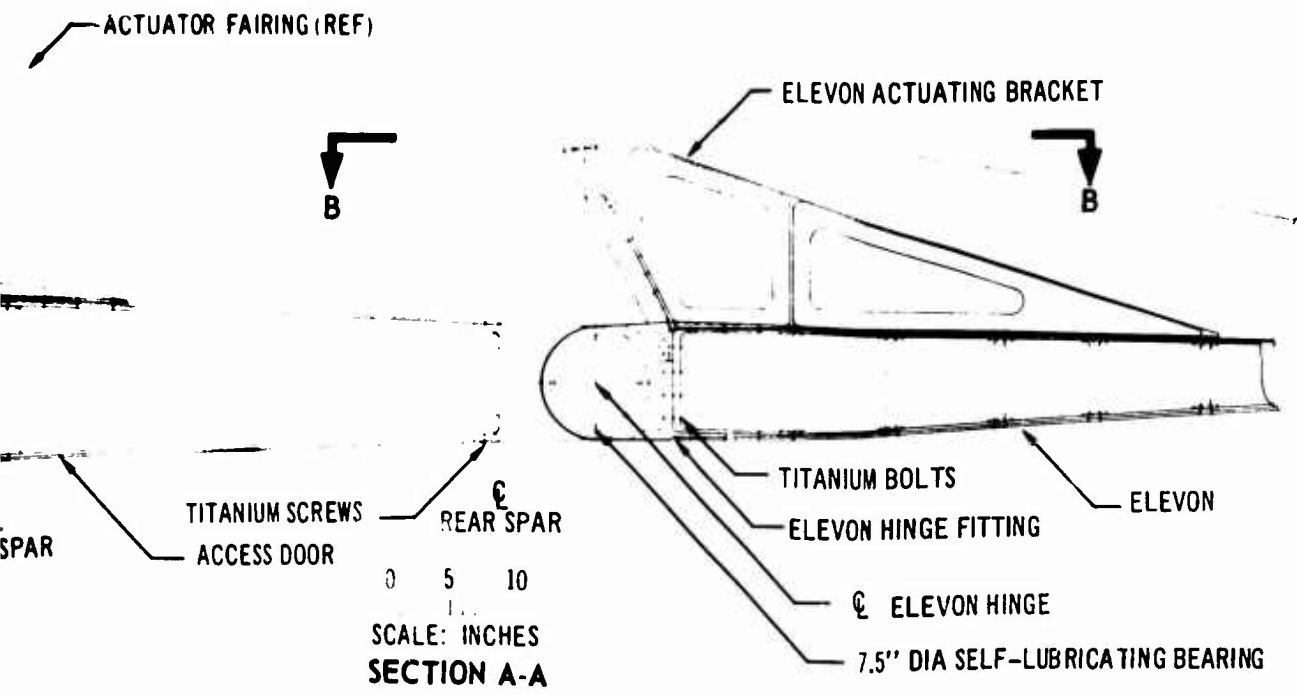
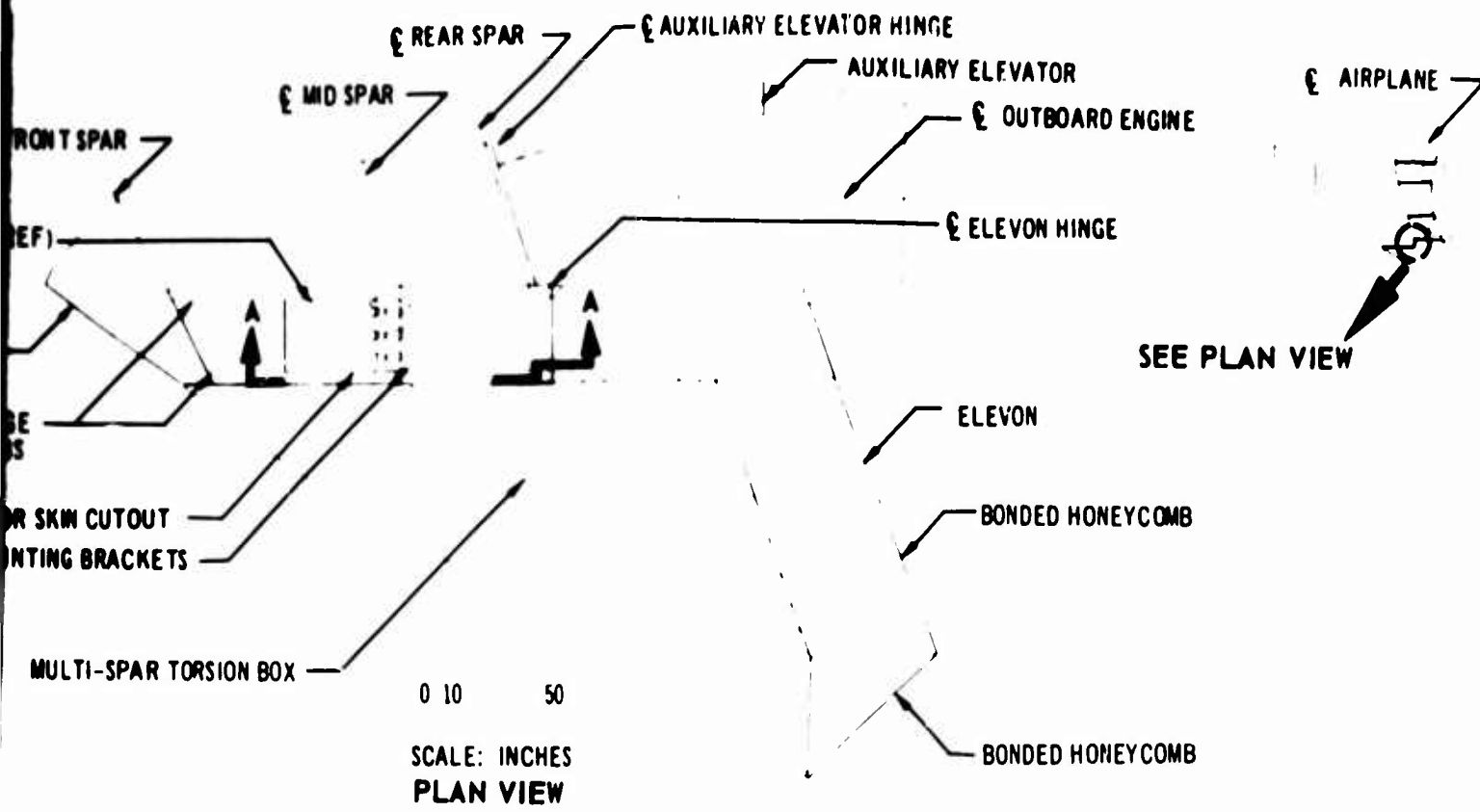
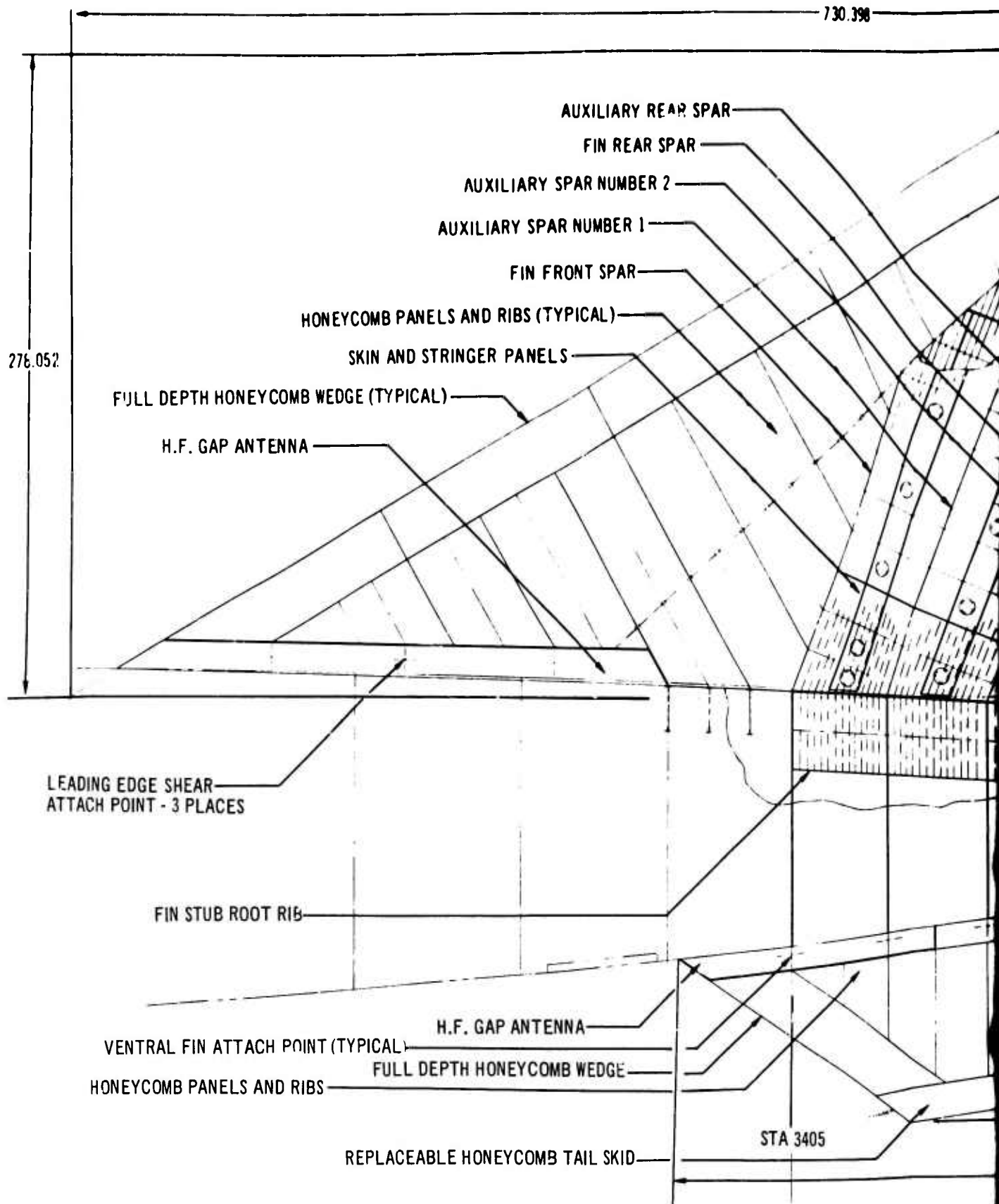
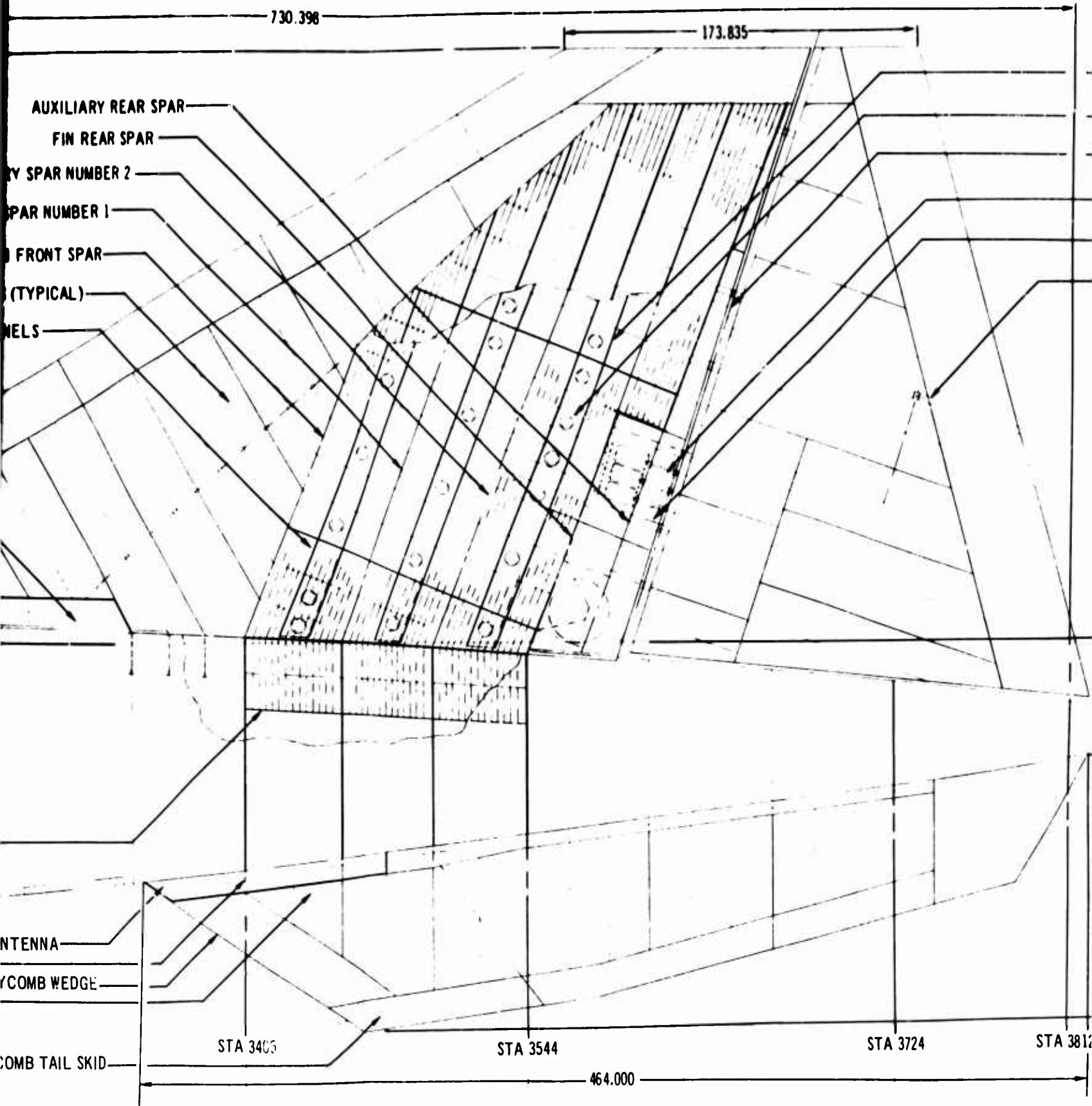


Figure 3-50. Elevon Support Structure

B

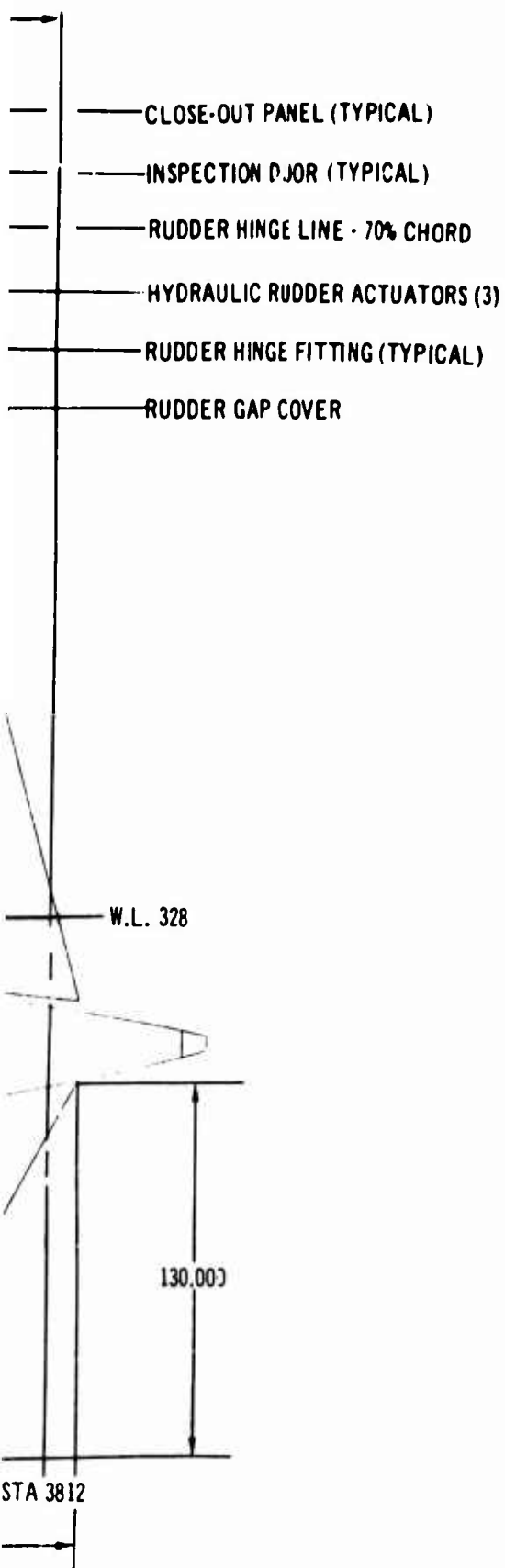


A



B





FIN DATA		
	VERTICAL	VENTRAL
AREA, SQUARE FEET	875	201
ASPECT RATIO	.615	
TAPER RATIO	.238	
LEADING EDGE SWEEP	60	
AIRFOIL	DOUBLE WEDGE	DOUBLE WEDGE
THICKNESS RATIO	2 1/2% @ 30% C 3% @ 70% C	3% @ 29 TO 66% C



Figure 3-51. Structural Diagram of Vertical and Ventral Fin

C

body by four spars and by continuous attachment of fin skin and stringers to body frames and skin.

The airfoils utilize a modified double wedge, resulting in tooling and fabrication economies while meeting aerodynamic performance requirements. The low-aspect-ratio fin, with its large root chord, results in good structural depth of the section, especially at the rear spar where the added depth can best be used for structural efficiency and for increased rudder-actuator moment arm.

The vertical and ventral fins are exposed to engine sonic levels as shown in Part C, Design Criteria, Loads, Aerodynamic Heating, Flutter (V2-B2707-7), of the Airframe Design Report. Maximum use is made of honeycomb panels because of their excellent resistance to high sonic levels. The skin stringer panels used on the vertical fin are designed for strength and are of adequate gage to withstand the sonic pressures. Extensive testing has been done to confirm the design, and test results are discussed in Part E, Structural Tests (V2-B2707-9), of the Airframe Design Report.

#### 3.4.1 Structural Box

The fin structural box has a riveted skin-stringer design as shown in Fig. 3-52. Access doors for inspection and repair are installed in one surface and are utilized for closeout during the manufacturing process. Multiple skin panels are used to ensure a fail-safe structure, and the multiple body attachments provide fail safety at the integral fin-to-body joint.

#### 3.4.2 Leading Edge

Lightweight bonded-honeycomb panels form the leading-edge cover. The panels are attached by mechanical fasteners to sine-wave-welded ribs. Panels on one side are removable for inspection. Hail and rain-erosion resistance are inherent in the design because of the sharp leading edge and excellent resistance of the titanium honeycomb panels.

#### 3.4.3 Rudder

A segmented rudder design with actuators on the lower segment allows structural deflection with minimum effect on actuation loads. The upper segment is driven by the lower segment by means of a fail-safe link. The rudder hinges and actuators are located to give maximum mechanical advantages (see Fig. 3-53). Fail safety is accomplished by multiple hinges and multiple arms.

Honeycomb panels form the cover for the rudder torque box, and support is provided by sine wave ribs except at concentrated load points. Assembly of all structure is by mechanical fasteners with one panel removable for inspection.

#### 3.4.4 Ventral Fin

The ventral fin design uses honeycomb panels supported on sine wave ribs (see Fig. 3-51). The lower edge of the ventral is a replaceable nonmetal rub strip attached to replaceable segments. This results in minimum replacement of parts if the ventral contacts the ground because of over rotation.

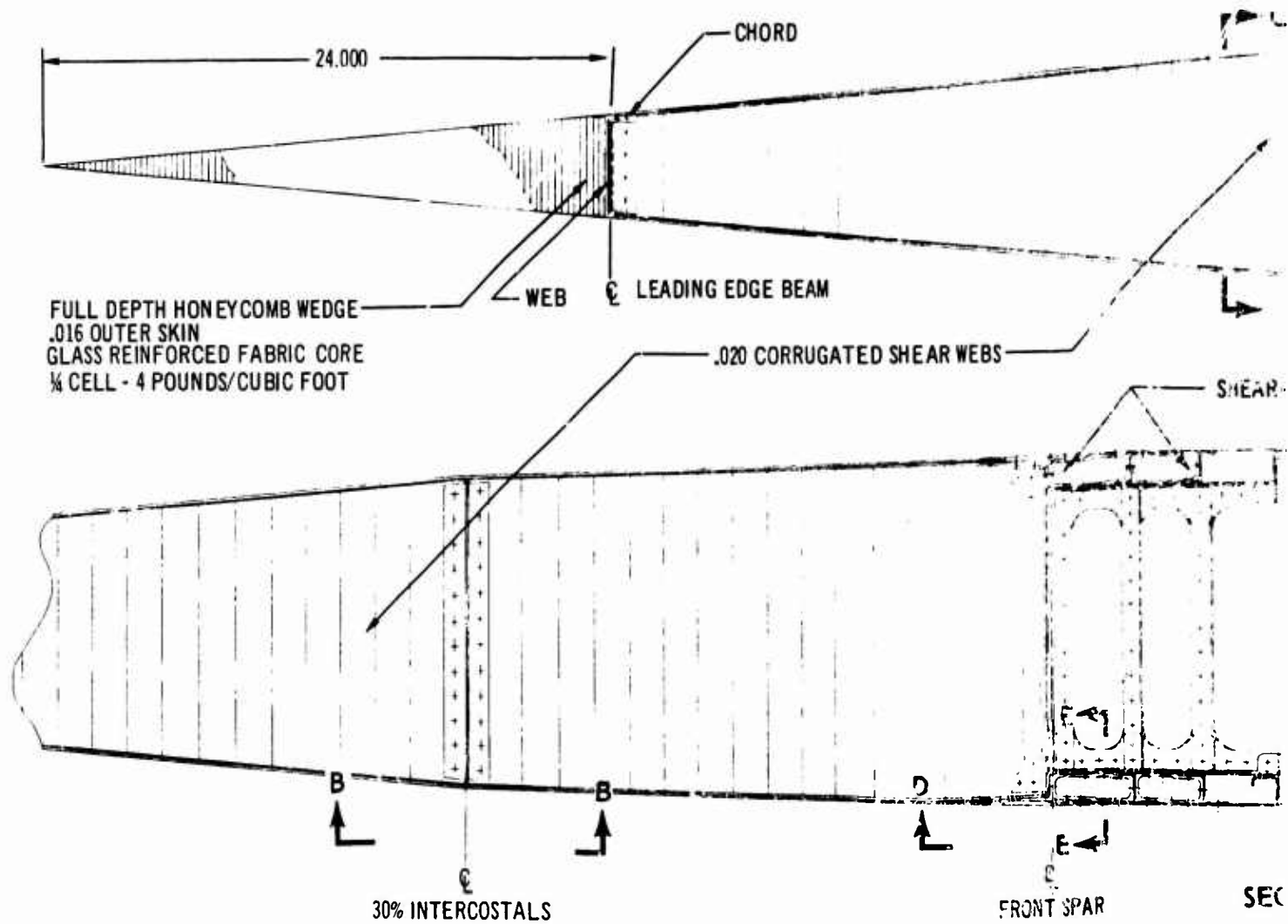
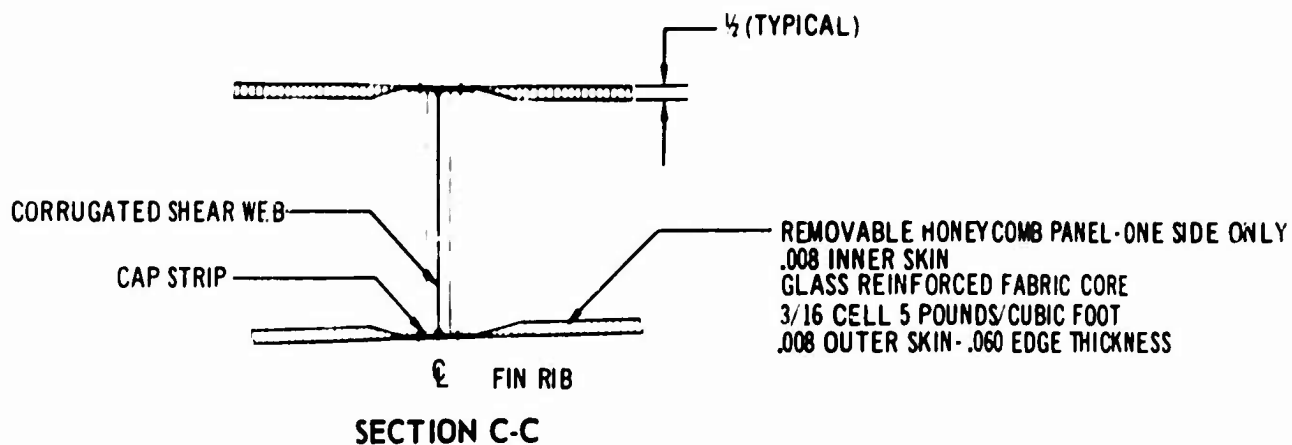
The ventral fin is attached to the body at multiple bulkheads and frames and is designed to be replaceable. The ventral fin is designed to fail before damage to primary fuselage structure. One surface has removable panels to allow access for inspection and repair.

### 3.5 LANDING GEAR

#### 3.5.1 General Features

The gear arrangement utilizes a conventional dual-wheel nose gear (shown in Fig. 3-54) together with the main gear system (shown in Fig. 3-55) that is similar in concept to that used on the 747 airplane. This arrangement has four individual main gears each mounting a four-wheel truck. The two forward main gears, which are attached to the wing-box front spar, retract forward and are stowed in the wing strake. The two rear main gears retract aft, are stowed within the body, and are attached to the wing-box rear spar. A manifold system on each side of the airplane equalizes the load between the forward and aft main gears. This system with the multiple gear, staggered arrangement provides the following advantages:

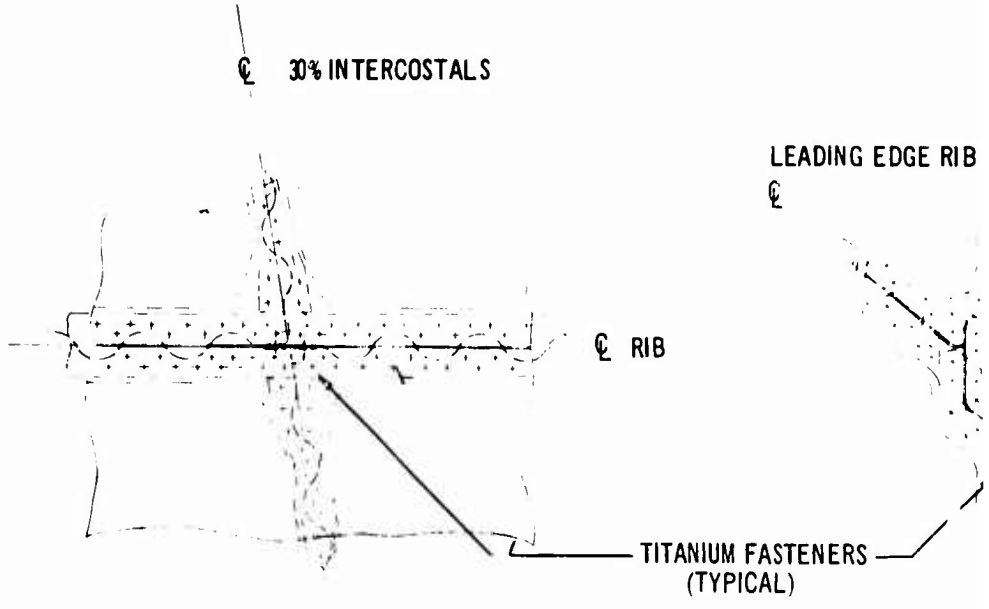
- Maximum operational safety because of main gear redundancy
- Minimum pavement loading under all operating conditions
- Compatibility with existing airport pavement
- Simplicity of gear design and components
- Maximum braking efficiency because of uniform



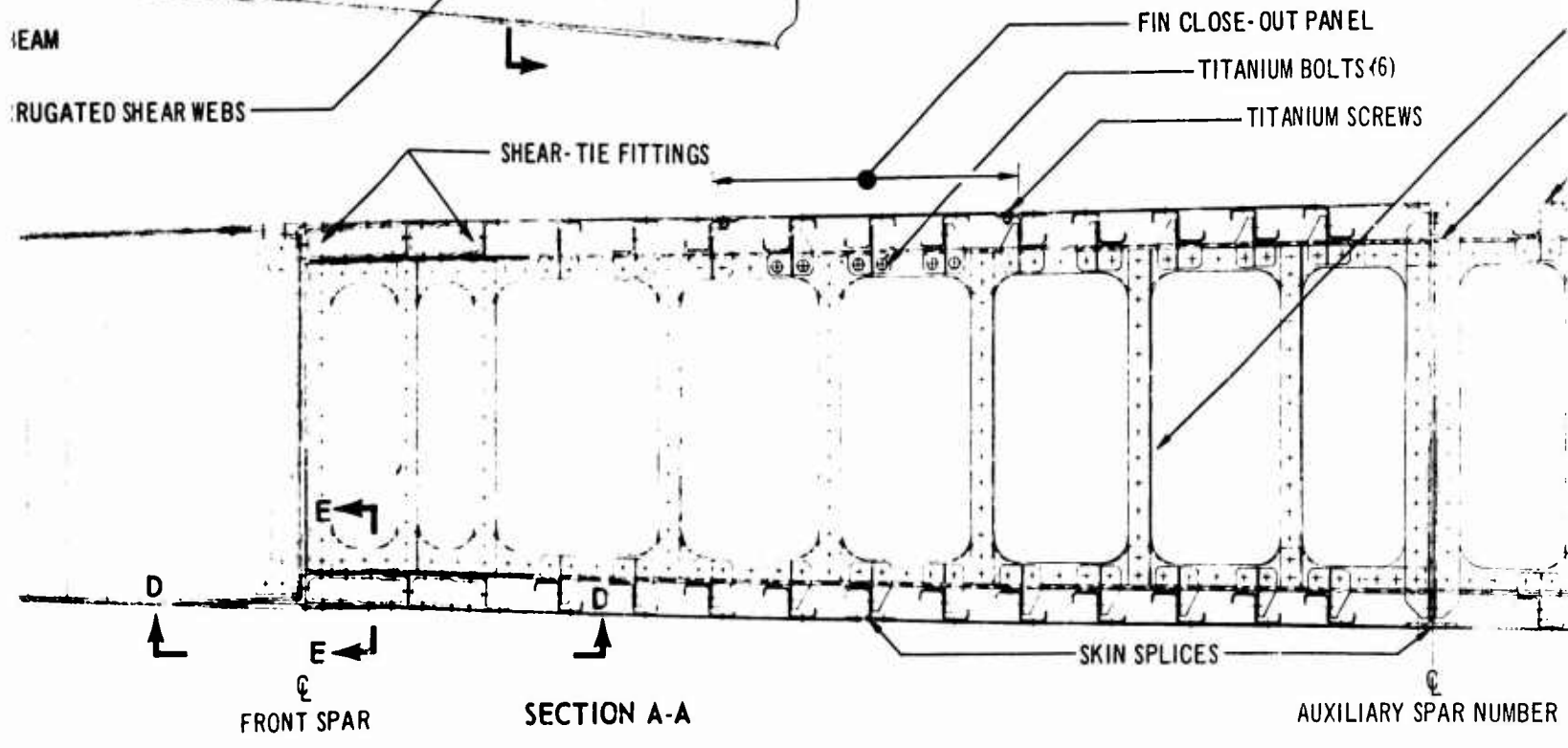
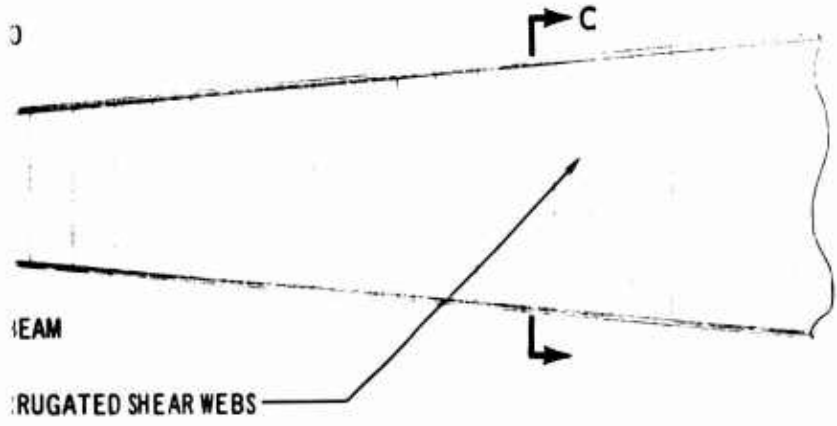
A

TYPICAL)

REMOVABLE HONEYCOMB PANEL - ONE SIDE ONLY  
.008 INNER SKIN  
GLASS REINFORCED FABRIC CORE  
3/16 CELL 5 POUNDS/CUBIC FOOT  
.008 OUTER SKIN - .060 EDGE THICKNESS



SECTION B-B



B

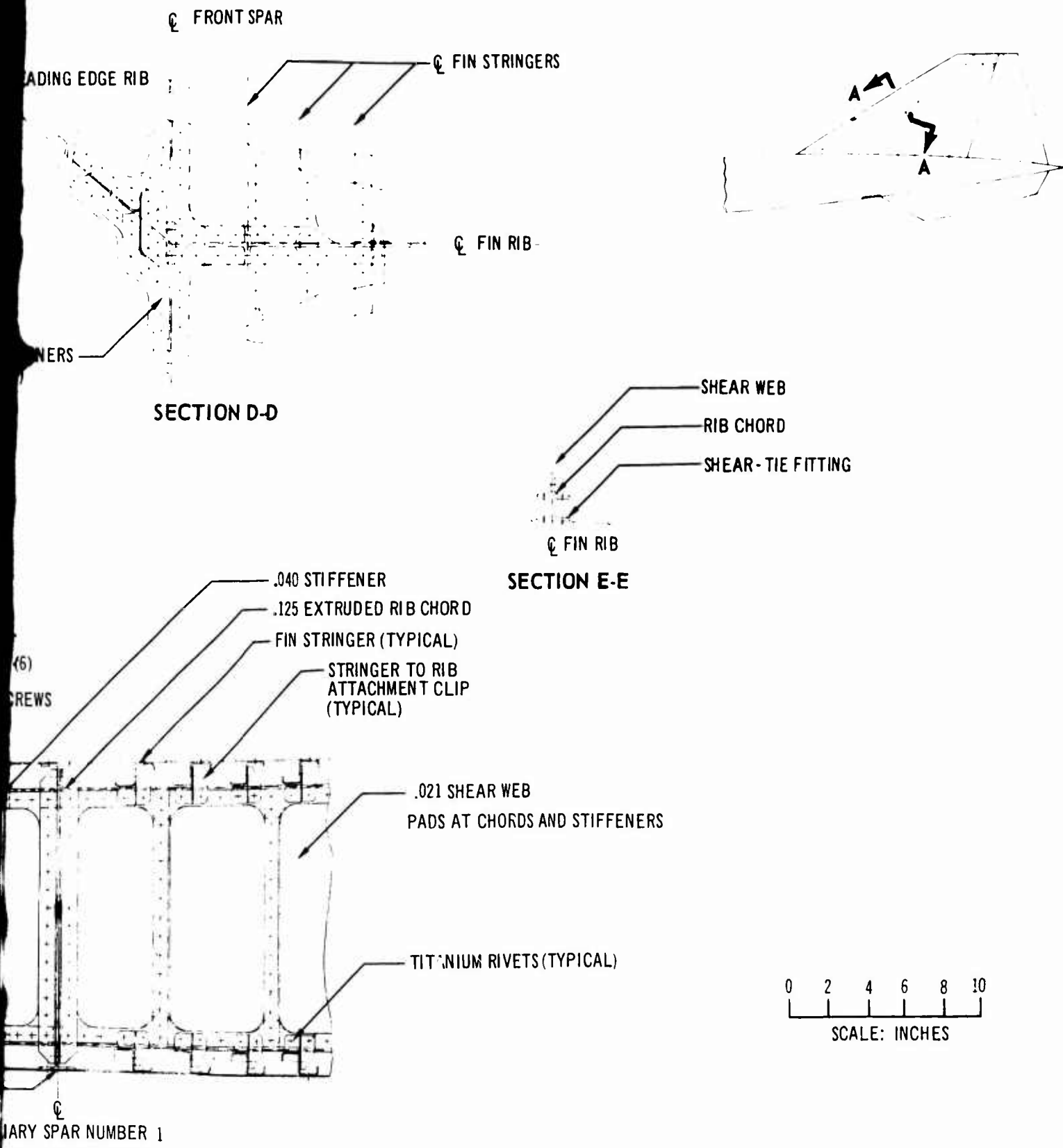
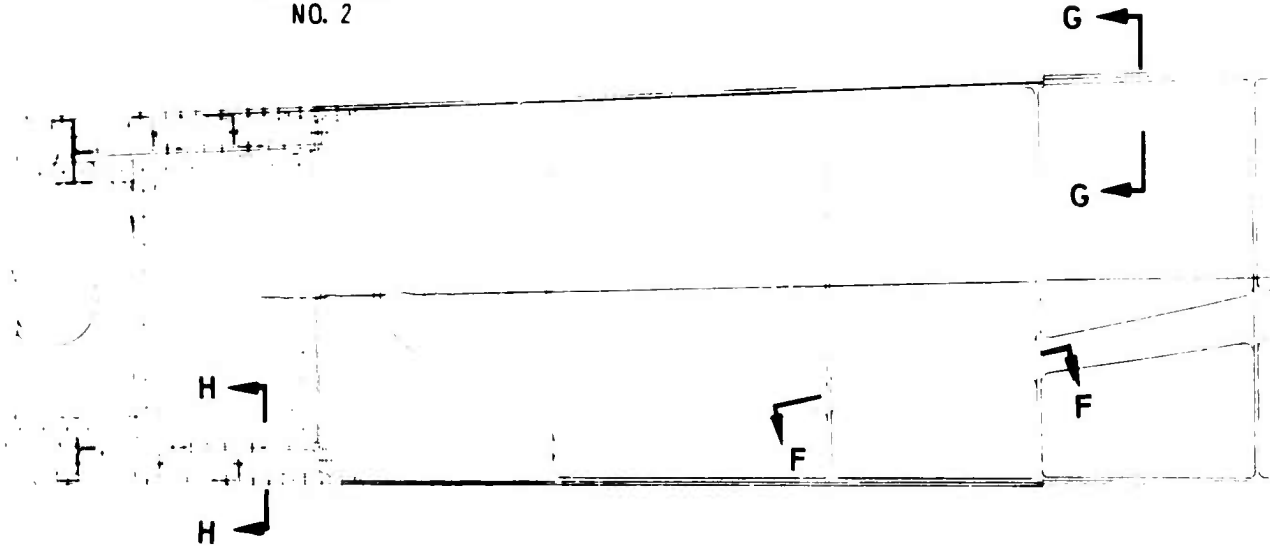


Figure 3-52. Vertical-Fin Structure

V2-B2707-6-2

C

Q  
AUX. SPAR  
NO. 2

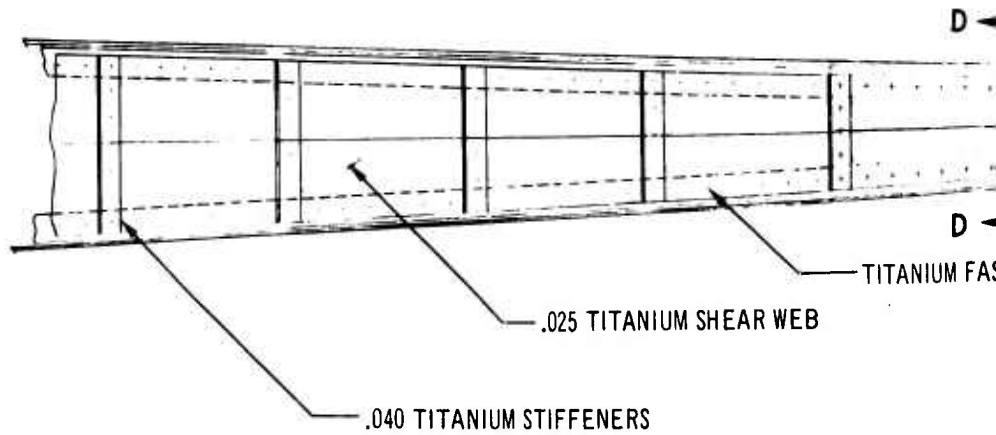


SECTION F-F

SECTION H-H

.005 INN  
SKIN (TYP)

.055 OUTER SKIN (TYP)



A

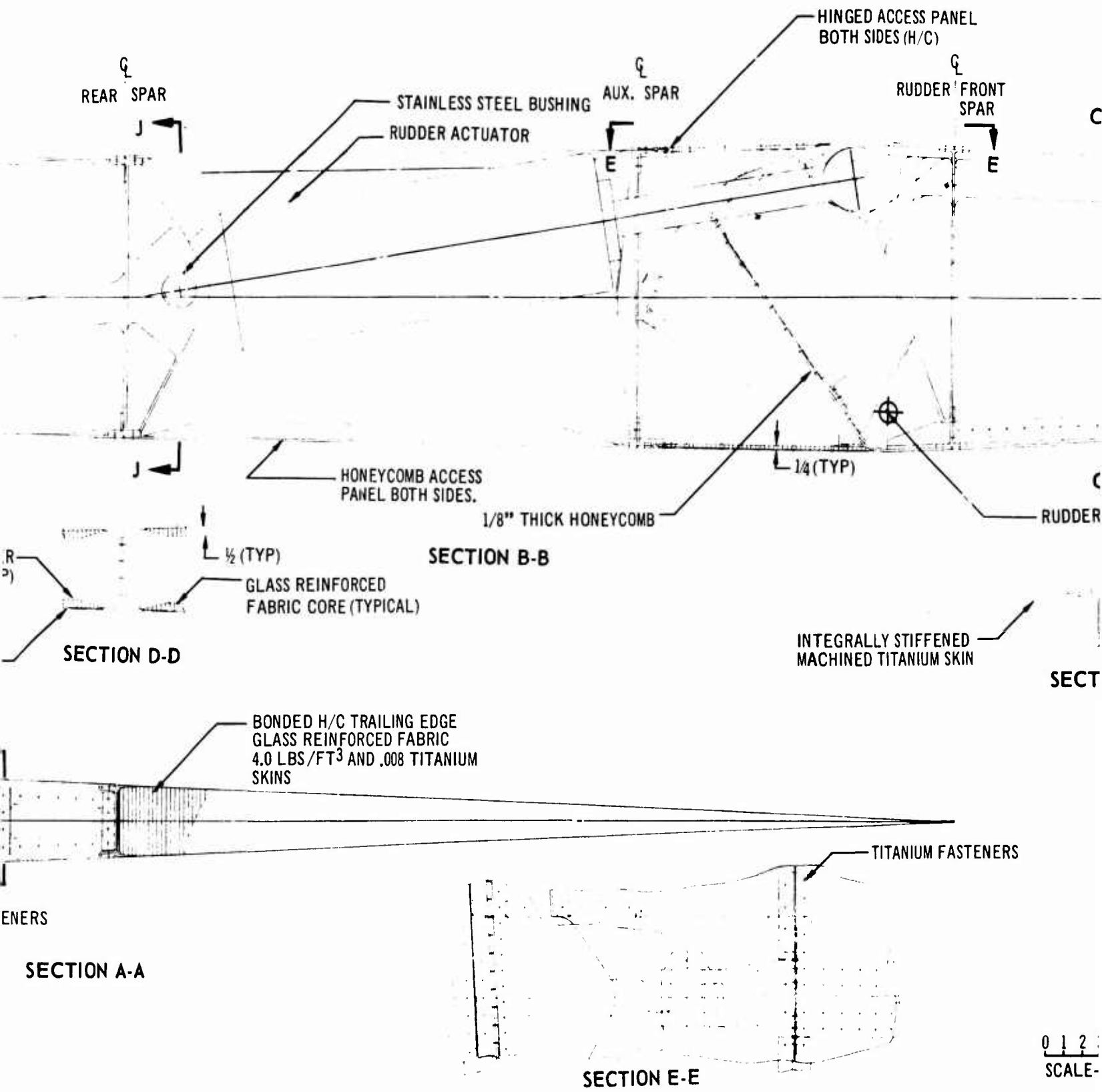


Figure 3-53. Vertical

B

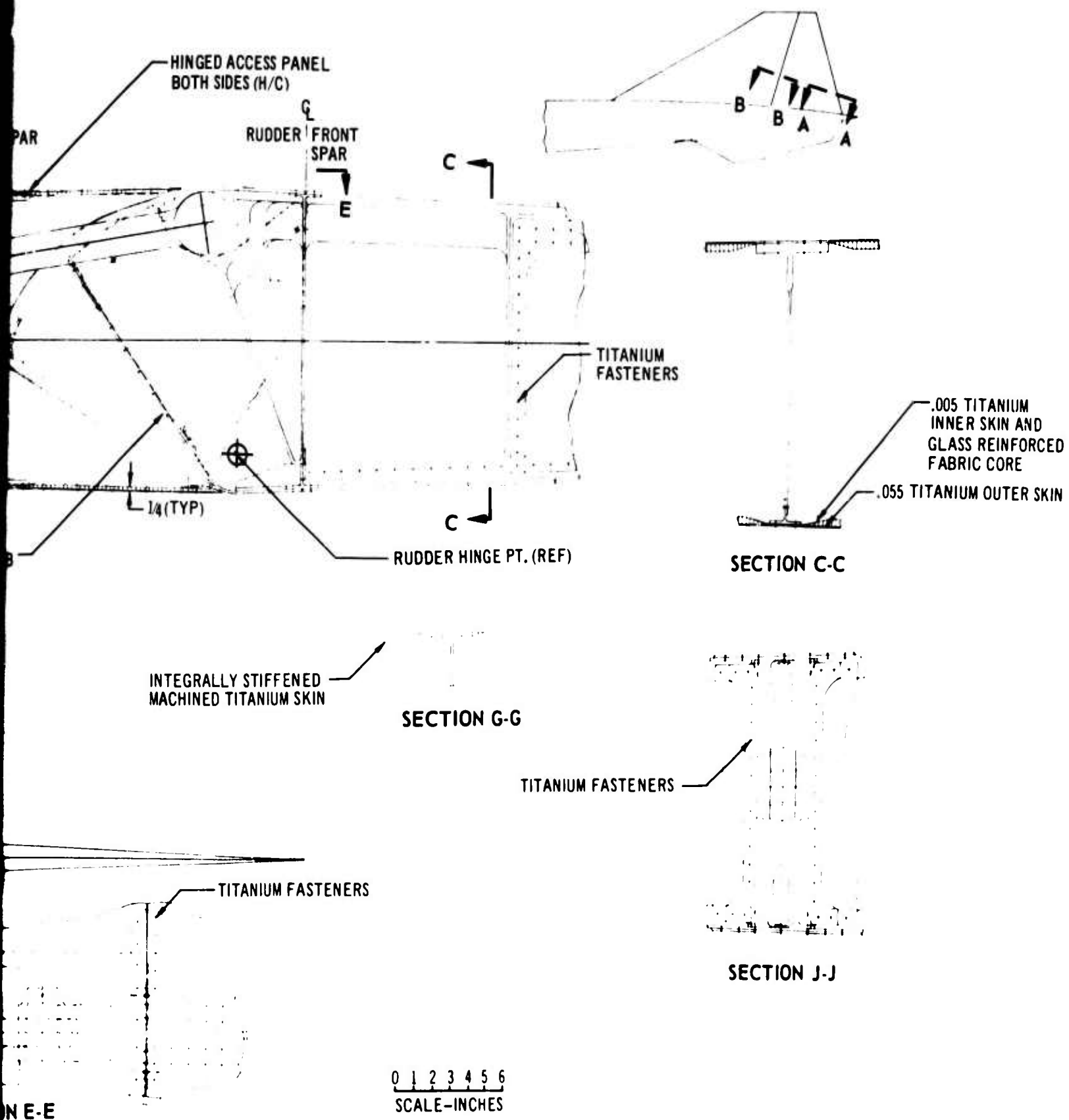
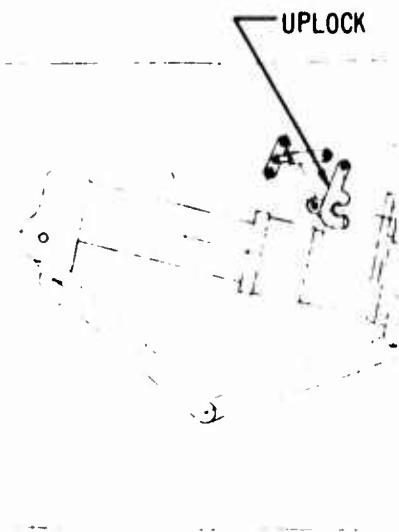
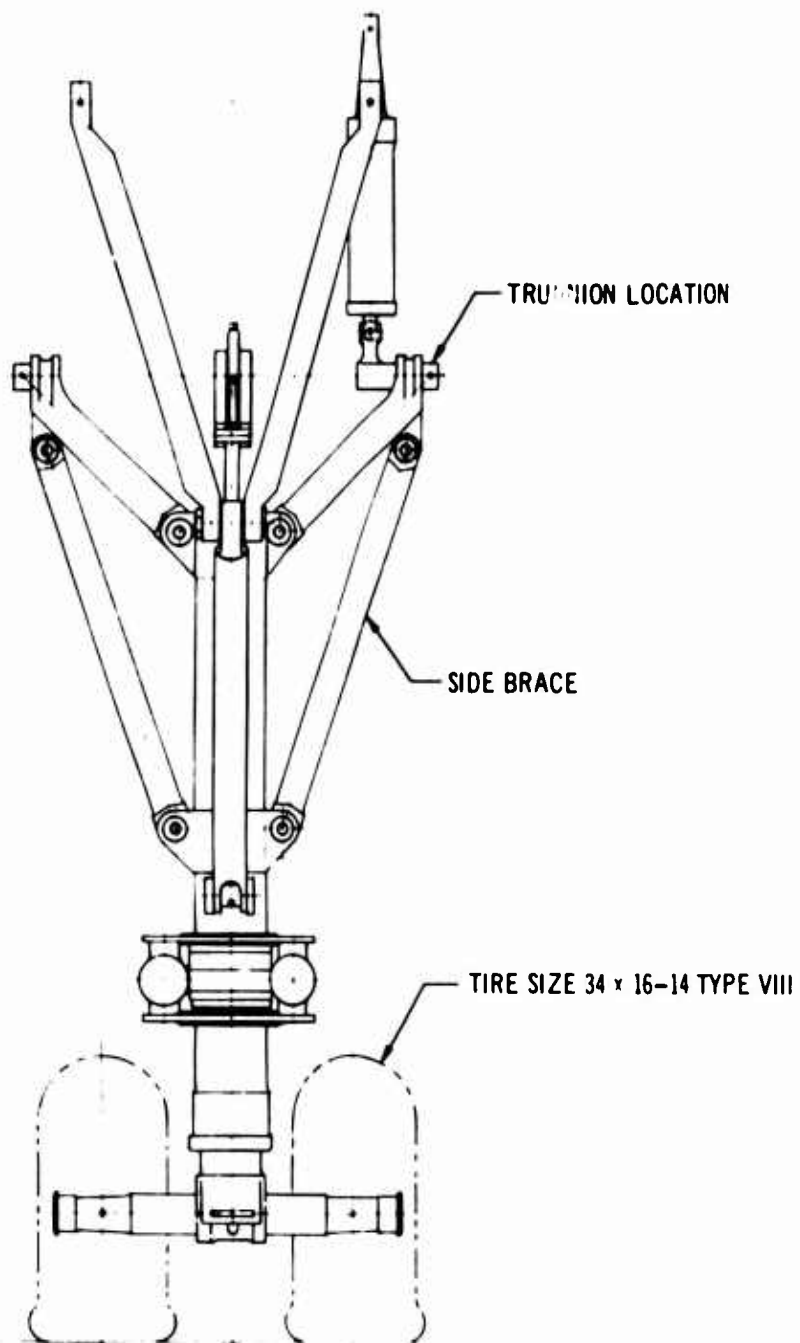


Figure 3-53. Vertical-Fin and Rudder Structure

C





← FOWARD →

0 10  
SCALE: IN

SECTION

A

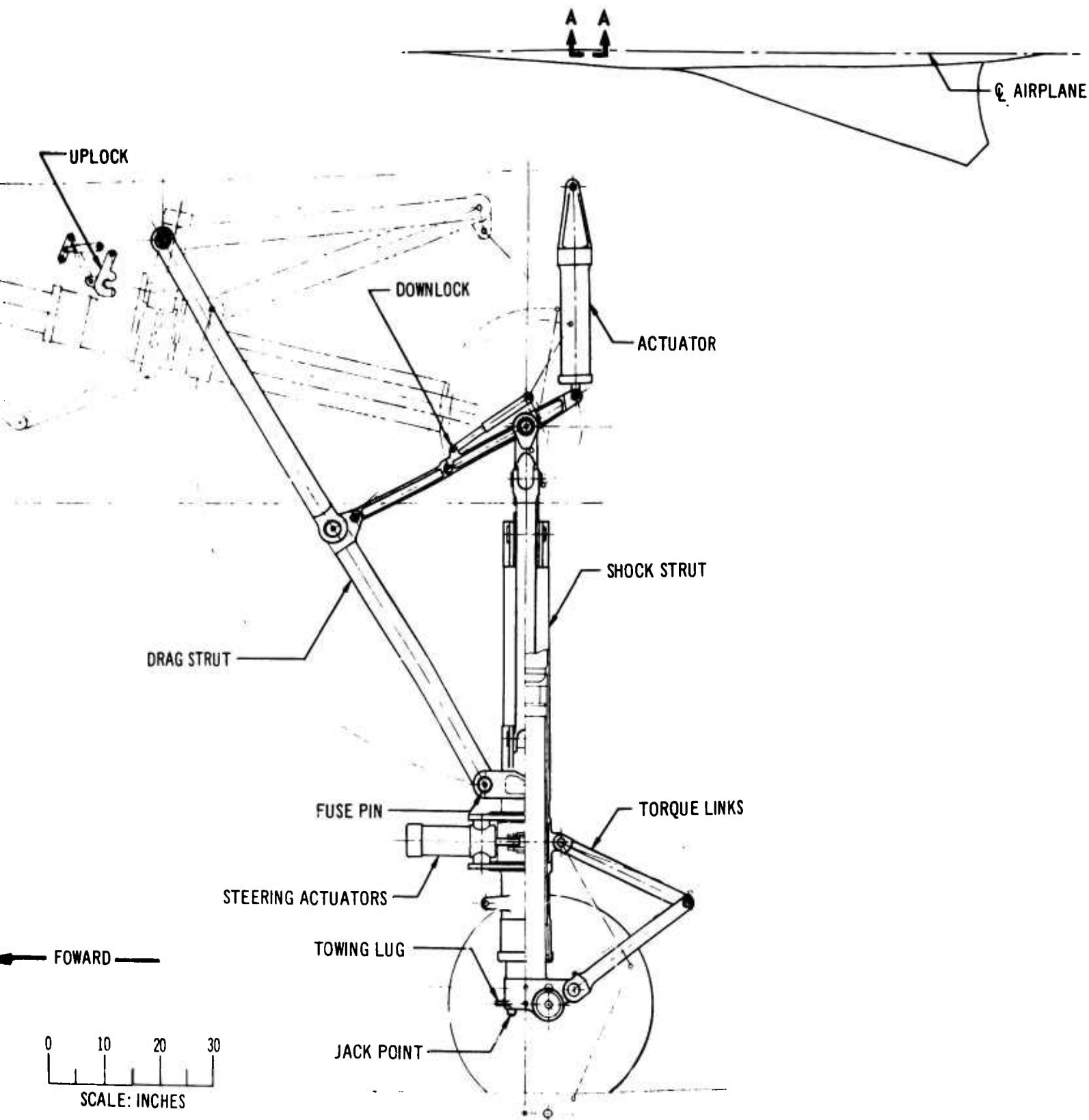
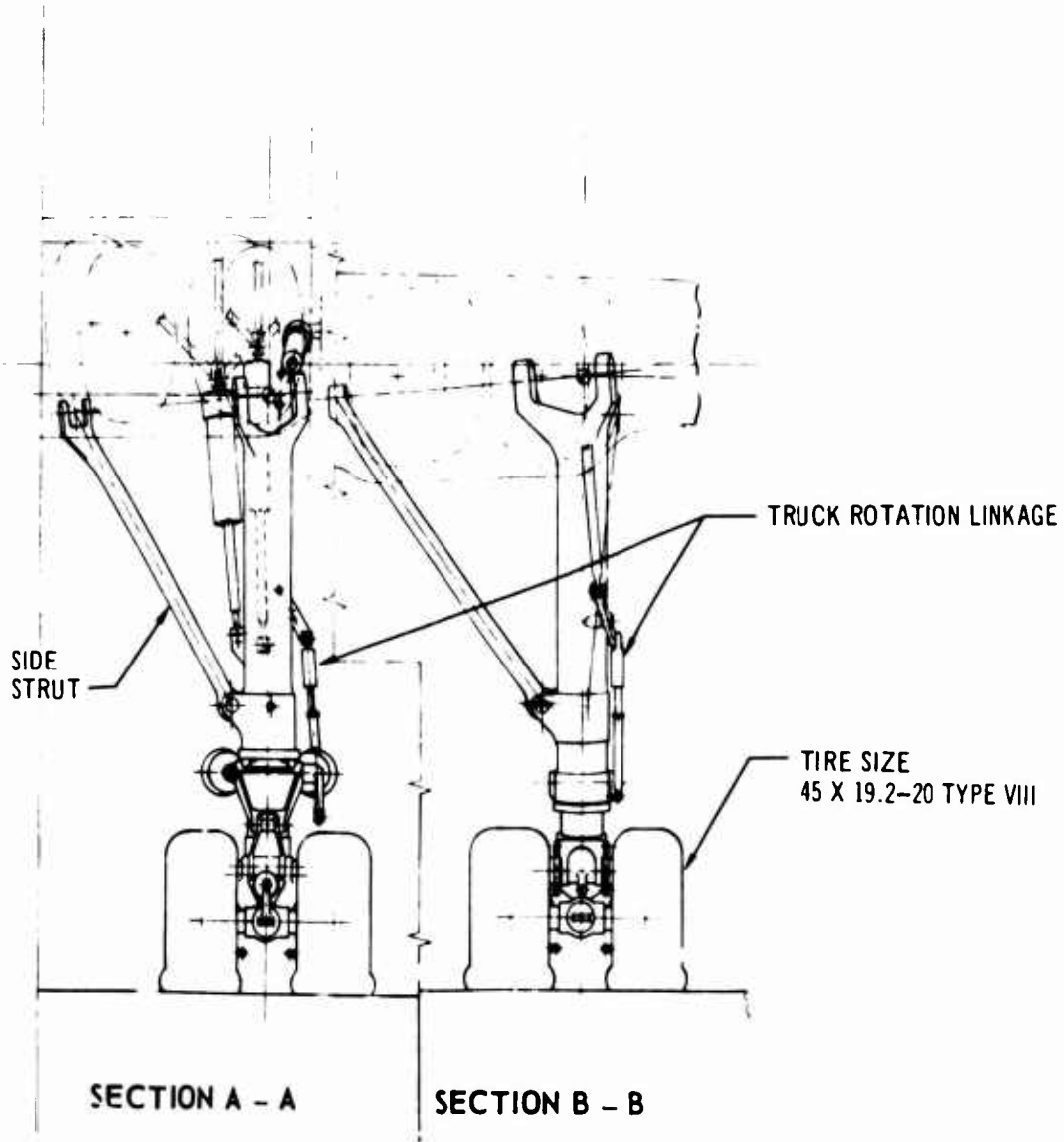


Figure 3-54. Nose Gear Arrangement

V2-B2707-6-2

B

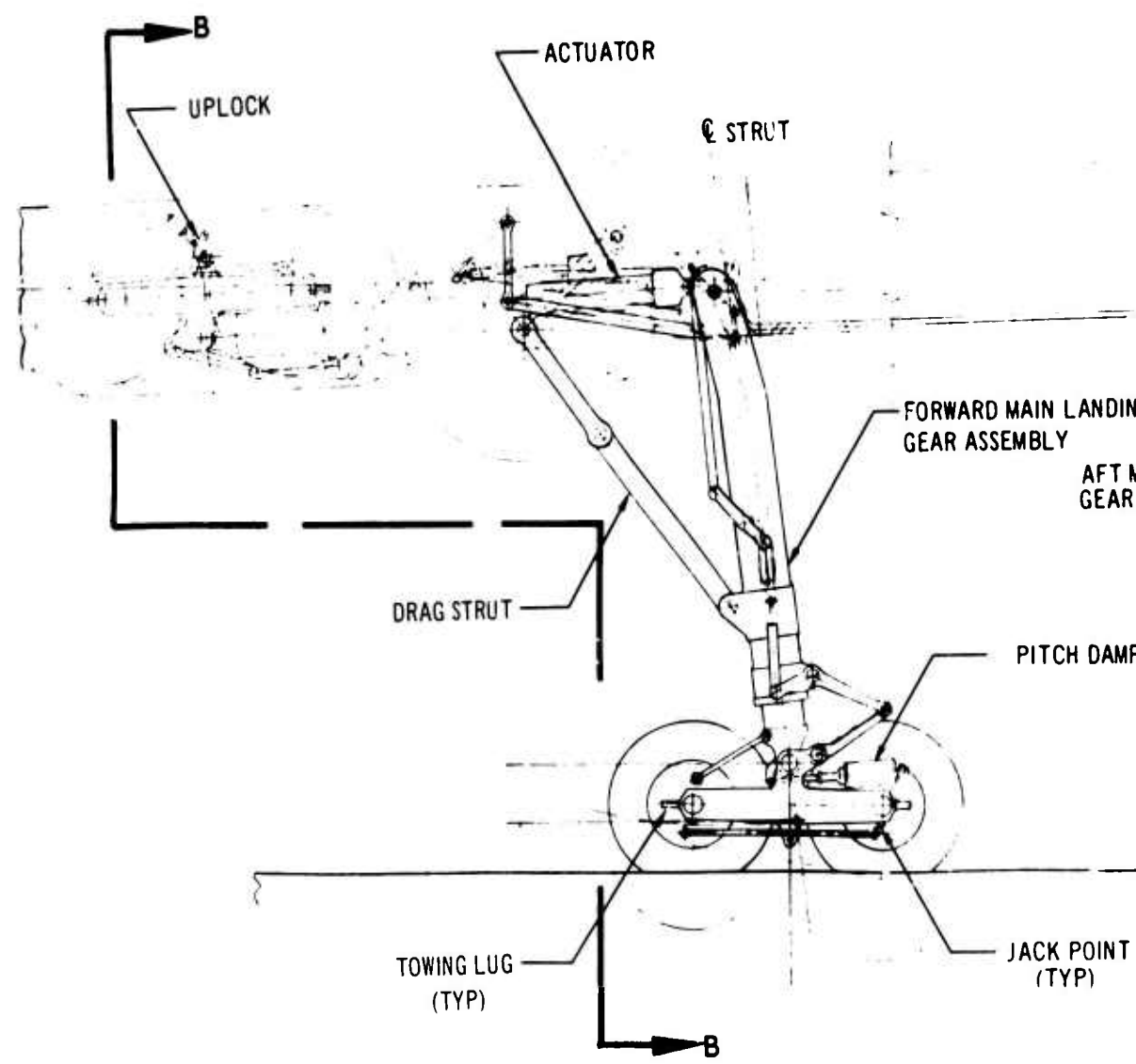
☉ AIRPLANE



A

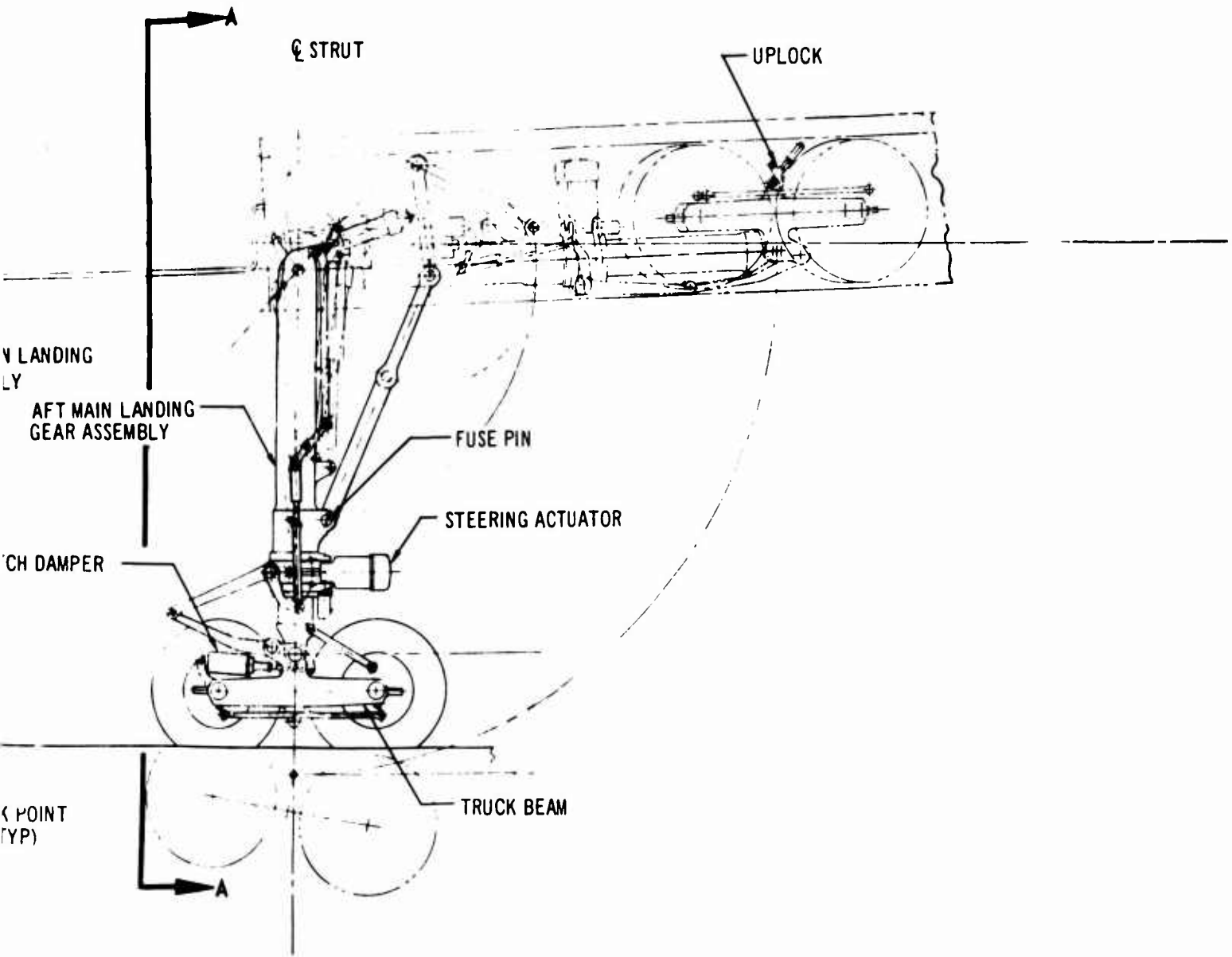
WHEEL ROTATION LINKAGE

ORIGINAL SIZE  
SCALE 19.2-20 TYPE VIII



B

FOR PLAN VIEW SEE SHEET 2



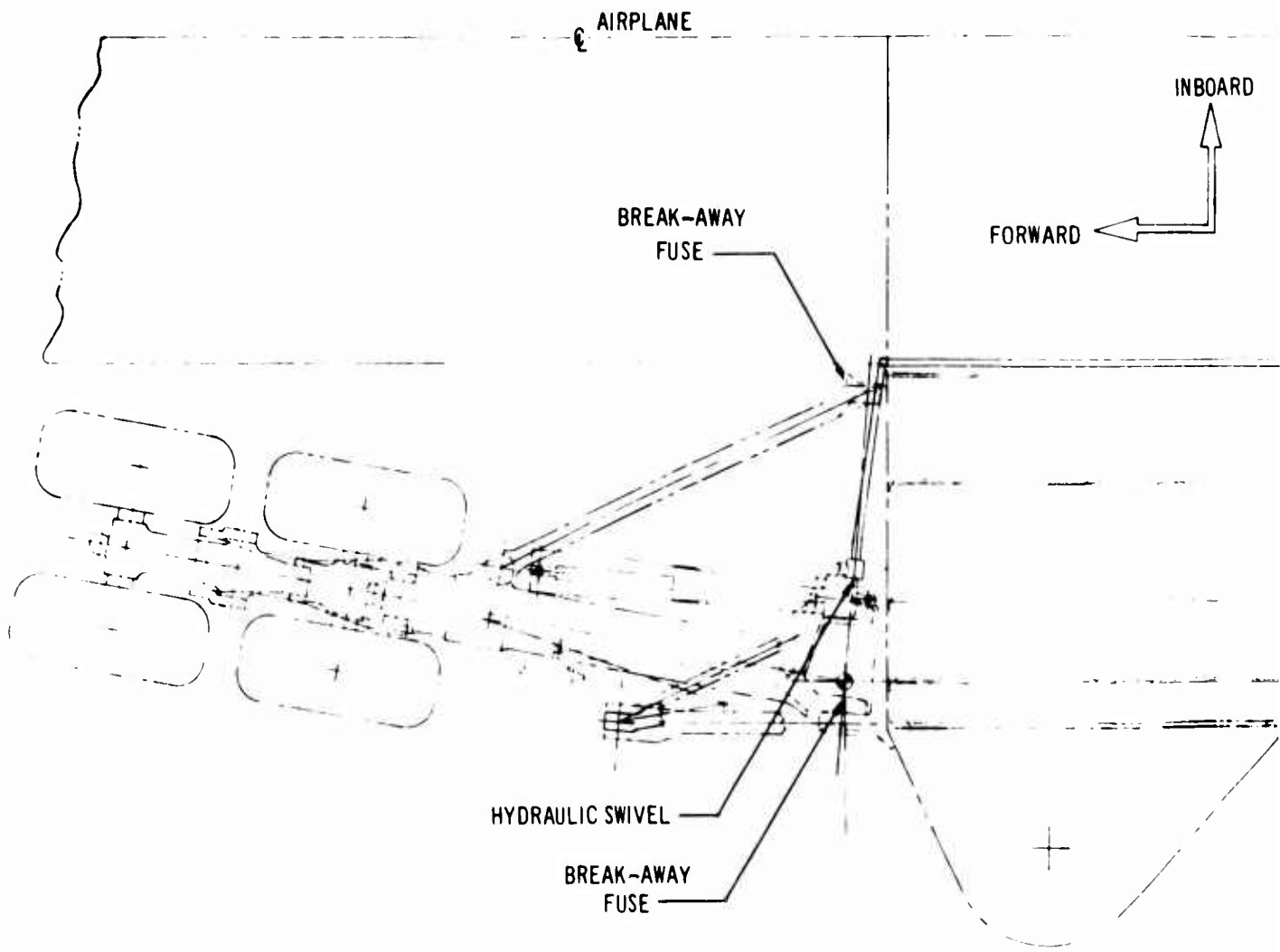
0 50 100  
SCALE: INCHES

Figure 3-55. Main Gear Arrangement

V2-B2707-6-2

C

HYDRAULI



PLAN VIEW

A

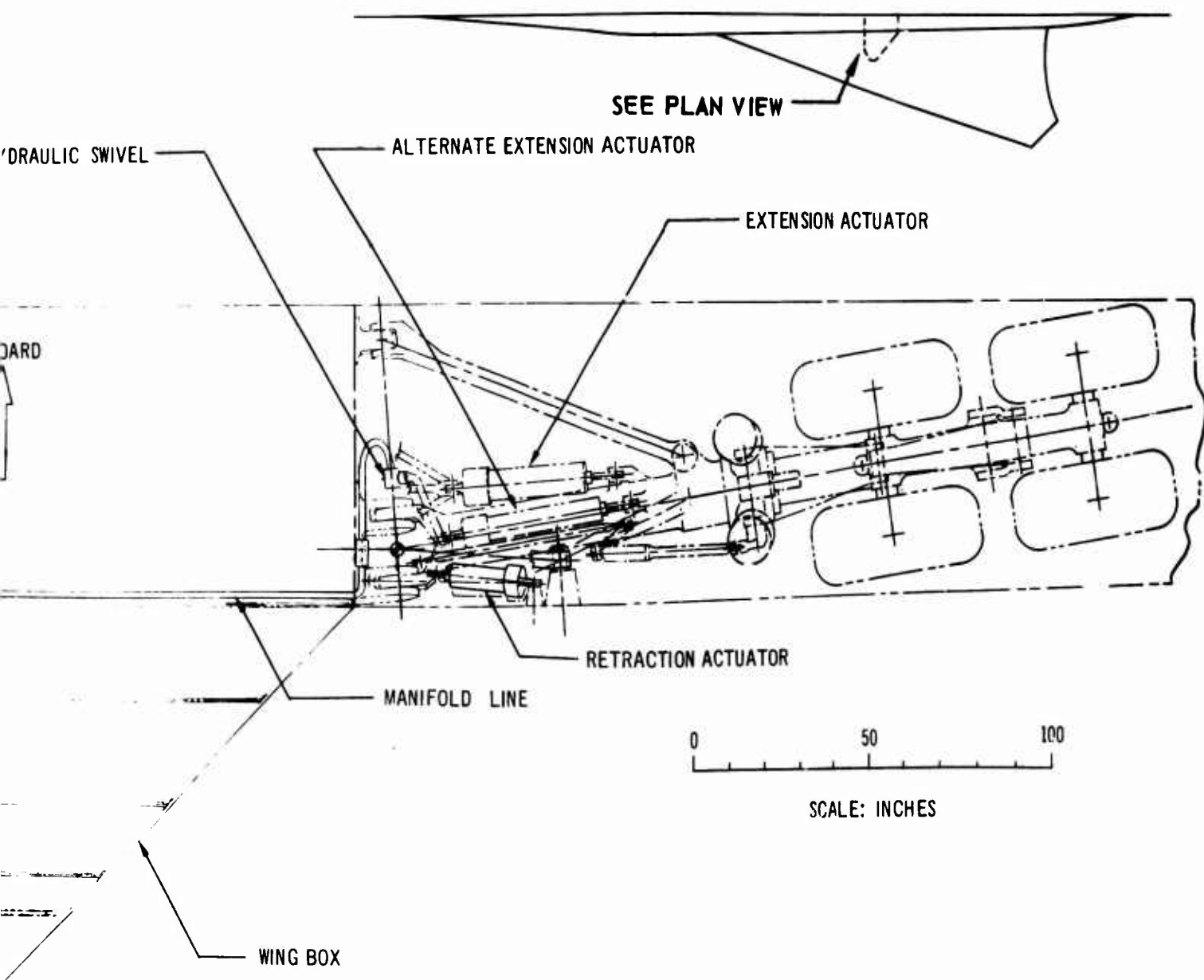


Figure 3-55. (Continued)

V2-B2707-6-2

B

- Minimum stowed volume
- Trunnion support mounted directly on the wing-box structure
- Soft landing with adequate lateral stability provided by multiple oleos.

Conventional air-oil shock struts are used on the main gears. Inflation pressures are similar to those used on present subsonic commercial airplanes allowing use of proved seals. The rear main-gear shock strut has a stroke of 40 in. and is designed to absorb landing energy for all normal landing conditions. With the aft gear retracted, the forward main gear can absorb full airplane landing energy at a reduced rate of descent of 6 ft/sec. The hydraulic manifold system interconnects the cylinders on the forward and aft main gears on each side of the airplane as shown in Fig. 3-56. A manifold piston above the air cylinders of each oleo equalizes the air pressure and load on the two interconnected gears. These pistons have limited travel which is sufficient to compensate for pavement unevenness. These pistons also ensure normal oleo function if manifold failure should occur.

The manifold system affects the dynamic characteristics of the airplane during takeoff and landing in the following manner. During the takeoff run when partial lift has been established, the airplane can be rotated to increase lift without overloading the aft gears. At touchdown, the aft main gear with its long stroke will absorb landing energy before the forward main gear makes contact with the runway. As the landing cycle proceeds, the load between the fore and aft main gears equalizes, helping to reduce nose gear loads as the nose gear contacts the runway. After nose gear contact, wing lift will be reduced by spoiler operation and full braking can be applied.

All gears are extended and retracted by hydraulic actuators and are retained in the up and down positions by hydraulically controlled locks. A separate hydraulic system unlocks the gear and door uplocks and powers the aft main gears into the down and locked position. This alternative hydraulic system uses separate hydraulic actuators that are completely independent of those used during normal operation. The forward main and nose gears free-fall into the down and locked position after release of the gear and door uplocks. The rear main-gear trucks are steerable to minimize tire scrubbing during turn maneuvers.

Steering is provided by linear hydraulic actuators and operates in conjunction with, and is controlled by, the nose-gear steering and control system. The steering angles of the nose and rear main gears allow a ground turn center within 15 ft of the main strut on the inside of the turn. During towing, steering power is supplied to the rear main gears from the standby hydraulic system, allowing full ground-handling capability.

The multiple gear arrangement provides a high degree of landing safety. The airplane can land on any three of the four main gears. In an emergency it can land on either the two forward or two aft main gears or on one gear on each side. When landing on the two forward gears the airplane would settle on the tail skid during the latter part of the landing run.

If ultimate design loads on the drag struts should be exceeded, fuse pins will allow the gears to rotate about the trunnions. These pins are located at the lower end of the drag struts where they are attached to the shock struts. The forward main gears will fold aft and are designed to separate without damaging the wing box. The side-brace fittings contain a breakaway pad at the upper attachment. The aft gears will fold under the body into the gear stowage area. The nose gear will also fold under the body.

### 3.5.2 Design Description

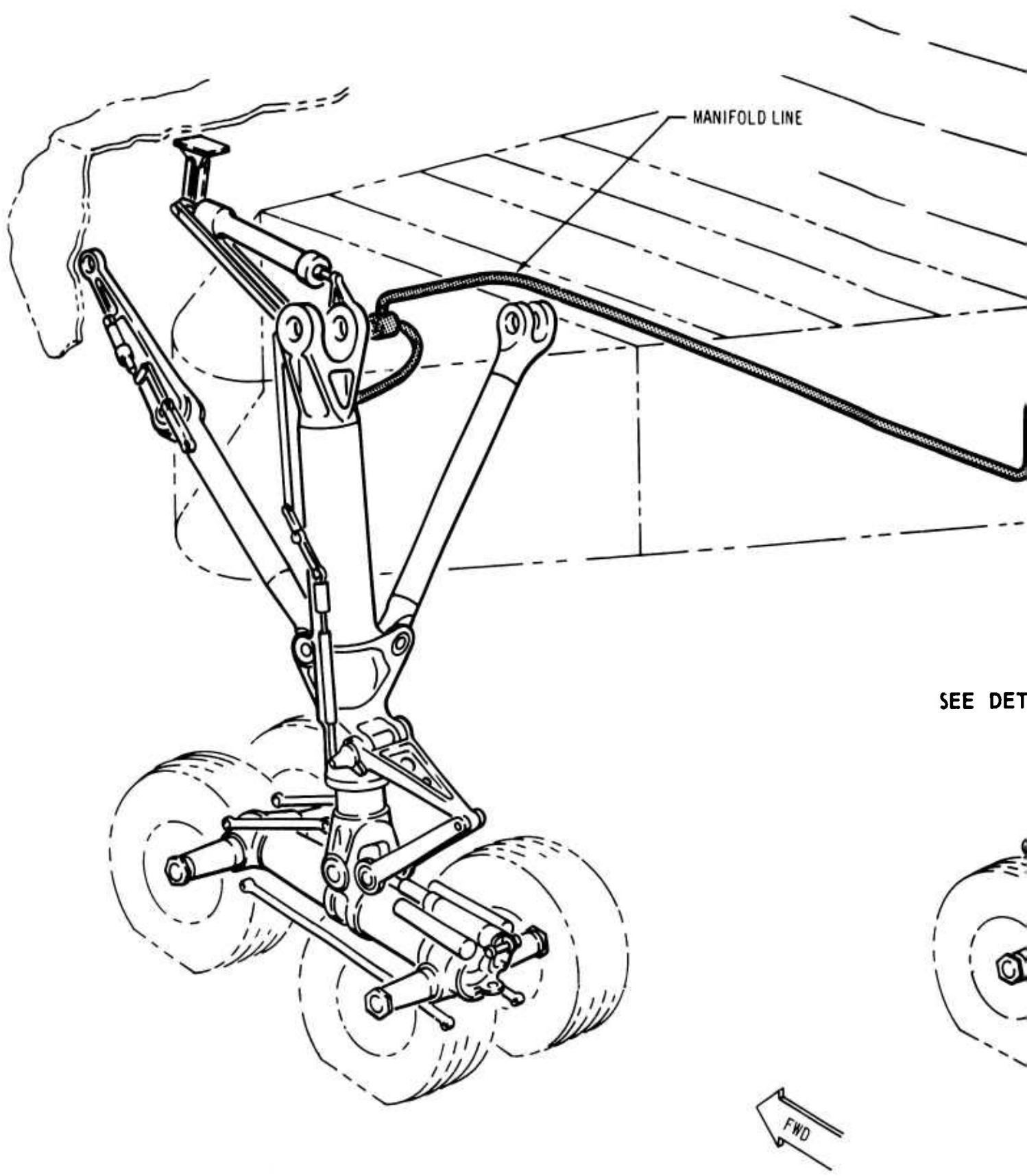
#### 3.5.2.1 Wheel-Well Environment

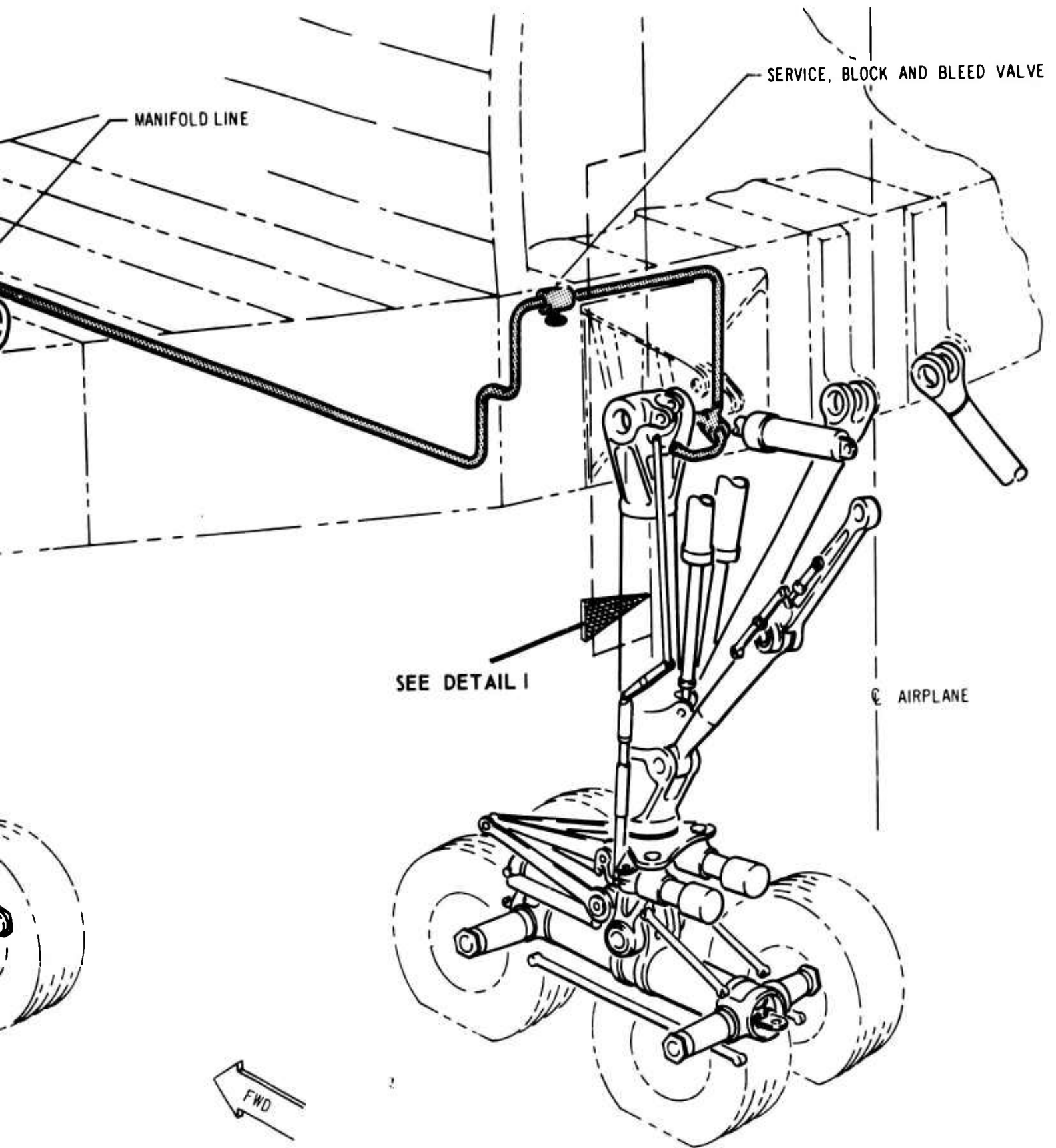
The wheel wells are cooled to protect landing gear components during supersonic flight. The cooling system (described in detail in Part A, Environmental Control, Electric, Navigation and Communications (V2-B2707-10), of the Systems Report) provides exhaust cabin air at approximately 115°F to the insulated wheel well. The system is designed to maintain tire temperatures below 180°F and gear component temperatures below 250°F. These temperatures allow usage of conventional materials for tires, the hydraulics system, and the structure.

#### 3.5.2.2 Main Landing Gear

The major structural parts are designed of 4340M-vacuum-arc remelt steel, heat treated from 270,000 to 300,000 psi. The use of the vacuum remelt process greatly improves physical properties, particularly fracture toughness. This material without the vacuum remelt process has had an excellent service record on the Boeing

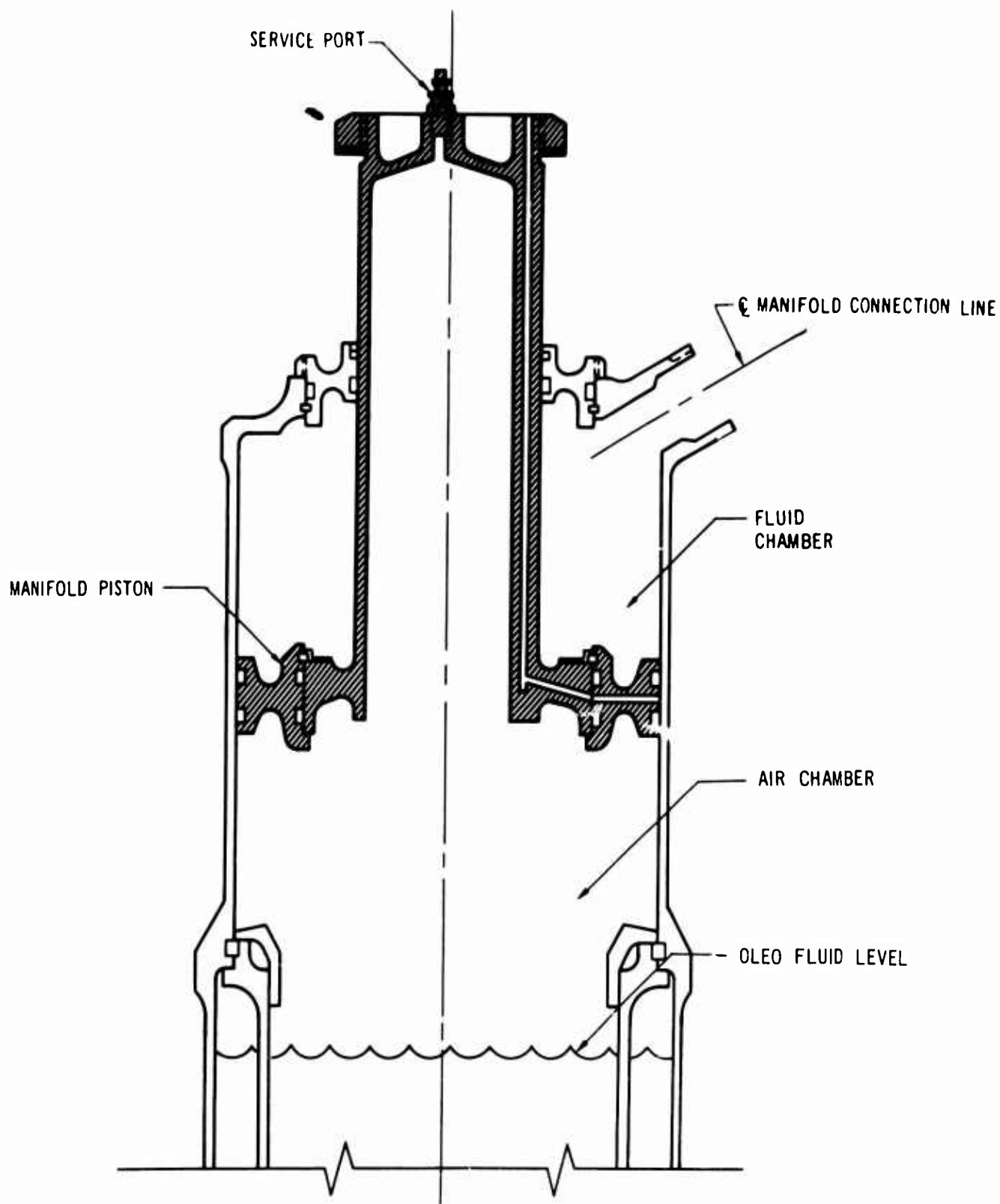






B

LVE



**DETAIL I**  
MANIFOLD CHAMBER TYPICAL ON ALL MAIN GEAR STRUTS

*Figure 3-56. Main Gear Manifold System*

V2-B2707-6-2

C

720 commercial jet airplane. The improved properties, together with the use of very exacting material specifications for material procurement, forging control, machining processes, heat treatment, and finishes guarantee a high degree of structural integrity. A discussion of the service history, design, and fabrication procedures is included in Boeing Document D6-17640 (Ref. 5).

The main-gear shock struts are braced by the side and drag struts to provide rigidity in all directions. The folding drag strut is retained in the down position by the down-lock linkage. The down-lock is designed to engage and lock without hydraulic assistance for all modes of operation. The truck beam is rotated about its pivot for stowage by a mechanical linkage. The truck is maintained in its correct attitude for landing by a truck pitch damper. Brake equalizing rods are used to eliminate truck pitching moments when the brakes are applied.

The aft main gears have a truck position lock that retains the truck in the fore and aft position during takeoff and landing when rudder pedal steering is being used.

Special structural features have been included in the design to improve service life and to simplify maintenance.

- Trucks are similar in spacing and loading to present commercial aircraft; therefore standard alligator jacks can be used.
- Nose gear axles are removable.
- Main gear axles are removable and interchangeable between positions.
- Truck beams utilize bushed holes for axle mounting.
- Axles are covered with protective sleeves in the area of the brake-mounting bushings and wheel bearings.
- All structural pin joints whether rotating or static have flanged bushings and are lubricated to reduce wear, galling, and corrosion, and to facilitate removal and repair.
- Shields are provided under the main-gear truck beams to protect them from damage.

- Tow lugs and jacking fittings are replaceable.
- Surfaces of all components are protected from corrosion by material selection, plating and paint.

The use of 16 individual brakes results in moderate brake temperatures and increased brake life. Brakes are conventional heat-sink disc type, hydraulically operated and housed within the wheel. The wheel is of conventional two-piece design manufactured from aluminum forgings and is designed for a roll life of 25,000 mi. Its strength and life characteristics will be verified by static limit and ultimate load tests and by roll tests at specific loads and distances. In addition, a fatigue analysis will be made for the main wheels using a load spectrum representative of actual ground-maneuvering conditions. The main gear wheels incorporate heat shields to protect the wheel and tire from brake heat following maximum energy stops. The wheel is also equipped with thermal plugs designed to release tire inflation air in the event of overheating. A Titanium wheel design is being investigated for possible improvement in weight and service life. A final choice will be made after review of weight, cost, and life data presented by wheel suppliers.

#### 3.5.2.3 Nose Gear

The nose gear as shown in Fig. 3-54 is similar in concept to that used on current commercial subsonic jets. Materials and construction are similar to those described for the main gear. The nose gear utilizes a conventional air-oil shock strut with a stroke of 18 in. The outer cylinder assembly includes pin-jointed structural trusses that attach to trunnions on the sides of the wheel well. Fore and aft loads are carried from the shock strut to the airframe structure through a folding drag strut. Nose wheel steering is accomplished by dual, linear, hydraulic actuators.

#### 3.5.2.4 Design Verification

Extensive photo stress techniques are used in the design of the landing gears. Following completion of the detail design, plastic replicas of the major structural members are fabricated. The parts are coated with a birefringent plastic. When the parts are loaded in a representative manner and viewed under polarized light, color patterns can be seen. The colors can be interpreted in terms of stress level within close limits

of accuracy. This will result in gear components with maximum structural efficiency and maximum life-to-weight ratio.

#### 3.5.2.5 Additional Data

Additional discussion of wheels, tires, brakes, steering, manifolding and retraction may be found in Part B, Hydraulics, Landing Gear, Auxiliary Systems (V2-B2707-11), of the Systems Report. Ground Maneuvering and flotation characteristics can be found in Operational Suitability, V4-B2707-1. Evaluation of other gear arrangements considered before selecting the present configuration is covered in System Engineering Report, V2-B2707-1.

### 3.6 STRUCTURAL INSPECTION AND REPAIR

#### 3.6.1 Inspection Methods, Applications, and Criteria

Inspection methods being used on commercial subsonic jets will be used on the B-2707. In addition, research and analysis of new inspection methods will be continued to take advantage of new technologies to improve airplane surveillance and reduce maintenance cost.

The nondestructive inspection procedures listed below are in use on Boeing subsonic jets. A detailed description of these methods and applications is contained in Boeing document D6-7170, Nondestructive Test Inspection Procedures for the Boeing Jet Transports (Ref. 6). A similar document will be prepared for the B-2707.

The primary method for inspection of structure will continue to be direct visual inspection. Indirect visual inspection by use of mirrors and boroscopes will be used in areas where access is limited. The B-2707 design project has considered maintainability as one of the prime design considerations. Access doors and openings are integrated into the structure.

The following common inspection methods will be used on the B-2707:

- X ray. Its principal application is for inspection of inaccessible airframe structure. One such application on the B-2707 will be the inspection of the leg of the lower-surface wing and stabilizer stringers which are covered by thermal insulation.
- Liquid penetrant. This method is used extensively on all structural parts.

- Magnetic particle inspection. This method is used for steel parts.
- Ultrasonic. This method is used for detecting flaws by high-frequency sound transmission through the part. It can be done either by immersion testing or by contact testing.
- Eddy current. This method has been used successfully in detecting cracks, originating in fastener holes, by use of a probe inserted in the hole.

A new inspection method under investigation is the use of liquid crystals for detecting bonding flaws in honeycomb panels. The method under development utilizes the unique characteristic of these compounds to respond to small changes in thermal environment with a reaction producing drastic color variations. The system is easily applied by brush or spray. The color transitions follow thermal changes rapidly and reverse with temperature and therefore are repeatable immediately. A bonding flaw or void area will have different thermal conductivity than the surrounding area, and this is indicated by a color change (see Figs. 3-57 and 3-58).

A promising new development for inspection of honeycomb panels is the sonic resonator. One of these instruments is being evaluated in the Model 737 program and the results of this evaluation will be applicable to B-2707 honeycomb structures. Preliminary results of this investigation are encouraging and appear to offer an opportunity to detect flaws at any location in the honeycomb by applying the probe to one surface. The equipment consists of a tunable signal-generator impedance bridge, amplifier, null detector, and a piezoelectric crystal probe. A photo of the instrument is shown in Fig. 3-59.

The instrument generates a low-frequency sound signal in a given structure and measures the acoustical impedance of the sound wave. This instrument can determine the location of a flaw in three dimensions. The dial on the instrument indicates whether the flaw is on the near or far surface.

Inspection criteria and schedules are established on subsonic jets during manufacturing and in service. Criteria for the B-2707 is patterned after this procedure. During manufacture, the inspection requirements are controlled by

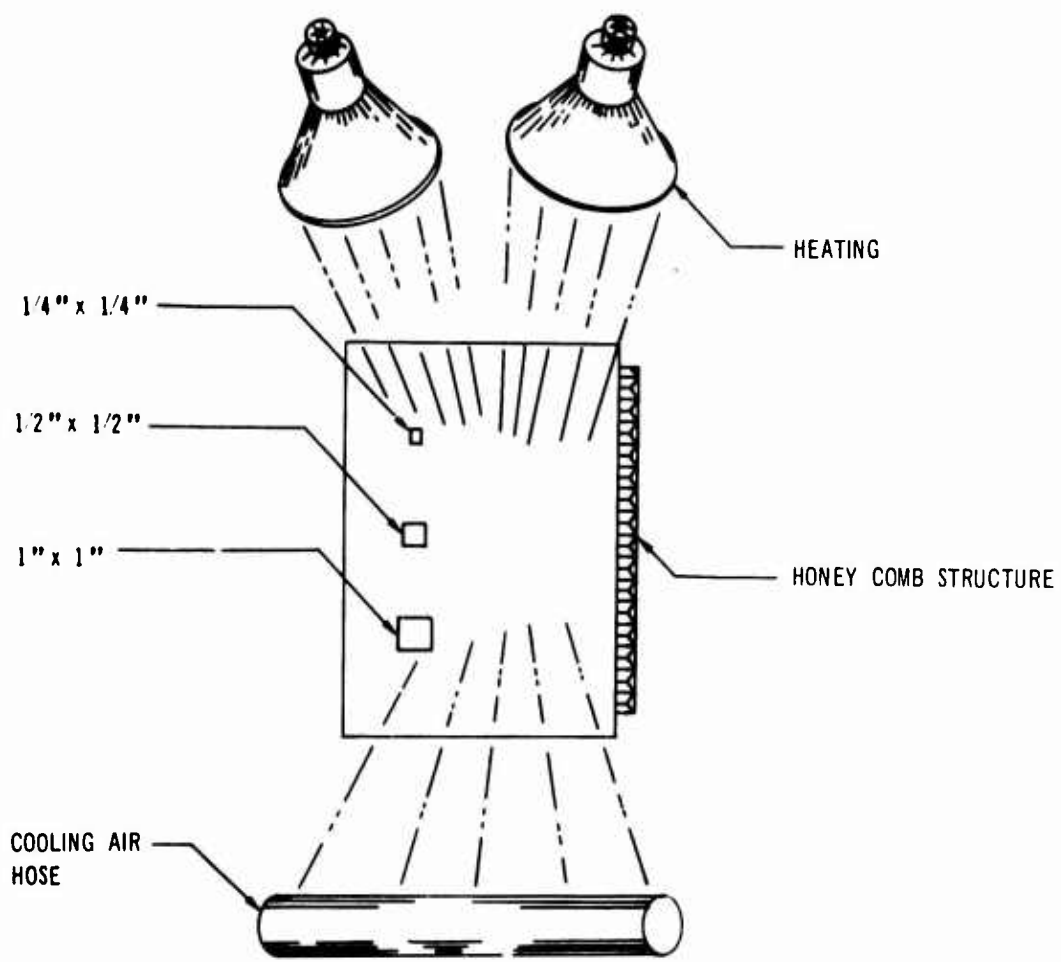


Figure 3-57. Flow Detection Setup



*Figure 3-58. Flaw Detection in Honeycomb Structure*

V2-B2707-6-2

**BLANK PAGE**



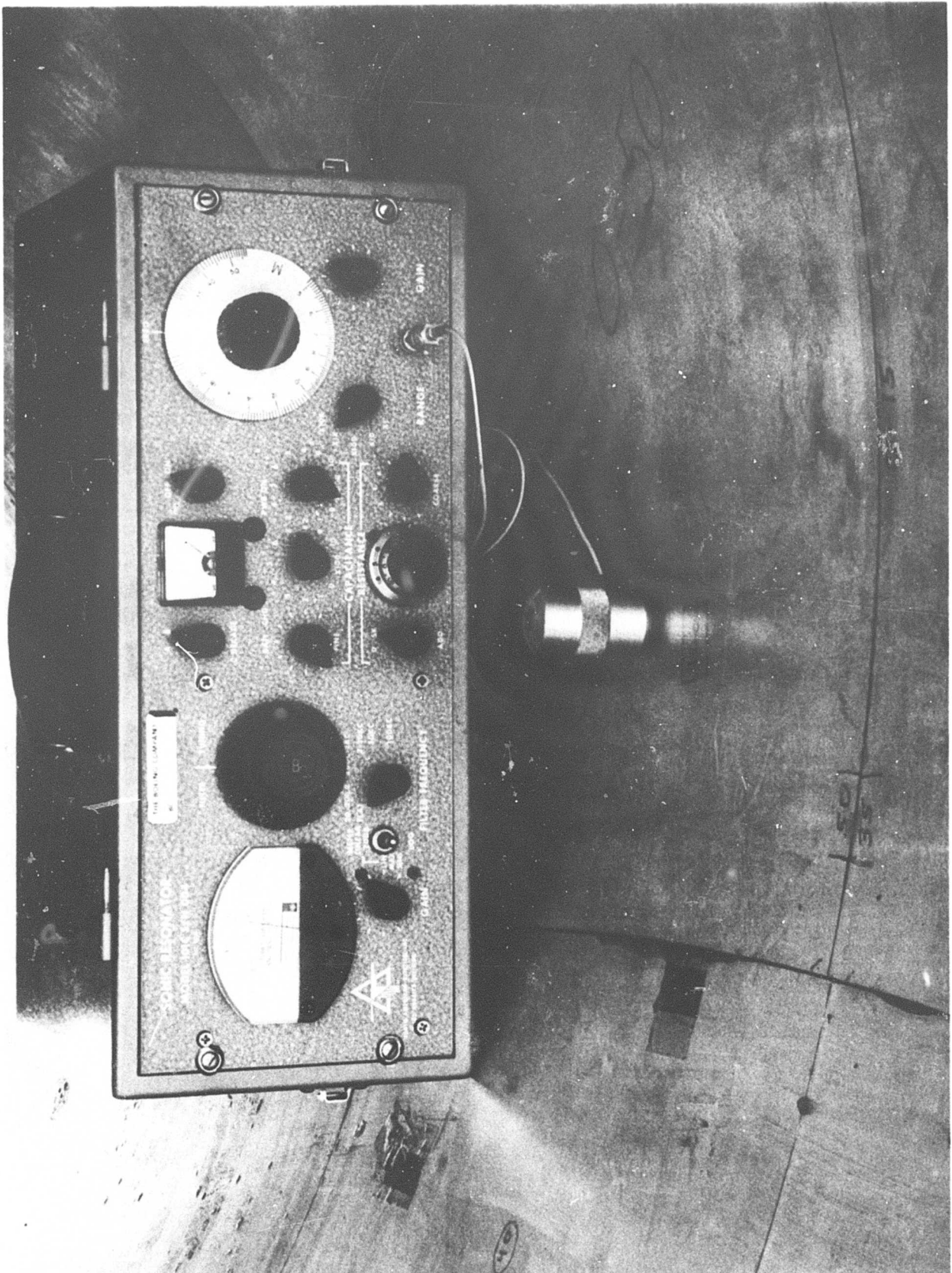


Figure 3-59. Sonic Resonator

engineering releases such as drawings and specifications. The Quality Control department is charged with the responsibility of inspection. During service, the scheduled inspections required to keep the airplane in a continuously safe-operating condition will be established in the FAA-airline negotiated B-2707 maintenance plan. The plan will be developed and presented in a maintenance planning data document that is described in the Product Support Program, V4-B2707-20. The application of this program to maintenance is described in Operational Suitability, V4-B2707-1.

The selection of a structural inspection interval for a specific structure is based on stress analysis, static and fatigue tests, environmental conditions, type of construction, and past experience. Each inspection requirement is defined in detail and the interval established for the inspections is considerably sooner than the occurrence of the earliest predicted service problem based on the above considerations. Some structure on all operator's fleet is inspected after a selected interval and other structure on some of the operator's fleet is inspected after every other interval. The sampling inspection technique has been used successfully and is considered a reliable method of detecting early defects.

Wear and rework tolerances will be established on parts subject to wear. Engineering will establish permissible wear limits commensurate with the parts function. This method is successfully used on subsonic jets today.

### 3.6.2 Structural Repair

Conventional techniques are applicable for accomplishing all structural repair on the B-2707. The airline mechanic will be able to perform repair tasks after updating his knowledge of tools, materials, and processes. This updating will be guided by maintenance manuals and by airline training programs conducted by the manufacturer. Damage will be evaluated and applicable repair determined from charts in structural repair documents.

Most bushings and bearings are replaceable without removal of major airplane components. They can be removed and installed with practices now used for the 707 and 727. The wing pivot is distinct and fully covered separately in Par. 3.1. The radome is the same durable type as used on the F-4 military airplane; scratches and gouges

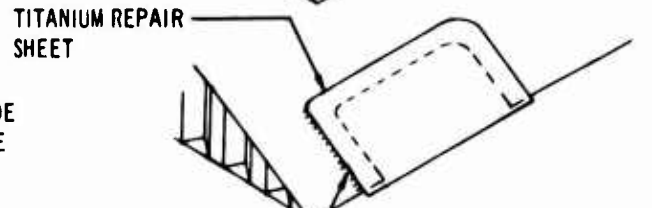
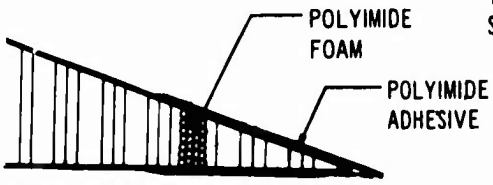
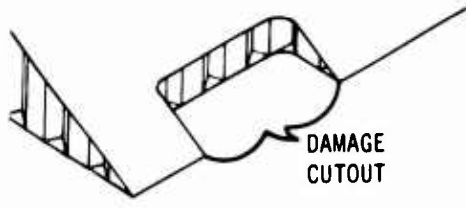
that can be restored with hand-applied sealant and roving are the probable extent of repair. Although sealant composition differs, repair procedures for integral wing and stabilizer-box fuel tank faults are the same as those for 707 and 727 transports and KC-135 tankers (with the additional requirement that the sealant be covered by insulation along tank floors of built-up construction). Fuel doors, passenger and cargo doors, dry-bay accesses, and aerodynamic surfaces have pressure seals that are retained in the same manner as on current commercial airplanes to enable rapid correction of any problems.

The prototype airplane test program and the static and fatigue tests of early production models will ensure correct repair procedure details. The manuals will be continually updated.

#### 3.6.2.1 Honeycomb Repair

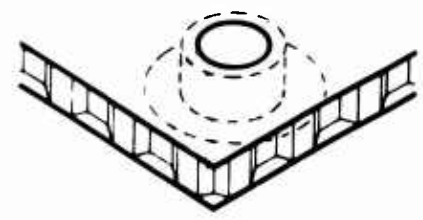
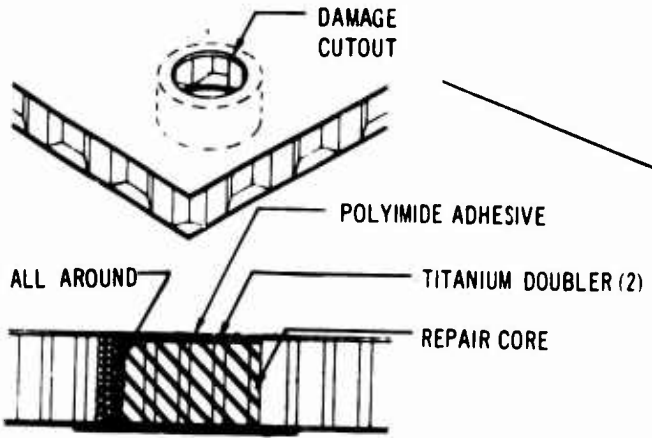
Honeycomb panels are used for airfoil surfaces, doors, panels, and other structure. Face sheets and edge doublers are of titanium with machined honeycomb cores of polyimide-reinforced glass fiber. For complex shapes, internal face sheets are sometimes made of polyimide glass fiber. Polyimide adhesives are used for assembly and are cured under pressure and temperature. Present subsonic-airplane bonding procedures are altered by the use of higher temperatures and pressures. Increased cleanliness is required. Production assembly is accomplished under closely controlled conditions of heating rates and adhesive-volatile evacuation. To fully restore structural strengths, permanent repairs must be similarly accomplished. Alternative repairs, which are heavier, can be done with heating blankets and vacuum pressure boxes. Concurrent with the prototype program, work is progressing in the development of field repair techniques that will enable faster structural repair. For repairs that are small relative to total panel size, the initial cure can be shortened to one hour, this initial cure will provide 80 percent of total bond strength, and postcure can be obtained during flight.

Several types of honeycomb damage repair are shown in Fig. 3-60. They are typical of B-2707 application and are similar to present repair procedures. Unique features are the polyimide adhesives and the core and face materials. Required bonding pressures will be limited to that achieved with vacuum methods (12 to 14 psi).

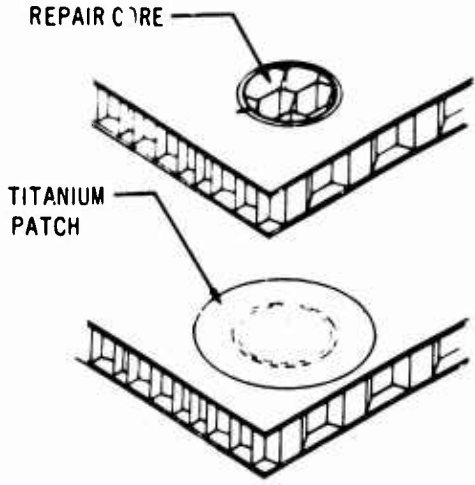
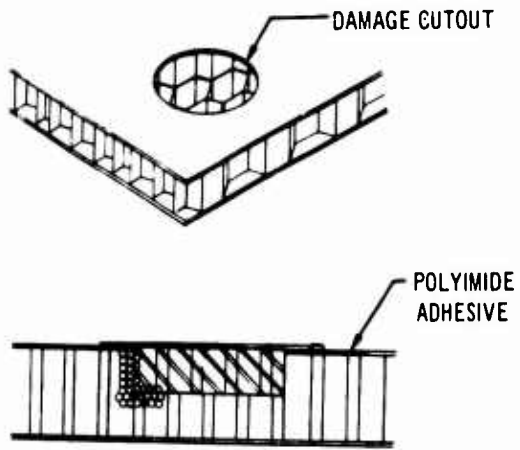


**REPAIR OF DAMAGE THRU BOTH FACE SHEETS**

SMOOTHER  
ROOM TEMPERATURE VULCANIZING



**FLUSH REPAIR**



**REPAIR OF DAMAGE TO OUTER FACE**

*Figure 3-60. Honeycomb Repair*

V2-B2707-6-2

### 3.6.2.2 Repair of Riveted and Bolted Titanium Construction

The conventional skin-stiffener structures assembled by rivets and bolts are repaired by techniques used on subsonic airplanes. Titanium-alloy replacement materials to match the damaged area and fasteners of titanium and A-286 steel will be used. Figure 3-61 shows typical repairs. Hole-drilling and rivet-driving techniques for the titanium materials have been developed. These methods will be refined during production as described in the Manufacturing Program V5-B2707-9. Maintenance manual data will be based on these developments.

### 3.6.2.3 Corrugated-Beam Repair

The empennage, wing, and fuselage utilize beams built up with a corrugated web welded to chord caps. The repair of a corrugated web requires the use of corrugated splice plates, riveted over the damaged web as shown in Fig. 3-62. Doublers required for patching damaged beam chords will match the shear web corrugations. Standard patches and doublers will be provided and be of sufficient size to allow fasteners outside the damaged area.

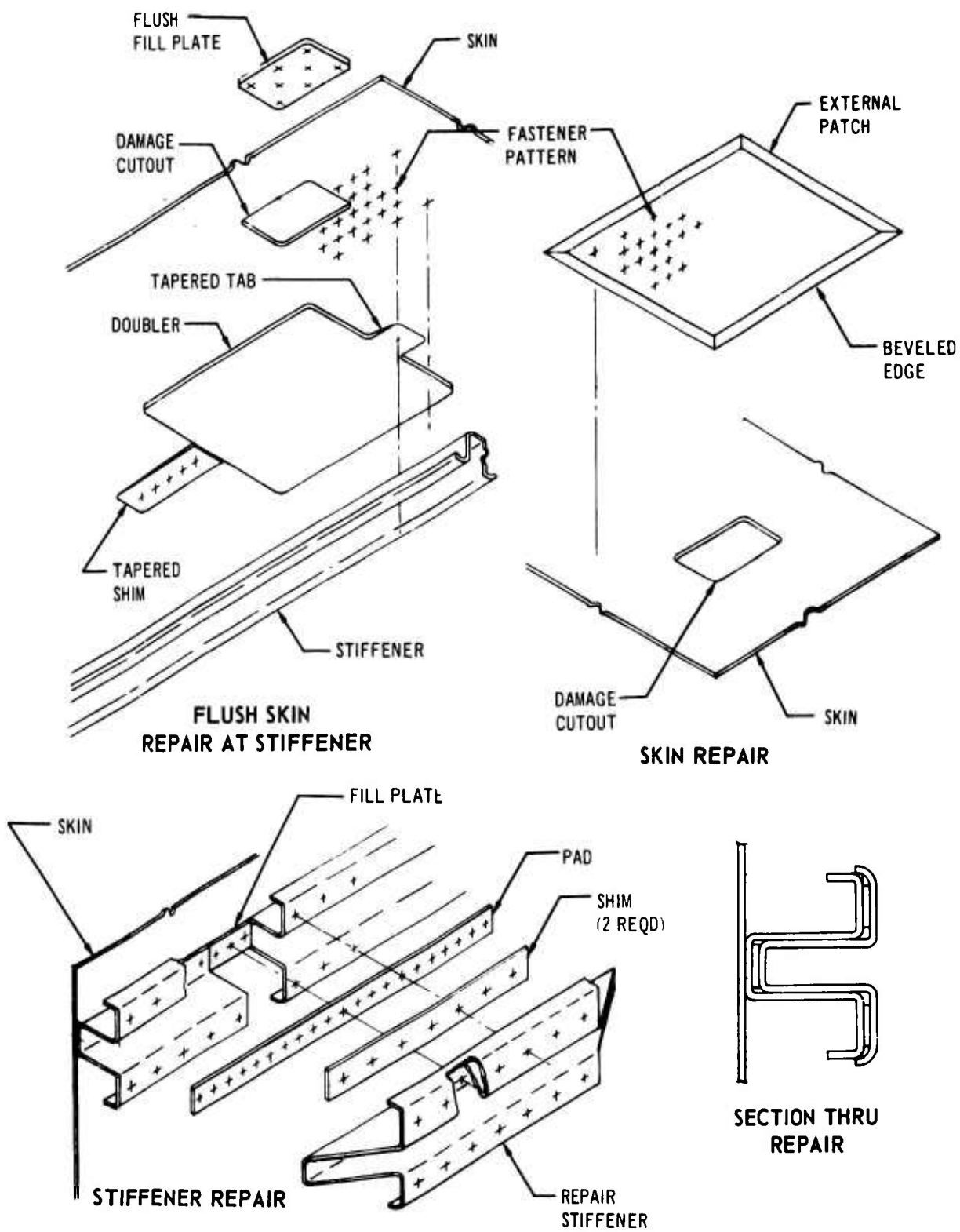
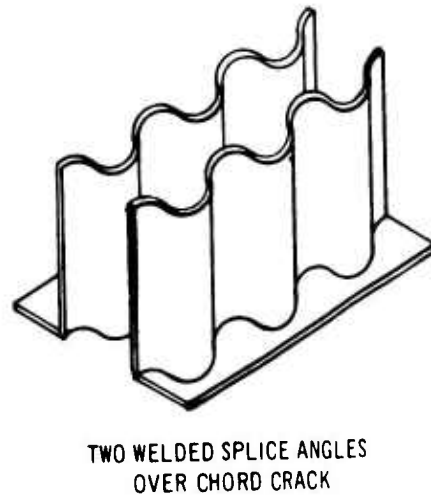
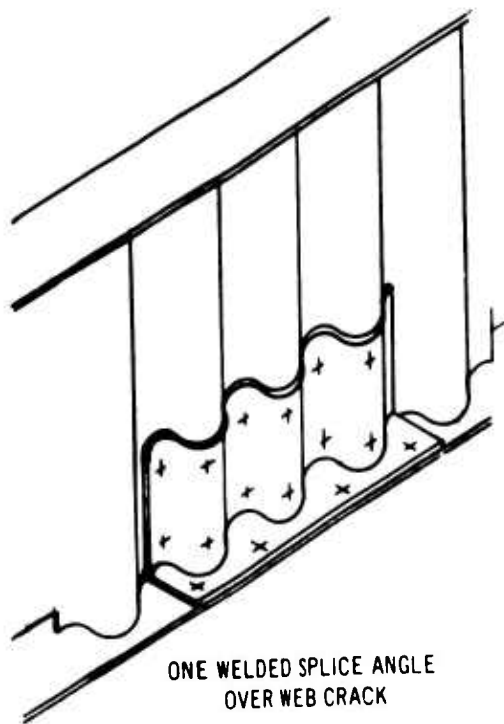


Figure 3-61. Skin and Stiffener Repair

V2-B2707-6-2



*Figure 3-62. Corrugated Beam Repair*

V2-B2707-6-2

## 4.0 STRESS ANALYSIS

This section presents a preliminary analysis of the B-2707 major structural components to depict stress levels, methods of analysis, member sizes, and allowable stresses. Fail-safe discussion and analysis, fatigue analysis, 1-g stress levels, and any unique structural requirements resulting from sonic or high-temperature effects are also included. Design criteria are presented in Part C, Design Criteria, Loads, Aerodynamic Heating, Flutter (V2-B2707-7); basic material properties in Part D, Materials and Processes (V2-B2707-8); and substantiating test data in Part E, Structural Tests (V2-B2707-9), all of the Airframe Design Report. Fatigue analysis including 1-g stress levels are presented in Sec. 5.0. Additional detail analysis data will be available at the on-site inspection to further substantiate the design.

### 4.1 METHODS OF ANALYSIS

Analysis techniques are similar for all of the major sections. Digital computers are used extensively to determine optimum structure arrangements, allowables, stresses, and margins of safety. Stresses are determined primarily by principal-axis beam theory with matrix force or redundant methods of analysis used to determine load and stress distributions in the more complex structures.

Several digital programs have been written for use in analysis of complex structural systems. These programs include the following:

**COSMOS** (Comprehensive Option Stiffness Method Organization System), a general purpose program for analysis of structures subjected to heating and loads using the direct stiffness method.

**SAMECS** (Structural Analysis Method for Evaluation of Complex Structures), a fully automated program for analysis of exceptionally large complex structures made up of plates and beams subjected to heating and loads and based on the direct stiffness method.

**ASTRA** (Advanced Structural Analyzer), a new generation COSMOS with capability to analyze

any size structure by automatically merging sub-structures, and having an improved library of structural elements and an improved method for handling boundary conditions.

**FUSARG** (Fuselage Analysis by the Argyris Force Method), a fully automated program designed for the analysis of a general class of fuselage structures that can be idealized to be composed of beam, rod, and shear panel elements subjected to heating and mechanical loads. Both the data generation and equation solution portion, ARGHOR III, have been designed to handle very large problems. This is a force method program.

**WINGEM** (Wing Generator Matrixes) an automated program for the analysis of a class of wing structures that can be idealized as an assembly of rods and shear panels subjected to mechanical loading. This is a force method program. The data generation and its solution program ARGHOR II OR III are designed to handle the solution of very complex problems.

**WING STRESS AND SAFETY MARGINS**, a program based on the theory of bending for the analysis of a limited class of wing structures.

**BODY STRESS AND SAFETY MARGINS**, a program based on the theory of bending for the analysis of a limited class of fuselage structures.

**TL-01**, a matrix interpretive scheme for the manipulation and arithmetic of large partitioned matrixes. The matrixes may be essentially of unlimited size.

Standard symbols of MIL-HDBK-5 (Ref. 7) are used to identify most quantities, and nonstandard symbols are identified where used. Detail descriptions of the typical analysis methods are included in the wing analysis section.

### 4.2 WING STRESS ANALYSIS

A stress analysis is presented in this document to verify the adequacy of the wing primary structure. The analysis of major components such as

pivot structure, outboard- and inboard-wing-portion bending material, strake, and wing box inside of the fuselage include design conditions, load and stress distributions, critical margins of safety, fail-safe features, and methods of analysis. Analysis of selected major components are given in the following sections.

#### 4.2.1 Structural Description

The wing structural arrangement is presented in Par. 4-2. The primary structure inboard and outboard of the pivot is fully cantilevered and constructed of semimonocoque beams of titanium 6Al-4V. The upper and lower panels are stiffened with Z extrusions. Spars webs are stiffened with formed or extruded sections. Inspar ribs are made of sine-wave corrugated webs with flat-plate chord members. Normal rib spacing is 27 in. in the primary box, but other spacing is used where required by concentrated loads.

The leading- and trailing-edge structure is cantilevered off the outboard primary box. The leading- and trailing-edge strake structure of the inboard wing portion is jointly supported by the wing and fuselage.

The wing and horizontal tail are designed for alignment at  $n = 1.0$  and nominal flight condition. Interconnect members that engage with the horizontal tail when the wing is in the full-aft position are cantilevered off the rear spars of the outboard wing portion. These members also serve as flap supports. The wing and horizontal-tail connection maintains alignment of the two surfaces for load conditions other than  $n = 1.0$ .

#### 4.2.2 Design Loads

Shear moment and torsion curves for wing design conditions are given in Figs. 4-1 through 4-5. The inboard portion of the movable wing is critical for the high-gross-weight, subsonic maneuver with  $\Lambda_{LE} 30$  deg. The outboard portion of the movable wing is critical for the start of cruise maneuver with  $\Lambda_{LE} 72$  deg.

The high-gross-weight, flaps-up, subsonic maneuver with  $\Lambda_{LE} 42$  deg. is the critical design condition for the pivot. The wing center section is critical for the high-gross-weight, flaps-down subsonic maneuver with  $\Lambda_{LE} 30$  deg. The wing inside of the fuselage is critical for several subsonic maneuver conditions at high gross weight. A low-gross-weight gust condition at time of

minimum fuel is the critical positive-bending condition for the strake. A full-fuel taxi condition gives the maximum negative-bending loading.

A comparison of the relative wing-panel material required for some of the design conditions is given in Fig. 4-6. This figure defines the critical condition along the wing span outboard of the pivot and is a means of showing the relative criticality of various flight conditions where the variables include external loading, thermal gradients, and elevated temperature effects on material properties.

#### 4.2.3 Design Allowables

Mostly the airplane is constructed of 6Al-4V material with mechanical fasteners as the primary method of attachment. The basic material properties and fastener allowables are taken from (Ref. 8). The properties of honeycomb panels and other materials used for special applications are shown with their analyses.

The basic material properties are used in calculating the allowable stress for each structural element. The calculations account for such variables as area distribution between skin and stringers, temperature, stress concentrations, column length, and other stability characteristics. Analytical methods of strength computation are also presented. Specific allowables for detailed structure are shown in the analysis of each major structural component.

Allowable tension and compression stresses for wing-bending material versus panel loading are shown in Fig. 4-7 for the selected skin-stringer panel construction. These allowables were determined using TEST DATA (see Part E, Structural Tests (V2-B2707-9), of the Airframe Design Report) and the analysis methods and criteria given in the following paragraphs. The compression allowables of Fig. 4-7 are based on 27-in. rib spacing and stringers with varying depths and spacing.

##### 4.2.3.1 Thermal Stresses

Elevated temperature allowables on structure subjected to aerodynamic heating are determined using basic allowables and the temperature profiles given in Part C, Design Criteria, Loads, Aerodynamic Heating, Flutter (V2-B2707-7), of the Airframe Design Report.

Thermal stresses ( $f_{th}$ ) for structural members subjected to thermal gradient environments are



V2-B2707-6-2

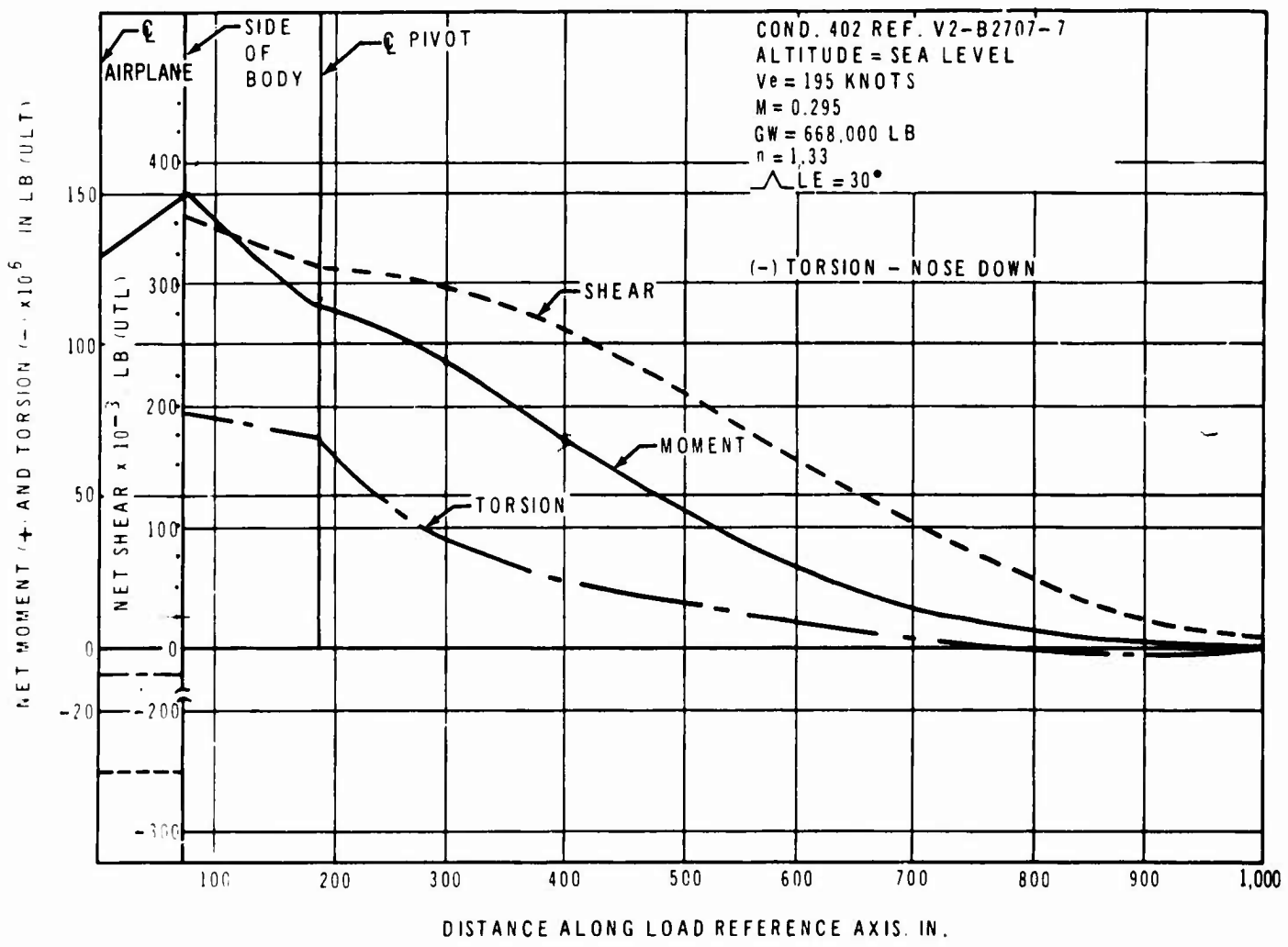


Figure 4-1. Ultimate Wing Loads, Flaps Down Steady Roll

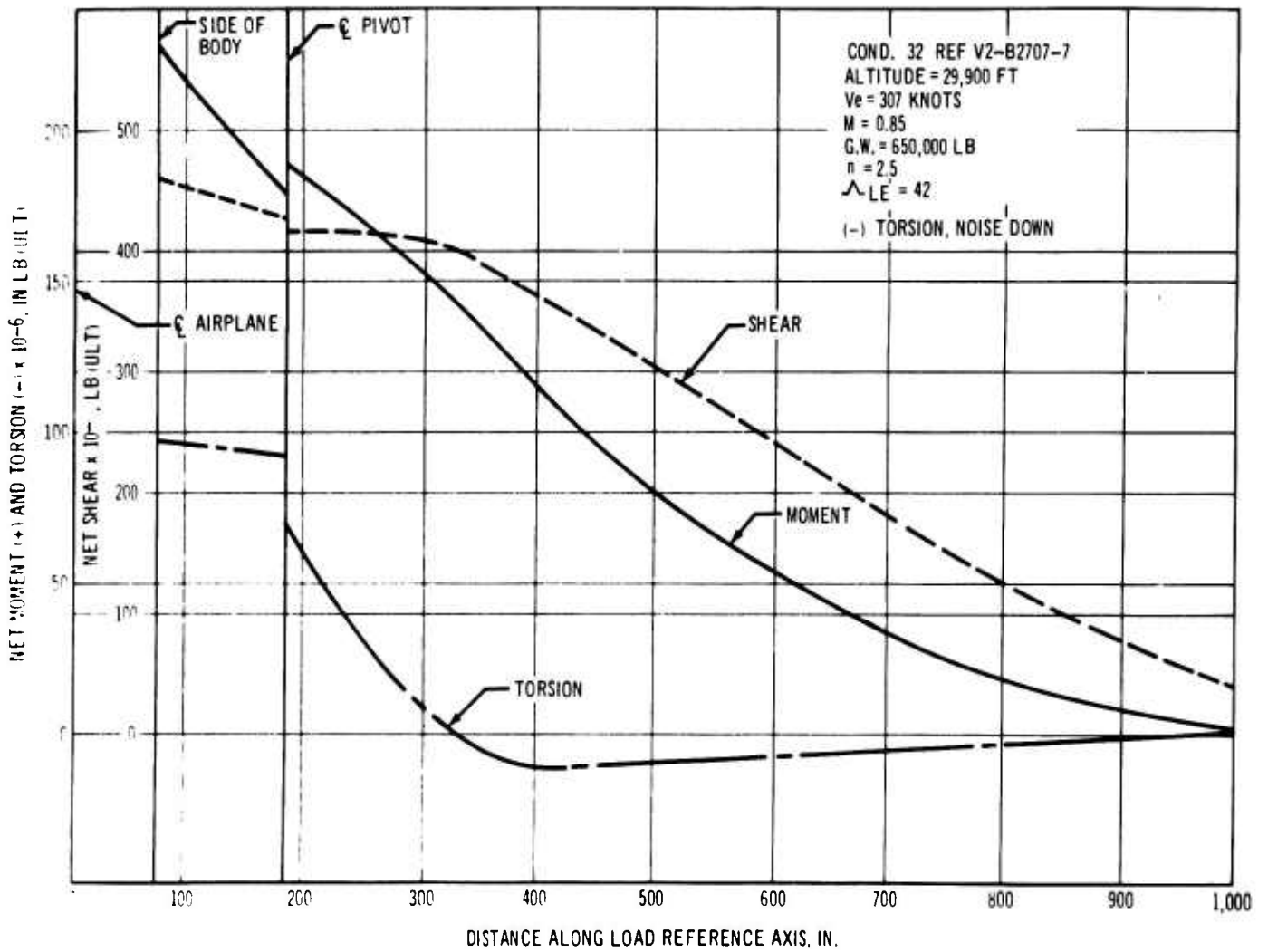


Figure 4-2. Ultimate Wing Loads, Subsonic Maneuver

*Verticals  
 @ PIVOT*

V2-B2707-6-2

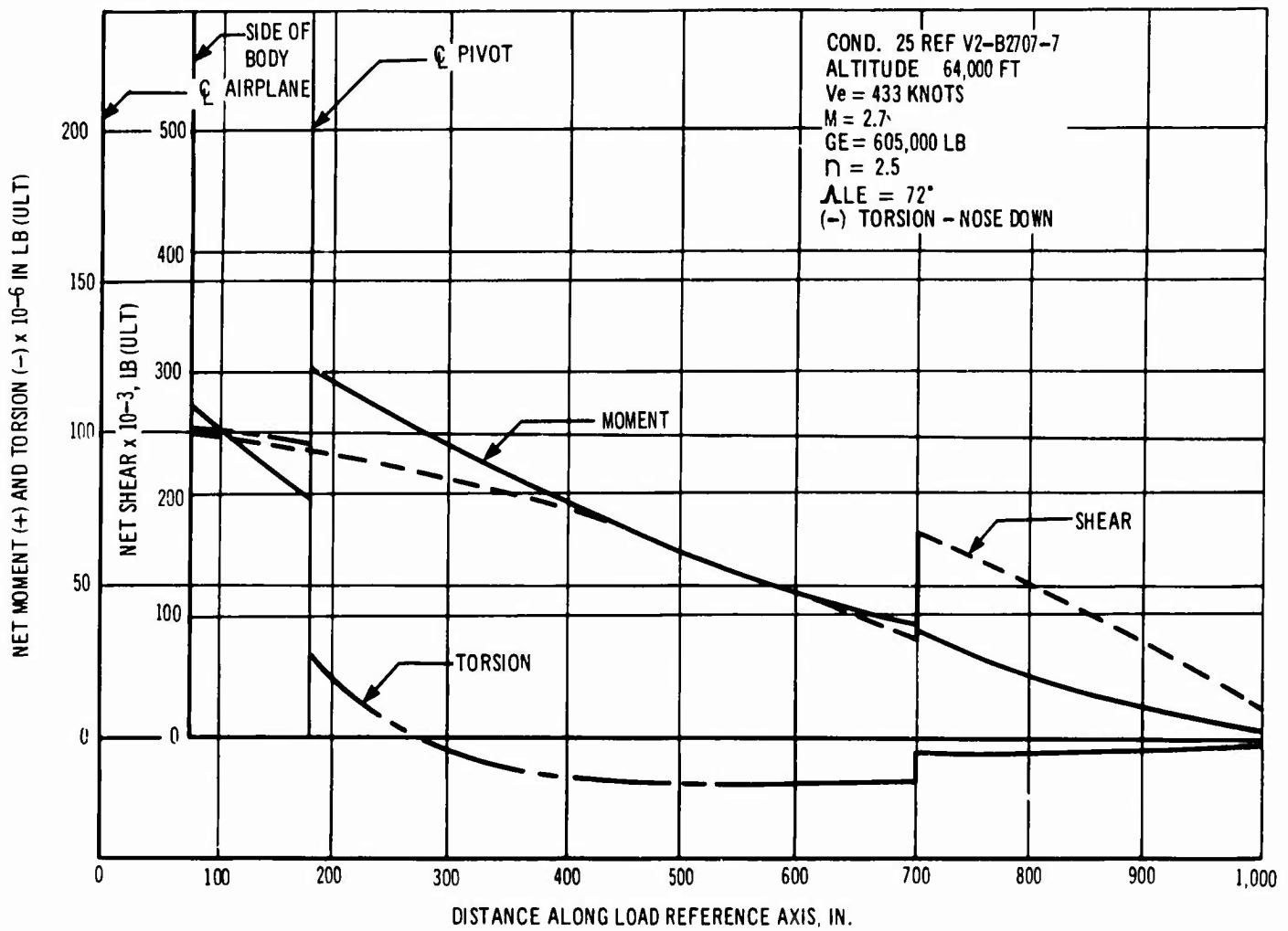


Figure 4-3. Ultimate Wing Loads, Start of Cruise Maneuver

VESIGAS  
 1. OUTBOARD PORTION OF MOVABLE WING

calculated using a relation of equal strain for each element of the section. The developed equation conservatively assumes that structural members have end-rotational restraint, that all strains are elastic, and that plane cross sections remain plane after the application of thermal gradients. Using  $E$  and  $\alpha$  consistent with the temperature of each element of the section, thermal stresses are calculated from the equation:

$$f_{th} = E \left[ -\alpha T + \frac{\sum E \alpha T A}{\sum E A} \right]$$

where the  $f_{th}$  = calculated thermal stress, psi

$\alpha$  = coefficient of thermal expansion, in./in./°F

$T$  = change in temperature from 70°F in °F

$A$  = section element area, in.<sup>2</sup>

In combination with ultimate mechanical stresses, thermal stresses are increased by a factor of 1.25 to account for temperature excursions above design conditions and the uncertainties of strain predictions caused by temperature on complex structure.

#### 4.2.3.2 Tension Allowables

The net area tension allowable is 98 percent of the material ultimate tension strength with 10 percent holeout. This reduction is slightly conservative because company tests on center-notched and bolted-joint specimens at room and elevated temperature have shown that titanium does not exhibit reduction in net material allowable at holes, as found for some aluminum alloys. These tests have indicated that 100-percent net area efficiency is obtained for 15 percent and greater holeout, with a slight reduction in efficiency for lesser percentage holeout. Reduced allowables or higher design factors are used when required by fatigue analysis results or by good design practices. An

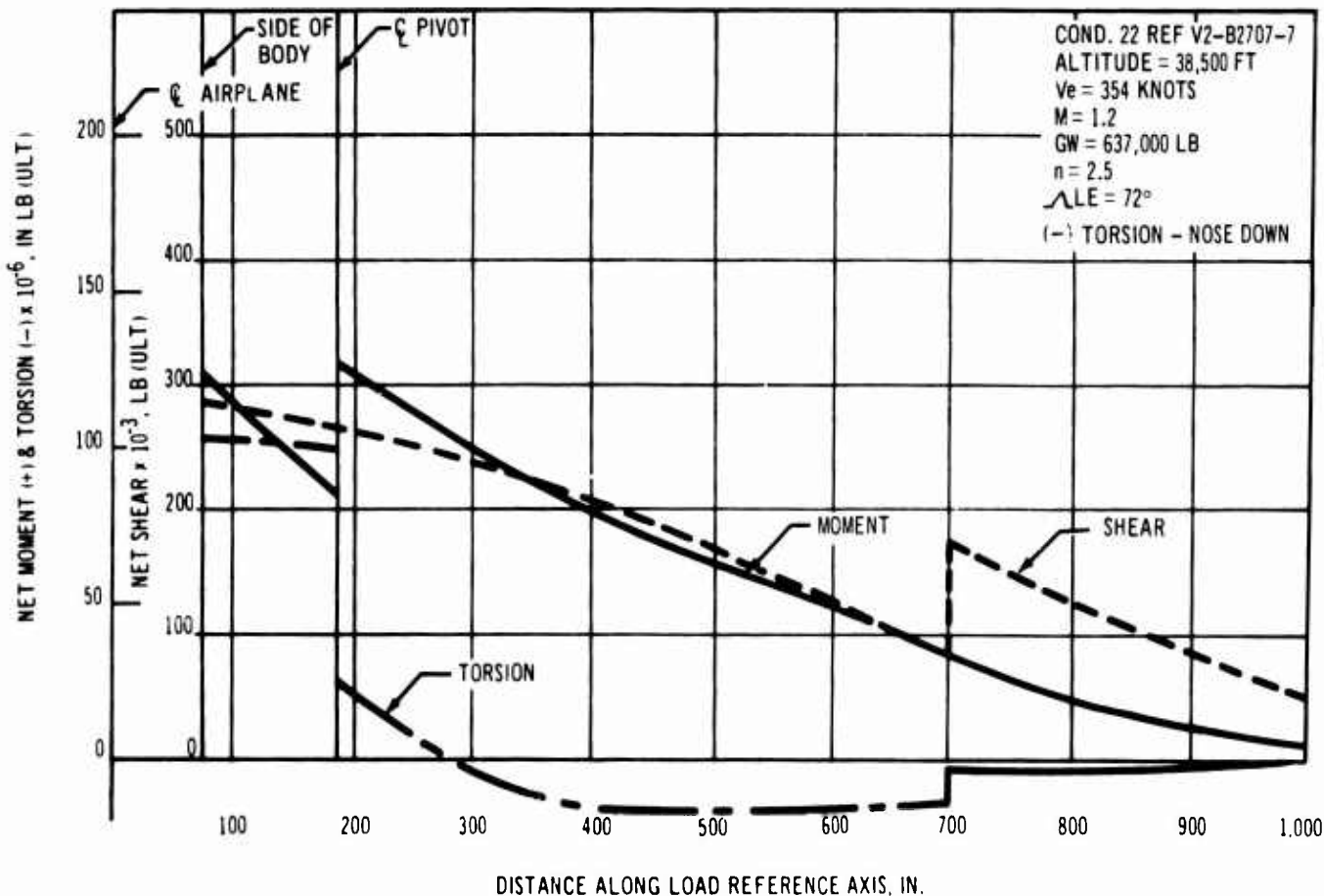


Figure 4-4. Ultimate Wing Loads - Transonic Maneuver

V2-B2707-6-2

allowance of 10 percent is made for holeout in sizing the wing lower-surface tension material.

Actual net area when greater than 10 percent holeout is used in individual component analysis. The design ultimate stress relation is

$$f_t + 1.25 f_{th} = F_t \text{ allowable}$$

The yield strength of titanium 6Al-4V is high relative to its ultimate strength. Therefore, any structure designed to meet ultimate load requirements will not exceed yield strength at limit load.

#### 4.2.3.3 Compression Allowables

Ultimate compression allowable stress is based on either column-allowable or the section-crip-

pling stress. Column allowables were determined from the Johnson-Euler equation.

$$F_c = F_{cc} \left[ 1 - \frac{F_{cc} \left( \frac{L}{p\sqrt{C}} \right)^2}{4\pi^2 E} \right]$$

The use of this equation has been substantiated by the test program described in Part E, Structural Tests (V2-B2707-9), of the Airframe Design Report. Columns are usually assumed to be pin-ended with a conservative fixity coefficient of one. In determining the section slenderness ratio, the amount of effective skin working with the section was calculated using the conventional effective width equation.

The allowable crippling strength of formed sections is determined using the analysis method of

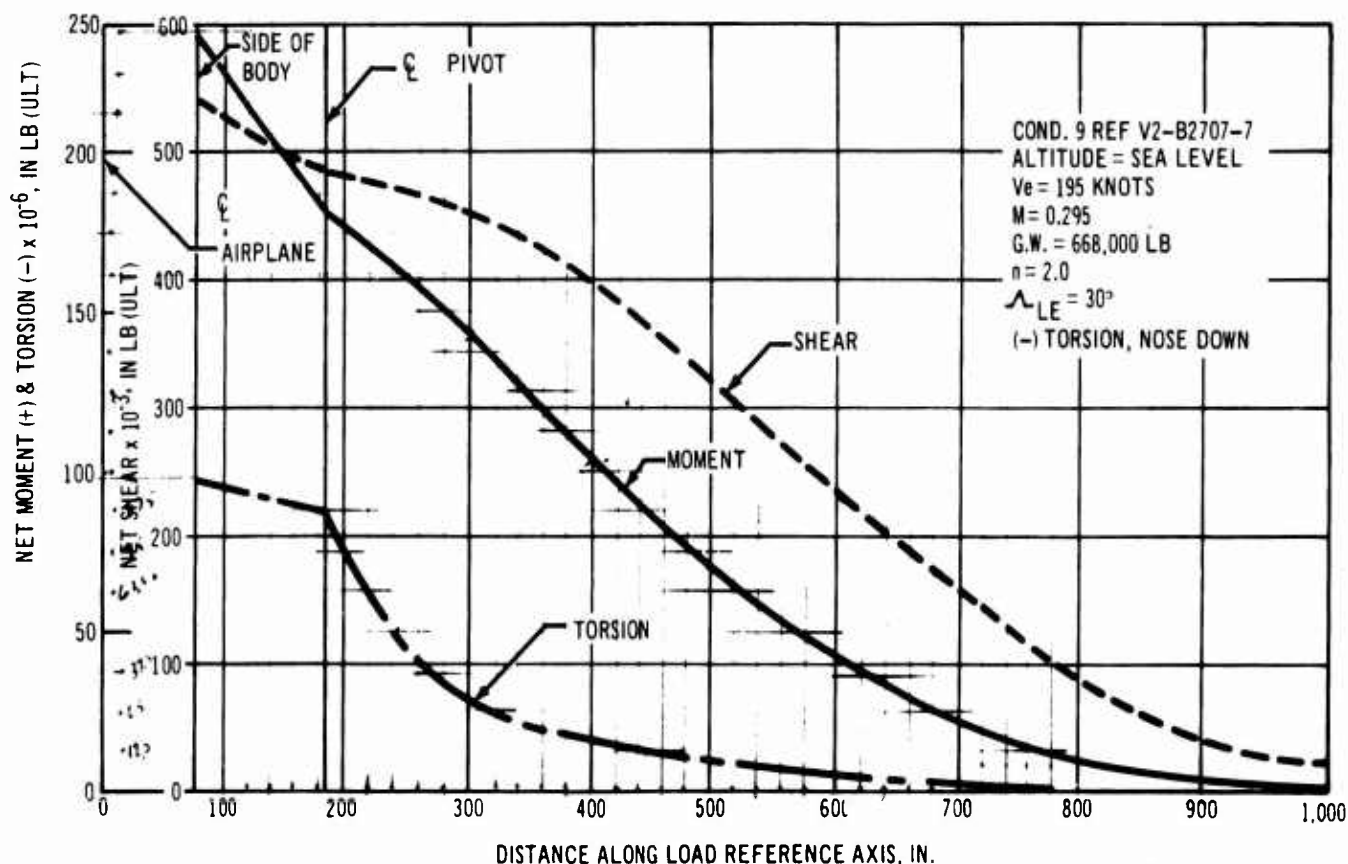
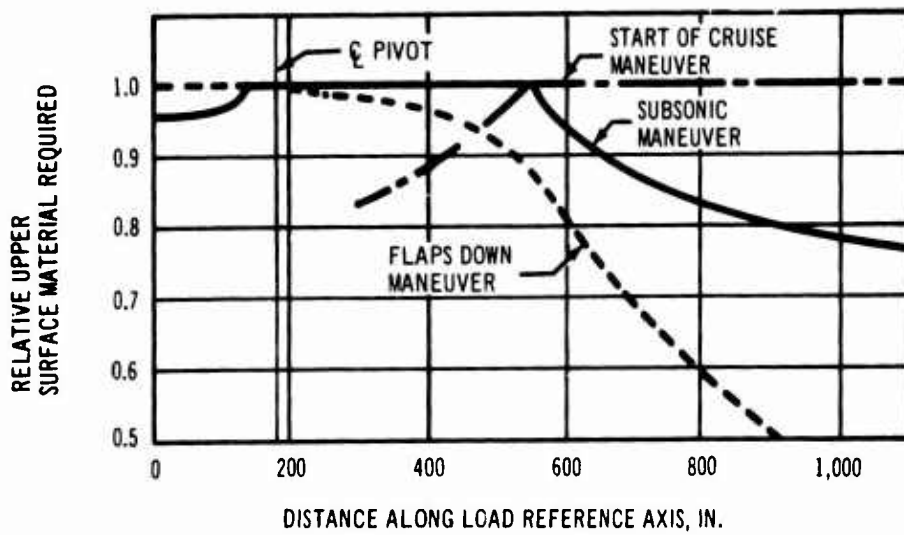


Figure 4-5. Ultimate Wing Loads, Flaps-Down Maneuver

*REMARKS*  
 1. INBOARD PORTION OF WING IS CRITICAL  
 2. WING INSIDE SECTION IS CRITICAL FOR SEVERAL SUBSONIC MANEUVER COND. @ HIGH GROSS WT.



REF. V2-B2707-6-1 FOR LOAD REFERENCE  
 AXIS LOCATION  
 REF. FIGS. 4-1 THRU 4-5 FOR DESCRIPTION  
 OF LOAD CONDITION

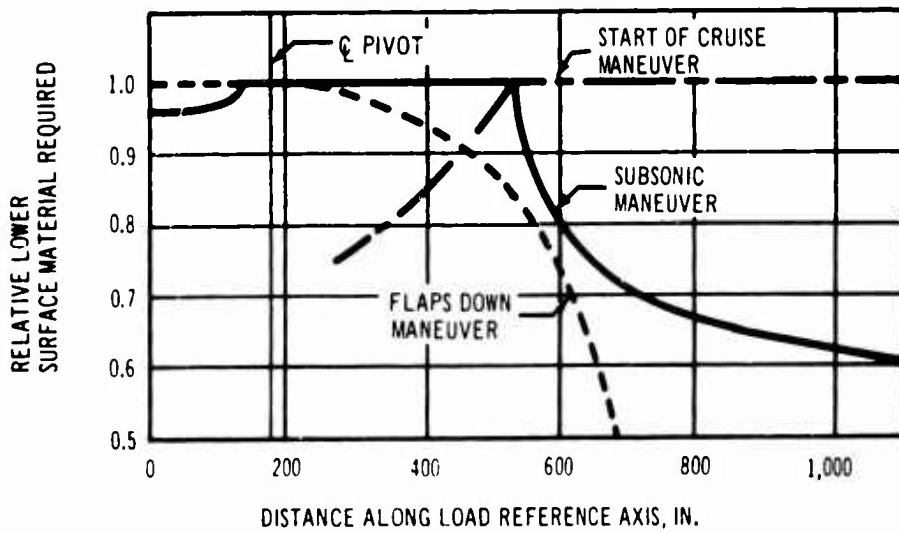


Figure 4-6. Comparison of Ultimate Wing-Design Conditions

V2-B2707-6-2

(Ref. 9). This method involves a summation of the crippling strengths of angle elements where the crippling strength of each element is found from:

$$F_{cc_n} = \frac{C \sqrt{F_{cy} E'}}{(b/T)^{0.75}}$$

where  $F_{cc_n}$  = element crippling strength, psi

$E'$  = reduced modulus, psi

$b'$  = element length, in.

$C$  = end restraint coefficient of element.

The allowable crippling stress for extruded or machined sections is calculated using the analysis method of Ref. 10,

$$F_{cc} = B \left[ \frac{gt^2}{A} \right]^m \sqrt{E^m F_{cy}^{2-m}}$$

where  $B$  and  $m$  are experimentally derived constants and  $g$  is a factor to reduce the section to a series of flanged elements. From the compression test program (V2-B2707-9), values of  $B = 0.64$  and  $m = 0.85$  resulted in excellent agreement between calculated and experimental crippling strengths. The crippling allowable of each element is determined from the above

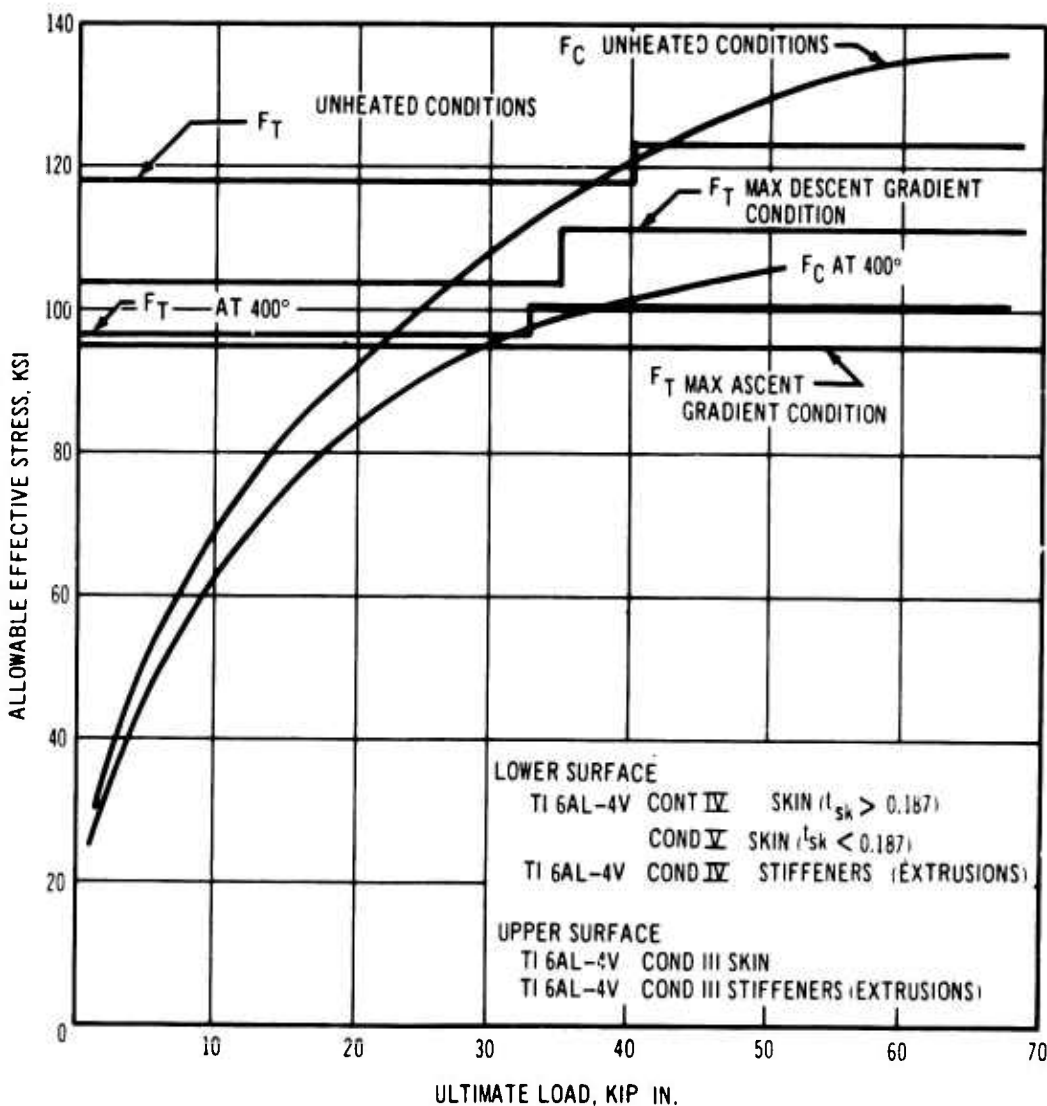


Figure 4-7. Wing Panel Allowables

*allowable stress is also dependent on temperature with varying degrees and spacing*

equation, and the allowable for the total section is determined as follows:

$$F_{cc} = \frac{F_{cc1} A_1 + F_{cc2} A_2 + \dots + F_{ccn} A_n}{A_1 + A_2 + \dots + A_n}$$

The required area for column critical sections is determined from the relation

$$[f_c \leq F_c]$$

The axial compression ( $f_c$ ) and thermal compressive stress ( $f_{th}$ ) are not permitted to exceed the crippling allowable of any segment

$$[f_c + 1.25 f_{th} \leq F_{cc}]$$

#### 4.2.3.4 Shear Allowables

All shear allowables for this analysis are determined from the ultimate shear strength of the material reduced by appropriate configuration factors based upon experimental values from similar structure. The ultimate, net-area, allowable shear stress for flat shear-resistant panels is 0.60  $F_{TU}$ ; for intermediate flat shear webs, it is 0.49  $F_{TU}$ . Required web stiffening will be approximately 50 percent with some variation from this value dependent on local requirements. Web-to-stiffener riveting will be sufficient to prevent web-stiffener attachment failure. The shear-web test program (V2-B2707-9) has verified the use of the design parameters for intermediate shear webs.

#### 4.2.3.5 Combined Stress Allowables

Principal stress theory is used to determine maximum stresses for combined shear and tension loading on shear-resistant panels. Maximum net stresses are not allowed to exceed material ultimate stresses previously discussed.

Combined shear and compression ultimate allowables for flat shear-resistant panels are conservatively combined by the following interaction formula:

$$\frac{f_c}{F_c} + \left[ \left( \frac{f_c}{F_c} \right)^2 + 4 \left( \frac{f_s}{F_s} \right)^2 \right]^{1/2} \leq 1.0$$

With the addition of thermal stresses, the equation becomes:

$$\frac{f_c + 1.25 f_{th}}{F_{cc}} + \left[ \left( \frac{f_c + 1.25 f_{th}}{F_{cc}} \right)^2 + 4 \left( \frac{f_s}{F_s} \right)^2 \right]^{1/2} \leq 1.0$$

#### 4.2.3.6 Buckling Criteria

To minimize aerodynamic drag, most skin surfaces are designed to remain unbuckled for normal one-factor cruise flight conditions. Buckling is permitted in some areas where thermal stresses peak for short periods of time and in areas where aerodynamic drag considerations are not significant and fatigue considerations permit. In integral fuel-tank areas, the design is such as to prevent buckling at limit load, which could cause fuel leakage.

#### 4.2.3.7 Fastener Allowables

Titanium 6Al-4V bolts, lockbolts, Taper Loks, and squeeze-driven rivets are used extensively. Fastener allowables are shown in Ref. 8.

### 4.2.4 Primary Wing Box

#### 4.2.4.1 Method of Analysis

Elementary bending theory for unsymmetrical beams is used to determine internal load distribution in the wing box. Shear flows are determined by  $VQ/I$  and  $T/2A$ . Wing cross sections are taken normal to the load reference axis. Stresses and margins of safety are determined using a digital computer program. The stress analysis computer program uses analysis theories confirmed by use on previous airplanes. This program was modified as necessary for the B-2707.

#### 4.2.4.2 Outboard Variable Sweep Portion of the Wing

Upper and lower surfaces are of conventional skin and Z-stiffener construction. The upper surface is titanium 6Al-4V Condition III material. The lower surface is Condition IV material because of its better fracture-toughness properties. Condition V material may be used where initial material gage is less than 0.187. Results of the wing fail-safe test program (V2-B2707-9) were used in selection of panel widths, skin-stringer



area ratios, and stringer spacing to provide fail-safe structure according to design criteria requirements of Part C, Design Criteria, Loads, Aerodynamic Heating, Flutter (V2-B2707-7), of the Airframe Design Report.

Printouts of computer data for sections that are located 315 and 715 in. outboard of the pivot measured along the load reference axis are presented in Tables 4-A, 4-B, and 4-C for the critical load conditions. Typical nomenclature is shown after the following paragraph. The given analysis and resulting margins of safety illustrate the methods employed and do not represent the final optimization of the section.

The results show that the subsonic maneuver for the inboard wing portion and the start of cruise-maneuver condition is critical for the outboard wing portion. With the wing in the aft position, local areas of the lower-surface trailing-edge structure in the immediate vicinity of the engine may be subjected to inlet buzz pressure. This pressure diminishes with distance from the inlet and obtains a maximum value of  $1.1 q$  immediately forward of the inlet. Local areas are reinforced for this condition.

ETA STA	Section perpendicular to assumed load reference axis, at which stresses are calculated, measured in percent semispan along the axis
LOAD COND.	Load condition number
$V_Z$	Beam shear load
$M_X$	Beam bending moment
T	Torsion about load reference axis
$V_X$	Chord shear load
$M_Z$	Chord bending moment
SEG. NO.	Segment number—assumes same number as stringer contained by segment. Zero refers to rear spar segment and 99 refers to front spar segment; the number 100 has been added to all upper surface numbers.

SKIN THICK.	Minimum skin thickness in segment effective in resisting shear stresses.
SEG. AREA	Segment area
AREA LOWER	Total lower surface cross-sectional area
AREA UPPER	Total upper surface cross-sectional area
*AREA E-LOWER	Sum of lower-surface-segment, cross-sectional areas multiplied by respective effectiveness factors
*AREA E-UPPER	Sum of upper-surface-segment, cross-sectional areas multiplied by respective effectiveness factors.
$I_X$	Moment of inertia about a line parallel to the wing reference plane through the section centroid and contained in the plane of cross section
$I_Z$	Moment of inertia about a line perpendicular to the wing reference plane through the section centroid and contained by the plane of cross section
$I_{XZ}$	Product of inertia
BAR ZE	Distance from wing reference plane to centroid of the effective segment
BAR XE	Distance from rear spar centerline to centroid of the effective segment
$I_{XE}$	Moment of inertia of effective section about a line parallel to the wing reference plane through the centroid of the effective segment and contained in the plane of cross section

$I_{ZE}$	Moment of inertia of effective section about a line perpendicular to the wing reference plane through the centroid of effective section and contained in the plane of cross section	SHEAR FLOW	Shear flow between segment (for example the shear flow shown at 4 occurs between segments 4 and 5); positive shear flow is clockwise.
$I_{XE ZE}$	Product of inertia of effective section	SHEAR STRESS	Shear stress (Each segment has a shear flow on both sides. The shear stress for a particular segment is equal to the maximum of its two shear flows divided by the skin thickness for that segment.)
TRUE J	Polar moment of inertia of the wing box		
2A	Twice the enclosed area of the section	SHEAR ALLOW	Shear allowable
$P_Z$	Beam shear adjustment because of slope of segment with wing reference plane	M.S. TEN.	Margin of safety for tension
$P_X$	Chord shear adjustment because of slope of stiffener with assumed-load reference axis	M.S. SHEAR	Margin of safety shear
		M.S. COMP.	Margin of safety for compression
		S.W. EFF.	Theoretical most efficient spar-web thickness
T. C. VZ	Torsion correction-adjustment for $P_Z$ torsion	*An effectiveness factor is used to account for reduced efficiency resulting from shear lag effects, which are caused by the geometry of the surface. Appropriate efficiency factors are obtained from analysis and comparison of data from tests of similar structures.	
T. C. VX	Torsion correction-adjustment for $P_X$ torsion	4.2.4.3 Wing Center Section Inside of Fuselage The structural description of the center section is given in Par. 3.2. Conventional wing construction is used except that the ribs are placed parallel to the spars. The upper surface is stabilized by the fuselage floor beams and intercostal ribs are provided to stabilize the lower surface. The locations for attachment of the main gears to the front and rear spars are shown in Fig. 4-8.	
T. E. EQUIB.	Torsion necessary to balance section	A redundant matrix force analysis is used to determine the surface-panel load distribution from wing bending. The wing torsion carried by differential bending at the pivot has been redistributed into the wing box at the side of the fuselage. The axial couple load at the pivot caused by wing-bending moment produces an eccentric loading condition on both the upper and lower surfaces. This eccentric loading	
STIFF AREA	Area of any stringers, spar chords, and spar webs that are included in a particular segment		
DIST. N. A.	Distance from the neutral axis to point of intersection of stringer centerline and wing contour		
SEG. LOAD	Segment load		
SEG. STRESS	Segment stress		
SKIN STRESS	Skin stress		
TEN. ALLOW	Tension allowable		

Table 4-A. Outboard-Wing-Portion Analysis, Subsonic Maneuver

MODEL 2707 WING SECTION PROPERTIES - STRESSES - MARGINS OF SAFETY  
50 IN. ALONG LOAD REFERENCE AXIS

R/12/66

ETA STA.	LCAC CONCD.	V Z	M X	T	V X	M Z	AREA LOWER	AREA UPPER	AREA ELLOWER	AREA FUPPER	S.W. EFF	TRUF-J.
C.500	32	302000.	8100000C.	90C0000.	0.	0.	34.130	38.485	34.130	38.485	0.150	20832.

I X	I Z	I XZ	BAR ZE	BAR XE	I XE	I ZE	I XE ZF	2A	P Z	P X	T.C. VZ	T.C. VX	T.C. FOIIR
14126.	100272.	-6677.8	-2.99	-53.95	14126.	100272.	-8677.8	6614	-93042.	4686.	546077.	668027.	25983352.

SEC. NO.	SKIN THICK	SEG. AREA	STIFF AREA	DIST N.A.	LOWER SURFACE SEG. LOAD	STRESS	SKIN STRESS	TENS. ALLOW	SHEAR FLOW	SHEAR STRESS	SHEA. ALLOW	M.S. TENS.	M.S. SHEAR
0	0.230	2.080	1.400	-17.536	214978.	103355.	107927.118000.	-1649.	9562.	77000.	0.08	0.41	
1	0.230	2.250	C.900	-17.442	231128.	102724.	104934.118000.	-1056.	7169.	77000.	0.12	0.45	
2	0.210	2.650	1.400	-16.950	267660.	99502.	102015.118000.	-370.	5030.	77000.	0.15	0.50	
3	0.210	2.250	C.900	-16.459	217732.	96770.	99041.118000.	189.	1760.	77000.	0.19	0.55	
4	0.210	2.370	0.900	-15.967	222283.	93790.	96061.118000.	761.	3623.	77000.	0.23	0.60	
5	0.210	2.250	C.900	-15.573	205656.	91403.	93674.118000.	1290.	6143.	77000.	0.25	0.63	
6	0.160	2.250	1.200	-15.179	199740.	88773.	91438.118000.	1805.	11279.	77000.	0.27	0.64	
7	0.160	2.550	1.000	-14.787	223788.	86405.	87069.118000.	2382.	14887.	77000.	0.29	0.64	
9	0.160	2.550	1.000	-14.001	211456.	81643.	84308.118000.	2929.	18305.	77000.	0.34	0.68	
10	0.110	1.650	C.900	-13.607	130772.	79256.	82072.118000.	3268.	29706.	77000.	0.29	0.52	
11	0.110	1.120	0.470	-13.416	87674.	78280.	80915.118000.	3495.	31774.	77000.	0.28	0.50	
12	0.110	1.120	C.470	-13.024	85015.	75906.	78541.118000.	3716.	33782.	77000.	0.30	0.49	
13	0.110	1.120	C.470	-12.833	83719.	74749.	77383.118000.	3934.	35763.	77000.	0.29	0.46	
14	0.090	1.360	0.750	-12.624	99523.	73178.	76176.118000.	4193.	46592.	77000.	0.20	0.28	
15	0.090	0.900	0.370	-12.350	64586.	71762.	74518.118000.	4362.	48466.	77000.	0.20	0.26	
16	0.050	0.900	0.370	-11.958	62450.	69388.	72144.118000.	4525.	50281.	77000.	0.20	0.24	
17	0.050	0.900	0.370	-11.767	61408.	68231.	70986.118000.	4686.	52068.	77000.	0.20	0.22	
18	0.050	0.900	0.370	-11.675	60634.	67371.	70429.118000.	4845.	53836.	77000.	0.19	0.20	
19	0.050	0.900	0.370	-11.383	59265.	65850.	68666.118000.	5001.	55568.	77000.	0.18	0.18	
20	0.050	0.770	0.370	-11.191	49809.	64687.	67504.118000.	5132.	57026.	77000.	0.18	0.16	
99	0.090	1.170	0.900	-11.158	73538.	62853.	67304.118000.	5326.	59181.	77000.	0.16	0.13	

UPPER SURFACE

199	0.120	1.280	C.800	4.342	-27686.	-21629.	-25929.90000.	5259.	44386.	87000.	0.55	0.48
123	0.120	1.040	C.400	5.414	-30255.	-29091.	-32472.70000.	5184.	43825.	87000.	0.33	0.46
122	0.120	1.380	C.600	6.555	-50182.	-36364.	-39331.70000.	5058.	43200.	87000.	0.22	0.43
121	0.140	1.150	0.400	7.663	-49123.	-42716.	-45986.75000.	4934.	36130.	87000.	0.27	1.03
120	0.140	1.090	C.400	8.585	-52643.	-48296.	-51567.75000.	4801.	35244.	87000.	0.19	0.49
119	0.140	1.150	0.460	9.406	-61262.	-53271.	-56542.80000.	4645.	34791.	87000.	0.18	0.46
118	0.140	1.150	C.460	10.225	-66989.	-58251.	-61522.80000.	4474.	33177.	87000.	0.17	0.42
117	0.140	1.210	C.460	10.951	-75777.	-62626.	-65896.88000.	4280.	31955.	87000.	0.15	0.40
116	0.140	1.630	C.800	11.659	-109859.	-67398.	-70144.92000.	3998.	30571.	87000.	0.14	0.47
115	0.160	1.465	C.600	12.368	-104495.	-71328.	-74416.92000.	3730.	24988.	87000.	0.15	0.44
114	0.160	1.385	C.600	12.889	-103163.	-74486.	-77574.92000.	3464.	23310.	87000.	0.17	0.42
113	0.160	1.385	0.600	13.412	-107544.	-77649.	-80737.92000.	3187.	21651.	87000.	0.10	0.40
112	0.160	1.385	C.600	13.933	-111917.	-80807.	-83895.92000.	2898.	19920.	87000.	0.07	0.47
111	0.160	1.465	C.600	14.255	-121234.	-82754.	-85842.94000.	2585.	18115.	87000.	0.08	0.47
110	0.160	1.950	1.005	14.663	-167143.	-85714.	-88318.94000.	2153.	16158.	87000.	0.05	0.45
109	0.200	1.780	0.700	14.972	-155254.	-87221.	-90068.100000.	1751.	10766.	87000.	0.12	0.44
108	0.200	1.680	0.700	15.194	-148785.	-88563.	-91409.100000.	1366.	4756.	87000.	0.11	0.47
107	0.200	1.680	0.700	15.316	-150030.	-89303.	-92150.100000.	976.	6828.	87000.	0.11	0.47
106	0.200	1.680	0.700	15.438	-151266.	-90039.	-92895.100000.	584.	4882.	87000.	0.11	0.46
105	0.200	1.780	0.700	15.659	-162657.	-91380.	-94227.100000.	161.	2919.	87000.	0.04	0.44
104	0.200	2.360	1.200	15.868	-215786.	-93130.	-95492.100000.	-411.	2054.	87000.	0.07	0.47
103	0.220	1.920	0.780	15.959	-179176.	-93321.	-95985.105000.	-877.	3988.	87000.	0.12	0.41
102	0.220	1.810	0.780	15.865	-167879.	-92751.	-95415.105000.	1315.	5977.	87000.	0.13	0.41
101	0.220	1.920	C.780	15.871	-178150.	-92786.	-95451.105000.	-1780.	8090.	87000.	0.12	0.40
100	0.220	1.780	1.100	15.864	-160519.	-91227.	-95405.120000.	-2199.	9996.	87000.	0.20	0.40

▷ CRITICAL MARGIN OF SAFETY FOR THIS SECTION

18.9

Table 4-B. Outboard-Wing-Portion Analysis, Flaps-Down Maneuver

MODEL 2707 WING SECTION PROPERTIES - STRESSES - MARGINS OF SAFETY  
500 IN. ALONG LOAD REFERENCE AXIS

R/12/66

ETA STA.	LCAC CCND.	V Z	M A	T	V X	M Z	AREA LOWER	ARFA UPPER	AREA ELLOWER	ARFA EUPPER	S.W. EFF	TRUE-I.
0.500	9	32000G.	7100C000.	-10000000.	0.	0.	34.130	38.485	34.130	38.485	0.150	20832.

I X	I Z	I Y	BAR ZE	BAR XE	I YC	I ZE	I XE	2A	P Y	P X	T.C. VZ	T.C. VX	T.C. EQUIB
14126.	100272.	-8677.6	-2.99	-53.95	14126.	100272.	-8677.8	6614	-81555.	4107.	478660.	585554.	29637749.

SEG. NO.	SKIN THICK	SEG. AREA	STIFF AREA	GIST N.A.	LOWER SURFACE SEG. LOAD	SEG. STRESS	SKIN STRESS	TENS. ALLOW	SHEAR FLOW	SHEAR STRESS	SHEAR ALLOW	M.S. TENS.	M.S. SHEAR
0	0.23C	2.080	1.400	-17.936	188437.	90595.	94603.118000.	-5006.	24503.	77000.	0.17	0.45	
1	0.230	2.250	C.900	-17.442	202594.	90042.	91979.118000.	-4329.	21767.	77000.	0.22	0.51	
2	0.210	2.650	1.400	-16.950	234615.	87218.	89421.118000.	-3545.	20616.	77000.	0.26	0.56	
3	0.210	2.250	C.900	-16.459	190851.	84823.	86814.118000.	-2906.	16880.	77000.	0.31	0.65	
4	0.210	2.370	C.900	-15.567	194840.	82211.	84202.118000.	-2254.	13839.	77000.	0.37	0.74	
5	0.210	2.250	C.900	-15.573	180267.	80119.	82109.118000.	-1649.	10732.	77000.	0.41	0.81	
6	0.160	2.250	1.200	-15.179	175081.	77814.	80149.118000.	-1062.	10309.	77000.	0.45	0.86	
7	0.160	2.590	1.000	-14.787	196160.	75737.	78073.118000.	-403.	6638.	77000.	0.50	0.94	
9	0.160	2.590	1.000	-14.001	185351.	71564.	73900.118000.	221.	2520.	77000.	0.59	1.08	
10	0.110	1.650	C.900	-13.607	114628.	69471.	71940.118000.	607.	5516.	77000.	0.63	1.12	
11	0.110	1.120	C.47C	-13.416	76850.	68616.	70925.118000.	866.	7873.	77000.	0.64	1.12	
12	0.110	1.120	0.470	-13.024	74519.	66535.	68844.118000.	1118.	10160.	77000.	0.68	1.15	
13	0.110	1.120	0.47C	-12.833	73383.	65521.	67830.118000.	1366.	12416.	77000.	0.68	1.13	
14	0.090	1.360	C.750	-12.624	87236.	64144.	66772.118000.	1661.	18456.	77000.	0.65	1.02	
15	0.090	0.900	0.370	-12.350	56613.	62903.	65318.118000.	1853.	20588.	77000.	0.66	0.99	
16	0.090	0.900	0.370	-11.958	54740.	60822.	63237.118000.	2039.	22652.	77000.	0.67	0.98	
17	0.090	0.900	0.370	-11.767	53827.	59807.	62223.118000.	2222.	24685.	77000.	0.67	0.94	
18	0.090	0.900	0.370	-11.675	53148.	59054.	61734.118000.	2403.	26695.	77000.	0.65	0.89	
19	0.090	0.900	0.370	-11.383	51948.	57721.	60189.118000.	2580.	28662.	77000.	0.65	0.85	
20	0.090	0.770	C.37C	-11.191	43660.	56701.	59170.118000.	2729.	30318.	77000.	0.64	0.82	
99	0.090	1.170	0.900	-11.158	64459.	55093	58995.118000.	2949.	32165.	77000.	0.60	0.75	

UPPER SURFACE

159	0.120	1.280	0.800	4.342	-24268.	-18959.	-22728.	90000.	2871.	24573.	87000.	1.46	2.21
123	0.120	1.040	0.400	5.414	-26520.	-25500.	-28419.	70000.	2785.	23924.	87000.	0.95	2.13
122	0.120	1.380	C.600	6.555	-43987.	-31875.	-34476.	70000.	2640.	23205.	87000.	0.73	2.01
121	0.140	1.150	0.400	7.663	-43059.	-37442.	-40309.	75000.	2498.	18857.	87000.	0.72	2.15
120	0.140	1.050	0.400	8.585	-46144.	-42334.	-45200.	75000.	2345.	17841.	87000.	0.58	2.02
119	0.140	1.150	C.460	9.406	-53659.	-46695.	-49561.	80000.	2166.	16749.	87000.	0.56	1.91
118	0.140	1.150	C.46C	10.229	-58719.	-51060.	-53926.	80000.	1971.	15474.	87000.	0.46	1.80
117	0.140	1.210	0.460	10.951	-66422.	-54894.	-57761.	88000.	1747.	14077.	87000.	0.51	1.71
116	0.140	1.630	C.800	11.659	-96296.	-59077.	-61519.	92000.	1427.	12493.	87000.	0.49	1.67
115	0.160	1.465	C.600	12.368	-91594.	-62522.	-65229.	92000.	1120.	8920.	87000.	0.44	1.57
114	0.160	1.385	C.600	12.689	-90476.	-65290.	-67997.	92000.	817.	7003.	87000.	0.39	1.51
113	0.160	1.385	C.600	13.412	-94267.	-68063.	-70770.	92000.	501.	5109.	87000.	0.34	1.43
112	0.160	1.385	C.600	13.933	-98101.	-70831.	-73538.	92000.	172.	3132.	87000.	0.30	1.36
111	0.160	1.465	0.600	14.255	-106267.	-72537.	-75244.	94000.	-186.	1160.	87000.	0.30	1.31
110	0.160	1.950	1.005	14.663	-146508.	-75132.	-77415.	94000.	-678.	4240.	87000.	0.25	1.23
109	0.200	1.780	C.700	14.972	-136087.	-76453.	-78948.	100000.	-1137.	5684.	87000.	0.30	1.18
108	0.200	1.680	0.700	15.194	-130417.	-77629.	-80124.	100000.	-1576.	7881.	87000.	0.27	1.13
107	0.200	1.680	0.700	15.316	-131508.	-78278.	-80773.	100000.	-2020.	10099.	87000.	0.25	1.09
106	0.200	1.680	0.700	15.438	-132591.	-78923.	-81418.	100000.	-2467.	12336.	87000.	0.23	1.05
105	0.200	1.780	0.700	15.659	-142576.	-80099.	-82594.	100000.	-2949.	14744.	87000.	0.20	0.98
104	0.200	2.360	1.200	15.868	-192652.	-81632.	-83702.	100000.	-3600.	18000.	87000.	0.16	0.91
103	0.220	1.920	C.780	15.959	-157055.	-81800.	-84135.	105000.	-4131.	18778.	87000.	0.20	0.89
102	0.220	1.810	C.780	15.865	-147153.	-81300.	-83636.	105000.	-4629.	21043.	87000.	0.19	0.86
101	0.220	1.920	C.780	15.871	-156156.	-81331.	-83667.	105000.	-5158.	23447.	87000.	0.16	0.81
100	0.220	1.760	1.100	15.864	-140737.	-79964.	-83627.	120000.	-5636.	25617.	87000.	0.29	0.77

Table 4-C. Outboard-Wing-Portion Analysis - Start of Cruise Maneuver

MODEL 2707 WING SECTION PROPERTIES - STRESSES - MARGINS OF SAFETY  
900 IN. ALONG LOAD REFERENCE AXIS

R/ 2/66

LOAD COND.	V Z	M X	T	V X	M Z	AREA LOWER	AREA UPPER	AREA ELLOWER	AREA EUPPER	S.W. EFF	TRUE-J.		
25	82000.	5000000.	2000000.	0.	0.	8.063	11.902	8.063	11.902	0.086	1954.		
I X	I Z	I XZ	BAR ZE	BAR XE	I XE	I ZE	I XE ZE	2A Z	P Z	P X	T.C. VZ	T.C. VX	T.C. EQUIB
1148.	6601.	-559.0	-3.60	-28.38	1148.	6601.	-559.0	1825	-20233.	907.	89807.	79110.	3555678.
SEG. NO.	SKIN THICK	SEG. AREA	STIFF AREA	DIST N.A.	LOWER SURFACE SEG. LOAD	UPPER SURFACE SEG. STRESS	SKIN STRESS	TENS. ALLOW	SHFAR FLOW	SHFAP STRESS	SHEAR ALLOW	M.S. TENS.	M.S. SHEAR
0	0.089	0.740	0.500	-11.000	61991.	87772.	89575.	97000.	-443.	10829.	63000.	0.07	0.37
1	0.080	0.676	0.260	-10.773	57257.	84699.	87723.	97000.	-52.	5540.	63000.	0.10	0.43
2	0.070	0.752	0.400	-10.466	61930.	82354.	85256.	97000.	372.	5312.	63000.	0.13	0.47
3	0.070	1.131	0.480	-10.018	88812.	78525.	81590.	97000.	980.	14000.	63000.	0.16	0.46
5	0.070	1.131	0.480	-9.201	81264.	71852.	74917.	97000.	1539.	21979.	63000.	0.20	0.45
6	0.070	0.729	0.400	-9.040	51420.	70535.	73600.	97000.	1892.	27034.	63000.	0.18	0.38
7	0.070	0.539	0.210	-8.833	37019.	68680.	71909.	97000.	2147.	30678.	63000.	0.17	0.33
8	0.070	0.539	0.210	-8.628	36115.	67003.	70231.	97000.	2397.	34239.	63000.	0.15	0.28
9	0.070	0.539	0.210	-8.423	35211.	65326.	68554.	97000.	2640.	37716.	63000.	0.14	0.24
10	0.070	0.567	0.210	-8.167	35899.	63315.	66461.	97000.	2889.	41266.	63000.	0.13	0.19
99	0.070	0.720	0.440	-7.844	42037.	58385.	63821.	97000.	3180.	45434.	63000.	0.11	0.13
UPPER SURFACE													
109	0.100	0.950	0.600	4.356	-26097.	-30702.	-35198.	74000.	3004.	31804.	71000.	0.43	0.95
114	0.100	0.528	0.257	4.709	-19073.	-34153.	-38076.	59000.	2882.	30044.	71000.	0.25	1.00
113	0.100	0.620	0.257	5.115	-23236.	-37478.	-41401.	59000.	2725.	28825.	71000.	0.20	1.00
112	0.100	0.621	0.257	5.522	-25294.	-40797.	-44720.	59000.	2553.	27248.	71000.	0.16	1.01
111	0.100	0.670	0.257	5.928	-29562.	-44122.	-48045.	59000.	2351.	25527.	71000.	0.12	1.03
110	0.100	0.942	0.500	6.419	-47137.	-48949.	-52954.	61000.	2029.	23511.	71000.	0.09	1.02
109	0.100	0.710	0.297	6.710	-35990.	-50676.	-54436.	61000.	1787.	20287.	71000.	0.09	1.09
108	0.100	0.660	0.297	6.916	-34558.	-52360.	-56120.	61000.	1545.	17821.	71000.	0.08	1.14
107	0.100	0.660	0.297	7.123	-35674.	-54051.	-57811.	61000.	1300.	15450.	71000.	0.07	1.17
106	0.100	0.660	0.297	7.229	-36246.	-54917.	-58677.	61000.	1050.	12998.	71000.	0.07	1.21
105	0.100	0.710	0.297	7.336	-39612.	-55791.	-59551.	61000.	777.	10504.	71000.	0.07	1.25
104	0.100	1.010	0.504	7.527	-58589.	-58009.	-61115.	61000.	373.	7775.	71000.	0.04	1.25
103	0.120	0.840	0.354	7.513	-49216.	-57400.	-60914.	64000.	40.	3110.	71000.	0.11	1.32
102	0.120	0.791	0.354	7.414	-44197.	-56590.	-60105.	64000.	-266.	2216.	71000.	0.13	1.36
101	0.120	0.840	0.354	7.215	-46189.	-54964.	-58478.	64000.	-586.	4883.	71000.	0.16	1.40
100	0.120	0.780	0.500	7.000	-40356.	-51739.	-56725.	74000.	-866.	7219.	71000.	0.40	1.43

▷ CRITICAL MARGIN OF SAFETY FOR THIS SECTION

produces an interaction between the two surfaces and a nonuniform load distribution across the center section, which results in additional shear in the inboard-wing-portion spars and ribs. The critical spar shears include this effect. A plot of the upper-surface end-load distribution at the side of the fuselage is shown in Fig. 4-9.

In addition to axial compression loads from wing bending, the upper surface must resist fuselage pressure loads. The skin-stringer segments beam the pressure loads to the fuselage floor beams, which transfer the load to the spanwise ribs and spars. The pressure load is then reacted at the side of the fuselage. Fuel loading on the lower surface is transferred in a similar manner.

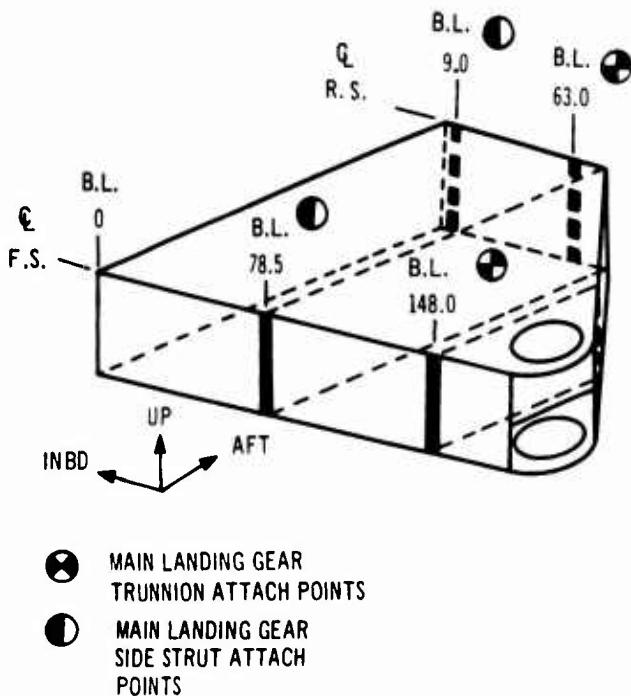
The critical load condition for the surfaces is a high-gross-weight, flaps-down maneuver condi-

tion with  $\Lambda$  LE 30 deg. without fuselage pressure. The inboard ribs are critical for the 2.5-factor cabin pressurization loading. Landing conditions give maximum rear spar shears. Front spar shears are critical for unsymmetrical flight loadings. A stress analysis for the upper surface and stress analysis for a typical rib is shown in Figs. 4-10 and 4-11, respectively.

#### 4.2.4.4 Wing Pivot Analysis

The wing pivot analysis and structural arrangement of the pivot is shown in Fig. 4-12. A description is given in Par. 3.2.

The primary wing loads are transferred across the pivot by upper- and lower-surface radial and thrust bearings. These bearing loads are distributed to a conventional torque box on each side of the pivot.



SEE PAR. 4.6. FOR LANDING GEAR LOADS ON THE WING  
**Figure 4-8. Landing Gear Attachment Locations on the Wing**

The concept of the B-2707 pivot is identical to that of the wing pivot being built for the pivot development test program (V2-B2707-9). Redundant analyses were made on component sections of the test pivot. Data from these analyses and strain gage data from the 36-in.-diameter bearing test (V2-B2707-9) were used in the determination of load distribution within the structure. The pivot structure was analyzed with these distribution aids. A description of the component redundant analysis and a more comprehensive redundant analysis of the test pivot are included in the following paragraphs. The comprehensive analysis was made after sizing of the test box was completed; the analysis validates the analysis methods used in the design.

The beam shear load is reacted by a thrust bearing at the upper surface between the outboard-wing-portion closure rib and the upper plug. This plug transfers the beam shear to the inboard curved spar. This curved spar carries 40 percent of the torsion load as determined from a

redundant element solution. The bending and torsional moments are transferred as couple loads on the radial bearings in the upper- and lower-pivot lugs. The torsional couple loads that produce differential bending in the lugs are assumed to be reacted by an  $M_y/I$  distribution in the surfaces at the first rib adjacent to the pivot centerline. This load is sheared out in the spars and surfaces at the rib 66 in. outboard of the pivot centerline and inboard at the side of the fuselage. The skins were designed to carry 100 percent of the torsion in differential bending in the redistribution area. The torsional effectivity of the curved spar in the inboard wing portion was neglected. The bending couple loads produce local effects in the lugs and wing surfaces in the redistribution area. A redundant analysis was used to determine the load intensity in these areas.

Shears in the torque boxes were determined from an idealized tapered box acted upon by beam shear, torsion, and differential bending.

Ultimate fail-safe design loads are 80 percent of limit load conditions, increased by a factor of 1.15 for dynamic effects, unless a lower value is substantiated by rational dynamic analysis. Fail-safe design features include multiple panel tension skins to prevent chordwise crack propagation and dual load-path lugs. A lug failure causes a change in the tension load path and induces shear in the adjacent spars and ribs. The lower lugs, the wing spars between the first and second ribs inboard of the pivot, and local areas of these ribs adjacent to the spars are critical for fail-safe conditions.

The wing surfaces and lugs are designed for a subsonic maneuver condition with  $\Lambda_{LE} = 42$  deg. The spars are critical for flaps-down maneuver condition with  $\Lambda_{LE} = 30$  deg. The maximum load intensity at the outboard and inboard lug to skin splices is shown in Fig. 4-13.

a. Redundant Analysis, Wing-Pivot Test Box  
 Redundant analysis was performed on the wing-pivot box being built for the pivot development test program (V2-B2707-9). The concept of the B-2707 airplane pivot is identical to the test pivot, and this analysis is adaptable to the B-2707 structural configuration.

The analyses were performed on an IBM 7094 using the COSMOS program (Ref. 11). COSMOS is based on the direct stiffness method of

structural analysis. The structure is idealized into an equivalent representation of finite elements with each finite element having the stiffness of the structure being represented. The stiffness matrix for the entire structure is obtained by direct merging of the individual element stiffness to satisfy force equilibrium and deformation compatibility at the nodes. The loading on the structure is represented by equivalent generalized forces applied at the nodes. The program obtains stresses, deflections, and flexibility data.

The COSMOS program was used in the analysis of selected components of the pivot test box. The results of these analyses are used in the design of the airplane pivot structure. The selected components analysed are as follows:

- Lower inboard lug  
The lower inboard lugs (idealized as one planar lug) were analyzed with the plug distributing the inplane bearing loads to the lugs. The aft-acting shear was reacted at the first rib location. Tension loads from

the outboard lug were reacted at the lug-to-inboard wing-splice. The lug was idealized as uniform plane stress plate elements superimposed on a 215-node grid. The circular plug was idealized as a circular frame subdivided into 10-deg. elements. This idealization permitted nonuniform bearing loads to be realistically represented. The plug-to-lug bearing loads were transmitted through very short axial elements. This provided a true radial loading. The axial members had negligible deformation so the plug and lug were constrained to deform similarly on the bearing surfaces.

- Inboard Box  
The above lug was used with a symmetrical spar element to obtain a box analysis. The inboard-wing-portion curved spar and the first rib are represented as spar elements. The spar element constrains the upper surface behavior to be antisymmetric with respect to the lower surface. The spar web deforms in shear and has compatible

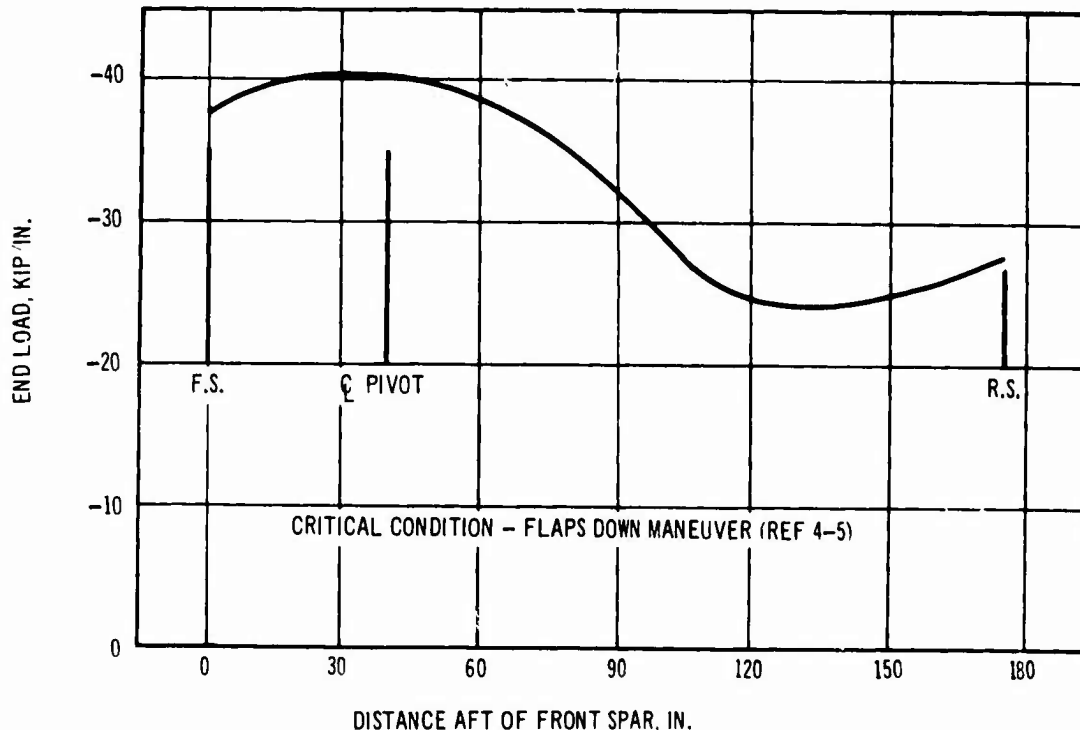


Figure 4-9. Upper Surface Panel End, WBL 77.4

UPPER SURFACE SKIN -  
 STRINGER SEGMENT, FIRST  
 BAY INSIDE OF BODY, 40  
 IN. AFT OF FRONT  
 SPAR

EFFECTIVE SECTION PROPERTIES

$$A = 1.37 \text{ IN.}^2$$

$$\bar{Y} = 0.82 \text{ IN.}$$

$$I_o = 1.36 \text{ IN.}^4$$

$$\rho = 0.99 \text{ IN.}$$

CRITICAL DESIGN CONDITION:  
 FLAPS DOWN MANEUVER  
 REF FIG. 4-5

ULTIMATE STRESS

$$f_c = \frac{197000}{1.37} = 144,000 \text{ PSI}$$

MATERIAL: Ti 6AL-4V, COND III

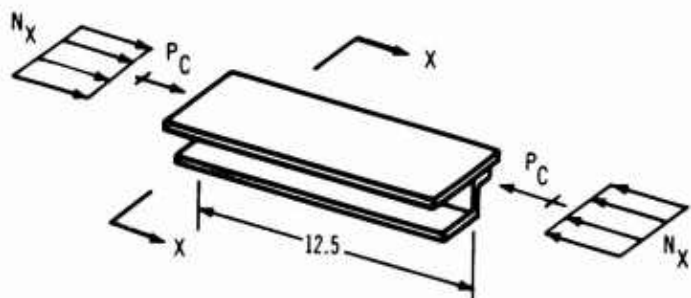
ALLOWABLE STRESS

$$F_c = 152,000 \text{ PSI}$$

$$\left(\frac{L}{\rho}\right)^2 - \left(\frac{12.5}{0.99}\right)^2 = 158$$

$$F_c = 152,000 - \frac{(152,000)^2 \cdot 158}{4(3.14)^2(16.4 \times 10^6)}$$

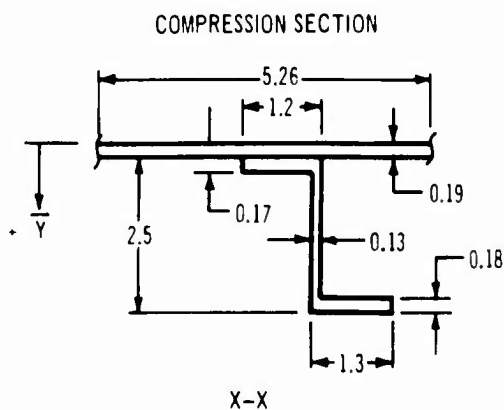
$$= 146,100 \text{ PSI}$$



$N_x$  - SEGMENT END LOAD PER  
 IN.  
 $P_c$  - TOTAL SEGMENT LOAD

$$M.S. = \frac{146,100}{144,000} - 1 = \underline{+0.01}$$

$N_x = 37,500 \text{ LB/IN}$  (REF FIG. 4-9)  
 STRINGER SPACING = 5.26 IN.  
 $P_c = 37,500(5.26) = 197,000 \text{ LB}$

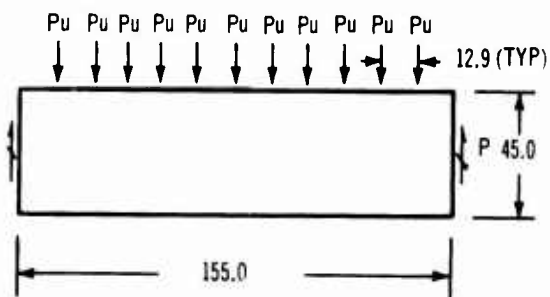


EFFECTIVE SKIN WIDTH = 3.43 IN.

Figure 4-10. Wing Upper-Surface Analysis, Center Section



CRITICAL DESIGN CONDITION:  
BODY PRESSURE ACTING ALONE



$$P = 11.12 (2.5) = 2.78 \text{ PSI}$$

FLOOR BEAM REACTIONS

$$P_u = 27.8 (44.25)(12.9) = 15,900 \text{ LB}$$

THEREFORE

$$V = \frac{15,900 (11)}{2} = 87,500 \text{ LB.}$$

$$q = \frac{87,500}{45.0} = 1950 \text{ LB/IN.}$$

ULTIMATE STRESS

$$t_{\text{WEB}} = 0.032 \text{ IN.}$$

$$f_s = \frac{1950}{0.032} = 61,000 \text{ PSI}$$

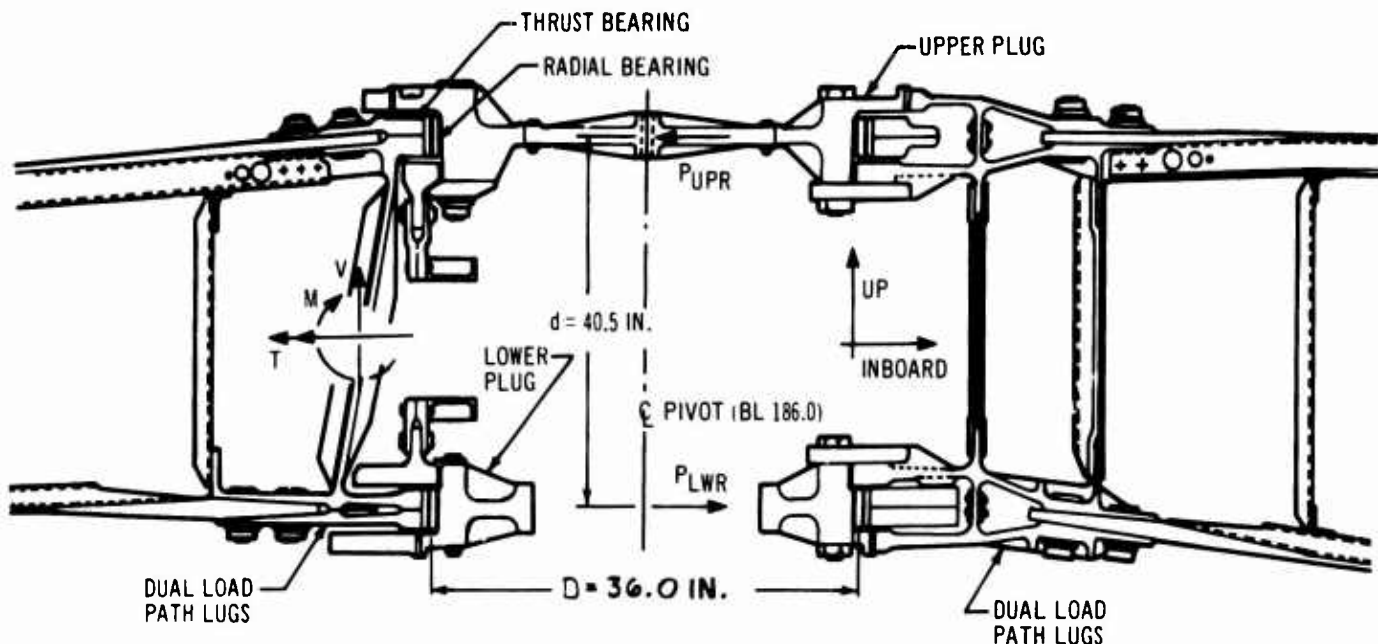
WEB MATERIAL: T1 GAL-4V, CONDI

ALLOWABLE SHEAR STRESS

$$F_{su} = 0.49 (129,000) = 63,700 \text{ PSI}$$

$$M.S. = \frac{63,700}{61,000} - 1 = +0.11$$

Figure 4-11. Spanwise Rib Analysis, Center Section



WING PIVOT BEARING ANALYSIS

CRITICAL COND.: SUBSONIC MANEUVER  
 GW = 647 KIPS  $\Lambda_{LE} = 42^\circ$   $N = 3.75$

$M = 80 \times 10^3$  N-KIPS (REF. FIG. 4-2)  
 $T = 92 \times 10^3$  IN-KIPS

AT  $\eta = 1.25$ ,  
 $M/2 = 5 \times 10^3$  IN-KIPS (REF. V2 B2707-7)

THE  $\eta = 1.0$  BEARING LOAD COMPUTED AT THE PIVOT  $\Phi$  IS  $1.10 \cdot \eta / N \cdot P_{ULT}$ .

AT  $\eta = 1.0$   $M/d = \frac{(1.10)(180 \times 10^3)}{(3.75)(40.5)} = 1305$  KIPS

$T/d = \frac{(1.10)(92 \times 10^3)}{(3.75)(40.5)} = 666$  KIPS

OFF ACT LOAD =  $\frac{13 \times 10^3}{2(1.25)(840)} = 62$  KIPS

THE MAXIMUM  $\eta = 1.0$  BEARING LOAD,

$P_{UPR} = 305 \rightarrow 666 \rightarrow 62 = 1506$  KIPS

A BEARING STRESS LEVEL UNDER 15 KSI WAS SELECTED TO OBTAIN GOOD SERVICE LIFE.

$t_{BRG} = 3.20$  IN  $D = 36.00$  IN

$f_{BRG} = \frac{1506}{(3.20)(36.00)} = 13.10$  KSI

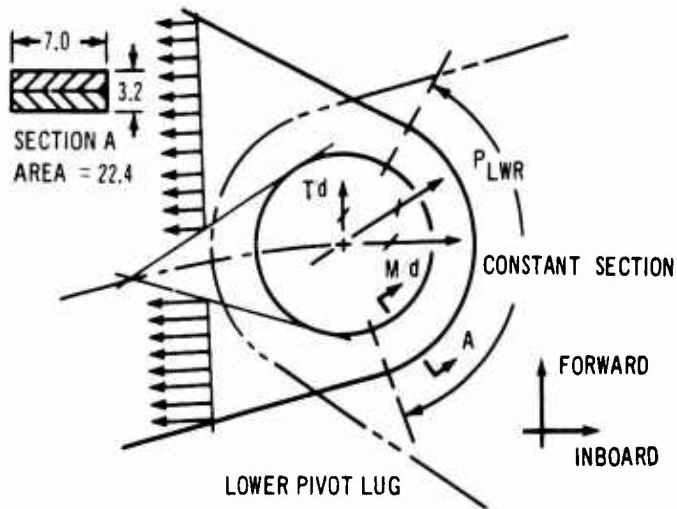
WING PIVOT TENSION LUG ANALYSIS  
 THE OUTBOARD WING LUGS ARE ANALYZED AS TYPICAL PIVOT TENSION LUGS.

CRITICAL COND.: SUBSONIC MANEUVER  
 GW = 647 KIPS  $\Lambda_{LE} = 42^\circ$   $N = 3.75$

$P_{LWR} = \frac{180 \times 10^3}{40.5} \rightarrow \frac{92 \times 10^3}{40.5} = 4990$  KIPS

THE PIVOT LUGS HAVE DUAL LOAD PATHS. UNDER FAILSAFE DESIGN CRITERIA AFTER A SINGLE TENSION ELEMENT FAILURE THE REMAINING LUG ELEMENT MUST BE CAPABLE OF WITHSTANDING 80% OF LIMIT LOAD CONSERVATIVELY INCREASED BY A 115 DYNAMIC FACTOR.

Figure 4-12. Wing Pivot Analysis



TAKING  $1/2 P_{LWR}$  ACROSS SECTION A

AT ULT. LOAD  $f_t = \frac{4990}{2(22.4)} = 111.5 \text{ KSI}$

AT  $1.15(.80)$  LIMIT LOAD (FAILSAFE)

$$f_t = \frac{(.92)(4990)}{(1.5)(2)(11.2)} = 136.5 \text{ KSI}$$

LUG MATERIAL IS TI-6AL-4V (COND. IV)  
 $F_{tu} = 138 \text{ KSI}$

M.S. =  $138.0 / 136.5 - 1.0 = +0.01$  ←

WING PIVOT SKIN/STR. ANALYSIS  
 THE ANALYSIS SHOWN FOR OUTBOARD WING PIVOT STRUCTURE IS TYPICAL FOR THE ENTIRE PIVOT REGION.

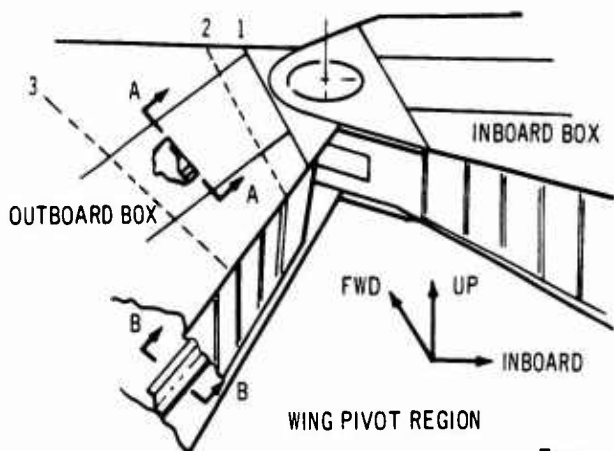


Figure 4-12. (Continued)

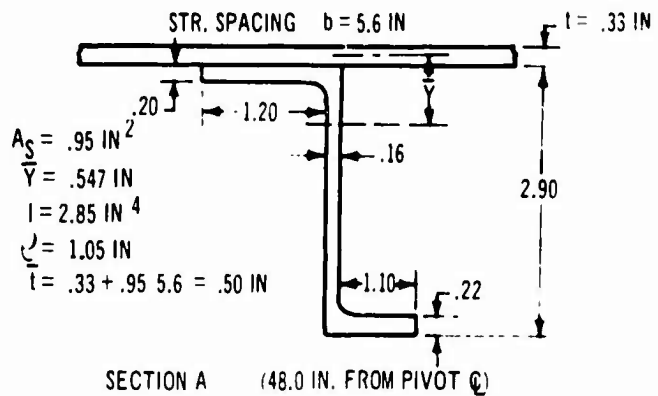
OUTBOARD PIVOT BOX

CRITICAL COND.: SUBSONIC MANEUVER  
 $GW = 647 \text{ KIPS}$   $\Lambda_{LE} = 42^\circ$   $N = 3.75$

UPPER SURFACE ANALYSIS

AT SECTION A THE MAXIMUM LOAD INTENSITY IS GIVEN BY AN ELLIPTICAL DISTRIBUTION OF THE  $M/d$  LOAD OVER A CENTRAL SEGMENT OF THE BOX WIDTH. THE LOAD INTENSITY IS  $660 \text{ K/IN}$

THE UPPER SURFACE COLUMN LENGTH BETWEEN RIBS (2) AND (3) IS  $240 \text{ IN.}$



UPPER SURFACE MATERIAL IS TI-6AL-4V (COND. III) - FOR EXTRUDED STR.  $F_{cc} = F_{cy} = 157 \text{ KSI}$

ALLOWABLE COLUMN STRESS IS GIVEN BY:

$$F_c = F_{cc} \left[ 1 - \frac{F_{cc} \left( \frac{L}{2\pi c} \right)^2}{4\pi^2 E} \right] \text{ WHERE } L = 24 \text{ IN, } C = 1 \text{ AND } E = 16.4 \times 10^3 \text{ KSI}$$

$$F_c = 136.0 \text{ KSI}$$

$$f_c = \frac{660 \text{ K/IN}}{.50 \text{ IN}} = 132.0 \text{ KSI}$$

M.S. =  $136.0 / 132.0 - 1.0 = +0.03$  ←

THE TOTAL NET SHEAR FLOW AT SECTION A IS COMPUTED TO BE  $6.1 \text{ K/IN.}$

$$f_s = \frac{6.1 \text{ K/IN}}{.33 \text{ IN}} = 18.5 \text{ KSI}$$

THE MAXIMUM PRINCIPAL COMPRESSIVE STRESS IS GIVEN BY:

$$f_{c1} = f_c/2 + \sqrt{(f_c/2)^2 + (f_s)^2}$$

$$f_{c1} = 135.5 \text{ KSI}$$

FOR COND III PLATE  $F_{CY} = 42 \text{ KSI}$

$$M.S. = 142.0/135.5 - 1.0 = +0.05 \leftarrow$$

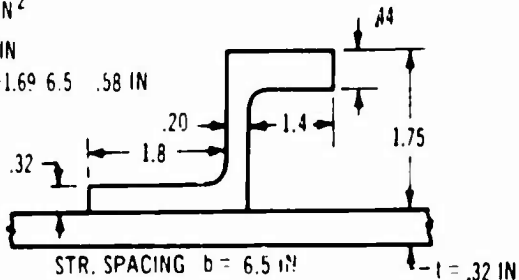
#### LOWER SURFACE ANALYSIS

AT SECTION B THE LOWER SURFACE END LOAD IS OBTAINED BY SUPERPOSITION OF THE WING BENDING MOMENT LOAD DISTRIBUTION AND THE DIFFERENTIAL BENDING DISTRIBUTION INDUCED IN THE COVER SKINS BY THE COUPLE REACTIONS TO THE WING TORSION. THE LOAD INTENSITY IS 490 K/IN.

$$A_c = 1.69 \text{ IN}^2$$

$$\bar{Y} = .346 \text{ IN}$$

$$I = .32 + 1.69 \cdot 6.5 \cdot .58 \text{ IN}^4$$



SECTION B (75.0 IN. FROM PIVOT Q)

THE GROSS STRESS LEVEL AT SECTION B IS DETERMINED BY:

$$f_t = \frac{490 \text{ K/IN}}{.58 \text{ IN}} = 84.5 \text{ KSI}$$

THE LOWER SURFACE SKIN MATERIAL IS T1-6AL-4V (COND. IV). FOR PLATE OVER .75 IN. THICK  $F_{tu} = 138 \text{ KSI}$ . AT 15% HOLES OUT  $F_t = .85 F_{tu} = 117 \text{ KSI}$ .

THE TOTAL NET SHEAR FLOW IS COMPUTED TO BE 18.8 KIPS/IN.

$$f_s = \frac{18.8 \text{ K/IN}}{.32 \text{ IN}} = 58.7 \text{ KSI}$$

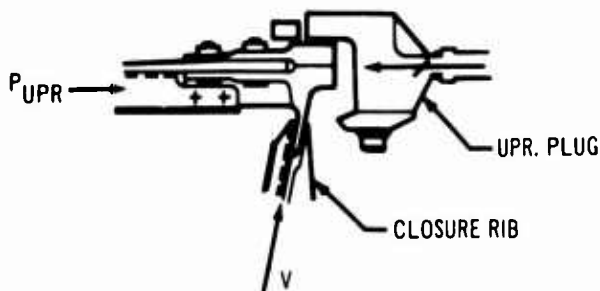
THE MAXIMUM PRINCIPAL TENSION STRESS IS GIVEN BY:

$$f_t = f_t/2 + \sqrt{(f_t/2)^2 + (f_s)^2} = 114.6 \text{ KSI}$$

$$M.S. = 117.0/114.6 - 1.0 = +0.02 \leftarrow$$

#### OUTBOARD WING CLOSURE RIB

TRANSFER OF THE OUTBOARD WING SHEAR LOAD TO THE UPPER PLUG AND THE INBOARD WING IS ACCOMPLISHED WITH A RESULTANT COMPRESSIVE REACTION AT THE CENTRAL SECTION OF THE CLOSURE RIB.



SHEAR TRANSFER LOAD PATH

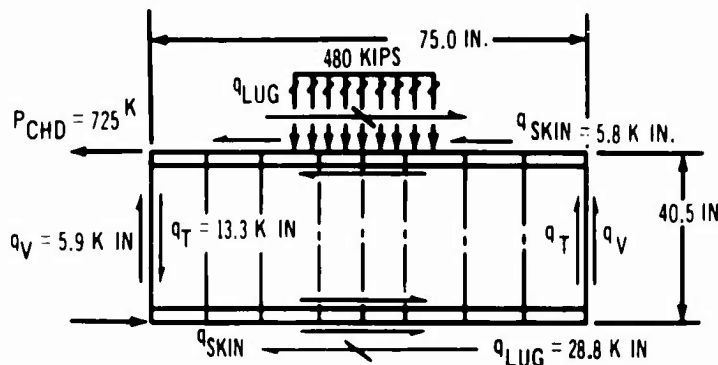
CRITICAL COND.: FLAPS DOWN MANEUVER  
GW = 670 KIPS  $\Lambda_{LE} = 30^\circ$  N = 3.0

$$V = 480 \text{ KIPS}$$

$$M = 174 \cdot 10^3 \text{ IN-KIPS (REF. FIG. 4-5)}$$

$$T = 87 \cdot 10^3 \text{ IN-KIPS}$$

THE RIB LOADS ARE SHOWN IN THE FOLLOWING SKETCH. ( $P_{CHD}$  AND  $q_{SKIN}$  ARE DUE TO DIFFERENTIAL BENDING.)



#### STIFFENER ANALYSIS

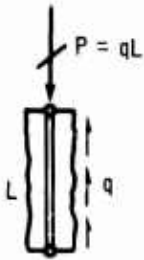
THE CRUSHING LOAD IS TAKEN PRIMARILY BY THE THREE CENTER STIFFENERS. THE CENTER ONE IS ASSUMED TO REACT 1/2 OF THE TOTAL LOAD.

THE STIFFENER LOAD,  $P = 240 \text{ KIPS}$

THE CENTER STIFFENER IS THEN ANALYZED AS A PINNED COLUMN

Figure 4-12. (Continued)

CONSERVATIVELY LOADED BY A UNIFORM SHEAR FROM THE RIB WEB.



$$L = 35.0 \text{ IN}$$

$$\rho = .48 \text{ IN}$$

$$A = 4.70 \text{ IN}^2 \quad \frac{L}{\rho \sqrt{C}} = 54.0$$

$$\frac{1}{\sqrt{C}} = .732$$

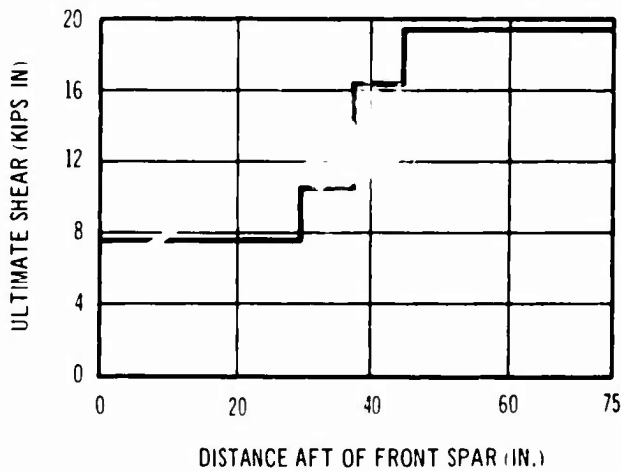
THE ALLOWABLE COLUMN STRESS,  $F_c = 55.0 \text{ KSI}$

$$f_c = \frac{240 \text{ KIPS}}{4.70 \text{ IN}^2} = 51.0 \text{ KSI}$$

$$\text{M.S.} = 55.0 / 51.0 - 1.0 = +0.07 \leftarrow$$

WEB ANALYSIS

THE MAXIMUM RIB SHEAR IS SHOWN IN THE FOLLOWING DIAGRAM.



AT THE REAR SPAR STIFFENER SPACING IS 10.0 IN. AND WEB  $t = .29 \text{ IN.}$  AT  $t/b = .029$ ,  $F_{SCR} = 67.0 \text{ KSI.}$

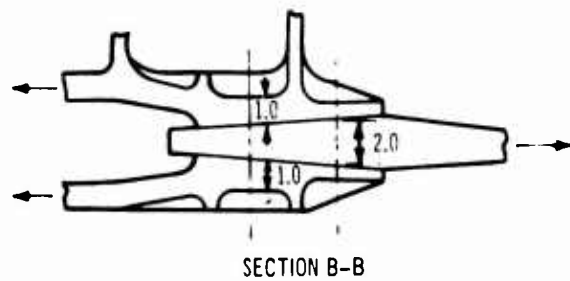
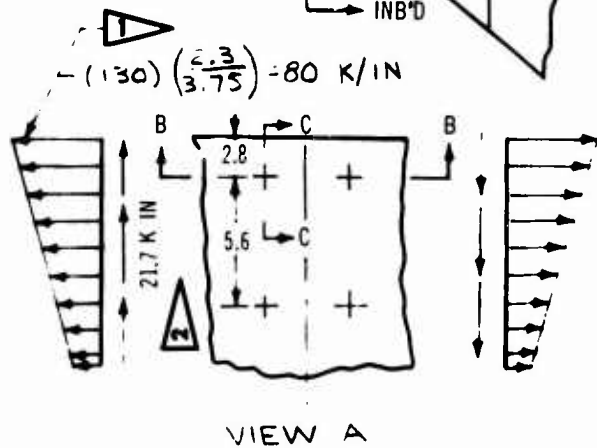
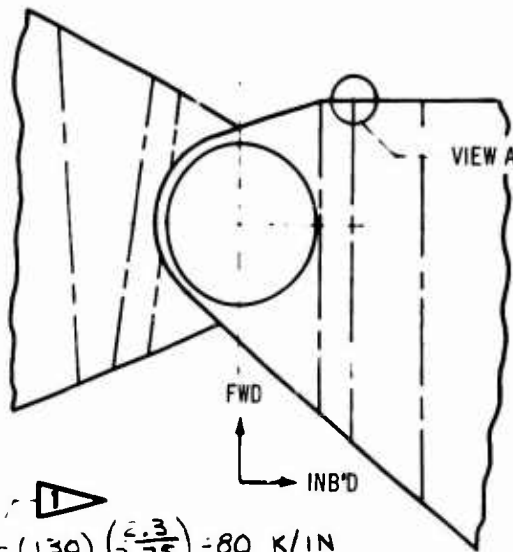
$$f_s = \frac{19.2 \text{ K/IN}}{.29 \text{ IN}} = 66.0 \text{ KSI}$$

AT 20% HOLEOUT,  $f_s = \frac{66.0}{1-.20} = 82.5 \text{ KSI}$

WEB MATERIAL IS TI-6AL-4V (COND. IV) FOR PLATE (OVER .188 THICK)  $F_{Su} = 90 \text{ KSI}$

$$\text{M.S.} = 90.0 / 82.5 - 1.0 = +0.09 \leftarrow$$

LOWER LUG - TO - INBOARD WING SPLICE



1 AVERAGE ULTIMATE LOAD INTENSITY AT SECTION C~C REF. FIG. A-13

2 THE SKIN SHEAR IS EQUAL TO THE FAILSAFE SPAR SHEAR AT SECTION C~C, REF. FIG. A-20

Figure 4-12. (Continued)

CRITICAL CONDITION:  
 SUBSONIC MANEUVER  $G_W = 647K$   
 $\alpha_{LE} = 42^\circ$   $N = 2.30$

THE LOWER LUGS ARE CRITICAL  
 FOR FAILSAFE LOADS

SECTION C~C

$$\text{TENSION LOAD} = (80)(5.6) = 448K$$

$$\text{SHEAR LOAD} = (21.7)(5.6) = 121K$$

$$\text{RESULTANT} = \sqrt{(448)^2 + (121)^2} = 466K$$

USE 2-17/8 IN. DIA. T1-6AL-4V  
 TAPER-LOK BOLTS (AVERAGE  
 DIA. = 1.94 IN.) WITH A 3/8 IN. DIA.  
 PILOT HOLE.  $F_{SU} = 90$  KSI  
 SINGLE SHEAR ALLOWABLE = 254 K.

$$\text{M.S.} = \frac{(2)(254)}{466} - 1 = +.09 \quad \leftarrow$$

LUG MATERIAL IS T1-6AL-4V  
 COND IV  $F_{TU} = 138$  KSI

36% HOLE OUT ALLOWS FOR  
 OVERSIZE 2 IN. DIA. TAPER-  
 LOK BOLTS

$$f_t = \frac{80}{(1)(1-.36)} = 125 \text{ KSI}$$

$$f_s = \frac{21.7}{(1)(1-.36)} = 34 \text{ KSI}$$

$$f_i = \frac{125}{2} + \sqrt{\frac{125}{2} + (34)^2} = 134 \text{ KSI}$$

$$\text{M.S.} = \frac{138}{134} - 1 = +.03 \quad \leftarrow$$

Figure 4-12. (Concluded)

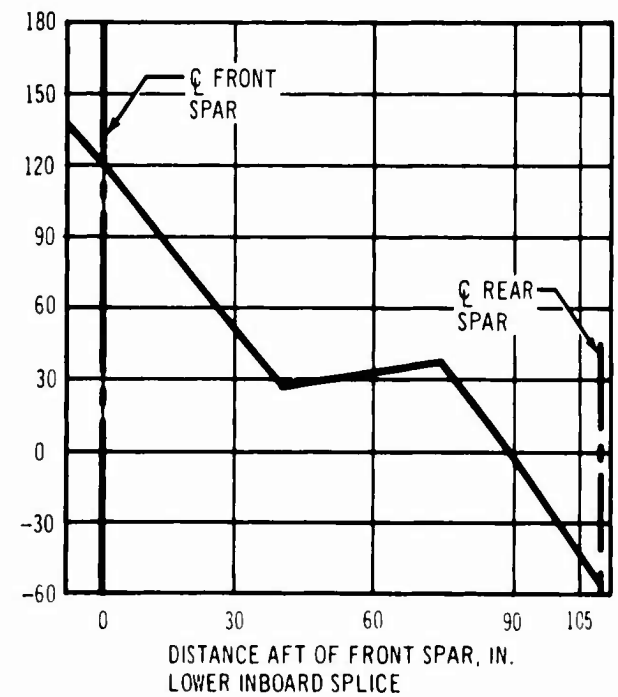
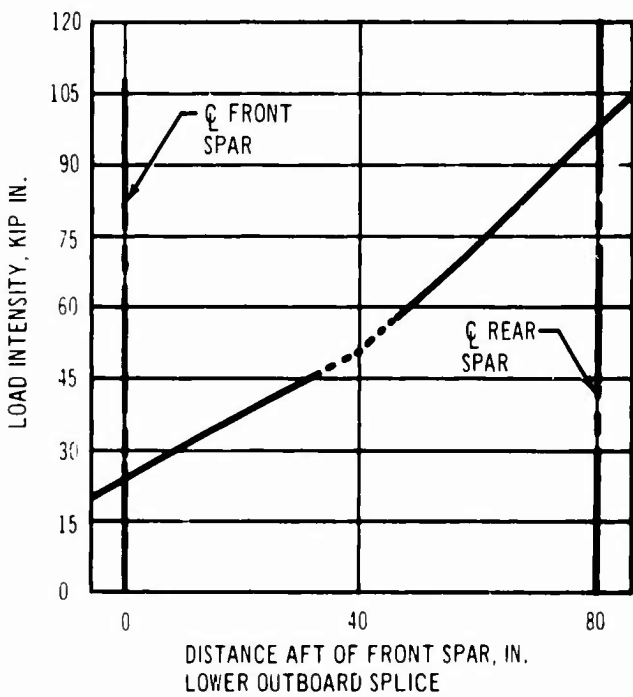
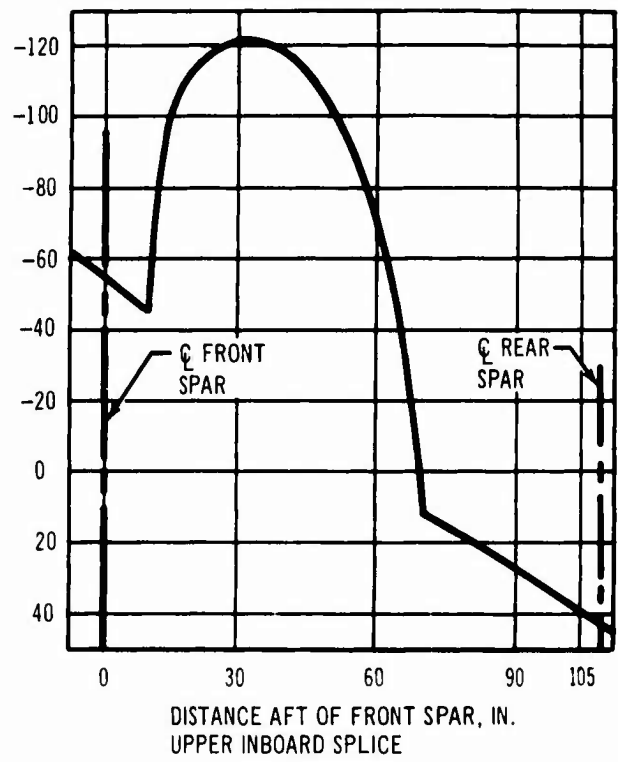
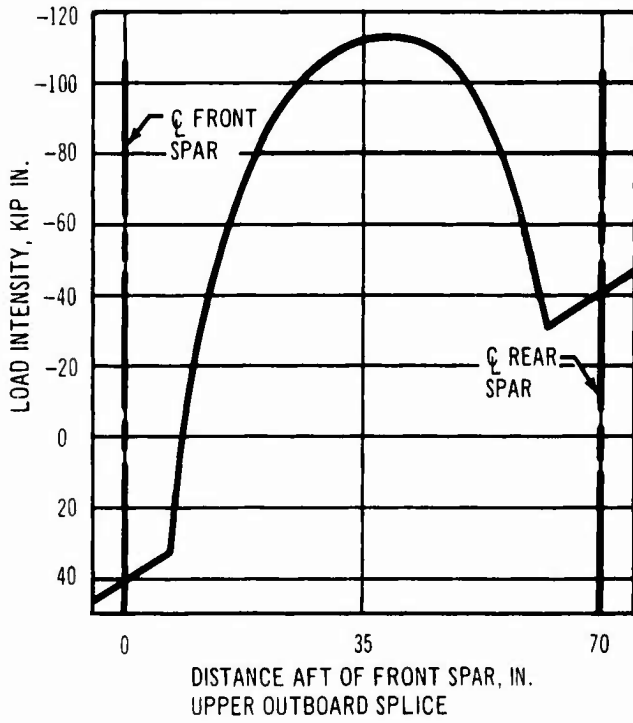


Figure 4-13. Pivot Lug to Wing Skin - Splice Loads

deflections with the box surfaces. The applied loads are reacted at the lug to inboard-wing-portion splices.

- **Inboard Upper and Lower Surfaces**  
The inboard-wing-portion upper and lower surfaces were separately analyzed to determine end-load distribution at several sections. An outboard acting load was applied at the centerline of the pivot and reacted at the side of the fuselage. The surfaces were idealized as planar orthotropic elements (the stiffener area was represented as an incremental thickness increase) on a 344-node grid.
- **Inboard-Wing-Portion Curved Spar**  
The inboard-wing-portion curved spar was analyzed as a beam (curved in planform) fixed against rotation at its juncture with the inboard front and rear spars. The effect of the surfaces on the spar were simulated by flanges with proper areas and moment of inertia in bending about a vertical axis. The web was idealized as uniform plane-stress plate elements. Three of these occur at a vertical section to more adequately represent the web bending-stress distribution. Web stiffeners and cutout framing members were idealized to carry axial load and bending moment normal to the plane of the web. These members accounted for unsymmetrical web stiffeners where applicable. Wing vertical shear loads were applied as point loads in one analysis and were distributed over a 60-deg. arc in another analysis. Torsional shear was applied at the juncture with the front spar and reacted at the rear spar juncture.

A comprehensive analysis was performed on an idealized representation of the structure from three ribs outboard to a point 160 in. inboard of the pivot centerline. The test specimen extends 100 in. inboard of the pivot centerline with the test jig structure extending further. Design ultimate loads were applied as an  $M_y/I$ ,  $VQ/I$ , and  $T/2A$  distribution on the outboard end of the structure. These loads were reacted by completely fixing the structure 160 in. inboard of the pivot centerline. Figure 4-14 illustrates the wing-pivot idealization with some of the 815-node grids and 1,054 elements. The lugs and wing surfaces are idealized as plate elements for inplane stiffnesses with superimposed beam

grillage representing out-of-plane stiffnesses. Ribs are idealized as plates with the equivalent area per inch for vertically oriented stresses and the basic web gage for shear and horizontally oriented stresses. This principle is also used on the stiffened surfaces. Spars are idealized as pure shear webs with flange-area increments representing the bending inertia equivalent to the web. The plug idealization principle is the same as used for the component analyses. The load transfer elements for the inplane bearing and vertical shear are axial load elements with stiffnesses compatible with the load transfer path.

b. **Comparison of Results Obtained by Conventional and Redundant Analysis Methods**

Data from the comprehensive analysis for the transonic maneuver condition is compared with that obtained from conventional and component redundant analysis. Figure 4-15 shows relative load intensity at the inboard, lower-surface, lug-to-skin splice at a location 38 in. inboard of centerline of pivot and also at 95 in. inboard of the centerline of the pivot. At the centerline of the lug-to-skin splice, the comprehensive analysis shows less load intensity at the front and rear spars. These differences occur because the comprehensive analysis also accounts for the torsional rigidity of the inboard-wing box in redistributing couple loads at the centerline of the pivot. The comprehensive analysis accounts for the interaction between the surfaces and spars; the analysis also indicates a more uniform end load on the surface 95 in. inboard of the centerline of the pivot than that obtained from a single-plate redundant analysis or a conventional method approach.

Relative inboard-wing spar shears are shown in Fig. 4-16. The comprehensive analysis shows the highest spars shears at the outboard end of the box. In the conventional method solution, the differential bending in the surfaces was assumed to shear out uniformly from the first rib to the fifth rib. The spar shears from the comprehensive solution indicate that the rate of change of load is not uniform, resulting in higher spar shears.

The curved-spar shear flows for the component analysis and comprehensive analysis are shown in Fig. 4-17. For design purposes, 40 percent of the  $T/2A$  torsional shear was applied to the



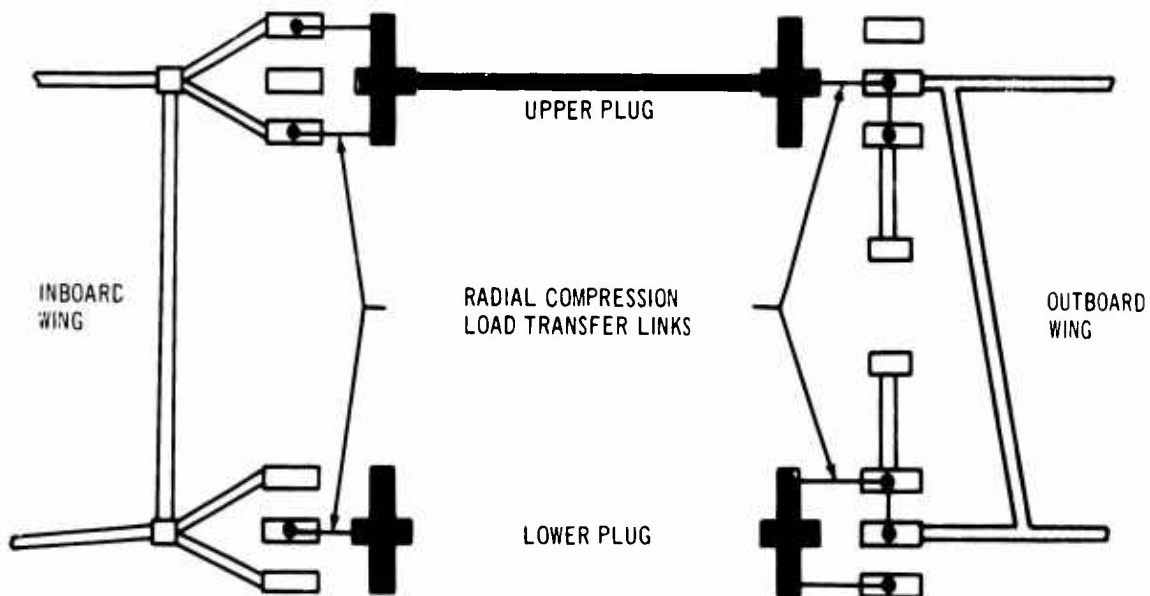
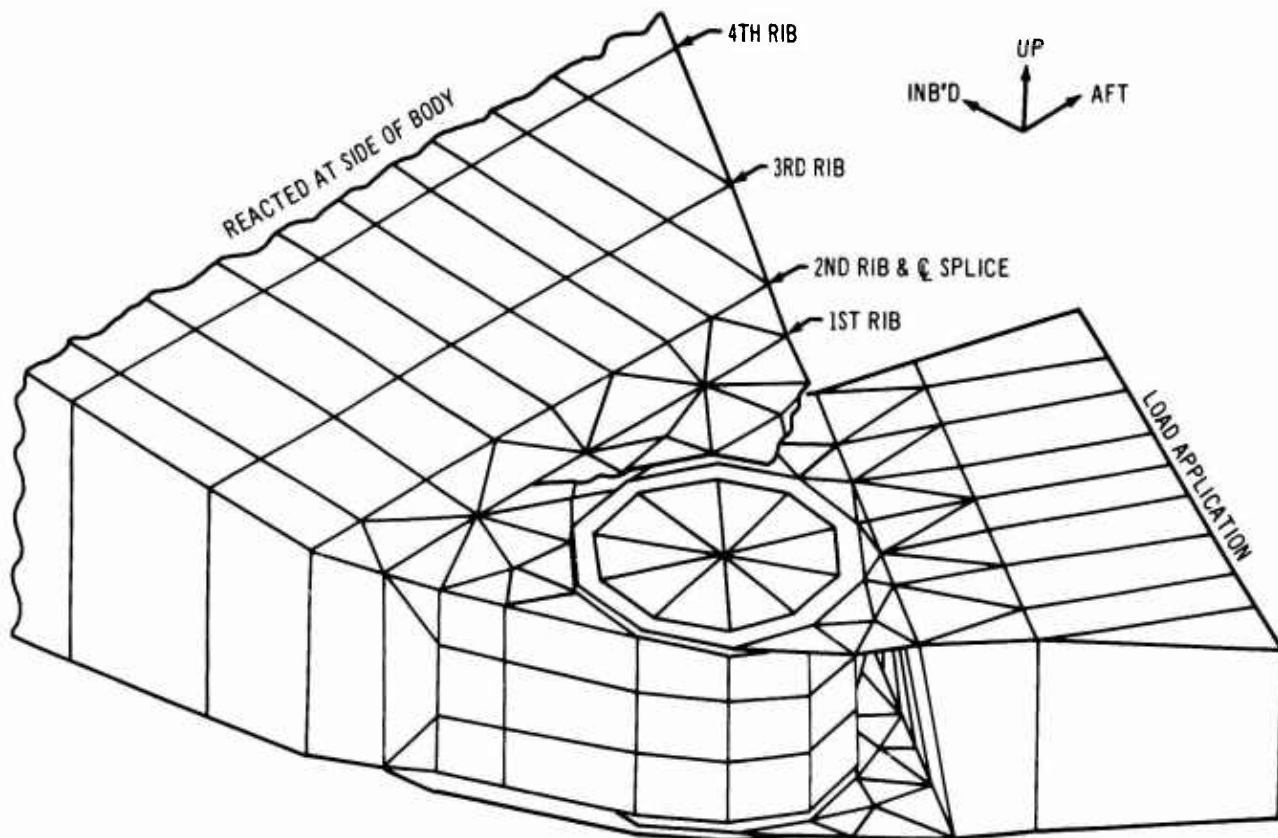


Figure 4-14. Wing Pivot Idealization

curved spar. The lower shears from the comprehensive analysis indicate that the curved spar is less than 40-percent effective in carrying  $T/2A$  torque, with the balance being carried in differential bending of the lugs.

The surface end load and spar shears obtained by the various methods of analysis show reasonable agreement. Analysis of other conditions at different wing-sweep positions are being made. The various overlapping assumptions made during

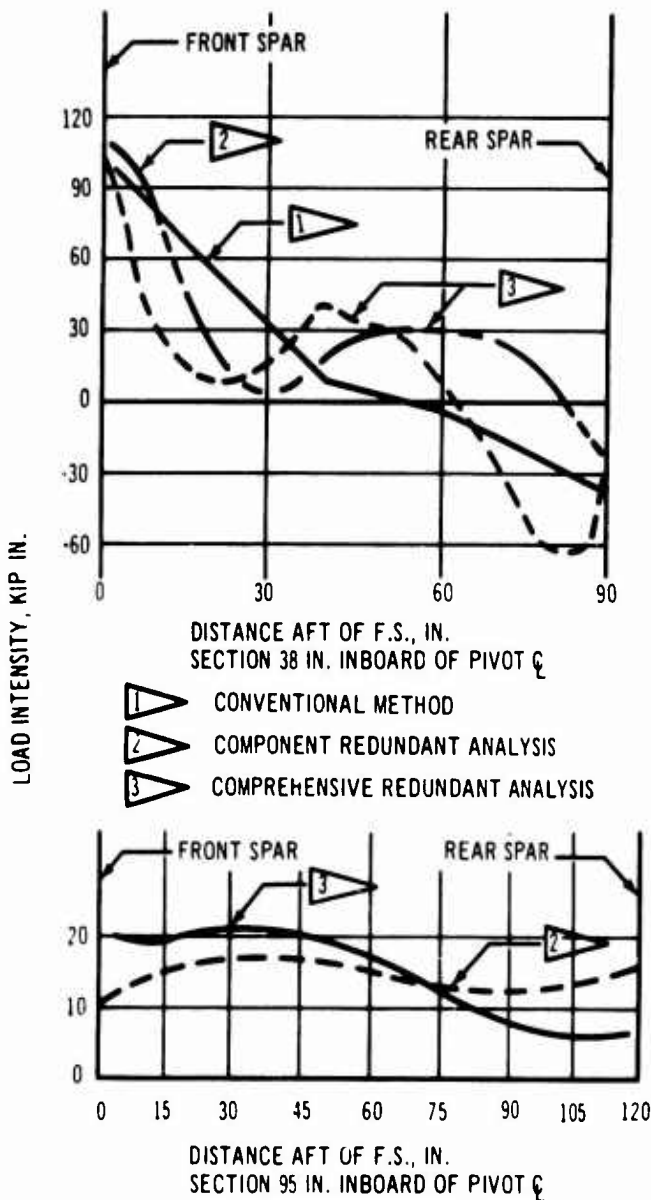


Figure 4-15. Relative Load Intensity, Inboard-Wing-Portion Lower Surface

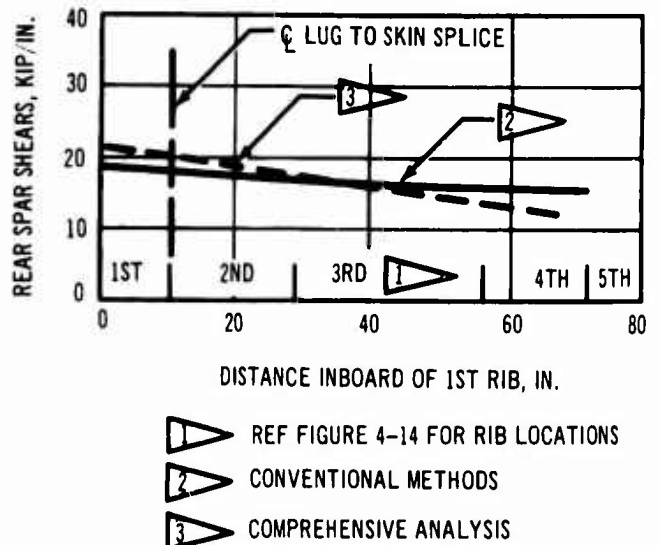
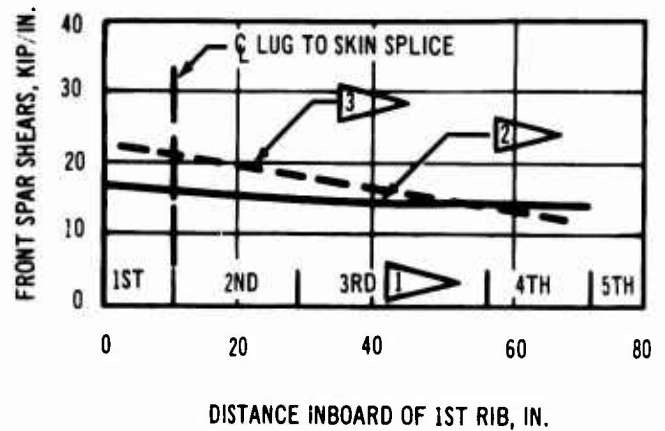


Figure 4-16 Relative Spar Shears Inboard Wing

the original analysis of the pivot test box resulted in structure capable of sustaining the larger loads indicated by the comprehensive analysis. The comprehensive analysis will be used to obtain load distribution, deflections, and flexibility data for design of the pivot region.

#### 4.2.4.5 Wing Spars

Front and rear spars are intermediate-type, stiffened, shear webs except in the pivot area where the spars are shear resistant. Titanium 6Al-4V, Condition V material is used for gages 0.187 and below, and Condition IV material used for gages 0.188 and greater. Web stiffeners are Condition IV.

Outboard-wing-portion spar shear flows for various design conditions are shown in Fig. 4-18. Analysis of a typical section of the rear spar web is shown in Fig. 4-19.

Critical spar shears from the centerline of the airplane to a distance 106 in. outboard of the centerline of the pivot are shown in Fig. 4-20. In the areas adjacent to the pivot, spars have large changes in shear flow resulting from the redistribution of wing torsion loads.

#### 4.2.4.6 Wing Ribs

The wing-fuselage closure rib redistributes wing loads into the fuselage. It also becomes an integral part of the fuselage side skin in distribution of fuselage shears and cabin-pressurization loads. The fuselage frames are connected through the wing to both the wing-fuselage closure rib and the longitudinal ribs of the center section. This provides a load path for fuselage pressure loads. The rib is also used as a tank end rib.

The high-gross-weight, flaps-down maneuver condition gives critical design loads for the rib. A rib analysis is shown in Fig. 4-21.

Typical inspar ribs are Titanium 6Al-4V, Condition III, sine-wave corrugated webs welded to flat-plate chord members. In addition to providing stabilization of the surface structure, these ribs redistribute airloadings. The sine-wave structure minimizes chordwise strains produced by elevated temperature environments. An analysis of a typical rib is shown in Fig. 4-22.

#### 4.2.4.7 Skin and Stiffener Splices

The chordwise skin-stiffener joints are fusion-welded butt type. Based on test data, the allowable stress of a fusion-welded butt joint is the same as the base material being spliced.

The spanwise skin splice locations are discussed in Par. 3.1. Mechanical fasteners are used in these splices. Splices are designed for 40,000-

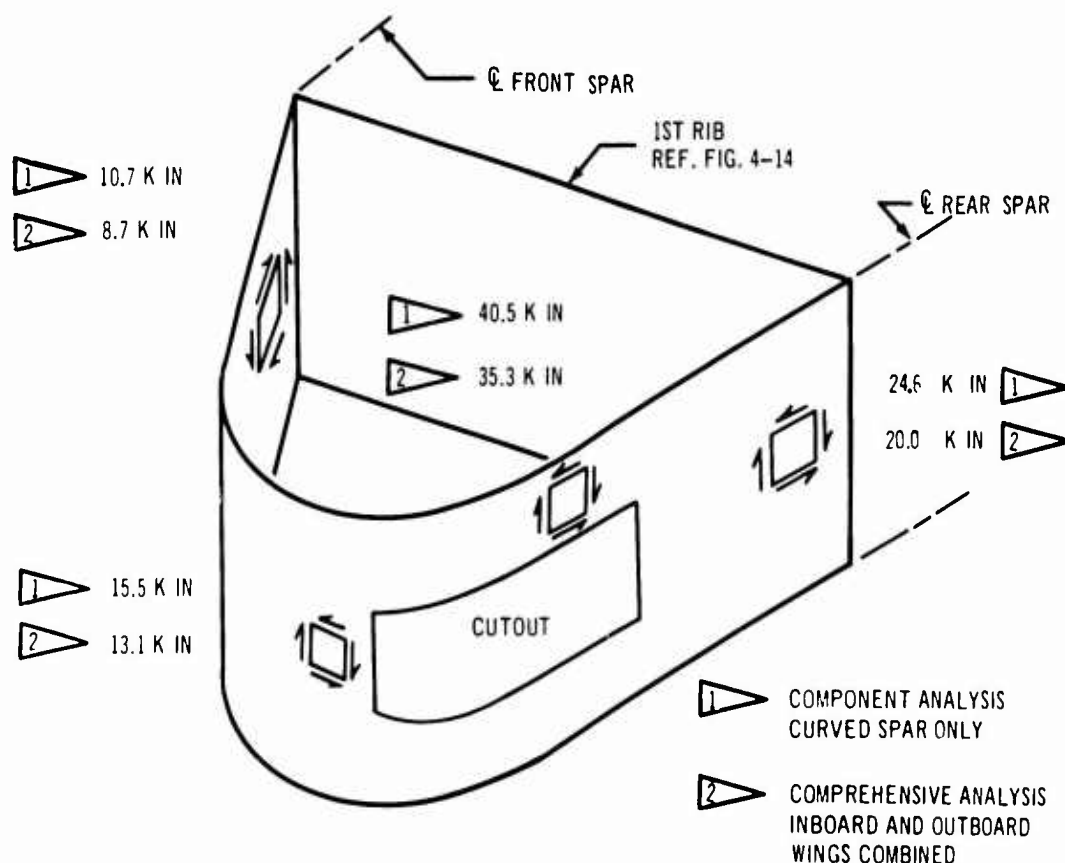


Figure 4-17. Inboard Curved Web Spar Shears

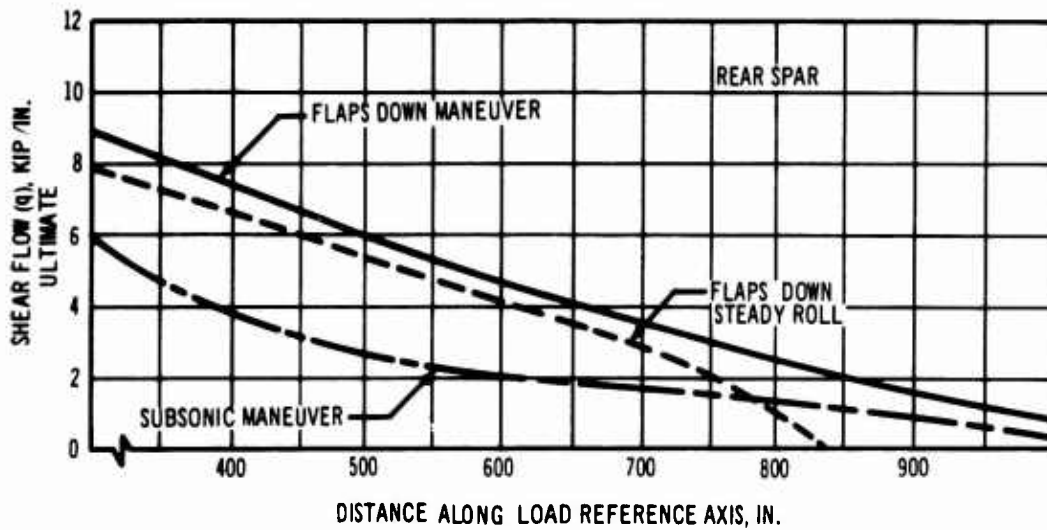
psi shear stress or ultimate applied shear, whichever is the higher.

On the lower surface, the number of splices was selected from fail-safe requirements. The splice members serve as tear stoppers with splice stringer area-to-skin area ratios required by fail-safe design.

Typical spanwise front and rear spar skin splices are shown in Fig. 4-23.

#### 4.2.4.8 Wing and Horizontal Tail Connection

When fully swept, the wing is joined to the horizontal tail by two probes supported by beams cantilevered off the rear spar. These probes engage sockets in the tail and maintain alignment



REF FIGURES 4-1 THRU 4-5  
FOR DESCRIPTION OF LOAD CONDITIONS  
REF V2-B2707-6-1 FOR LOAD REFERENCE AXIS DESCRIPTION.

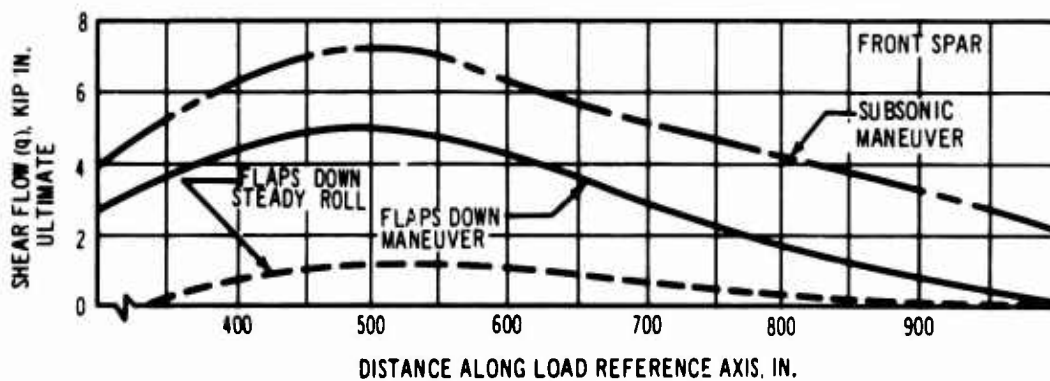


Figure 4-18. Outboard-Wing-Portion Spar Shear

V2-B2707-62

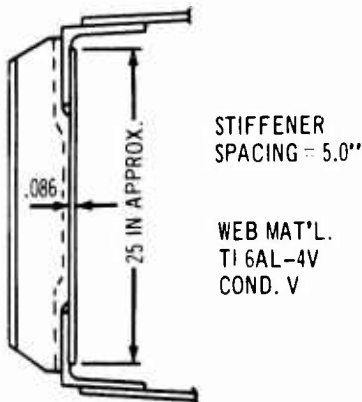
**BLANK PAGE**

**BLANK PAGE**

CRITICAL COND.  
 FLAPS DOWN ~ GW = 670K  
 N = 3.0, M = .295, V = 195 KTS.  
 (REF FIG. 4-18)

SECTION @ 702" ALONG  
 THE LOAD REFERENCE  
 AXIS

REAR SPAR



$$f = 3500 \text{ #/IN (ULT.)}$$

$$F_c = (.49)(134,000) = 65,700 \text{ #/IN} \triangleright$$

$$MS = \frac{(65,700)(.086) - 1}{3500}$$

$$= .62$$

WEB-CHORD RIVETING  
 $\frac{3}{16}$  A 256 RIVETS (BK RIVETS)  
 AT 1.10 - 2 ROWS

$$f_{RIVETS} = \frac{(2)(2540)}{1.10} = 4610 \text{ #/IN}$$

$$MS = \frac{4610}{3500} - 1 = .25 \leftarrow$$

$\triangleright$  REF PAR 4.2 3.4

Figure 4-19. Outboard-Wing-Portion Spar Analysis

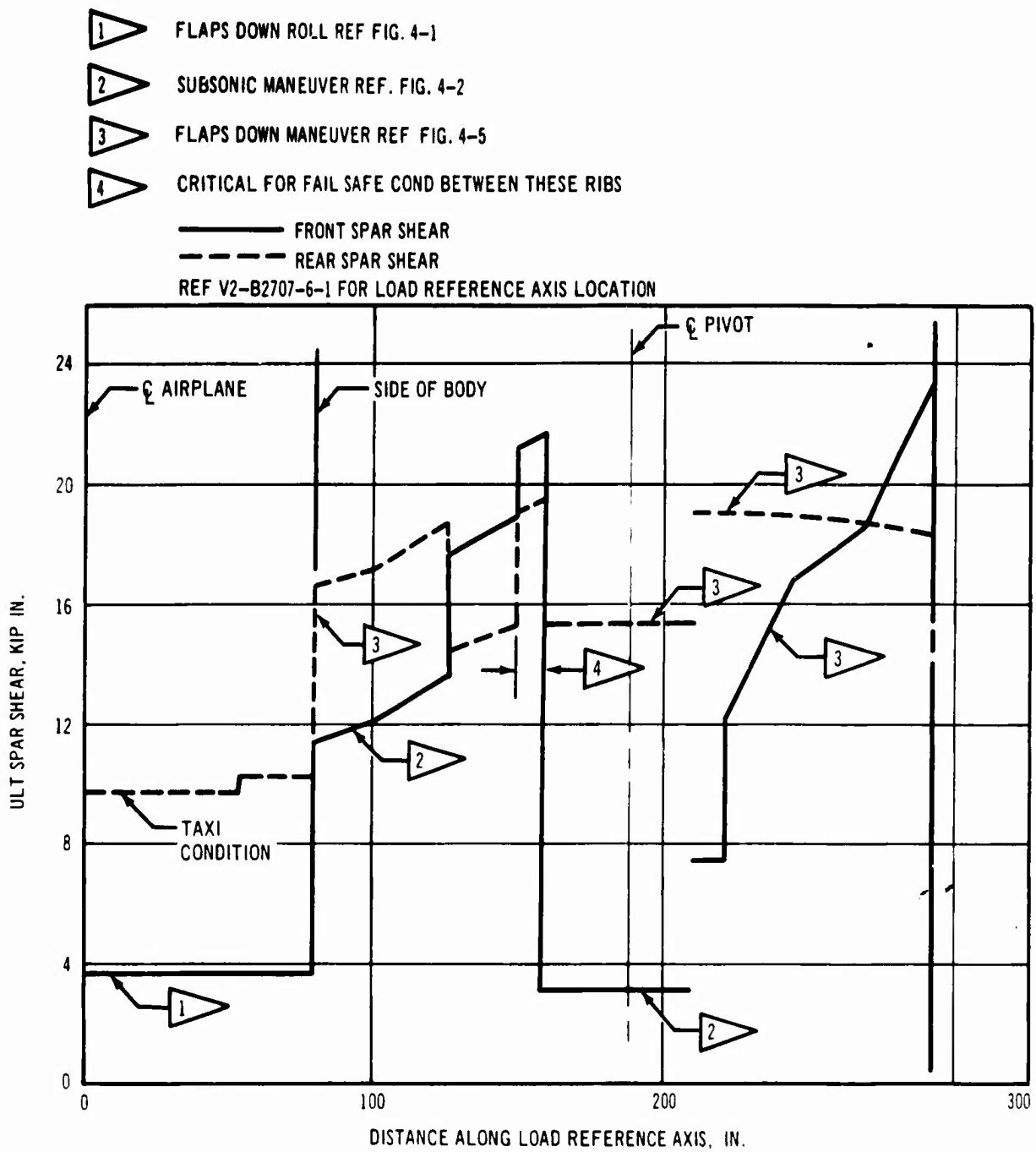


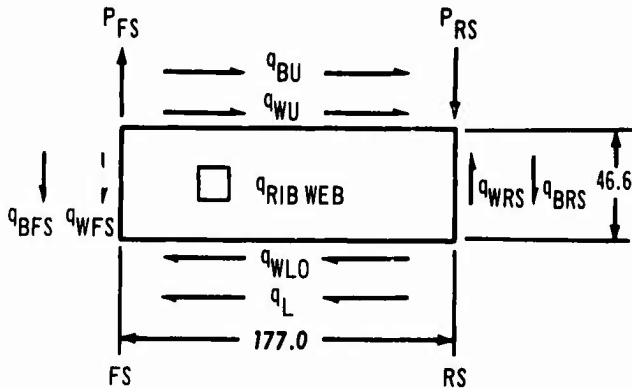
Figure 4-20. Wing Spar Shears

V2-B2707-6-2



CRITICAL DESIGN CONDITION:  
FLAPS DOWN MANEUVER  
REF FIG 4-5

SHEAR IN THE RIB DUE TO  
REDISTRIBUTION OF WING  
LOADS INTO THE BODY



SUBSCRIPTS  
FS — FRONT SPAR  
RS — REAR SPAR  
L — LONGERON  
LO — LOWER  
U — UPPER  
B — BODY  
W — WING

FROM BODY ANALYSIS

$P_{FS}$  = 1890 #/IN  
 $P_{BU}$  = 1890 #/IN  
 $P_{BFS}$  = 1010 #/IN  
 $P_{BRS}$  = 2710 #/IN

FROM WING ANALYSIS

$q_{WLO}$  = 4300 #/IN  
 $q_{WU}$  = 4300 #/IN  
 $q_{WFS}$  = 9350 #/IN  
 $q_{WRS}$  = 17090 #/IN

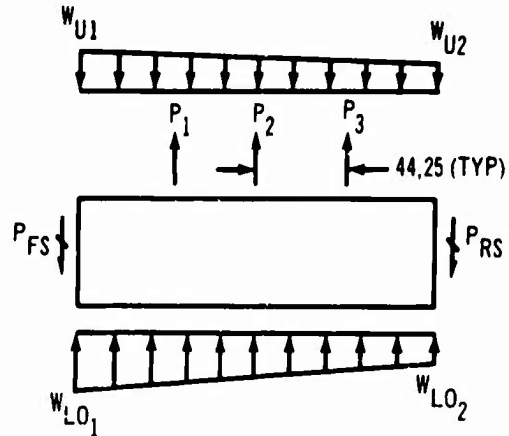
THEREFORE

$$q_{RIB\ WEB} = 4300 + 1890 = 6190 \# / IN$$

$$P_{RS} = [790 - 2710 - 6190] 46.6 = 381000 \#$$

$$P_{FS} = [3350 + 1010 - 6190] 46.6 = 194000 \#$$

SHEAR IN THE RIB FROM BUILT  
IN SURFACE CURVATURE OF  
THE CENTER SECTION LESS  
FUEL WEIGHT



\* LOAD DUE TO LARGER CURVATURE ON THE LOWER SURFACE THAN ON THE UPPER SURFACE IN THE CENTER SECTION LESS FUEL WEIGHT  
 $W_U$  — UPPER SURFACE CURVATURE LOAD  
 $W_{LO}$  — LOWER SURFACE CURVATURE LOAD LESS FUEL WEIGHT

RIB CRUSHING LOADS

$P_{RS}$  = 34700 #       $W_{U1}$  = 1270 #/IN  
 $P_{FS}$  = 24600 #       $W_{U2}$  = 619 #/IN  
 $P_{B1}$  = 14400 #       $W_{LO1}$  = 1534 #/IN  
                                  $W_{LO2}$  = 851 #/IN

THEREFORE

$$P_{RS} = \frac{34700(44.25) + 24600(88.5) + 14400(132.75)}{177.0} + \frac{(815 - 619)(177)(88.5) + (683 - 651)(88.5)(59.0)}{177.0}$$

$$= 53100 \#$$

$$P_{FS} = 34700 + 24600 + 14400 - 53100 + (815 - 619)177 + (683 - 651)88.5 = 64100 \#$$

THE FORWARD END OF THE RIB IS CRITICAL FOR COMBINED LOADING

Figure 4-21 Wing-Fuselage Closure Rib Analysis

$$h_e = 45.0 \text{ IN.}$$
$$q_{FS} = \frac{64100}{45.0} = 1420 \text{ #/IN}$$

TOTAL WEB SHEAR

$$q_{FS} = 1420 + 6190 = 7610 \text{ #/IN}$$
$$t_{WEB} = .10 \text{ IN}$$
$$f_s = \frac{7610}{.10} = 76100 \text{ PSI}$$

WEB MATERIAL: TL 6AL-4V, COND III

ALLOWABLE STRESS  
INTERMEDIATE TYP WEB

$$F_{su} = .49(162000) = 79400 \text{ PSI}$$

$$M.S. = \frac{79400}{76100} - 1 = +.04$$

Figure 4-21. (Concluded)

V2-B2707-6-2

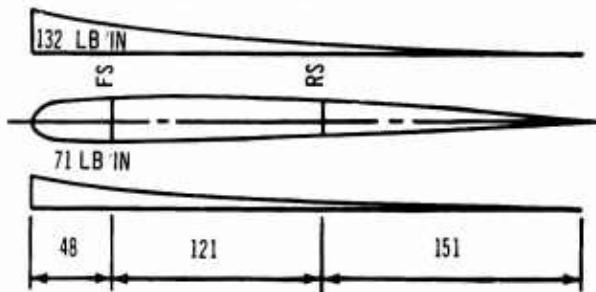
ANALYSIS OF TYPICAL INSPAR WING RIB

CRITICAL CONDITION: SUBSONIC MANEUVER,  $\Lambda_{LE} = 42^\circ$ ,  $M = .85$ ,  $N = 3.75$ , G.W. = 647<sup>k</sup>  
 AVERAGE PRESSURE = 2.5<sup>psi</sup> (ULTIMATE)

ASSUME PARABOLIC AIR LOAD DISTRIBUTION ALONG CHORD (CP AT 25% CHORD)

ASSUME 65% OF AIR LOAD ON UPPER SURFACE, 35% ON LOWER SURFACE.

RIB LOCATED APPROXIMATELY 330" OUTBD. OF  $\phi$  PIVOT. 2.7" RIB SPACING.



BENDING CURVATURE LOADS:

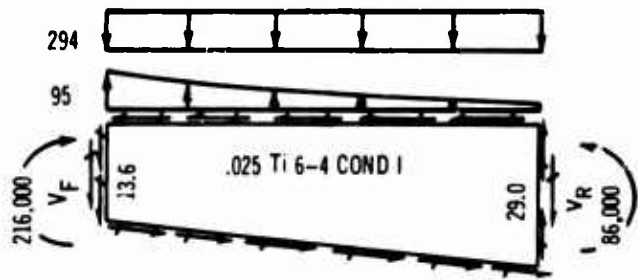
$P = \frac{M^2}{2yh_xEI}$  WHERE  $y$  = DISTANCE FROM N.A. TO BENDING MAT'L. CENTROID.  
 $h_x$  = DIST. BETWEEN SPARS.

$$\frac{EI}{M} = \frac{210 \times 10^9}{75 \times 10^6} = 2880$$

$$P = \frac{75 \times 10^6}{(2)(3.9)(121)(2880)} = 10.9 \text{ psi}$$

$$u = (10.9)(27) = 294 \text{ psi}$$

REF. FIG. 4-2



$$q_T = \frac{216,000 - 86,000}{(2)(21.3)(121)} = 25 \text{ psi}$$

$$V_F = 6510 \text{ psi} \quad V_R = 4490 \text{ psi}$$

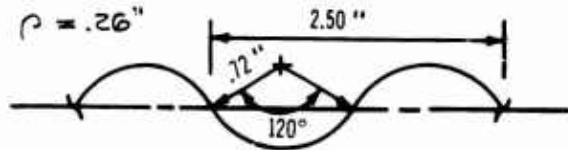
$$q_{WEB} = \frac{(1" \text{ FWD. OF REAR SPAR})}{24.0} = \frac{4410 - (25)(29.0)}{24.0} = 157 \text{ psi}$$

$$f_s = \frac{157}{.025} = 6270 \text{ psi}$$

$$f_c = \frac{294}{.0302} = 9720 \text{ psi}$$

$$\epsilon = .0302 \text{ psi}$$

$$\rho = .26 \text{ psi}$$



TYPICAL WEB CORRUGATION

$F_{scr}$  (GENERAL STABILITY CRITICAL)

$$= .76 K E_n \left(\frac{t}{a}\right)^2 \left(\frac{2R}{t}\right)^{3/2} f(\phi)$$

$$= (.76)(8.0)(164)(10^6)(1.0) \left(\frac{.025}{24.0}\right)^2 \left(\frac{1.44}{.025}\right)^{3/2} (.237)$$

$$= 10,960 \text{ psi}$$

$$F_c = \frac{\pi^2 E_T}{(4\rho)^2} = \frac{(9.14)^2 (164)(10^6)}{(576)(.26)^2} = 18,000 \text{ psi}$$

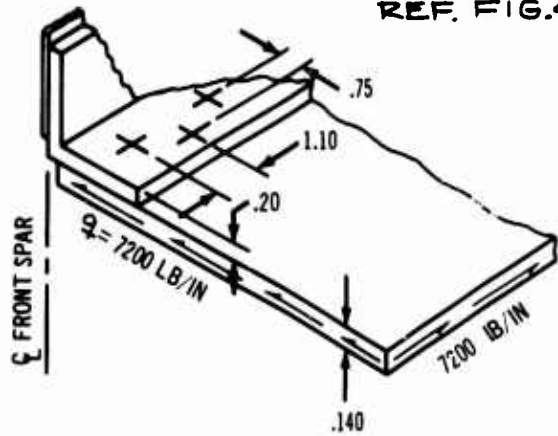
$$MS = \frac{2}{\frac{9720}{18000} + \left[\frac{9720}{18000}\right]^2 + 4 \left[\frac{6270}{10960}\right]^2}^{-1}$$

$$= .11$$

CHORD DEPTH AT REAR SPAR

Figure 4-22. Typical Inspar Rib Analysis

500" ALONG LOAD REFERENCE  
 AXIS - SUBSONIC MAN-  
 EUVER  
 REF. FIG. 4-18



TLV 100-4  $\frac{1}{4}$  TI 6-4 TAPER LOKS  
 SHEAR ALLOWABLE = 4650\*

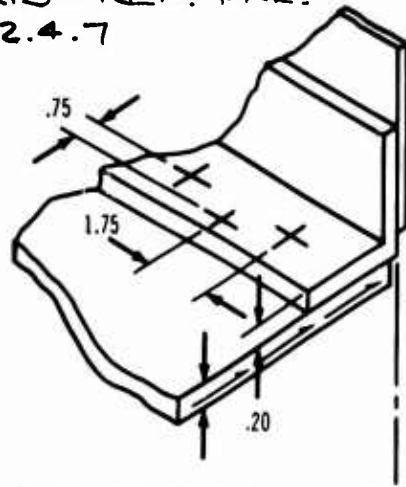
$$MS = \frac{(2)(4650)}{(7200)(1.10)} - 1 = \underline{.17}$$

$$f_{NET} = \frac{(7200)(1.10)}{(1.10 - .25)(.140)} = 66,600\%*$$

NOT CRITICAL

700" ALONG LOAD REFERENCE  
 AXIS - REF. PAR.

4.2.4.7



$$q = (40,000)(.20) = 8000\%*$$

TLV 100-5  $\frac{5}{16}$  TI 6-4 TAPER-LOKS  
 SHEAR ALLOWABLE = 7300\*

$$MS = \frac{(2)(7300)}{(8000)(1.75)} - 1 = \underline{.04}$$

Figure 4-23. Skin Splice Analysis

of the wing and tail. The wing and horizontal tail are designed to provide vertical position alignment at  $n = 1.0$  at normal flight conditions. The probes are designed to react loads produced from differential loadings of the wing and horizontal tail. Gaps are provided to allow movement in the chordwise direction. The outboard probe is designed to bottom out and prevent excessive chordwise wing deflection.

During actuation, the inboard probe is first to engage. Loading of the inboard probe for deviations from the  $n = 1.0$  condition brings the wing and tail into closer alignment at the outboard probe. The inboard probe is designed for the actuation case with only the inboard probe engaged. The support beam is common with the flap track supports and is designed by flap loads except in the area near the probe fitting.

The outboard probe is designed by loads occurring at  $+2.5\text{-g}$  limit and  $-1.0\text{ g}$  limit with the  $-1.0\text{ g}$  limit being most severe. Loads incurred from the tail surfaces are relieving to the wing structure.

The roller support fitting and fitting attach forgings are not critical to the safety of the airplane; however, a multiple path fail-safe concept is used. The probe support analysis is shown in Fig. 4-24.

#### 4.2.5 Wing Strake

The strake is a multicelled box with spanwise ribs, a leading-edge spar, and sandwich-construction cover panels. Strake volume is divided into three integral fuel compartments by tank end ribs. Structural arrangement of the strake is shown in Par. 3.1. Additional fore and aft compartmentation to limit the fuel head for crash landing conditions is achieved by restricted orifices.

Strake ribs coincide with fuselage frames. Shear and moment continuity across the fuselage is provided at each rib-frame intersection. Ribs have sine-wave corrugated webs. The front-spar and wheel-well walls are of conventional stiffened-web design.

The strake structure is critical for a variety of conditions. The surfaces are critical for a fuel vent malfunction during refueling. The vent system is designed to limit tank pressures to  $7.5\text{ psig}$  limit. Ultimate  $6\text{-g}$  crash loadings

create the critical longitudinal design forces for the bulkheads and spars.

Strake loads are modified by fuselage-strake interaction effects of body bending and temperature. The critical positive bending condition for the ribs and leading edge spar is a low-gross-weight gust condition with minimum strake fuel. The critical negative bending condition is a 2-g-limit taxi condition with full-strake fuel. Design shear and moments for the strake are shown in Figs. 4-25 and 4-26.

Analysis of typical structural components of the strake are shown in Fig. 4-27 and 4-28.

#### 4.2.6 Wing Sweep Actuator

The basic structural design concept of the actuator is shown in Fig. 4-29 and is similar to that used on the stabilizer jackscrew on the 707, 720, and 727 airplanes. A complete description of the actuator is given in Part B, Hydraulics, Landing Gear, Auxiliary Systems (V2-B2707-11), of the Systems Report. The actuator gear box is located on the inboard end of the screw and is gimbal mounted to the fixed wing structure. Support of the outboard end of the screw is provided by a gimbal-mounted nut attached to the movable wing.

Actuation is provided by three hydraulic motors supplying power to a gear system through a dual torque tube. The gear system is designed to maintain full-output torque, at reduced rotational velocity, for partial failures of the power system. Failure of one power system will result in a reduction of output rotational velocity of one third. The rotational velocity is one third of design with the failure of two power systems.

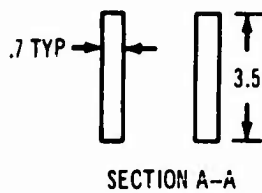
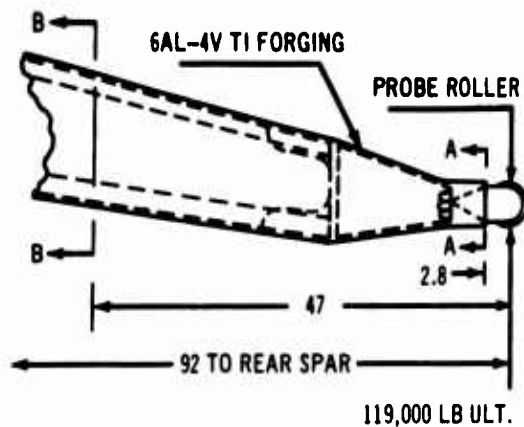
Axial screw loads are transmitted through three separate ball-bearing circuits, each contacting four screw threads. The torque brake prevents screw rotation during holding. The torque brake is designed for two times the maximum torque developed from the screw thread load.

Dual load paths are maintained throughout the gear box, drive-train system, and screw. Figure 4-29 identifies the dual load paths.

Static conditions produce the maximum design loads as shown in Fig. 4-30. Sweep rotation design moments are given in Design Criteria, Loads, Aerodynamic Heating, Flutter (V2-B2707-7) of the Airframe Design Report.

# ANALYSIS OF PROBE SUPPORT

CONDITION 24 ~ START OF CRUISE  
 ~ NEGATIVE MANEUVER CRITICAL



$$M_{AA} = 119,000 \times 2.8 = 333,000 \text{ " LB ULT.}$$

$$f_b = \frac{6M}{bh^2} = \frac{6 \times 333,000}{2 \times .7 \times 3.5^2} = 116,200 \text{ */d"}$$

$$f_s = 119,000 / 1.4 \times 3.5 = 24,300 \text{ */d"}$$

$$F_{TU} = 110,000 \text{ */d" AT } 450^\circ \text{ F } \blacktriangleright$$

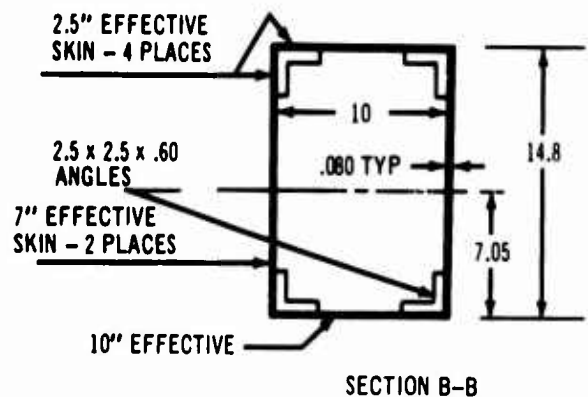
$$F_{TY} = 96,000 \text{ */d" AT } 450^\circ \text{ F}$$

K FACTOR FOR RECTANGULAR SECT = 1.5

$$F_{BU} = F_{TU} + (K-1)F_{TY} \text{ RE} = 1.2$$

$$F_{BU} = 110,000 + (1.5-1)96,000 = 158,000 \text{ */d"}$$

$$\text{MARGIN OF SAFETY} = \frac{158,000}{116,200} - 1 = .36$$



LOWER FIBER TENSION.

$$I_{NA} = 550 \text{ IN}^4$$

$$M_{BB} = 119,000 \times 47 = 5,590,000 \text{ " LB}$$

$$f_t = \frac{5,590,000 \times 7.05}{550} = 71,600 \text{ */d"}$$

GROSS AREA EFFICIENCY FACTOR = .88

$$f_t = 71,600 / .88 = 81,500 \text{ */d"}$$

$$F_{TU} = 107,000 \text{ */d"}$$

$$\text{MARGIN OF SAFETY} = \frac{107,000}{81,500} - 1 = .31$$

THE BOX BEAM CONFIGURATION  
 ALLOWS FOR FAIL SAFE DESIGN  
 THE BEAM CAN SUPPORT 80%  
 LIMIT LOAD WITH ONE ANGLE  
 FAILED.

UPPER ANGLE

$$\bar{y} = 14.8 - 7.05 - 8.4 = 6.91$$

$$f_c = \frac{5,590,000 \times 6.91}{550 \cos 15^\circ} = 72,800 \text{ */d"}$$

$$b = 2.5 - .30 = 2.2$$

$$b/t = 2.2 / .60 = 3.67$$

$$F_{CC} = 108,000 \text{ */d"}$$

$$\text{MARGIN OF SAFETY} = \frac{108,000}{72,800} - 1 = .48$$

$\blacktriangleright$  IN LIEU OF FORGING;  
 PROPERTIES FOR COND IV  
 PLATE ( $t > .75$ ) ARE USED.

Figure 4-24. Wing-Horizontal Tail Probe Analysis

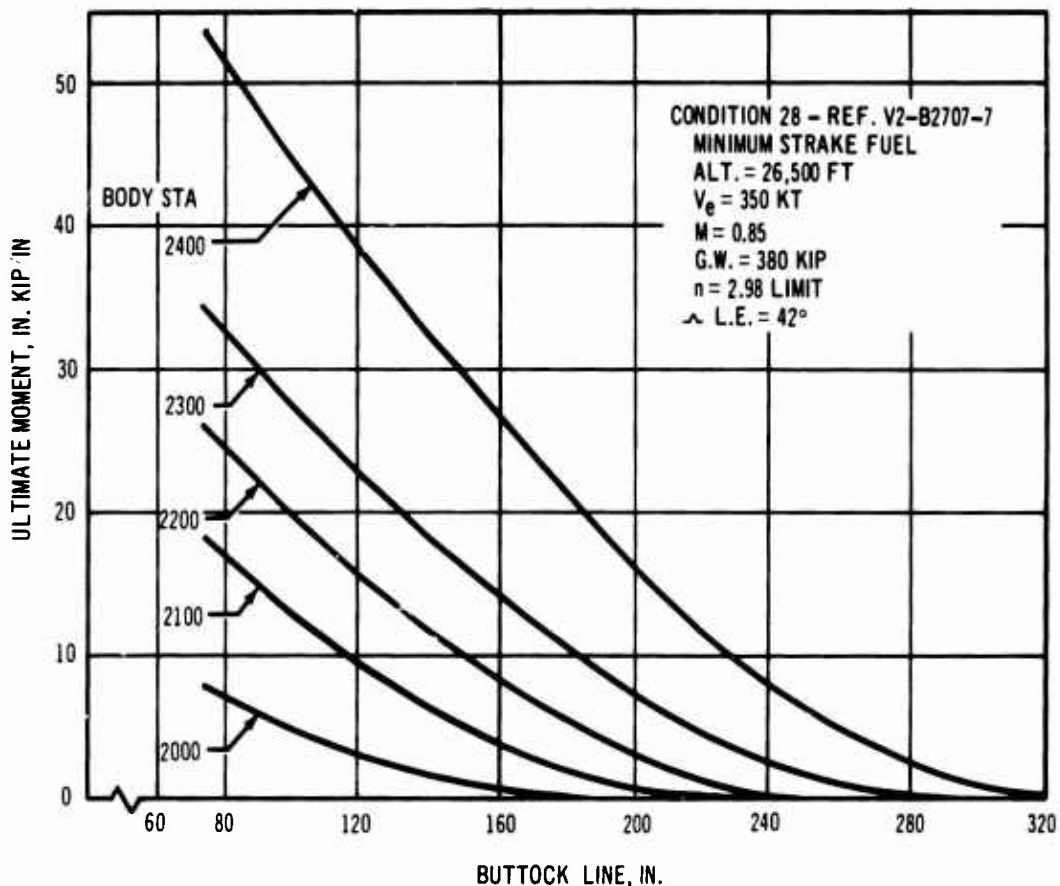
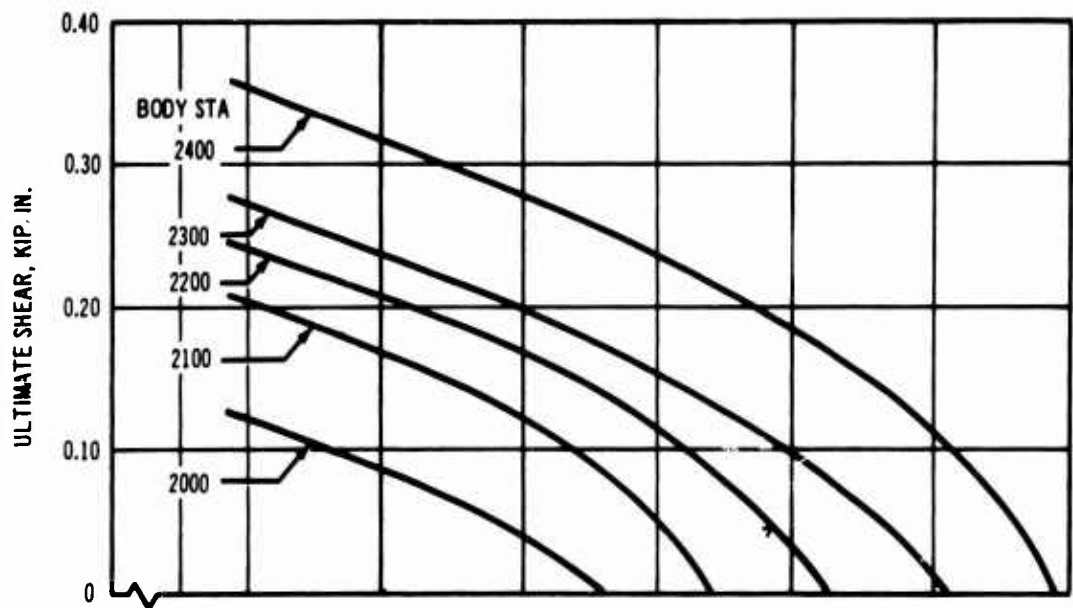


Figure 4-25. Strake Shear and Moment, Gust Condition

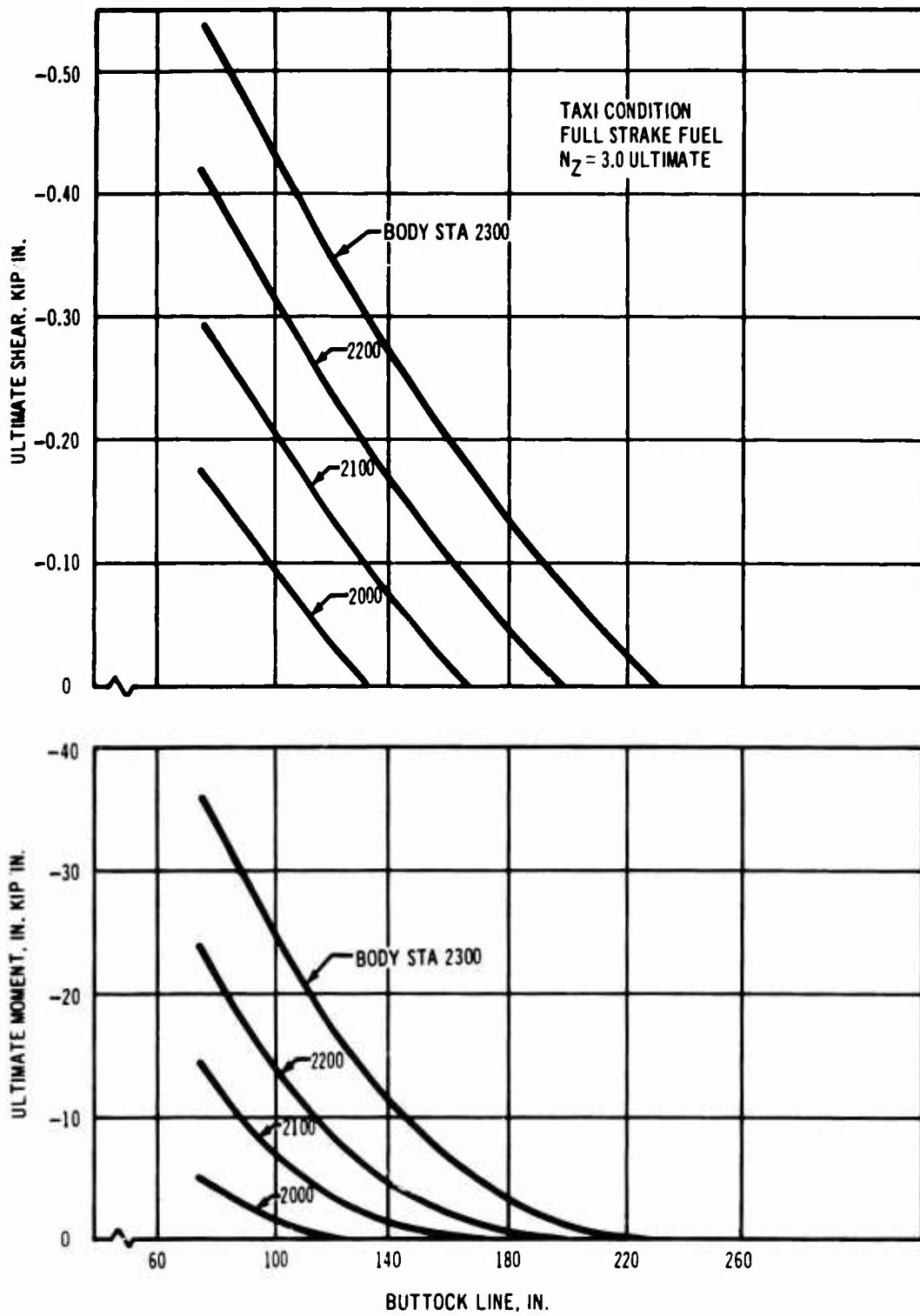


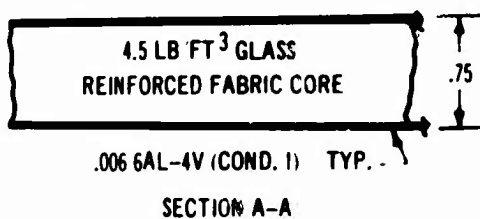
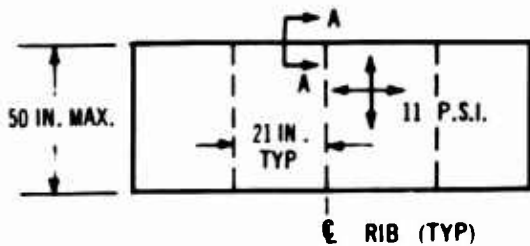
Figure 4-26. Strake Shear and Moment, Taxi Condition

V2-B2707-6-2



## SURFACE STRUCTURE

THE CRITICAL LOAD CONDITION IS AN ULTIMATE REFUELING OVERPRESSURE OF 11 P.S.I.G. RESULTING FROM A VENT VALVE MALFUNCTION.



### CONDITION I ALLOWABLES:

$$F_{tu} = 139 \text{ KSI}$$

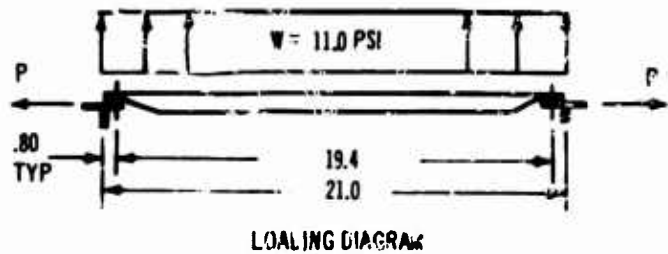
$$F_{cy} = 138 \text{ KSI.}$$

$$E_c = 16.4 \times 10^3 \text{ KSI.}$$

$$F_c/E_T = .0038$$

$$E_T = 16.4 \times 10^3$$

$$F_c = 62.3 \text{ KSI.}$$



$$M_{MAX.} = WJ^2 (1 - \text{SECH } U/2)$$

$$P = (50 - 1.75)(11) / 2 = 266 \text{ LB./IN.}$$

$$I = 2(.006)(.372)^2 = .00164 \text{ IN}^4/\text{IN.}$$

$$J = [EI/P]^{0.5}$$

$$= [16.4 \times 10^6 \times 16.6 \times 10^{-6} / 266]^{0.5}$$

$$= \sqrt{102.5} = 10.1$$

$$U/2 = L/2J = 19.4/2 \times 10.1 = 0.956$$

$$\text{SECH } U/2 = 0.668$$

$$M_{MAX} = 11(102.5)(1 - 0.668) = 375 \text{ IN.-LB./IN.}$$

$$f_b = \pm 375 / .744(.006) = \pm 84.0 \text{ KSI}$$

$$f_a = 266 / .012 = 22.2 \text{ KSI}$$

$$f_{TENS} = 84.0 + 22.2 = 106.2 \text{ KSI}$$

$$f_{COMP} = 84.0 - 22.2 = 61.8 \text{ KSI}$$

$$MS(\text{COMP}) = (62.5/61.8) - 1$$

$$= +.01 \leftarrow$$

△ UPPER SURFACE .75 IN.  
LOWER 1.00 IN.

Figure 4-27. Strake Surface Analysis

**RIB STRUCTURE:**

**INTERNAL PRESSURE CONDITION:**  
 6 G ULTIMATE FUEL HEAD. 5%  
 ASSUMED MLLAGE SPACE.  $\rho_{FUEL}$   
 = .029 LB/IN.<sup>3</sup>  
**RIB SHEAR AND BENDING CONDITION:**  
 THREE G TAXI  $\blacktriangleright$

**LOADS:**

$$p = 6(.029)(21)(.95) = 3.47 \text{ PSI - ULT. (6 G FUEL HEAD)}$$

**TAXI CONDITION  $\blacktriangleright$ :**  
 (BODY STA. 2300, BL 74.0)

$$V = -.54 \text{ KIPS/IN - ULT.}$$

$$M = -38.0 \text{ IN-KIPS/IN - ULT.}$$

**WEB:**  
 THE CORRUGATED WEB THICKNESS  
 REQUIRED TO RESIST TRANSVERSE  
 PRESSURE IS .032 IN.  $R=2.0$  IN.

THE ALLOWABLE COMPRESSION  
 STRESS,  $F_c = 0.20 E t / R = 52.5$  KSI

$$f_c = M c / I - P / A$$

$$M = w L^2 / 8 = \frac{3.47(50)^2}{8} = 1085 \text{ IN-KIPS/IN}$$

$$c / I = \frac{2.0}{2(.156)(.032)(2.0)^2} = .0498$$

$$M c / I = 1085(.0498) = 54.0 \text{ KSI}$$

$$P / A = \frac{21(3.47)}{1.21(.032)} = 1.9 \text{ KSI}$$

$$f_c = 54.0 - 1.9 = 52.1 \text{ KSI}$$

$$M.S. = 52.5 / 52.1 - 1.0 = +0.01 \leftarrow$$

**RIB LOWER CAP:**

$$P = \frac{38(21)}{49.8} = 16.0 \text{ KIPS}$$

$$b / t = 1.50 / .085 = 17.7 \text{ (REF. VIEW B)}$$

$$F_{cc} = 63.0 \text{ KSI}$$

$$f_c = \frac{16.0}{3.0(.085)} = 63.0 \text{ KSI}$$

$$M.S. = 63.0 / 63.0 - 1.0 = 0.00 \leftarrow$$

$\blacktriangleright$  REF. FIG. 4-26

$\blacktriangleright$  1.21 = WRAP FACTOR

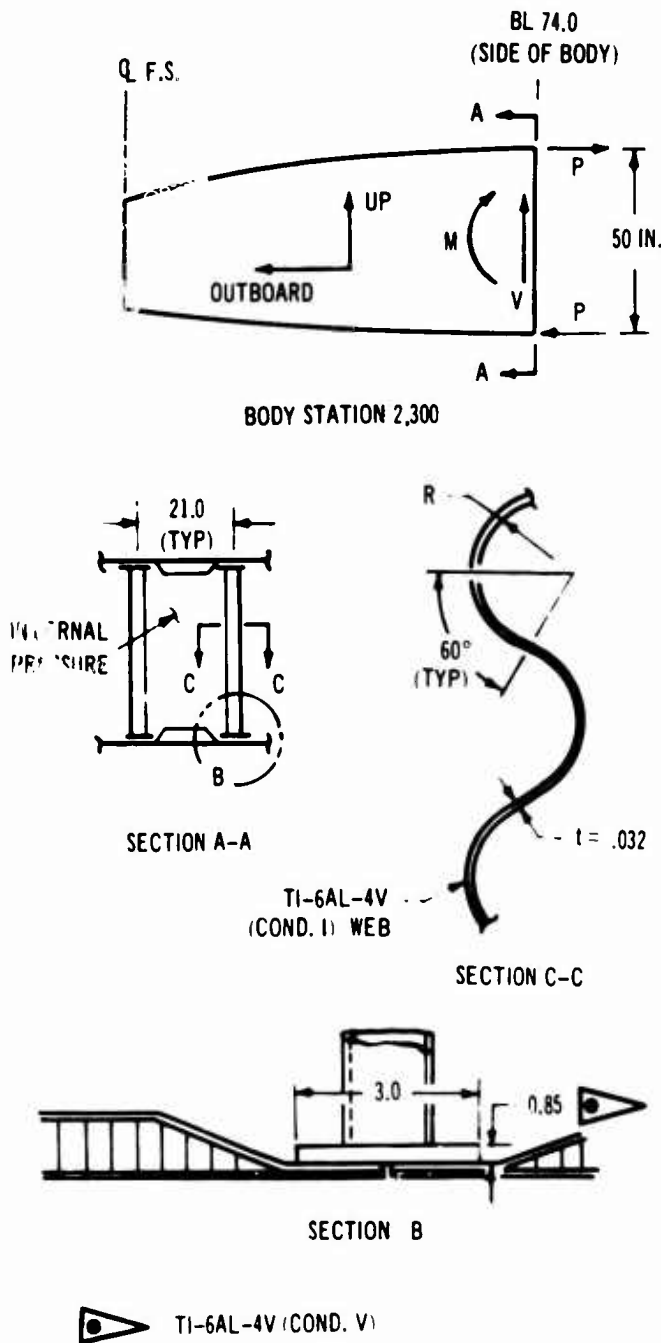
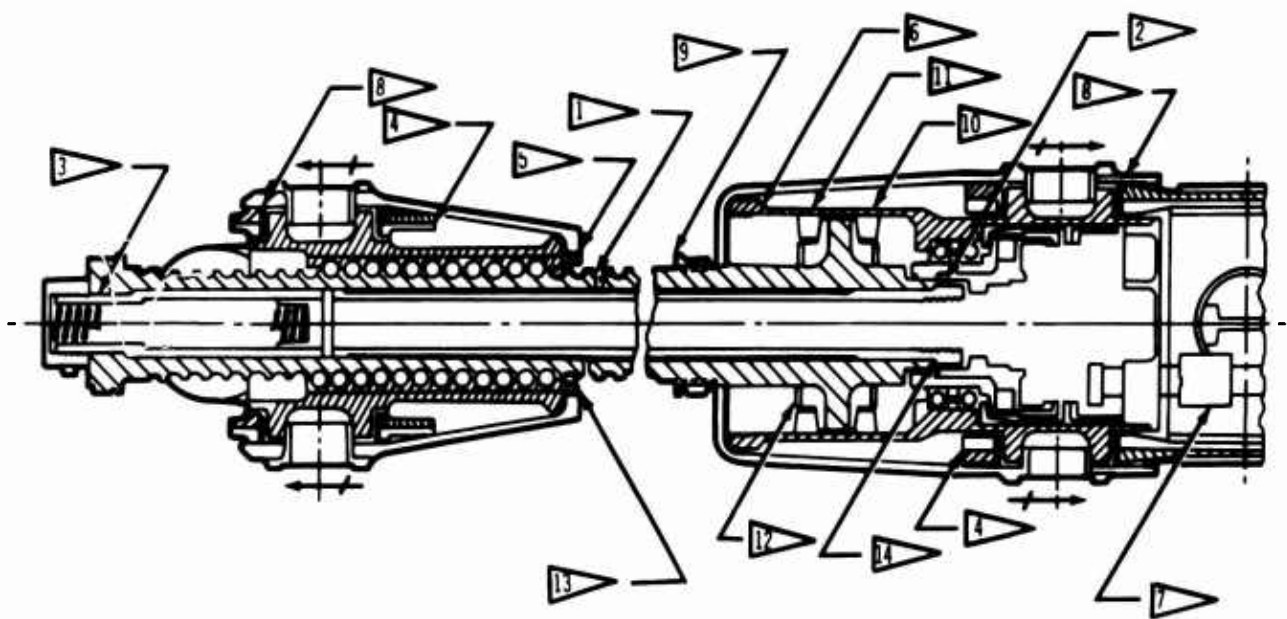


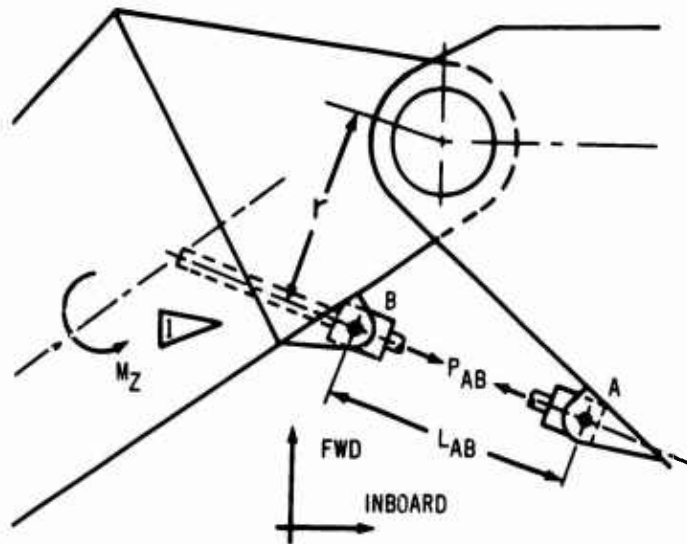
Figure 4-28. Strake Rib Analysis



- |   |   |
|---|---|
| <p>1 DUAL LOAD PATH SCREW - WITH TENSION FAILURE AT THE THREAD ROOT. LOAD IS TRANSFERRED TO SECONDARY ROD AT 14</p> <p>2 WITH SCREW FAILURE, TORQUE FROM GEARBOX IS TRANSMITTED DIRECTLY TO SECONDARY ROD BY SPLINES</p> <p>3 TORQUE FROM SECONDARY ROD IS TRANSMITTED TO SCREW BY SPLINE IF SCREW FAILS</p> <p>4 DUAL LOAD PATH GIMBALS (2 PLACES)</p> <p>5 DUAL LOAD PATH NUT</p> | <p>6 DUAL LOAD PATH GEARBOX HOUSING</p> <p>7 DUAL INPUT TORQUE TUBES</p> <p>8 DUAL BEARINGS TO PREVENT SEIZURE</p> <p>9 TORQUE STOPS (2 PLACES)</p> <p>10 THRUST BEARING (COMPRESSION)</p> <p>11 THRUST BEARING (TENSION)</p> <p>12 TORQUE BRAKE</p> <p>13 TRIPLE BALL CIRCUITS</p> |
|---|---|

Figure 4-29. Structural Arrangement, Wing Sweep Actuator

WING SWEEP ACTUATOR LOADS



CONDITION	HOLDING (MAX. TENSION)	HOLDING (MAX. COMP.)
$\Lambda_{LE} \sim$ DEGREES	42	30
$M_z \sim$ IN-KIPS (ULT)	-85,500	+67,500
$r \sim$ INCHES	84.0	81.0
$P_{AB} \sim$ KIPS (ULT)	+1018.0	-833.0
$L_{AB} \sim$ INCHES	103.0	120.0

REF. V2 B2707-7

Figure 4-30. Ultimate Design Loads, Wing Sweep Actuator

### 4.3 FUSELAGE STRESS ANALYSIS

#### 4.3.1 Structural Description

The basic structure of the fuselage is a semi-monocoque shell of conventional skin-stringer surface supported by internal frames and bulkheads. Structural arrangement of the fuselage is shown in Sec. 3.2.

The fuselage is a complete torque box of either one or two cells for its entire length. Continuity of the torque section around local cutouts to

accommodate windows, doors, and access openings is maintained by reinforcement of local structure.

Forward of the lower-deck fuel tanks, the entire fuselage is pressurized. Aft of this point, a cabin pressure floor extends to the stabilizer rear spar to provide an unpressurized area for the fuselage fuel tanks, wing center section, rear main gear, equipment bays, and stabilizer center section. The pressure floor is supported by continuous longitudinal floor beams, with

floor beam support provided by lower-deck bulkheads. Lateral floor beams at fuselage frame locations are used when both upper and lower sections of the fuselage are pressurized.

An integral structural attachment is provided between the fuselage structure and the wing and stabilizer structure. The fuselage frames and floor structure provide continuous carry-through structure for the wing strake. The wing and horizontal-stabilizer spars provide integral parts of the main-fuselage-attachment bulkheads except that the rear stabilizer spar is pin connected.

#### 4.3.2 Fuselage Design Loads

The critical design conditions for the fuselage,

shown in Table 4-D and Figs. 4-31 and 4-32, are based on criteria presented in Part C, Design Criteria, Loads, Aerodynamic Heating, Flutter (V2-B2707-7), of the Airframe Design Report. Forward of the wing front spar, the fuselage is designed by either dynamic landing, takeoff taxi, or internal cabin-pressure loads. The effects of nose-gear impact are included in the dynamic landing loads. No elevated temperature flight conditions are critical for the forward fuselage.

Subsonic maneuver and fin gust are the critical vertical- and side-load conditions for the aft fuselage. Portions of the aft fuselage are critical for maneuvers at elevated temperature.

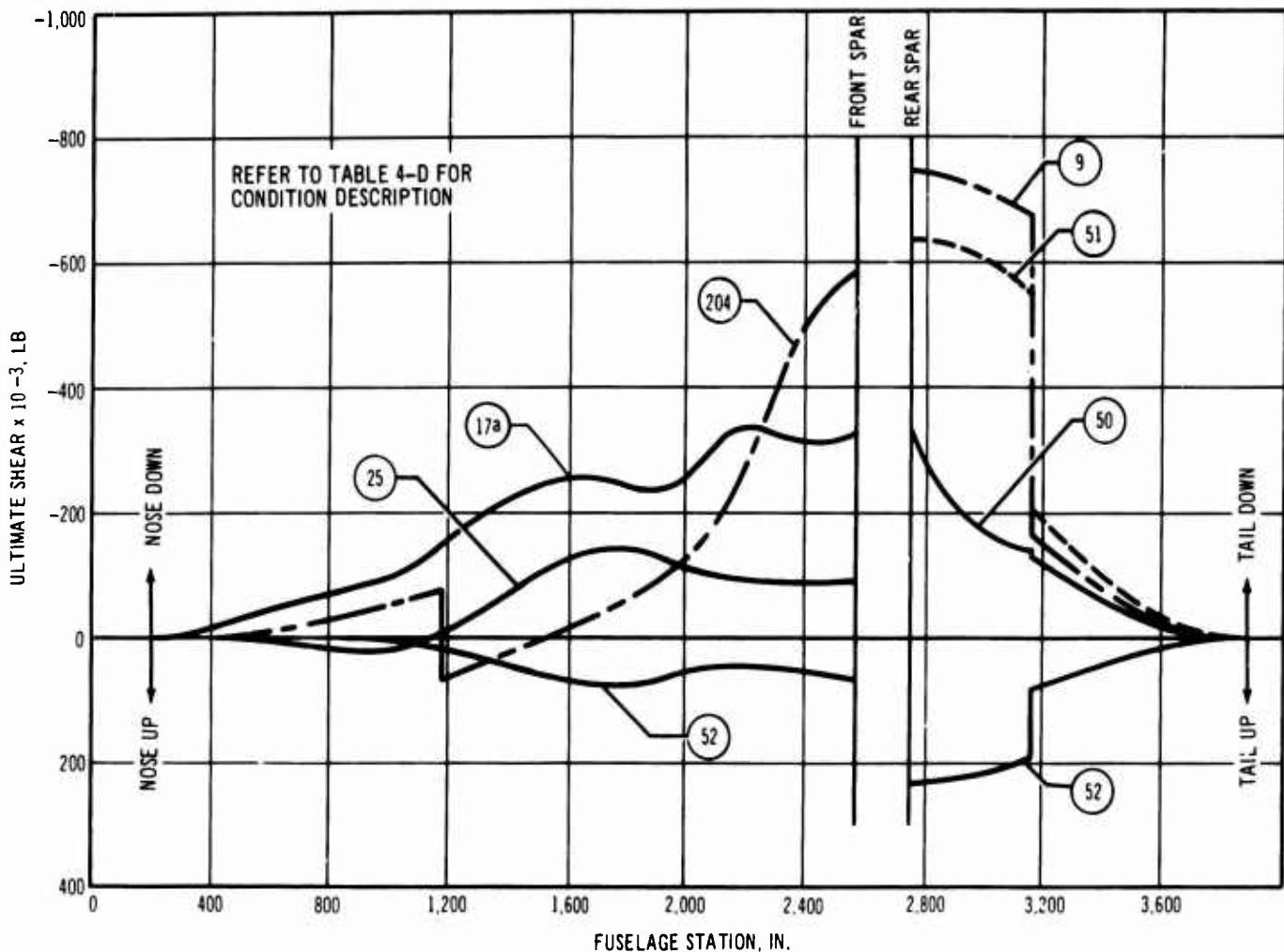


Figure 4-31. Fuselage Ultimate Vertical Shear

Table 4-D. Fuselage Design Conditions

Condition No.	Condition Description	$\alpha$ LE	M	Alt.	G.W.	$n_{cg}$
		(Deg.)	(No.)	( $10^{-3}$ ft)	(kips)	
9	Flaps-down maneuver	30	0.295	S.L.	668.	2.0
17a	Dynamic-landing negative bending	30	0.211	S.L.	430.	2.6
25	Supersonic $V_A$ Maneuver (fwd cg)	72	2.7	64.0	605.	2.5
28	Vertical gust	42	0.90	26.6	380.	2.32
50	Supersonic $V_A$ Maneuver (aft cg)	72	2.7	64.0	605.	2.5
51	Subsonic, Positive $V_A$ Maneuver	42	0.90	33.0	648.	2.5
52	Subsonic, Negative $V_A$ Maneuver	42	0.90	33.0	648.	-1.0
204	Takeoff Taxi	30	--	S.L.	675.	2.0

Fuselage nominal operating cabin pressure is 11.12 psi and maximum relief valve setting is 12.34 psi. An ultimate design pressure of 2.5 times the nominal operating pressure, acting alone, is used. In regions of stress concentration, such as cutouts, windows, and doors, an ultimate design pressure of 3 times nominal operating pressure is used. An ultimate design pressure of 2 times nominal operating pressure is used in conjunction with flight loads.

These factors are higher than those required by FAR 25 (Ref. 13) and conservatively account for cabin pressure and external aerodynamic forces.

Design load criteria for floor structure and fuel bulkheads are contained in V2-B2707-7.

#### 4.3.3 Fuselage Design Allowables

Mechanical properties of fuselage structural materials and allowable strength of structural elements are taken from Ref. 8. Tension allowables, for riveted structure, are based on a net area efficiency of 98 percent or on a gross area efficiency of 88 percent for 10 percent holeout or less. Gross area efficiency is 85 percent for 15 percent holeout, and decreases linearly with increase in holeout. Allowable, gross-section, effective tension stress versus ultimate tension load per inch is shown plotted

in Fig. 4-33. The cutoff on the left in the figure represents 0.032-skin and 0.025-hat-section stiffeners, 1.25 in. deep, and 5 in. on center. Solid curves represent heat-treated stiffeners and mill-annealed skins, while the dashed lines represent mill-annealed skin and stiffeners. Mill-annealed stiffeners are an alternative material choice in areas that are not compression-critical.

Compression allowables for upper- and lower-surface stiffeners are based on 1.25-in.-deep Z- and hat sections attached to an effective width of skin. The stiffener crippling stress is based on the method of Needham (Ref. 9) and is used in the Johnson-Euler column equation to

determine the allowable column stress, as discussed in Par. 4.2. For any given column load, there is a combination of stiffener gage and skin gage that results in a minimum cross-sectional area. This area is used to establish the allowable, gross-area, effective compression stress versus compression load per inch curve, shown in Fig. 4-34. The cutoff on the left represents 0.032-in.-skin and 0.025 Z-section stiffeners, 1.25 in. deep, and 3 in. on center.

The ultimate allowable net area shear stress for shear-resistant flat and curved panels is  $0.60 F_{TU}$  and  $0.48 F_{TU}$ , respectively. The ultimate, allowable net-area shear stress for

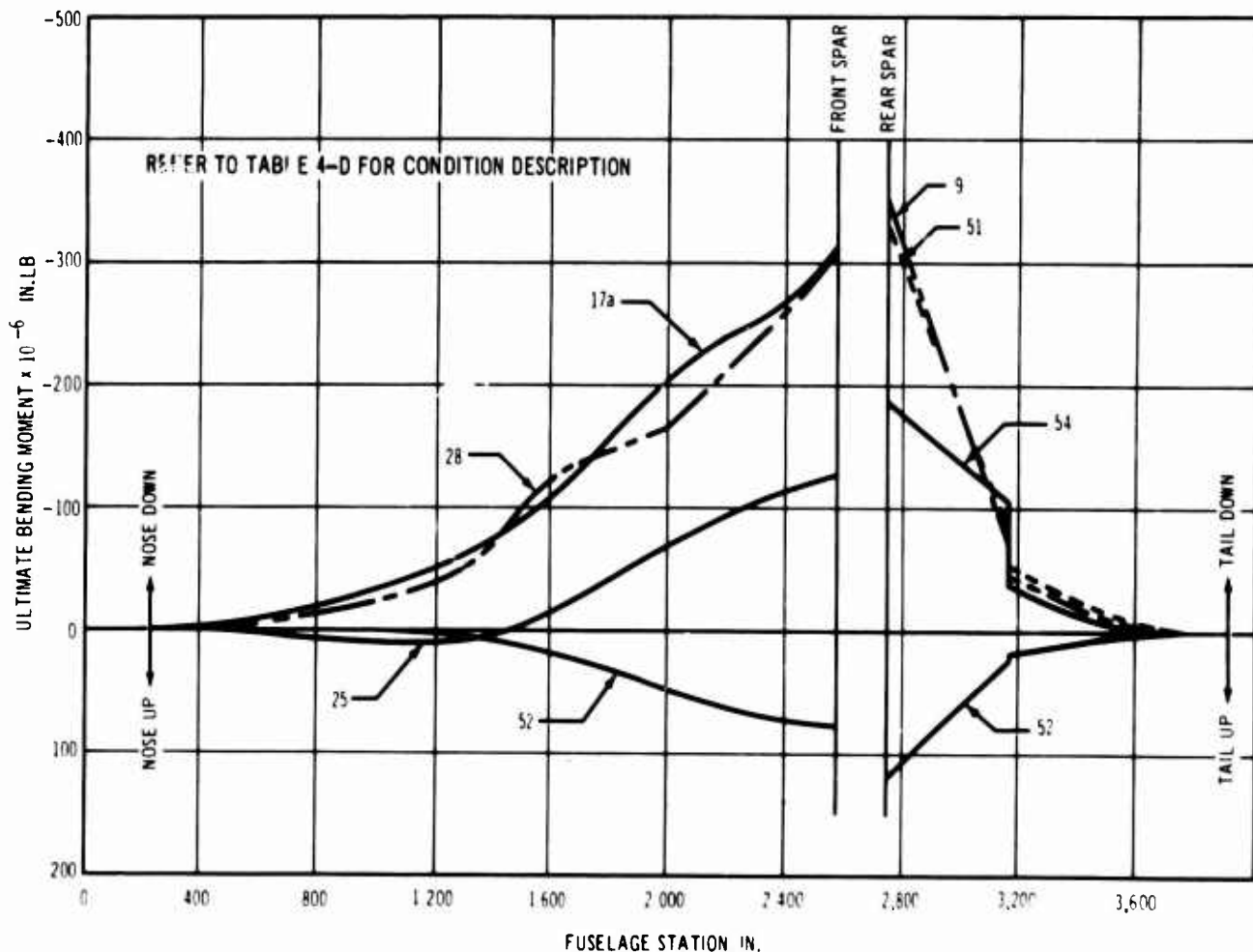


Figure 4-32. Fuselage Ultimate Vertical Bending Moment

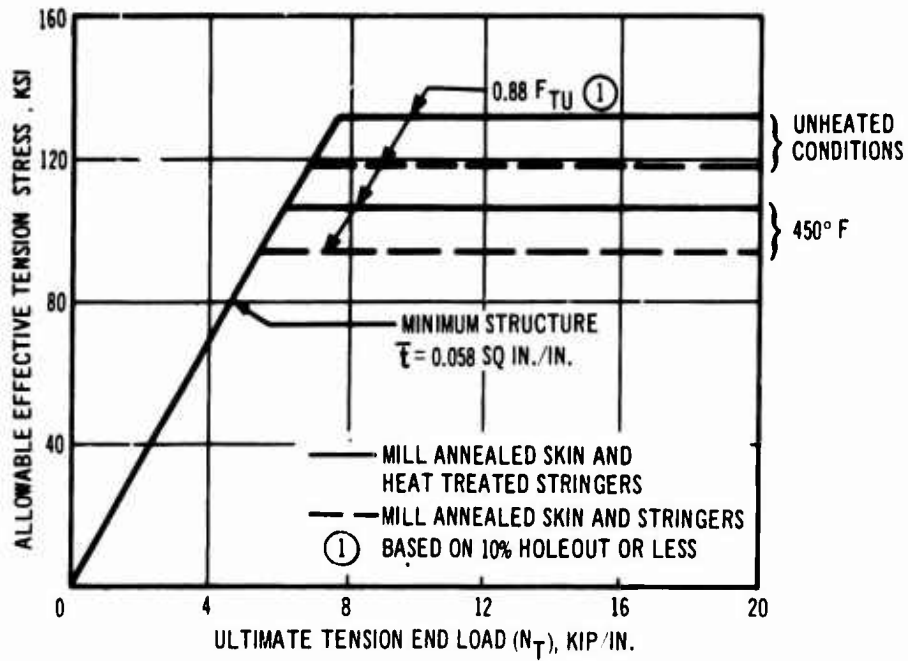


Figure 4-33. Fuselage Tension Allowables

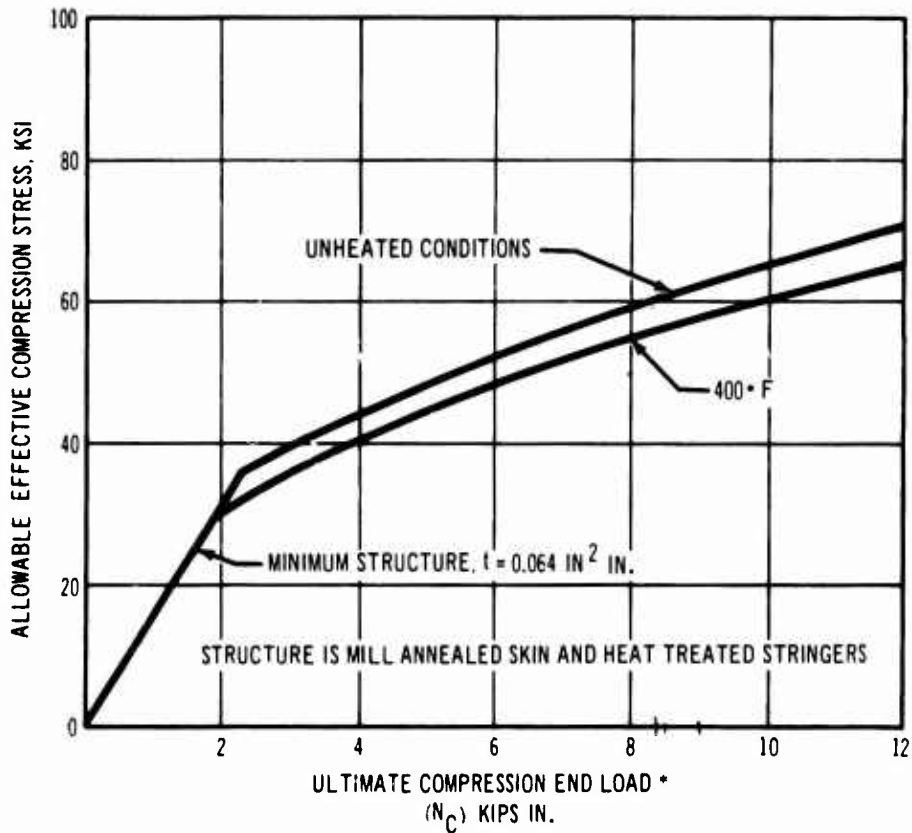


Figure 4-34. Fuselage Lower Surface Panel Compression Allowables

V2-B2707-6-2



semitension field-flat and curved panels is  $0.49 F_{TU}$  and  $0.39 F_{TU}$ , respectively. Gross-area shear stresses, based on 10 percent hole-out or less, are 10 percent below these values. The critical shear-buckling stress for curved panels is determined from Ref. 14.

$$F_{SCR} = 5.25 \eta E \left( \frac{t}{b} \right)^2 + \left[ \frac{\pi}{4} \left( \frac{Rt}{L^2} \right)^{1/4} \left( \frac{Et}{R} \right) \right]$$

- where  $F_{SCR}$  = critical buckling stress, psi  
 $b$  = stringer spacing, inches  
 $\eta$  =  $(E_T/E)^{1/2}$ , plasticity reduction factor  
 $E$  = modulus of elasticity, psi  
 $E_t$  = tangent modulus of elasticity, psi  
 $t$  = skin thickness, inches  
 $L$  = frame spacing, inches  
 $R$  = radius of shell, inches

The critical shear-buckling stress of pressurized curved plates is derived from the interaction equation of Ref. 15 for curved plates:

$$F_{SCR(P)} = F_{SCR} \left( 1 - \frac{P}{P_0} \right)^{1/2}$$

- where  $F_{SCR(P)}$  = critical buckling stress of pressurized curved panel, psi  
 $P$  = cabin internal pressure, psi (positive)  
 $P_0$  = critical external radial pressure, psi (negative)

The allowable effective shear stress versus shear load per inch curve is shown in Fig. 4-35. The cutoff on the left of this figure represents 0.032 skin and 0.025 Z-section stiffeners, 1.25 in. deep and 5 in. on center.

#### 4.3.4 Fuselage Semimonocoque

##### 4.3.4.1 Forward Fuselage, Sta 1199

Forward of Sta 1934, the entire fuselage is pressurized, including equipment and cargo compartments located below the floor. At Sta 1199 considerations of skin crack propagation for 11.12 psi nominal operating pressure, have resulted in fuselage skins being designed thicker than the 0.032-in. minimum gage. These thicker skins, together with stiffeners of equal gage, produce low shear and bending stresses during ground operations and flight maneuvers (see Fig. 4-36). The maximum design condition at this station is dynamic landing at a sink speed of 10 fps.

Fail safety is provided by the multiload paths available in semimonocoque structure. Body skins are reinforced at every frame with a tear strap. Fail safety of this structure has been demonstrated with a full-size fuselage test (see Part E, Structural Tests (V2-B2707-9), of the Airframe Design Report).

##### 4.3.4.2 Forward Fuselage, Sta 1934

Aft of Sta 1934, the fuselage is divided into a pressurized passenger compartment and a series of unpressurized fuel tanks below the floor. Skin thickness above the floor is determined by cabin pressure. Between the upper and lower surface of the wing strake, the fuselage side skin carries vertical shear loads and its minimum gage (0.032 in.). Below the strake, the lower skin is sized by panel flutter requirements because the stabilizing effect of cabin pressure is not present in the unpressurized fuel tanks. Stringers are spaced to stabilize the skins and sized to carry bending loads, in conjunction with the skin (see Fig. 4-37).

The critical load condition is dynamic landing at  $V_{SINK} = 10$  fps and 430 kips gross weight.

Next in severity is vertical gust at Mach 0.90, 380 kips gross weight. Large margins of safety exist for elevated temperature maneuver conditions as shown by the analysis (Fig. 4-37).

##### 4.3.4.3 Forward Fuselage, Sta 2396

Fuselage structure is similar to that at Sta 1934 except that skin and stiffener thickness are heavier to carry the higher shear and bending loads. Fuselage frames above the floor are designed by overall fuselage-shell bending

stability requirements; those below the floor are designed by fuel tank pressures occurring during a malfunction of the fuel-tank shutoff valve. Lower-fuselage section bulkheads are located at every third frame to minimize fuel slosh loads and to contain the fuel during a forward crash condition. The upper skin surface is designed for tension loads resulting from vertical bending combined with pressure. The lower skin surface is designed by vertical bending only and is critical in compression. The side skin panels are designed by the vertical shear loads (see Fig. 4-38).

The critical load conditions are takeoff taxi, vertical gust at Mach 0.90 and 380 kips gross weight, and dynamic landing at  $V_{SINK} = 10$  fps.

Fail-safe design in this area is similar to that of other sections of the fuselage.

#### 4.3.4.4 Rear-Spar Fuselage Bulkhead

The rear spar fuselage bulkhead consists of the rear-spar shear web in the center wing, a machined ring frame in the upper lobe above the wing, and a forged fitting attaching the rear spar to the machined frame at the side of the fuselage

(see Par. 3.2). Wing vertical loads, consisting of rear-spar vertical shears and wing root torsional shears, are applied to the bulkhead and carried into the fuselage skin. The bulkhead must also conform to the rotation of the wing, caused by flexure, and the resulting lateral displacement of the bulkhead at the upper and lower surface of the wing.

Critical design conditions for the bulkhead include a symmetrical pitchup and maneuvers, rolling pullout maneuvers, and fin gust loads. The analysis that follows is for Condition 9,  $n = 2$  factors limit, flaps-down maneuver at maximum gross weight (see Fig. 4-39).

Fail-safe conditions at the bulkhead above the wing will result in rear spar and wing root-rib upward loads being carried in direct compression in the fitting. Downward-acting loads will be carried forward and aft in the side of the fuselage and introduced into the fuselage by the adjoining frames.

#### 4.3.4.5 Aft Fuselage, Sta 2765

The aft fuselage is frame- and stringer-supported monocoque. In the area where lower surface cutouts are provided for main landing gear doors

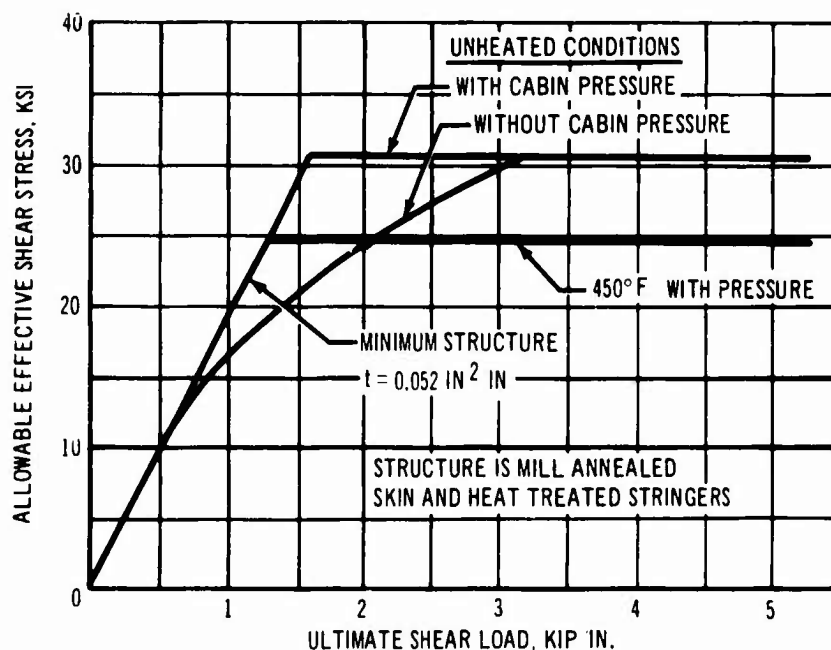
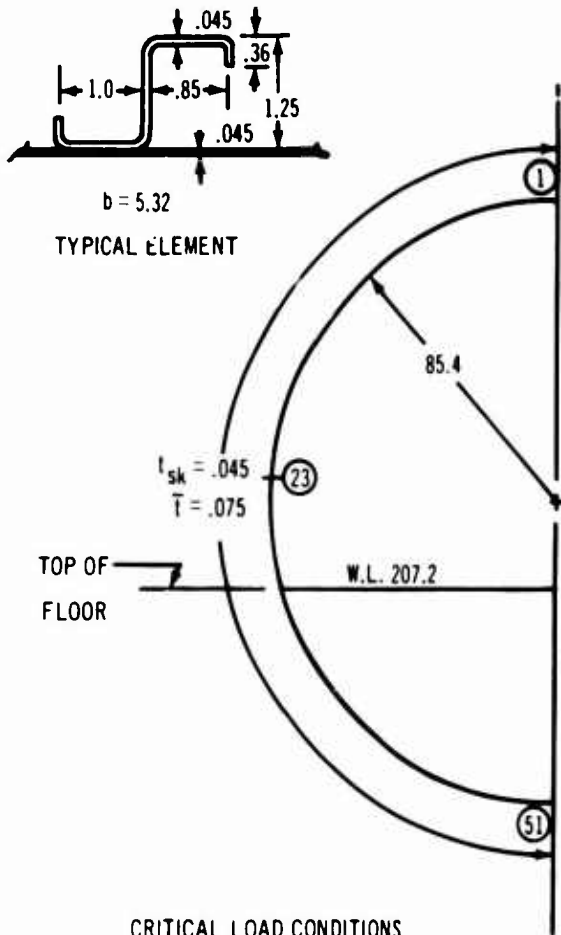


Figure 4-35. Fuselage Side Panel Shear Allowables

V2-B2707-6-2



CRITICAL LOAD CONDITIONS

CONDITION	V <sub>Z</sub>	M <sub>Y</sub>
17a	150 KIPS	50 x 10 <sup>6</sup> IN-LBS

BODY SECTION PROPERTIES

PROPERTY	ELEM	I (IN.)
A <sub>NET</sub> = 32.9 IN <sup>2</sup>	1	70.6
A <sub>GROSS</sub> = 40.2 IN <sup>2</sup>	23	1.8
I <sub>Y</sub> = 105764. IN <sup>4</sup>	51	-98.6

Z = 0 @ W.L. = 244.8

ELEMENT #1 MAX. TENSION

STIFF TI 6A-4V COND III  
SKIN TI 6A-4V MILL ANNEAL

$$F_{TU} = 139000(.95) = 132000 \text{ PSI}$$

TENS. STRESS FROM BEND.

$$f_{TB} = 33400 \text{ PSI}$$

TENS. STRESS FROM PRESS.

$$f_{TP} = 12450 \text{ PSI}$$

$$f_s = 33400 + 12450 = 45850$$

$$M.S. = \frac{132}{45.85} - 1 = \underline{.87}$$

ELEMENT #23 MAX. SHEAR

SKIN TI 6A-4V MILL ANNEAL

$$F_{Su} = 139000(.37) = 51400 \text{ PSI}$$

$$q = 580 \text{ #/IN}$$

$$f_s = \frac{580}{.045} = 12900 \text{ PSI}$$

$$M.S. = \frac{51.4}{12.9} - 1 = \underline{HIGH}$$

ELEMENT #51 MAX. COMP.

STIFF TI 6A-4V COND. III  
SKIN TI 6A-4V MILL ANNEAL

$$F_c = F_{c0} \left[ 1 - \frac{F_{c0}(L/R)^2}{4T^2 E} \right] \quad L = L/R = 21.0$$

C = 1.0  
E = 16.4 x 10<sup>6</sup>

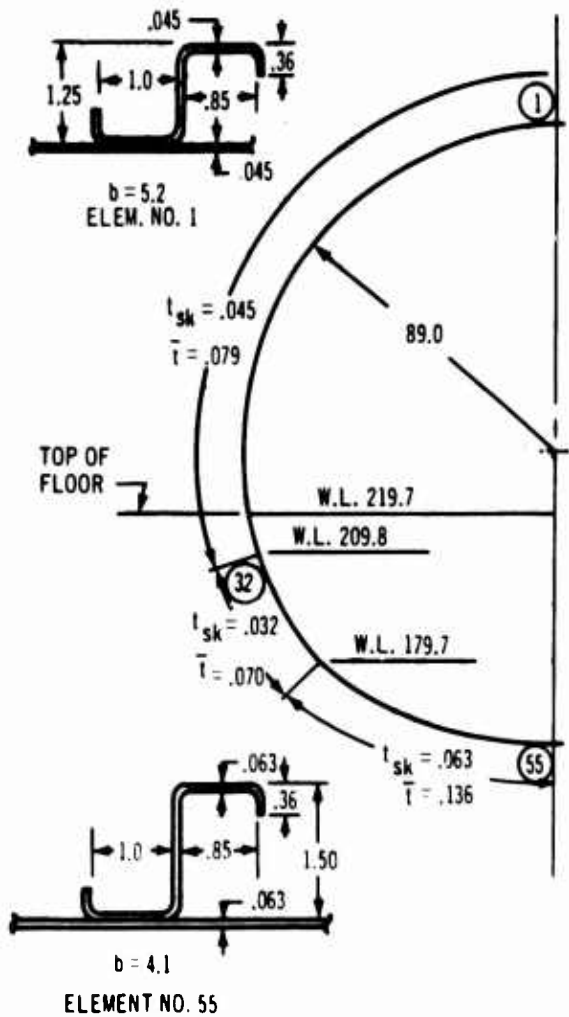
$$F_c = 75000 \text{ PSI}$$

$$f_c = 46600 \text{ PSI}$$

$$M.S. = \frac{75.0}{46.6} - 1 = \underline{.61}$$

\* FACTOR FOR HOLE OUT.

Figure 4-36. Forward Fuselage Analysis, Station 1199



MOD. SECTION PROPERTIES

	ELEM.	Z
$A_{NET} = 44.32 \text{ IN}^2$	1	90.2
$A_{GROSS} = 51.92 \text{ IN}^2$	32	-31.8
$I_Y = 173570. \text{ IN}^4$	55	-82.6
$\bar{E} = 0 \text{ @ W.L. } 236.04$		

ELEMENT #1 TENSION CRIT.

STIFF T<sub>6</sub> 6A-4V COND. III  
SKIN T<sub>6</sub> 6A-4V MILL ANNEAL.

$$F_{Tu} = 139000 (.95) = 132000 \text{ PSI}$$

TENS. STRESS FROM BEND.

$$f_{tB} = 98700 \text{ PSI. (COND. 17)}$$

TENS. STRESS FROM PRESS.

$$f_{tp} = 9820 \text{ PSI.}$$

$$f_t = 98700 + 9820 = 108520 \text{ PSI}$$

$$MS = \frac{132.0}{108.52} = 1.22$$

ELEMENT #32 SKIN SHEAR CRIT.

SKIN T<sub>6</sub> 6A-4V MILL ANNEAL.

$$F_{Su} = 139000 (.37) = 51400 \text{ PSI}$$

$$g = 785 \text{ #/IN (COND. 17)}$$

$$f_s = \frac{785}{.032} = 24600 \text{ PSI}$$

$$MS = \frac{51.4}{24.6} = 1.09$$

ELEMENT #55 COMP. CRIT.

STIFF T<sub>6</sub> 6A-4V COND. III

SKIN T<sub>6</sub> 6A-4V DUPLEX ANNEAL

$$F_c = F_{cc} \left[ 1 - \frac{F_{cc} (L/r)^2}{4\pi^2 E} \right] \quad L' = L/r = 21.0$$

$$F_c = 97000 \text{ PSI} \quad E = 16.4 \times 10^6$$

$$f_c = 90400 \text{ PSI (COND. 17)}$$

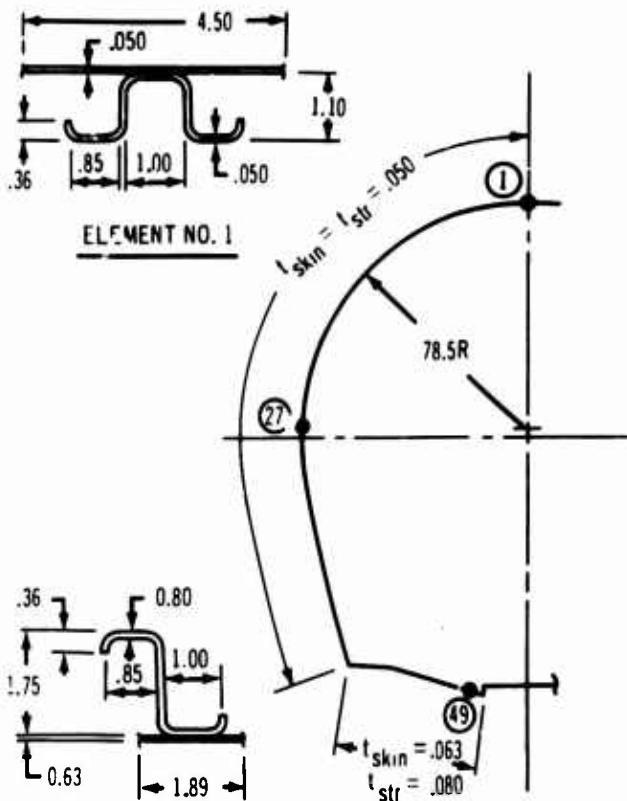
$$MS = \frac{97.0}{90.4} = 1.07$$

CRITICAL LOAD CONDITIONS

COND.	$V_x$	$M_x$
17	$235.0 \times 10^3$	$190.0 \times 10^6$
25	$125.0 \times 10^3$	$75.0 \times 10^6$

• FACTOR FOR RIVET HOLES

Figure 4-37. Forward Fuselage Analysis - Station 1934



ELEMENT NO. 1

ELEMENT # 49

BODY SECTION PROPERTIES:

$A_{NET} = 57.94 \text{ IN.}^2$        $Z = 0 \text{ @ W.L. 240.7}$   
 $A_{GROSS} = 68.73 \text{ IN.}^2$        $Q_{MAX} = 779.16 \text{ IN.}^3$   
 $I_Y = 205,628 \text{ IN.}^4$

ELEM	Z
1	88.2
27	2.5
49	-75.5

CRITICAL LOAD CONDITIONS:

COND.	$V_Z$ (KIPS)	$M_Y$ (IN-KIPS)
DYN. LDG NEG. BEND.	315	270,000
T.O. TAXI	495	150,000
START CRUISE MAN.	86	110,000

ELEMENT #1 - TENSION CRITICAL

STIFFENER: TI 6-4 COND. III  
 SKIN: TI 6-4 COND. I (MILL ANNEAL)

$F_{TU} = .95 \times 139 = 132 \text{ KSI}$

TENSION STRESS DUE TO BENDING:

$f_{TB} = 116 \text{ KSI}$

TENSION STRESS DUE TO PRESSURE:

$f_{TP} = 8.7 \text{ KSI}$

TOTAL TENSION STRESS:

$f_T = 124.7 \text{ KSI}$

$M.S. = \frac{132}{124.7} - 1 = .06$

ELEMENT #27 - SKIN SHEAR CRITICAL

SKIN: TI 6-4 COND. I (MILL ANNEAL)

$t = .050"$

$F_{SU} = .37 \times 139 = 51.5 \text{ KSI}$

$f_S = 37.6 \text{ KSI}$

$M.S. = \frac{51.5}{37.6} - 1 = .37$

ELEMENT #49 - COMPRESSION CRITICAL

STIFFENER: TI 6-4 COND. III

SKIN: TI 6-4 COND. II (DUPLIX ANN.)

$F_c = F_{cc} \left[ 1 - \frac{F_{cc} \left( \frac{L}{\rho r} \right)^2}{4\pi^2 E} \right]$        $L = 21"$   
 $C = 1$

$F_c = 107 \text{ KSI}$

$E = 16 \times 10^6 \text{ PSI}$

$F_{cc} = 132.1 \text{ KSI}$

$f_c = 99 \text{ KSI}$

$\rho = .70$

$M.S. = \frac{107}{99} - 1 = .08$

Figure 4-38. Forward Fuselage Analysis, Station 2396

EXTERNAL LOADS (ULTIMATE)  
LOAD CONDITION 9

NODE NO.	Y IN.	Z IN.	g LB/IN
1	0	106.60	0
2	23.92	102.81	1,575
3	45.49	91.82	3,000
4	62.62	74.69	4,120
5	73.61	53.12	4,850
6	77.40	29.20	5,100
7	77.40	19.47	5,100
8	77.40	9.73	5,100
9	77.40	0	5,100

EXTERNAL (ENFORCED) DEFLECTIONS  
LOAD CONDITION 9  
NODE 9:  $\delta Y = -.5$  IN.  
 $\delta \theta = -.02$  RAD.

INTERNAL LOADS (ULTIMATE)  
M = MOMENT AT NEUTRAL AXIS  
+M INDICATES TENSION AT  
INNER CAP.  
P = AXIAL LOAD AT NEUTRAL AXIS  
+P INDICATES TENSION  
V = SHEAR

LOAD CONDITION 9

NODE NO.	M IN. · KIP	P KIPS	V KIPS
1	973.6	98.47	—
2	366.2	47.93	40.91
3	-98.2	1.68	42.61
4	-908.7	-9.36	14.38
5	-1,005.5	-196.73	48.54
6	403.4	-305.65	97.57
7	1,464.4	-341.80	137.52
8	2,980.0	-390.99	143.63
9	4,609.9	-440.61	143.63

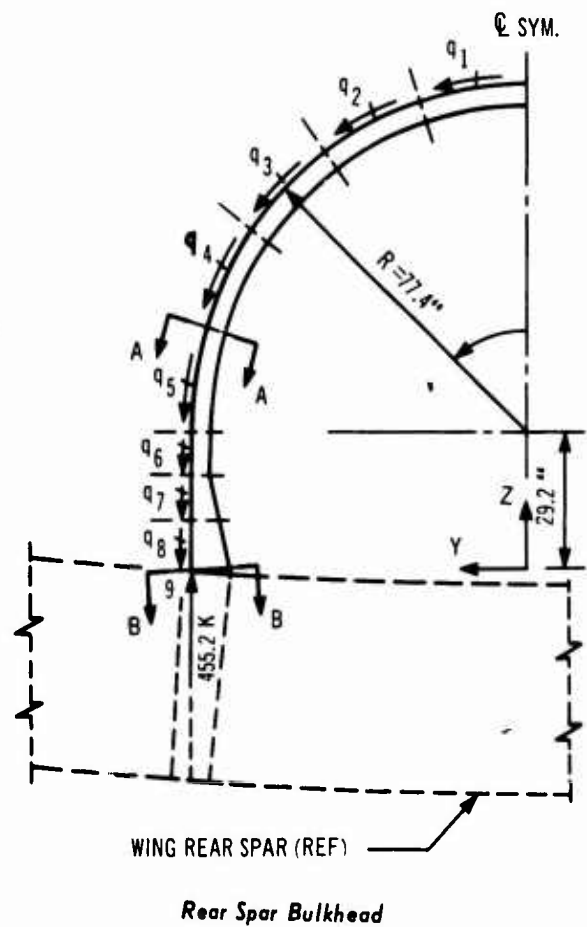
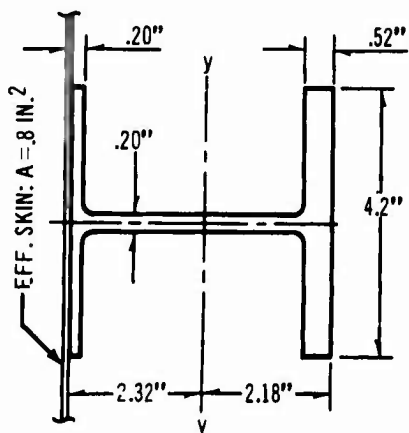
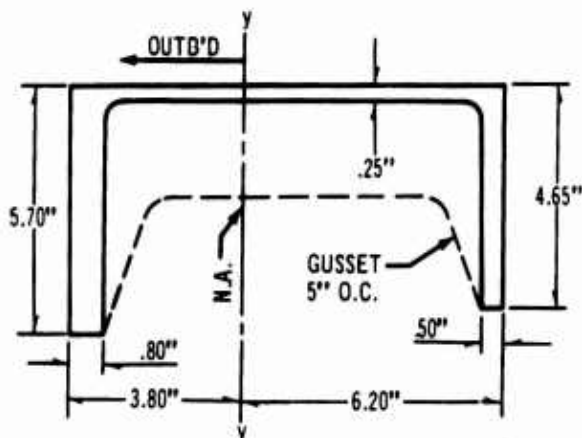


Figure 4-39. Rear-Spar Fuselage Bulkhead

SECTION A-A (NODE 5)  
SECTION PROPERTIES



SECTION B-B (NODE 9)  
SECTION PROPERTIES



$$A = 4.58 \text{ IN}^2$$

$$I_{yy} = 17.65 \text{ IN}^4$$

MATERIAL: T16AL-4V, COND. III

LOADS AND STRESSES

$$M = -1005.5 \text{ IN-KIPS.}$$

$$P = -196.73 \text{ KIPS}$$

$$f_a = \frac{-1005.5 \times 1.92}{17.65} = -109,200 \text{ PSI}$$

$$P/A = \frac{-196.73}{4.58} = -42,800 \text{ PSI}$$

$$f_c = -109,200 - 42,800 = -152,000 \text{ PSI.}$$

$$F_{cc} = -152,000 \text{ PSI}$$

$$M.S. = \frac{152}{152} - 1.0 = .00 \quad \leftarrow$$

$$A = 9.14 \text{ IN}^2$$

$$I_{yy} = 133.83 \text{ IN}^4$$

MATERIAL: T16AL-4V, FORGING, COND. III

LOADS AND STRESSES

$$M = 4610 \text{ IN-KIPS.}$$

$$P = -440.6 \text{ KIPS.}$$

$$f_a = \frac{4610 \times 3.4}{133.83} = -102,100 \text{ PSI}$$

$$P/A = \frac{-440.6}{9.14} = -48,300 \text{ PSI.}$$

$$f_c = -102,100 - 48,300 = -150,400 \text{ PSI.}$$

$$F_{cc} = -152,000 \text{ PSI}$$

$$M.S. = \frac{152.0}{150.4} - 1.0 = +.01 \quad \leftarrow$$

Figure 4-39. (Concluded)

and equipment access doors, two lower longerons carry lower-surface axial loads. Maximum positive flight maneuvers produce design compression loads in the lower longeron, with maximum negative maneuvers applying tension loads equal to approximately 40 percent of the maximum compression loads. Aft fuselage torsion caused by fin gust is carried by a torsion cell composed of the upper lobe and the pressure web below the floor and by differential bending of the sides. The upper skin is designed by shear loads from fin gust, the side panels by vertical shear loads, and the pressure web by torsion caused by fin gust (see Fig. 4-40).

The critical vertical load conditions are the  $n = 2$  factors limit, flaps-down maneuver at maximum gross weight and the  $n = 2.5$  factors limit maneuver at Mach 0.90. The critical side-load condition in the aft fuselage is fin gust at Mach 1.2.

Fail-safe provisions are provided by the inherent multiplicity of load paths in semimonocoque structure. The lower longeron is divided into five longitudinal segments to avoid wing-flexure-induced bending stresses, at the point that it crosses the lower surface of the wing. This approach also provides multiload path structure and meets fail-safety requirements without added weight.

#### 4.3.4.6 Fuselage Aft of Sta 3405

The fuselage aft of the aft pressure bulkhead (Sta 3405) is of frame and longeron construction with several bulkheads to support fin and fuel loads. Titanium skins are used between Sta 3405 and 3544. Sandwich panels form the external surfaces aft of Sta 3544. Bulkheads at Sta 3451 and aft are of sandwich construction. The primary structure in the aft fuselage is strength designed, and there is no additional structure required to meet the sonic fatigue environment and criteria shown in V2-B2707-7.

Aft fuselage loads are shown in Fig. 4-41 for the critical condition of landing at takeoff gross weight with aft-fuselage fuel tanks full. The same figure shows analysis at three body locations aft of Sta 3405. A typical bulkhead analysis at Sta 3451 is shown in Fig. 4-42 for fin loads and 12-g fuel thrust loads.

#### 4.3.5 Wing-to-Fuselage Joint

The wing center section inside the fuselage has a 177-in. chord and a 155-in. span.

Cabin pressure loads are carried by the front and rear spars and by three additional spars located between the main spars. These five spars also carry fuel-slosh loads as well as fuel-pressure loads caused by a crash condition. The aft main gear trunnion is located aft of the rear spar and inboard of the side of the fuselage. It is supported by an inboard and outboard fitting on the rear spar. The outboard fitting is combined with the rear spar-to-fuselage fitting.

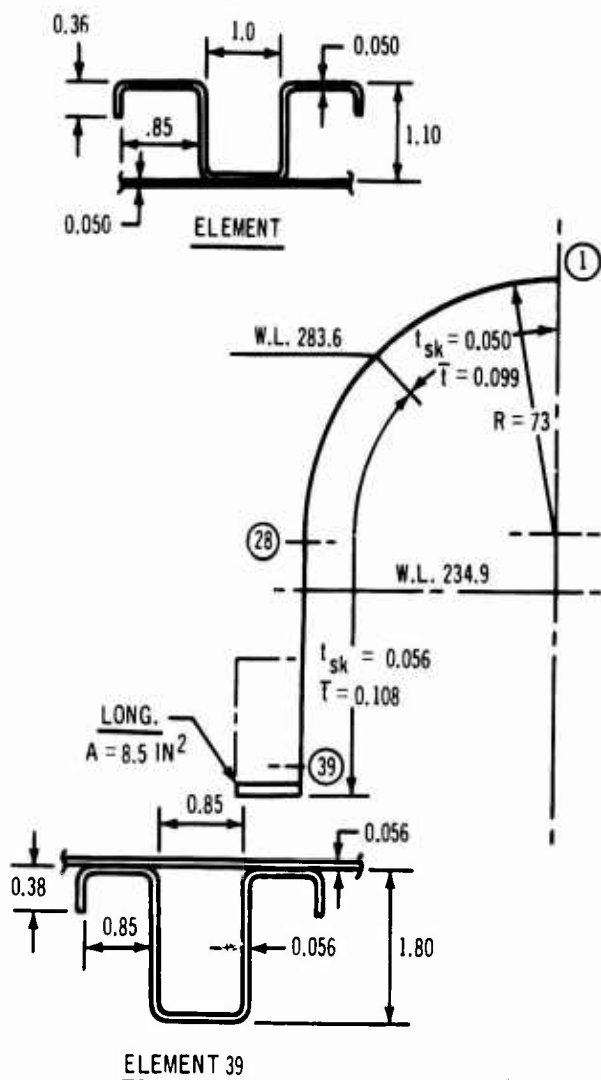
Cabin pressure loads help reduce wing fitting loads, resulting in lower wing-to-fuselage vertical loads. Hence, the critical design condition for the wing-to-fuselage fittings occurs with an unpressurized cabin. The fuselage structure must also have proper stiffness distribution to accommodate wing flexure with minimum induced stresses. Fuselage structure is arranged to progressively reduce the deformation caused by wing flexure, both forward and aft of the wing center section.

The wing is attached to the fuselage by titanium forgings bolted to the front and rear spar at the side of the fuselage. The forgings extend the full depth of the wing and about 36 in. above the upper surface of the wing. The forgings are tapered above the wing and attach to a ring frame, which provides the required flexibility.

The fuselage is flat-sided below the upper lobe, with the wing rib coinciding with the side of the fuselage. The entire side of the fuselage is utilized for vertical shear distribution. Because the wing is 50 in. deep compared to a fuselage depth of 160 in., approximately 40 percent of the wing vertical shear is carried directly into the fuselage, resulting in lighter front and rear spar-to-fuselage fittings. All intermediate fuselage frames between spars are bolted through the wing, providing load continuity for vertical loads, caused by cabin pressure, and deflection continuity between the front and rear spar fittings and the inspar frames, resulting in low induced stresses.

In the event of failure of either front or rear spar fitting, up-load from the wing will be carried in the fittings in direct compression. Down-load, caused by negative maneuvers, combined with cabin pressure, are carried forward and aft of the spars to adjacent fuselage frame and bulkhead structure. Inspar fuselage frames adjacent to the additional center-





CRITICAL LOAD CONDITIONS

COND	V <sub>Z</sub>	M <sub>Y</sub>
9	745 K	330,000 IN-K
50	315 K	180,000 IN-K

BODY SECTION PROPERTIES

A<sub>NET</sub> = 59.9 IN<sup>2</sup> I<sub>Y-Y</sub> = 764,200 IN<sup>4</sup>  
 A<sub>GROSS</sub> = 63.2 IN<sup>2</sup> N.A. = W.L. 248.25

ELEMENT	W. L.
1	335.8
28	245.9
39	176.2

ELEMENT NO. 1

TENSION CRITICAL  
 STIFF. TL 6-4 COND II  
 SKIN TL 6-4 MILL ANNEAL

$$F_{TU} = 138,000(0.95) = 132,000 \text{ PSI}$$

TENSION STRESS-BENDING

$$f_{tB} = 112,500 \text{ PSI}$$

TENSION STRESS-PRESSURE

$$f_{tP} = 7,700 \text{ PSI}$$

TOTAL TENSION STRESS

$$f_{tTOTAL} = 120,200 \text{ PSI}$$

COND. 9 MS. =  $\frac{132.0}{120.2} - 1 = 0.09$

ELEMENT NO. 28 SKIN SHEAR CRIT.

SKIN TL 6-4 DUPLEX ANNEAL

$$f_s = 43,900 \text{ PSI}$$

$$F_{SU} = 49,600 \text{ PSI}$$

COND. 9 M.S. =  $\frac{49.6}{43.9} - 1 = 0.13$

ELEMENT NO. 39 COMPRESS. CRIT.

STIFF TL 6-4 COND. II

SKIN TL 6-4 DUPLEX ANNEAL

$$F_c = F_{CC} \left[ 1 - \frac{F_{CC} \left( \frac{L'}{r} \right)^2}{4\pi^2 E_c} \right] \quad L = 210 \text{ IN.}$$

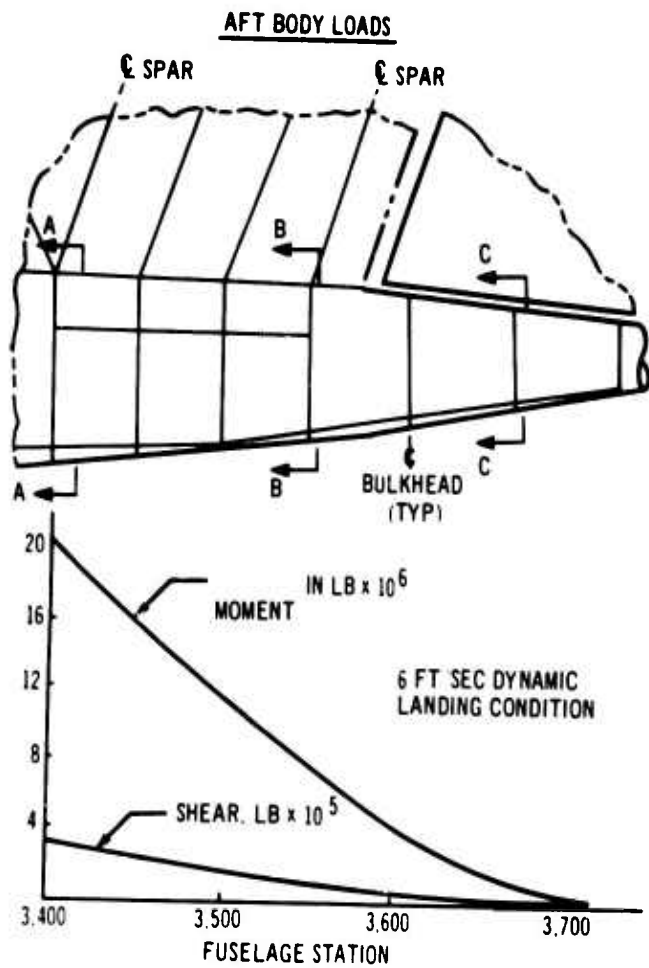
$E_c = 16.4 \times 10^6$

$$F_c = 87,000 \text{ PSI}$$

$$f_c = 86,000 \text{ PSI}$$

COND. 9 MS. =  $\frac{87.0}{86.0} - 1 = 0.01$

Figure 4-40. Aft Fuselage Analysis, Station 2765



LONGERON COMPRESSIVE STRESS

$$f_c = \frac{20.0 (10^6) (66.4)}{13260} = 100,000 \text{ PSI.}$$

$$F_c = 114,000 \text{ PSI}$$

$$M.S. = \frac{114000}{100000} - 1 = 0.14$$

AT SECTION B-B THE BODY IS A CYLINDER OF 84.81 IN. DIA. WITH 5.0 IN. FRAME SPACING AND A 0.60 SQ. IN. LONGERON AREA.

$$M = 9.68 (10^6) \text{ IN-LB.}$$

$$Z = 87.0 \text{ IN.}^3$$

$$f_{\text{LONGERON}} = \frac{9.68 (10^6)}{87} = 111,000 \text{ PSI.}$$

$$M.S. = \frac{114000}{111000} - 1 = 0.025$$

INTERMEDIATE FRAME STIFFNESS REQUIRED FOR SHELL PANEL STABILITY BASED ON SHANLEY EQUATION

$$I = \frac{MD^2}{16000EL}$$

AT STA. 3405

$$I = \frac{20.0 (10^6) (84.8)^2}{1600 (16) (10^6) (5)} = 0.114 \text{ IN.}^4$$

$$I_{\text{ACT}} = 0.146 \text{ IN.}^4$$

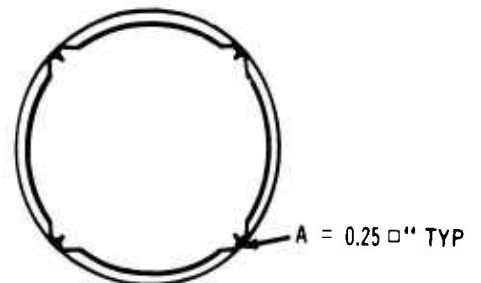
$$M.S. = \frac{0.146}{0.114} - 1 = 0.28$$

BENDING SECTION THROUGH AFT HONEYCOMB CONICAL SECTION

STA 3,664

$$R = 30.2$$

$$M = 0.16 \times 10^6 \text{ IN LB}$$



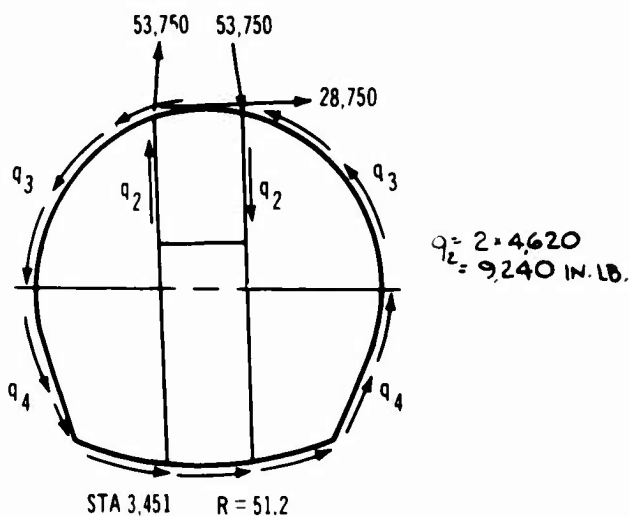
TAKING BENDING IN LONGERONS ONLY,

$$I = \{2(0.25) [30.2 \cos 45^\circ]^2\} (2) = 450 \text{ IN.}^4$$

$$f_c = \frac{1.2 (10^6) (21.21)}{450} = 56,000 \text{ PSI.}$$

Figure 4-41. Aft Fuselage Analysis, Aft of Station 3405

BULKHEAD ANALYSIS



TORQUE APPLIED TO BULKHEAD  
 =  $53,750 \times 20 + 9240 \times 30 \times 20 + 28,750 \times 51.2$   
 =  $8.00 \times 10^6$  IN LB.

BALANCING SHEAR FLOWS

$$q_3 = \frac{T}{2A} + \frac{S}{2D} = \frac{8.0 \times 10^6}{2\pi \times 51.2^2} + \frac{28,750}{2 \times 102.4} = 625 \frac{\text{LB}}{\text{IN}}$$

$$q_4 = \frac{T}{2A} - \frac{S}{2D} = 345 \frac{\text{LB}}{\text{IN}}$$

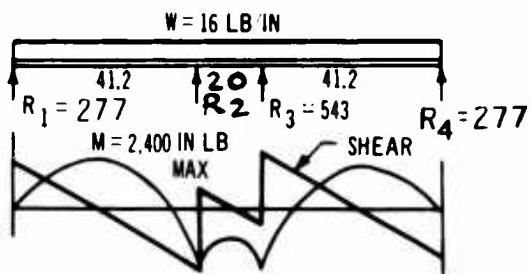
VERTICAL STIFFENERS MUST REDISTRIBUTE THE LOADS APPLIED TO THE BULKHEAD FROM THE FIN ROOT TO THE HONEYCOMB PANELS ALONG THE ENTIRE LENGTH OF THE STIFFENERS.

BULKHEAD STA 3451 PRESSURE LOAD

THIS LOADING WILL DESIGN THE MAJOR PORTION OF THE BULKHEAD. THE LOADING IS CAUSED BY THE FUEL HEAD DURING A 12 G CRASH CONDITION.

$$p = \frac{50 \times 46 \times 12}{1728} = 16 \text{ PSI}$$

TAKING A STRIP OF THE HONEYCOMB PANEL AT THE MAXIMUM HALF WIDTH AND CHECKING AS A SIMPLE SUPPORTED CONTINUOUS BEAM.



FOR 2 IN. -.013 FACES HONEYCOMB

$$f_c = \frac{2,400}{2 \times .013} = 92,500 \text{ PSI}$$

$$F_c = 100,000 \text{ PSI}$$

$$M.S. = 100,000 / 92,500 - 1.0 = 0.08$$

Figure 4-42. Aft Fuselage Analysis, Station 3451

wing spars have sufficient strength because of cabin-pressure load requirements to carry the maximum limit down-load. A fuel-tank bulk-head and high-strength frame, which provides an alternative load path for down-loads on the front spar, is located 40 in. forward of the front spar. A wheel-well floor support bulk-head and high-strength frame, which provide an alternative load path for down-loads on the rear spar, is located 36 in. aft of the rear spar.

A wing-body internal loads analysis has been developed to encompass all wing primary structure inboard of the wing pivots and all fuselage primary structure from one frame forward of the horizontal tail to five frames forward of the wing front spar. This analysis permits a comprehensive determination of wing interaction with the body throughout the central section. Included are effects of landing gear loads in stowed and extended positions, inboard flap loads for various flap positions, pivot actuator loads for all wing sweeps, and the effects of doors, windows, access panels, and wheel-well cutouts on distribution of load in the structure.

This structure is analyzed using the finite-element direct stiffness method. The structure, idealized as an assembly of plate and beam elements intersecting at nodes, is loaded along beam elements and at nodes by external and internal forces. These forces are caused by surface air loads, internal pressurization, inertia loads, and control surface loads. Thermal gradients are applied along, across, and through plate and beam elements. Internal plate and beam element forces and node deflections are obtained as a result of applied loads and temperatures and the structural redundancies.

Figure 4-43 is an abbreviated display of the mathematical model centerline diagram of the section. Solid lines represent boundaries of plate elements and the offset centerlines of beam elements to which plate elements are attached. There are 1,899 nodes, 2,191 plate elements, and 2,978 beam elements in the center-section mathematical model. Internal loads and deflections are determined for symmetrical and for unsymmetrical load conditions.

Plate elements are capable of inplane stretching and shear, and out-of-plane bending and shear. Plates may be isotropic or ortho-

tropic, stiffened or sandwich, buckled or unbuckled. Plate temperature may be uniform or vary linearly between nodes and through the plate thickness. Beam elements are capable of stretching, shear, bending, and torsion, may be pinned and/or fixed arbitrarily at their ends, may be offset with respect to their nodes in any direction and to any degree, may be straight or curved, and may vary arbitrarily in section properties (continuously and discontinuously) between nodes. Beam elements may be loaded continuously or discontinuously between nodes by all components of moments and shears and may be subjected to thermal gradients in any direction through their cross sections as well as along their lengths.

This wing-fuselage internal loads and deflection analysis will be combined with similar solutions for the horizontal tail-fuselage and the forward fuselage.

#### 4.3.6 Crew Compartment

##### 4.3.6.1 Structural Description

The crew compartment structure incorporates windows with sills, posts, and frames to support the windows and to redistribute the loads around the window cutouts. Outside of the window area, semimonocoque structure employing longerons with closely spaced frames or stringers with larger frames spacing is used. The basic structural material used throughout the crew compartment is titanium 6Al-4V.

##### 4.3.6.2 Internal Loads

The windows, window sills, window posts, frames and skins of the crew compartment form a highly redundant structure that is analyzed by the COSMOS digital computer program. A separate airloads panel program was used to distribute panel loading to the nodes. The grid of structural elements employed in the programs is shown in Fig. 4-44.

The crew compartment is designed primarily by internal pressure, thermal, and dynamic landing loads. The stress analysis of typical members using loads from the COSMOS program are included in this document. The critical loads are for the 3-factor pressure condition with material allowables reduced because of elevated temperature.

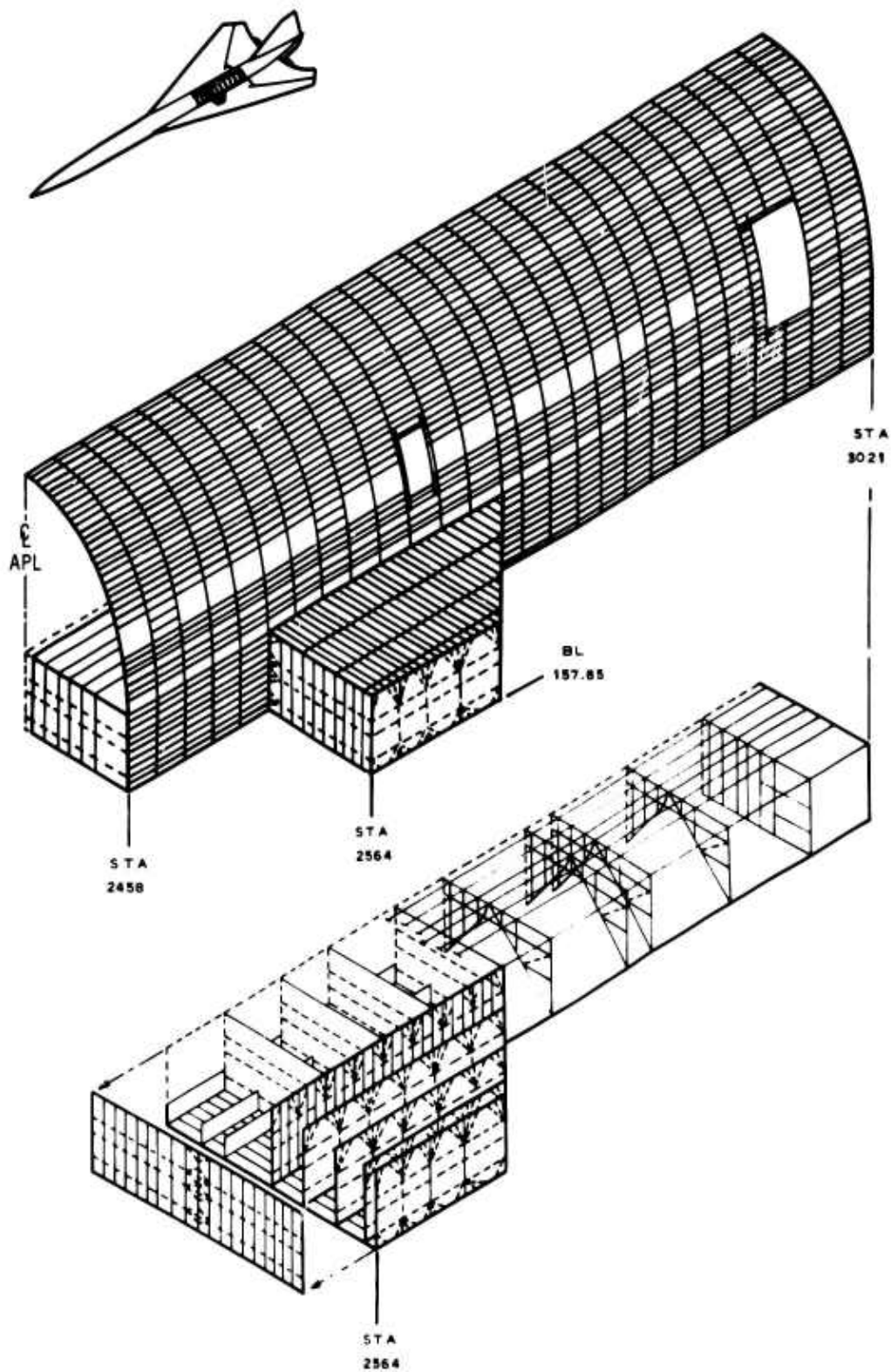


Figure 4-43. Wing-to-Fuselage Internal Loads Analysis, Mathematical Model

V2-B2707-6-2

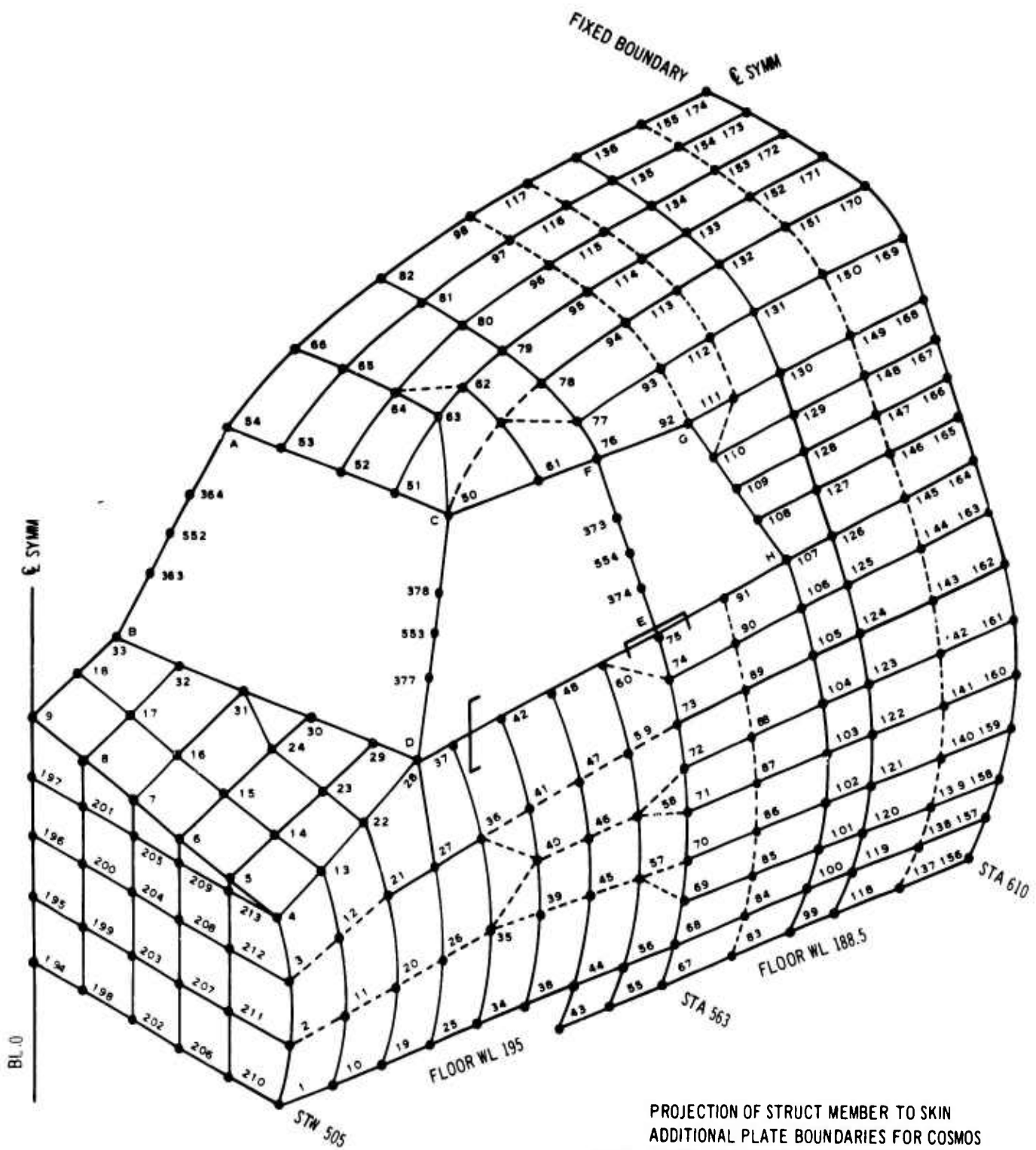


Figure 4-44. Phase II-C Crew Compartment Idealized Structure

V2-B2707-62

#### 4.3.6.3 Analysis

Detail analyses are presented for typical sections of the Phase II-C crew compartment in Fig. 4-45. This test structure is representative of the B-2707 crew compartment. Fail-safety of the crew compartment is achieved by designing each load-carrying member as an assembly of two or more elements.

#### 4.3.7 Moveable Nose

The moveable nose is a monocoque structure composed of titanium skins and longerons (see Par. 3.2). Frames are at 7-inch spacing extending from the aft end of the radome to a hinge point located on the fuselage at Sta 607.5. Because large window cutouts are located above the upper longerons, only the area below the upper longerons is considered effective in carrying monocoque bending. The area above the upper longerons is designed to carry local air loads. Actuation of the moveable nose is accomplished by means of a jack screw supported from the fuselage forward pressure bulkhead.

The section is designed by the nose-gear-up landing run-out with maximum braking effort. Local structure is designed by external aerodynamic air pressure combined with the maximum thermal environment. Analysis of the moveable nose is shown in Fig. 4-46.

#### 4.3.8 Floor Beams and Pressure Web

The passenger cabin floor and pressure web is supported on longitudinal, corrugated, shear web beams. These beams are supported every third frame. Both beams and pressure webs are made of titanium 6Al-4V (Condition D). Each beam is analyzed as a continuous beam with its top and bottom flanges stabilized by the floor panels and pressure webs respectively. Room temperature allowables are used for all computations because the floor beams are within the temperature-conditioned cabin.

The design conditions investigated consisted of 2.5 factors on cabin pressure alone, 2 factors pressure and flight loads, forward crash loads, fuel tank pressure effects, and thermal interaction forces.

Thermal stresses, induced by the heated fuselage skin, were investigated using the model shown in Fig. 4-47 and the COSMOS program. In the mathematical model, a circular fuselage with the floor at mid-height was used. Stringer areas are assumed lumped at 15 deg intervals except

for the first 20 in. on either side of the skin-floor intersection where actual stringer areas were used. Actual floor beam areas and a 0.020 pressure web are used for the floor. The results of this calculation show that the beam and pressure web are strong enough to support all thermally induced loads. Maximum tension stress in the pressure web and floor beams is 21,600 psi because of thermal effects. The web consists of panels 21 by 11 in. with a 2 by 0.02 in. doubler adhesive bonded at all floor beams and frames. Two 1 by 0.02 in. doublers are adhesive bonded between frames. These doublers serve as tear straps.

Thorough trade studies were conducted on the various types of floor beams. These studies showed that the corrugated shear web is the lightest (Ref. 4).

In the event of failure of one floor beam, each adjacent beam has sufficient strength to carry the severed beam's load. The pressure web has sufficient strength to carry the load over to the adjacent beams. Maximum beam stress level caused by 1 factor cabin pressure and thermal effects is limited to 37,000-psi tension. Maximum longitudinal-pressure web stress caused by 1 factor cabin pressure is 33,350-psi tension (21,600 psi caused by thermal effects, and 11,750 psi caused by membrane tension). Maximum lateral-pressure web stress is 41,350-psi tension (3,150 psi caused by thermal effects and 38,200 psi caused by membrane tension). This structure has been tailored to these stress levels to meet service-life requirements.

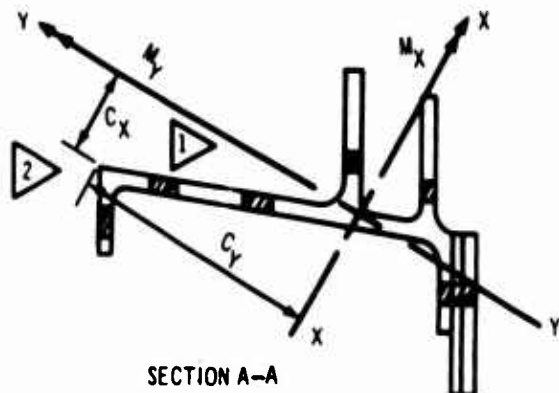
#### 4.3.9 Windows

The primary pressure-carrying panel of each window in the crew compartment is a laminate employing two panes of chem-tempered glass as the primary load-carrying members and utilizing a plug-type installation. An outer monolithic pane of glass is employed as a secondary pressure fail-safe path and is attached to supporting structure by a flush retainer ring. The polyvinyl-butyl interlayer of the main windshield provides the required bird-impact resistance.

The passenger window assembly is composed of three panes, consisting of two load-carrying panes, and one inner nonstructural pane. The outer, or fail-safe pane is 0.8-in. chill-tempered soda lime glass. The center basic pressure pane is 0.125-in. chem-tempered glass.

## DF SILL

CRITICAL CONDITION: 3.0 FACTOR  
INTERNAL PRESSURE = 33.36 PSI  
SECTION A-A IS THE CRITICAL  
SECTION (SEE FIG. )



NET SECTION PROPERTIES: X & Y ARE  
PRINCIPAL AXES.  $I_x = 1.50 \text{ IN}^4$ ,  $I_y = 0.80 \text{ IN}^4$   
 $A = 1.19 \text{ IN}^2$ ,  $C_x = 0.98$ ",  $C_y = 2.78$ "

### STRESS ANALYSIS

LOADS AT SECTION A-A:  $P = +18,300 \text{ LB}$

$M_x = 21,930 \text{ IN-LB}$ ,  $M_y = 5750 \text{ IN-LB}$

$P/A = 18,300/1.19 = +15,400 \text{ PSI}$

$M_x C_y / I_x = 21,930(2.78)/1.50 = +40,700 \text{ PSI}$

$M_y C_x / I_y = 5,750(0.98)/0.80 = +7,100 \text{ PSI}$

$f_t = 15,400 + 40,700 + 7,100 = +63,200 \text{ PSI}$

$F_t = 107,000 \text{ PSI AT } 350^\circ \text{ F}$

M.S. =  $107.0/63.2 - 1 = +0.69$  ← M.S.

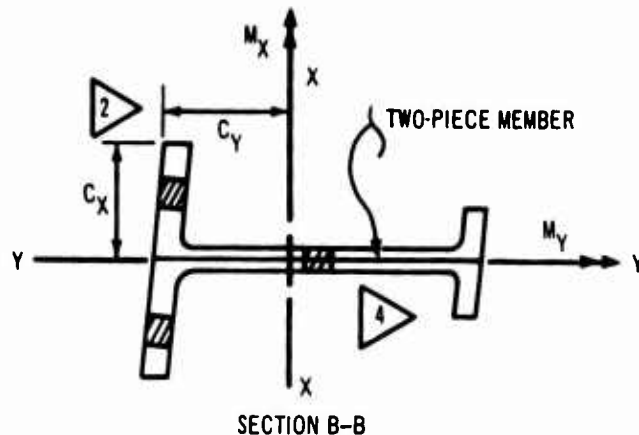
Ti-6Al-4V COND I BAR STOCK

POINT OF CRITICAL TENSILE STRESS

INCLUDES 5% CONC. FACTOR

## EF POST

CRITICAL CONDITION: 3.0 FACTOR  
INTERNAL PRESSURE, 33.36 PSI  
SECTION B-B IS THE CRITICAL  
SECTION (SEE FIG. )



NET SECTION PROPERTIES: X & Y ARE  
PRINCIPAL AXES.  $I_x = 3.21 \text{ IN}^4$ ,  $I_y = .37 \text{ IN}^4$   
 $A = 1.46 \text{ IN}^2$ ,  $C_x = 1.30$ ",  $C_y = 1.54$ "

### STRESS ANALYSIS

LOADS AT SECTION B-B:  $P = +33,320^*$

$M_x = 79,030 \text{ IN-LB}$ ,  $M_y = 2910 \text{ IN-LB}$

$P/A = 33,320/1.46 = +22,800 \text{ PSI}$

$M_x C_y / I_x = 79,030(1.54)/3.21 = +37,900 \text{ PSI}$

$M_y C_x / I_y = 2910(1.30)/.37 = +10,200 \text{ PSI}$

$f_t = 22,800 + 37,900 + 10,200 = 70,900 \text{ PSI}$

$F_t = 102,000 \text{ PSI @ } 450^\circ \text{ F}$

M.S. =  $102.0/70.9 - 1 = +.44$  ← M.S.

Ti-6Al-4V COND I PLATE STOCK

THE ABOVE MARGIN OF SAFETY

IS HIGH BECAUSE THE EF POST

IS LIGHTLY STRESSED IN

ORDER TO REDUCE THE

DEFLECTION OF THIS MEMBER

Figure 4-45. Crew Compartment Analysis



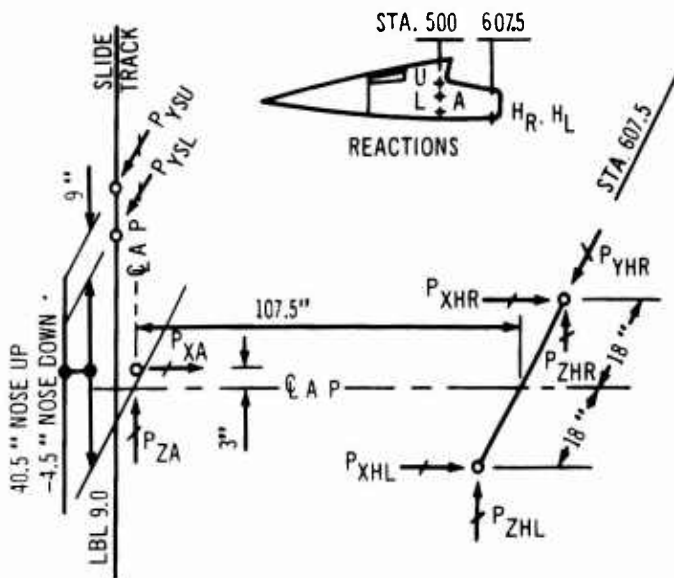
# CRITICAL LOAD CONDITIONS

1. DYN LANDING:  $V_3 = 10/\text{SEC}$ , G.W. = 430 KIP.
2. NEG. MAN:  $M = 90$ ,  $V_{MO}$ ,  $\delta_{NOSE} = 21^\circ$ ,  $n = -1.0$
3. YAWED FLIGHT:  $M = 90$ ,  $V_{MO}$ ,  $\delta_{NOSE} = 21^\circ$ ,  $n = 0$
4. NOSE GEAR UP LANDING, MAX. BRAKING

# ACTUATOR AND HINGE LOADS

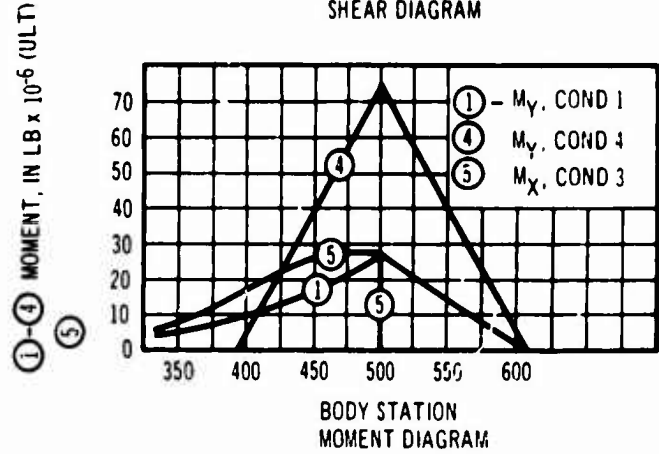
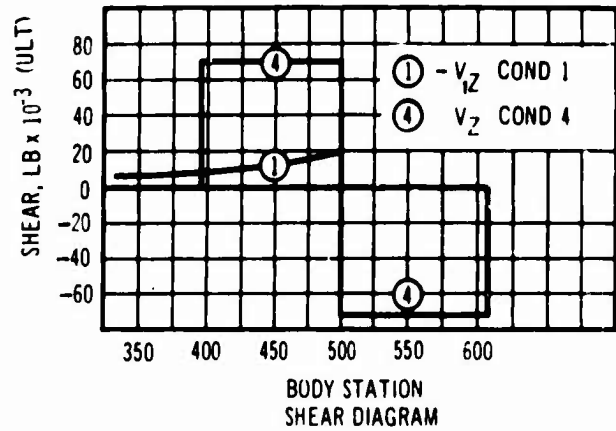
## OVERLAPING ASSUMPTIONS

- A) ALL SIDE LOAD REACTED BY SLIDE TRACK.
- B) SIDE LOAD REACTED BY SLIDE TRACK AND RIGHT HINGE.



## REACTIONS ~ KIPS

COND.	$P_{SU}$	$P_{SL}$	$P_{YA}$	$P_{ZA}$	$P_{YHR}$	$P_{ZHR}$	$P_{YHL}$	$P_{ZHL}$	$P_{XR}$	$P_{YR}$	$P_{ZR}$
1	—	—	-45.4	6.8	-3.4	-3.4	—	—	14.2	14.2	—
2	—	—	56.5	-8.5	4.2	4.2	—	—	-8.0	-8.0	—
3-A	-24.8	38.0	37.3	-5.6	-11.1	16.2	—	—	-3.5	-3.5	—
3-B	-1.0	40.8	37.3	-5.6	2.8	2.8	-4.7	-5.5	-5.0	—	—
4	—	—	142.0	-21.3	10.2	10.2	—	—	35.0	35.0	—



## MONOCOQUE BENDING: STA. 500

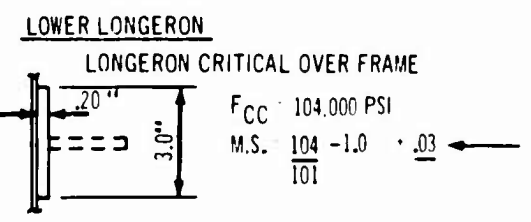
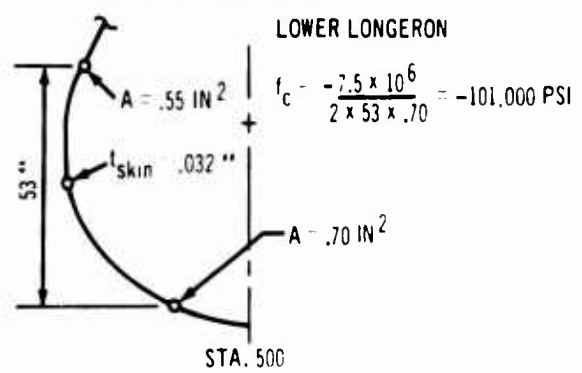
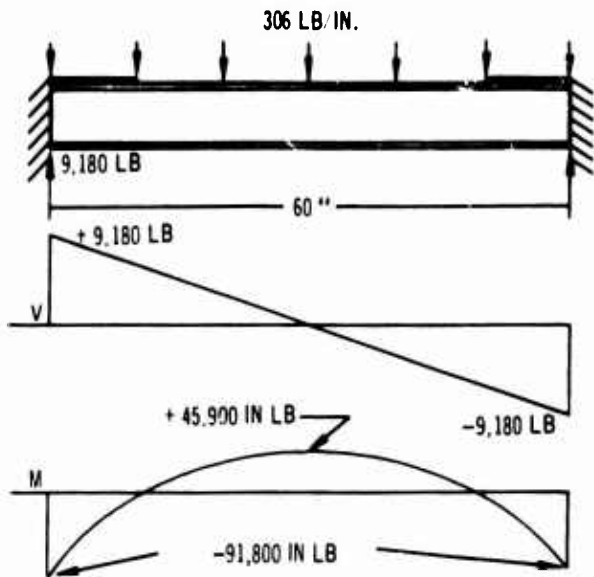


Figure 4-46. Analysis of Movable Nose

THE ANALYSIS SHOWN FOR ONE FLOOR BEAM & PRESSURE WEB IS TYPICAL FOR ENTIRE CABIN FLOOR IN SECT. 45. (ASSUME 11" BEAM SPACING)

$$\text{LOAD/INCH ON BEAM} = (2.5)(11.12)(11) = 306 \frac{\text{LB}}{\text{IN}}$$



**CORRUGATED BEAM WEB**

BEAM WEB HAS 60° CORRUGATIONS WITH A .70" RADIUS. WEB IS LOCAL STABILITY CRITICAL.

$$F_{S,ALL} = 1.55 \eta_T \sqrt{2} E (t/2R)^{3/2} \triangleright$$

$$= 60,000 \text{ PSI}$$

$$f_s = \frac{V}{dt} = \frac{9180}{(.025)(8)}$$

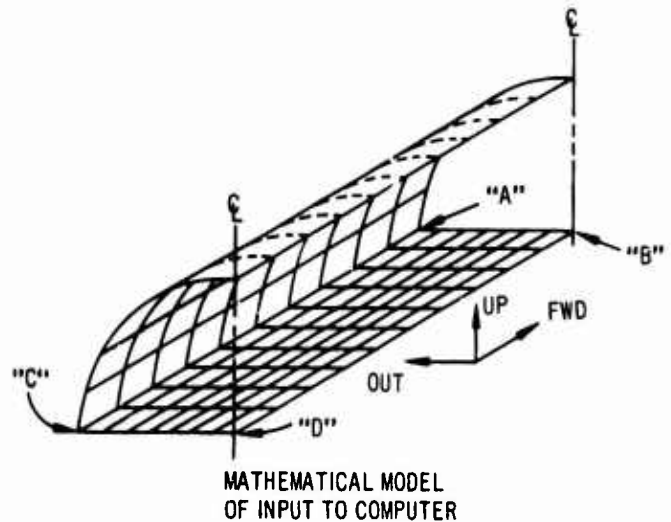
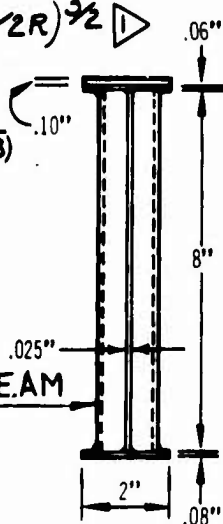
$$= 45,900 \text{ PSI}$$

$$M.S. = \frac{60,000}{45,900} - 1$$

$$= .30$$

CUT AT END OF BEAM

$\triangleright$  SEE REF 16



FLOOR BEAMS

	"A" TO "B"				
	22,438	12,118	7,542		
	21,289	14,933	10,134	6,793	
TO "C"	17,987	14,048	10,170	6,964	4,335
	14,639	12,034	9,086	6,381	4,066
	9,902	7,706	5,539	3,615	2,000
	7,872	6,265	4,592	3,057	1,718
	4,829	3,594	2,441	1,383	
	2,569	1,759	1,012		

SHEAR STRESSES, (PSI), IN PRESSURE WEB DUE TO THERMAL EXPANSION OF THE FUSELAGE

Figure 4-47. Analysis of Floor and Pressure Web

The inner, or passenger accommodation liner, is acrylic sheet.

The cab No. 2 window, window sills, window panes, window seals, and local supporting structure, which make up a highly redundant structure, are analyzed employing the SAMECS digital computer program.

The displacement and rotation of structure adjacent to the window and window frame subassembly (as obtained from the crew compartment internal loads analysis) are forced, at node points surrounding the mathematical model, to simulate the deformation of the crew compartment structure beyond the window model. Thermal gradients and pressure corresponding to these forced displacements and rotations are applied to the window model. All windows in the prototype cab will be similarly analyzed (see Fig. 4-48).

Because of the hazard to crew and passengers from sudden decompression of an airplane at 70,000 ft caused by the loss of any one of the crew compartment windows, all of the crew windows incorporate dual fail-safe paths. The primary pressure-carrying panel of each window in the crew compartment is a laminate employing two panes of chem-tempered glass, with each pane capable of carrying 1.5 factors on the operating pressure. An outer monolithic pane of glass employed in the window assembly is also capable of carrying 1.5 factors on the operating pressure. Because the passenger windows have considerably smaller area than the crew compartment windows, they have a single fail-safe design. The main pressure-carrying pane of chem-tempered glass is designed to three factors on the operating pressure. The external fail-safe pane has sufficient strength to carry 4.9 factors on cabin pressure. The fail-safe adequacy of this two-pane design has been substantiated by an extensive test program (V2-B2707-9).

#### 4.3.10 Nose Radome

The nose radome is a filament-wound, polyimide-impregnated, fiberglass conical shell structure. A slip-cast ceramic cap is bonded to the nose to provide rain-erosion resistance. The radome is designed to take monocoque bending, distributed air loads, and internal pressurization. The wall thicknesses are based on electrical transmissivity requirements; thus margins of safety for loads are large. The

critical load condition is as follows: dive maneuver, Mach = 2.7, n = 2.5 limit, with external pressure p = 3.5 psi (see Fig. 4-49).

#### 4.3.11 Fuselage Frames

Fuselage frames are continuous rings attached to the longitudinal stringers through clips. Shear tie connections are used between the skin and frame in some areas for localized shear transfer.

Fuselage frames are designed for loads resulting from stability requirements, internal and external pressure, thermal gradients, lower-lobe fuel-cell supports, and strake loads.

Frame stiffness requirements to prevent fuselage general instability are based on Shanley's equation modified to account for the stabilizing effect of the floor.

$$I_{\text{req'd}} = \frac{3}{4} C_f \frac{MD^2}{EL}$$

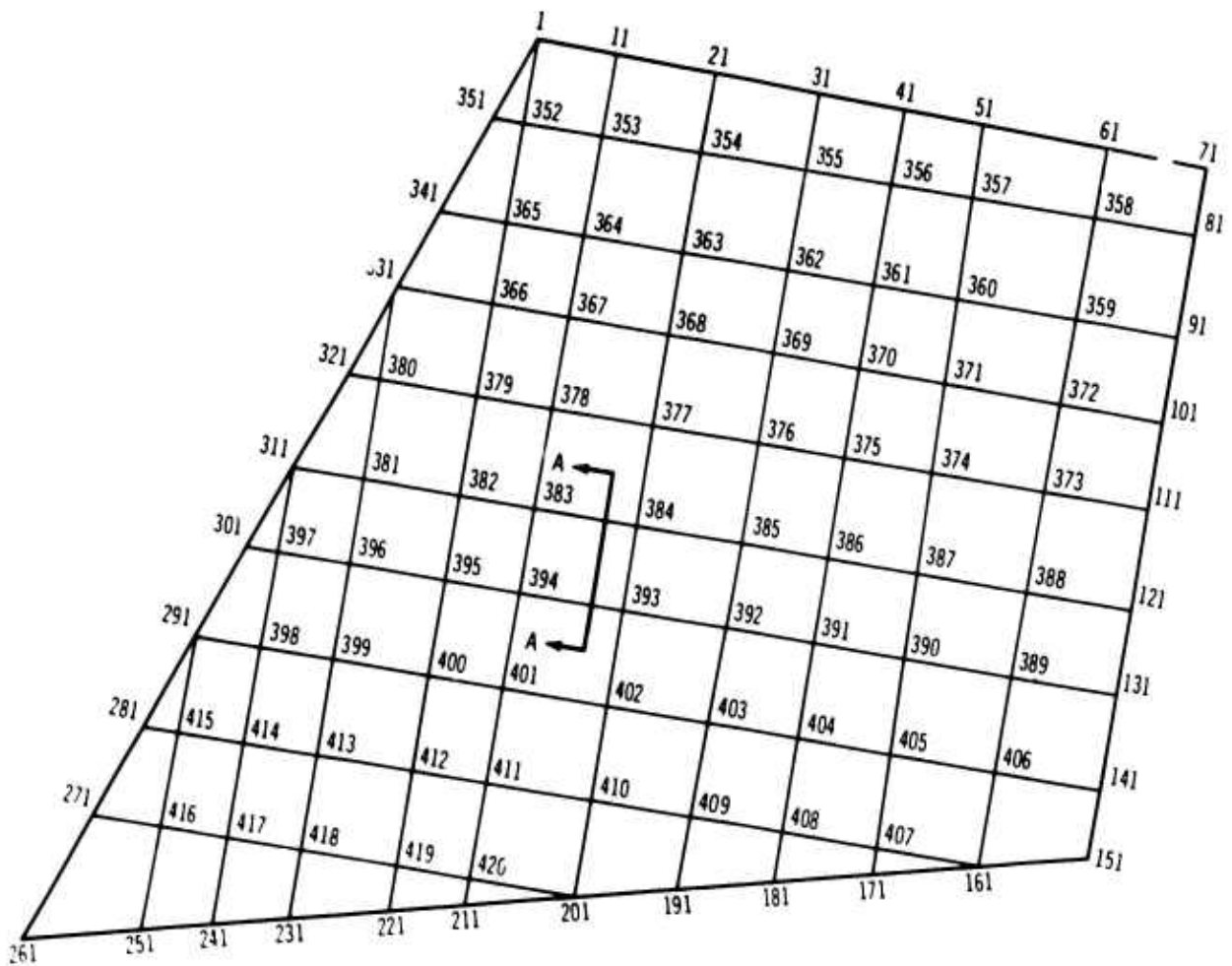
where:

- E = Modulus of elasticity of frame, psi
- I = Moment of inertia of frame, in.<sup>4</sup>
- C<sub>f</sub> = Empirical stability constant
- M = Fuselage bending moment, in. lb
- D = Diameter of fuselage, in.
- L = Frame spacing

Based on NACA test data, a value of C<sub>f</sub> = 6.25 x 10<sup>-5</sup> results in frame stiffness sufficient to give assurance of prevention of general instability failures.

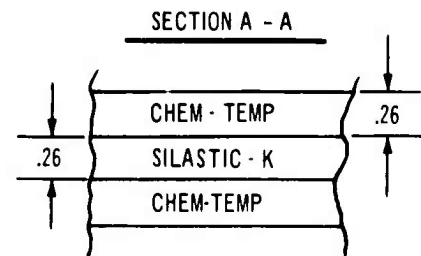
In general, the frames are critical for the fuselage stability requirements. The wing strake loads are critical for local frame structure below the cabin floor.

An analysis of the frame at Sta 2200 is shown in Fig. 4-50. This frame supports a 21-in. section of the strake. The conditions of maximum strake up-load and maximum strake down-load are analyzed. Fuselage crushing loads are superimposed. The critical up-load is vertical gust at Mach = 0.90 and 380 kips gross weight. The critical down-load is takeoff taxi, n = 2 factors limit.



CRITICAL CONDITION: 3.0 FACTOR  
INTERNAL PRESSURE, 33.36 PS.I.

DUE TO THE 300° TEMPERATURE,  
THE INTERLAYER IS ASSUMED  
TO HAVE NO SHEAR CAPA-  
BILITY AND EACH GLASS  
PANE IS ASSUMED TO ACT  
INDEPENDENTLY AND CARRYS  
1.5 FACTOR PRESSURE .



$M_y$  AT SECTION A - A = 410 IN-LB/IN.

$$f_b = 6M/t^2 = (6)(410)/(.26)^2$$

$$f_b = 36,400 \text{ PSI.}$$

$$F_b = 40,000 \text{ PSI.}$$

$$M.S. = 40/36.4 - 1 = 0.1 \leftarrow$$

Figure 4-48. Crew Compartment Window Analysis

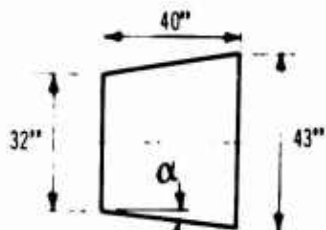
V2-B2707-6-2

CRITICAL CONDITION: DIVE MAN;  
 $M = 2.7$ ;  $n = 2.5$ ; WITH EXTERNAL  
 PRESSURE;  $P = 3.5$  PSI

CRITICAL BENDING MOMENT

SHELL ANALYZED BY DIVISION  
 INTO FRUSTRUMS OF CONES.

CRITICAL FRUSTRUM FROM  
 STA 295 - STA. 335



$$M_{CR} = F_B \pi R^2 t$$

$$P = \frac{R}{\cos \alpha} = 16.2; t_{MIN.} = 0.29; L' = 40.5''$$

$$\frac{P}{t} = \frac{16.2}{0.29} = 56; \frac{L'}{P} = \frac{40.5}{16.2} = 2.5$$

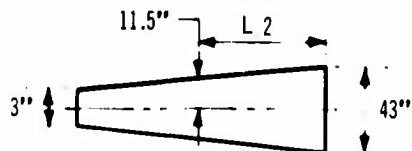
$$F_B = 20,000 \text{ PSI}; \triangleright$$

$$M_{CR} = 20,000 \pi (16)^2 (0.29)$$

$$M_{CR} = 4.66 \times 10^6 \text{ IN.} \#$$

CRITICAL EXTERNAL PRESSURE

SHELL ANALYZED AS A CONE 145" LONG



$$P_{CR} = \frac{K_y \pi^2 E t^3}{e_{AVG.} L^2 12(1-\mu)}$$

$$Z = \frac{L^2}{e_{AVG.} t} \sqrt{1-\mu^2}$$

$$L = 136''; E = 2.0 \times 10^6; \mu = 0.20$$

$$Z = \frac{(136)^2}{11.5(0.29)} \sqrt{1-(0.20)^2} = 5430$$

$$K_y = 70 \triangleright$$

$$P_{CR} = \frac{70 \pi^2 (2.0 \times 10^6) (0.29)^3}{15 (146)^2 12 (1-0.2^2)} = 9,15 \text{ PSI}$$

BUCKLING INTERACTION

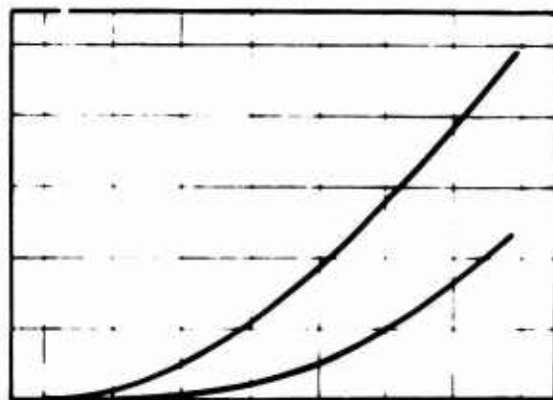
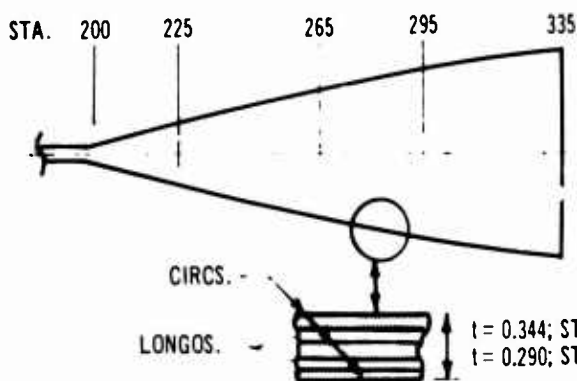
$$R_B^{1.2} + R_P^{1.2} \leq 1.0; \text{ PAGE C 8.23 } \triangleright$$

$$\text{WHERE: } R_B = \frac{M}{M_{CR}} \quad \& \quad R_P = \frac{P}{P_{CR}}$$

$$\left(\frac{4.4 \times 10^5}{4.66 \times 10^6}\right)^{1.2} + \left(\frac{3.5}{9.15}\right)^{1.2} = 0.323 < 1.0$$

M.S. LARGE ~ SHELL DESIGNED  
 FOR TRANSMISSIVITY.

NOSE RADOME



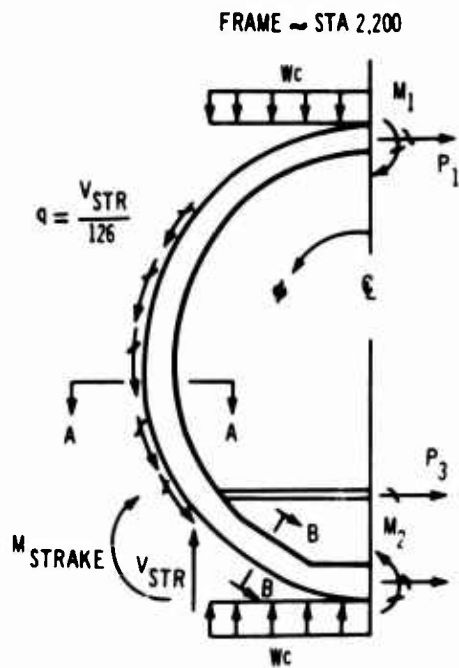
FAIL SAFE DISCUSSION

THE CONSTRUCTION OF THE NOSE  
 RADOME, 5 PLYS., IS FAIL SAFE,  
 SINCE WITH ANY PLY REMOVED:

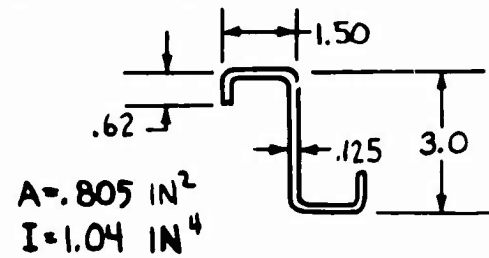
$$\left(\frac{3.9 \times 10^5}{2.3 \times 10^6}\right)^{1.2} + \left(\frac{2.33}{5.4}\right)^{1.2} = 0.36 < 1.0$$

AT LIMIT LOADS.

Figure 4-49. Nose Radome Analysis



UPPER FRAME - SECT. A-A



FOR BODY STABILITY

$$I_{REQ'D} = \frac{3}{4} \frac{C_F M D^2}{E L}$$

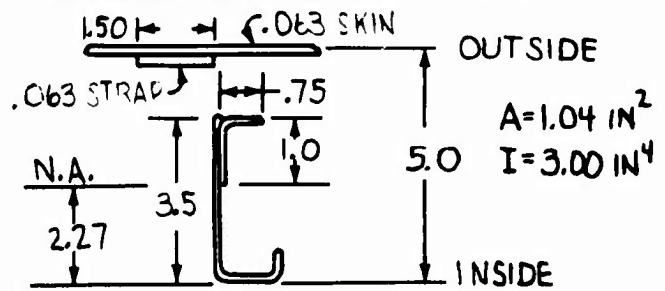
$C_F = 1/16000$   
 $M = 244 \times 10^6 \text{ IP}$   
 $D = 170 \text{ IN}$   
 $E = 16 \times 10^6 \text{ psi}$   
 $L = 21 \text{ IN}$

$$I_{REQ'D} = 0.98$$

$$\frac{I}{I_{REQ'D}} = 1.06$$

COND. →	VERTICAL GUST	T.O. TAXI
LOAD (ULT)		
$M_{STRAKE}$ , IN-K	546	-504
$V_{STRAKE}$ , KIPS	.50	-.86
$W_c$ , LB IN	23.9	2.6
$M_1$ , IN-KIPS	-7.1	7.1
$P_1$ , KIPS	-1.1	-.7
$M_2$ , IN-KIPS	-74.2	62.0
$P_2$ , KIPS	9.6	-10.3
$P_3$ , KIPS	-8.4	-5.0

LOWER FRAME - SECT B-B



COMPRESSION ON OUTSIDE SKIN CRITICAL.

T.O. TAXI COND.

$M = -90 \text{ IN-KIPS}$  (COMP. OUTSIDE)

$P = -6.1 \text{ K}$

$$f_{OUT} = \frac{M C}{I} + \frac{P}{A} = -84.9 \text{ KSI}$$

$F_{CR \text{ SKIN}} = -92.5 \text{ KSI}$  (INTER-RNET BUCKLE)

$$M.S. = .09$$

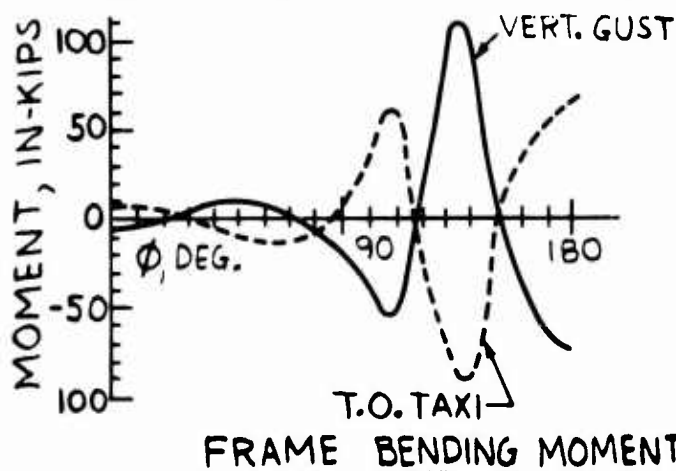


Figure 4-50. Typical Fuselage Frame Analysis

#### 4.4 EMPENNAGE STRESS ANALYSIS

##### 4.4.1 Horizontal Stabilizer

Detail structural diagram and descriptions are shown in Par. 3.4.

##### 4.4.1.1 Analysis Methods

The primary structure is analyzed as a two-cell box with skin stiffener covers similar to those used on the wing box. Skin-to-stiffener area ratios are higher than in the wing to obtain additional torsional stiffness. Higher than normal tension margins of safety are obtained because of the added skin area. The higher skin area is greater than optimum for a normal fail-safe design on higher tension stressed structure. This is more than offset by the resultant lower stress levels that also produce a long-life fatigue design. Fail safety is also provided by limiting the skin panel width.

The all-movable tip elevons are analyzed as a multispar structure with nonbuckling titanium sheet covers. The corrugated web spars stabilize the covers and carry the shear. The elevon is connected to the aft face of the rear spar of the horizontal stabilizer by means of two multi-piece fail-safe hinge fittings mounted on stream-wise ribs. The trailing edge, leading edge, and tip region are analyzed in a conventional manner similar to sandwich construction on the fin as described in Par. 4.4.2.4.

##### 4.4.1.2 Design Loads

Shear moment and torsion curves for the stabilizer design maximum up- and down-bending flight conditions are shown in Fig. 4-51. The inboard sections are critical in down-bending for a subsonic maneuver condition. Local regions are critical for the wing interconnect and jacking loads; and engine, elevon, and actuator attachments. Lower surface areas near the engine inlet are designed by local pressures occurring during engine external compression and buzz. The forward spar is generally critical for thrust inertia factors on fuel for crash-landing conditions. Other spars are critical for primary-bending conditions and local attachment loads.

Control surface loads and actuator and hinge reactions are shown in Fig. 4-52.

##### 4.4.1.3 Allowables

Because of the similarity of the stabilizer and wing construction, the wing allowables presented

in Par. 4.2.3 are applicable to the stabilizer with modification for the different skin-to-stiffener ratios.

##### 4.4.1.4 Analysis

The stress analysis is the same as that described for the wing, Par. 4.2.4. Analyses of typical cover panels ribs, engine support, wing interconnect, and outboard elevon structures are presented in Figs. 4-53, 4-54, and 4-55.

##### 4.4.2 Fin

Detail structure arrangements and discussions are presented in Par. 3.4.

##### 4.4.2.1 Analysis Methods

The primary box utilizes multispar construction and skin-stringer panels that are analyzed as conventional box beams. This analysis is applicable everywhere except locally at the back-up structure for the rudder actuator system, where integrally machined skins and ribs are used in the aft bay. The location of the actuator pack allows the complete fin box above the actuator and forward of the hinge line to be used effectively in providing torsional stiffness. Intercostals located along the 30 percent chord line carry leading-edge panel loads to the ribs. Shear from the lower forward leading edge is collected by the rib located along the top of the high-frequency gap antenna, and then transmitted to the top of the body through three pin joints mounted on stub ribs extending from the top of the body.

##### 4.4.2.2 Design Loads

The fin structure is generally critical for the transonic maneuver conditions combined with descent thermal gradients. The critical shear moments and torsions are shown in Figs. 4-56 and 4-57.

##### 4.4.2.3 Design allowables

The construction of the fin is similar to the wing. The allowables given in Pars. 4.2.3 and 4.3.3 are used for the fin.

##### 4.4.2.4 Analysis

The criteria and analysis methods are similar to those presented in Par. 4.2. Redundant analysis of the composite fin-body structure was done to determine overall load distribution. Conventional box-bending analysis of a typical fin section is shown in Fig. 4-58. Leading-edge sections and internal rib analyses are shown in Fig. 4-59. The empennage body juncture analysis is presented in Fig. 4-60.

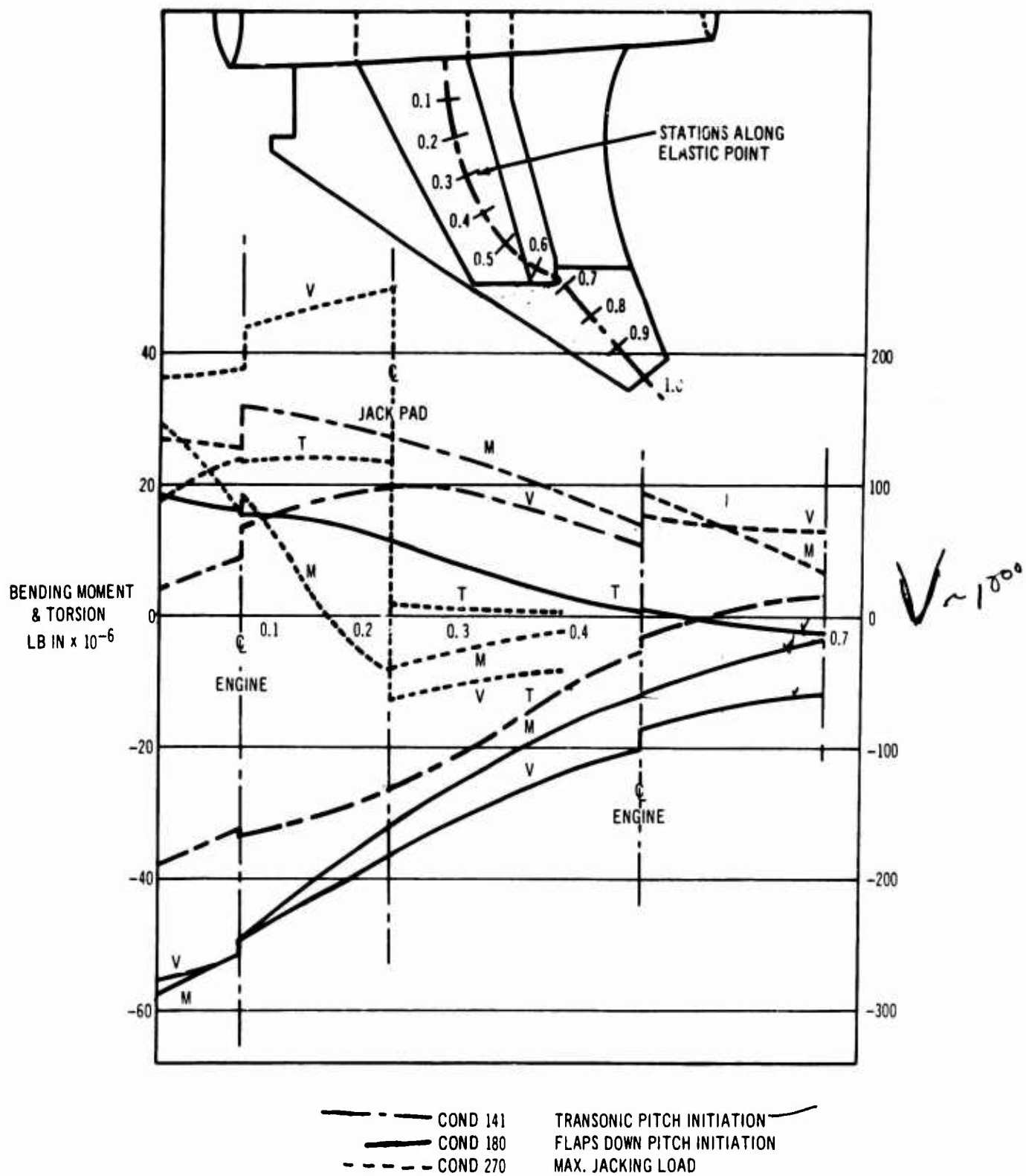
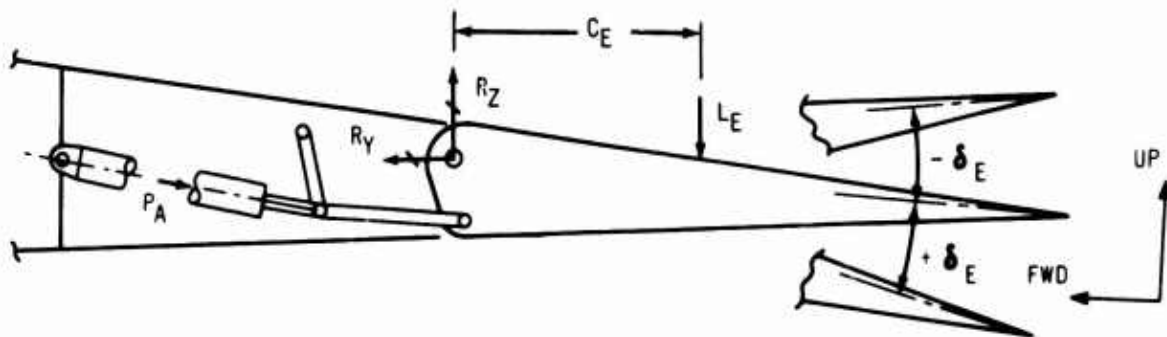


Figure 4-51. Horizontal-Stabilizer Ultimate Design Loads

V2-B2707-6-2





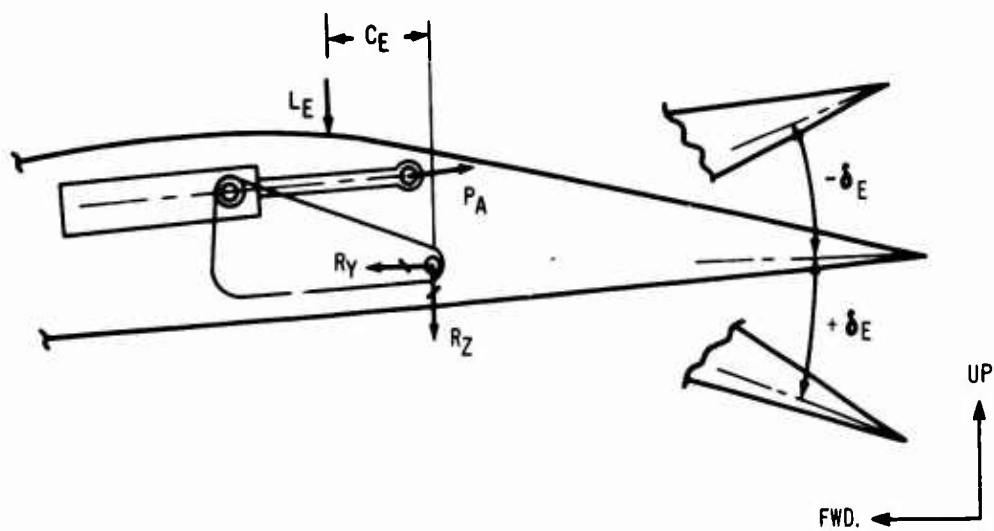
TYPICAL ACTUATOR LOADS & HINGE REACTIONS  
(9 ACTUATORS & 4 HINGES)

CONDITION		TRANSONIC PITCH INITIATION $M = 1.2$ $V_e = 354$
$\delta_E$	DEGREES	-30
S	FT. <sup>2</sup>	108.3
$L_E$	KIPS ULT.	135
$C_E$	INCHES	59.5
HINGE MOMENT	IN-KIPS ULT.	8030
$P_A$ LOAD ACT.	KIPS ULT.	189
$R_Y$ LOAD HINGE	(MAX.) KIPS ULT.	540
$R_Z$ LOAD HINGE	(MAX.) KIPS ULT.	23.6

ELEVATOR CONTROL SYSTEM LOADS

Figure 4-52. Horizontal-Tail Control Surface Loads

TIP ELEVON CONTROL SYSTEM LOADS

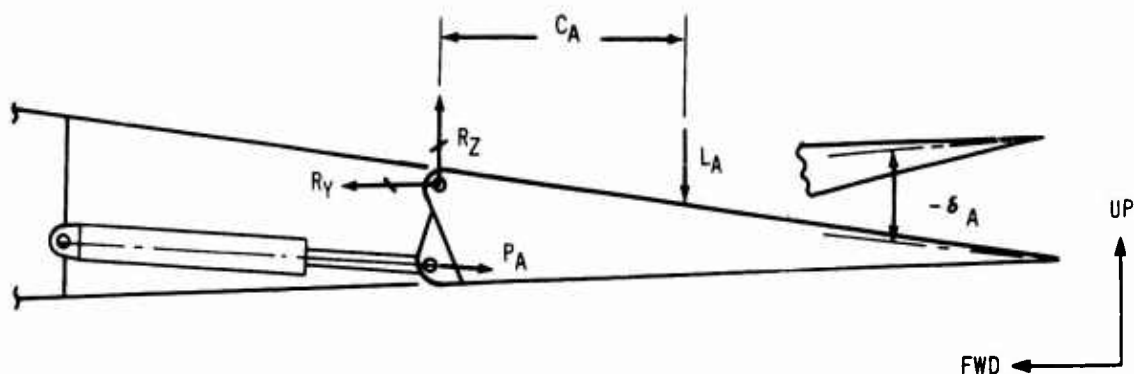


TYPICAL ACTUATOR LOADS & HINGE REACTIONS  
(3 ACTUATORS & 2 HINGES)

CONDITION		ROLL INITIATION $M = .85$ $V_e = 438$
$\delta_E$	DEGREES	-30
S	FT. <sup>2</sup>	193.95
$L_E$	KIPS ULT.	122.1
$C_E$	INCHES	12.1
HINGE MOMENT		IN-KIPS ULT. 1476
$P_A$ LOAD ACT.	KIPS ULT.	29.5
$R_y$ LOAD HINGE (MAX.)	KIPS ULT.	44.3
$R_z$ LOAD HINGE (MAX.)	KIPS ULT.	6.0

Figure 4-52 (Continued)

AUXILIARY ELEVATOR CONTROL SYSTEM LOADS  
(INBOARD)

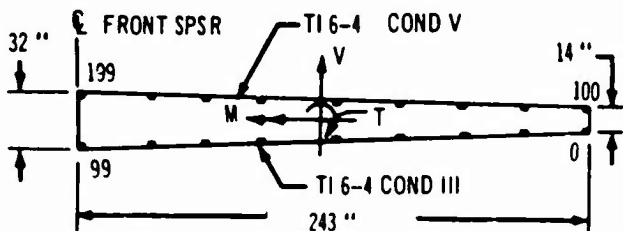


TYPICAL ACTUATOR LOADS & HINGE REACTIONS  
(3 ACTUATORS & 2 HINGES)

CONDITION		FLAP PLACARD TAKEOFF PITCH INITIATION $M = .34$ $v_e = 225$
$\delta_A$	DEGREES	-30
S	FT. <sup>2</sup>	70
$L_A$	KIPS ULT.	19.4
$C_A$	INCHES	45
HINGE MOMENT	IN-KIPS ULT	873
$P_A$ LOAD ACT.	KIPS ULT.	58.6
$R_Y$ LOAD HINGE (MAX.)	KIPS ULT.	149.5
$R_Z$ LOAD HINGE (MAX.)	KIPS ULT.	6.5

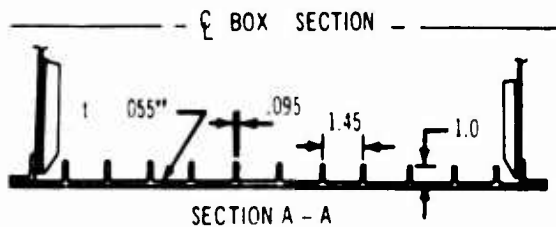
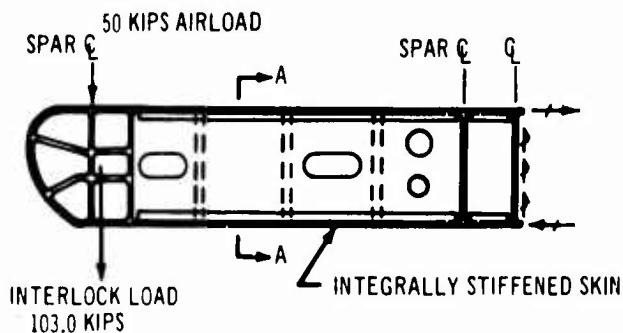
Figure 4-52. (Concluded)

ANALYSIS  
PRIMARY BOX  
SECTION AT BODY SIDE



THE AREA OF THE 'ZEE' STIFFENED PANELS IS IDEALIZED AS ACTING AT EQUALLY SPACED NODES ON EACH SURFACE. SUMMARIES OF THE CRITICAL DESIGN CONDITIONS, STRESSES AND MARGINS OF SAFETY AS PRODUCED BY THE COMPUTER PROGRAM ARE SHOWN IN FIGS. 2c, 2d AND 2e.

WING INTERLOCK RIBS  
DESIGN CONDITION: A COND. 24. NEG MAN'VER



COVER LOADING  $W' = \frac{M}{wh} = \frac{3.86 \times 10^6}{18 \times 24} = 8950 \text{ #/IN}$   
 $f_{COMP} = \frac{1.45 \times 8950}{175} = 74500 \text{ PSI}$   
 $f_{SKIN} = KE \left(\frac{t}{b}\right)^2 = 75100 \text{ PSI}$

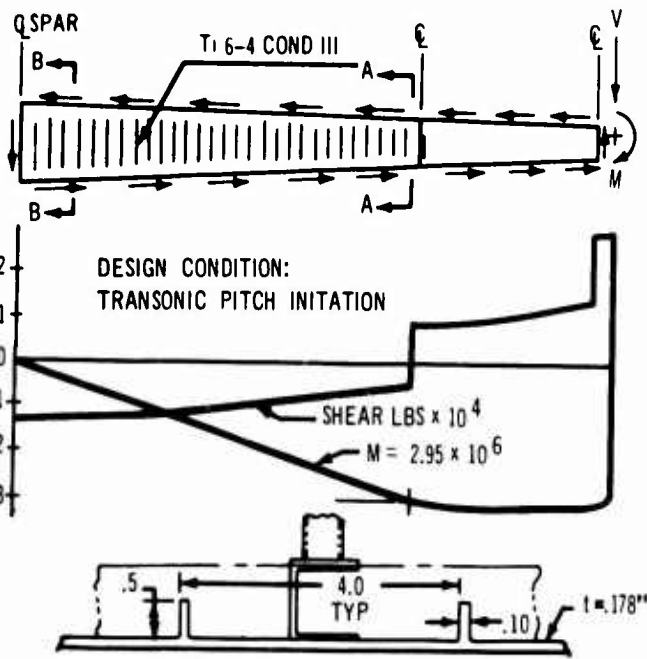
M.S. =  $75100 / 74500 - 1 = .01$

RIB WEB AT SECTION A-A  
 $q = V/h = 2250 \text{ #/IN}$

$q_{ULT ALLOW.} = .49 F_{TU@450} \times t_w$   
 $= .49 \times 134000 \times .805 \times .065$   
 $= 2390 \text{ #/IN}$

M.S. =  $2390 / 2250 - 1 = .06$

ELEVATOR HINGE RIB @  $\eta = .36$



SECTION A-A LOWER SKIN AS SHOWN  
SECTION B-B SIMILAR

COVER LOADING =  $\frac{2.95 \times 10^6}{44 \times 12.6} = 5330 \text{ #/IN}$

.178 SKIN WITH INTEGRAL RIBS @ 4"

$P_{STIFF} = 4 \times 5330 = 21320 \text{ #}$

$P_{CR} = 5.5 \times 16.4 \times 10^6 \times .0081 / 5.5^2 = 24200$

M.S. =  $24200 / 21320 - 1.0 = .13$

RIB MAX WEB SHEAR AT B-B

$q = 690 \text{ #/IN}$

$q_{ALL} = .55 E_c \left(\frac{t}{R}\right)^{3/2} = 770 \text{ #/IN FOR .02" CORRUGATED WEB}$

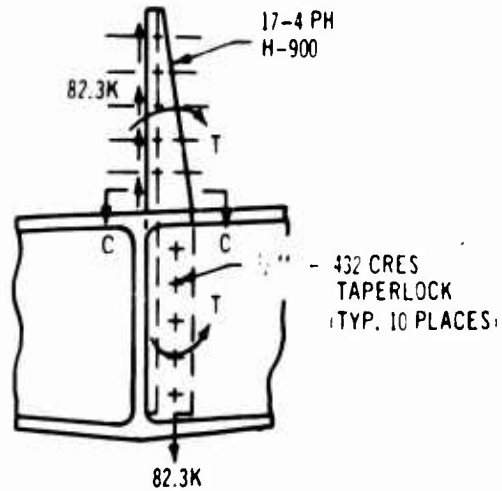
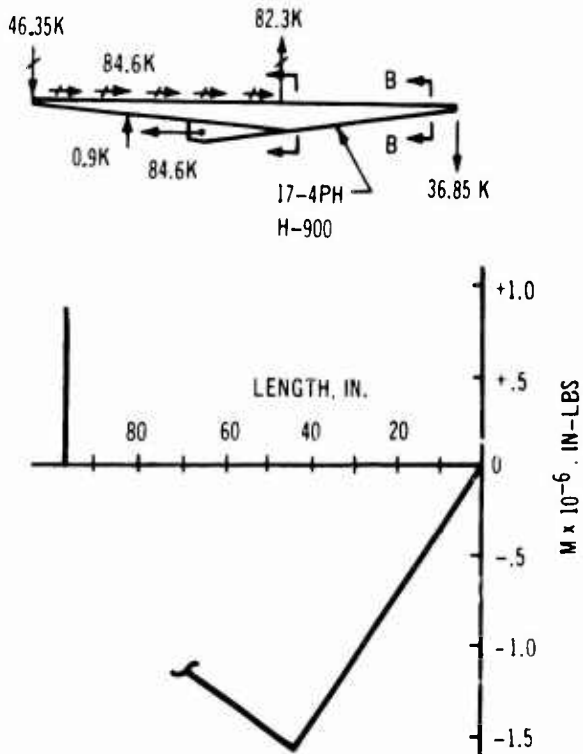
M.S. =  $770 / 690 - 1.0 = .12$

Figure 4-53. Stabilizer Stress Analysis

OUTBOARD ENGINE ATTACHMENT BEAM

BEAM ATTACHMENT ANGLE AT REAR SPAR

2.5 G MANEUVER + GYROSCOPIC LOADS

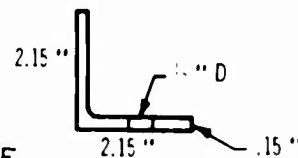


SECTION C-C

$$f_T = \frac{82.3K}{.538} = 153 \text{ KSI}$$

$$F_{TU} = 159 \text{ KSI @ } 600^\circ\text{F}$$

$$M.S. = +.04$$



BOLTS

$$\text{SHEAR LOAD}_{MAX} = \sqrt{\left(\frac{V}{5}\right)^2 + \left(\frac{T}{\sum Y_i^2}\right)^2} = 17.56 \text{ KIPS}$$

$$\text{ALLOW SHEAR} = 19.1 \text{ KIPS @ } 600^\circ\text{F}$$

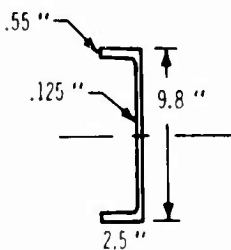
$$M.S. = +.09$$

$$\text{BEARING LOAD}_{MAX} = 17.56 \text{ KIPS}$$

$$\text{BEARING ALLOWABLE} = 18.05 \text{ KIPS @ } 600^\circ\text{F}$$

$$M.S. = +.03$$

SECTION A-A



$$I_x = 65.4 \text{ IN}^4$$

$$f_{Y_{MAX}} = \frac{15.85K(4.9)}{65.4} = 118.8 \text{ KSI}$$

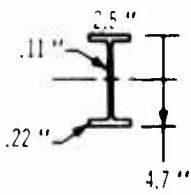
$$F_{CY} = 125.5 \text{ KSI @ } 600^\circ\text{F}$$

$$M.S. = +.06$$

$$f_{S_{MAX}} = \frac{36.85K \times 7.54}{65.4 \times .125} = 340 \text{ KSI}$$

$$F_{SU} = 93.5 \text{ KSI @ } 600^\circ\text{F}$$

$$M.S. = \text{HIGH}$$



$$I_x = 6.25 \text{ IN}^4$$

$$f_{Y_{MAX}} = \frac{276.5K(2.35)}{6.25} = 104 \text{ KSI}$$

$$F_{CY} = 106.8 \text{ KSI @ } 750^\circ\text{F}$$

$$M.S. = +.08$$

$$f_{S_{MAX}} = \frac{36.85K(1.48)}{6.25(.110)} = 79.5 \text{ KSI}$$

$$F_{SU} = 82.4 \text{ KSI @ } 750^\circ\text{F}$$

$$M.S. = +.04$$

Figure 4-53. (Concluded)

FTA STA.	LOAD COND.	V Z	M X	T	V X	M Z	AREA LOWER	AREA UPPER	AREA ELOWER	AREA EUPPER	S.W. EFF	TRUE-J.	
0.000	180	-279100.	-57800000.	18200000.	-0.	-0.	38.862	38.862	31.876	31.876	0.107	27175.	
I X	I Z	I XZ	BAR ZE	BAR XE	I XE	I ZE	I XE ZE	2A	P Z	P X	T.C. VZ	T.C. VX	T.C. EQUIB
11749.	354864.	0.0	0.00	-141.02	9345.	299829.	0.0	11637	93643.	-21079.	1170104.	-1.10E 07	-4.17E 07

LOWER SURFACE

SEG. NO.	SKIN THICK	SEG. AREA	STIFF AREA	DIST N.A.	SEG. LOAD	SEG. STRESS	SKIN STRESS	COMP. ALLOW	SHEAR FLOW	SHEAR STRESS	SHEAR ALLOW	M.S. COMP.	M.S. SHEAR
0	0.110	2.700	2.700	-7.000	-101363.	-37542.	-42954.	82000.	4508.	43723.	69500.	0.11	0.43
1	0.110	0.001	0.001	-7.900	-45.	-44852.	-47549.	82000.	4508.	40982.	69500.	0.08	0.47
2	0.110	0.001	0.001	-9.800	-53.	-53492.	-56052.	82000.	4508.	40981.	69500.	-0.00	0.40
3	0.110	2.800	2.800	-10.700	-146085.	-52173.	-59912.	82000.	4052.	40979.	69500.	0.01	0.37
4	0.110	7.440	2.760	-11.400	-446392.	-59999.	-62448.	82000.	2644.	36833.	69500.	-0.01	0.44
5	0.110	7.440	2.760	-12.700	-471562.	-63382.	-65694.	82000.	1136.	24032.	69500.	0.10	0.71
6	0.110	7.440	2.760	-14.000	-484538.	-65126.	-67273.	82000.	-432.	10326.	69500.	0.22	0.98
7	0.110	7.440	2.760	-15.300	-497146.	-66821.	-68830.	82000.	-2060.	18723.	69500.	0.12	0.77
99	0.110	3.600	3.600	-16.000	-193886.	-53857.	-69032.	82000.	-2702.	24564.	69500.	0.23	0.64

UPPER SURFACE

SEG. NO.	SKIN THICK	SEG. AREA	STIFF AREA	DIST N.A.	SEG. LOAD	SEG. STRESS	SKIN STRESS	TENS. ALLOW	SHEAR FLOW	SHEAR STRESS	SHEAR ALLOW	M.S. TENS.	M.S. SHEAR
199	0.105	3.600	3.600	16.000	193886.	53857.	69043.	118000.	-2100.	25733.	58000.	0.52	0.35
107	0.105	7.440	2.980	15.300	497146.	66821.	68841.	118000.	-537.	20002.	58000.	0.59	0.46
106	0.105	7.440	2.980	14.000	484538.	65126.	67285.	118000.	1004.	9562.	58000.	0.72	0.66
105	0.105	7.440	2.980	12.700	471562.	63382.	65707.	118000.	2522.	24023.	58000.	0.60	0.43
104	0.105	7.440	2.980	11.400	446392.	59999.	62462.	118000.	3979.	37894.	58000.	0.47	0.18
103	0.105	2.800	2.800	10.700	146085.	52173.	59926.	118000.	4460.	42479.	58000.	0.44	0.12
102	0.105	0.001	0.001	9.800	53.	53492.	56066.	118000.	4460.	42480.	58000.	0.50	0.14
101	0.105	0.001	0.001	7.900	45.	44852.	47565.	118000.	4461.	42482.	58000.	0.63	0.19
100	0.105	2.700	2.700	7.000	101363.	37542.	42969.	118000.	4810.	45805.	58000.	0.64	0.15

Figure 4-54. Stresses and Margins of Safety, Stabilizer Stress Analysis

ETA STA.	LOAD COND.	V Z	M X	T	V X	M Z	AREA LOWER	AREA UPPER	AREA ELOWER	AREA EUPPER	S.W. EFF	TRUF-J.	
0.000	141	16300.	26300000.	-38000000.	-0.	-0.	38.862	38.862	31.876	31.876	0.107	27175.	
I X	I Z	I XZ	BAR ZE	BAR XE	I XF	I ZE	I ZE	2A Z	P X	P X	T.C. VZ	T.C. VX	T.C. FOUR
11749.	354864.	0.0	0.00	-141.02	9345.	299829.	0.0	11637	-42609.	9591.	-532418.	4988256.	-5914936.

SEG. NO.	SKIN THICK	SEG. AREA	STIFF AREA	DIST N.A.	SEG. LOAD	SEG. STRESS	SKIN STRESS	TENS. ALLOW	SHEAR FLOW	SHEAR STRESS	SHFAR ALLOW	M.S. TFNS.	M.S. SHFAR
0	0.110	2.700	2.700	-7.000	46122.	17082.	19545.142000.	-2461.	22369.	69500.	3.15	1.85	
1	0.110	0.001	0.001	-7.900	20.	20409.	21636.142000.	-2461.	22369.	69500.	2.98	1.80	
2	0.110	0.001	0.001	-9.800	24.	24340.	25505.142000.	-2461.	22370.	69500.	2.69	1.70	
3	0.110	2.800	2.800	-10.700	66471.	23740.	27261.142000.	-2533.	23026.	69500.	2.52	1.60	
4	0.110	7.440	2.760	-11.400	203116.	27301.	28415.142000.	-2747.	24973.	69500.	2.31	1.42	
5	0.110	7.440	2.760	-12.700	214569.	28840.	29892.142000.	-2944.	26947.	69500.	2.10	1.26	
6	0.110	7.440	2.760	-14.000	220473.	29633.	30610.142000.	-3179.	28997.	69500.	1.96	1.13	
7	0.110	7.440	2.760	-15.300	226210.	30405.	31319.142000.	-3390.	30821.	69500.	1.83	1.01	
99	0.110	3.600	3.600	-16.000	88222.	24506.	31411.142000.	-3469.	31539.	69500.	1.79	0.97	

UPPER SURFACE

SEG. NO.	SKIN THICK	SEG. AREA	STIFF AREA	DIST N.A.	SEG. LOAD	SEG. STRESS	SKIN STRESS	COMP. ALLOW	SHFAR FLOW	SHFAR STRESS	SHFAR ALLOW	M.S. COMP.	M.S. SHEAR
199	0.105	3.600	3.600	16.000	-88222.	-24506.	-31416.	66400.	-3372.	33041.	58000.	0.28	0.59
107	0.105	7.440	2.980	15.300	-226210.	-30405.	-31324.	66400.	-3131.	32112.	58000.	0.21	0.62
106	0.105	7.440	2.980	14.000	-220473.	-29633.	-30616.	66400.	-2904.	29817.	58000.	0.28	0.73
105	0.105	7.440	2.980	12.700	-214569.	-28840.	-29898.	66400.	-2692.	27659.	58000.	0.35	0.84
104	0.105	7.440	2.980	11.400	-203116.	-27301.	-28421.	66400.	-2500.	25639.	58000.	0.44	0.98
103	0.105	2.800	2.800	10.700	-66471.	-23740.	-27267.	66400.	-2439.	23808.	58000.	0.60	1.11
102	0.105	0.001	0.001	9.800	-24.	-24340.	-25511.	66400.	-2439.	23229.	58000.	0.60	1.19
101	0.105	0.001	0.001	7.900	-20.	-20409.	-21643.	66400.	-2439.	23229.	58000.	0.72	1.26
100	0.105	2.700	2.700	7.000	-46122.	-17082.	-19552.	66400.	-2404.	23229.	58000.	0.82	1.30

Figure A-54. (Continued)

FTA STA.	LOAD COND.	V	M	T	V	M	AREA LOWER	AREA UPPER	AREA FLOWER	AREA EUPPER	S.W. EFF	TRUF-J.	
0.000	270	182000.	30500000.	17800000.	-0.	-0.	38.862	38.862	38.862	38.862	0.107	27175.	
I	I	I	BAR	BAR	I	I	I	2A	P	P	T.C.	T.C.	T.C.
X	Z	XZ	ZE	XE	XE	ZE	XE ZE	Z	Z	X	VZ	VX	EQUIB
11749.	354864.	0.0	0.00	-147.93	11749.	354864.	0.0	11637	-48761.	11014.	-559204.	5912071.	27768769.

SFG. NO.	SKIN THICK	SEG. AREA	STIFF AREA	DIST N.A.	SEG. LOAD	SEG. STRESS	SKIN STRESS	TENS. ALLOW	SHEAR FLOW	SHEAR STRESS	SHEAR ALLOW	M.S. TENS.	M.S. SHEAR
0	0.110	2.700	2.700	-7.000	42547.	15758.	18030.	142000.	-660.	7577.	69500.	5.83	4.90
1	0.110	0.001	0.001	-7.900	19.	19211.	20366.	142000.	-660.	6000.	69500.	5.45	4.88
2	0.110	0.001	0.001	-9.800	24.	24143.	25299.	142000.	-660.	5999.	69500.	4.33	3.96
3	0.110	2.800	2.800	-10.700	67384.	24066.	27635.	142000.	-372.	5998.	69500.	3.92	3.61
4	0.110	7.440	2.760	-11.400	210531.	28297.	29452.	142000.	535.	4864.	69500.	3.70	3.48
5	0.110	7.440	2.760	-12.700	235640.	31672.	32827.	142000.	1562.	14197.	69500.	2.73	2.20
6	0.110	7.440	2.760	-14.000	260749.	35047.	36202.	142000.	2708.	24616.	69500.	1.92	1.27
7	0.110	7.440	2.760	-15.300	285859.	38427.	39577.	142000.	3973.	36121.	69500.	1.33	0.69
99	0.110	3.600	3.600	-16.000	116262.	32295.	41394.	142000.	4497.	40835.	69500.	1.14	0.52

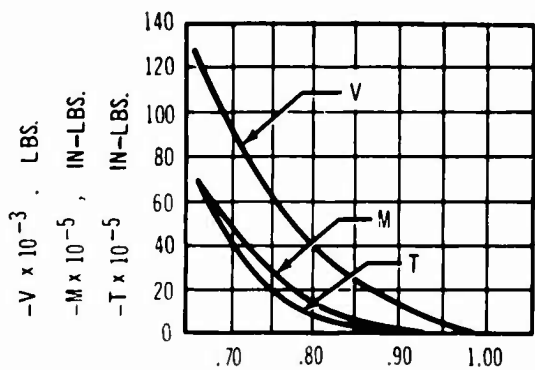
UPPER SURFACE													
SFG. NO.	SKIN THICK	SEG. AREA	STIFF AREA	DIST N.A.	SEG. LOAD	SEG. STRESS	SKIN STRESS	COMP. ALLOW	SHEAR FLOW	SHEAR STRESS	SHEAR ALLOW	M.S. COMP.	M.S. SHEAR
199	0.105	3.600	3.600	16.000	-116262.	-32295.	-41401.	66400.	3995.	42779.	58000.	-0.02	0.22
107	0.105	7.440	2.980	15.300	-285859.	-38427.	-39584.	66400.	2763.	38043.	58000.	-0.01	0.35
106	0.105	7.440	2.980	14.000	-260749.	-35047.	-36709.	66400.	1631.	26311.	58000.	0.27	0.82
105	0.105	7.440	2.980	12.700	-235640.	-31672.	-32834.	66400.	598.	15529.	58000.	0.67	1.57
104	0.105	7.440	2.980	11.400	-210531.	-28297.	-29459.	66400.	-334.	5698.	58000.	1.23	2.67
103	0.105	2.800	2.800	10.700	-67384.	-24066.	-27642.	66400.	-635.	6047.	58000.	1.56	2.84
102	0.105	0.001	0.001	9.800	-24.	-24143.	-25305.	66400.	-635.	6048.	58000.	1.55	3.14
101	0.105	0.001	0.001	7.900	-19.	-19211.	-20373.	66400.	-635.	6049.	58000.	2.10	3.90
100	0.105	2.700	2.700	7.000	-42547.	-15758.	-18736.	66400.	-833.	7938.	58000.	2.34	3.83

Figure 4-54. (Concluded)

V2-B2707-6-2

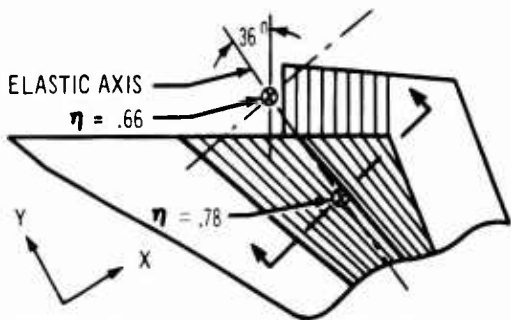
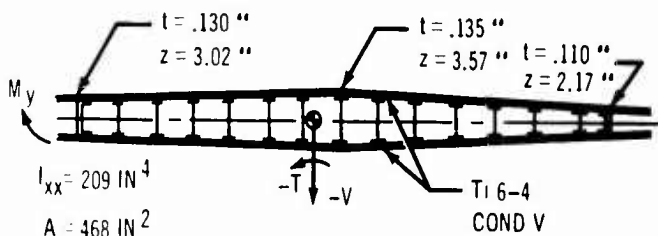


ELEVONS  
DESIGN CONDITION  
SUBSONIC ROLL INITIATION



STRENGTH ANALYSIS

SECTION AT  $\eta = .78$   
 $-V = 48.14$  KIPS  
 $-M_x = 2,040$  IN-KIPS  
 $-T = 1,230$  IN-KIPS



SURFACE PANEL AT ELASTIC AXIS

$$f_x = \frac{M_y}{2zt} = 7.45 \text{ KSI} \quad F_x = 13.9 \text{ KSI} \quad R_x = .535$$

$$f_y = \frac{M_x z}{I_{xx}} = 34.8 \text{ KSI} \quad F_y = 46.1 \text{ KSI} \quad R_y = .755$$

$$f_s = \frac{T}{2At} = 9.7 \text{ KSI} \quad F_s = 58.0 \text{ KSI} \quad R_s = .167$$

$$\text{M.S.} = \frac{1}{\sqrt{R_x^2 + R_y^2 + R_s^2}} - 1 = +.06$$

Figure 4-55. Elevon Stress Analysis

FRONT SPAR

(SHEAR RESISTANT WEB BONDED TO L.E. HONEYCOMB CORE,  $t = .025$ " )

$$q_{\text{TORQUE}} = 1320 \text{ LB/IN}$$

$$q_s = 430 \text{ LB/IN}$$

$$q_{\text{TOTAL}} = 1750 \text{ LB/IN}$$

$$f_s = 70.0 \text{ KSI}$$

$$F_s = .60 \times .85 \times 157K = 80.0 \text{ KSI}$$

$$\text{M.S.} = +.14$$

INTERMEDIATE SPAR

(CORRUGATED WEB,  $t = .025$ " )

$$q_{\text{TORQUE}} = 0$$

$$q_s = 820 \text{ LB/IN}$$

$$q_{\text{TOTAL}} = 820 \text{ LB/IN}$$

$$f_s = 32.8 \text{ KSI}$$

$$F_s = .55 E_c \left(\frac{t}{A}\right)^{1/2} = 36.2 \text{ KSI}$$

$$\text{M.S.} = +.10$$

ELEVATORS

THE ELEVATORS ARE SIMILAR IN SIZE, SHAPE, AND DESIGN LOADS, TO THE RUDDERS WHICH ARE ANALYZED IN SECTION -

#### 4.4.3 Rudder

Structural diagrams and discussion of the rudder are shown in Par. 3.4.

##### 4.4.3.1 Structural Analysis

The rudder consists of two sections, the lower section driving the upper by means of fail-safe connection. This separation reduces the induced loads when the rudder is rotated with a deflected fin and also reduces the power required to drive the rudder. The honeycomb-sandwich panel covers on the rudder box provide high torsional stiffness and minimum gage structure that gives a low rudder mass moment of inertia. The upper rudder section is supported by two hinges so arranged that no load is induced by fin bending.

The hinges on the lower rudder section are designed for air loads combined with deflection-induced loads. All hinges and rudder structure are designed with multiload paths to provide fail-safety.

##### 4.4.3.2 Design Loads

The rudder is designed for the transonic rudder-kick-condition loads as shown in Fig. 4-61. Actuator and hinge reactions are shown in Fig. 4-62.

##### 4.4.3.3 Analysis

Stress analysis is presented for typical rudder sandwich surfaces and support structure in Fig. 4-61.

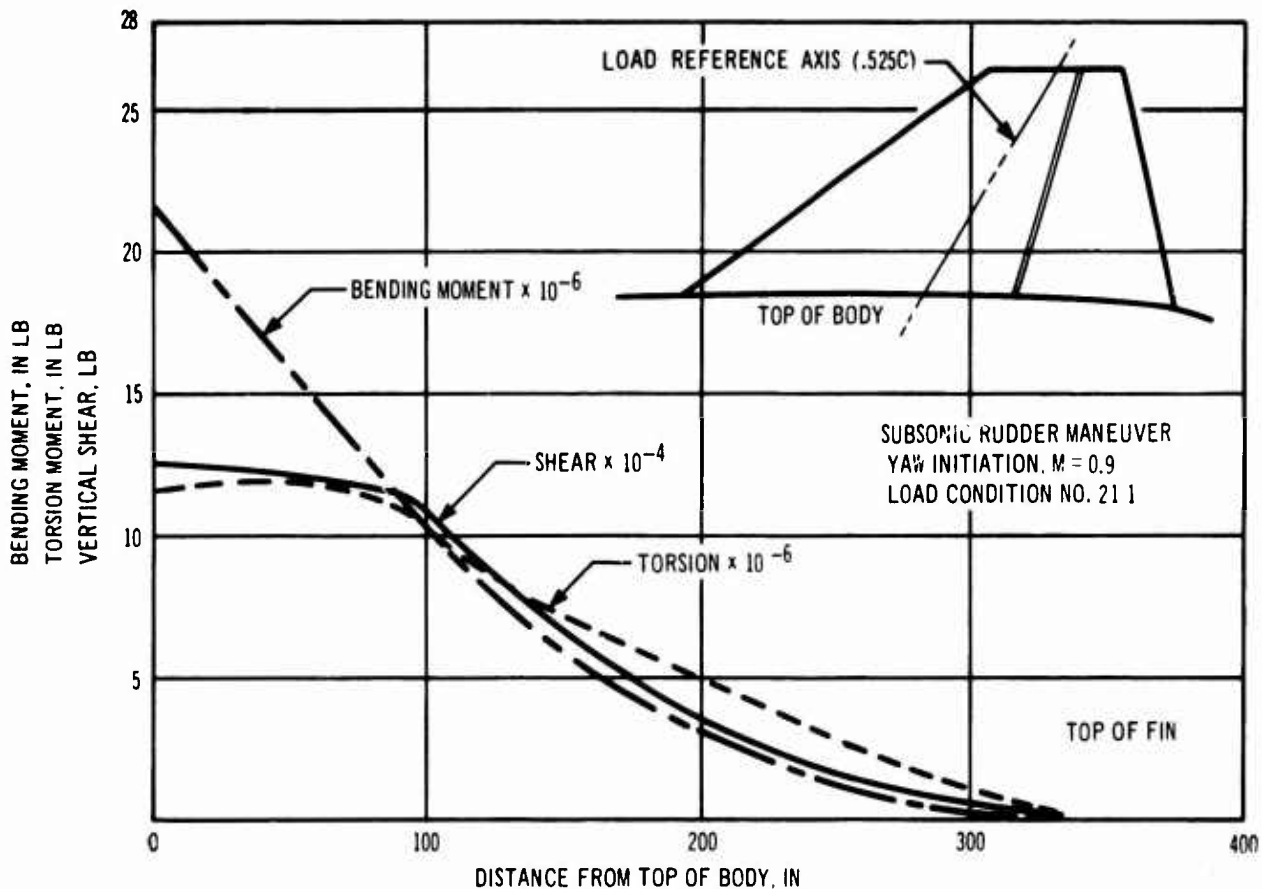


Figure 4-56. Ultimate Fin Loads, Yaw Initiation Condition

V2-B2707-6-2

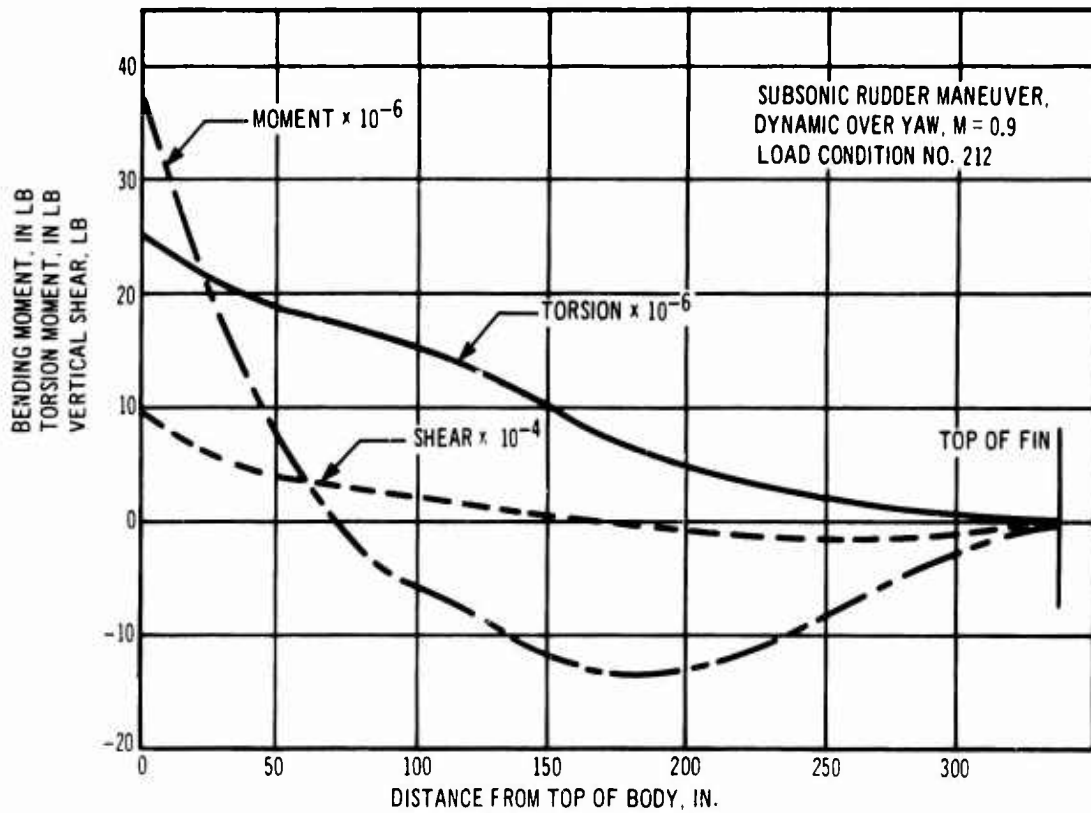
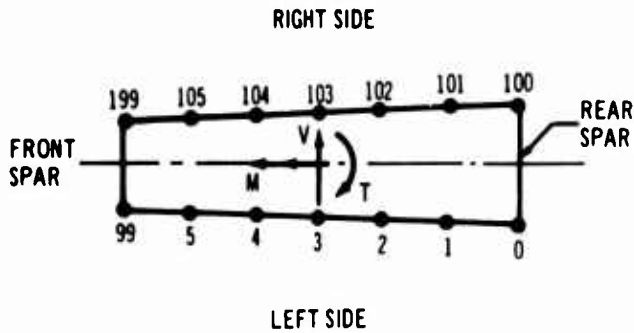


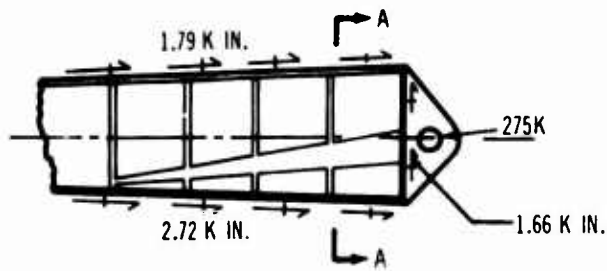
Figure 4-57. Ultimate Fin Loads, Dynamic Overyaw Condition

BEAM SOLUTION OF TYPICAL FIN SECTION ( $\eta = .5$ )



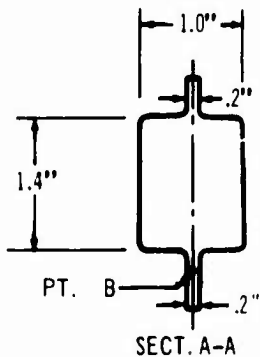
THE AREA OF THE ZEE STIFFENED PANELS IS IDEALIZED AS ACTING AT 6 EQUALLY SPACED NODES ON EACH SURFACE.

ACTUATOR RIB ANALYSIS



CRITICAL CONDITION:

2.5 FACTORS ON ACTUATOR CAPACITY



CHORD STRESS AT SECT. A-A

CHORD LOAD = 206K

EFFECTIVE AREA = 1.6 IN<sup>2</sup>

CHORD STRESS = 129 KSI

SHEAR STRESS IN WEB

ADJACENT TO CHORD AT

POINT (B) =  $\frac{2.72}{0.2}$

= 13.6 KSI

PRINCIPAL SHEAR STRESS

=  $\sqrt{\left(\frac{129.0}{2}\right)^2 + (13.6)^2} = 65.8$  KSI

F<sub>s</sub> = 0.60 × 134 = 80.6 KSI

PRINCIPAL COMPRESSIVE STRESS

=  $\frac{129.0}{2} + 65.8 = 130.3$  KSI

F<sub>cy</sub> = 132 KSI

M.S. =  $\frac{132}{130.3} - 1 = +.01$

Figure 4-58. Fin Stress Analysis

V2-B2707-6-2

FTA STA.	LOAD COND.	V Z	M X	T	V X	M Z	AREA LOWER	AREA UPPER	AREA FLOWER	AREA FUPPER	S.W. EFF	TRUF-J.
0.400	2	62400.	4960000.	5920000.	-0.	-0.	20.175	20.175	20.175	20.175	0.072	2041.

I X	I Z	I XZ	BAR ZF	BAR XF	I XF	I ZE	I XF ZF	2A Z	P Z	P X	T.C. VZ	T.C. VX	T.C. EQUIB
1339.	68355.	0.0	0.00	-73.33	1339.	68355.	0.0	3368	-19444.	0.	122377.	-0.	5241647.

SEF. NO.	SKIN THICK	SEG. AREA	STIFF AREA	DIST N.A.	SEG. LOAD	SEG. STRESS	SKIN STRESS	TENS. ALLOW	SHFAR FLOW	SHFAR STRESS	SHFAR ALLOW	M.S. TENS.	M.S. SHFAR
0	0.063	0.485	0.485	-7.750	6951.	14333.	28586.119000.	218.	3456.	47200.	3.10	2.21	
1	0.063	3.380	1.660	-7.400	49504.	26480.	27290.119000.	993.	15754.	47200.	2.45	1.26	
2	0.063	3.380	1.660	-6.800	81993.	24258.	25068.119000.	1702.	27020.	47200.	1.81	0.58	
3	0.067	3.680	1.820	-6.170	80684.	21925.	22727.119000.	2401.	35832.	47200.	1.43	0.26	
4	0.075	4.090	2.020	-5.500	79525.	19444.	20231.119000.	3089.	41188.	47200.	1.27	0.11	
5	0.087	4.770	2.360	-4.850	81264.	17036.	17801.119000.	3723.	43593.	47200.	1.23	0.06	
99	0.094	0.390	0.390	-4.450	3207.	8222.	16307.119000.	2870.	40642.	47200.	1.40	0.14	

UPPER SURFACE

SEF. NO.	SKIN THICK	SEG. AREA	STIFF AREA	DIST N.A.	SEG. LOAD	SEG. STRESS	SKIN STRESS	COMP. ALLOW	SHFAR FLOW	SHFAR STRESS	SHFAR ALLOW	M.S. COMP.	M.S. SHFAR
100	0.094	0.390	0.390	4.450	-3207.	-8222.	-16307.	73000.	3723.	40642.	47200.	0.09	0.14
105	0.093	4.770	2.190	4.850	-81264.	-17036.	-17790.	71000.	3089.	40780.	47200.	0.01	0.13
104	0.080	4.090	2.150	5.500	-79525.	-19444.	-20231.	60000.	2401.	38614.	47200.	0.00	0.19
103	0.067	3.680	1.820	6.170	-80684.	-21925.	-22727.	55000.	1702.	35832.	47200.	0.02	0.26
102	0.063	3.380	1.660	6.800	-81993.	-24258.	-25068.	53000.	993.	27020.	47200.	0.18	0.58
101	0.063	3.380	1.660	7.400	-89504.	-26480.	-27290.	53000.	218.	15754.	47200.	0.50	1.26
100	0.063	0.485	0.485	7.750	-6951.	-14333.	-28586.	53000.	158.	3456.	47200.	2.46	2.21

I X	I Z	I XZ	BAR ZF	BAR XF	I XF	I ZE	I XF ZF	2A Z	P Z	P X	T.C. VZ	T.C. VX	T.C. EQUIB
1339.	68355.	0.0	0.00	-73.33	1339.	68355.	0.0	3368	-5023.	0.	31591.	-0.	-1113730.

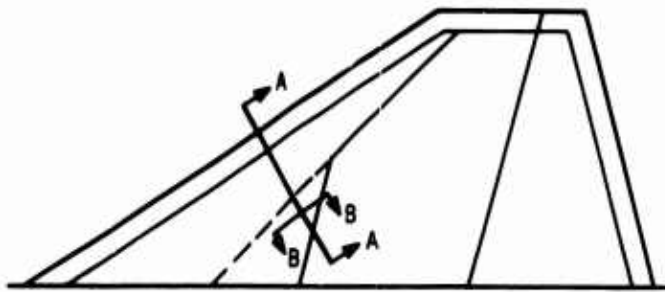
SEF. NO.	SKIN THICK	SEG. AREA	STIFF AREA	DIST N.A.	SEG. LOAD	SEG. STRESS	SKIN STRESS	TENS. ALLOW	SHFAR FLOW	SHFAR STRESS	SHFAR ALLOW	M.S. TENS.	M.S. SHFAR
0	0.063	0.485	0.485	-7.750	1794.	3699.	7377.119000.	2776.	44591.	47200.	1.46	0.05	
1	0.063	3.380	1.660	-7.400	23098.	6834.	7043.119000.	2632.	44388.	47200.	1.48	0.06	
2	0.063	3.380	1.660	-6.800	21160.	6260.	6469.119000.	2481.	41775.	47200.	1.64	0.13	
3	0.067	3.680	1.820	-6.170	20822.	5658.	5865.119000.	2333.	37030.	47200.	1.97	0.27	
4	0.075	4.090	2.020	-5.500	20523.	5018.	5221.119000.	2186.	31101.	47200.	2.52	0.91	
5	0.087	4.770	2.360	-4.850	20971.	4396.	4594.119000.	2037.	25130.	47200.	3.32	0.87	
99	0.094	0.390	0.390	-4.450	827.	2122.	4208.119000.	2031.	21669.	47200.	3.98	1.17	

UPPER SURFACE

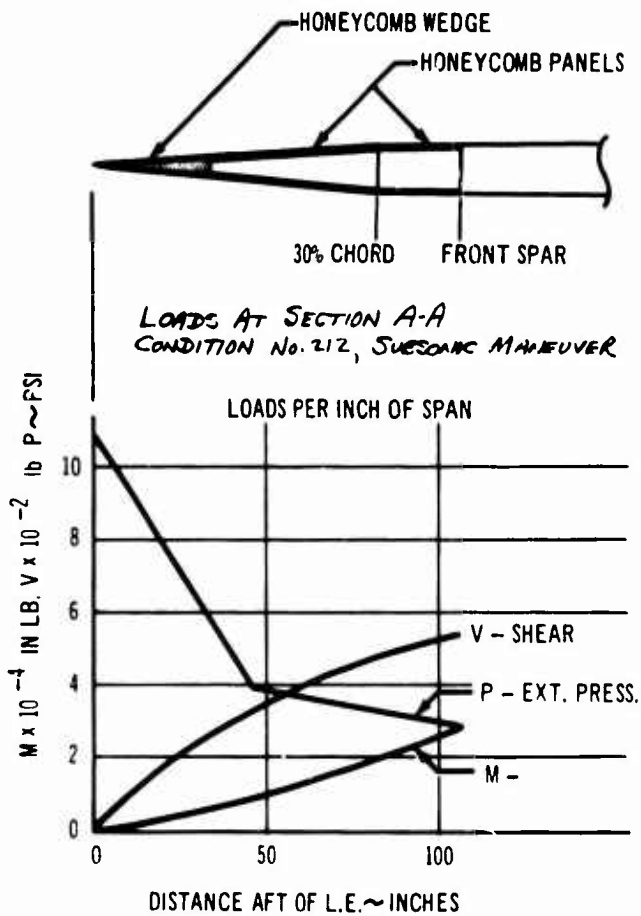
SEF. NO.	SKIN THICK	SEG. AREA	STIFF AREA	DIST N.A.	SEG. LOAD	SEG. STRESS	SKIN STRESS	COMP. ALLOW	SHFAR FLOW	SHFAR STRESS	SHFAR ALLOW	M.S. COMP.	M.S. SHFAR
100	0.094	0.390	0.390	4.450	-827.	-2122.	-4208.	73000.	2037.	21669.	47200.	1.11	1.17
105	0.093	4.770	2.190	4.850	-20971.	-4396.	-4591.	71000.	2186.	23509.	47200.	0.89	1.00
104	0.080	4.090	2.150	5.500	-20523.	-5018.	-5218.	60000.	2333.	29158.	47200.	0.51	0.61
103	0.067	3.680	1.820	6.170	-20822.	-5658.	-5865.	55000.	2481.	37030.	47200.	0.19	0.27
102	0.063	3.380	1.660	6.800	-21160.	-6260.	-6469.	53000.	2632.	41775.	47200.	0.06	0.13
101	0.063	3.380	1.660	7.400	-23098.	-6834.	-7043.	53000.	2776.	44388.	47200.	-0.01	0.06
100	0.063	0.485	0.485	7.750	-1794.	-3699.	-7377.	53000.	2809.	44591.	47200.	0.02	0.05

Figure 4-58. (Continued)

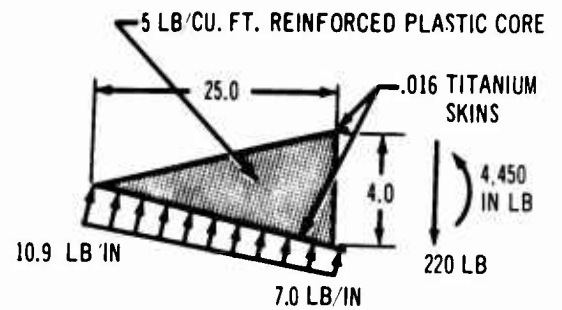
VERTICAL FIN LEADING EDGE



SECTION A-A



HONEY COMB WEDGE



$$\phi = \text{CHAMF SLOPE} = \tan^{-1} \frac{4}{25} = 4.6^\circ$$

TITANIUM FACING STRESS

$$\text{AVERAGE LOAD/IN} = \frac{M}{h \cos \phi} = \frac{4450}{4 \times .996} = 1120 \text{ lb/in}$$

$$\text{MAX LOAD DUE TO VARIATION IN BACKUP STIFFNESS} = 1.5 \times 1120 = 1680 \text{ lb/in}$$

CRITICAL FOR FACE WRINKLING  
ALLOWABLE STRESS = .75 Fcy

$$\text{M.S.} = \frac{12000 \times .75 \times .016}{1680} - 1 = +.10$$

WEDGE EDGE MEMBER BOND



$$\text{BOND STRESS} = \frac{1680}{.8} = 2100 \text{ psi}$$

ALLOWABLE STRESS = 2500 psi

$$\text{M.S.} = \frac{2500}{2100} - 1 = +.19$$

WEDGE TO PANEL ATTACHMENT



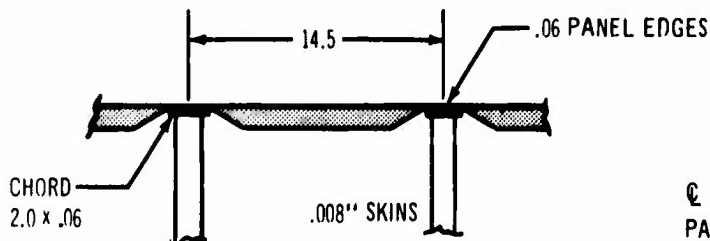
$$\text{BOLT LOAD} = 1120 \times 1 = 1120 \text{ lb}$$

ALLOWABLE LOAD = 1380 lb

$$\text{M.S.} = \frac{1380}{1120} - 1 = +.23$$

Figure 4-59. Fin Leading-Edge Stress Analysis

PANELS AND CHORDS (SECTION B-B)



1 IN. LONG 1\"/>
$$LOAD = \frac{A}{h} \times 145 = \frac{22500 \times 145}{73.5} = 4300^*$$

$$AREA = 11.5 \times .06 + 4 \times .06 = .44 \text{ IN}^2$$

$$COMPRESSION STRESS = \frac{23900}{.44} = 54300 \text{ PSI}$$

CRIPPLING ALLOWABLE (HULL)

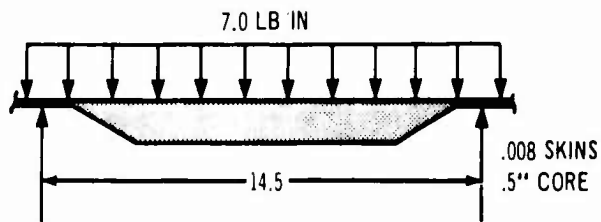
$$k_c = 1.0 / .06 = 16.7$$

$$F_{cc} = 55,000 \text{ PSI @ } 350^\circ\text{F}$$

$$M.S. = \frac{55000}{54300} - 1 = +.01$$

PANEL BENDING DUE TO AIRLOAD

CRITICAL AT 1\"/>

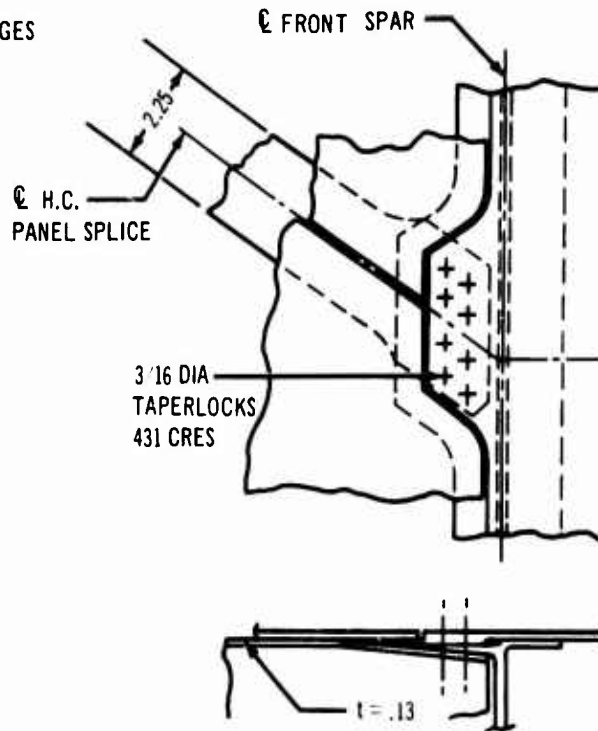


$$MOMENT ON 1" STRIP = \frac{7 \times 14.5^2}{8} = 184 \text{ IN}^2$$

$$FACE STRESS = \frac{184}{.5 \times .008} = 46,000 \text{ PSI}$$

NOT CRITICAL

ATTACHMENT OF LEADING EDGE TO FRONT SPAR



LOCKETS

ASSUME AIR HOLE CARRIES 10% OF LINE HOLE STRESS

$$LOAD = \frac{A}{h} \times 145 = \frac{7 \times 2740 \times 145}{14}$$

$$LOAD = 25600^*$$

$$LOAD/BLT = 25600 / 8 = 3200^* / \text{BLT}$$

$$ALLOWABLE LOAD/BLT = 3400^*$$

$$M.S. = \frac{3400}{3200} - 1 = +.06$$

RIB CHORD

$$CHORD STRESS = \frac{25600}{.5 \times .13} = 87500 \text{ PSI}$$

CRIPPLING ALLOWABLE

$$k_c = 1.1 \times 7 / .13 = 5.7$$

$$F_{cc} = 100,000 \text{ PSI @ } 350^\circ\text{F}$$

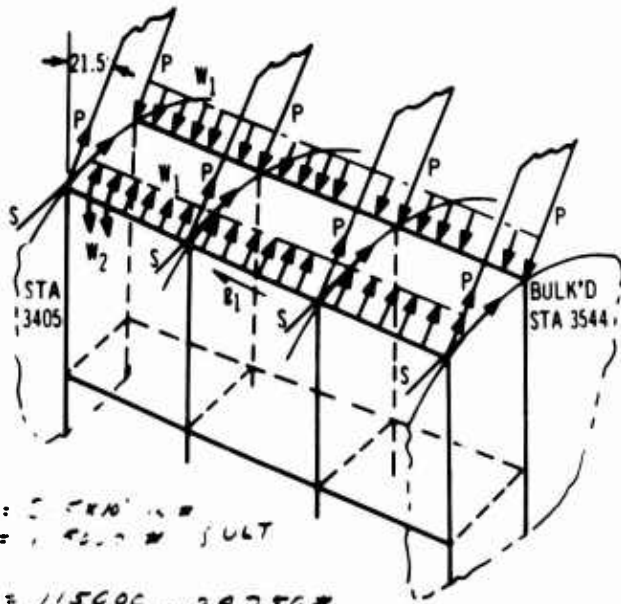
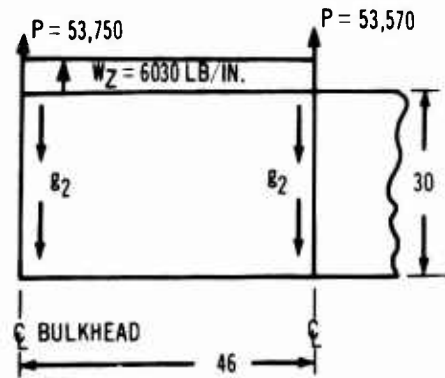
$$M.S. = \frac{100000}{87500} - 1 = +.05$$

Figure 4-59 (Continued)

### FIN TO BODY CONNECTION

FIN SHEAR WILL BE TAKEN EQUALLY BY THE FOUR SPARS. THE BENDING MOMENT WILL BE TAKEN BY THE COVERS AND THE SPARS IN AN 80-20 DISTRIBUTION RESPECTIVELY. THE FIN STUB WILL REDISTRIBUTE THESE LOADS TO THE BODY BULKHEADS.

### FIN STUB LOADS



$M = 2 \text{ FRONTS} \times \text{SULT}$   
 $V = 1 \text{ REAR} \times \text{SULT}$

$$S = \frac{115000}{4} = 28,750 \#$$

$$W_1 = \frac{60 \times 21.5 \times 10^6}{20 \times 133} = 6470 \#/\text{IN}$$

$$W_2 = 6470 \cos 21.5^\circ = 6030 \#/\text{IN}$$

$$W_3 = 6470 \sin 21.5^\circ = 2370 \#/\text{IN}$$

SPAR CAP LOADS

$$P = 20 \times 21.5 \times 10^6 = 53,750 \#$$

$$B_2 = \frac{6030 \times 46}{2 \times 30} = 4620 \#/\text{IN}$$

$$C = .09$$

$$Q_{\text{OUT}} = 4730 \#/\text{IN}$$

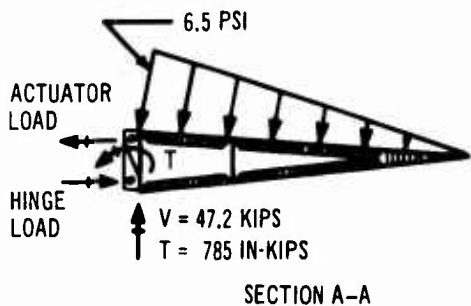
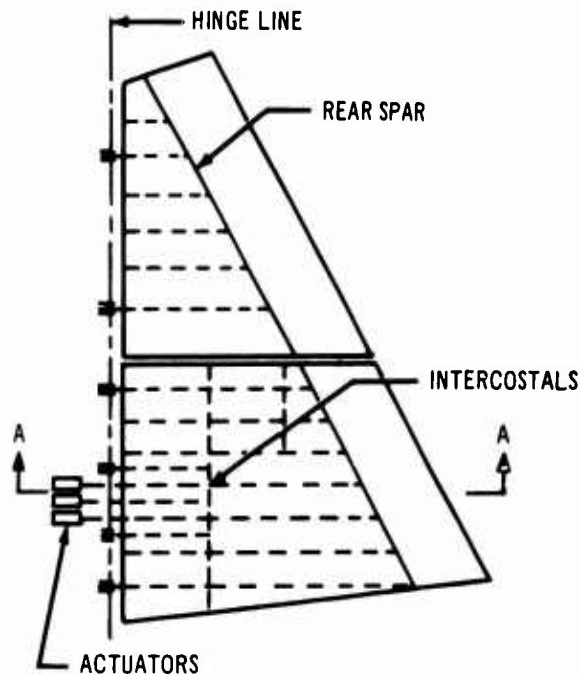
$$M.S. = \frac{4730}{4620} - 1 = .03$$

Figure 4-60. Stress Analysis of Fin-to-Fuselage Joints



CRITICAL CONDITION:

TRANSONIC MANEUVER,  $M = 1.2$ ,  
 RUDDER ANGLE =  $8^\circ$ .



STRENGTH ANALYSIS:

FRONT SPAR SHEAR WEB AT SECT. A-A

$$q = \frac{V}{h} - \frac{T}{2A}$$

$$= \frac{47.2}{18.8} - \frac{785}{2 \times 1960} = 2.31 \text{ KIPS/IN.}$$

MAT'L = T<sub>1</sub>-6AL-4V, COND. I

FOR  $T = 400^\circ\text{F}$

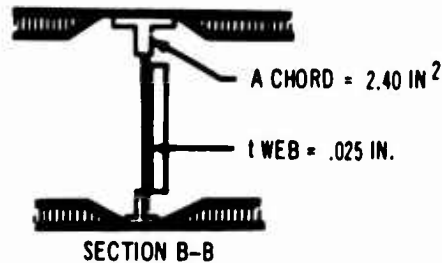
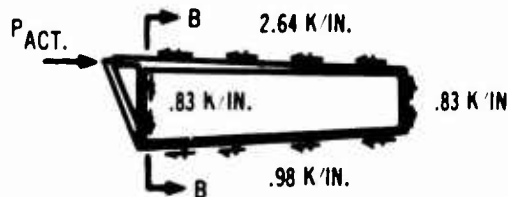
$$F_b = .49 \times F_{tu} \times .82 = 53.7 \text{ KSI}$$

FOR  $t = .045$ "

$$q_{\text{ALLOW.}} = 53.7 \times .045 = 2.41 \text{ K/IN}$$

$$\text{M.S.} = \frac{2.41}{2.31} - 1 = \underline{+0.04}$$

TYPICAL ACTUATOR RIB



SHEAR WEB AT SECT. B-B

$$t = .025 \text{ IN.}$$

$$q = 0.83 \text{ K/IN.}$$

$$q_{\text{ALLOW.}} = 53.7 \times .025 = 1.34 \text{ K/IN.}$$

$$\text{M.S.} = \frac{1.34}{0.83} - 1 = \underline{+0.60}$$

RIB CHORD AT SECT. B-B

CHORDS ARE DESIGNED FOR 2.5 FACTORS ON ONE ACTUATOR LOAD CAPACITY.

$$P_{\text{ACT.}} = 275 \text{ KIPS}$$

Figure 4-61. Rudder Stress Analysis

V2-B2707-6-2

TENSILE STRESS

$$f_t = \frac{P_{ACT.}}{A_{CHORD}} = \frac{275}{2.40} = 115 \text{ KSI}$$

MAT'L = Ti-6AL-4V EXTRUSION,  
COND. IV

FOR 15% AREA OUT

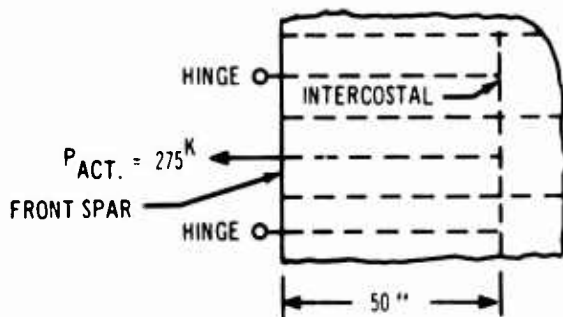
$$F_t = 0.85 \times 136 = 115 \text{ KSI}$$

$$M.S. = \frac{115}{115} - 1 = \underline{0.0}$$

COVER PANEL

HONEYCOMB SANDWICH PANELS  
NEAR THE ACTUATORS ARE  
DESIGNED FOR 2.5 FACTORS  
ON THE LOAD CAPACITY OF  
ONE ACTUATOR.

$$P_{ACT.} = 275 \text{ KIPS}$$



THE 275<sup>K</sup> LOAD IS REACTED  
IN THE 50 IN. FORWARD  
CELL.

$$q = \frac{275}{100 \times 50} = 2.75 \text{ K/IN.}$$

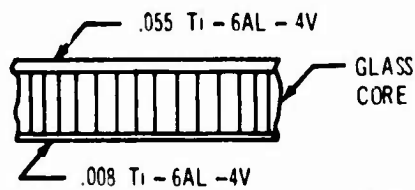


Figure 4-61. (Concluded)

$$f_s = \frac{2.75}{.055 + .008} = 43.7 \text{ KSI}$$

TENSILE STRESS INDUCED  
FROM RIB BENDING

$$f_t = 115 \text{ KSI}$$

MAX. PRINCIPAL SHEAR STRESS

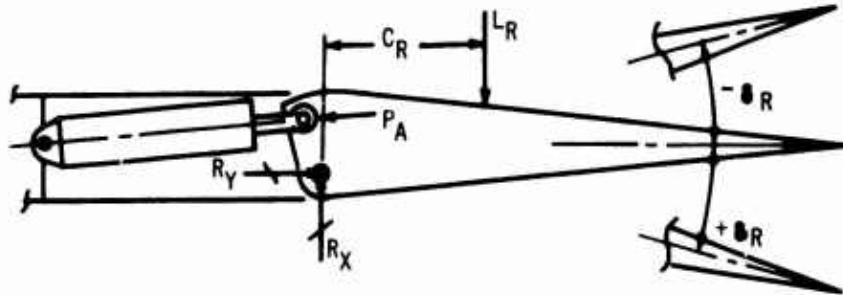
$$\tau = \sqrt{\left(\frac{115}{2}\right)^2 + (43.7)^2} = 72.2 \text{ KSI}$$

FOR Ti-6AL-4V, COND. I  
AT 70° F,

$$F_{SU} = 79 \text{ KSI}$$

$$\therefore M.S. = \frac{79}{72.2} - 1 = \underline{+0.07}$$

RUDDER CONTROL SYSTEM LOADS  
(UPPER & LOWER RUDDER)



TYPICAL ACTUATOR LOADS & HINGE REACTIONS  
(3 ACTUATORS & 6 HINGES)

CONDITION		SUBSONIC YAW INITIATION	TRANSONIC YAW INITIATION
		M = .90 Ve = 350	M = 1.2
$\theta_R$	DEGREES	-15	-8
$L_R$ (UPPER)	KIPS ULT.	28.8	—
$C_R$ (UPPER)	INCHES	30	—
$L_R$ (LOWER)	KIPS ULT.	63.4	—
$C_R$ (LOWER)	DEGREES	45	—
HINGE MOMENT	IN-KIP ULT.	3,715	7,000
$P_A$ LOAD/ACT	KIPS ULT.	98.2	181.2
$R_X$ LOAD/HINGE (MAX)	KIPS ULT.	24.3	47.0
$R_Y$ LOAD/HINGE (MAX)	KIPS ULT.	145.0	268.0

ULTIMATE HINGE MOMENT LIMITED TO 7,000 IN-KIPS. HIGHER MOMENTS WILL RESULT IN A RELIEF VALVE OPENING, AND THE ACTUATOR WILL BLOW BACK UNTIL A MOMENT OF 7,000 IN-KIPS IS REACHED.

Figure 4-62. Rudder Actuator and Hinge Loads

## 4.5 LANDING GEAR STRESS ANALYSIS

### 4.5.1 Landing Gear Analysis

Stress analysis and loads are presented for the main and nose landing gear. Typical component section analyses are presented to show cross-section sizes and design approaches.

A complete landing gear arrangement and design discussion is presented in Par. 3.6. The B-2707 utilizes a conventional dual-wheel nose gear and four truck-type main gears, each similar to existing 707 and 720 gears. The forward and outboard main gears are supported from the front spar of the wing pivot box and the aft inboard main gears from the rear spar to provide a short load path to existing rigid structure. The aft main gear on one side of the airplane is hydraulically connected to the forward main gear on the same side, resulting in equal vertical loads on these two gears. This hydraulic manifold has a 6-in. travel. Because the manifold is stroke limited, loss of manifold pressure results only in the two main gears on that side compressing 6 in. in length and forming conventional gears. Besides the obvious fail-safe and flotation advantages, this gear arrangement will improve passenger ride and reduce fatigue damage caused by taxiing over uneven pavement.

Analysis methods developed for the 747, which has a similar landing gear configuration, were used for the B-2707. The main-gear shock strut strokes have been selected for improved structural efficiency. Landing impact loads are primarily reacted on the 40-in. stroke aft main gears, which extend below the shorter-stroke forward main gears at normal touchdown. The forward main gears have the capability of absorbing the landing impact of a 6 ft/sec descent velocity emergency landing without the use of rear main gears.

Drop tests will demonstrate the energy-absorbing capabilities and substantiate the landing load factors. Static and fatigue tests of the complete gear will verify structural integrity. Photostress testing on full-size plastic models will be used during the design phase to define and eliminate areas of high stress and to optimize weight. A complete description of the landing gear test program is in V2-B2707-9.

### 4.5.2 Design Ultimate Ground Loads

The design ultimate ground loads are calculated according to the criteria of V2-B2707-7.

Most of the primary nose-gear structure is designed by landing loads. The axles are critical for the nose-gear yaw conditions and the drag brace for forward towing.

The aft main-gear axles, truck beam, side strut, and part of the inner and outer cylinders are designed by ground turn. Parts of the inner cylinder and the drag brace are critical for landing loads. The outer cylinder is partially designed by the pivoting condition.

The forward main gear components are critical for the same conditions as the aft main gear except for the drag brace and inner cylinder, which are designed by braked roll and ground turn. Because of its short stroke and relative position, the forward main gear is not critical for landing conditions.

General arrangement diagrams for the nose, aft, and forward main gears are shown in Figs. 4-63, 4-64, and 4-65. The critical design ultimate loads and internal reactions are shown in Tables 4-E, 4-F, and 4-G.

### 4.5.3 Material and Allowable Stress

The landing gear is designed primarily of 4340M vacuum arc remelted steel, which is procured to an exacting Boeing material specification, and heat treated to 270 ksi. Titanium will be used in some locations. This material is selected because of its excellent strength and fracture toughness (Phase III document V2-B2707-8). Allowable design stresses are according to Ref. 7.

### 4.5.4 Nose Landing Gear

The nose landing gear analysis is presented in Fig. 4-66.

### 4.5.5 Aft Main Landing Gear Analysis

The aft main landing gear analysis is presented in Fig. 4-67.

### 4.5.6 Forward Main Landing Gear

The forward main landing gear analysis is presented in Fig. 4-68.

NOTE: POSITIVE LOADS  
AND REACTIONS  
ACTING AS SHOWN

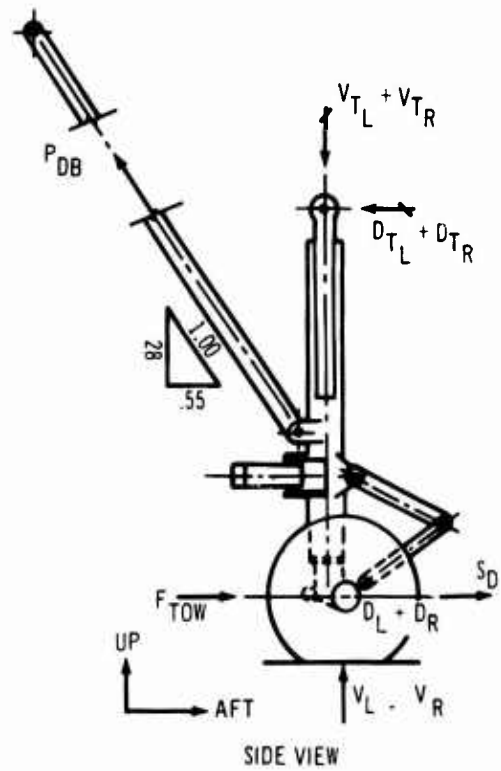
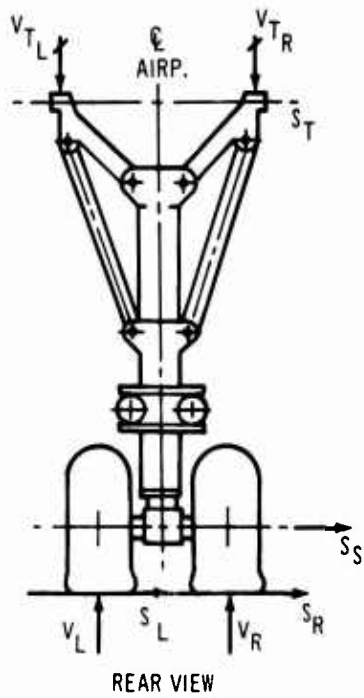
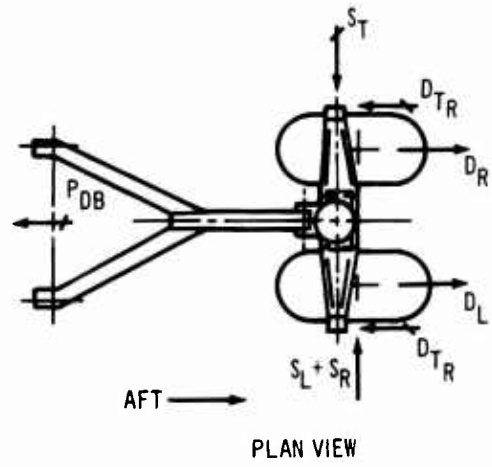


Figure 4-63. Nose-Landing-Gear General Arrangement

NOTE: POSITIVE LOADS AND REACTIONS ARE ACTING AS SHOWN

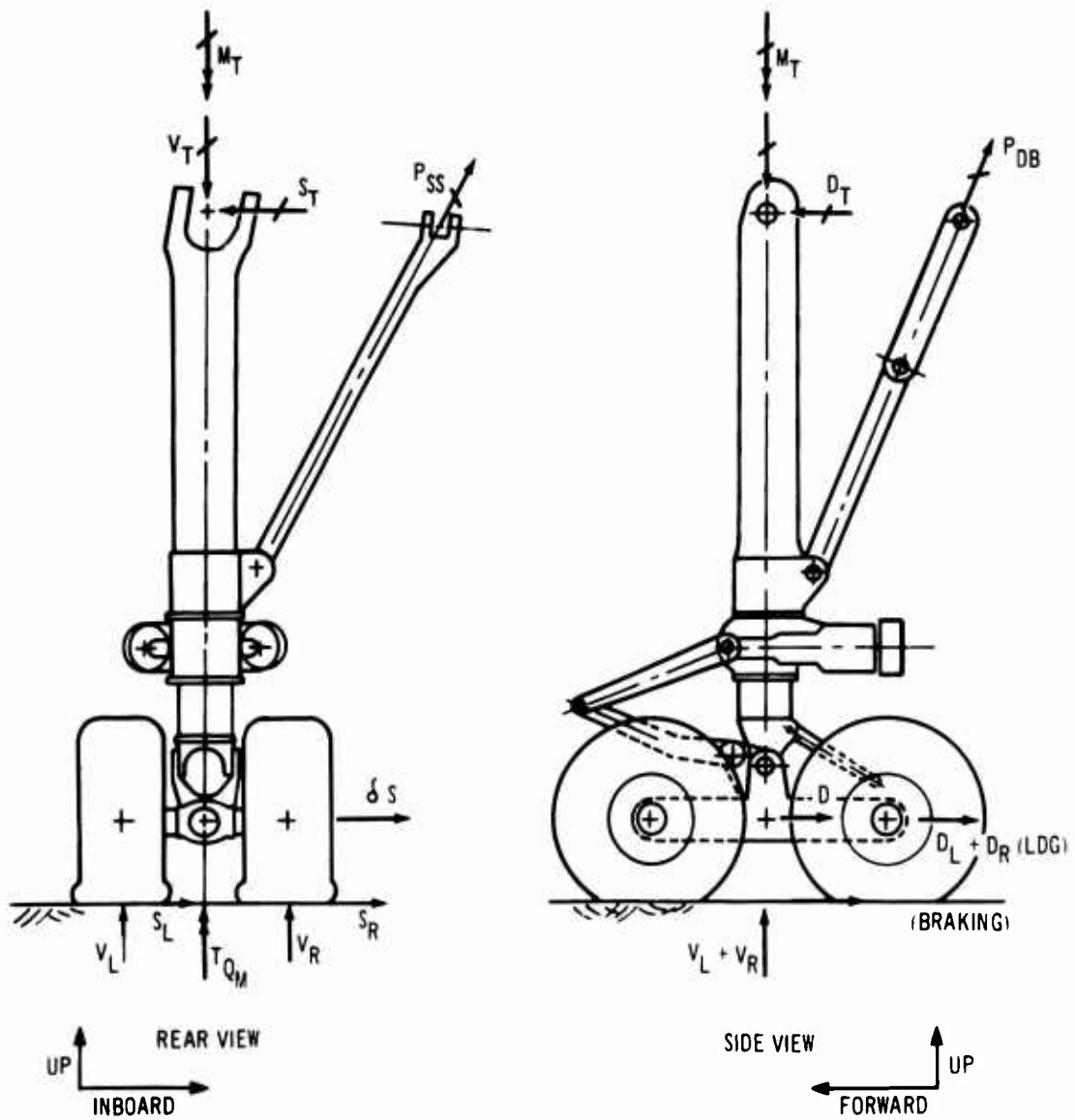


Figure 4-64. Aft-Main-Landing-Gear General Arrangement

V2-132707-62

NOTE: POSITIVE LOADS AND REACTIONS ARE ACTING AS SHOWN

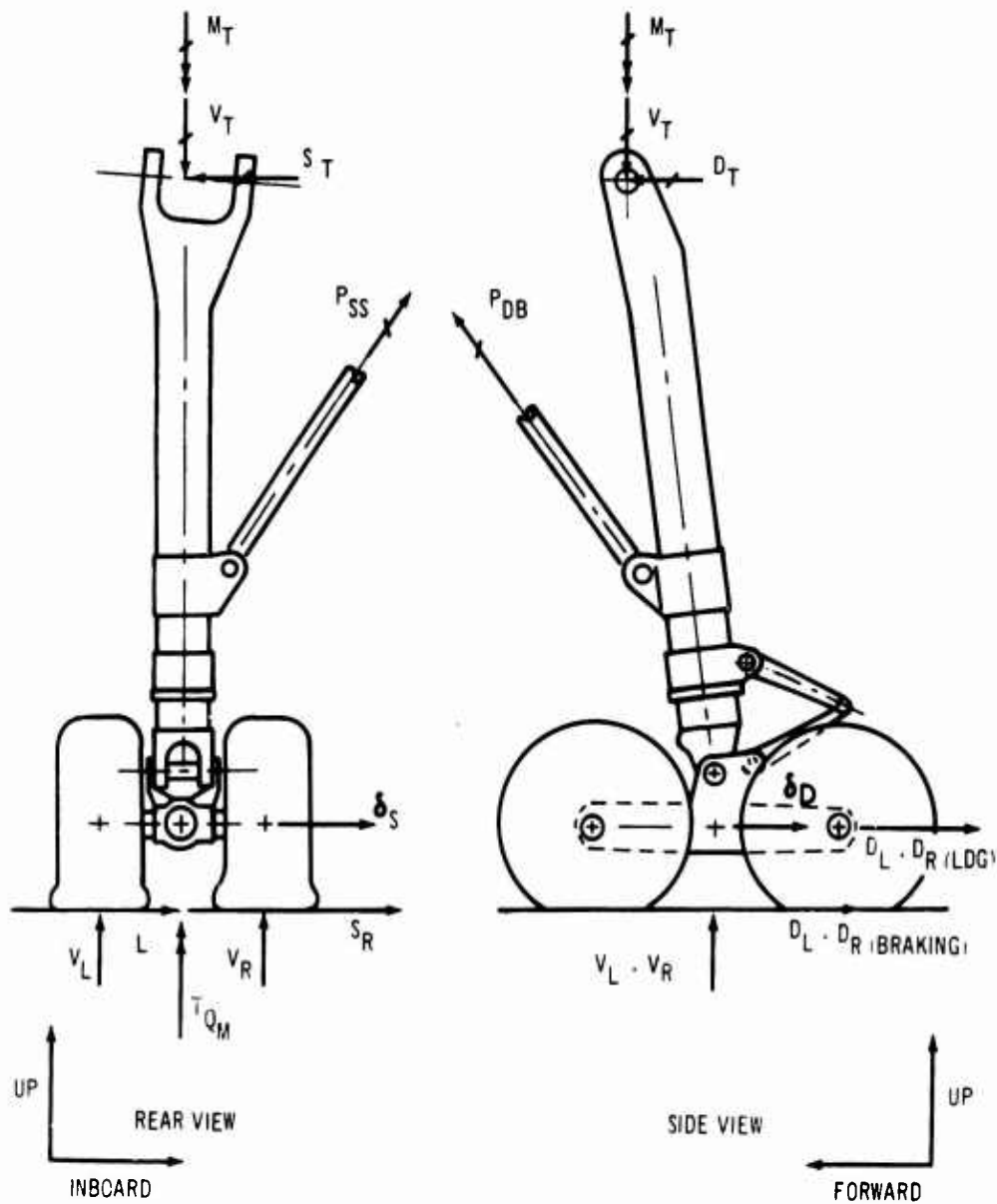


Figure 4-65. Forward-Main-Landing-Gear General Arrangement

Table 4-E. Nose-Landing-Gear Ultimate Reactions

CONDITION	DIST.	V <sub>L</sub>	V <sub>R</sub>	D <sub>L</sub>	D <sub>R</sub>	S <sub>L</sub>	S <sub>R</sub>	S <sub>D</sub>	S <sub>S</sub>	P <sub>DB</sub>	V <sub>TL</sub>	V <sub>TR</sub>	D <sub>TL</sub>	D <sub>TR</sub>	S <sub>T</sub>
YAW UNSYM. BRAKING	S-S	59	59	0	0	13	13	0	2.0	13	0	178	-2	-6	26
	F-O	95	0	0	0	14	0	0	0	10	49	54	-2	-4	14
	O-F	0	95	0	0	0	14	0	2.0	10	-14	117	-2	-4	14
YAW-STATIC	S-S	36	36	0	0	29	29	0	4.0	8	-99	177	3	-7	58
	F-O	72	0	0	0	29	0	0	2.0	8	-8	86	1	-5	29
	O-F	0	72	0	0	0	29	0	3.0	8	-54	132	1	-5	29
3 POINT BRAKED ROLL	S-S	79	79	0	0	0	0	0	0	17	86	86	-5	-5	0
	6-4	94	63	0	0	0	0	0	0	17	96	77	-5	-5	0
	4-6	63	94	0	0	0	0	0	0	17	77	96	-5	-5	0
	F-O	116	0	0	0	0	0	0	-1.0	13	102	25	-4	-4	0
	O-F	0	116	0	0	0	0	0	1.0	13	25	102	-4	-4	0
TOWING-FORWARD	S-S	36	36	F <sub>TOW</sub> = 152		0	0	-6.0	0	-384	-122	-122	30	30	0
	6-4	43	29	= 152		0	0	-6.0	0	-384	-117	-126	30	30	0
	4-6	29	43	= 152		0	0	-6.0	0	-384	-126	-117	30	30	0
	F-O	72	0	= 91		0	0	-4.0	-1.0	-278	-34	-81	16	19	0
	O-F	0	72	= 91		0	0	-4.0	1.0	-278	-81	-34	19	16	0
TOWING-LEFT	S-S	36	36	F <sub>TOW</sub> = 152		0	0	6.0	0	399	200	200	-34	-34	0
	6-4	43	29	= 152		0	0	6.0	0	399	204	196	-34	-34	0
	4-6	29	43	= 152		0	0	6.0	0	399	196	204	-34	-34	0
	F-O	72	0	= 91		0	0	4.0	-1.0	243	160	112	-20	-23	0
	O-F	0	72	= 91		0	0	4.0	1.0	243	112	160	-23	-20	0
TOWING-SIDE	S-S	36	36	0	0	F <sub>TOW</sub> = 54		0	5.0	0	-83	155	0	0	54
	6-4	43	29	0	0	= 54		0	5.0	6	-81	157	-2	-2	54
	4-6	29	43	0	0	= 54		0	5.0	-6	-85	153	2	2	54
	F-O	72	0	0	0	= 33		0	2.0	29	-26	121	-8	-8	33
	O-F	0	72	0	0	= 33		0	4.0	-29	-52	101	8	8	33
BOEING CONDITION +SPIN-UP	S-S	76	76	53	53	0	0	5.0	0	350	220	220	-44	-44	0
	6-4	91	61	64	64	0	0	5.0	0	350	229	211	-50	-37	0
	4-6	61	91	64	64	0	0	5.0	0	350	211	229	-37	-50	0
	F-O	91	0	64	0	0	0	3.0	-1.0	207	199	103	-4	-46	0
	O-F	0	91	0	64	0	0	3.0	1.0	207	103	199	-46	-4	0
BOEING CONDITION +SPIN-UP BACK	S-S	76	76	-38	-38	0	0	-4.0	0	-221	-18	-18	29	29	0
	6-4	91	61	-45	-30	0	0	-4.0	0	-221	-8	-27	19	29	0
	4-6	61	91	-30	-45	0	0	-4.0	0	-221	-27	-8	29	19	0
	F-O	91	0	-45	0	0	0	-3.0	-1.0	-130	-22	-38	2	28	0
	O-F	0	91	0	-45	0	0	-3.0	1.0	-130	-38	-22	28	2	0

NOTE: ALL LOADS & REACTIONS ARE IN KIIPS  
 ALL DEFLECTIONS (S<sub>D</sub>, S<sub>S</sub>) ARE IN INCHES.  
 ALL SIDE LOADS ARE REVERSIBLE.



Table 4-F. Aft-Main-Gear Ultimate Reactions

CONDITION	DIST.	V <sub>L</sub>	V <sub>R</sub>	D <sub>L</sub>	D <sub>R</sub>	S <sub>L</sub>	S <sub>R</sub>	T <sub>GM</sub>	δ <sub>0</sub>	δ <sub>3</sub>	P <sub>DB</sub>	P <sub>SS</sub>	V <sub>T</sub>	D <sub>T</sub>	S <sub>T</sub>	M <sub>T</sub>
TAKE OFF TAXI	5-5	243	243	0	0	0	0	0	0	0	0	0	486	0	0	0
	6-4	292	194	↑	↑	↑	↑	↑	↑	↑	4	38	523	↑	18	↑
	4-6	194	292	↓	↓	↓	↓	↓	↓	↓	-4	-38	449	↓	-18	↓
	F-0	243	0	↑	↑	↑	↑	↑	↑	↑	10	97	357	↑	46	↑
	0-F	0	243	↓	↓	↓	↓	↓	↓	↓	-10	-97	149	↓	-46	↓
2 POINT BRAKED ROLL	5-5	127	127	88	88	0	0	0	5.0	0	-693	-40	-418	-93	6	0
	6-4	152	101	88	70	↑	↑	↑	4.5	↑	-622	-16	-304	-83	14	340
	4-6	101	152	70	88	↓	↓	↓	4.5	↓	-625	-57	-371	-83	-5	-340
	F-0	253	0	88	0	↑	↑	↑	2.5	↑	-338	81	14	-47	47	1670
	0-F	0	253	0	88	↓	↓	↓	2.5	↓	-358	-121	-182	-47	-46	-1670
GROUND TURN	5-5	238	238	0	0	119	119	2620	0	4.0	-88	826	-335	-3	-157	2620
	0-F	90	270	0	0	30	60	2080	0	2.0	-41	-365	50	-1	-94	2080
	0-2F	0	336	0	0	0	67	1340	0	1.5	-39	-367	22	-1	-108	1340
+ PIVOT	5-5	122	122	0	0	0	0	6580	0	0	0	0	244	0	0	6580
	6-4	146	97	0	0	0	0	6580	0	0	2	19	264	0	9	6580
	4-6	97	146	0	0	0	0	6580	0	0	-2	-19	224	0	-9	6580
- PIVOT	5-5	122	122	0	0	0	0	6580	0	0	0	0	244	0	0	-6580
	6-4	146	97	0	0	0	0	6580	0	0	2	19	264	0	9	-6580
	4-6	97	146	0	0	0	0	6580	0	0	-2	-19	224	0	-9	-6580
REVERSE BRAKING	5-5	122	122	-67	-67	0	0	0	-4.0	0	527	30	754	70	-4	0
	6-4	146	97	-67	-54	0	0	0	-3.5	0	526	49	717	64	7	-250
	4-6	97	146	-54	-67	0	0	0	-3.5	0	522	12	670	64	-11	250
2 POINT LEVEL +SPIN-UP	5-5	128	128	91	91	0	0	0	6.0	0	-723	-42	-446	-98	5	0
	6-4	153	102	109	73	↑	↑	↑	6.0	0	-720	-21	-424	-98	15	690
	4-6	102	153	73	109	↓	↓	↓	6.0	0	-724	-62	-464	-98	-5	-690
	F-0	153	0	109	0	↑	↑	↑	3.5	-1.5	-416	42	-192	-55	-6	1910
	0-F	0	153	0	109	↓	↓	↓	3.5	1.5	-431	-94	-325	-55	-30	-1910
TAIL DOWN +SPIN-UP	5-5	138	138	61	61	0	0	0	4.0	0	-487	-28	-197	-67	4	0
	6-4	165	111	73	49	↑	↑	↑	4.0	0	-484	-7	-165	-67	14	460
	4-6	111	165	49	73	↓	↓	↓	4.0	0	-485	-50	-210	-67	-7	-460
	F-0	165	0	73	0	↑	↑	↑	2.5	-1.0	-217	56	-40	-38	37	1310
	0-F	0	165	0	73	↓	↓	↓	2.5	1.0	-293	-89	-183	-38	-33	-1310
TAIL DOWN +SPRING- BRK	5-5	126	126	-85	-85	0	0	0	-5.5	0	675	39	907	92	-5	0
	6-4	151	100	-102	-68	↑	↑	↑	-5.5	0	678	60	928	92	5	-650
	4-6	100	151	-68	-102	↓	↓	↓	-5.5	0	673	19	888	92	-15	650
	F-0	151	0	-102	0	↑	↑	↑	-3.5	-1.0	404	89	600	52	29	-2040
	0-F	0	151	0	-102	↓	↓	↓	-3.5	1.0	390	-43	471	52	-35	2040
DRIFT - RIGHT	5-5	64	64	-32	-32	51	51	0	-2.0	2.0	211	-330	32	31	-63	-130
	6-4	77	51	-38	-25	61	41	0	-2.0	2.0	212	-320	41	30	-58	-160
	0-F	0	77	0	-38	0	61	0	-2.0	2.0	129	-229	-13	18	-52	-170
DRIFT - LEFT	5-5	64	64	-32	-32	-39	-39	0	-2.0	-2.0	276	277	624	32	44	30
	4-6	51	77	-25	-38	-30	-47	0	-2.0	-2.0	277	267	634	33	49	-90
	F-0	77	0	-38	0	-47	0	0	-2.0	-2.0	167	199	345	19	13	-170

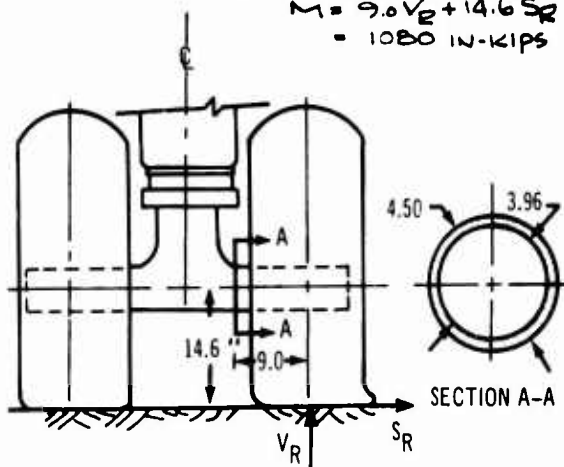
NOTE: ALL LOADS & REACTIONS ARE IN KIPS & INCH-KIPS  
ALL DEFLECTIONS (δ<sub>0</sub>, δ<sub>3</sub>) ARE IN INCHES.

Table 4-G. Forward-Main-Gear Ultimate Reactions

CONDITION	DIST.	V <sub>L</sub>	V <sub>R</sub>	D <sub>L</sub>	D <sub>R</sub>	S <sub>L</sub>	S <sub>R</sub>	TQ <sub>M</sub>	δ <sub>D</sub>	δ <sub>S</sub>	P <sub>DB</sub>	P <sub>SS</sub>	V <sub>T</sub>	D <sub>T</sub>	S <sub>T</sub>	M <sub>T</sub>
TAKE OFF TAXI	5-5	243	243	0	0	0	0	0	0	0	197	29	668	-121	-2	0
	6-4	292	194	↑	↑	↑	↑	↑	↑	↑	200	61	695	-126	17	↑
	4-6	194	292	↑	↑	↑	↑	↑	↑	↑	195	-3	640	-117	-21	↑
	F-0	243	0	↓	↓	↓	↓	↓	↓	↓	105	93	482	-72	45	↓
	0-F	0	243	0	0	0	0	0	0	0	98	-64	270	-53	-47	0
2 POINT BRAKED ROLL	5-5	127	177	88	88	0	0	0	5.0	0	703	104	900	-255	-7	0
	6-4	152	101	88	70	↑	↑	↑	4.5	↑	643	111	858	-238	4	340
	4-6	101	152	70	88	↑	↑	↑	4.5	↑	640	78	829	-233	-16	-340
	F-0	253	0	88	0	↑	↑	↑	2.5	↑	409	141	695	-171	44	1670
	0-F	0	253	0	88	↑	↑	↑	2.5	↑	376	-22	553	-148	-51	-1670
GROUND TURN	5-5	238	238	0	0	119	119	2620	0	4.0	139	-649	61	-29	-159	7380
	0-F	90	270	0	0	30	60	2080	0	2.0	122	-273	235	-44	-83	3880
	0-F	0	336	0	0	0	67	1340	0	1.5	112	-278	201	-42	-108	2680
+ PIVOT	5-5	122	122	0	0	0	0	6580	0	0	100	15	336	-61	-1	6580
	6-4	146	97	0	0	0	0	6580	0	0	100	31	349	-59	9	6580
	4-6	97	146	0	0	0	0	6580	0	0	98	-2	321	-58	-11	6580
- PIVOT	5-5	122	122	0	0	0	0	6580	0	0	100	15	336	-61	-1	6580
	6-4	146	97	0	0	0	0	6580	0	0	100	31	349	-59	9	6580
	4-6	97	146	0	0	0	0	6580	0	0	98	-2	321	-58	-11	6580
REVERSE BRAKING	5-5	122	122	-67	-67	0	0	0	-4.0	0	-358	-53	-85	86	-66	0
	6-4	146	97	-67	-54	0	0	0	-3.5	0	-312	-31	-31	89	12	250
	4-6	97	146	-54	-67	0	0	0	-3.5	0	-314	-62	-58	74	-7	250
2 POINT LEVEL +SPIN-UP	5-5															
	6-4															
	4-6															
	F-0															
	0-F															
TAIL DOWN +SPIN-UP	5-5															
	6-4															
	4-6															
	0-F															
TAIL DOWN +SPIN-UP BACK	5-5															
	6-4															
	4-6															
	0-F															
DRIFT - RIGHT	5-5															
	0-F															
DRIFT - LEFT	5-5															
	0-F															
<p><b>NOTE:</b> FORWARD MAIN GEAR IS NOT CRITICAL FOR ANY NORMAL LANDING LOADS.</p>																
<p><b>NOTE:</b> ALL LOADS &amp; REACTIONS ARE IN KIPS &amp; INCH-KIPS. ALL DEFLECTIONS (δ<sub>D</sub>, δ<sub>S</sub>) ARE IN INCHES.</p>																

STRESS ANALYSIS  
NOSE GEAR AXLE  
 SECTION A-A

CONDITION: NOSE GEAR YAW-  
 STATIC + FLAT TIRE.  
 LOADS:  $V_R = 72.0$  } REF. TABLE  
 $S_R = 29.0$  } 4-E  
 $M = 9.0V_R + 14.6S_R$   
 $= 1080$  IN-KIPS



SECTION PROPERTIES:  
 O.D. = 4.50 AREA = 3.6  
 I.D. = 3.96  $D/t = 10.7$

MATERIAL & ALLOWABLES:  
 4340M STEEL @ 270 KSI  
 $F_{TU} = 270$  KSI  
 $\frac{M}{D^3} = 13.0$  (REF. 8)

STRESS & M.S.

$$\frac{M}{D^3} = \frac{1080}{4.5^3} = 12.0$$

$$f_T = \frac{S_R}{AREA} = \frac{29.0}{3.6} = 8.1 \text{ KSI}$$

$$M.S. = \frac{1}{R_b + R_T} - 1$$

$$= \frac{1}{\frac{12.0}{13.0} + \frac{8.1}{270.0}} - 1$$

$$= +.04 \leftarrow$$

STRESS ANALYSIS  
NOSE GEAR INNER CYLINDER  
 SECTION AT & LOWER BEARING

CONDITION:  
 BOEING CONDITION LANDING  
 + SPIN-UP - 60-40 DIST.

LOADS:  
 $V_L = 91.0$  } REF TABLE  
 $V_R = 61.0$  } 4-E  
 $D_L = 64.0$   
 $D_R = 42.0$

$$M_s = (4.0 + \delta_0)(V_L + V_R) + 21.85(D_L + D_R)$$

$$= (4.0 + 5.0)(152) + 21.85(106)$$

$$= 3690$$

$$M_b = 15.00(V_L - V_R)$$

$$= 15.00(91 - 61)$$

$$= 450$$

$$M_R = M_s + M_b$$

$$= 3690 + 450$$

$$= 3700 \text{ IN-KIP}$$

SECTION PROPERTIES:

O.D. = 7.00 AREA = 8.2  
 I.D. = 6.22  $D/t = 18.0$

MATERIAL & ALLOWABLES  
 4340M STEEL @ 270 KSI  
 $F_{TU} = 270$  KSI  
 $\frac{M}{D^3} = 12.0$  (REF. 8)

STRESS & M.S.

$$\frac{M}{D^3} = \frac{3700}{7^3} = 10.8$$

$$f_c = \frac{V_L + V_R}{AREA} = \frac{152}{8.2} = 18.6$$

$$M.S. = \frac{1}{R_b + R_c} - 1$$

$$= \frac{1}{\frac{10.8}{12.0} + \frac{18.6}{270.0}} - 1$$

$$= +.02 \leftarrow$$

Figure 4-66. Nose-Landing-Gear Analysis

**STRESS ANALYSIS**  
**NOSE GEAR OUTER CYLINDER**  
**SECTION AT UPPER BRG. (LDG)**

**CONDITION:**  
 BOEING LANDING + SPIN-UP 60-60

**LOADS:**  
 $V_L = 91.0$   
 $V_R = 61.0$   
 $D_L = 64.0$   
 $D_R = 42.0$   
 $S_L = S_R = 0$   
 $\delta_0 = 5.0"$

REF. TABLE  
 4-E

$$M_s = 42.75(D_L + D_R) + (A_0 + \delta_0)(V_L + V_R)$$

$$= 5900 \text{ IN-K}$$

$$M_D = 15.00(V_L - V_R) = 450 \text{ IN-K}$$

$$M_E = M_s + M_D = 5950 \text{ IN-K}$$

$$M_V = 15(D_L - D_R) = 330 \text{ IN-K}$$

P = INTERNAL PRESSURE  
 $= \frac{V_L + V_R}{\text{AREA}} = \frac{91 + 61}{.786(7.30)^2} = 36 \text{ KSI}$

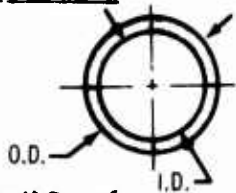
**SECTION PROPERTIES**

$$O.D. = 8.70$$

$$I.D. = 7.30$$

$$D/t = 18.2$$

$$t = .45$$



**MATERIALS & ALLOWABLES**

4340M STEEL @ 270 KSI

$$M/D_3 = 12.0 \text{ } \left. \begin{array}{l} \text{REF. B} \\ \text{TQ/D_3} = 11.5 \end{array} \right\}$$

$$F_{TU} = 270 \text{ KSI}$$

**STRESS & M.S.**

$$M/D_3 = \frac{M_E}{8.2} = 10.9 \quad R_b = .912$$

$$TQ/D_3 = \frac{M_V}{8.2} = 0.6 \quad R_{VT} = .052$$

$$f_{INT.} = \frac{P(O.D.)}{2t} = 32.7 \quad R_{INT} = .121$$

$$M.S. = \frac{1}{[R_b^2 + R_{VT}^2 + R_{INT}^2 - R_{INT}(R_b)]^{.5}}$$

$$= +.02 \leftarrow$$

**STRESS ANALYSIS**  
**NOSE GEAR UPPER SIDE STRUT**  
**SECTION 24.0" FROM TRUNION**

**CONDITION:**  
 BOEING LANDING + SPIN-UP 60-60

**LOADS:**

$$V_T = 229.0$$

$$S_T = 0$$

$$D_T = -50.0$$

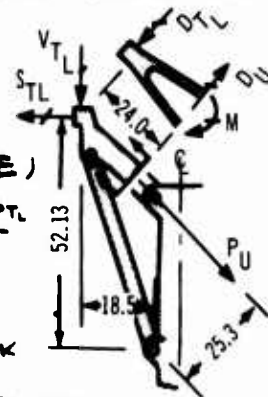
(REF. TABLE 4-E)

$$P_U = \frac{18.5V_T + 52.15S_T}{25.30}$$

$$= 167.0$$

$$M = 24.0 D_T$$

$$= -1200 \text{ IN-K}$$



**SECTION PROPERTIES**

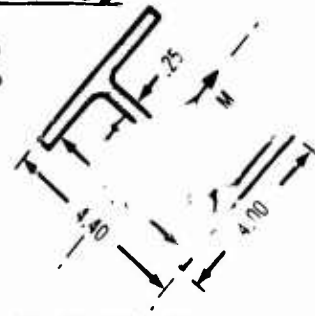
$$\text{AREA} = 3.40$$

$$I_{x-x} = 11.30$$

$$K = \frac{2Q}{3/c} = 1.10$$

$$Q = 2.31$$

$$c = 2.20$$



**MATERIALS & ALLOWABLES**

4340M STEEL @ 270 KSI

$$F_{TU} = 270 \text{ KSI}$$

$$F_b = 292 \text{ KSI (FOR } K = 1.10)$$

**STRESS & M.S.**

$$f_b = \frac{M_c}{I} = \frac{(1200)(2.20)}{11.30} = 234 \text{ KSI}$$

$$f_T = \frac{P_U}{\text{AREA}} = \frac{167}{3.40} = 49.0 \text{ KSI}$$

$$M.S. = \frac{1}{R_b + R_T} - 1$$

$$= \frac{1}{\frac{234}{292} + \frac{49}{270}} - 1$$

$$= +.02 \leftarrow$$

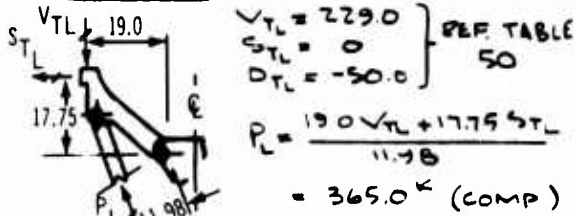
Figure 4-66.(Continued)

FIGURE D.3

STRESS ANALYSIS  
NOSE GEAR LOWER SIDE STRUT

CONDITION: BOEING LANDING  
SPIN-UP 60-40

LOADS



SECTION PROPERTIES

$OD = 5.00$      $AREA = 2.58$   
 $ID = 4.65$      $I = 7.50$   
 $D/R = 28.5$      $\rho = 1.70$

MATERIALS & ALLOWABLES

4340M STEEL @ 270 KSI

$E = 29.0 \times 10^6$

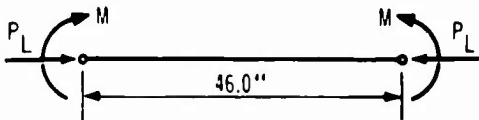
$F_{CL} = F_{CY} = 223.0$

$$F_c = F_{CL} - \frac{F_{CL}^2 [L/\rho C]^2}{4 \pi^2 E}$$

= 190.0 KSI FOR  $L/\rho C = 27.2$

$M/D_3 = 7.2$  (REF. B)

STRESS & M.S.



$$M = (59\%) P_L = 18.3 \text{ K (ASSUMED)}$$

$$M' = 1.05 M = 19.3 \text{ K FOR } \sqrt{\frac{PL^3}{8I}} = 1.5$$

$$M/D_3 = 19.3/5^3 = 1.55$$

$$F_c = \frac{P_L}{AREA} = \frac{365}{2.58} = 141 \text{ KSI}$$

$$M.S. = \frac{1}{R_b + R_c} = 1$$

$$= \frac{1}{\frac{1.55}{7.2} + \frac{141}{190}} = 1$$

$$= \underline{+0.04} \leftarrow$$

STRESS ANALYSIS  
NOSE GEAR DRAG BRACE

CONDITION: FORWARD TOWING

LOADS:  $P_{DB} = .384 \text{ K (COMP)}$   
(REF. TABLE 4-E)

SECTION PROPERTIES

$OD = 5.00$      $AREA = 2.83$   
 $ID = 4.62$      $I = 8.25$   
 $D/R = 26.4$      $\rho = 1.68$

MATERIALS & ALLOWABLES

4340M STEEL @ 270 KSI

$E = 29 \times 10^6$  } DM 84 DI

$F_{CY} = 223$  } SECTION 22.1

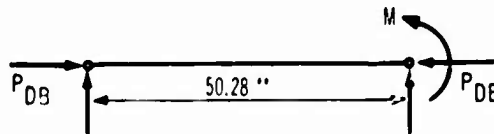
$F_{CL} = F_{CY}$  (ASSUMED)

$$F_c = F_{CL} - \frac{F_{CL}^2 [L/\rho C]^2}{4 \pi^2 E}$$

= 182 KSI FOR  $L/\rho C = 30.0$

$M/D_3 = 7.8$  (REF. B)

STRESS & M.S.



$$M = (59\%) P_{DB} = 19.2 \text{ (ASSUMED)}$$

$$M' = 1.10 M = 21.2 \text{ K FOR } \sqrt{\frac{PL^3}{8I}} = 2.0$$

$$M/D_3 = \frac{21.2}{5^3} = 1.70$$

$$F_c = \frac{P_{DB}}{AREA} = \frac{384}{2.83} = 136 \text{ KSI}$$

$$M.S. = \frac{1}{R_b + R_c} = 1$$

$$= \frac{1}{\frac{1.70}{7.80} + \frac{136}{182}} = 1$$

$$= \underline{+0.03} \leftarrow$$

Figure 4-66 (Concluded)


STRESS ANALYSIS

AFT MAIN - INNER CYLINDER  
SECTION AT & LWR. 826 (STATIC)

CONDITION  
GROUND TURN 50-50

LOADS  
 $V_L = V_R = 238$  } REF  
 $S_L = S_R = 119$  } TABLE 4-F  
 $TQ_M = 2620$   
 $P_a = \text{TORSION LINK APPL LOAD}$   
 $= TQ_M / r_o = 87.8$   
 $M = 53.9(9.43) + 6_s(V_L + V_R) + 6 P_a$   
 $= 15.2 \text{ IN-K}$   
 $P = \text{INTERNAL PRESSURE}$   
 $= \frac{V_L + V_R}{\frac{\pi}{4}(12)^2} = 4.2 \text{ KSI}$

SECTION PROPERTIES  
 $OD = 12.00$   
 $ID = 10.86$   
 $D/t = 21.0$   
 $A = 20.14$



MATERIAL & ALLOWABLES  
 4340 M STEEL @ 270 KSI  
 $F_{UT} = 270$  } REF 8  
 $M/D_3 = 10.0$

STRESS & M.S.  
 $M/D_3 = \frac{15.2}{12^3} = 8.8 \quad R_b = .880$   
 $f_{HT} = \frac{P(OD)}{2t} = 45.0 \quad R_T = .167$   
 $M.S. = \frac{1}{[R_b^2 + R_{HT}^2 - R_b(R_{HT})]^2} - 1$   
 $= +.03 \leftarrow$

NOTE: SEE FWD MAIN GEAR SECTION FOR ANALYSIS OF THE TRUCK BEAM & AXLES, FOR BOTH THE FWD & AFT MAIN GEARS.

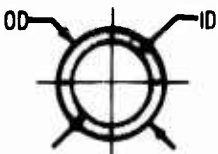
STRESS ANALYSIS

AFT MAIN - OUTER CYLINDER  
SECTION 76.0' FROM & TRUNNION

CONDITION  
GROUND TURN 50-50

LOADS  
 $V_L = V_R = 238$  } REF  
 $V_T = -335$  } TABLE 4-F  
 $S_T = -157$   
 $D_T = -3$   
 $M_T = 2620$   
 $M_p = 76.0 (S_T + D_T) = 12.0$   
 $P = \text{INTERNAL PRESSURE}$   
 $= 4.2 \text{ KSI (SEE INNER CYLINDER)}$

SECTION PROPERTIES  
 $OD = 13.36$   
 $ID = 12.60$   
 $D/t = 35.2$   
 $AREA = 19.0$



MATERIAL & ALLOWABLES  
 4340 M STEEL @ 270 KSI  
 $F_{UT} = 270$  } REF 8  
 $M/D_3 = 5.7$   
 $T/D_3 = 6.4$

STRESS & M.S.  
 $M/D_3 = \frac{M_p}{OD^3} = 5.0 \quad R_b = .890$   
 $T/D_3 = \frac{M_T}{OD^3} = 1.1 \quad R_{ST} = .173$   
 $f_T = \frac{V_T}{AREA} = 23.7 \quad R_T = .088$   
 $f_{HT} = \frac{P(OD)}{2t} = 73.5 \quad R_{HT} = .272$   
 $M.S. = \frac{1}{[(R_b + R_T)^2 + R_{ST}^2 + R_{HT}^2 - R_{HT}(R_b + R_T)]^2} - 1$   
 $= +.02 \leftarrow$

Figure 4-67. Aft Main Landing Gear Analysis

STRESS ANALYSIS

AFT MAIN - SIDE STRUT

CONDITION

GROUND TURN 50-50

LOADS

$P_{SS} = -826^k$  (REF TABLE 4-F)

SECTION PROPERTIES

$CL = 7.00$  AREA = 5.96  
 $IL = 6.44$  I = 33.2  
 $L/D = 25.0$   $\rho = 2.37$

MATERIALS & ALLOWABLES

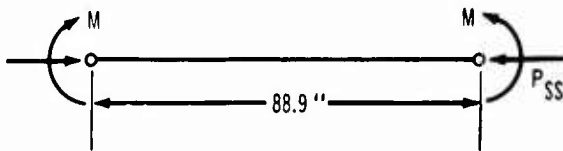
A516M STEEL @ 270 KSI

$F_u = 223$  } REF. 8  
 $M/D = 0.5$  }

$F_{CC} = F_{CY}$  (ASSUMED)

$F_c = F_{CC} - \frac{F_{CC}^2 \left[ \frac{L}{\rho E} \right]^2}{4\pi^2 E}$   
 $= 162.0 \text{ KSI}$  FOR  $\frac{L}{\rho E} = 37.5$

STRESS & M.S.



$M = 1.4\% P_{SS} = 82.6$  (ASSUMED)

$M' = 2.72 M = 225$  FOR  $\sqrt{\frac{PL^3}{EI}} = .6$

$M/D = \frac{225}{7.3} = .95$

$f_c = \frac{P_{SS}}{AREA} = \frac{826}{5.96} = 138.0$

M.S. =  $\frac{1}{R_b + R_c} = -1$

=  $\frac{1}{\frac{.95}{8.9} + \frac{138}{162}} = -1$

= + .05 ←

STRESS ANALYSIS

AFT MAIN - ORDG BRACE

CONDITION

LEVEL LANDING  
 + SPIN-UP

LOADS

$P_{DB} = -724^k$  (REF TABLE 4-F)

SECTION PROPERTIES

OD = 6.00 AREA = 7.36  
 ID = 3.14 I = 28.9  
 $\rho = 1.98$

MATERIALS & ALLOWABLES

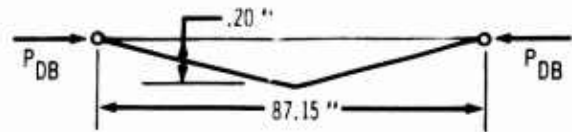
A516M STEEL @ 270 KSI

$E = 29 \times 10^6$  } REF. 8  
 $F_u = 223$  }

$F_u = F_{CC} = F_{CY}$  (ASSUMED)

$F_c = F_{CC} - \frac{F_{CC}^2 \left[ \frac{L}{\rho E} \right]^2}{4\pi^2 E}$   
 $= 138.0 \text{ KSI}$  FOR  $\frac{L}{\rho E} = 43.7$

STRESS & M.S.



ASSUME .20 MISALIGNMENT

$M = .20 P_{DB} = 144.8 \text{ IN-K}$

$f_c = \frac{P_{DB}}{AREA} = 99.0$   $R_c = .712$

$M' = \frac{M}{1 - R_c} = \frac{144.8}{.288} = 520 \text{ IN-K}$

$f_b = \frac{M'c}{I} = 54.0$   $R_b = .240$

M.S. =  $\frac{1}{R_b + R_c} = -1$

= + .04 ←

Figure 4-67. (Concluded)

STRESS ANALYSIS

FWD MAIN - INNER CYLINDER  
SECTION AT & LWR BRG (STATIC)

CONDITION

GROUND TURN 50-50

LOADS:

$$\left. \begin{aligned} V_L = V_R = 258 \\ S_L = S_R = 119 \\ TQM = 2620 \end{aligned} \right\} \text{REF. TABLE 4-G}$$

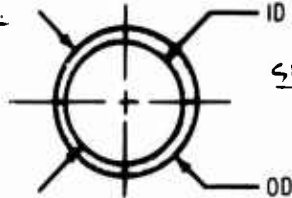
$$P_A = \text{TORSION LINK APEX LOAD} \\ = TQM / 80.0 = 87.5^k$$

$$M = 50(S_L + S_R) + d_b(V_L + V_R) + 6.0 P_A \\ = 14.4 \text{ IN-KIPS}$$

$$P = \text{INTERNAL PRESSURE} \\ = \frac{V_L + V_R}{\text{AREA}} = \frac{476}{\frac{\pi}{4}(12.0)^2} = 4.2 \text{ KSI}$$

SECTION PROPERTIES:

$$\begin{aligned} \text{OD} &= 12.00 \\ \text{ID} &= 10.92 \\ D/t &= 27.2 \end{aligned}$$



MATERIAL & ALLOWABLES:

$$\begin{aligned} &4340 \text{M STEEL @ 270 KSI} \\ &F_{TU} = 270 \text{ KSI} \\ &M/D_3 = 9.6 \end{aligned} \left. \right\} \text{REF. 8}$$

STRESS & M.S.:

$$M/D_3 = \frac{14.4}{12^3} = 8.4 \quad R_b = .872$$

$$f_{HT} \approx \frac{P(\text{OD})}{2t} = 46.6 \quad R_{HT} = .173$$

$$M.S. = \frac{1}{[R_b^2 + R_{HT}^2 - R_b(R_{HT})]} - 1$$

$$= \underline{+ .03} \leftarrow$$

STRESS ANALYSIS

FWD MAIN - OUTER CYLINDER  
SECTION AT & UPR BRG (STATIC)

CONDITION

GROUND TURN 50-50

LOADS:

$$\left. \begin{aligned} V_T = 61 \\ S_T = -149 \\ D_T = -25 \\ M_T = 7380 \end{aligned} \right\} \text{REF TABLE 4-G}$$

$$M_3 = 65 D_T + 14(V_T)$$

$$= -780 \text{ IN-K}$$

$$M_0 = 65.5 S_T + 5 \sin T^{\circ} (M_T)$$

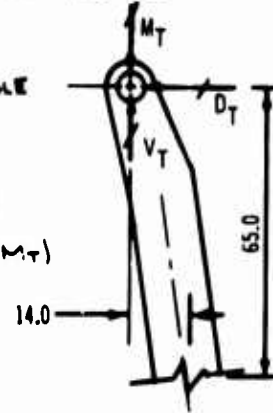
$$= 9300 \text{ IN-K}$$

$$M_2 = M_0 + M_3$$

$$= 9400 \text{ IN-K}$$

$$TQ = \cos T^{\circ} M_T$$

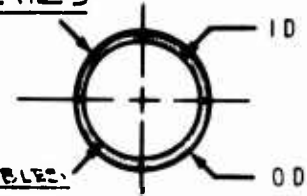
$$= 7380 \text{ IN-K}$$



$$P = 4.2 \text{ KSI (REF. INNER CYL. ANALYSIS)}$$

SECTION PROPERTIES:

$$\begin{aligned} \text{OD} &= 13.45 \\ \text{ID} &= 12.60 \\ D/t &= 31.8 \\ t &= .429 \end{aligned}$$



MATERIAL & ALLOWABLES:

$$\begin{aligned} &4340 \text{M STEEL @ 270 KSI} \\ &M/D_3 = 6.4 \\ &TQ/D_3 = 6.8 \\ &F_{TU} = 270 \text{ KSI} \end{aligned} \left. \right\} \text{REF 8}$$

STRESS & M.S.:

$$M/D_3 = \frac{M_2}{\text{OD}^3} = 3.9 \quad R_b = .610$$

$$T/D_3 = \frac{TQ}{\text{OD}^3} = 6.8 \quad R_T = .448$$

$$f_{HT} \approx \frac{P(\text{OD})}{2t} = 76.0 \quad R_{HT} = .280$$

$$M.S. = \frac{1}{[R_b^2 + R_{HT}^2 + R_T^2 - R_{HT}(R_b)]} - 1$$

$$= \underline{+ .04} \leftarrow$$

Figure 4-68. Forward-Main-Landing-Gear Analyses



STRESS ANALYSIS

FWD MAIN - AXLES  
SECTION 12.2" FROM & WHL.

CONDITION  
GROUND TURN + FLAT

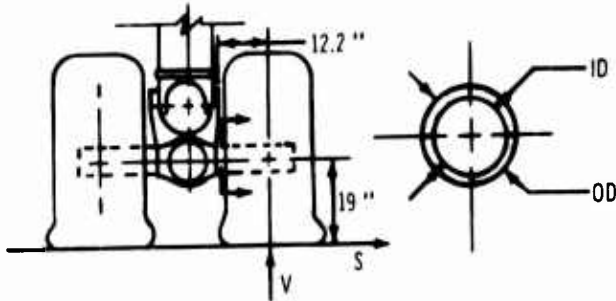
LOADS

$V_L = 90$   
 $V_R = 270$   
 $S_L = 30$   
 $S_R = 60$   
 $TQM = 2080$

REF TABLE  
4-G

$V = \frac{V_L + V_R}{2} = 180$   
 $S = \frac{S_L + S_R}{2} + \frac{TQM}{56} = 92$

$M = 12.2V + 19.0S = 3950 \text{ "K}$



SECTION PROPERTIES

OD = 6.00 AREA = 9.4  
ID = 4.90 D/t = 10.9

MATERIAL & ALLOWABLES

4340M STEEL @  $F_{TU} = 270$   
 $M/D^3 = 19.4$  (REF 8)

STRESS & M.S.

$M/D^3 = \frac{3950}{6.0^3} = 18.4$   $R_b = .950$

$f_t = \frac{S}{\text{AREA}} = 9.8$   $R_t = .035$

$M.S. = \frac{1}{R_b + R_t} - 1$

$= +.01$

STRESS ANALYSIS

FWD MAIN - TRUCK BEAM  
SECTION 23" FROM AXLE &

CONDITION

GROUND TURN 50-50

LOADS

$V_L = V_R = 238$   
 $S_L = S_R = 119$   
 $TQM = 2620$

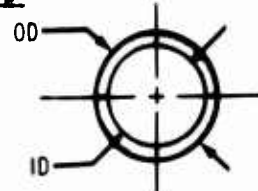
REF TABLE  
4-G

$V = \frac{V_L + V_R}{2} = 238$   
 $S = \frac{S_L + S_R}{2} + \frac{TQM}{56} = 166$

$M = 23.0(V \rightarrow S) = 6180$   
 $TQ = 19.0(S) = 3150$

SECTION PROPERTIES

OD = 10.00  
ID = 9.30  
D/t = 28.6



MATERIALS & ALLOWABLES

4340M STEEL @  $F_{TU} = 270$  KSI  
 $M/D^3 = 7.3$   
 $T/D^3 = 7.6$

REF 8

STRESS & M.S.

$M/D^3 = \frac{6180}{10^3} = 6.18$   $R_b = .848$

$T/D^3 = \frac{3150}{10^3} = 3.15$   $R_{ST} = .415$

$M.S. = \frac{1}{(R_b^2 + R_{ST}^2)^{.5}} - 1$

$= +.05$

NOTE: SINCE THE TRUCK BEAM AND AXLES USED ON THE DFT MAIN GEAR ARE ESSENTIALLY IDENTICAL THE TRUCK BEAM & AXLE ANALYSIS FOR THE FWD MAIN GEAR ALSO APPLY TO THE DFT MAIN GEAR.

Figure 4-68. (Continued)

STRESS ANALYSIS

FWD MAIN - SIDE STRUT

CONDITION

GROUND TURN 50-50

LOADS:

$$P_{SS} = -649.0 \text{ K (REF TABLE 4-G)}$$

SECTION PROPERTIES

$$\begin{aligned} OD &= 7.00 & AREA &= 5.3 \\ ID &= 6.50 & I &= 30.9 \\ D/4 &= 28.0 & r &= 2.34 \end{aligned}$$

MATERIALS & ALLOWABLES

4340M STEEL @ 270 KSI  
E = 29 x 10<sup>6</sup>

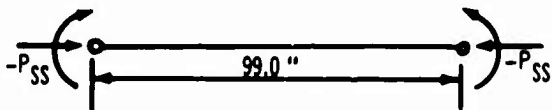
$$F_c = F_y = 223.0 \text{ (ASSUMED)}$$

$$F_c = F_c - \frac{F_c^2 [L/r]^2}{4\pi^2 E}$$

$$= 147.0$$

$$M/OD = 7.3 \text{ (REF. B)}$$

STRESSES & M.S.



$$M = 10\% P_{SS} = 64.9 \text{ K (ASSUMED)}$$

$$M' = 4.5M = 292.0 \text{ K FOR } \sqrt{\frac{PL}{EI}} = 2.7$$

$$M'/OD = \frac{292}{75} = 0.82$$

$$f_c = \frac{P_{SS}}{AREA} = \frac{649}{5.3} = 123.0 \text{ KSI}$$

$$M.S. = \frac{1}{R_b + R_c} - 1$$

$$= \frac{1}{\frac{0.82}{7.30} + \frac{123}{147}} - 1$$

$$= \underline{\underline{+0.05}} \leftarrow$$

STRESS ANALYSIS

FWD MAIN - DEAG BRACE

CONDITION

REVERSE BRAKING 50-50

LOADS

$$P_{DB} = -345.0 \text{ K (REF TABLE 4-G)}$$

SECTION PROPERTIES

$$\begin{aligned} OD &= 6.00 & I &= 16.8 \\ ID &= 5.55 & r &= 2.03 \\ AREA &= 4.07 \end{aligned}$$

MATERIALS & ALLOWABLES

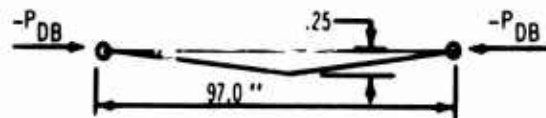
4340M STEEL @ 270 KSI

E = 29 x 10<sup>6</sup> } REF. B

$$F_c = F_b = F_y \text{ (ASSUMED)}$$

$$F_c = F_c - \frac{F_c^2 [L/r]^2}{4\pi^2 E} = 124.0$$

STRESSES & M.S.



ASSUME .25 MIS-ALIGNMENT  
M = .25 P<sub>DB</sub> = 89.5 IN-K

$$f_c = \frac{P_{DB}}{AREA} = 89.2 \quad R_c = .710$$

$$M' = 3.45 M \text{ FOR } \frac{1}{1 - R_c} = 3.45$$

$$M' = 3.45 (89.5) = 309 \text{ IN-K}$$

$$f_b = \frac{M'c}{I} = 55.0 \text{ KSI} \quad R_b = .246$$

$$M.S. = \frac{1}{R_c + R_b} - 1$$

$$= \underline{\underline{+0.04}} \leftarrow$$

Figure 4-68. (Concluded)

## 4.6 PROPULSION POD STRESS ANALYSIS

### 4.6.1 Structural Description

The four propulsion pods are suspended from the lower surface of the horizontal stabilizer. Each engine pod is attached to the stabilizer support structure by a three-point suspension system, two points at the forward engine-mounting position and a single point at the rear mount. The three-point suspension is very similar to subsonic jet-mounting installations. The General Electric Company engine has a fourth attachment point on the forward engine-mount structure to carry engine thrust loads to the support structure. The forward mount structure, operating in an estimated thermal environment of 550° F, is fabricated from 17-4PH stainless steel forgings. The aft mount structure operates in a higher thermal environment and is fabricated from forgings of Rene' 41 heat-treated to 170,000 psi. The Rene' 41 may be replaced with Inconel 718. Radial expansion of the engine is accommodated at both mounts by linkage between the engine and the mounting structure. Axial expansion is accommodated by the two hinges in the aft mount structure.

The mount fasteners are designed to shear and allow clean separation of the propulsion package from the airplane without damaging fuel cells in the case of:

- Extreme engine deceleration because of internal engine damage.
- Ditching.
- Extreme drag forces caused by contacting an obstruction.

The variable-geometry engine inlet, fabricated of 6Al-4V annealed titanium, is mounted forward of and supported by the forward engine flange. Tension support is provided by four pairs of attaching bolts between the inlet aft frame and the forward engine flange. Shear loads are transferred to the engine by a conical flange that is an integral part of the forward engine flange. The titanium inlet cowling consists of circumferential frames supporting the inner and outer skins with longitudinal members utilized to reinforce the cutout for bypass and access doors. The cowling leading-edge assembly incorporates chem-milled stiffening to resist hailstone damage. Allowances are provided for anti-icing air orifices on the cowling lip. The inlet centerbody

consists of a center structural tube which is cantilevered from four supporting struts mounted within the aft part of the inlet cowling. The structural tube supports the centerbody spike, the centerbody actuator, and the movable segments which form the variable centerbody contours.

The engine side cowl panels, made in three removable sections, are fabricated of circumferentially stiffened sheet construction in 6Al-4V annealed titanium where temperatures are less than 600 F. Similar construction of stainless steel or Hastalloy X material is used in the aft cowl portions exposed to a higher temperature environment, as shown in Part C, Design Criteria, Loads, Aerodynamic Heating, Flutter (V2-B2707-7) of the Airframe Design Report. The stiffening rings or corrugations are fastened to the skin with bonding and riveting. The flush-type latches, mounted at the ends of circumferential frames, are of similar design to the latches in current use on Boeing 720 airplanes.

### 4.6.2 Engine Mount Loads

Engine mounting reactions are shown in Table 4-H for the GE engine and in Table 4-I for the P&WA engine for all conditions defined in V2-B2707-7.

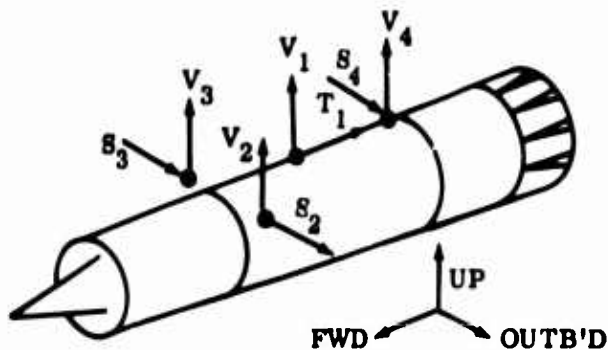
### 4.6.3 Engine Mount Analysis

Analysis is shown for the critical load conditions for the forward and aft mounts for both GE and P&WA engines in Figs. 4-69 through 4-72.

### 4.6.4 Inlet Loads

Critical design pressures in the inlet are shown in Table 4-J. Normal operating pressures are multiplied by a factor of 2.5 to obtain ultimate design pressures. A factor of 2.0 is used for cruise unstart conditions. A factor of 1.5 is used for abnormal conditions of upset or incorrect bypass door positioning. The inlet components critical for each condition are identified in the table. Most components are critical for the high internal pressures occurring in an upset condition (Mach = 2.9). The forward inlet cowling and aft pressure baffle are critical for lower than atmospheric pressures in the inlet during ground operation. Normal operation at near idle power with the takeoff bypass doors closed is generally the critical ground condition. Abnormal ground operation, at full takeoff power with

Table 4-M. Engine Mount Reactions (GE)

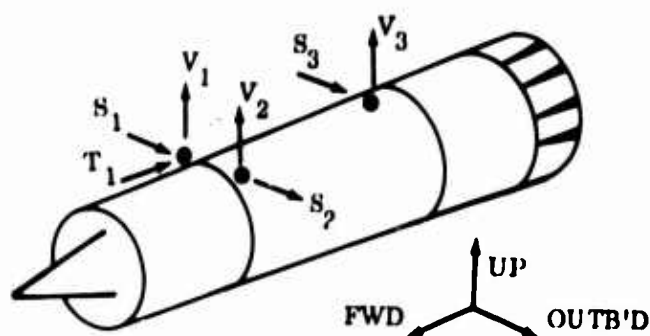


Cond. No.	Condition		V <sub>1</sub>	T <sub>1</sub>	V <sub>2</sub>	S <sub>2</sub>	V <sub>3</sub>	S <sub>3</sub>	V <sub>4</sub>	S <sub>4</sub>
1	Landing	6.0V	0	0	14.3	6.6	+18.3	-6.6	50.5	0
2	Landing	-4.0V	0	0	-12.2	-4.4	-12.2	4.4	-33.7	0
3	Supersonic Maneuver	6.0V + 1.5 Tm	51.5	89.3	-11.1	-4.2	-11.1	4.2	57.8	0
4	Supersonic Maneuver	-4.0V + 1.5 Tm	51.5	89.3	-41.6	-15.2	-41.6	15.2	26.4	0
5	Fatigue	3.0V + 3.0 Tm	103.0	178.5	-49.7	-18.2	-49.7	18.2	39.9	0
6	Fatigue	3.0 Tm	103.0	178.5	-58.8	-21.5	-58.8	21.5	14.6	0
7	Maneuver	2.5S	0	0	-23.9	-8.7	23.9	-6.2	0	-21.1
8	Maneuver	-2.5S	0	0	23.9	8.7	-23.9	6.2	0	21.1
9	Gyroscopic	1.5 V + 1.5 Tm + My	51.5	89.3	-20.2	-7.4	-29.4	24.7	20.0	-17.3
10	Gyroscopic	1.5 V + 1.5 Tm - My	51.5	89.3	-29.4	-10.8	-20.2	-6.5	20.0	17.3
11	Gyroscopic	3.75 V + 1.5 Tm + Mp	51.5	89.3	-29.5	-10.9	-29.5	10.9	61.9	0
12	Gyroscopic	3.75 V + 1.5 Tm - Mp	51.5	89.3	-6.5	-2.5	-6.5	2.5	15.9	0
13	Supersonic Maneuver	1.5 Tm + Aero (s)	51.5	89.3	-52.3	-19.1	-6.5	-4.7	7.3	-5.9
14	Supersonic Maneuver	1.5 Tm - Aero (s)	51.5	89.3	-6.5	-2.5	-52.3	26.3	7.3	5.9
15	Transonic Maneuver	1.5 Tm + Aero (T)	51.5	89.3	-59.5	-21.7	0.7	-20.2	7.3	7.8
16	Transonic Maneuver	1.5 Tm - Aero (T)	51.5	89.3	0.7	0.1	-59.5	41.8	7.3	-7.8
17	Wheels-up Landing	9.0D	75.3	130.5	-51.7	-18.8	-51.7	-18.8	28.1	0
18	Pitching	-6.0D	-50.2	-87.0	34.5	12.5	34.5	-12.5	-18.7	0
19	Reverse Thrust	3.0 V + 3.0 Tr	-40.0	-69.3	32.1	11.7	32.1	-11.7	19.6	0
20	Engine Seizure	Mr	0	0	-74.8	-27.3	74.8	27.3	0	0

V = weight of propulsion pod acting vertically  
 D = weight of propulsion pod acting forward  
 S = weight of propulsion pod acting laterally  
 Tm = maximum engine thrust  
 Tr = maximum engine reverse thrust  
 Aero (s) = total aerodynamic load acting on propulsion pod (Supersonic)  
 Aero (T) = total aerodynamic load acting on propulsion pod (Transonic)  
 My = gyroscopic yawing moment  
 Mp = gyroscopic pitching moment  
 Mr = engine rolling moment induced by stoppage of critical rotating mass in .3 sec.

All loads are in kips  
 All loads are ultimate  
 Force directions shown as positive

Table 4-1. Engine Mount Reaction (P&WA)



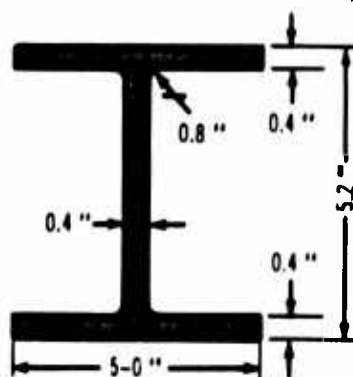
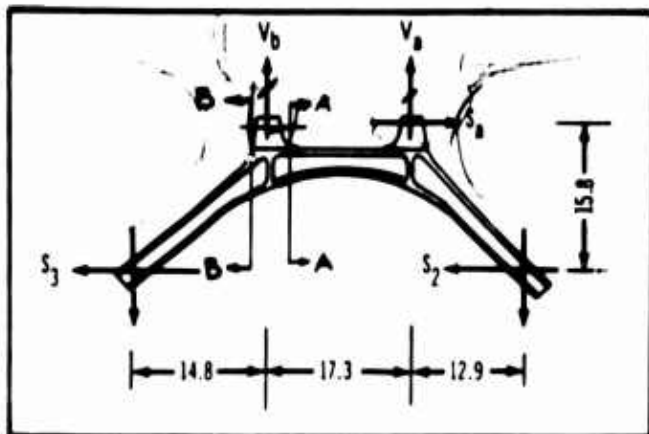
Cond. No.	Condition		$V_1$	$S_1$	$T_1$	$V_2$	$S_2$	$V_3$	$S_3$
1	Landing	6.0V	18.2	0	0	18.2	0	47.6	0
2	Landing	-4.0V	-12.2	0	0	-12.2	↑	-31.8	0
3	Supersonic Maneuver	6.0V + 1.5 Tm	15.1	10.1	84.6	-4.2	↑	73.0	-10.1
4	Supersonic Maneuver	-4.0V + 1.5 Tm	-15.3	10.1	84.6	-34.6	↑	-6.4	-10.1
5	Fatigue	3.0V + 3.0 Tm	3.0	20.3	169.2	-35.7	↑	74.7	-20.3
6	Fatigue	3.0 Tm	-6.1	20.3	169.2	-44.8	↑	50.9	-20.3
7	Maneuver	2.5S	72.1	-15.2	0	-72.1	↑	0	-19.8
8	Maneuver	-2.5S	-72.1	15.2	0	72.1	↑	0	19.8
9	Gyroscopic	1.5 V + 1.5 Tm + My	8.1	24.0	84.6	-24.4	↑	37.3	-24.0
10	Gyroscopic	1.5 V + 1.5 Tm - My	-5.1	-3.8	84.6	-11.2	↑	37.3	3.8
11	Gyroscopic	3.75 V + 1.5 Tm + Mp	-0.9	10.1	84.6	-20.2	↑	73.7	-10.1
12	Gyroscopic	3.75 V + 1.5 Tm - Mp	17.5	10.1	84.6	-1.8	↑	36.7	-10.1
13	Supersonic Maneuver	1.5 Tm + Aero (s)	42.7	-21.6	84.6	-68.2	↑	25.4	-5.3
14	Supersonic Maneuver	1.5 Tm - Aero (s)	-48.9	41.8	84.6	23.4	↑	25.4	-14.9
15	Transonic Maneuver	1.5 Tm + Aero (T)	44.5	49.1	84.6	-70.0	↑	25.4	15.6
16	Transonic Maneuver	1.5 Tm - Aero (T)	-50.7	69.3	84.6	25.2	↑	25.4	-35.8
17	Wheels-up Landing	9.0D	-19.3	15.5	126.0	-34.9	↑	54.2	-15.5
18	Ditching	-6.0D	12.9	-10.3	-84.0	23.3	↑	-36.1	10.3
19	Reverse Thrust	3.0 V + 3.0 Tr	13.7	-6.4	-53.5	23.4	↑	4.9	6.4
20	Engine Seizure	Mr	45.0	0	0	-45.0	0	0	0

V = weight of propulsion pod acting vertically  
 D = weight of propulsion pod acting forward  
 S = weight of propulsion pod acting laterally  
 Tm = maximum engine thrust  
 Tr = maximum engine reverse thrust  
 Aero (s) = total aerodynamic load acting on propulsion pod (Supersonic)  
 Aero (T) = total aerodynamic load acting on propulsion pod (Transonic)  
 My = gyroscopic yawing moment  
 Mp = gyroscopic pitching moment  
 Mr = engine rolling moment induced by stoppage of critical rotating mass in .3 sec.

All loads are in kips  
 All loads are ultimate  
 Force directions shown as positive

FORWARD ENGINE MOUNT (G.E.)

SECTION ~~B-B~~  
 CRITICAL CONDITION NO. 16  
 $1.5 T_M - Z(AERO)(T)$



$b^2/t = 1.55/1.4 = 3.88$   
 USE  $F_{TU} = 163 \text{ KSI}$

$S(\text{req'd}) = M/F_{TU}$   
 $= 1257/163$   
 $= \underline{7.71 \text{ IN.}^3}$

$I(\text{req'd}) = S_C = (7.71)(2.45) = \underline{18.9 \text{ IN.}^4}$

$I(\text{ACT.}) = \frac{(5.0)(4.9)^3 - (4.7)(4.1)^3}{12} = \underline{22.0 \text{ IN.}^4}$

M.S. =  $\frac{I(\text{ACT.})}{I(\text{req'd})} - 1 = 0.16$

DESIGN CONDITIONS AND TEMPERATURE

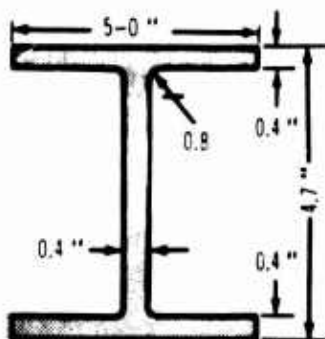
COND NO	$V_2$	$S_2$	$V_3$	$S_3$	ENGINE CASE TEMP
14	-6.5	-8.5	-52.3	26.3	550°F
15	-59.5	-21.7	0.7	-20.2	550°F
16	0.7	0.1	-59.5	41.8	550°F
20	-71.8	27.3	-71.8	27.3	550°F

D- REF TABLE 316-A

SECTION A-A — CRITICAL CONDITION NO 16

$\Sigma S = 0 \quad S_a = 41.9$   
 $\Sigma M = 0 \quad V_a = 90.6$   
 $\Sigma V = 0 \quad V_b = -149.6$

$M_a = 62 V_3 - 14 V_b - 11.3 S_3 = -1257 \text{ IN.}^2$

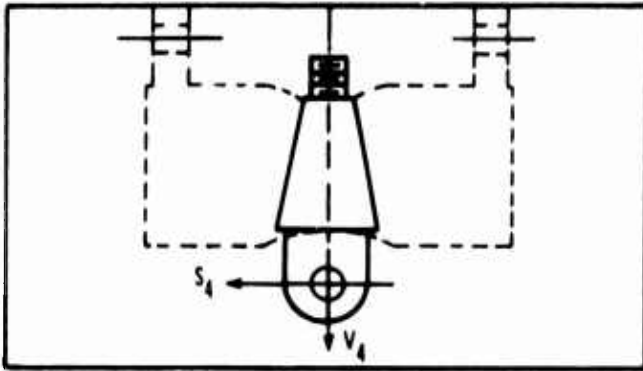


$I(\text{ACT.}) = \frac{(5.0)(4.2)^3 - (4.6)(3.4)^3}{12} = \underline{15.8 \text{ IN.}^4}$

M.S. =  $\frac{I(\text{ACT.})}{I(\text{req'd})} - 1 = .00$

Figure 4-69. Forward Engine Mount Analysis (GE)

AFT ENGINE MOUNT (G.F.)



DESIGN CONDITIONS & TEMPERATURES

COND NO.	CONDITION	V <sub>4</sub>	S <sub>4</sub>	ENGINE CASE TEMP
9	GYROSCOPIC	20.0	-17.3	1,200° F
10	GYROSCOPIC	20.0	+17.3	1,200° F
14	GRYOSCOPIE	61.9	0	1,200° F

REF. TABLE 21.1  
 BOLT: 160 KSI (TENSION), 95 KSI (SHEAR)  
 USE 3/4" Ø BOLT

$$V_4 = 61.9 \text{ K} \quad P_{\text{ALLOW}} = 2(41,950) = 83.9 \text{ K}$$

LUG OF CONE

SHEAR TEAR OUT  $F_{\text{SU}} = 92 \text{ KSI ALLOW}$   
 $A_s = (.95)(1.50 - .75) = .712 \text{ in}^2$   
 $T_s = P/A_s = 61.9/7.12 = 87 \text{ KSI} < 92 \text{ KSI}$   
 $M.S. = T_s/F_{\text{SU}} - 1 = 0.06$

BENDING:  $F_{\text{TU}} = 146$

$$M = (17.3)(1.7) = 29.4 \text{ in} \cdot \text{K}$$

$$S = bh^2/6 = (.95)(1.50)^2/6 = 0.356 \text{ in}^3$$

$$f = M/S = 29.4/3.56 = 82.6 \text{ KSI} < 146$$

TOP BOLT:

$$d = 7/8", \quad F_{\text{TU}} = 146 \text{ KSI}$$

$$P_{\text{ALLOW}} = 70 \text{ OK} > 61.9 \text{ K}$$

$$M.S. = \frac{P_{\text{ALLOW}}}{P} - 1 = 0.13$$

CONE BEARING

$$\Sigma F = 0 \quad F_1 \cos \theta - F_2 \cos \theta + S_4 = 0$$

$$\Sigma M = 0 \quad 2.8 F_1 - 5.5 F_2 + 7.7 S_4 = 0$$

$$\cos \theta = .976$$

$$.964 F_2 = 29.9 \quad F_2 = 31.0$$

$$F_1 = -17.7 + 31.0 \quad F_1 = 13.3$$

$$A_1 = 1/2 (2)(.9 + 1.7) = 2.5 \text{ in}^2$$

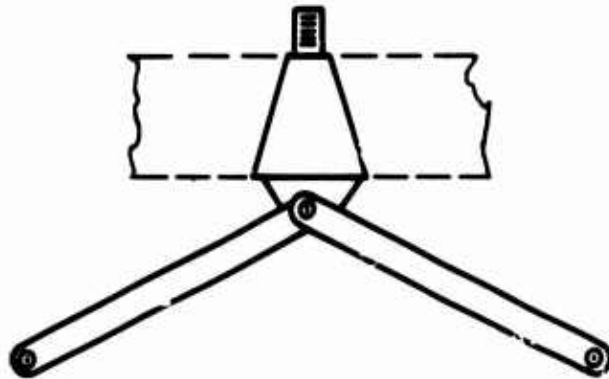
$$A_2 = 1/2 (2)(1.7 + 2.5) = 4.2 \text{ in}^2$$

$$W_1 = \frac{2 F_1}{A_1} = \frac{(2)(13.3)}{2.5} = 11 \text{ KSI} < 280$$

$$W_2 = \frac{2 F_2}{A_2} = \frac{(2)(31.0)}{4.2} = 15 \text{ KSI} < 280$$

Figure 4-70. Aft Engine Mount Analysis (GE)

AFT ENGINE MOUNT (P&W)



DESIGN CONDITIONS & TEMPERATURES

COND NO.	CONDITION	V <sub>3</sub>	S <sub>3</sub>	ENGINE CASE TEMP
5	FATIGUE	74.7	-20.3	900° F
16	TRANSONIC MANEUVER	25.4	-35.8	900° F
18	DITCHING	-36.1	+10.3	900° F

LINKS - CRITICAL CONDITIONS

COND. NO. 5 P = 960\*

COND. NO. 18 P = 462\*

BOLTS - LINK TO ENGINE, LINK TO CONE

BOLTS SHEAR 160 KSI (TENSION), 95 KSI (SHEAR)

USE 7/8" Ø BOLT

P (ELBOW) = (2)(571) = 1142\*

M.S. = 114/96.0 - 1 = 0.188

LINKS

A<sub>3</sub> = (.90)(2)(.6) = 1.08 IN<sup>2</sup>

SHEAR-TEAR OUT

$$T_s = P/A_s = 96.0/1.08 = 89.0 \text{ KSI} < 101$$

$$M.S. = F_{su}/T_s - 1$$

$$= \frac{101}{89} - 1 = 0.14$$

TENSION: A<sub>T</sub> = (.9)(.75) = 0.675 IN<sup>2</sup>

$$\sigma_T = P/A_T = 96.0/0.675 = 142 \text{ KSI}$$

$$M.S. = F_{Tu}/\sigma_T - 1 = \frac{151}{142} - 1 = 0.11$$

COMP.

$$F_c = F_{cc} - \frac{3F_c^2}{\pi E} \left( \frac{L}{h(\text{min})} \right)^2$$

$$F_c = 117 - \frac{(117)^2(11)^2(3)}{(9.85 \times 10^6)(.75)^2}$$

$$A_c = 1.08 \text{ IN}^2$$

$$\sigma = P_c/A_c = 46.2/1.08 = 42.8 \text{ KSI} < 79.4$$

CONE

LLG. SHEAR TEAR OUT: F<sub>su</sub> = 101

$$A_s = (2)(.6)(.7) = 0.84 \text{ IN}^2$$

$$T_s = V_4/A_s = 74.7/0.84 = 89.0$$

$$M.S. = \frac{101}{98} - 1 = 0.14$$

BENDING

$$M = S_4 L = (35.1)(1.3) = 45.5 \text{ IN. KIP}$$

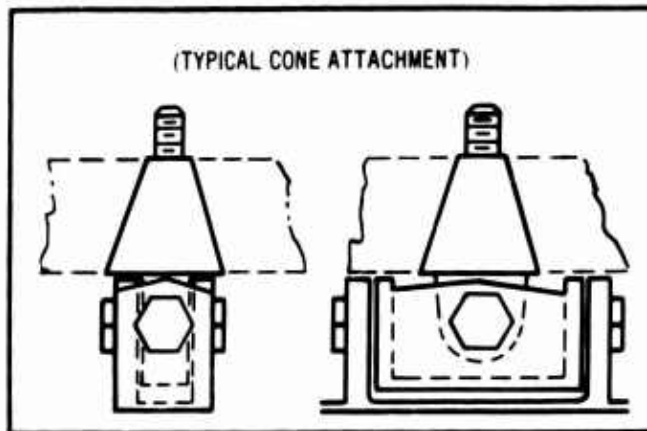
$$S = \frac{bh^2}{6} = \frac{(.7)(.4)^2}{6} = 0.67 \text{ IN}^3$$

$$\sigma_p = M/S = 45.5/0.67 = 68 \text{ KSI} < 157$$

Figure 4-71. Aft Engine Mount Analysis (P&WA)



FORWARD ENGINE ANALYSIS



AFT MOUNT ANALYSIS (CONT)

TOP BALL: 1" φ

$$\sum S = 0 \quad F_1 \cos \theta - F_2 \cos \theta + S_4 = 0$$

$$\sum M = 0 \quad 2.4 F_1 - 5.2 F_2 + 6.2 S_4 = 0$$

$$\cos \theta = .284 \quad \theta = .972$$

$$F_1 = 143 \quad F_2 = 311$$

$$P = \sqrt{F_1^2 + (F_2 + F_1) \cos \theta} = 541 \text{ K}$$

$$P(\text{LBRCH}) = 16.5 \text{ K}$$

$$M.S. = \frac{16.5}{541} = 1 - 0.16$$

DESIGN CONDITIONS & TEMPERATURES

COND NO.	V <sub>1</sub>	S <sub>1</sub>	T <sub>1</sub>	V <sub>2</sub>	ENGINE CASE TEMP
6	-6.1	20.3	169.2	-44.8	500° F
15	44.5	-49.1	84.6	-70.0	500° F
16	50.7	69.3	84.6	25.4	500° F

GIMBALL FITTING

CRITICAL - COND No. 16

$$I_{xx} = 2.01 \text{ IN}^4$$

$$I_{yy} = 2.56 \text{ IN}^4$$

$$C_x = 1.4''$$

$$C_y = 1.72''$$

$$M_{xx} = 87.5 \text{ IN} \cdot \text{K}$$

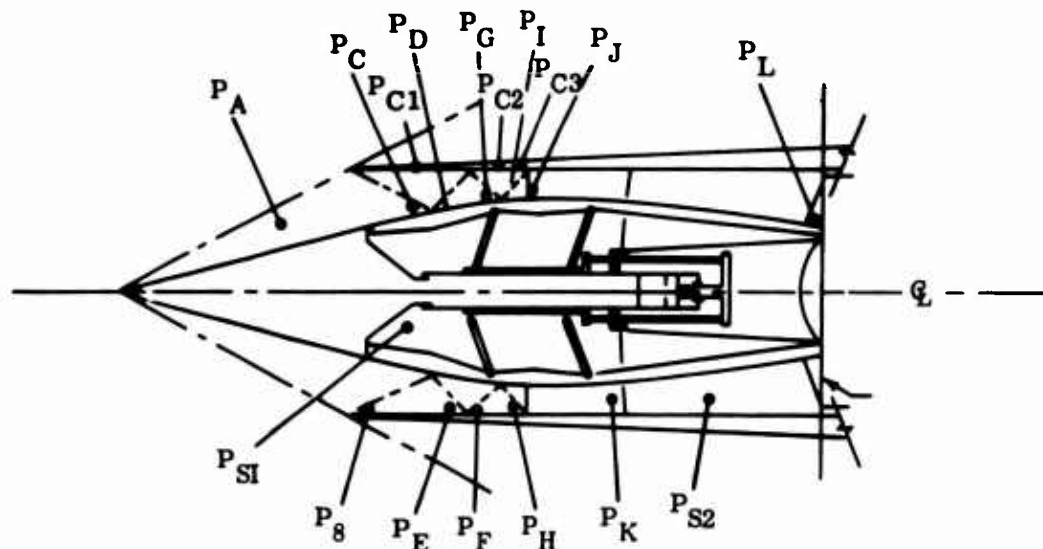
$$M_{yy} = 119.5 \text{ IN} \cdot \text{K}$$

$$\sigma = \frac{M_{xx} C_x}{I_{xx}} + \frac{M_{yy} C_y}{I_{yy}} = 147 \text{ KSI} \angle 16.5^\circ$$

$$M.S. = \frac{16.5}{147} = 1 = 0.12$$

Figure 4-72. Forward Engine Mount Analysis (P&WA)

Table 4-J Inlet Design Pressures



INLET OPERATING PRESSURES, PSI

A/P Mach.	Alt.	Condition	C' Body Radius	P <sub>AMB</sub>	P <sub>LOC</sub>	P <sub>T</sub>	P <sub>A</sub>	P <sub>B</sub>	P <sub>C</sub>	P <sub>D</sub>	P <sub>E</sub>	P <sub>F</sub>	P <sub>G</sub>
2.9	52,000	a. Int. & External Compression	23.46	1.53	1.53	46.3	2.85	3.46	2.85	7.48	7.06	15.1	10.8
2.9	52,000	b. Ext. Compression	14.50	1.53	1.53	46.3	2.85	2.85	20.2	20.1	19.7	19.5	19.7
0.0	S. L.	c. Sub-sonic Drs. Closed	23.46	14.7	14.7	14.7	14.7	10.32	10.32	11.20	9.71	8.70	9.64
0.0	S. L.	d. Sub-Sonic Drs. Closed	14.50	14.7	14.7	14.7	14.7	8.70	8.70	8.70	9.47	10.83	11.05

INLET OPERATING PRESSURES, PSI (Con't)

A/P Mach.	Alt.	Condition	C' Body Radius	P <sub>H</sub>	P <sub>I</sub>	P <sub>J</sub>	P <sub>K</sub>	P <sub>L</sub>	P <sub>C1</sub>	P <sub>C2</sub>	P <sub>C3</sub>	P <sub>S1</sub>	P <sub>S2</sub>
2.9	52,000	a. Int. & External Compression	23.46	14.5	11.6	30.8	31.8	33.6	8.13	6.2	16.6	14.2	13.2
2.9	52,000	b. Ext. Compression	14.50	19.9	21.7	23.6			10.7	10.7	10.7	11.4	10.3
0.0	S. L.	c. Sub-Sonic Drs. Closed	23.46	9.7	10.3	8.90			11.91	11.70	11.70	8.70	8.70
0.0	S. L.	d. Sub-Sonic Drs. Closed	14.50	11.12	11.4	9.90			12.07	12.80	12.80	9.47	9.47

- Cond. a. Designs Centerbody Wedge Beams, Support Struts
- Cond. b. Designs Nose Cone, Actuator, Actuator Linkage
- Cond. c. Designs Inlet Cowl, Aft Pressure Baffle
- Cond. d. Designs Inlet Cowl, Aft Pressure Baffle

Design Pressure Factors:  
 1.5 Factor on Conditions a., b. and d.  
 2.5 Factor on Condition c.

All inlet stress analyses are based on the GE engine. Inlet stress analyses for the P&W engine would be similar and give results which are very close to those indicated for the GE engine.

the normally open doors inadvertently closed, was also checked and is slightly more critical than the normal condition on some components. Normal takeoff and flight conditions and cruise unstart and buzz conditions were investigated and found to be less critical than those shown.

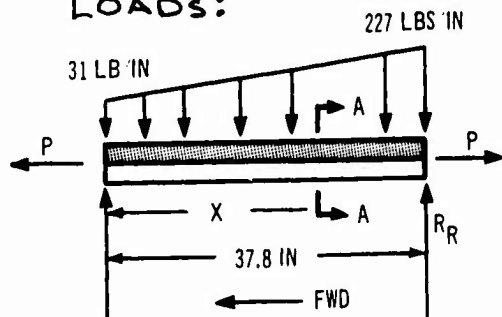
## INLET CENTERBODY

### OUTER CENTER WEDGE/ANALYSIS

#### DESIGN CONDITION:

CONDITION 1 - MACH.  
2.9, INTERNAL -  
EXTERNAL PRESSURE  
(REF. TABLE 4-K)

#### LOADS:



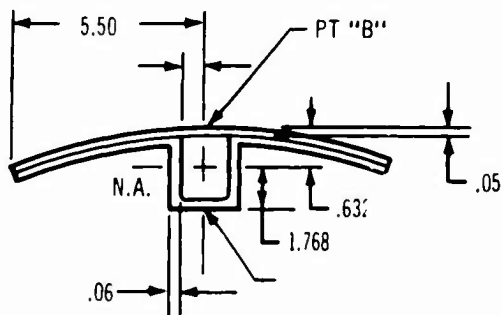
$$N = 1.5 \text{ (FOR DESIGN COND. 1)}$$

$$R_L = 1.5(1820) = 2730 \text{ lbs}$$

$$R_R = 1.5(3056) = 4584 \text{ lbs}$$

$$P = 1.5(183) = 275 \text{ lbs}$$

#### GEOMETRY:



AT X = 21.2

4-73. Inlet Centerbody Wedge Analysis

Inlet mount loads are shown in Table 4-K for all conditions defined in V2-B2707-7.

#### 4.6.5 Inlet Analysis

Analysis is shown for the critical load conditions on the inlet centerbody and the inlet cowl in Figs. 4-73 through 4-77.

#### SECTION PROPERTIES

@ A-A

$$A = 1.50 \text{ IN}^2$$

$$I = .72 \text{ IN}^4$$

#### MATERIALS & ALLOWABLES

(a) TITANIUM

(T<sub>1</sub>-6AL-4V, COND 1)

(b) AT 500°F

$$F_{TY} = 88000 \text{ PSI}$$

$$F_{CC} = 50000 \text{ PSI}$$

#### STRESSES & MARGIN OF SAFETY

THE CRITICAL SECTION IS A-A, THE POINT OF THE MAXIMUM BEAM MOMENT.

$$M_{A-A} = 1.5(23400)$$

$$= 35100 \text{ IN-LBS}$$

$$f = \frac{P}{A} \pm \frac{Mc}{I}$$

AT POINT "B"

$$f = 30250 \text{ PSI}$$

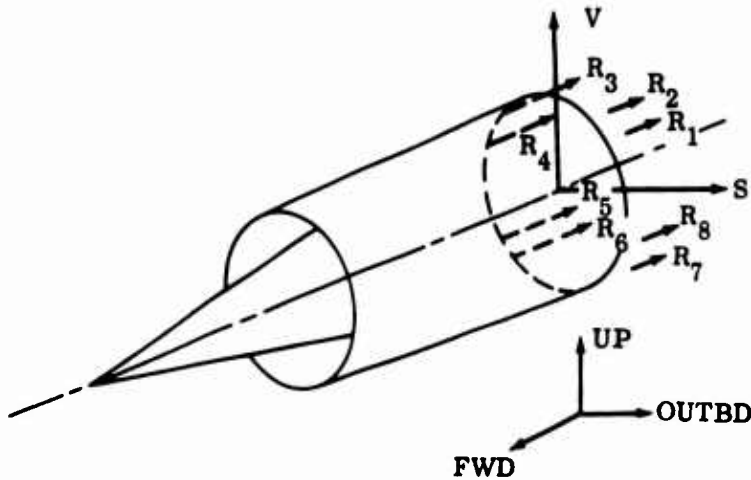
$$M.S. = \frac{50000}{30250} - 1 = +.65$$

AT POINT "C"

$$f = 86370 \text{ PSI}$$

$$M.S. = \frac{88000}{86370} - 1 = +.02$$

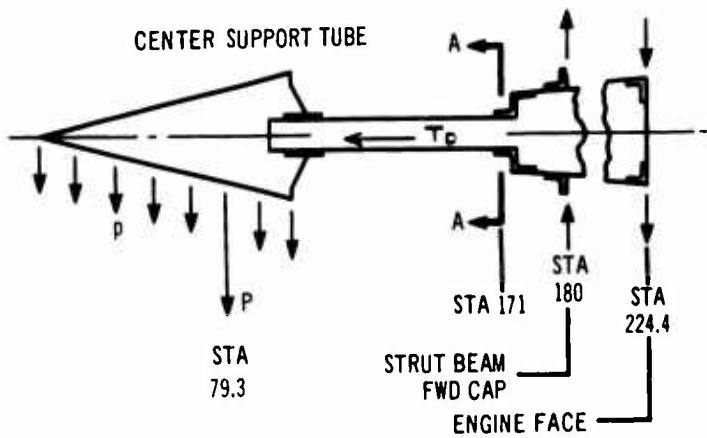
Table 4-K. Inlet Mount Reactions



V = Wt. of inlet acting vertically downward  
 D = Wt. of inlet acting forward  
 S = Wt. of inlet acting laterally  
 Aero (s) = total aerodynamic load acting on inlet (Supersonic)  
 Aero (T) = total aerodynamic load acting on inlet (Transonic)  
 $T_D$  = inlet internal pressure net thrust load at  $M = 2.90$   
 $T_{s-u}$  = inlet internal pressure net thrust load at  $M = 2.70$  (normal oper.) or at  $M = 2.35$  (normal oper.); whichever is greater  
 $T_{u-u}$  = inlet internal pressure net thrust load at  $M = 2.70$  or  $M = 2.35$  (unstart-up); whichever is greater  
 $T_t$  = inlet internal pressure net thrust load at  $M = 1.40$

Cond. No.	Condition		$\Sigma V$	$\Sigma S$	$R_1$	$R_2$	$R_3$	$R_4$	$R_5$	$R_6$	$R_7$	$R_8$
1	Landing	6.0V	13.1	0	3.6	4.5	4.5	3.6	-3.6	-4.5	-4.5	-3.6
2	Landing	-4.0V	-8.7	0	-2.4	-3.0	-3.0	-2.4	2.4	3.0	3.0	2.4
3	S'sonic Maneuver	6.0V + 1.5 $T_D$	13.1	0	11.3	12.3	12.3	11.3	4.2	3.3	3.3	4.2
4	S'sonic Maneuver	-4.0V + 1.5 $T_D$	-8.7	0	5.4	4.8	4.8	5.4	10.1	10.7	10.7	10.1
5	S'sonic Maneuver	3.75V + 2.5 $T_{s-u}$	8.2	0	10.2	10.7	10.7	10.2	5.7	5.1	5.1	5.7
6	S'sonic Maneuver	3.75V + 2.0 $T_{s-u}$	8.2	0	4.3	4.9	4.9	4.3	-0.1	-0.7	-0.7	-0.1
7	Maneuver	2.5S	0	5.5	1.9	1.5	-1.5	-1.9	-1.9	-1.5	1.5	1.9
8	Maneuver	-2.5S	0	-5.5	-1.9	-1.5	1.5	1.9	1.9	1.5	-1.5	-1.9
9	Emergency Landing	9.0D	0	0	2.5	2.5	2.5	2.5	2.5	2.5	2.5	2.5
10	Ditching	-6.0D	0	0	-1.6	-1.6	-1.6	-1.6	-1.6	-1.6	-1.6	-1.6
11	S'sonic Maneuver	1.5 $T_D$ + Aero (s)	0	13.9	15.4	13.8	1.3	-3	-3	1.3	13.8	15.4
12	S'sonic Maneuver	1.5 $T_D$ - Aero (s)	0	-13.9	-3	1.3	13.8	15.4	15.4	13.8	1.3	-3
13	Transonic Maneuver	1.5 $T_t$ + Aero (T)	0	23.0	13.6	10.7	-10.9	-13.8	-13.8	-10.9	10.7	13.6
14	Transonic Maneuver	1.5 $T_t$ - Aero (T)	0	-23.0	-13.8	-10.9	10.7	13.6	13.6	10.7	-10.9	-13.8

Cond. No.	Condition		$\Sigma V$	$\Sigma S$	$R_1$	$R_2$	$R_3$	$R_4$	$R_5$	$R_6$	$R_7$	$R_8$
1	Landing	6.0V	16.7	0	4.3	5.3	5.3	4.3	-4.3	-5.3	-5.3	-4.3
2	Landing	-4.0V	-10.5	0	-2.9	-3.5	-3.5	-2.9	2.9	3.5	3.5	2.9
3	S'sonic Maneuver	6.0V + 1.5 $T_D$	15.7	0	14.4	15.3	15.3	14.4	5.8	4.5	4.5	5.8
4	S'sonic Maneuver	-4.0V + 1.5 $T_D$	-10.5	0	7.2	6.6	6.6	7.2	12.9	13.6	13.6	12.9
5	S'sonic Maneuver	3.75V + 2.5 $T_{s-u}$	9.8	0	12.9	13.5	13.5	12.9	7.5	7.0	7.0	7.5
6	S'sonic Maneuver	3.75V + 2.0 $T_{s-u}$	9.8	0	5.4	6.0	6.0	5.4	0.1	-0.5	-0.5	0.1
7	Maneuver	2.5S	0	6.6	2.2	1.8	-1.8	-2.2	-2.2	-1.8	1.8	2.2
8	Maneuver	-2.5S	0	-6.6	-2.2	-1.8	1.8	2.2	2.2	1.8	-1.8	-2.2
9	Emergency Landing	9.0D	0	0	2.9	2.9	2.9	2.9	2.9	2.9	2.9	2.9
10	Ditching	-6.0D	0	0	-2.0	-2.0	-2.0	-2.0	-2.0	2.0	-2.0	-2.0
11	S'sonic Maneuver	1.5 $T_D$ + Aero (s)	0	15.5	16.9	15.7	4.5	3.3	3.3	4.5	15.7	16.9
12	S'sonic Maneuver	1.5 $T_D$ - Aero (s)	0	-15.5	3.3	4.5	15.7	16.9	16.9	15.7	4.5	3.3
13	Transonic Maneuver	1.5 $T_t$ + Aero (T)	0	25.0	15.2	12.5	-11.7	-14.4	-14.4	-11.7	12.5	15.2
14	Transonic Maneuver	1.5 $T_t$ - Aero (T)	0	-25.0	-14.4	-11.7	12.5	15.2	15.2	12.5	-11.7	-14.4



### CENTER SUPPORT TUBE

#### DESIGN CONDITIONS:

COND. 13 - TRANSONIC  
SIDE LOAD ON THE  
NOSE CONE. (REF.  
FIG. 3.1.6.1-1)

#### LOADS:

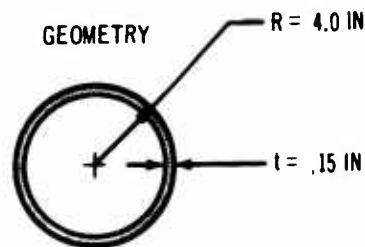
$T_D = 0$  (THE SUPPORT TUBE  
DOES NOT REACT  
ANY EXPULSION  
LOADS)

$$p = 2.2 \text{ psi (ULT.)}$$

$$P = p A$$

WHERE  $A = 933 \text{ in}^2$  -  
THE PROJECTED AREA  
OF THE NOSE CONE.

$$P = 2050 \text{ lbs}$$



#### SECTION A-A

#### MATERIALS & ALLOWABLES

(a) TITANIUM  
(Ti-6AL-4V, COND 1)

(b) @ 500° F

$$F_{TU} = 105000 \text{ PSI}$$

$$F_{CC} \sim 26000 \text{ PSI}$$

#### STRESSES & MARGIN OF SAFETY

THE CRITICAL SECTION IS  
A-A, THE POINT OF  
MAXIMUM MOMENT

$$Q_{A-A} = 2050 \text{ lbs}$$

$$M_{A-A} = 2050(171-79.3) \\ = 188000 \text{ in-lbs}$$

$$f_{SHR} = \frac{Q_{A-A}}{\pi R t} = 1980 \text{ PSI}$$

$$f_b = \pm \frac{M}{\pi R^2 t} = 25000 \text{ PSI}$$

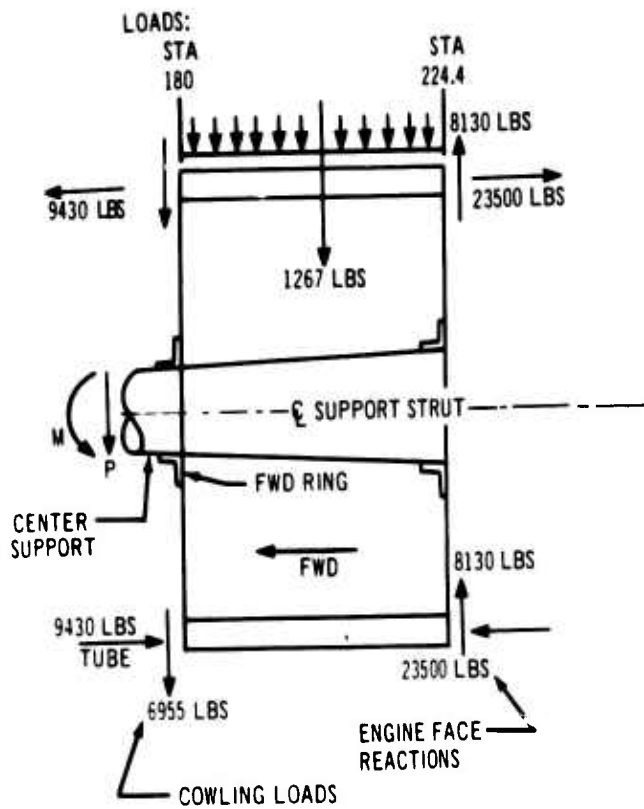
$$M.S. = \frac{26000}{25000} - 1 = +.04$$

Figure 4-74. Inlet Centerbody Support-Tube Analysis

# INLET SUPPORT STRUT

## DESIGN CONDITION:

COND. 13, TRAN-SONIC SIDE PRESSURE ON THE INLET.  
(REF. FIG. 3.1.6.1-1)



M & P ARE NOSE CONE LOADS

$$M = 146200 \text{ IN lbs}$$

$$P = 1452 \text{ lbs}$$

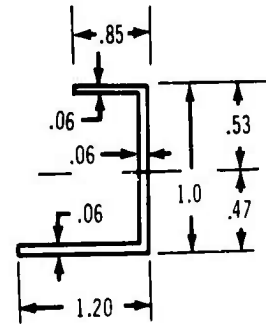
## STRESS ANALYSIS

CHECK THE FWD. RING. ASSUME THE RING AS THE FWD. CAP OF THE STRUT BEAM. THE MOMENT AT THE BEAM & WILL BE REACTED AS A COUPLE LOAD IN THE CAPS OF THE STRUT BEAM.

$$M_{\text{FWD CAP}} = 100360 \text{ IN lbs}$$

$$\text{CAP LOAD} = \frac{MOM}{444} = 2260 \text{ lbs.}$$

## GEOMETRY:



SECTION A-A  
( $\phi = 45^\circ$ )

$$A = .17 \text{ IN}^2$$

$$I = .02 \text{ IN}^4$$

$$R = 6.6 \text{ IN}$$

## MATERIAL & ALLOWABLES:

(a) TITANIUM  
(Ti-6AL-4V, COND 1)

(b) @ 500° F

$$F_{TU} = 105 \text{ KSI}$$

$$F_{CC} = 74 \text{ KSI}$$

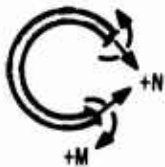
Figure 4-75. Forward Ring Analysis of Inlet Support Strut

## INLET SUPPORT STRUT (CONTD)

STRESSES:

$$M_{A-A} = K_M P R$$

$$N = K_N P$$



WHERE

$$\phi = 45^\circ$$

$$K_M = -.15916$$

$$K_N = .47746$$

$$P = 2571 \text{ lbs}$$

$$R \sim 6.6 \text{ in.}$$

$$M = 2375 \text{ in-lbs}$$

$$N = 1080 \text{ lbs}$$

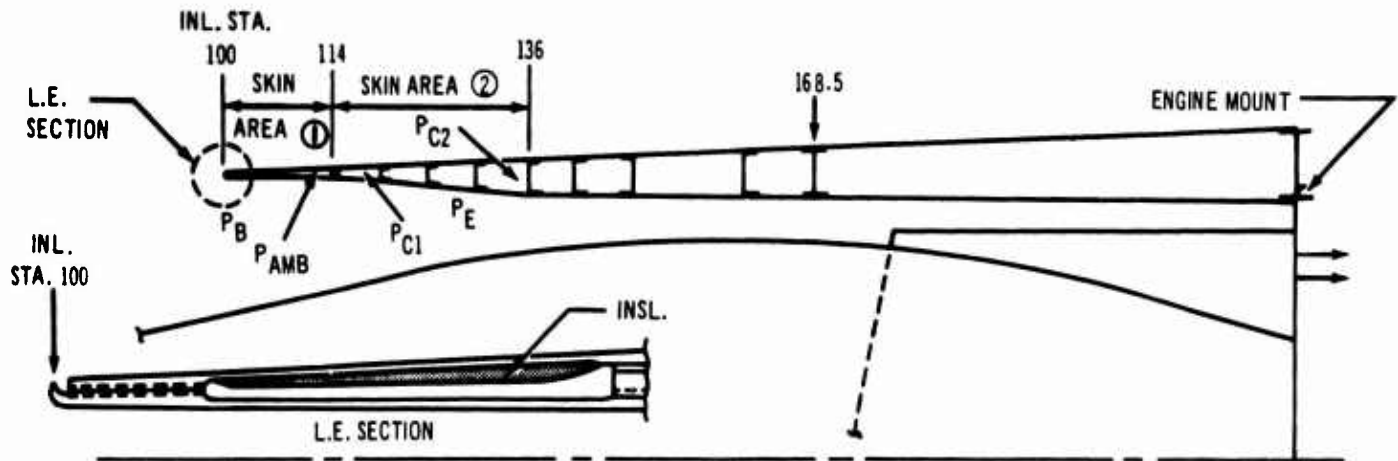
$$f_{A-A} = \frac{N}{A} + \frac{M_c}{I}$$

$$f_{A-A} = 65800 \text{ PSI}$$

$$M.S. = \frac{74000}{65800} - 1 = +.12$$

Figure 4-75 (Concluded)

V2-B2707-6-2



SKIN EXTERNAL PRESSURE, BUCKLING LOADS, REF. INLET DESIGN PRESSURES

SKIN AREA NO.	LOAD COND.	P <sub>AMB</sub>	P <sub>B</sub>	P <sub>E</sub>	P <sub>C1</sub>	P <sub>C2</sub>	LOAD FACTOR	ΔP-ULT.
1 INSIDE	d.	14.7	8.7				1.5	9.0
2 OUTSIDE	c.	14.7				12.6	2.5	5.2
2 INSIDE	c.			11.0	13.0		2.5	5.0

STRESS AND M.S.

$$P_{ALL} = F_{CR} \frac{x_{eff}}{r}$$

$$M.S. = \frac{P_{ALL}}{\Delta P_{ULT}} - 1 =$$

SKIN AREA NO.	(PSI)	M.S.
1 INSIDE	12.8	+ .42
2 OUTSIDE	6.5	+ .25
2 INSIDE	5.2	+ .04
2 INSIDE BLEED AREA	6.35	+ .27

MATERIAL AND ALLOWABLES

T1 - 6 AL - 4V, COND. 1, A, TEMP. RM.

$$F_{CY} = 132 \text{ KSI}$$

$$E_C = 16.4 \times 10^3 \text{ KSI}$$

$$F_{CR} = \frac{K_Y \pi^2 E_C}{12(1 - \nu_e^2)} \left(\frac{x}{L}\right)^2$$

SECTION PROPERTIES

$$Z_L = \frac{L^2}{r^2} \sqrt{1 - \nu_e^2}$$

SKIN AREA NUMBER	L	T	x	Z <sub>L</sub>	K <sub>Y</sub>	F <sub>CR</sub> KSI
INSIDE	3.5	31.2	.040	9.35	5.2	10.0
OUTSIDE	7.0	32.5	.045	32.5	7.6	4.7
2 INSIDE	7.0	30.0	.040	39.0	8.0	3.9
2 INSIDE BLEED AREA	7.0	30.0	.045	34.6	7.2	4.4



FOR .04" DIA. BLEED HOLES AT .30" SPACING

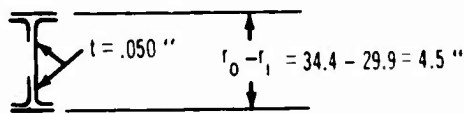
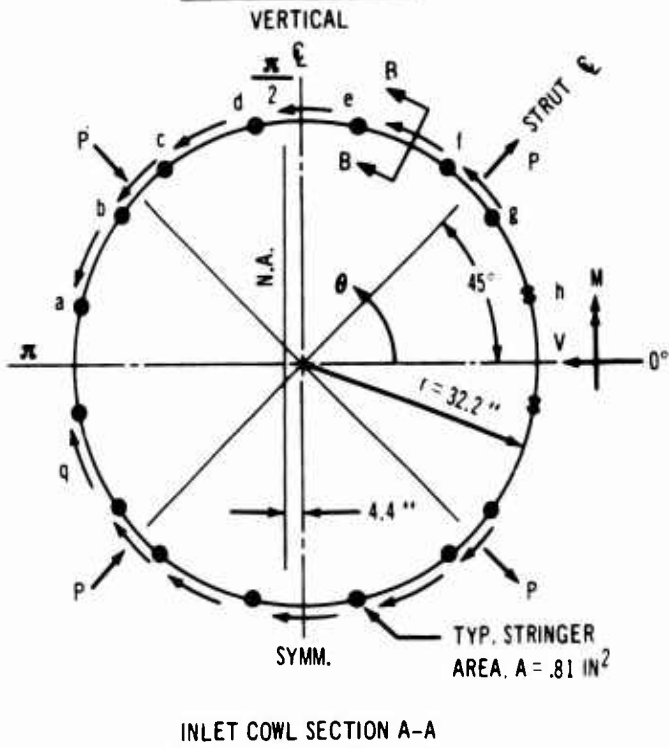
$$r_{eff} = \frac{.26}{.30} x$$

Figure 4-76. Inlet Cowl Analysis

V2-B2707-6-2



2. FRAME, INL STA 168.5



TYP SECTION B-B

SACS  
 TRANSONIC SIDE PRESSURE AS PER (E. 1)  
 SEC. A-A:  
 $V = \pm 18.1 \text{ KIPS}$ ,  $M = \pm 703 \text{ IN-KIPS}$   
 TRFN:  
 $F = \pm \frac{18.1}{4 \times .707} = \pm 6.4 \text{ KIPS}$   
 $M_{MAX} = \pm .59 \text{ PY} \times \frac{\pi}{4} = \pm 32.1 \text{ N-KIPS}$   
 $S_{MAX} = \pm .009 \text{ P} = \pm 4.2 \text{ KIPS}$   
 $N_{MAX} = \pm .478 \text{ P} = \pm 3.1 \text{ KIPS}$   
 $\gamma = \pm \frac{V}{A} = \dots$

SECTION PROPERTIES

$I_{A-A} = 2450 \text{ IN}^4$   
 $A_{B-B} = .54 \text{ IN}^2$   
 $I_{B-B} = 1.67 \text{ IN}^4$   
 $\frac{I}{C} = \frac{32.2}{2.25} = 14.3 > 10 \quad \leftarrow \text{OK}$

△ CURVED BEAM EFFECT, NEGLIGIBLE

MATERIAL & ALLOWABLES

TI-6AL-4V, COND. 1, A : TEMP. = 500°F  
 $F_{TU} = 105.0 \text{ KSI}$   
 $F_{CY} = 94.3 \text{ KSI}$   
 $F_{SU} = 61.5 \text{ KSI}$   
 $E_c = 14.3 \times 10^3 \text{ KSI}$

WEB (B-B) W/ STIFFENERS AT STRUT STRINGERS, A.E. b, c, f ± z

$\frac{a}{b} = 2 ; K_s = 11.3$   
 $\frac{t}{x \sqrt{K_s}} = 25 ; \frac{F_s}{G_T} = .0056$   
 $F_{SCR} = 20.5 \text{ KSI}$

SKIN, OUTER

$L \approx l = \pi (34.4) \frac{25}{180} = 14$   
 $Z_b = \frac{L^2}{\gamma x} \sqrt{1 - \nu_e^2} = 121 ; K_s = 47$   
 $F_{SCR} = \frac{K_s \pi^2 E_c}{12 (1 - \nu_e^2)} \left(\frac{x}{b}\right)^2 = 6.28 \text{ KSI}$

STRESS & M.S.

FLANGE, SEC. B-B

$\Sigma f = \pm \left( \frac{M C}{I} + \frac{N}{A} \right) = 50 \text{ KSI}$

WEB

$f_s = \pm \frac{S}{A_{WEB}} = \pm 20 \text{ KSI}$

M.S. =  $\frac{20.5}{20} - 1 = \pm .03 \quad \leftarrow$

Figure 4-77. Inlet Cowl Frame and Rig Analysis

FRAME INLET STA. 168.5 CON'T

STRESS & M.S., SKIN

STR.	A <sub>f</sub>	Y	A <sub>F</sub> Y	Σ A <sub>f</sub> Y	Q <sub>AV.</sub>
b	.41	27.1	11.0	11.0	82
c	.41	21.2	8.6	19.6	145
d	.41	15.2	6.2	25.8	191
e	.41	2.6	1.1	26.9	199
f	.41	-11.4	-4.6	22.3	165
"	.41	-24.0	-9.7		
	.41	-30.0	-12.2	12.6	93

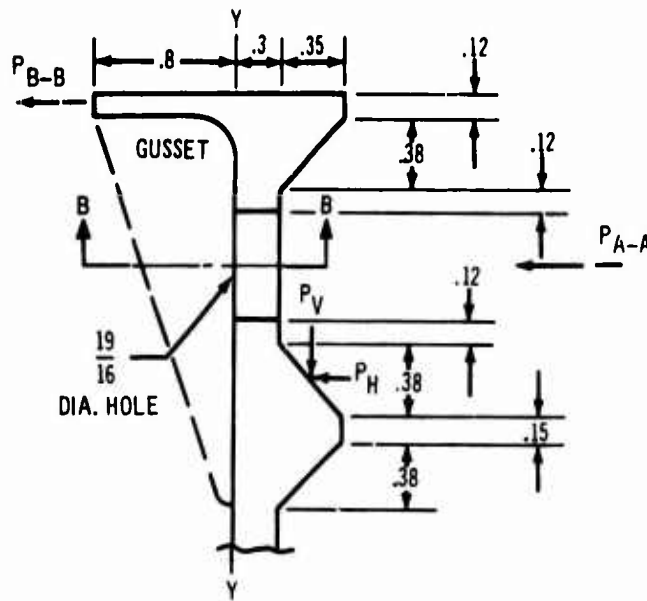
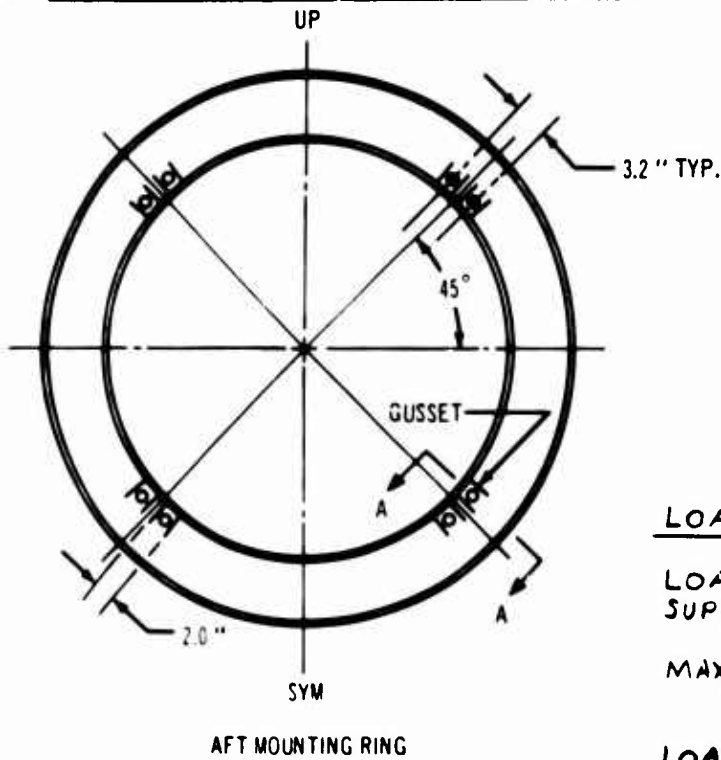
$$q_{MAX.} = \frac{199 \times 1.05}{2} = 105 \text{ LB/IN}$$

OUTER SKIN

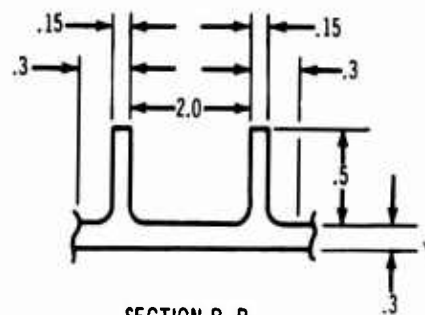
$$t_s = \frac{105}{.045} = 2.34 \text{ KSI}$$

$$M.S. = \frac{6.28}{2.34} - 1 = +1.68$$

3. AFT MOUNTING RING & ATTACHMENTS



SECTION A-A, THICKNESSES LOCAL, INS



SECTION B-B

LOADS

LOAD CONDITION II, TABLE 3.7.4.1-B  
SUPERSONIC MANEUVER, 1.5 T<sub>0</sub> + Σ AERO (S)

MAX. P<sub>BOLT</sub> APPLIED = 16.9 KIPS +  
HEEL-TOE ACTION

LOAD DISTRIBUTION IS ASSUMED TO  
VARY AS "I" AND INVERSELY AS  
MOMENT ARM FOR SECTIONS A-A  
AND B-B.

ASSUME: P<sub>w</sub> = 1/2 P<sub>B-B</sub> WHERE:  
P<sub>B-B</sub> = FLANGE LOAD  
P<sub>A-A</sub> = GUSSET LOAD, 2 GUSSETS

Figure 4-77. (Continued)

V2-B2707-6-2

AFT MOUNTING RING & ATTACHMENTS CONT

SECTION PROPERTIES

SECTION A-A:

$$A = .902 \text{ IN}^2$$
$$\bar{Y} = .185 \text{ IN}$$
$$I = .0634 \text{ IN}^4$$

SECTION B-B:

$$A = .87 \text{ IN}^2$$
$$\bar{Y} = .219 \text{ IN}$$
$$I = .0285 \text{ IN}^4$$

MATERIAL & ALLOWABLES

Ti-6AL-4V, COND. 1, A : TEMP. = 500°F

$$F_{TU} = 105.0 \text{ KSI}$$
$$F_{CY} = 94.3 \text{ KSI}$$
$$F_{ORU} = 185.0 \text{ KSI}$$

BOLT, EW8 T815,  $\frac{9}{16}$ "  $\phi$ , Ti-ALLOY

$$P_{ALL} = .83 \times 27.8 = 23 \text{ KSI}$$

STRESS & M.S.

$$P_{A-A} + P_{B-B} = 16.9 \text{ KIPS ULT.}$$

$$P_{B-B} = \frac{.0285}{.0285 + .0634} \times 16.9 = 5.25 \text{ KIPS}$$

$$P_{A-A} = 16.9 - 5.25 = 11.65 \text{ KIPS}$$

$$f_{A-A} = \frac{11.65 \times \frac{1}{2} \times 1 \times .985}{.0634} = 90.6 \text{ KSI}$$

$$M.S. = \frac{105}{90.6} - 1 = +.16 \leftarrow$$

$$f_{B-B} = \frac{5.25 \times .92 \times .58}{.0285} + \frac{\frac{1}{2} \times 5.25}{.87}$$

$$= 101.42 \text{ KSI}$$

$$M.S. = \frac{105}{101.42} - 1 = +.03 \leftarrow$$

$$P_{BOLT} = 16.9 + \frac{1}{2} \times 5.25 = 19.6 \text{ KIPS}$$

$$M.S. = \frac{23}{19.6} - 1 = +.17 \leftarrow$$

Figure 4-77 (Concluded)

V2-B2707-6-2

## 5.0 FATIGUE ANALYSIS

A preliminary fatigue analysis has been completed for the B-2707. The analysis results provide data on the fatigue life of the airframe, design stress requirements for fatigue, and the significance of mission and loading parameters on fatigue life. The analysis was accomplished for a spectrum of predicted B-2707 usage and associated loadings for selected locations on the wing, body and empennage. The results are summarized in Par. 5.5.

### 5.1 FATIGUE CRITERIA

The airframe of the B-2707 will have a design service life of at least 50,000 flight hr. Achievement of this goal means that none of the primary structure will experience fatigue cracking sufficient to warrant significant design modification during this period. With normal maintenance and inspection, the fatigue life can be extended indefinitely.

The structure shall be designed and analyzed for the design service life multiplied by a scatter factor. The scatter factor shall be four except for the following situation. Parts that can be readily inspected and replaced, and where sufficient redundancy exists so safety is not compromised, can be designed to a scatter factor of two.

In addition to fulfilling the requirements of this criteria, full advantage will be taken of a comparative approach like that being used on the 747. This approach is based on an integration of fatigue analysis, test, and service experience from the large fleets of contemporary Boeing commercial airplanes. Much available data are being used to relate fatigue cracking of airline operations (and, equally important, absence of fatigue cracking) to locations and times predicted by analyses and tests. Retroactive checking tests are also made. Extrapolation of this experience to the SST can be accomplished by the relationships between design stresses, operating stresses, structural fatigue quality, and fatigue environment. As a further aid in life prediction and design development, a microstress analysis method has been developed and is being adapted to rapid design usage by computer

methods. This method has proven successful in analytically predicting fatigue failure locations and relative fatigue quality.

### 5.2 FATIGUE ENVIRONMENT

The fatigue environment consists of the airplane usage and the resulting loads and temperatures.

A study was made to establish predicted B-2707 operational usage. Flight distances and relative frequencies were determined for integration of the B-2707 into the route structure of nine airlines. An average use for the nine airlines was calculated, and is shown in Fig. 5-1. Operational flying was assumed to comprise 96 percent of the total B-2707 flight hours. The remaining 4 percent was assumed to be used for pilot training and check flights.

The loading environment used in the fatigue analysis was that resulting from gusts, maneuvers, landing impact, runway roughness, and pressure and thermal gradients. Gust data used in prior SST fatigue analyses were based on the discrete gust atmospheric definition presented in Ref. 17. More recent data for the higher altitudes, presented in Ref. 18, indicates less severe turbulence than that of Ref. 17. The more conservative gust spectrum of Ref. 17 was retained for this analysis and is shown in Fig. 5-2. For subsequent fatigue analyses of the B-2707, the power spectral density approach will be used to determine the airplane response to turbulence.

Flight maneuver spectra are based on unpublished data obtained from subsonic commercial jet transport flying. These data were received as an informal transmittal from the NASA and cover about 7,400 operational flights (7.5 times  $10^6$  nmi) and 1,400 training and check flights (0.4 times  $10^6$  nmi). The derived maneuver load-factor exceedance curves for operational B-2707 flights are shown in Fig. 5-3.

Landing impact data for the fatigue analysis were obtained from Ref. 19. This reference presents probability distributions for both sink speed and cg acceleration for subsonic commercial aircraft. The sink speed probability distribution

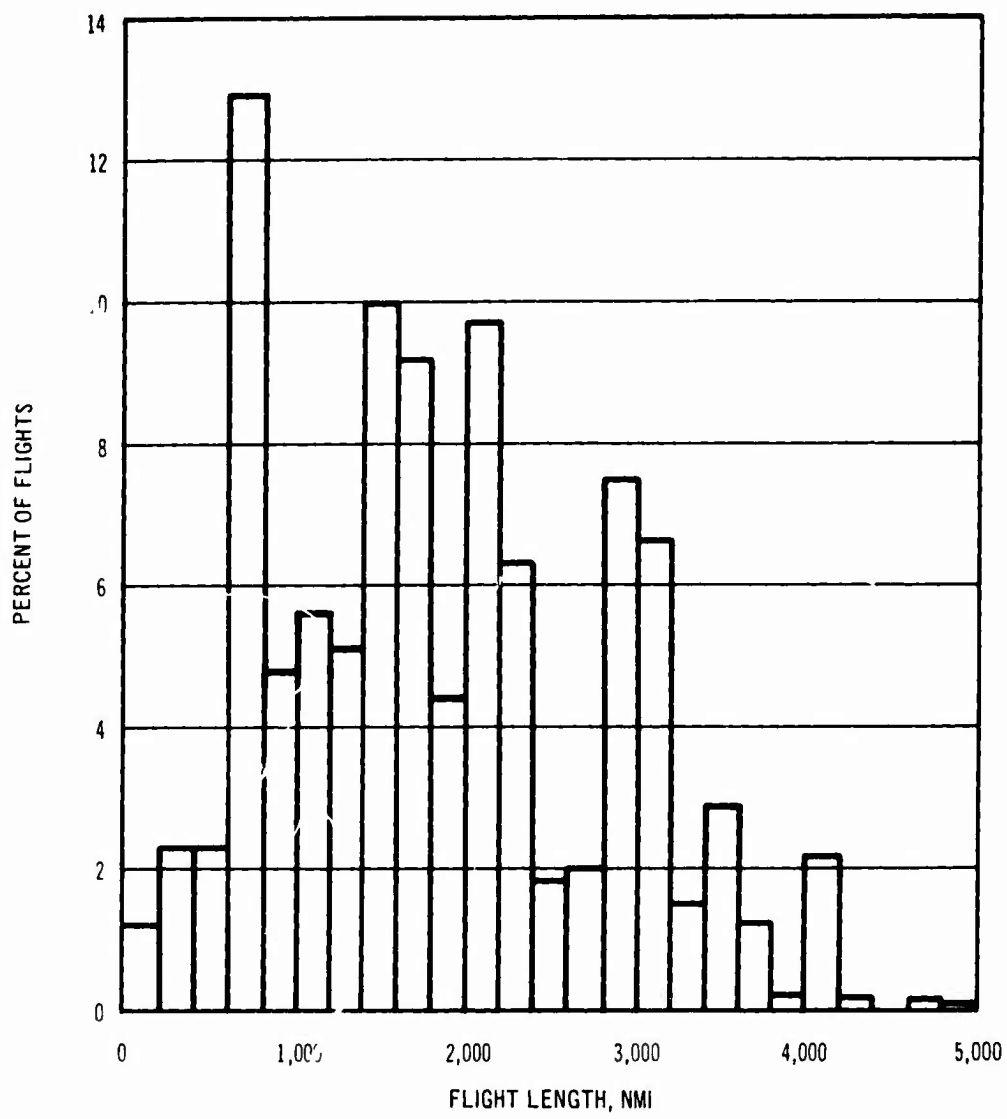


Figure 5-1. Operational Flight Length Distribution

V2-B2707-6-2

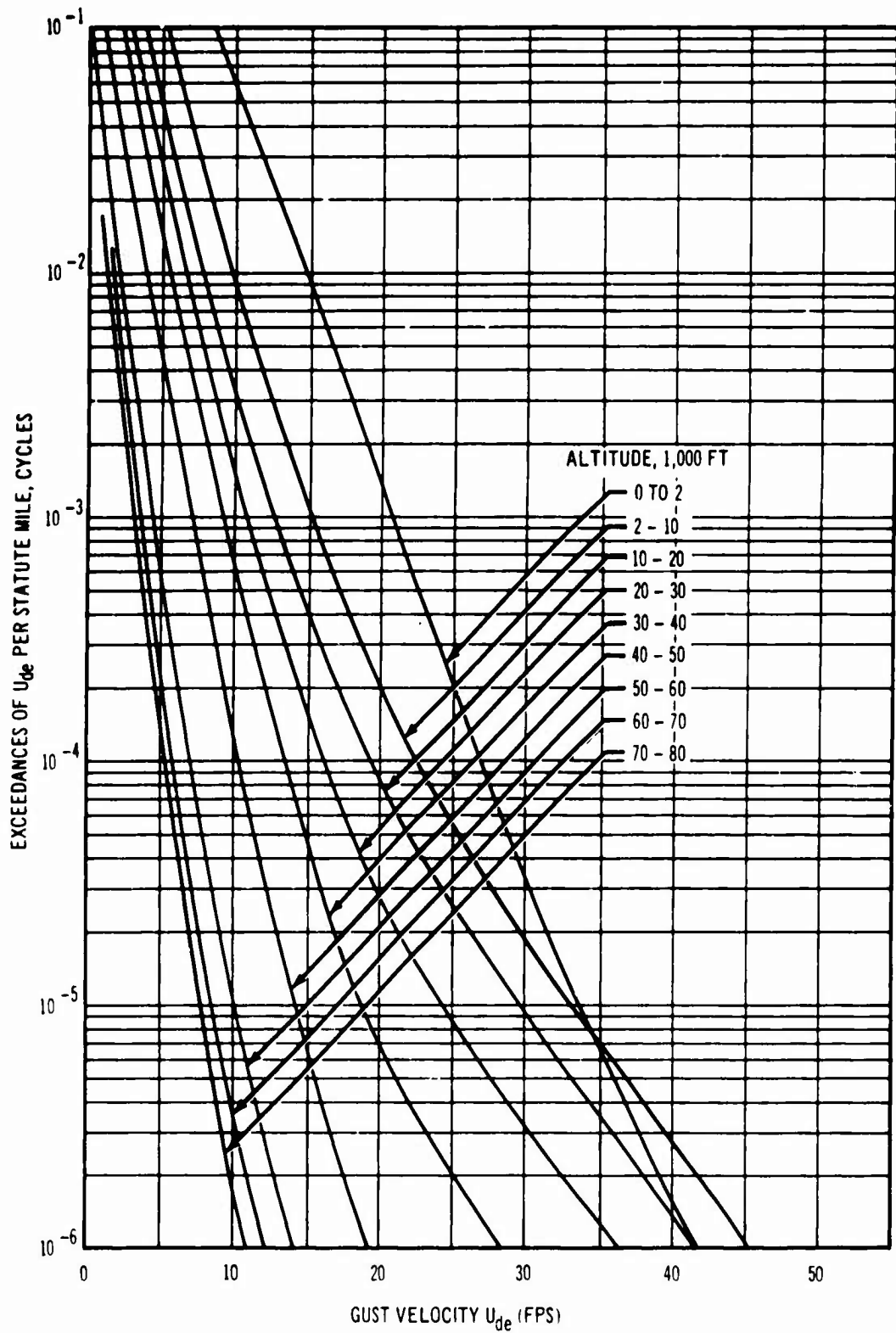


Figure 5-2. Gust Spectrum

V2-B2707-6-2

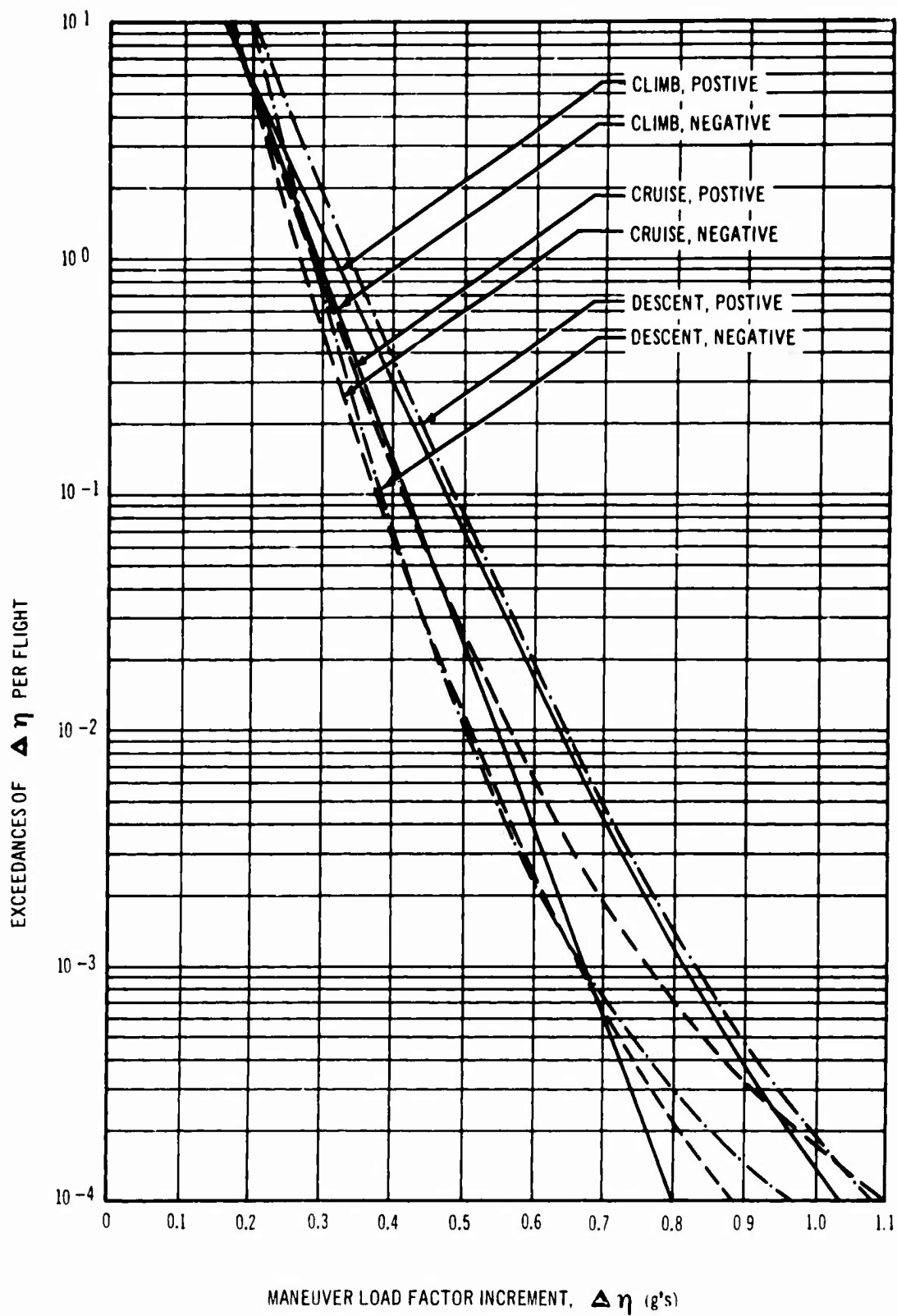


Figure 5-3. Operational Flight Maneuver Spectrum

V2-B2707-6-2

as being the most applicable for predicted SST ground contact conditions and is shown in Fig. 5-4.

Taxi incremental load factor data in Ref. 20 were used for airframe fatigue damage caused by runway roughness. The taxi spectrum is shown in Fig. 5-5.

Stresses caused by body pressure were calculated based on a 6000-ft cabin pressure altitude.

Structural temperatures were calculated for standard day conditions by the methods described in Part C, Design Criteria, Loads, Aerodynamic Heating, Flutter (V2-B2707-7) of the Airframe Design Report. The thermal stresses caused by the temperature gradients were calculated and included as contributions to the total 1-g stresses.

### 5.3 S-N CURVES

S-N curves have been derived from the results of extensive development fatigue testing for a variety of structural details. Three families of curves were selected for use in this analysis, and are designated as S-N No. 1, S-N No. 2, and S-N No. 3. Each represents a quality level of fatigue resistance representative of specific structural details.

S-N No. 1 represents the fatigue resistance of stiffener runouts, access door panels, and Taper-Lok spanwise splices. It is used in the analysis of the skin for the wing lower surface, horizontal-tail upper surface and vertical tail, and is shown in Fig. 5-6. S-N No. 2 represents the attachment of a machined stiffener free flange to a rib chord. It is used for the analysis of the stiffener free flange for the wing lower surface and the horizontal-tail upper surface and is shown in Fig. 5-7. S-N No. 3 represents the skin in the skin-stiffener-split tear strap construction in the thin-gage forebody area, the skin in an aftbody longitudinal skin splice, and the connections to the stiffener webs of the shear ties to the frames or ribs for the fuselage and the vertical tail. S-N No. 3 is shown in Fig. 5-8.

### 5.4 FATIGUE ANALYSIS PROCEDURE

The fatigue analysis was accomplished by integrating the fatigue damage from the total flight environment using the linear cumulative fatigue damage method. The typical structural

locations at which the analyses were made are representative of the total B-2707 configurations and show the most critical fatigue areas. Eight analysis locations are presented:

- Movable-wing lower surface at midspan.
- Movable-wing lower surface near root (just outboard of pivot-affected area).
- Wing center section lower surface.
- Forebody crown area (30 percent of body length).
- Forebody crown area (50 percent of body length).
- Aftbody crown area.
- Horizontal-tail upper surface near root.
- Vertical tail near root.

These locations represent the general fatigue-critical areas of the airframe. By analyzing at these locations and by using S-N curves representative of repetitive structural details, any reductions in allowable design stresses necessary to satisfy fatigue-life requirements can be determined. From the amount of reduction in design stress (if required) and the area of structure affected, increments of airframe weight necessary to satisfy the fatigue criteria can be calculated.

For each analysis location, the fatigue damage was calculated for a 3,500-nmi flight and for a 1,700 nmi flight. The mission profiles for these two operational missions are shown in Figs. 5-9 and 5-10.

The fatigue analysis for the movable-wing lower surface near the root is described to illustrate the procedure. The 3,500-nmi mission was divided into 24 segments. The segments were selected to be compatible with the gust altitude bands and sufficiently small so that average values of gross weight, speed, altitude, wing sweep, and temperature would be representative of conditions within a segment. For each segment, the one-factor mechanical stress, the thermal stress, the stress change for a unit gust, and the stress change for a unit maneuver-load-factor increment were calculated. The fatigue damage caused by the stress variations resulting from gusts, maneuvers, landing



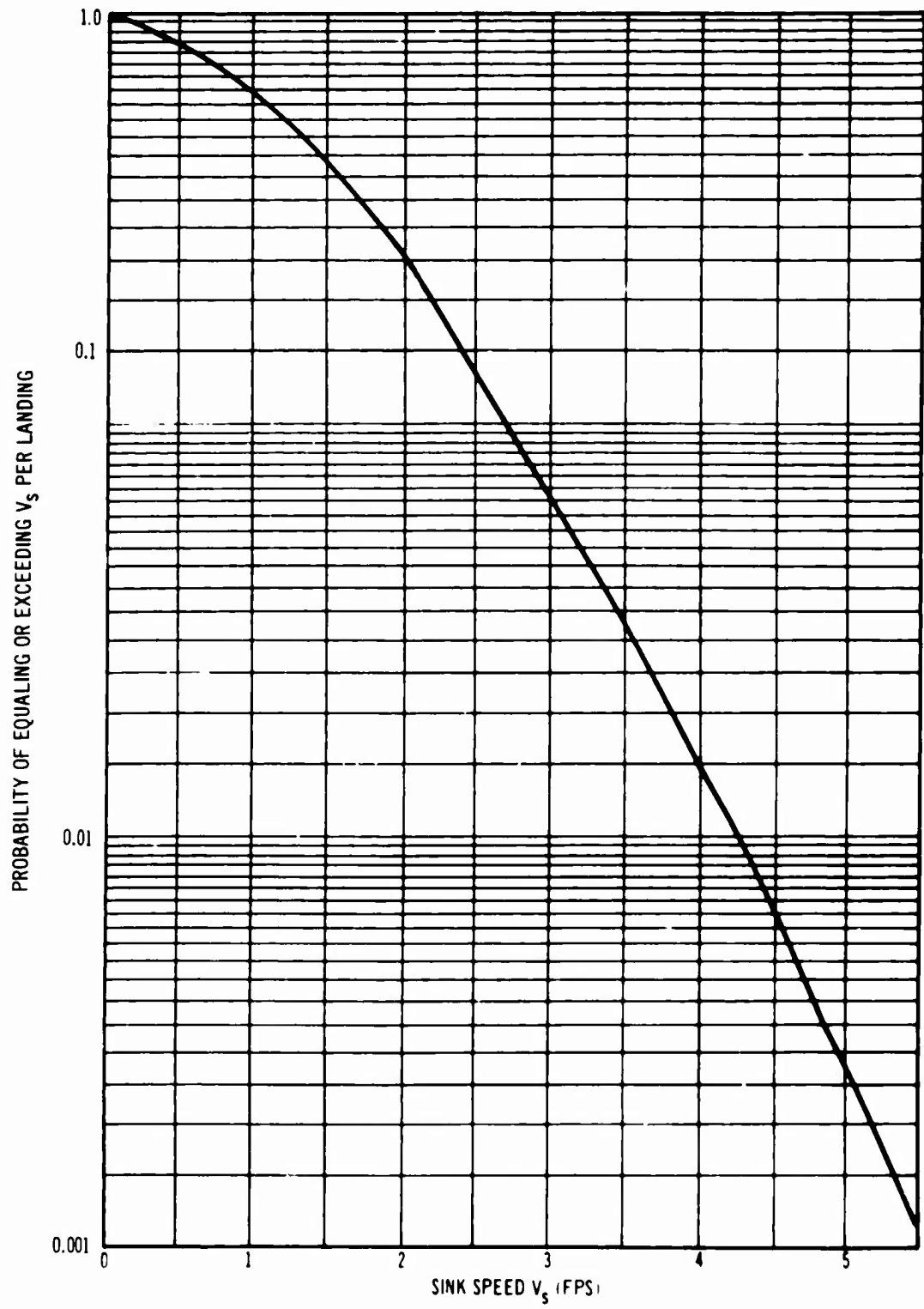


Figure 5-4. Sink Speed Spectrum

V2-B2707-6-2

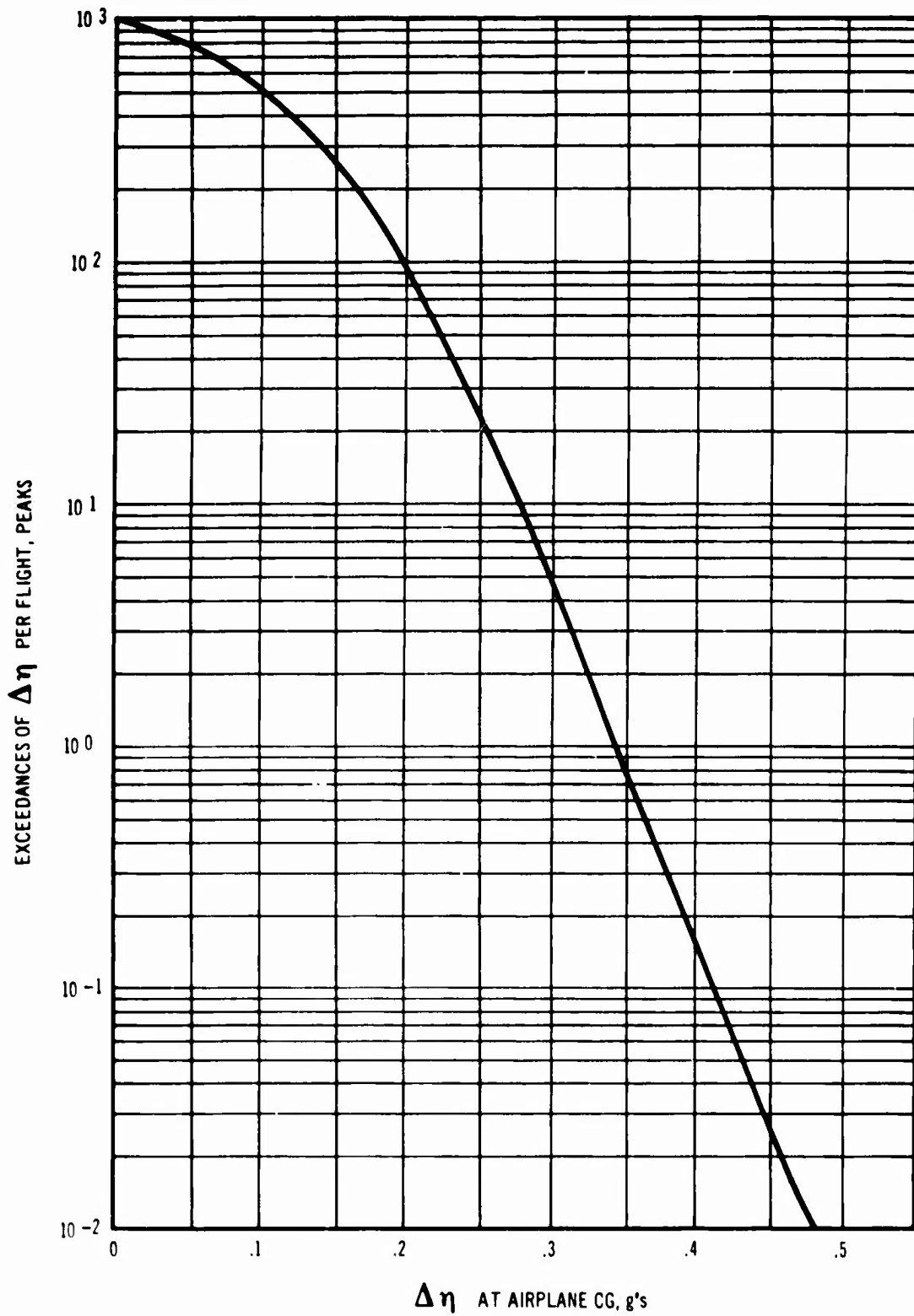


Figure 5-5. Taxi - Load Factor Spectrum

V2-B2707-6-2

impact, or runway roughness was calculated for each segment containing that environment.

For this analysis location (and most other locations of the airframe), most of the fatigue damage is caused by ground-air-ground (GAG) cycle and a similar secondary, or thermal, cycle, caused primarily by a significant variation of the one-factor flight stress. The GAG cycle is defined as the stress cycle varying between the maximum and minimum stresses statistically experienced once per flight. The secondary cycle is established in a similar manner for subportions of the flight. This method is illustrated, for the skin, in Fig. 5-11. The fatigue damage from all sources is then added together to provide a total fatigue damage for the flight, as shown in Table 5-A.

A similar procedure was followed for the 1,700-nmi mission. From the fatigue damage per flight for these missions, and from the pattern of

damage variation with flight length established by previous analyses, a plot was prepared showing the fatigue damage as a function of flight length. This plot is presented in Fig. 5-12. The number of flights of each length, from 100 to 4,900-nmi in 200-mile increments, was determined from the distribution of Fig. 5-1 for 48,000 hr of operational flying. Multiplying the number of flights of each length by the damage per flight, and summing the products for all of the flight lengths, gave the total damage for operational flights. The damage caused by training flights was calculated by using the same ratio between total training flight damage and total operational flight damage as established by prior analyses. Any error resulting from this simplification would be small because there are only 2,000 hr of training flights as compared to 48,000 hr of operational flights. The fatigue damage summation and resulting fatigue life are shown in Table 5-B.

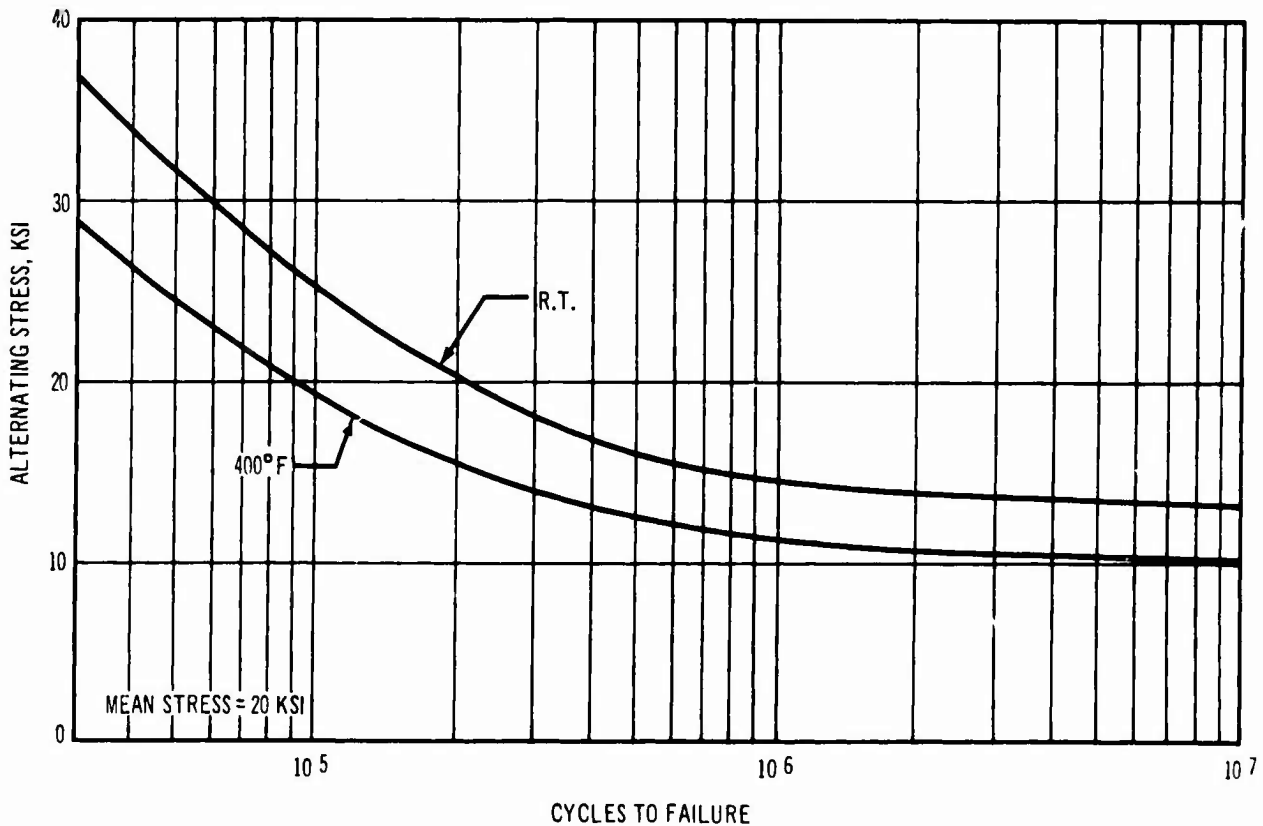


Figure 5-6. S-N No. 1

Because the calculated fatigue life of 548,000 hr is greater than the design requirement, no reduction in the allowable design stress, below that used for static sizing, is required. If the calculated fatigue life had been less than the required life, the analysis would have been repeated for a reduced allowable design stress. By repeating the analysis for different values of allowable stress, the relationship between fatigue life and allowable design stress could be determined. The design stress that would give the required life could then be established from a plot of this relationship. This is illustrated in Fig. 5-13.

In order to evaluate the primary contributions to the airframe weight required by fatigue considerations, this preliminary analysis has emphasized evaluation of the basic structure of the airframe. Structural joints are also potential fatigue-critical items. Satisfactory fatigue life can be developed for the joints by suitable local pad-up (as a part of good detail design). The total contribution of this local incremental weight to the airframe weight is small when compared to that which would result from a reduction in the allowable design stress for general areas of the structure. Therefore, the weight increment for joint fatigue requirements

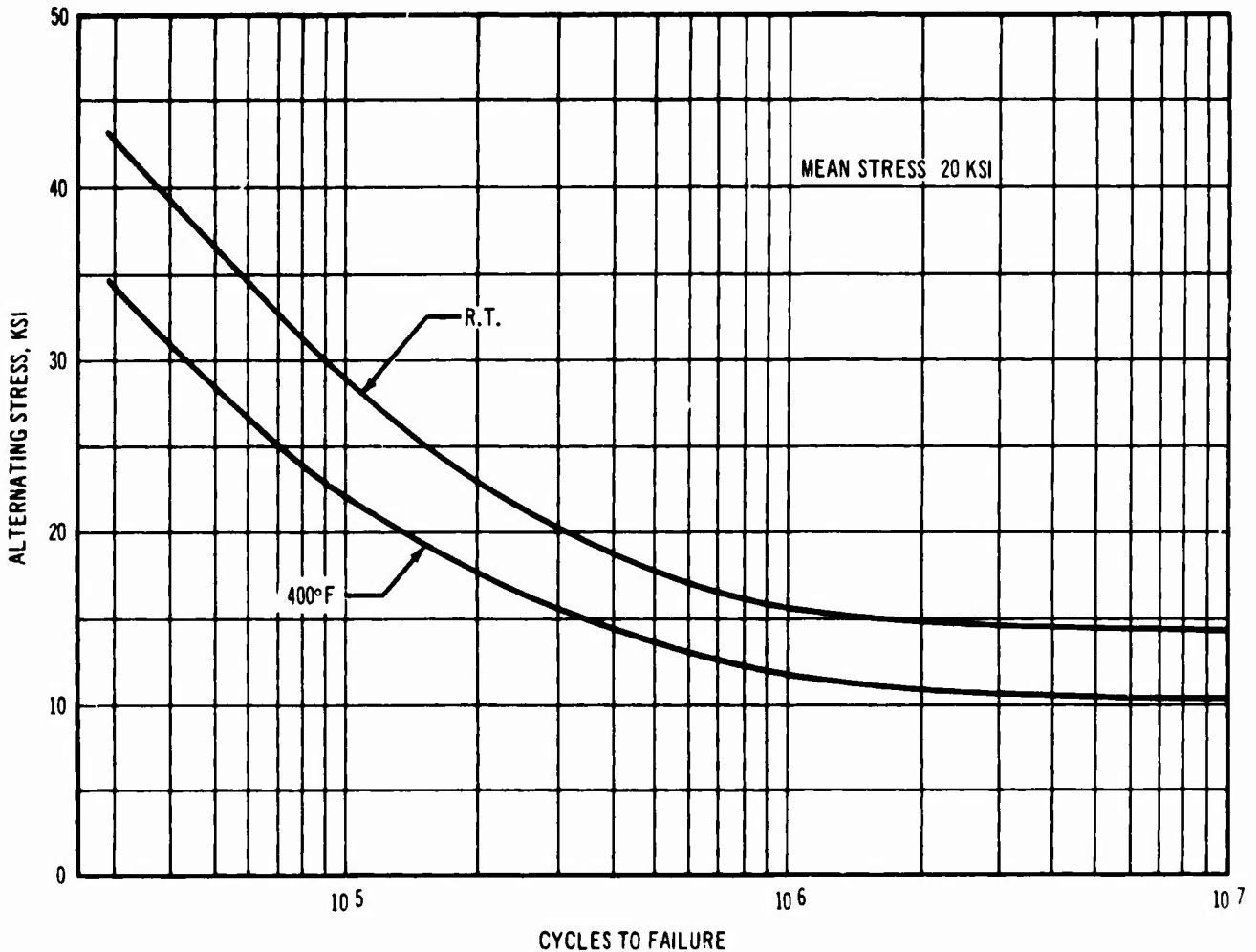


Figure 5-7. S-N No. 2

was estimated from the results of prior fatigue analyses and from consideration of the size of the B-2707 relative to the size of the SST models previously analyzed.

### 5.5 FATIGUE ANALYSIS RESULTS

The calculated fatigue lives for the analysis locations are summarized in Table 5-C. For each analysis section, the fatigue life for a skin element and a stiffener element is shown for structure sized by static strength requirements. Except for the wing-center-section lower surface skin, all of the fatigue lives exceed the maximum analysis requirement of 200,000 hr (scatter factor of four). In order to conservatively show 200,000 hr life for the center section, a reduction in design stress to 90 percent of that permitted for static sizing is required. This results in a 50-lb weight increment for the center section basic structure. The weight increment for the joint areas is 110 lb, giving a

total fatigue weight increment of 160 lb, which is included in the weight statement.

For all of the analysis locations, almost all of the calculated fatigue damage was caused by the GAG and secondary cycles. Variations about the mean stress caused by gusts, maneuvers, landing impact cycles, and runway roughness did not contribute significant fatigue damage. They did, however, contribute significantly to maximum and minimum stresses for the GAG and secondary cycles.

### 5.6 ONE-G STRESSES

The variations of 1-g stresses with time during the flight were plotted for the 3,500-nmi mission. For each of the eight analysis locations, the 1-g mechanical stresses were determined along with the total stresses resulting from mechanical and thermal stresses for both the skin and the stiffener. These are shown in Figs. 5-14 through 5-21.

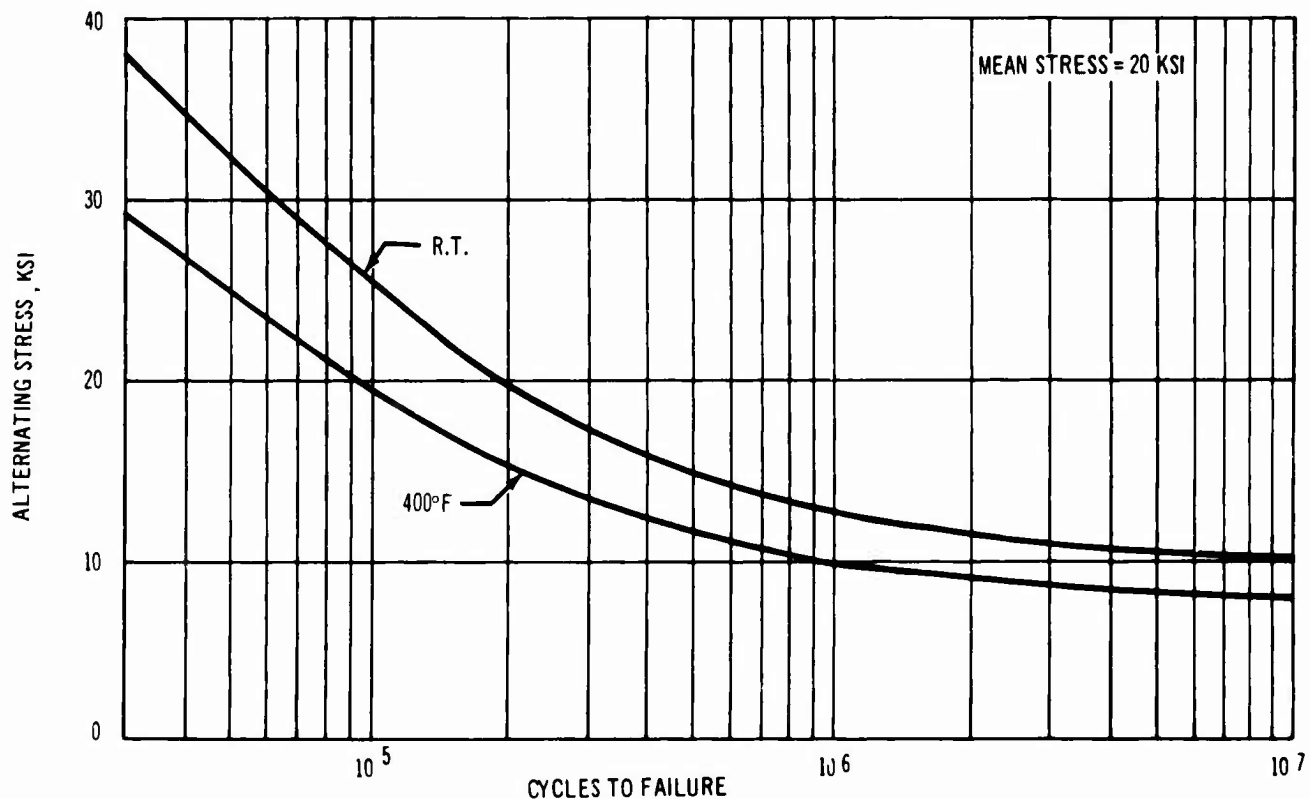


Figure 5-8. S-N No. 3

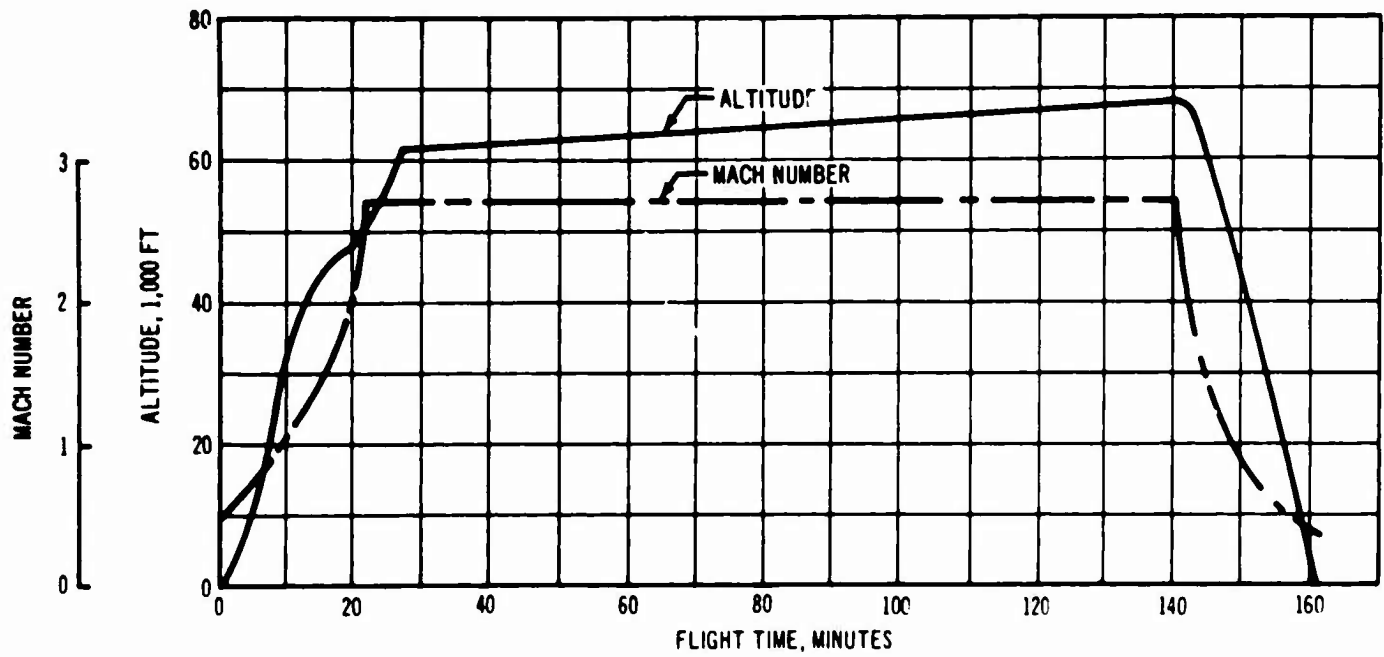


Figure 5-9. 3,500 Nmi Mission Profile

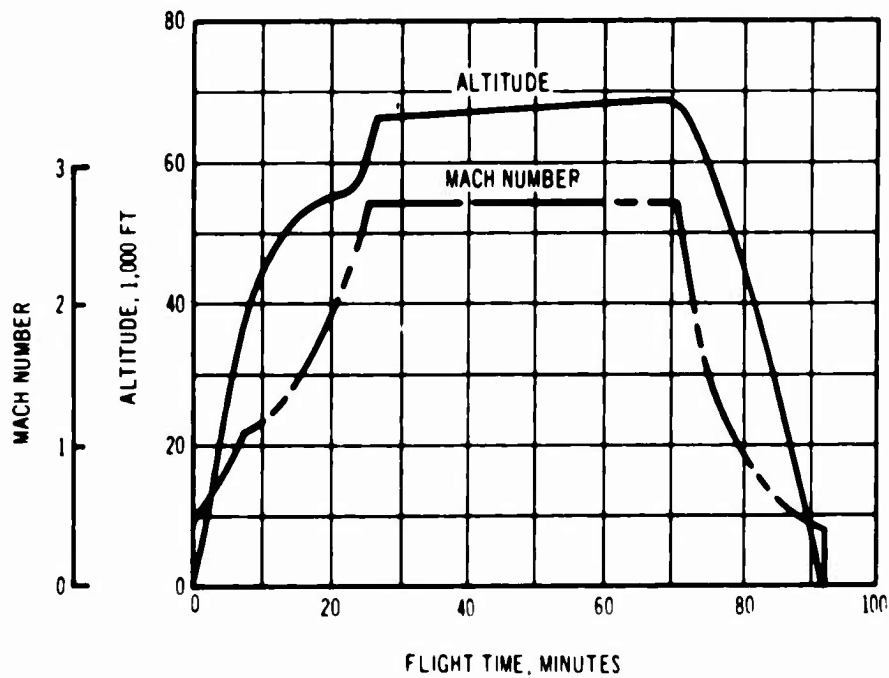


Figure 5-10. 1,700-Nmi Mission Profile

V2-F2707-6-2

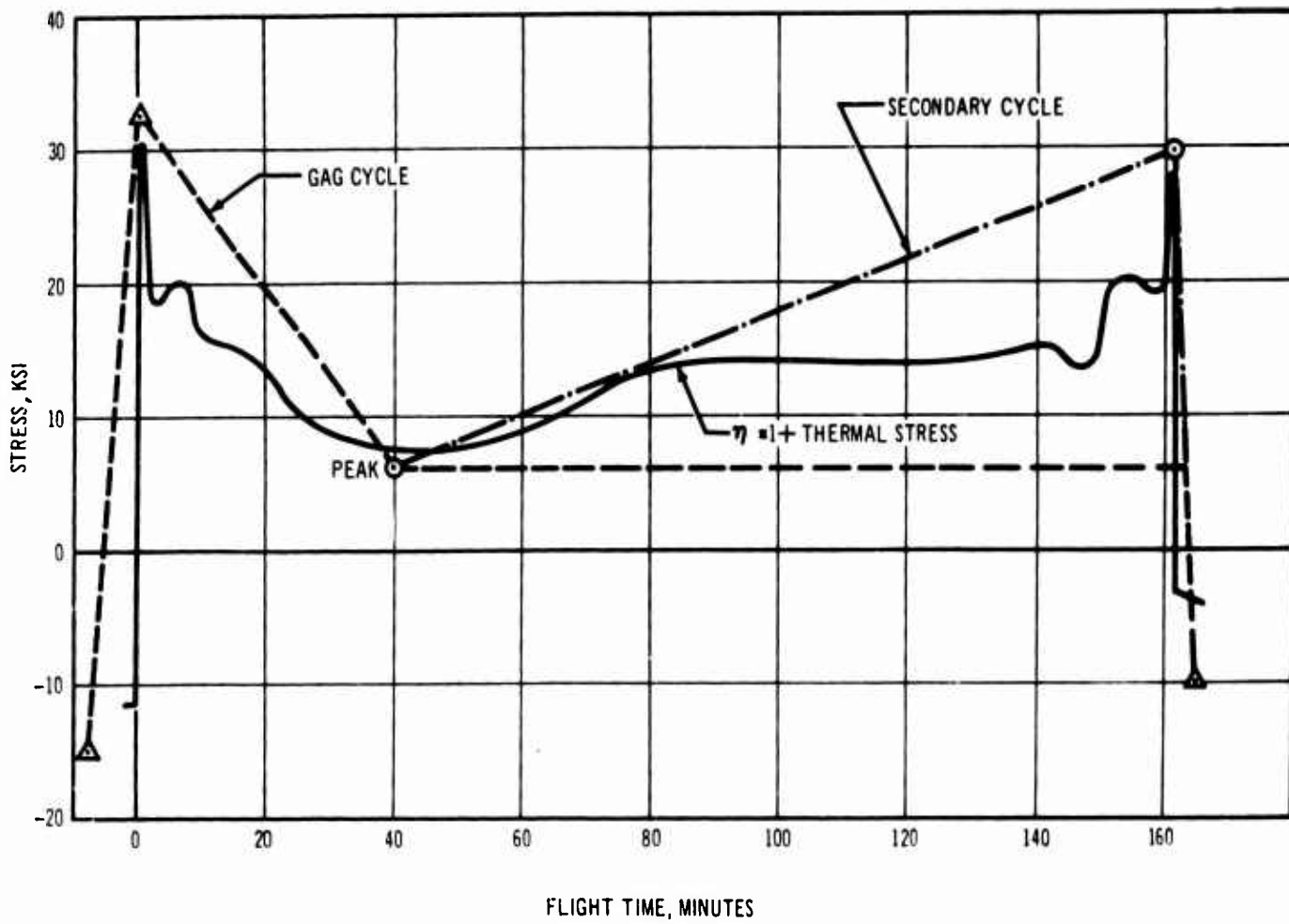


Figure 5-11. Illustration of GAG and Secondary Cycle

Table 5 - A. Fatigue-Damage Summary For Wing Lower-Surface Skin (Root) for 3500-NMI Mission

Flight Segment				Fatigue Damage in 1,000 Flights, Percent					
No.	Altitude, 10 <sup>3</sup> FT	Mach No.	Flap Position	Taxi	Gust	Maneuver	Landing Impact	Gag Cycle	Secondary Cycle(s)
1		Taxi		0.	---	---	---		
2	1.0	0.30	Down	---	0	0	---		
3	1.0	0.45	Up	---	0	0	---		
4	5.7	0.57	↑	---	0.00002	0	---		
5	15.0	0.68		---	0.00004	0	---		
6	23.0	0.81		---	0.00004	0	---		
7	28.5	0.90		---	0.00002	0	---		
8	35.7	1.10		---	0	0	---		
9	42.5	1.38		---	0	0	---		
10	47.5	1.83		---	0	0	---		
11	55.2	2.40		---	0	0	---		
12	61.5	2.70		---	0	0	---		
13	64.5	2.70		---	0	0	---		
14	67.0	2.70		---	0	0	---		
15	65.5	2.04		---	0	0	---		
16	55.0	1.22		---	0	0	---		
17	45.0	0.90		---	0	0	---		
18	35.5	0.75		---	0	0	---		
19	25.5	0.60		---	0.00001	0	---		
20	15.0	0.50	↓	---	0.00002	0	---		
21	6.0	0.38	Up	---	0.00001	0	---		
22	1.0	0.26	Down	---	0	0	---		
23	Landing Impact			---	---	0	0.		
24	Taxi			0.	---	---	---		
Totals				0.	0.00016	0.	0.	0.465	0.02306
Total Damage In 1,000 Flights = 0.4882 Percent									
Total Damage Per Flight = 0.000488 Percent									



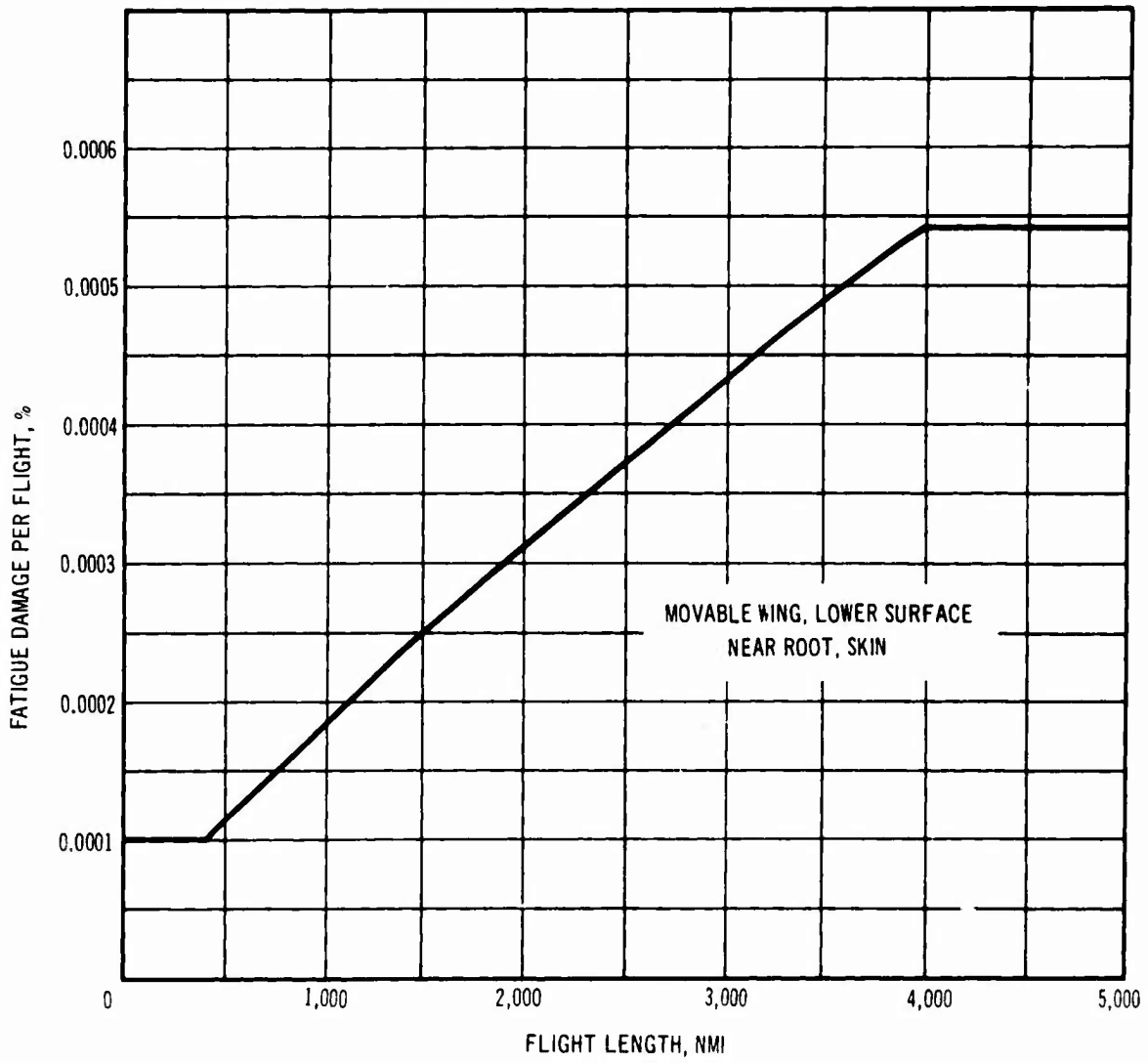


Figure 5-12. Fatigue-Damage Variation With Operational Flight Length

Table 5 - B. Fatigue Damage Summary

Structural Location: Movable Wing, Lower Surface Near Root, Skin

Flight Length, NMI	No. of Flights per 48,000 Hr of Operational Flights	Fatigue Damage per Flight, Percent	Fatigue Damage per 48,000 Hr of Operational Flights
100	345	0.000100	0.035
300	661	0.000100	0.066
500	661	0.000115	0.076
700	3,707	0.000143	0.530
900	1,380	0.000180	0.248
1,100	1,609	0.000195	0.314
1,300	1,466	0.000220	0.323
1,500	2,874	0.000250	0.719
1,700	2,644	0.000272	0.719
1,900	1,265	0.000295	0.373
2,100	2,788	0.000320	0.892
2,300	1,811	0.000350	0.634
2,500	517	0.000370	0.191
2,700	575	0.000395	0.227
2,900	2,156	0.000420	0.906
3,100	1,897	0.000440	0.835
3,300	431	0.000460	0.198
3,500	833	0.000490	0.408
3,700	345	0.000510	0.176
3,900	57	0.000530	0.030
4,100	575	0.000545	0.313
4,300	57	0.000545	0.031
4,500	0	0.000545	0.000
4,700	57	0.000545	0.031
4,900	29	0.000545	0.016
$\Sigma =$			8.291

Damage for Training Missions = 0.829  
 Total Damage for 50,000 Hours = 9.120

Fatigue Life, Hours = 548,000

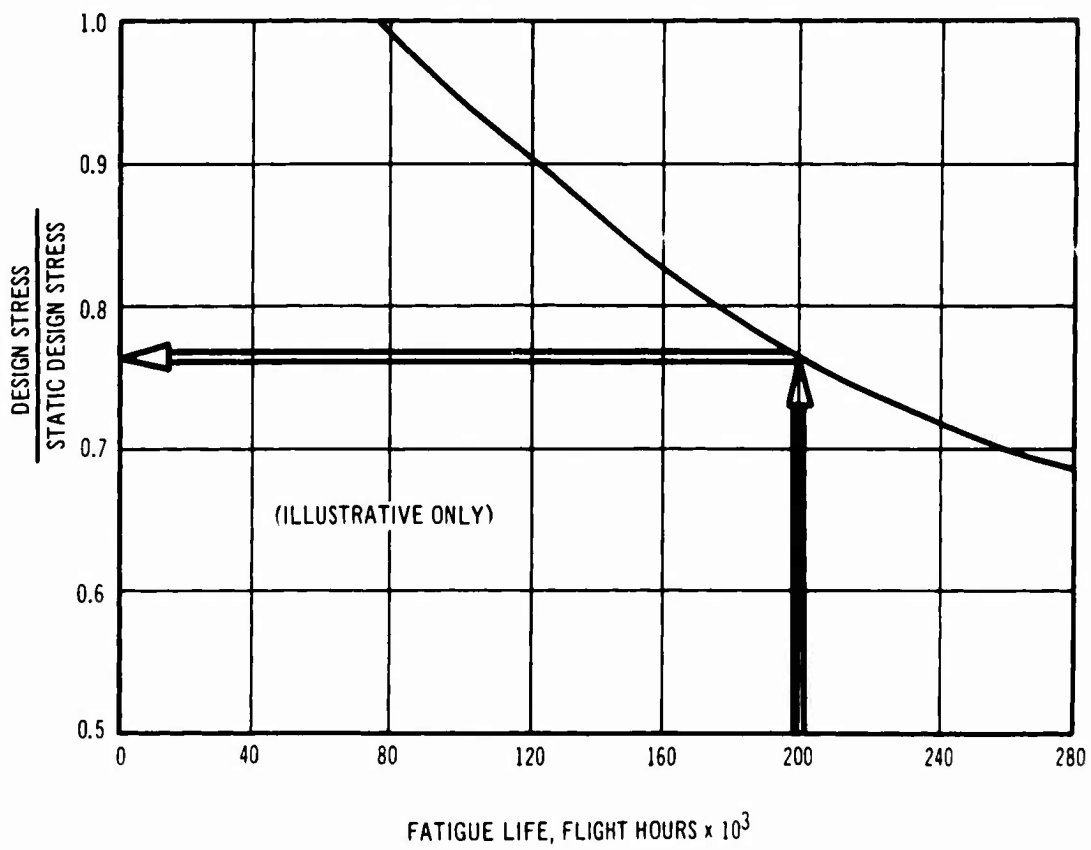


Figure 5-13. Design Stress Determination for Fatigue Life

Table 5 - C. Fatigue Life Summary

Location		Structural Element	Fatigue Life For Static Design, Hours	Fatigue Life Design Service Life
Movable Wing Lower Surface	Root	Skin	548,000	11.0
		Stiffener	652,000	13.0
	Midspan	Skin	2,500,000	50.0
		Stiffener	500,000	10.0
Wing Center Section Lower Surface		Skin	135,000*	2.7*
		Stiffener	318,000	6.4
Forward Body Crown	30% Body Length	Skin	∞	>100
		Stiffener	∞	>100
	50% Body Length	Skin	∞	>100
		Stiffener	∞	>100
Aft Body Crown		Skin	590,000	11.8
		Stiffener	295,000	5.9
Horizontal Tail Upper Surface at Root		Skin	590,000	11.8
		Stiffener	11,800,000	>100
Vertical Tail at Root		Skin	∞	>100
		Stiffener	808,000	16.0

\*Design stress subsequently reduced to 0.90 static design stress. This provides 200,000 hr fatigue life and a ratio of four between fatigue life and design service life.

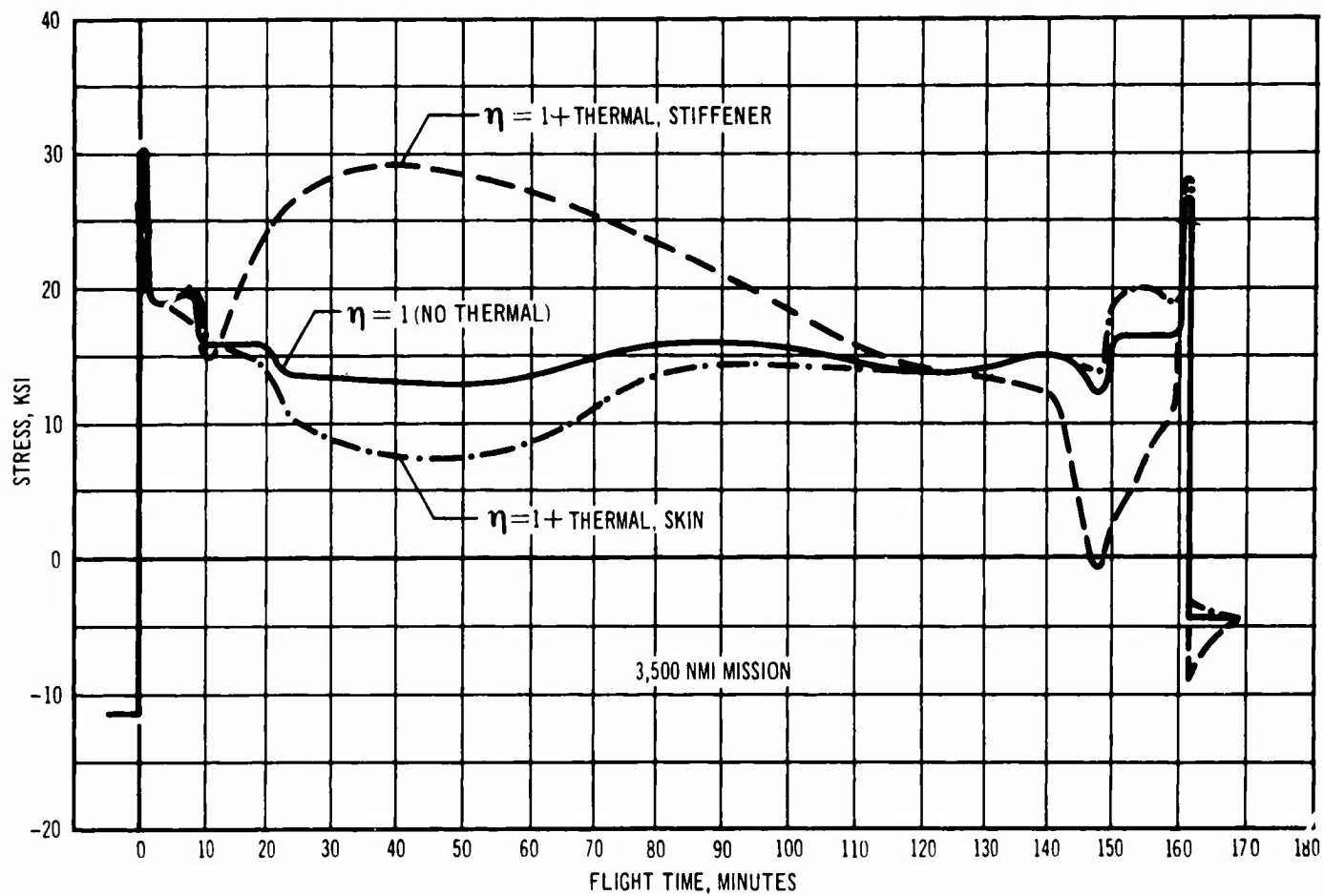


Figure 5-14. One-g Stress History, Movable-Wing Lower Surface At Root

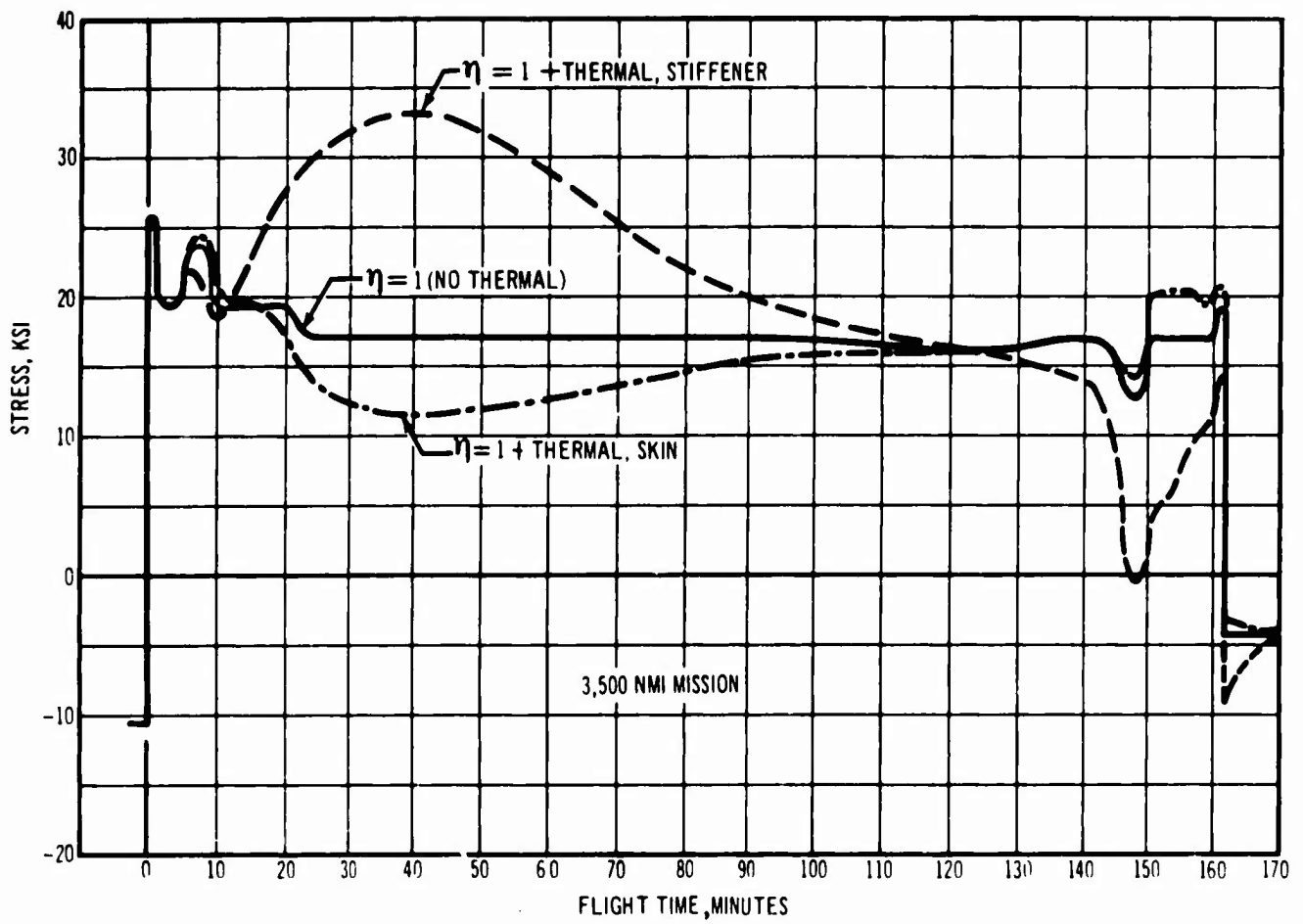


Figure 5-15. One-g Stress History, Movable-Wing Lower Surface At Midspan

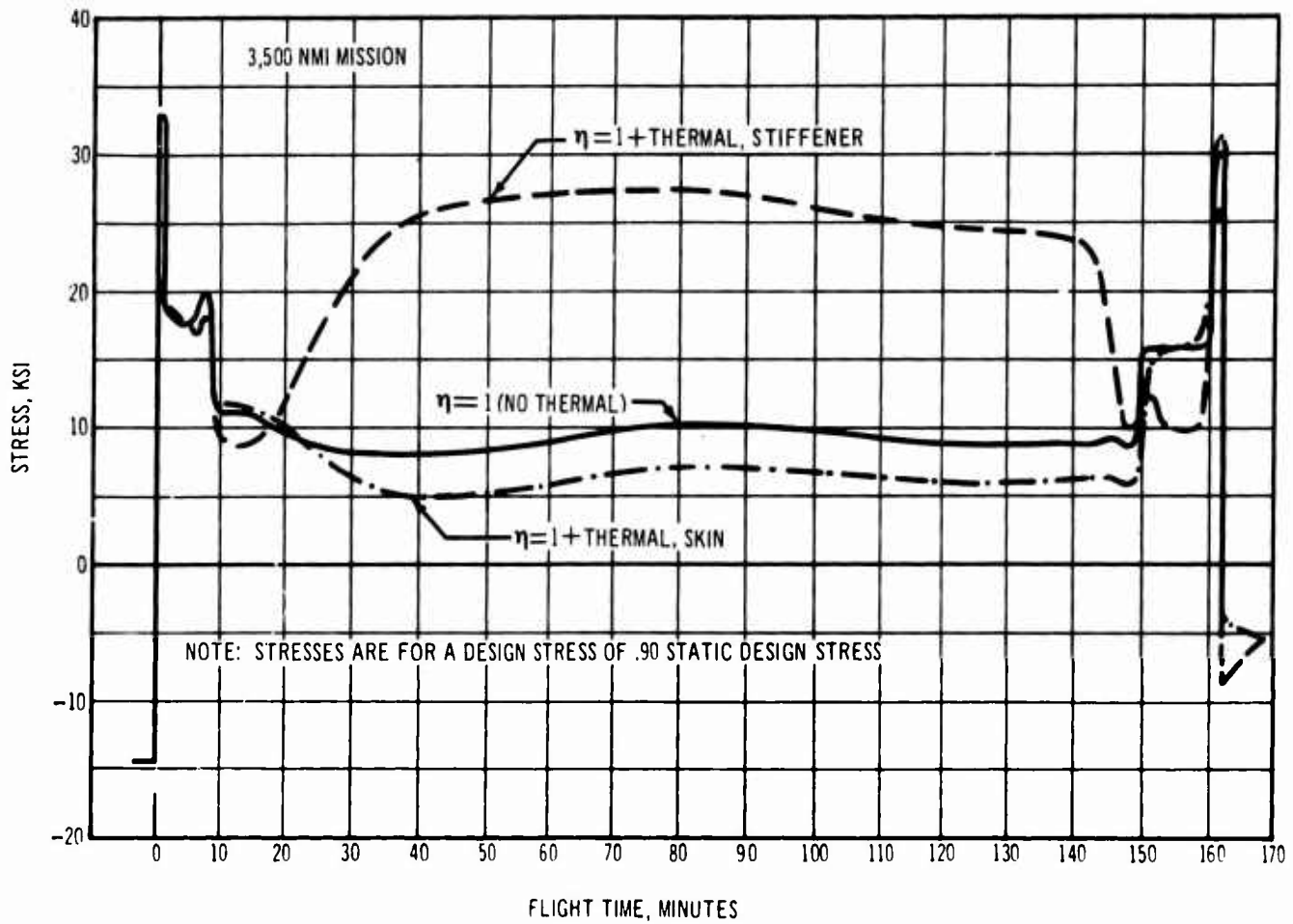


Figure 5-16. One-g Stress History, Wing-Center-Section Lower Surface

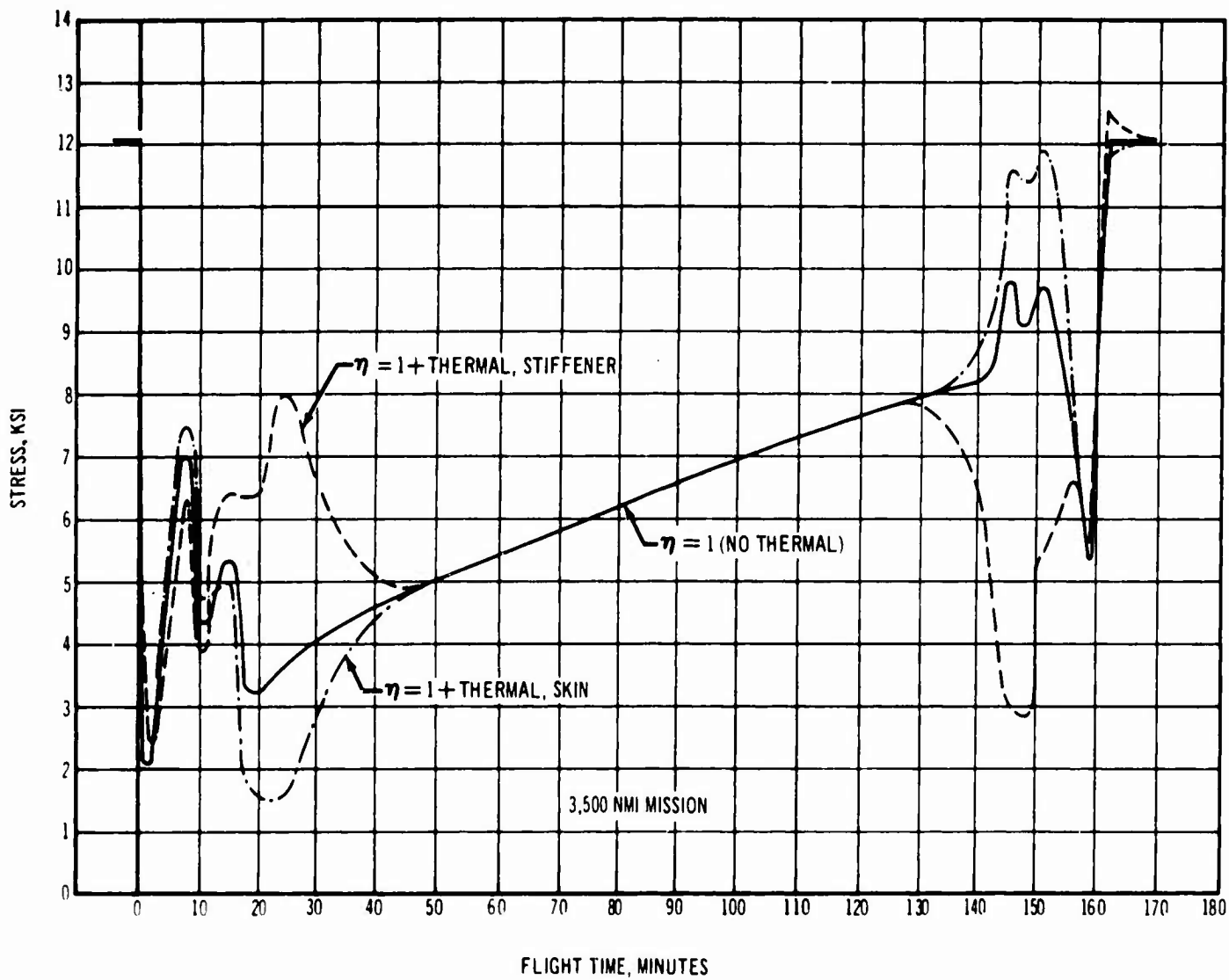


Figure 5-17. One-g Stress History, Forward-Fuselage Crown (30 Percent Fuselage Length)

V2-B2707-6-2



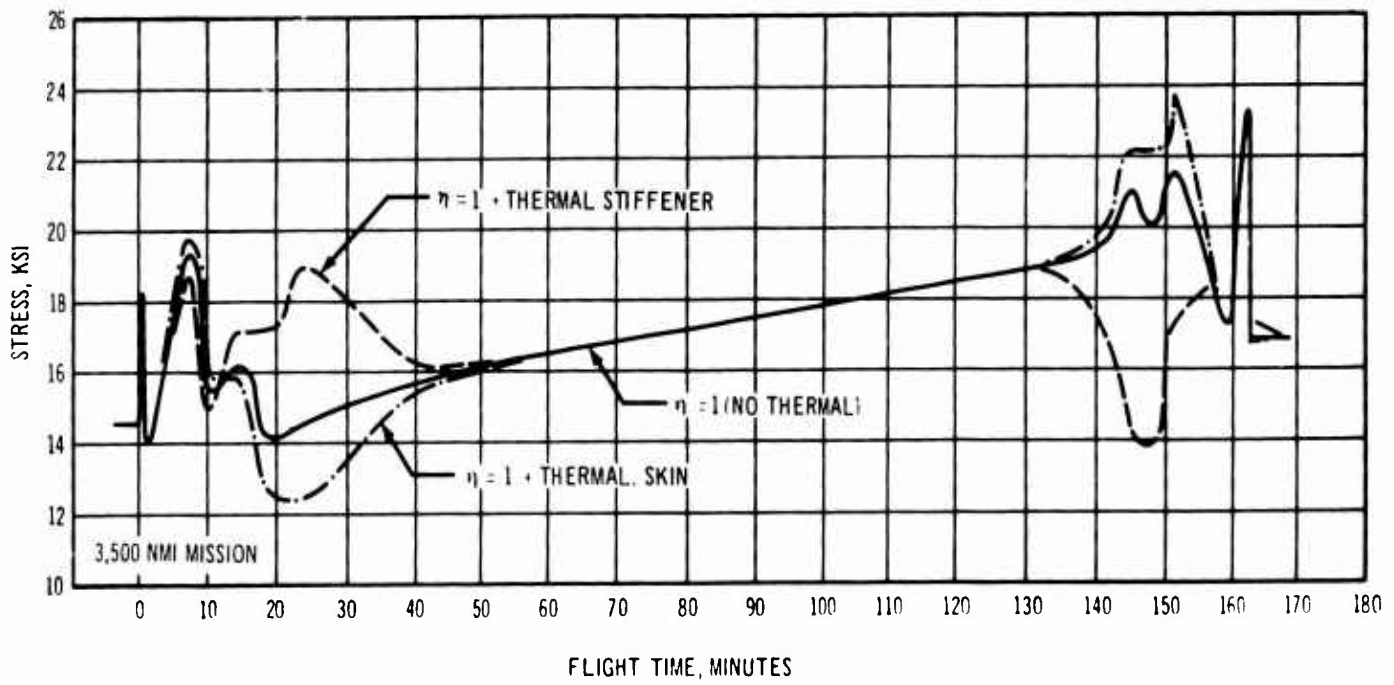


Figure 5-18. One-g Stress History, Forward-Fuselage Crown (50 Percent Fuselage Length)

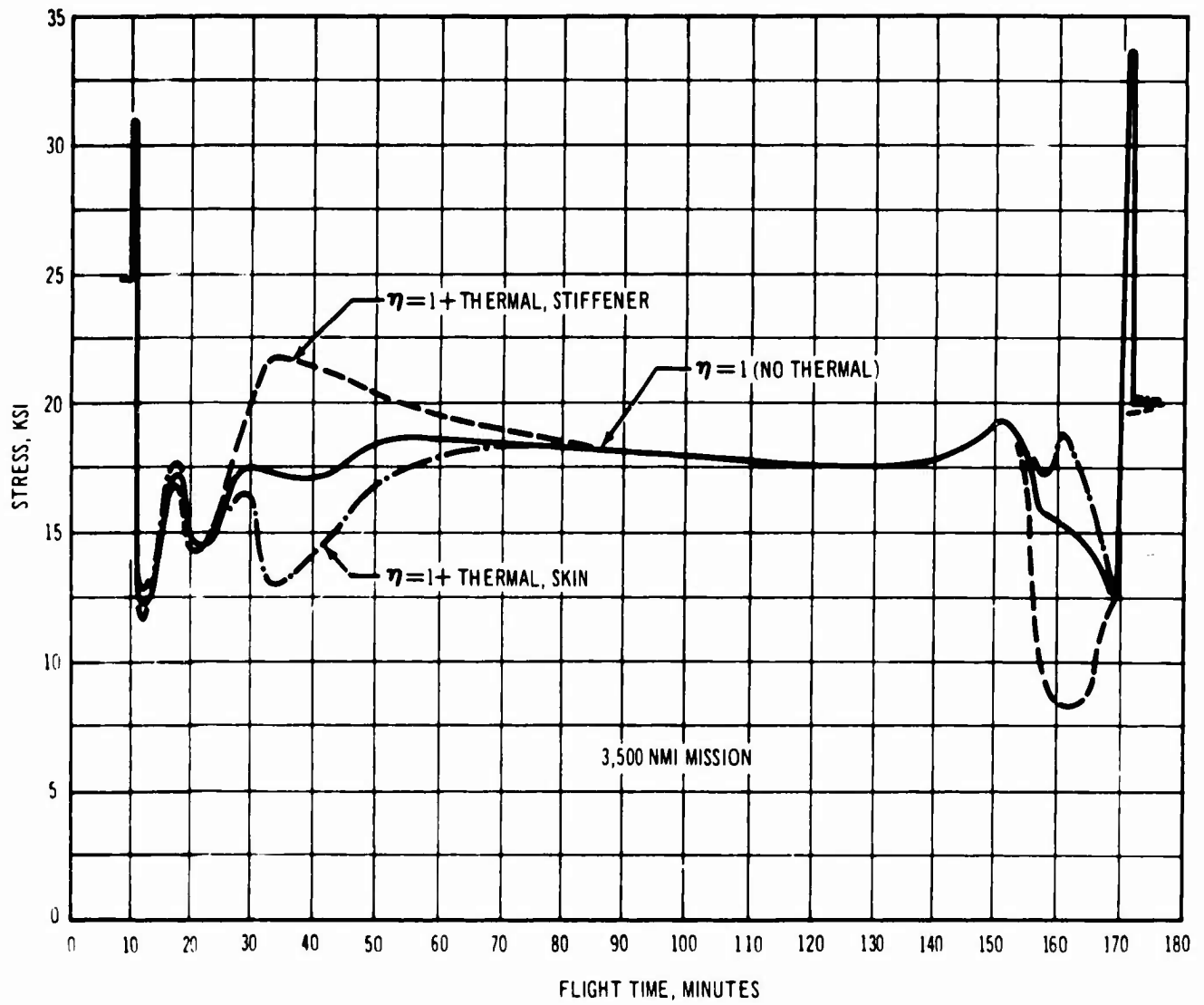


Figure 5-19. One-g Stress History, Aft Fuselage Crown

V2-B2707-6-2

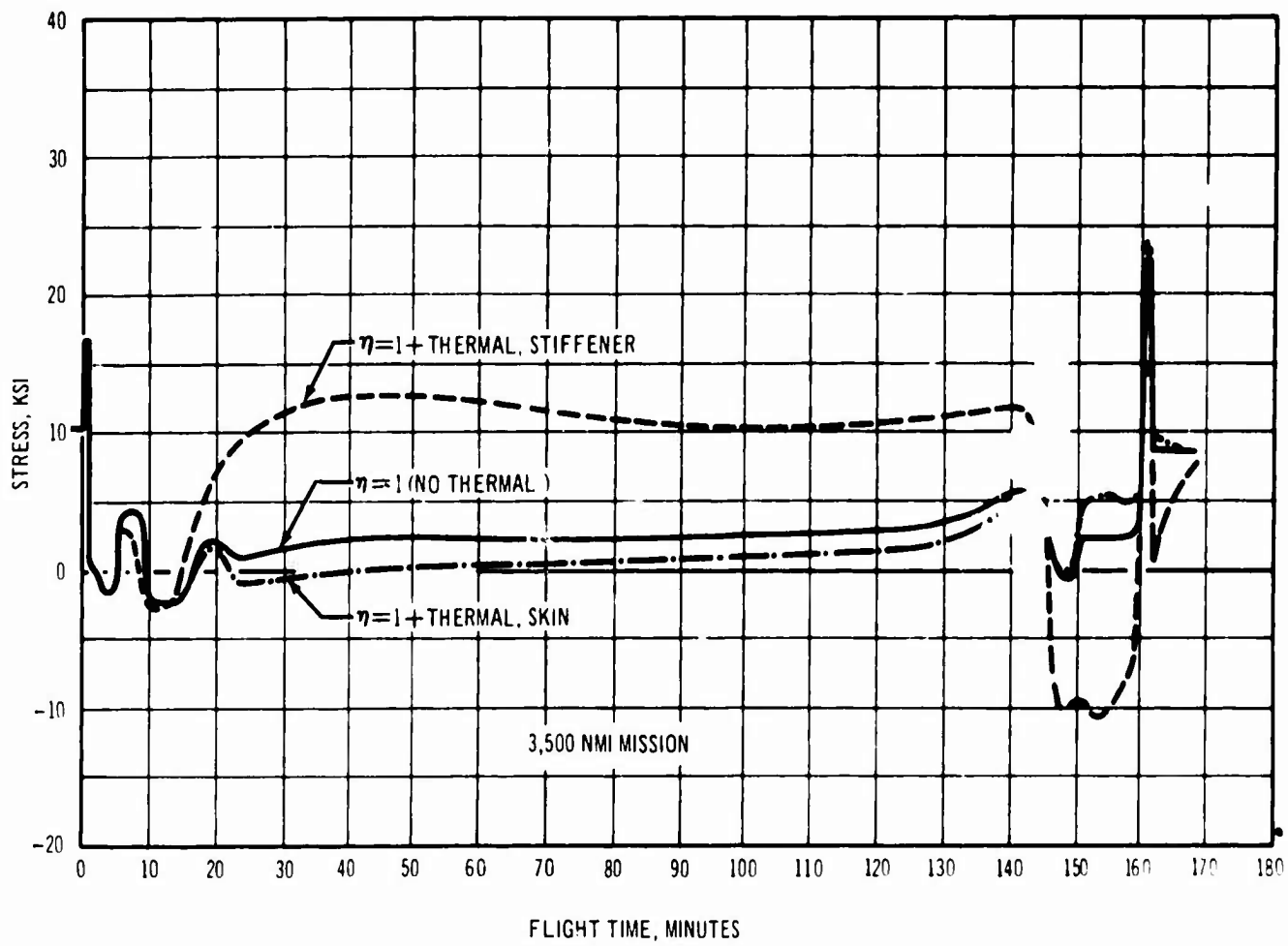


Figure 5-20. One-g Stress History, Horizontal-Tail Upper Surface at Root

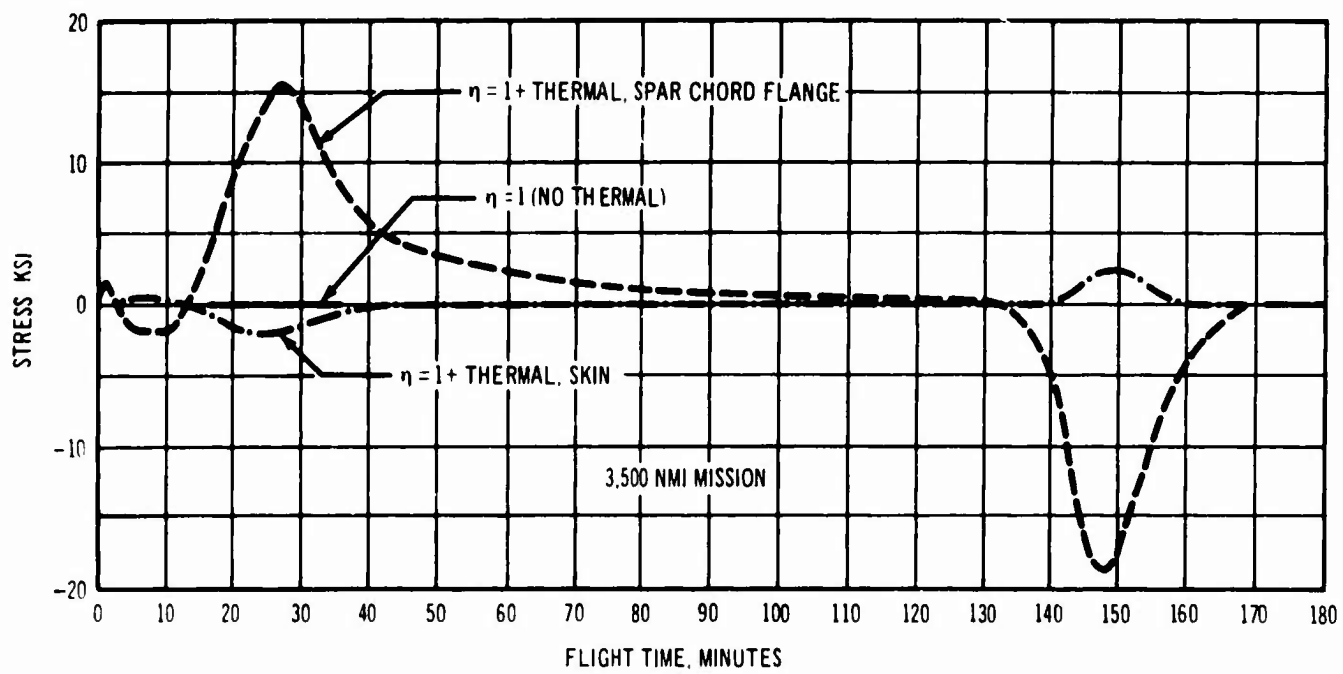


Figure 5-21. One-g Stress History, Vertical Tail at Root

## REFERENCES

The following documents are available at The Boeing Company, SST Division:

1. Wing Pivot Designs and Analysis for a Supersonic Transport, FDL-TDR 64-57, Vol. 1 April 1966
2. Lightning Protection for Supersonic Transport, D6-A10257-1, The Boeing Company, 1 September 1966
3. Electrical Bonding and Grounding Design Requirements for the B-2707 Airplane, D6-A10236-1, The Boeing Company, September 1966
4. SST Engineering Trade Studies Summary, D6-10187-1, The Boeing Company, in Press
5. The Use of High-Strength 4340 M Steel for SST Landing Gear Components, D6-17640, The Boeing Company, 23 April 1965
6. Nondestructive Test Inspection Procedures for the Boeing Jet Transports, D6-7170, The Boeing Company, 1 September 1966
7. Metallic Materials and Elements for Flight Vehicular Structures, MIL Handbook 5, March 1959 With Revisions
8. Design Manual, D-5000, The Boeing Company, Current Issue
9. R. A. Needham, "The Ultimate Strength of Aluminum-Alloy Formed Structural Shapes in Compression," *Journal of the Aeronautical Sciences*, April 1954
10. G. Gerard, "The Crippling Stress of Compression Elements," *Journal of Aeronautical Sciences*, Vol. 25, January 1958
11. COSMOS, A Computer Program for Structural Analysis, D2-4513, The Boeing Company, 26 January 1962, Rev. 16 October 1964
12. D. J. Peery, Aircraft Structures, McGraw-Hill, New York, 1950, pp.321 to 323
13. Airworthiness Standards: Transport Category Airplanes, Part 25, Federal Aviation Regulations
14. M. A. Melcon and A. F. Ensrud, "Analysis of Stiffened Curved Panels Under Shear and Compression," *Journal of the Aeronautical Sciences*, February, 1953
15. G. Gerard and H. Becker, Handbook of Structural Stability, Part III — Buckling of Curved Plates and Shells, NACA Technical Note 3783, August 1957
16. H. D. Emero and L. Spunt "Wing Box Optimization Under Combined Shear and Bending," *Journal of Aircraft*, March-April 1966
17. T. Coleman and J. Stickle, "Turbulence Environment for Supersonic Transports," *Society of Experimental Test Pilots, Quarterly Review — Supersonic Transport Symposium*, Vol. V, No. 4, 29-30 September 1961, pp. 144-160

References (Concluded)

18. R. Steiner, "A Review of NASA High-Altitude Clear Air Turbulence Sampling Programs," *Journal of Aircraft*, Vol. 3, No. 1, January-February 1966, pp. 48-52
19. Staff of Langley Airworthiness Branch, Operational Experiences of Turbine-Powered Commercial Transport Airplanes, NASA TND 1392, National Aeronautics and Space Administration, Washington, October, 1962
20. B. Milwitzky, Study of Taxiing Problems Associated with Runway Roughness, NASA Memo 2-21-59L, National Aeronautics and Space Administration, Washington, March 1959